

Dissertation zur Erlangung des Doktorgrades
der Fakultät für Chemie und Pharmazie
der Ludwig-Maximilians-Universität München



**Structure-Reactivity Relationships in Reactions
of 1,3-Diarylallyl Derivatives and of the
Corresponding Palladium Complexes**

Konstantin Troshin

aus

St. Petersburg, Russland

2012

Erklärung

Diese Dissertation wurde im Sinne von §7 der Promotionsordnung vom 28. November 2011 von Herrn Prof. Dr. Mayr betreut.

Eidesstattliche Versicherung

Diese Dissertation wurde selbständig und ohne unerlaubte Hilfe erarbeitet.

München, 20.09.2012

.....
Konstantin Troshin

Dissertation eingereicht am	20.09.2012
1. Gutachter	Prof. Dr. Herbert Mayr
2. Gutachter	Prof. Dr. Manfred Heuschmann
Mündliche Prüfung am	26.10.2012

Für meine Familie

Danksagung

Zuallererst möchte ich mich bei Herrn Prof. Dr. Herbert Mayr bedanken, der mir die Möglichkeit gegeben hat in seiner Gruppe zu promovieren. Seine unschätzbare Betreuung, die einem viel Raum für Kreativität und Entwicklung eigener Ideen lässt, hat mich allezeit dazu motiviert für jedes chemische Problem, was im Rahmen meiner Forschung entstand, eine Lösung zu suchen, was mir hoffentlich mit dieser Dissertation auch gelungen ist. Ohne sein Vertrauen zu den Mitarbeitern sowie seine stetigen Diskussions- und Hilfsbereitschaft wäre das nicht möglich gewesen.

Ich danke Herrn Prof. Dr. Manfred Heuschmann für die Bereitschaft, das Zweitgutachten meiner Arbeit zu übernehmen, sowie allen Mitgliedern des Prüfungsausschusses für ihre Teilnahmebereitschaft.

Bei Dr. Armin R. Ofial bedanke ich mich für zahlreiche Diskussionen und Vorschläge hinsichtlich meiner Publikationen und anderer Forschungsangelegenheiten.

Brigitte Janker, Nathalie Hampel und Hildegard Lipfert danke ich für die Chemikalien- und Gerätebestellung, synthetische Unterstützung und Erledigung organisatorischer Dinge.

Bei Herrn Prof. Dr. Paul Knochel möchte ich mich für die Erlaubnis bedanken, die HPLC Geräte seines Arbeitskreises zu benutzen, sowie für die Beratung hinsichtlich der Synthese optisch aktiver Allylalkohole. Für die Hilfe, die ich anfangs bei der Bedienung dieser Geräte gebraucht habe, danke ich Julia Tsvik.

Meiner F-Praktikantin Anna Kalinnik danke ich für die Mitarbeit. Obwohl ihre Daten es nicht geschafft haben, in die Publikationen und diese Dissertation zu kommen, haben sie mir bei der Entwicklung meiner Vorstellungen über die Ionenpaarung sehr geholfen.

Mein weiterer Dank gilt den Mitarbeitern der analytischen Abteilung der Fakultät Chemie und Pharmazie, die für die zügige Bearbeitung meiner Aufträge gesorgt haben.

Für das angenehme Arbeitsklima, das in all den Jahren meiner Promotion herrschte, danke ich allen ehemaligen und aktuellen Mitgliedern des Arbeitskreises. Besonders möchte ich mich bei den (Ex-)Kollegen bedanken, die mich nicht nur während der Arbeitszeit, sondern auch bei den zahlreichen Aktivitäten außerhalb der Forschung, begleitet haben: Dr. Nicolas Streidl, Dr. Markus Horn, Dr. Tanja Kanzian, Dr. Roland Appel, Dr. Sami Lakhdar, Johannes Ammer, Tobias Nigst, Dominik Allgäuer, Hans Laub, Alexander Wagner, Elija Wiedemann und Ivo Zenz. Ich hoffe, dass die entstandenen Freundschaften das Ende dieser Arbeit lange überdauern!

Für die zügige und effiziente Durchsicht dieser Dissertation bedanke ich mich bei Johannes Ammer, Anna Antipova, Hans Laub, Tobias Nigst, Alexander Wagner, Ivo Zenz und Dominik Allgäuer.

Meinen Landsmännern (oder fast Landsmännern) – Dr. Evgeny Larionov, Vasily Mezhnev, Dr. Aliaksei Putau, Varvara Morozova, und insbesondere Dr. Boris Maryasin und Anna Antipova, – die mich kürzer oder länger während meiner Promotion begleitet haben, danke ich für die zahlreichen "Russenpartys" und "Russenausflüge", bei den ich jede Menge Spaß aber auch was zum Nachdenken hatte. Auch in diesem Fall hoffe ich, dass wir uns nicht aus den Augen verlieren, unabhängig davon in welchen Ländern und Städten unsere zukünftigen Arbeitsstellen sich befinden mögen.

Zuletzt möchte ich mich bei allen Mitgliedern meiner Familie bedanken, die mich während meiner Arbeit auf die eine oder andere Weise unterstützt haben, insbesondere bei meinen Großeltern, meinem Onkel und, natürlich, bei meiner Mutter und meinem Stiefvater. Meiner Familie, und insbesondere meiner Mutter, die seit meiner Geburt immer alles Mögliche und Unmögliche getan hat, um mich zu unterstützen, ist diese Arbeit gewidmet.

Publications

[1] **Electrophilicities of Symmetrically Substituted 1,3-Diarylallyl Cations**

Troshin, K.; Schindele, C.; Mayr, H. *J. Org. Chem.* **2011**, *76*, 9391-9408

[2] **How does Palladium Coordination Affect the Electrophilicities of Allyl Cations?**

Development of a Robust Kinetic Method for Following Reactions of

$[(\eta^3\text{-Diarylallyl})\text{Pd}(\text{Ph}_3\text{P})_2]^+$ with Nucleophiles

Troshin, K.; Mayer, P.; Mayr, H. *Organometallics* **2012**, *31*, 2416-2424

[3] **(*R,E*)-3-(4-Chlorophenyl)-1-phenylallyl 4-nitrobenzoate**

Troshin, K.; Mayer, P.; Mayr, H. *Acta Crystallogr., Sect. E: Struct. Rep. Online* **2012**, *68*, o2549

[4] **Ion Pair Dynamics: Solvolyses of Chiral 1,3-Diarylallyl Carboxylates as a Case Study**

Troshin, K.; Mayr, H. *J. Am. Chem. Soc.*, submitted

Conference Contribution

Dec 2009

12th Kyushu International Symposium on Physical Organic Chemistry, Fukuoka, Japan

Poster: "Electrophilicities and Electrophilicities of Symmetrical 1,3-Diarylallyl Cations"

Table of Contents

Chapter 1. Summary	1
1. General	1
2. Electrophilicities of Symmetrically Substituted 1,3-Diarylallyl Cations	2
3. Ion Pair Dynamics: Solvolyses of Chiral 1,3-Diarylallyl Carboxylates as a Case Study	4
4. Electrofugalities of Symmetrical 1,3-Diarylallyl Cations	6
5. How Does Palladium Coordination Affect the Electrophilicities of Allyl Cations? Development of a Robust Kinetic Method for Following Reactions of $[(\eta^3\text{-Diarylallyl})\text{Pd}(\text{PPh}_3)_2]^+$ with Nucleophiles	8
Chapter 2. Introduction	12
1. Allyl Derivatives in Synthetic and Mechanistic Investigations	12
2. Allylic Rearrangements and Ion Pairs in $\text{S}_{\text{N}}1$ Solvolyses	13
3. Linear Free Energy Relationships	16
4. Objectives	18
5. References	20
Chapter 3. Electrophilicities of Symmetrically Substituted 1,3-Diarylallyl Cations	24
1. Introduction	24
2. Results and Discussion	25
2.1. Synthesis of 1,3-Diarylallyl Cations 1(a-i)	25
2.2. Product Studies	27
2.3. Kinetic Experiments	32
2.4. Determination of the Electrophilicity Parameters E	34
2.5. Quantum Chemical Calculations	37
2.6. Comparison with Benzhydryl Cations	42
3. Conclusions	43
4. Experimental Section	44
4.1. General	44
4.2. Synthetic Procedures	44
4.3. Product Studies	53
4.4. Determination of the Rate Constants	65
4.5. Kinetic Measurements	66
4.5.1. Reactions of (<i>E</i>)-1,3-bis(3,5-difluorophenyl)allyl cation (1a)	66
4.5.2. Reactions of (<i>E</i>)-1,3-bis(3-difluorophenyl)allyl cation (1b)	68
4.5.3. Reactions of (<i>E</i>)-1,3-bis(4-bromophenyl)allyl cation (1c)	69
4.5.4. Reactions of (<i>E</i>)-1,3-bis(4-chlorophenyl)allyl cation (1d)	71
4.5.5. Reactions of (<i>E</i>)-1,3-diphenylallyl cation (1e)	72
4.5.6. Reactions of (<i>E</i>)-1,3-di- <i>p</i> -tolylallyl cation (1f)	73
4.5.7. Reactions of (<i>E</i>)-1,3-bis(4-methoxyphenyl)allyl cation (1g)	73
4.5.8. Reactions of (<i>E</i>)-1,3-bis(4-dimethylaminophenyl)allyl cation (1h)	75

4.5.9. Reactions of (<i>E</i>)-1,3-bis(julolidin-9-yl)allyl cation (1i)	76
4.6. Computational Results	79
4.6.1. Conformational analysis	79
4.6.2. Calculated energies	84
5. Supplementary Section	88
6. References	93
Chapter 4. Ion Pair Dynamics: Solvolyses of Chiral 1,3-Diarylallyl Carboxylates as a Case Study	97
1. Introduction	97
2. Results	101
2.1. Synthesis and Chromatographic Separation of the Model Compounds	101
2.2. Kinetic Experiments	103
3. Discussion	110
A Comprehensive View on Solvolyses of Allyl Carboxylates	118
4. Conclusions	126
5. Experimental Section	127
5.1. General	127
5.2. Synthetic Procedures	127
5.3. NMR Product Studies	130
5.4. HPLC Kinetic Measurements	131
5.4.1. General procedure	131
5.4.2. HPLC calibration	134
5.4.3. Kinetics of the solvolysis reactions	136
5.5. Isomerization of 3 and 4 in the Presence of Acids	174
5.6. Reaction of the Free Cation 6 with 60% Aq Acetone	174
5.7. Determination of the Microscopic Rate Constants	175
5.7.1. Direct solution	175
5.7.2. Steady state approximation	180
5.7.3. Fitting of the experimental values	182
5.7.4. M-files used for parameter optimization	202
5.8. NPA Calculation for the Cation 6 (B3LYP/6-31G(d,p))	211
5.9. Thermal Ellipsoid Plot for (<i>R</i>)- 1	212
6. Appendix. Solvolyses of (<i>R</i>)-1 and (<i>S</i>)-1 in the Presence of Tetrabutylammonium Benzoate	213
6.1. Discussion	213
6.2. Experimental Section	214
6.2.1. Synthesis of (<i>E</i>)-3-(4-chlorophenyl)-1-phenylallyl benzoate	214
6.2.2. HPLC kinetic measurements	214
7. References	227
Chapter 5. Electrofugalities of Symmetrical 1,3-Diarylallyl Cations	233
1. Introduction	233
2. Results and Discussion	234
2.1. Synthesis of the Substrates	234
2.2. Kinetic Experiments	235
2.3. Winstein-Grunwald Analysis	241
2.4. Hammett Analysis	243

2.5. Determination of the Electrofugality Parameters	244
2.6. Comparison of 1,3-Diarylallyl and Benzhydryl Cations	246
2.7. Electrophilicity–Electrofugality Relationships	249
2.8. Parallel S _N 1 and S _N 2 Mechanisms in Reactions of 1a -Br with Amines	250
2.9. Changes of Solvolysis Mechanisms of Allyl Derivatives	251
3. Conclusions	254
4. Experimental Section	254
4.1. General	254
4.2. Synthetic Procedures	255
4.3. Kinetic Measurements	258
4.3.1. Calibration curves	259
4.3.2. Solvolyses of 1a -LG	260
4.3.3. Solvolyses of 1b -LG	268
4.3.4. Solvolyses of 1c -LG	269
4.3.5. Solvolyses of 1d -LG	271
4.3.6. Solvolyses of 1e -LG	274
4.3.7. Solvolyses of 1f -LG	278
4.3.8. Solvolyses of 1g -LG	283
4.3.9. Solvolyses of 1h -LG	284
5. Supplementary Section	285
5.1. Hammett Correlations	285
5.1.1. 1,3-Diarylallyl chlorides	285
5.1.2. 1,3-Diarylallyl 3,5-dinitrobenzoates	286
5.1.3. 1,3-Diarylallyl 4-nitrobenzoates	288
5.1.4. Electrofugality parameters E_f	289
5.2. Electrofugalities vs Calculated Gas-Phase Methyl Anion Affinities (MP2FC/6-31+G(2d,p)//B3LYP/6-31G(d,p) level of theory)	289
5.3. Winstein-Grunwald Correlations for Benzhydryl Systems	290
5.4. Determination of the S _N 2C ⁺ Region for the Solvolysis of 1,3-Diarylallyl 4-Nitrobenzoates	291
6. References	292
Chapter 6. How Does Palladium Coordination Affect the Electrophilicities of Allyl Cations? Development of a Robust Kinetic Method for Following Reactions of $[(\eta^3\text{-Diarylallyl})\text{Pd}(\text{PPh}_3)_2]^+$ with Nucleophiles	295
1. Introduction	295
2. Results and Discussion	297
2.1. Synthesis of the Complexes 1(a–c)	297
2.2. Kinetic Investigations	297
2.3. Four-Component-System for Determining The Rates of the Reactions of $[(\eta^3\text{-Allyl})\text{Pd}(\text{PPh}_3)_2]^+$ with Amines	302
2.4. Determination of Electrophilicity Parameters E for 1(a–c)	306
2.5. Comparison of the Allylpalladium Complexes 1(a–c) with the Free Diarylallyl Cations 5(a–c)	309
3. Conclusions	311
4. Experimental Section	312
4.1. General	312
4.2. Synthetic Procedures	313

4.3. Product Studies	314
4.4. Estimation of the Equilibrium Constant of the Ligand Exchange (K_E) between 1a and Benzylamine (2g)	316
4.5. Kinetic Measurements	318
4.6. ESI Experiments	342
4.6.1. Sample preparation and settings	342
4.6.2. Spectra	342
4.7. Thermal Ellipsoid Plot for the Compound 1b -TfO	344
5. Supplementary Section	345
6. References	347

Chapter 1. Summary

1. General

Rates of many electrophile-nucleophile combinations were shown to follow the linear free energy relationship (eq 1), where nucleophiles are characterized by the nucleophilicity and sensitivity parameters N and s_N , and the reactivities of electrophiles are quantified by the electrophilicity parameter E .

$$\log k (20\text{ }^\circ\text{C}) = s_N(N + E) \quad (1)$$

An analogous approach (eq 2) was also proposed for the reverse reactions. In eq 2, the first-order rate constants of bond heterolyses (k_1) are correlated with two solvent-dependent nucleofuge-specific parameters – sensitivity s_f , and nucleofugality N_f – and one solvent-independent electrofuge-specific parameter E_f .

$$\log k_1 (25\text{ }^\circ\text{C}) = s_f(N_f + E_f) \quad (2)$$

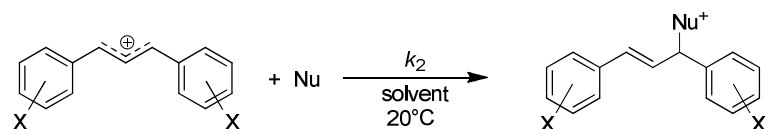
This thesis was designed to examine the applicability of eqs 1 and 2 for the corresponding reactions of 1,3-diarylallyl derivatives.

As unique information on ion pair dynamics during S_N1 reactions can be obtained by studying transformations of asymmetric allyl derivatives, such a system should be investigated by employing modern analytical methods.

2. Electrophilicities of Symmetrically Substituted 1,3-Diarylallyl Cations

Kinetics of the reactions of nine symmetrically substituted 1,3-diarylallyl cations with different nucleophiles were studied photometrically in dichloromethane, acetonitrile, and DMSO solutions (Scheme 1).

Scheme 1.



The resulting second-order rate constants k_2 were found to correlate with N and s_N parameters, which have previously been derived from the reactions of the corresponding nucleophiles with benzydrylium ions, showing the applicability of eq 1 (Figure 1).

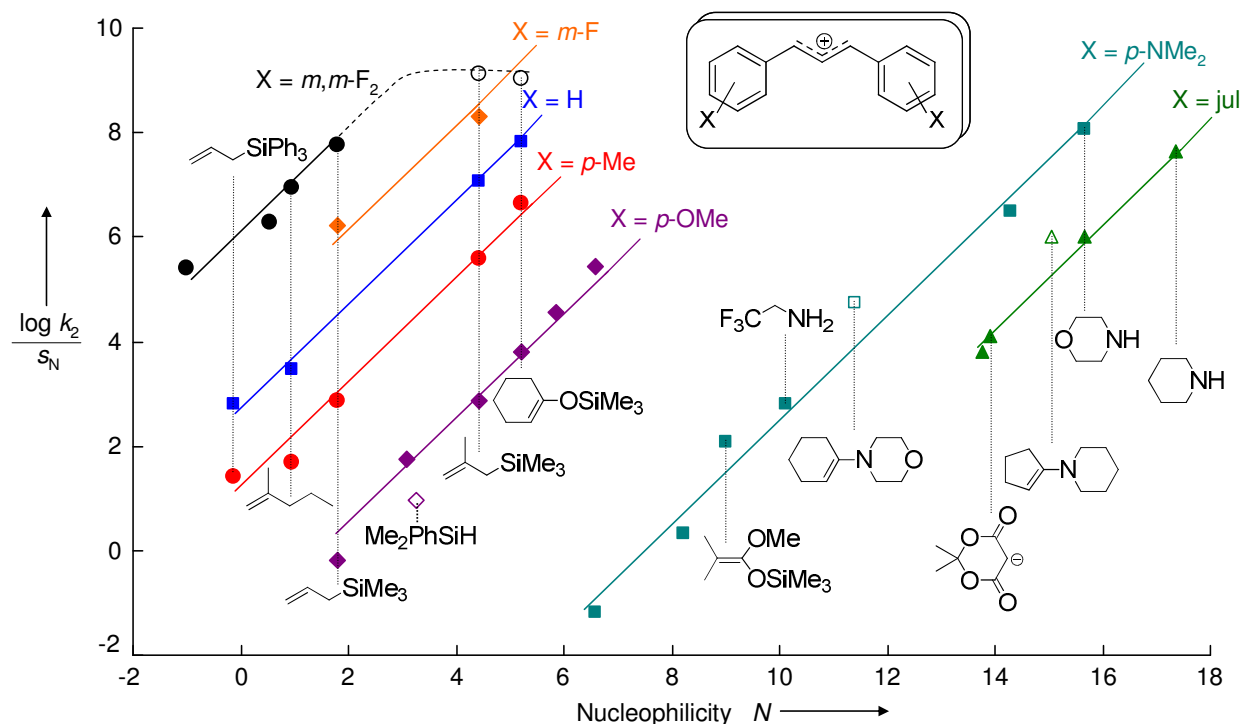


Figure 1. Plot of $(\log k_2)/s_N$ versus N for the reactions of the 1,3-diarylallyl cations with various nucleophiles. The data points shown with open symbols were not used for the determination of electrophilicity parameters E of the corresponding cations. The abbreviation jul is defined in Figure 2.

The electrophilicity parameters E of the investigated 1,3-diarylallyl cations were derived from these correlations and compared with the electrophilicities of analogously substituted benzhydrylium ions (Figure 2a). The reactivity range covered by 1,3-diarylallyl cations studied in this work (16 orders of magnitude) is slightly smaller than that for analogously substituted diarylmethyl cations. A linear correlation was observed between the E values of benzhydrylium ions and their vinylogs (Figure 2b).

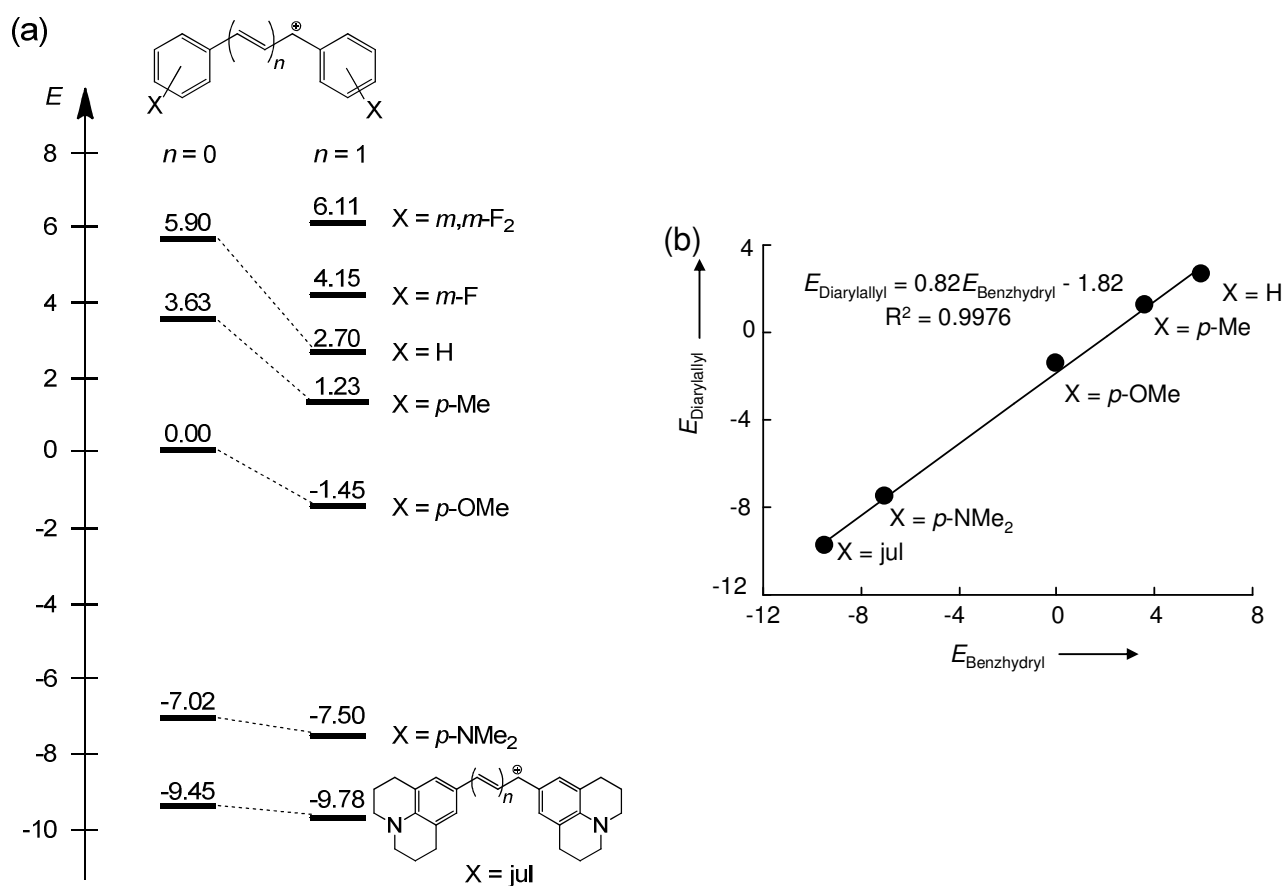


Figure 2. Electrophilicities E of the 1,3-diarylallyl cations compared with those of the corresponding benzhydrylium ions.

Good linear correlations were found between the electrophilicities E and the quantum chemically calculated gas-phase methyl anion affinities of the allyl cations and the σ^+ constants of the substituents X . These correlations may be employed to estimate reactivities of further 1,3-diarylallyl cations.

3. Ion Pair Dynamics: Solvolyses of Chiral 1,3-Diarylallyl Carboxylates as a Case Study

Chiral HPLC was used to follow the time-dependent concentrations of all four isomeric esters (two regioisomeric pairs of enantiomers) and all four isomeric alcohols generated during the hydrolysis of enantiopure 1-(4-chlorophenyl)-3-phenylallyl and 3-(4-chlorophenyl)-1-phenylallyl 4-nitrobenzoates in 60 % aq acetone in the presence and absence of external nucleophiles (Figure 3, for formulae see Scheme 2).

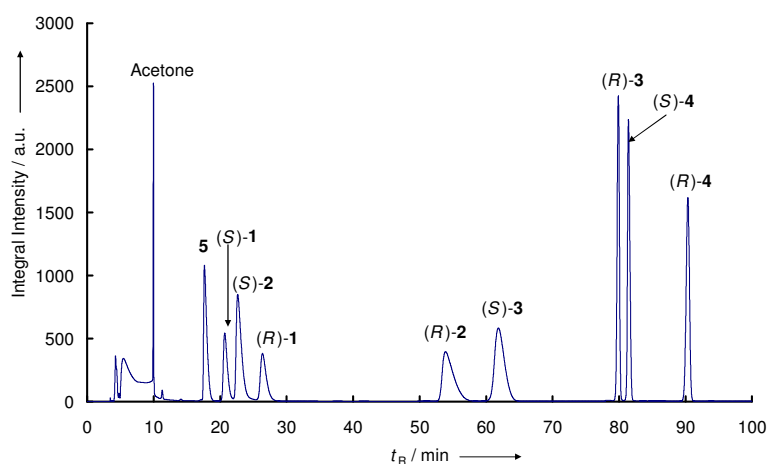
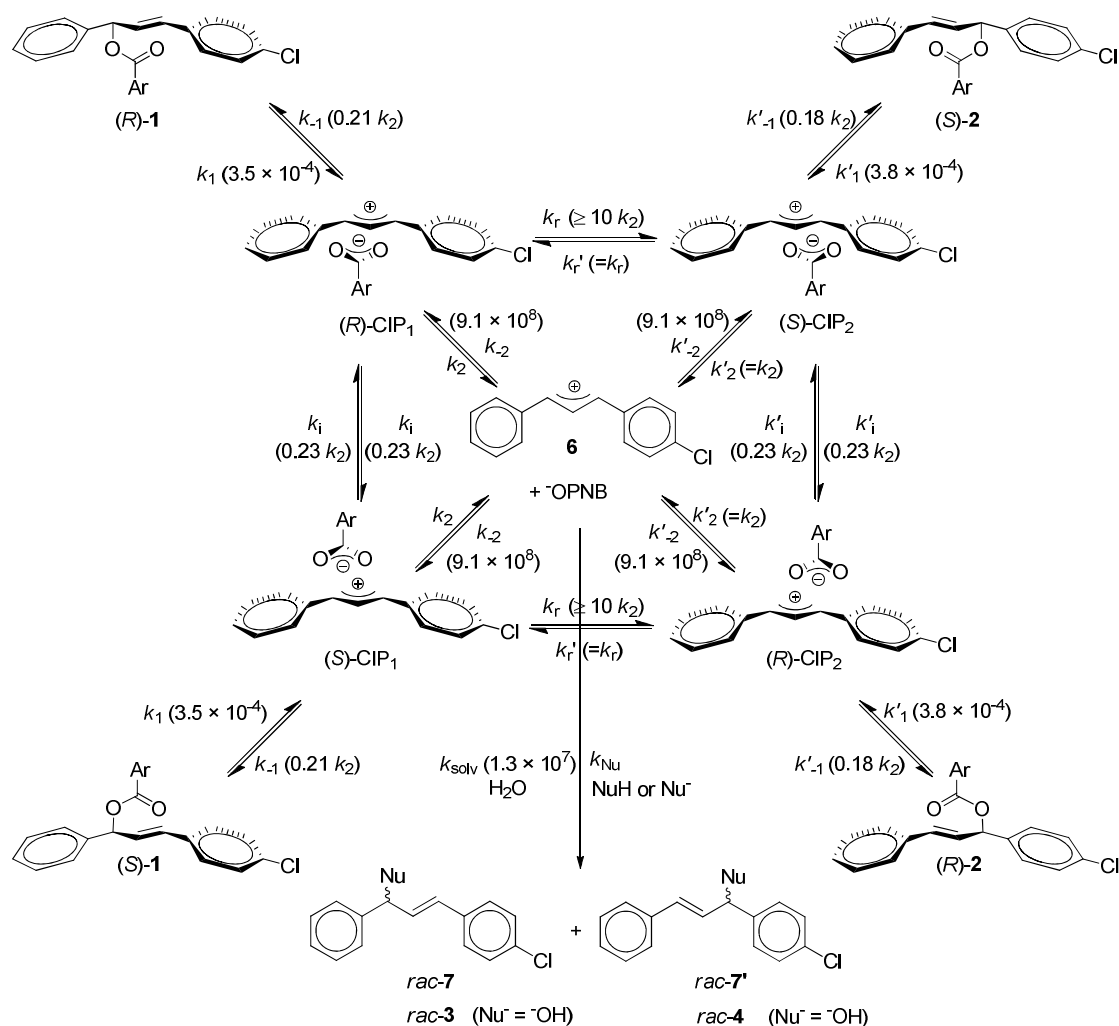


Figure 3. Chromatogram of an artificial mixture of racemic **1-4** and (*E*)-1-(4-methylphenyl)-3-phenylprop-2-en-1-one (**5**) (internal standard). For formulae see Scheme 2.

Combination of these results with the directly measured rate constant for the reaction of the laser-flash photolytically generated 1-(4-chlorophenyl)-3-phenylallyl cation with water in aqueous acetone provided a complete mechanistic scheme for this solvolysis cascade. As depicted in Scheme 2, the slowest step is the initial ionization leading to the contact ion pairs ($k_1 = 3.5 \times 10^{-4} \text{ s}^{-1}$, $k'_1 = 3.8 \times 10^{-4} \text{ s}^{-1}$). Suprafacial migration of the 4-nitrobenzoate anion ($k_r = k'_r > 10k_2$) is the most likely transformation of the contact ion pair, followed by dissociation ($k_2 = k'_2$) and, finally, inversion ($k_i = k'_i = 0.23k_2$) and ion pair collapse ($k_{-1} = 0.21k_2$, $k'_{-1} = 0.18k_2$). This sequence explains the partial stereospecificity of internal return, i.e., the fact that (*S*)-**2** is the major product among the rearranged esters during solvolysis of (*R*)-**1** and vice versa.

Scheme 2. Mechanism for the Solvolysis of Allyl 4-Nitrobenzoates **1** and **2**.^a

^a The rate constants shown in parentheses result from the simulations of experimental data based on the mechanism depicted in this scheme. All first-order rate constants as well as the pseudo-first-order rate constant k_{solv} are given in s^{-1} and correspond to 60% aq acetone at 25 °C. Second-order rate constants k_{-2} and k'_{-2} are given in $\text{M}^{-1} \text{s}^{-1}$. $\text{}^- \text{OPNB}$ = 4-nitrobenzoate.

The results of this work were combined with previously determined electrophilicity parameters E for 1,3-diarylallyl cations to analyze the role of internal and external return in solvolyses of 1,3-diarylallyl 4-nitrobenzoates. While the parent 1,3-diphenylallyl 4-nitrobenzoate ($E = 2.7$) is predicted to solvolyze with 16% internal and 11% external return, the contribution of external return increases, and the contribution of internal return decreases with increasing stabilization (decreasing electrophilicity E) of the allyl cations (Figure 4).

Eq 1 can be used to estimate the role of internal and external return also for other substrates.

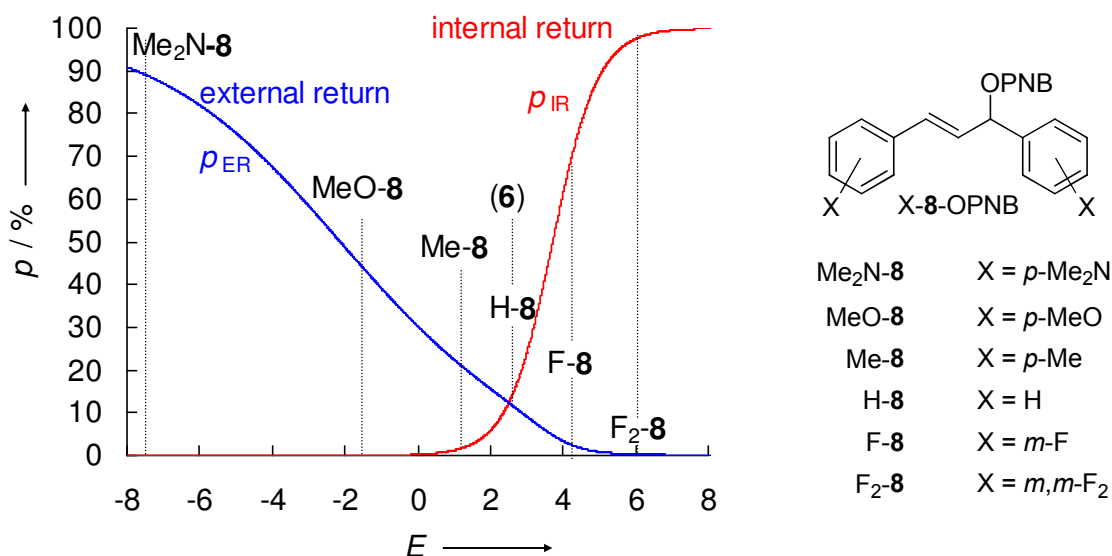
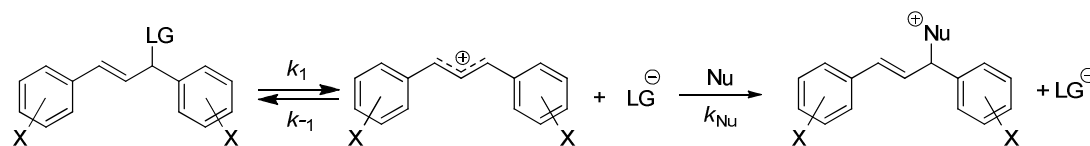


Figure 4. Dependencies of probabilities of internal and external return (p_{IR} and p_{ER}) for solvolyses of 1,3-diarylallyl 4-nitrobenzoates in 60% aq acetone (25 °C) on the E values of the corresponding cations for $[\text{OPNB}^-] = 5 \text{ mM}$. $\text{OPNB}^- = 4\text{-nitrobenzoate}$.

4. Electrofugalities of Symmetrical 1,3-Diarylallyl Cations

Heterolysis rate constants k_1 of halides and carboxylates derived from eight differently substituted 1,3-diarylallyl cations have been determined in various solvents (Scheme 3).

Scheme 3.



Though eq 2 was found to predict heterolysis rates of 1,3-diarylallyl bromides, chlorides and carboxylates with an accuracy of factor 5 from a single set of E_f parameters and the benzhydrylium-based nucleofuge-specific parameters N_f and s_f , systematic deviations are evident. Thus, the 1,3-diarylallyl carboxylates react generally faster while the 1,3-diarylallyl chlorides react generally more slowly than calculated by eq 2 from the benzhydrylium-based nucleofuge-specific parameters N_f and s_f , when both types of leaving groups were used to determine the electrofugality parameters E_f (Figure 5).

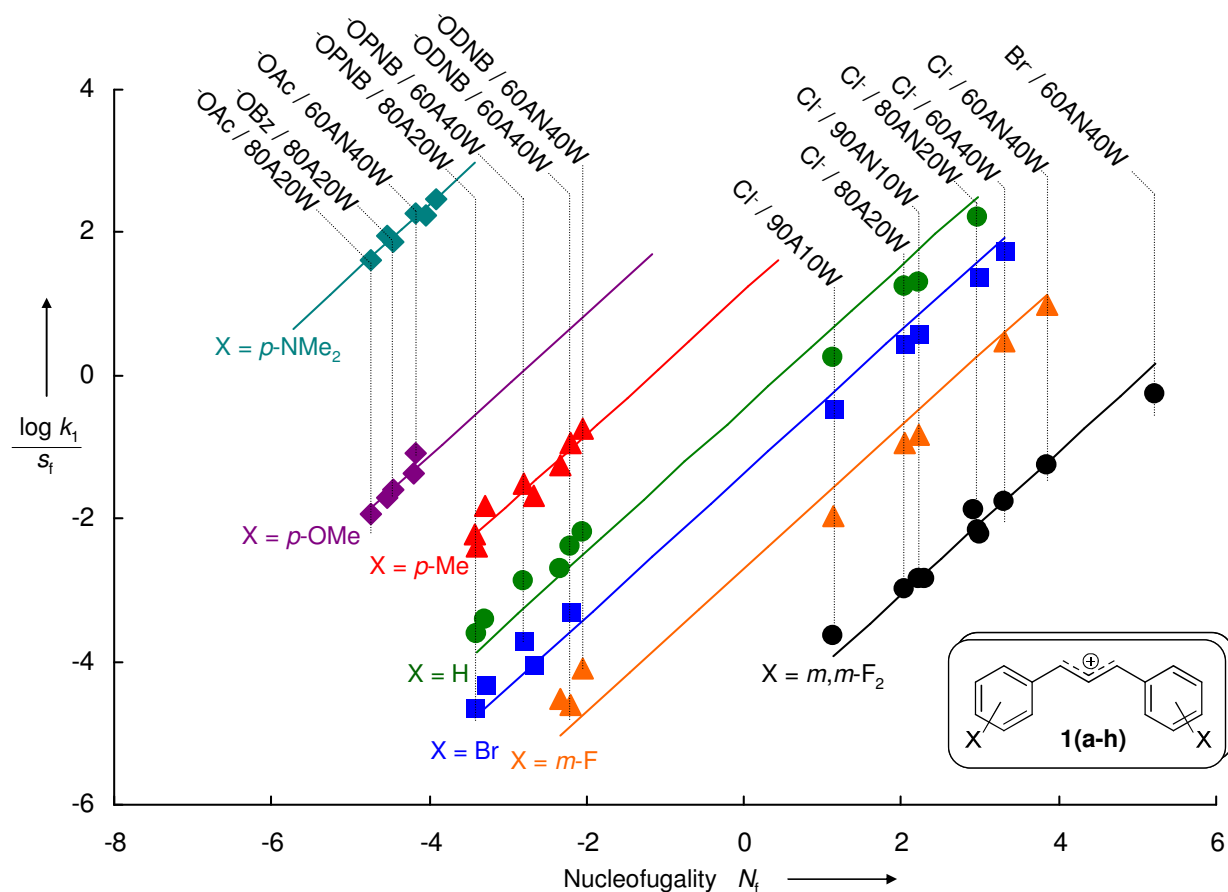


Figure 5. Plot of $(\log k_1)/s_f$ versus N_f for solvolyses of 1,3-diarylallyl derivatives in various solvents. Abbreviations used for the solvents are: A – acetone, AN – acetonitrile, W – water. All solvent ratios are given in % v/v. Abbreviations for leaving groups are: $^-$ OPNB = 4-nitrobenzoate, $^-$ ODNB = 3,5-dinitrobenzoate.

As in the benzhydryl and trityl series, solvolyses of 1,3-diarylallyl bromides and chlorides have significantly larger Winstein-Grunwald m -values than carboxylates, which have been explained by late and early transition states. Substituent variation affects solvolysis rates of 1,3-diarylallyl derivatives significantly less than those of benzhydryl derivatives (Figure 6a). As the intrinsic barriers for heterolyses of 1,3-diarylallyl derivatives are lower than those for the corresponding benzhydryl heterolyses, one comes to the conclusion that 1,3-diarylallyl derivatives ionize faster than benzhydryl derivatives of same electrophilicity E and that 1,3-diarylallylium ions react faster with nucleophiles than benzhydryl cations of equal electrofugality E_f . The reactivity parameters E (Figure 2) and E_f (Figure 6a) have been combined to derive the full mechanistic spectrum of 1,3-diarylallyl solvolyses (Figure 6b).

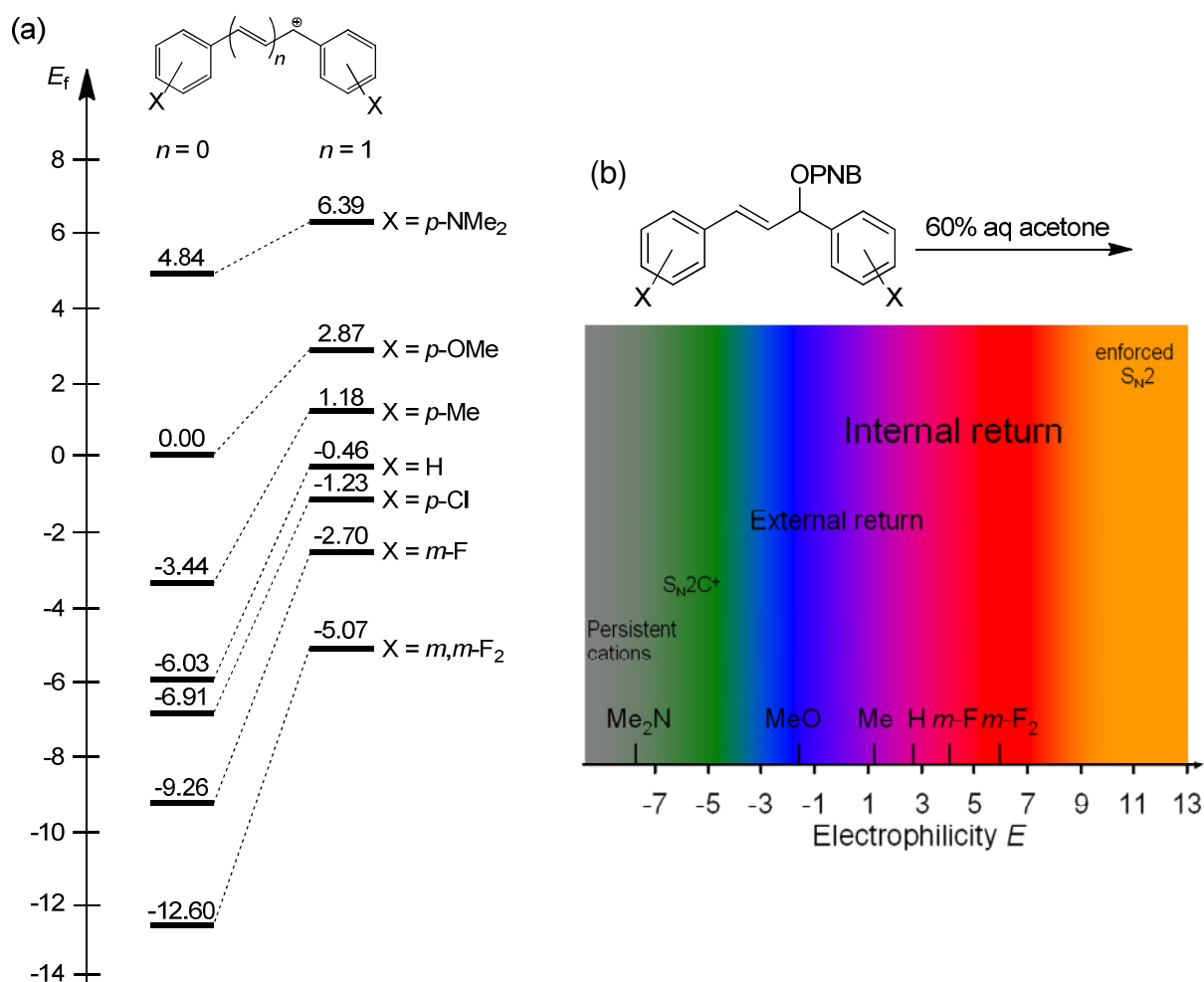


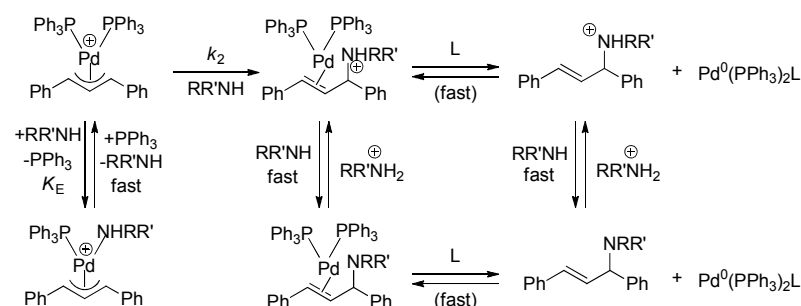
Figure 6. (a) Electrofugalities E_f of the 1,3-diarylallyl cations compared with those of the corresponding benzhydrylium ions. (b) Comprehensive spectrum of 1,3-diarylallyl 4-nitrobenzoate solvolysis in 60 % aq acetone ($[\text{OPNB}] = 5 \text{ mM}$).

5. How Does Palladium Coordination Affect the Electrophilicities of Allyl Cations? Development of a Robust Kinetic Method for Following Reactions of $[(\eta^3\text{-Diarylallyl})\text{Pd}(\text{PPh}_3)_2]^+$ with Nucleophiles

Kinetics of the reactions of $[(\eta^3\text{-1,3-diarylallyl})\text{Pd}(\text{PPh}_3)_2]^+$ complexes with carbanions, enamines, amines, and triphenylphosphine have been investigated photometrically in dichloromethane, DMSO, and acetonitrile solutions at 20 °C. Amines were found to react

both at palladium (substitution of PPh_3) and at the allyl ligands (Scheme 4) causing complex and poorly reproducible kinetics.

Scheme 4. Mechanism for Amination of Allylpalladium Complexes.



Excellent reproducibility of the second-order rate constants for the attack at the allyl ligand was achieved when the reactions were studied in the presence of traces of PPh_3 and fumaronitrile (Figure 7).

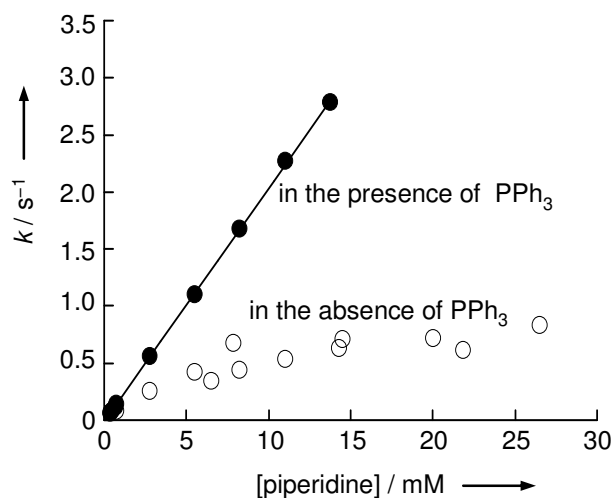


Figure 7. Correlation between the pseudo-first-order rate constants k_{obs} for the decay of absorbance at $\lambda = 360$ nm (absorption maximum of the complex) during the reaction of $[(\eta^3\text{-1,3-diphenylallyl})\text{Pd}(\text{PPh}_3)_2]^+\text{BF}_4^-$ with piperidine (used in excess) in the absence (open symbols) and presence of PPh_3 (filled symbols) and the amine concentration (acetonitrile, 20°C).

The second-order rate constants k_2 for the attack of nucleophiles at the allyl ligands were found to follow the correlation described by eq 1. The resulting electrophilicity parameters E

of $[(\eta^3\text{-}1,3\text{-diarylallyl})\text{Pd}(\text{PPh}_3)_2]^+$ are compared with the reactivities of other important classes of electrophiles in Figure 8.

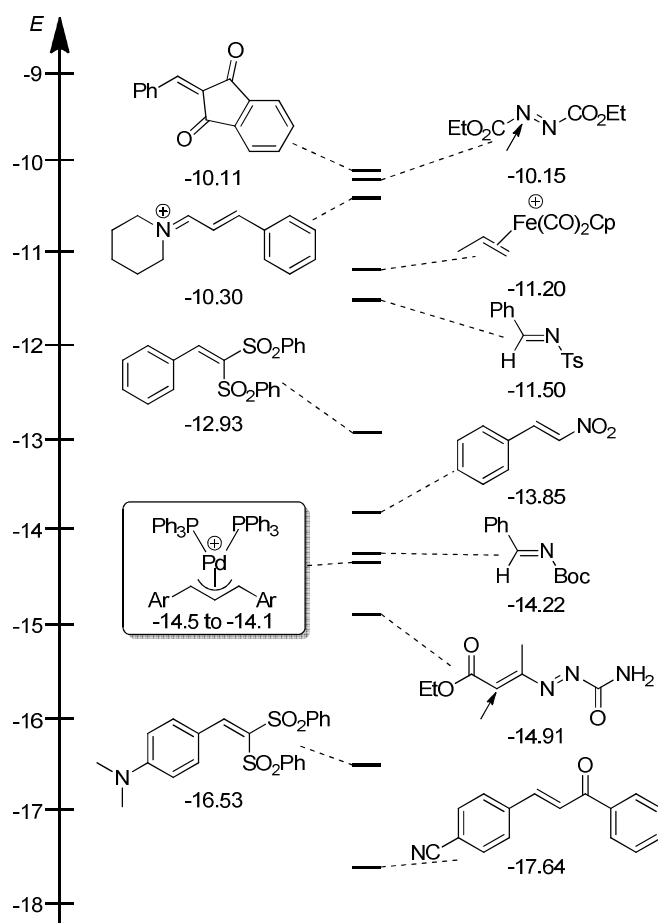


Figure 8. Comparison of the electrophilicities of the $\eta^3\text{-}1,3\text{-diarylallyl}$ palladium complexes and electron-deficient π -systems of similar reactivity.

While the electrophilicities of the free 1,3-bis(3,5-difluorophenyl)allyl ($E = 6.11$) and the 1,3-bis(4-dimethylamino-phenyl)allyl cations ($E = -7.50$) differ by more than 13 orders of magnitude, the electrophilicities of the corresponding $\text{Pd}(\text{PPh}_3)_2$ complexes were found to be almost independent of the nature of the substituents ($E \approx -14$), showing that $\text{Pd}(\text{PPh}_3)_2$ coordination reduces the electrophilic reactivities of allyl cations by 7-20 orders of magnitude (Figure 9).

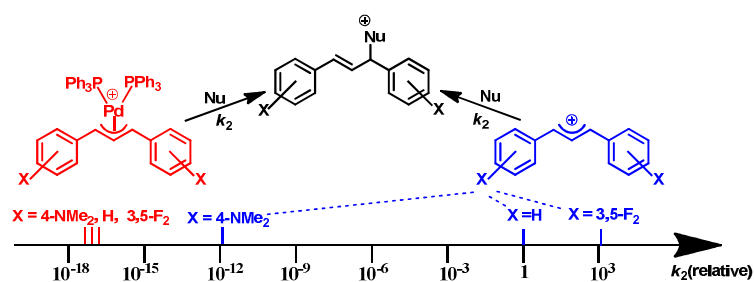


Figure 9. Electrophilicities of $[(\eta^3\text{-1,3-diarylallyl})\text{Pd}(\text{PPh}_3)_2]^+$ in comparison with the reactivities of the corresponding free carbenium ions.

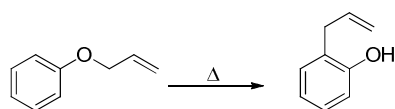
Since the reactivities of the allylpalladium complexes $[(\eta^3\text{-RCHCHCHR})\text{PdL}_2]^+$ are obviously not related to the reactivities of the free allyl cations $[\text{RCHCHCHR}]^+$, the designation of the former species as “palladium-stabilized allyl cations” may be misleading.

Chapter 2. Introduction

1. Allyl Derivatives in Synthetic and Mechanistic Investigations

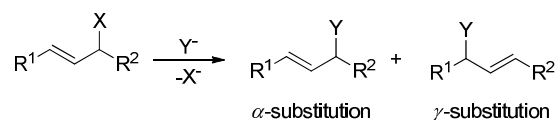
Allyl derivatives were discovered by Wertheim, who isolated diallyl sulfide from garlic oil in 1844,¹ and have been a subject of extensive studies since that time. Apart from practical applications (for instance, in fragrance industry)² and the presence of the allyl group in natural products such as alkaloids, steroids, and terpenes, the interest in allyl derivatives is due to the unique chemical transformations of allyl systems. The first example of a different behavior of allyl and alkyl derivatives was given by Claisen, who found that allyl phenyl ethers undergo rearrangement to the allyl phenols upon heating (Claisen rearrangement, Scheme 1)³, which was also the first pericyclic reaction⁴ reported in the literature.

Scheme 1. Claisen Rearrangement.



The recognition of the ability of allyl systems to undergo “anomalous” transformations triggered further investigations of the reactivities of allyl derivatives.⁵ In many cases, nucleophiles were found to attack not only the carbon atom connected to the leaving group (α -substitution) but also the terminal carbon of the double bond (γ -substitution) giving rise to mixtures of products, or, in some cases, even exclusively to γ -substitution products (Scheme 2).

Scheme 2. α - and γ -Substitution in Allyl Derivatives.



Hughes' and Ingold's mechanistic model of aliphatic nucleophilic substitution reactions (1920–1930s),⁶ explained why the monomolecular reaction pathway (S_N1) can be accompanied by allylic rearrangement: The allyl cation, which is formed in the rate-determining step, can be attacked by the nucleophiles at both allyl termini.

In 1938, Bergmann,⁷ Winstein,⁸ and Hughes⁹ independently suggested that, in addition to conventional S_N2 reactions, allyl derivatives may undergo bimolecular substitutions of

another type. This mechanism, where the nucleophilic attack at the γ -position, the departure of the leaving group, and the shift of the double bond proceed simultaneously directly leading to a γ -substitution product, was termed S_N2' . Its occurrence and stereochemistry have been a topic of long and controversial discussions in the literature.¹⁰

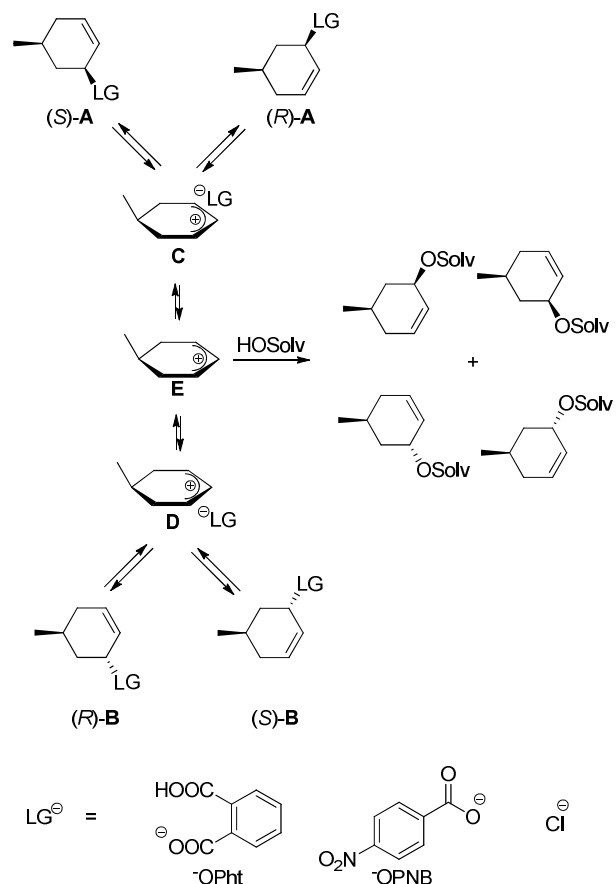
The discovery of many new reactions, which are specific for allyl derivatives, was stimulated by the search for stereoselective transformations, in particular those mediated by metals. Examples include allylations using chiral allylboronates,¹¹ Sharpless epoxidation of allyl alcohols,¹² Tsuji–Trost reactions,¹³ and copper-catalyzed allylations.¹⁴

2. Allylic Rearrangements and Ion Pairs in S_N1 Solvolyses

Investigations on the S_N1 solvolyses have shown that these reactions can be accompanied by internal rearrangements of the substrates, which are independent of the concentration of the anionic leaving group.¹⁵ This observation led to the introduction of the concepts of contact (intimate) ion-pairs and internal return, which expanded the mechanistic variety of unimolecular substitution reactions. The studies on transformations of optically active allyl derivatives performed by Goering and coworkers were an important contribution to the development of the theory of ion-pairing and will, therefore, be discussed in detail.

Since the *cis/trans* isomerizations of optically active *cis*- and *trans*-5-methylcyclohex-2-enyl 2-carboxybenzoates (**A** \rightleftharpoons **B**, LG = OPht, Scheme 3) in acetonitrile were found to proceed significantly more slowly than the racemizations (*(S)*-**A** \rightleftharpoons (*(R)*-**A** and (*(S)*-**B** \rightleftharpoons (*(R)*-**B**),¹⁶ Goering proposed the formation of ion-pair intermediates (**C**, **D**), in which the anion remains on the same face of the allyl cation as in the substrate. The collapse of these ion pairs (internal return) either regenerates the starting materials or leads to their enantiomers by attack of the anion at the other allylic terminus. The *cis/trans*-isomerization, which requires the migration of the leaving group to the other face of the allyl cation, was proposed to proceed via dissociation of the initial ion pairs to an achiral carbocationic intermediate (**E**) that can be attacked by the leaving group from both faces (Scheme 3).¹⁶

Scheme 3. Ion Pair Mechanism Proposed by Goering for Solvolyses and Rearrangements of *Cis*- and *Trans*-5-Methyl-2-Cyclohexenyl Derivatives.^a



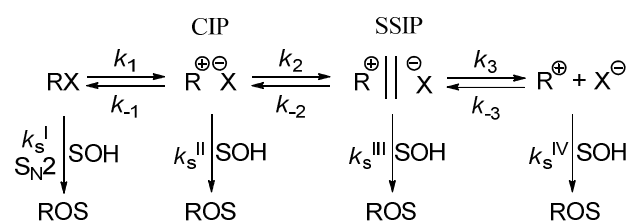
^a The descriptors (*R*)- and (*S*)- for the configuration of the C5 atom (connected to the methyl group) are omitted.

The hydrolyses of *cis*- and *trans*-5-methylcyclohex-2-enyl 2-carboxybenzoates (**A**, **B**, $\text{LG} = \text{OPht}$)¹⁷ and 4-nitrobenzoates (**A**, **B**, $\text{LG} = \text{OPNB}$)¹⁸ in aqueous acetone as well as the ethanolyses and acetolyses of *cis*- and *trans*-5-methylcyclohex-2-enyl chlorides (**A**, **B**, $\text{LG} = \text{Cl}$)¹⁹ were rationalized on the basis of this mechanism. In none of these cases, *cis/trans* isomerization of the non-reacted substrates was detected, and the polarimetric rate constant (racemization plus solvolysis) was always larger (factor of 1.1 – 5.1) than the titrimetric rate constant (solvolysis only). Based on a later study on the solvolyses of deuterated 2-cyclohexenyl 4-nitrobenzoates and 3,5-dinitrobenzoates, Goering concluded that the contact ion pairs (CIPs) have unsymmetrical structures, i.e., the leaving group in the CIPs is still closer to the carbon from which it departs (there are, therefore, two structures of type **C** and two structures of type **D**).²⁰ This conclusion was later supported by Thibblin, who argued that allyl cation-molecule pairs also have unsymmetrical structures.²¹

In contrast to the situation described for symmetrical allyl systems in Scheme 3, racemization of unsymmetrical allyl derivatives implies migration of the leaving group to the other face of the allyl cation. As solvolyses of *trans*-3-methyl-1-phenylallyl and *trans*-1-methyl-3-phenylallyl 4-nitrobenzoates in aqueous acetone were later observed to be accompanied by approximately 70% racemization of the unsolvolyzed esters, Goering concluded that the previously investigated stereochemical behavior of cyclohexenyl derivatives (Scheme 3) was largely dominated by conformational phenomena, which are absent in acyclic derivatives.²²

Apart from Goering's studies on the stereochemistry of allylic rearrangements, the problem of ion-pairing was addressed also by many other investigators: Detailed studies on solvent and salt effects in solvolysis reactions led Winstein²³ to the formulation of the ion-pair mechanism depicted in Scheme 4, which has commonly been used to rationalize solvolysis reactions, though the terms contact ion pairs (CIP) and solvent separated ion pairs (SSIP) comprise a variety of structural arrangements.

Scheme 4. Classical Winstein Scheme for Solvolysis Reactions.²³



A further attempt to generalize the ion-pair mechanism was undertaken by Snee,²⁴ who suggested that S_N2 reactions might proceed via initial reversible formation of ion pairs followed by their trapping by nucleophiles instead of the classical concerted mechanism. Detailed analyses of systems, where competing reactions with solvent and added nucleophiles occur, demonstrated, however, that the presence of two independent reaction pathways (S_N1 for solvent and S_N2 for nucleophile) accounts for the experimental data significantly better than Snee's general ion pair mechanism.²⁵

A breakthrough in our understanding of solvolysis reactions, as well as of nucleophilic aliphatic substitutions in general, came through the investigations of Jencks, Richard, and Tsuji,²⁶⁻²⁸ who used clock methods to determine rate constants for the attack of solvents on the intermediate carbocations. These authors were not only able to identify the change from S_N1 to S_N2 mechanisms²⁶ but also clarified the dynamics of ion pair dissociation²⁷ and recombination.²⁸

3. Linear Free Energy Relationships

As the number of chemical transformations available to synthetic chemists increased, it became necessary to find a way of classifying organic structures in terms of their reactivities in order to predict whether a certain combination of substrate and reagent would lead to the formation of a desired product within acceptable time. Since it was realized that most organic transformations involve elementary reactions between electron-deficient and electron-rich species, which were termed electrophiles and nucleophiles by Ingold,²⁹ the search for a quantitative description of organic reactivity mainly focussed on electrophile-nucleophile combinations.

One of the first examples of structure-reactivity relationships was reported in 1953 by Swain and Scott, who showed that the rates of the S_N2 reactions can be described by the linear free energy relationship (eq 1).³⁰

$$\log k/k_0 (25\text{ }^\circ\text{C}) = s n \quad (1)$$

In this approach, the parameter n accounts for the reactivities of nucleophiles, the electrophile-specific parameter s reflects sensitivity of an electrophile towards variation of the nucleophile, and k_0 represents the first-order rate constant of the hydrolysis of this electrophile in pure water.

In 1972, Ritchie found that the rate constants of the reactions of various anionic nucleophiles and methanol with several tritylium, aryldiazonium, and aryltropylium ions correlate with the rate constants of the corresponding reactions with water (k_w) according to eq 2, which employs only one nucleophile-specific parameter N_+ .³¹

$$\log k/k_w (23\text{ }^\circ\text{C}) = N_+ \quad (2)$$

Attempts to expand this approach to other electrophiles and nucleophiles revealed the limitations of eq 2, as significant deviations were found for certain electrophile-nucleophile combinations.³²

In 1994, Mayr and Patz developed a linear free energy relationship (eq 3), where nucleophiles are characterized by the solvent-dependent nucleophilicity and sensitivity parameters N and s_N and the reactivities of electrophiles are quantified by the solvent-independent electrophilicity parameter E .³³

$$\log k (20\text{ }^\circ\text{C}) = s_{\text{N}}(N + E) \quad (3)$$

The scope of eq 3 has been greatly expanded over the last 18 years and covers now 40 orders of magnitude in reactivity. Many important classes of nucleophiles, such as amines,³⁴ heterocyclic arenes,^{35,36} hydride donors,³⁷ enamines,^{36,38} NHC carbenes,³⁹ organic solvents and solvent mixtures,⁴⁰ organoboron compounds,⁴¹ phosphorus and sulfur ylides,⁴² silyl enol ethers and ketene acetals,^{36,43,44} as well as electrophiles, such as aldehydes,⁴⁵ azodicarboxylates,⁴⁶ imines,⁴⁵ iminium ions,^{44,47} metal π -complexes,^{36,44,48} and nitrostyrenes⁴⁹ were characterized by eq 3 leading to the most comprehensive nucleophilicity and electrophilicity scales presently available.⁵⁰

Linear free energy relationships were also applied to characterize the reactivities in $S_{\text{N}}1$ solvolyses – another important transformation in organic chemistry.

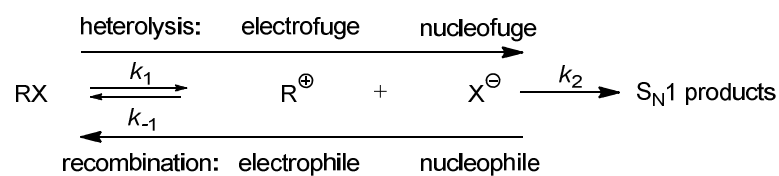
One of the first attempts to quantify the rates of unimolecular solvolyses in various solvents was undertaken by Grunwald and Winstein, who proposed a correlation (eq 4), where the solvents are characterized by their ionizing powers Y , and the substrates by the sensitivity parameters m and the rate constants of their solvolyses in 80% v/v aq ethanol (k_0).⁵¹

$$\log k/k_0 (25\text{ }^\circ\text{C}) = m Y \quad (4)$$

Subsequently, it was demonstrated that predictions based on parameters Y derived from the rates of solvolyses of $^t\text{BuCl}$ in the corresponding solvents – reference reactions in the original work of Grunwald and Winstein – are rather of qualitative than of quantitative character when other substrates (alkyl tosylates, benzyl derivatives, etc.) are considered. This resulted in the construction of numerous scales of solvent ionizing power referring to certain classes of substrates.⁵²

A linear free energy relationship (eq 5) analogous to eq 3 was developed by the groups of Mayr and Kronja.⁵³ In this approach, the rates of bond heterolyses are correlated with two solvent-dependent nucleofuge-specific parameters – sensitivity s_{f} , and nucleofugality N_{f} – and one solvent-independent electrofuge-specific parameter E_{f} . The terms nucleofuge and electrofuge are closely related to the terms nucleophile and electrophile, as illustrated in Scheme 5.

$$\log k_1 (25\text{ }^\circ\text{C}) = s_{\text{f}}(N_{\text{f}} + E_{\text{f}}) \quad (5)$$

Scheme 5. Simplified S_N1 Mechanism.^a

^a Without consideration of ion-pairing.

Eq 5 was shown to be applicable to various types of transformations of benzhydryl derivatives (benzhydrylium ions were used as reference electrophiles and electrofuges in eqs 3 and 5, respectively) involving initial bond heterolysis: from the classical S_N1 reactions with irreversible generation of the carbenium ions ($k_1, k_{-1}[\text{X}^-] \ll k_2$, Scheme 5) over S_N1 reactions with common ion return ($k_1 \ll k_{-1}[\text{X}^-] \approx k_2$) to S_N2C⁺ reactions ($k_1 > k_{-1}[\text{X}^-], k_2$).⁵⁴

4. Objectives

As there are numerous examples of synthetic and mechanistic applications employing allyl cations, including studies performed in recent time,⁵⁵ it was of interest whether this class of carbenium ions can be treated by eqs 3 and 5. 1,3-Diarylallyl cations, which are structurally related to benzhydrylium ions, the reference electrophiles and electrofuges for the development of eqs 3 and 5, respectively, appeared to be the most proper subjects for such an investigation. Therefore, it was a goal of this thesis to elucidate the applicability of eqs 3 and 5 to symmetrically substituted 1,3-diarylallylium ions⁵⁶ and to compare their reactivities as electrophiles and electrofuges.

As Goering's studies on the stereochemistry of allylic rearrangements were limited to the analytical methods available at the time of his research (1950–1970s), it was a further objective to use the advantages of modern chiral HPLC for gaining insight into the mechanism of the solvolyses of optically active unsymmetrically-substituted 1,3-diarylallyl derivatives and to quantify ion pair dynamics and internal return. These data should be combined with electrophilicities and electrofugalities of 1,3-diarylallyl cations to provide a comprehensive view on solvolyses of the corresponding derivatives and to predict the solvolysis mechanism for a certain substrate (S_N2, S_N1 or S_N2C⁺) as well as the extent of internal and external (common ion) return in the corresponding S_N1 reactions.

η^3 -Allylpalladium complexes, the key intermediates in the Tsuji–Troost allylations,¹³ can be formally seen as “palladium-stabilized allyl cations”. Therefore, it was of interest to study the reactivities of differently substituted species of this type and compare them with those of the

corresponding free carbocations. $[(\eta^3\text{-1,3-Diarylallyl})\text{Pd}(\text{PPh}_3)_2]^+\text{X}^-$ complexes appeared to be the most proper choice for these investigations, since examples of kinetic studies on electrophiles of this type had been already given in the literature.⁵⁷ Exploratory kinetic investigations of the reactions of these species with amines showed, however, that significant deviations from the second-order rate law are observed when the amine concentration exceeds a certain level. Therefore, it was a further objective of this thesis to rationalize this unexpected behavior of amines and develop a method for following reactions of $[(\eta^3\text{-1,3-diarylallyl})\text{Pd}(\text{PPh}_3)_2]^+$ with nucleophiles. The resulting procedure should be applied for the determination of the electrophilicity parameters of differently substituted $(\eta^3\text{-1,3-diarylallyl})$ palladium complexes, which should be compared with the E values of the corresponding free 1,3-diarylallylium ions.

As most parts of this thesis have already been published or submitted for publication, individual introductions will be given at the beginning of each chapter. In order to identify my contribution to multiauthor publication described in the Chapter 3, only the kinetic and synthetic experiments, which were performed by me, are described in the corresponding Experimental Section.

5. References

- (1) Wertheim, T. *Ann. Chem. Pharm.* **1844**, 3, 289–315.
- (2) See for instance: (a) Clapp, J. J.; Kaye, C. M.; Young, L. *Proceedings of the Biochemical Society* **1969**, 114, 6–7. (b) Politano, V. T.; Isola, D. A.; Lalko, J.; Api, A. M. *International Journal of Toxicology* **2006**, 25, 183–193 and references therein.
- (3) Claisen, L. *Ber. Dtsch. Chem. Ges.* **1912**, 45, 3157–3166.
- (4) Epiotis, N. D. *Angew. Chem.* **1974**, 86, 825–868.
- (5) See for instance (a) Kremers, F.; Roth, F.; Tietze, E.; Claisen, L. *J. Prakt. Chem.* **1922**, 105, 65–92. (b) Ziegler, K. *Ber. Dtsch. Chem. Ges.* **1925**, 58, 359–361. (c) Straus, F.; Ehrenstein, M. *Liebigs Ann. Chem.* **1925**, 442, 93–118.
- (6) (a) Cleave, J. L.; Hughes, E. D.; Ingold, C. K. *J. Chem. Soc.* **1935**, 236–244 and references therein. (b) Hughes, E. D.; Ingold, C. K. *J. Chem. Soc.* **1935**, 244–255.
- (7) Bergmann, E.; Sprinzak, Y. *Helv. Chim. Acta.* **1937**, 20, 590–621.
- (8) Winstein, S. *PhD Dissertation*, California Institute of Technology, 1938.
- (9) Hughes, E. D. *Trans. Faraday Soc.* **1938**, 34, 185–202.
- (10) (a) Bordwell, F. G. *Acc. Chem. Res.* **1970**, 3, 281–290. (b) Bordwell, F. G.; Mecca, T. G. *J. Am. Chem. Soc.* **1972**, 94, 5829–5837. (c) Magid, R.M. *Tetrahedron*, **1980**, 36, 1901–1930.
- (11) Herold, T.; Hoffmann, R. W. *Angew. Chem. Int. Ed. Engl.* **1978**, 17, 768–769.
- (12) Johnson, R.; Sharpless, K. B. Catalytic Asymmetric Epoxidation of Allylic Alcohols. In *Catalytic Asymmetric Synthesis*, 2nd Edition, Ojima, I, Ed.; Wiley, New York, 2000, pp 231–280.
- (13) Trost, B. M.; Van Vranken, D. L. *Chem. Rev.* **1996**, 96, 395–422.
- (14) Alexakis, A.; Bäckvall, J. E.; Krause, N.; Pàmies, O.; Diégues, M. *Chem. Rev.* **2008**, 108, 2796–2823.
- (15) (a) Young, W. G.; Winstein, S.; Goering, H. L. *J. Am. Chem. Soc.* **1951**, 73, 1958–1963. (b) Winstein, S.; Schreiber, K. C. *J. Am. Chem. Soc.* **1952**, 74, 2165–2170. (c) Winstein, S.; Schreiber, K. C. *J. Am. Chem. Soc.* **1952**, 74, 2171–2178.
- (16) Goering, H. L.; Blanchard, J. P.; Silversmith, E. F. *J. Am. Chem. Soc.* **1954**, 76, 5409–5418.
- (17) Goering, H. L.; Silversmith, E. F. *J. Am. Chem. Soc.* **1955**, 77, 1129–1133.
- (18) (a) Goering, H. L.; Silversmith, E. F. *J. Am. Chem. Soc.* **1955**, 77, 6249–6253. (b) Goering, H. L.; Takahashi Doi, J. *J. Am. Chem. Soc.* **1960**, 82, 5850–5854.
- (19) Goering, H. L.; Nevitt, T. D.; Silversmith, E. F. *J. Am. Chem. Soc.* **1955**, 77, 5026–5032.

- (20) Kantner, S. S.; Humski, K.; Goering, H. L. *J. Am. Chem. Soc.* **1982**, *104*, 1693–1697.
- (21) Thibblin, A. *J. Chem. Soc., Perkin. Trans.* **1987**, *11*, 1629–1632.
- (22) (a) Goering, H. L.; Koermer, G. S.; Linsay, E. C. *J. Am. Chem. Soc.* **1971**, *93*, 1230–1234. (b) The importance of conformational factors for 5-methylcyclohex-2-enyl system is demonstrated in: Goering, H. L.; Josephson, R. R. *J. Am. Chem. Soc.* **1962**, *84*, 2779–2785.
- (23) Winstein, S.; Klinedinst Jr., P. E.; Robinson, G. C. *J. Am. Chem. Soc.* **1961**, *83*, 885–895.
- (24) Sreen, R. A. *Acc. Chem. Res.* **1973**, *6*, 46–53.
- (25) McLennan, D. J. *Acc. Chem. Res.* **1976**, *9*, 281–287.
- (26) Richard, J. P.; Jencks, W. P. *J. Am. Chem. Soc.* **1984**, *106*, 1383–1396.
- (27) Richard, J. P.; Jencks, W. P. *J. Am. Chem. Soc.* **1984**, *106*, 1373–1383.
- (28) (a) Tsuji, Y.; Mori, T.; Richard, J. P.; Amyes, T. L.; Fujio, M.; Tsuno, Y. *Org. Lett.*, **2001**, *3*, 1237–1240. (b) Teshima, M.; Tsuji, Y.; Richard, J. P. *J. Phys. Org. Chem.* **2010**, *23*, 730–734.
- (29) Ingold, C. K. *Recl. Trav. Chim. Pays.–Bas.* **1929**, *42*, 797–812.
- (30) Swain, C. G.; Scott, C. B. *J. Am. Chem. Soc.* **1953**, *75*, 141–147.
- (31) Ritchie, C. D. *Acc. Chem. Res.* **1972**, *5*, 348–354.
- (32) Ritchie, C. D. *Can. J. Chem.* **1986**, *64*, 2239–2250.
- (33) Mayr, H.; Patz, M. *Angew. Chem. Int. Ed. Engl.* **1994**, *33*, 938–957.
- (34) (a) Brotzel, F.; Chu, Y. C.; Mayr, H. *J. Org. Chem.* **2007**, *72*, 3679–3688. (b) Phan, T. B.; Nolte, C.; Kobayashi, S.; Ofial, A. R.; Mayr, H. *J. Am. Chem. Soc.* **2009**, *131*, 11392–11401. (c) Phan, T. B.; Breugst, M.; Mayr, H. *Angew. Chem. Int. Ed.* **2006**, *45*, 3869–3874. (d) Minegishi, S.; Mayr, H. *J. Am. Chem. Soc.* **2003**, *125*, 286–295. (e) Kanzian, T.; Nigst, T. A.; Maier, A.; Pichl, S.; Mayr, H. *Eur. J. Org. Chem.* **2009**, 6379–6385. (f) Baidya, M.; Kobayashi, S.; Brotzel, F.; Schmidhammer, U.; Riedle, E.; Mayr, H. *Angew. Chem. Int. Ed.* **2007**, *46*, 6176–6179. (g) Ammer, J.; Baidya, M.; Kobayashi, S.; Mayr, H. *J. Phys. Org. Chem.* **2010**, *23*, 1029–1035. (h) Nigst, T. A.; Antipova, A.; Mayr, H. *J. Org. Chem.*, ASAP (doi 10.1021/jo301497g).
- (35) (a) Lakhdar, S.; Westermaier, M.; Terrier, F.; Goumont, R.; Boubaker, T.; Ofial, A. R.; Mayr, H. *J. Org. Chem.* **2006**, *71*, 9088–9095. (b) Kempf, B.; Hampel, N.; Ofial, A. R.; Mayr, H. *Chem.—Eur. J.* **2003**, *9*, 2209–2218. (c) Nigst, T. A.; Westermaier, M.; Ofial, A. R.; Mayr, H. *Eur. J. Org. Chem.* **2008**, 2369–2374.
- (36) Mayr, H.; Bug, T.; Gotta, M. F.; Hering, N.; Irrgang, B.; Janker, B.; Kempf, B.; Loos, R.; Ofial, A. R.; Remennikov, G.; Schimmel, H. *J. Am. Chem. Soc.* **2001**, *123*, 9500–9512.

- (37) Horn, M.; Schappele, L. H.; Lang–Wittkowski, G.; Mayr, H.; Ofial, A. R. *Chem.—Eur. J.* **2012**, accepted.
- (38) (a) Kanzian, T.; Lakhdar, S.; Mayr, H. *Angew. Chem. Int. Ed.* **2010**, *49*, 9526–9529. (b) Lakhdar, S.; Maji, B.; Mayr, H. *Angew. Chem. Int. Ed.* **2012**, *51*, 5739–5742. (c) Kempf, B.; Hampel, N.; Ofial, A. R.; Mayr, H. *Chem.—Eur. J.* **2003**, *9*, 2209–2218. (d) Dilman, A. D.; Ioffe, S. L.; Mayr, H. *J. Org. Chem.* **2001**, *66*, 3196–3200.
- (39) Maji, B.; Breugst, M.; Mayr, H. *Angew. Chem. Int. Ed.* **2011**, *50*, 6915–6919.
- (40) (a) Phan, T. B.; Mayr, H. *Can. J. Chem.* **2005**, *83*, 1554–1560. (b) Minegishi, S.; Kobayashi, S.; Mayr, H. *J. Am. Chem. Soc.* **2004**, *126*, 5174–5181. (c) Phan, T. B.; Nolte, C.; Kobayashi, S.; Ofial, A. R.; Mayr, H. *J. Am. Chem. Soc.* **2009**, *131*, 11392–11401. (d) Ammer, J.; Nolte, C.; Mayr, H. *J. Am. Chem. Soc.* **2012**, *134*, 13902–13911.
- (41) Berionni, G.; Maji, B.; Knochel, P.; Mayr, H. *Chem. Sci.* **2012**, *3*, 878–882.
- (42) (a) Appel, R.; Mayr, H. *Chem.—Eur. J.* **2010**, *16*, 8610–8614. (b) Appel, R.; Loos, R.; Mayr, H. *J. Am. Chem. Soc.* **2009**, *131*, 704–714. (c) Appel, R.; Hartmann, N.; Mayr, H. *J. Am. Chem. Soc.* **2010**, *132*, 17894–17900.
- (43) (a) Tokuyasu, T.; Mayr, H. *Eur. J. Org. Chem.* **2004**, 2791–2796. (b) Laub, H.; Yamamoto, H.; Mayr, H. *Org. Lett.* **2010**, *12*, 5206–5209. (c) Laub, H. A.; Gladow, D.; Reissig, H.–U.; Mayr, H. *Org. Lett.* **2012**, *14*, 3990–3993.
- (44) Mayr, H.; Kempf, B.; Ofial, A. R. *Acc. Chem. Res.* **2003**, *36*, 66–77.
- (45) Appel, R.; Mayr, H. *J. Am. Chem. Soc.* **2011**, *133*, 8240–8251.
- (46) Kanzian, T.; Mayr, H. *Chem.—Eur. J.* **2010**, *16*, 11670–11677.
- (47) (a) Lakhdar, S.; Tokuyasu, T.; Mayr, H. *Angew. Chem. Int. Ed.* **2008**, *47*, 8723–8726. (b) Lakhdar, S.; Ammer, J.; Mayr, H. *Angew. Chem. Int. Ed.* **2011**, *50*, 9953–9956. (c) Lakhdar, S.; Appel, R.; Mayr, H. *Angew. Chem. Int. Ed.* **2009**, *48*, 5034–5037
- (48) Dulich, F.; Müller, K.–H.; Ofial, A. R.; Mayr, H. *Helv. Chim. Acta* **2005**, *88*, 1754–1768.
- (49) Zenz, I.; Mayr, H. *J. Org. Chem.* **2011**, *76*, 9370–9378.
- (50) An actual database of reactivity parameters E , N , and s_N can be found at:
www.cup.lmu.de/oc/mayr/DBintro.html.
- (51) Grunwald, E.; Winstein, S. *J. Am. Chem. Soc.* **1948**, *70*, 846–854.
- (52) (a) Bentley, T. W.; Carter, G. E. *J. Am. Chem. Soc.* **1982**, *104*, 5741–5747.
- (53) Denegri, B.; Minegishi, S.; Kronja, O.; Mayr, H. *Angew. Chem. Int. Ed.* **2004**, *43*, 2302–2305.

(54) (a) Mayr, H.; Ofial, A. R. *Pure. Appl. Chem.* **2009**, *81*, 667–683. (b) Streidl, N.; Denegri, B.; Kronja, O.; Mayr, H. *Acc. Chem. Res.* **2010**, *43*, 1537–1549.

(55) Rueping, M.; Uria, U.; Lin, M.-Y.; Atodiresei, I. *J. Am. Chem. Soc.* **2011**, *133*, 3732–3735.

(56) Initial studies on electrophilicities of (*E*)-1,3-bis(4-(dimethylamino)phenyl)allylium and (*E*)-1,3-bis(4-methoxyphenyl)allylium ions were performed by Schindele (Schindele, C. *Dissertation*, Ludwig-Maximilians-Universität, München, 2002).

(57) (a) Kuhn, O.; Mayr, H. *Angew. Chem., Int. Ed.* **1999**, *38*, 343–346. (b) Amatore, C.; Bahsoun, A. A.; Jutand, A.; Mensah, L.; Meyer, G.; Ricard, L. *Organometallics.* **2005**, *24*, 1569–1577.

Chapter 3. Electrophilicities of Symmetrically Substituted 1,3-Diarylallyl Cations

Konstantin Troshin, Claus Schindele, and Herbert Mayr^a

J. Org. Chem. **2011**, *76*, 9391–9408

1. Introduction

Nucleophilic substitutions of allyl derivatives not only give products where the nucleofuge is directly displaced by the nucleophile but also may proceed with allylic rearrangement.¹ While concerted S_N2' reactions are rare or do not exist,² allylic rearrangements via addition–elimination reactions are well-established.³ Of particular interest are allylic rearrangements via intermediate allyl cations, i.e., S_N1 reactions. Because of the possibility of internal return at both termini of the allylic system, allyl solvolyses provide detailed information on the nature of ion pairs, which cannot be derived from solvolyses of other S_N1 substrates.

Goering's pioneering studies on the solvolyses of optically active allyl derivatives using titrimetric, polarimetric, and isotope exchange methods made it possible to differentiate various steps of the multistep solvolytic processes.⁴ However, a comprehensive model, which explains the mechanistic changes caused by structural modifications of the substrates and the solvent, remained elusive.

In recent work, we have demonstrated that knowledge of the absolute rate constants for the reactions of carbocations with leaving groups (ion recombination) and other nucleophiles (e.g., solvents) allows one not only to predict whether solvolyses will proceed with or without common ion return⁵ but also to define the border between S_N1 and S_N2 mechanisms.⁶ Key to these analyses was the linear free energy relationship (eq 1), where *E* is an electrophilicity parameter, *N* is a nucleophilicity parameter, and *s_N* is a nucleophile-specific sensitivity parameter (previously termed *s*).⁷

$$\log k_2(20\text{ }^\circ\text{C}) = s_N(N + E) \tag{1}$$

^a Several kinetic measurements and synthetic transformations presented in this chapter and the corresponding publication were performed by Dr. Carmen Nitu, Dr. Thomas Singer, and Dr. Claus Schindele. In order to identify my contribution to this publication, only data obtained by me are presented in the experimental part of the chapter.

By defining diarylmethyl (benzhydryl) cations and a set of C-nucleophiles as reference compounds we have succeeded in arranging a large variety of electrophiles and nucleophiles in electrophilicity and nucleophilicity scales.^{8–10}

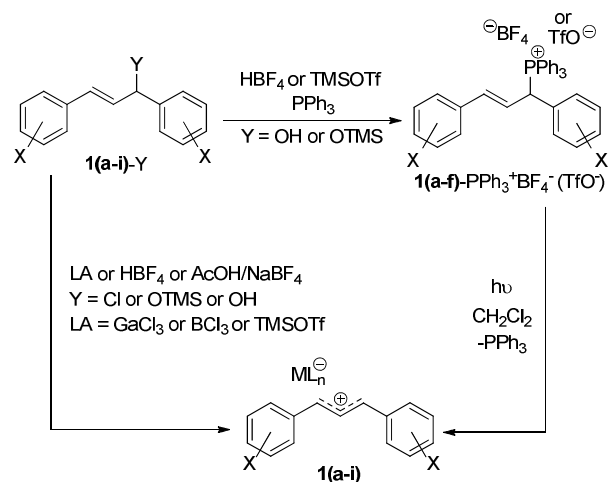
We have now studied the reactions of nine symmetrically substituted 1,3-diarylallyl cations **1(a–i)** with nucleophiles **2(a–u)** in order to derive the electrophilicity parameters E of these carbocations, which we will employ in subsequent work for elucidating solvolysis mechanisms⁴ of allyl derivatives and for investigating the effect of palladium coordination in the intermediates of Tsuji–Trost reactions.¹¹ The resulting E parameters can also be used for designing new synthetic procedures as well as for better understanding of known reactions via intermediate 1,3-diarylallyl cations, e.g., catalytic S_N1-type reactions of alcohols, which are relevant for designing environmentally benign processes.¹²

2. Results and Discussion

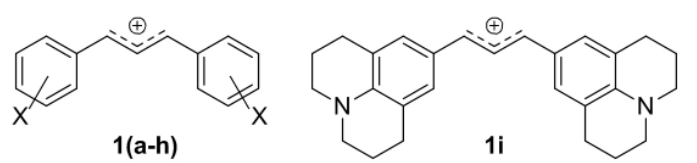
2.1. Synthesis of 1,3-Diarylallyl Cations **1(a–i)**

Cations **1(a–f)** cannot be stored as stable salts; they were generated in solution either by treatment of the corresponding chlorides **1-Cl** or trimethylsilyl ethers **1-OTMS** with Lewis acids or by laser-flash photolysis of the corresponding phosphonium salts **1-PPh₃⁺BF₄⁻** or **1-PPh₃⁺TfO⁻** as illustrated in Scheme 1.¹³ The diarylallyl tetrafluoroborates **1(g–i)-BF₄** were obtained as stable salts by treatment of the corresponding alcohols **1(g–i)-OH** with HBF₄·OEt₂ or AcOH/NaBF₄ as described in the Experimental Section. All allyl cations **1(a–i)** were characterized by UV–vis spectroscopy (Table 1).

Scheme 1. Generation of Allyl Cations **1(a–i)**.^a



^aFor definition of X see Table 1.

Table 1. Cations 1(a–i) and Their UV–Vis Maxima in Different Solvents.


X	conditions	λ_{\max}/nm	$\log \varepsilon$
1a <i>m,m</i> -F ₂	1a -OH/conc. H ₂ SO ₄	496	-
1b <i>m</i> -F	1b -OH/conc. H ₂ SO ₄	500	-
1c <i>p</i> -Br	1c -Cl/GaCl ₃ /CH ₂ Cl ₂	551	≈ 5.16
	1c -OH/conc. H ₂ SO ₄	527	-
1d <i>p</i> -Cl	1d -OH/AcOH	530	-
1e H	1e -OTMS/TMSOTf/CH ₂ Cl ₂	503	5.16
	1e -OH/AcOH	488	-
1f <i>p</i> -Me	1f -OTMS/TMSOTf/CH ₂ Cl ₂	532	5.25
1g <i>p</i> -OMe	1g -BF ₄ /CH ₂ Cl ₂	578	5.26
1h <i>p</i> -NMe ₂	1h -BF ₄ /CH ₃ CN	693	5.31
	1h -BF ₄ /CH ₂ Cl ₂	704	-
1i jul ^a	1i -BF ₄ /CH ₃ CN	730	5.34
	1i -BF ₄ /CH ₂ Cl ₂	740	-

^a For structure see heading of this table.

As shown in Figure SX1 of the Supplementary Section (p 88), the UV–Vis spectrum of cation **1e**, generated photolytically from (*E*)-(1,3-diphenylallyl)triphenylphosphonium triflate in dichloromethane, was identical to that of **1e**, generated from (*E*)-((1,3-diphenylallyl)oxy)trimethylsilane and trimethylsilyl triflate in the same solvent.

In addition, the stable cations **1(g–i)** were identified by NMR spectroscopy and HRMS (see Experimental Section). ¹H NMR spectra of **1h**-BF₄ taken at different temperatures allow determination of the barrier of rotation around the C2–C3 bond in the allyl cation **1h** (Figure 1). From the coalescence temperature¹⁴ of H^a and H^{a'} at -10 °C and for H^b and H^{b'} at -20 °C one derives rotational barriers of 50.5 ± 2 and 52 ± 2 kJ mol⁻¹, respectively. The structure of **1h**-BF₄ was also confirmed by X-ray analysis.¹⁵

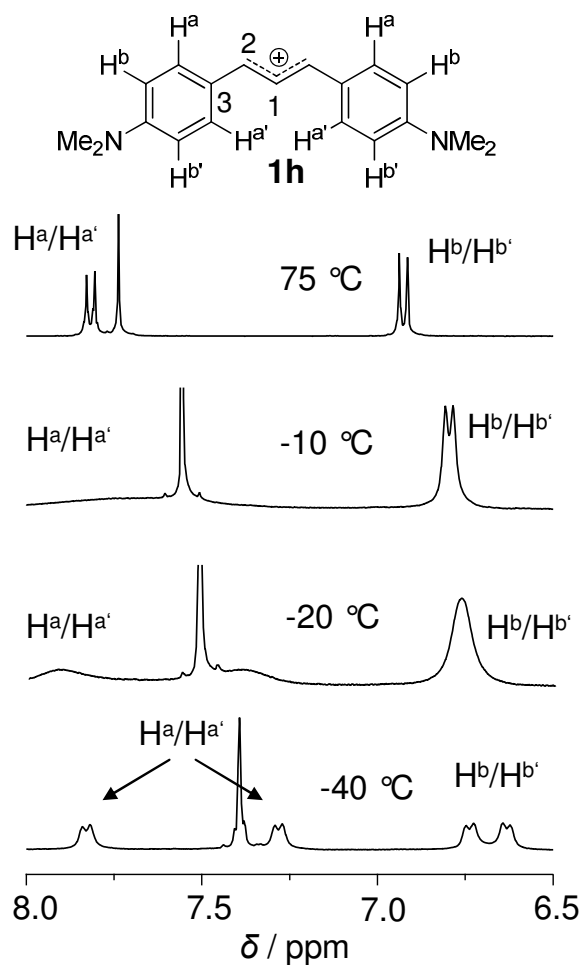


Figure 1. ^1H NMR spectra of **1h**- BF_4 taken at different temperatures.

2.2. Product Studies

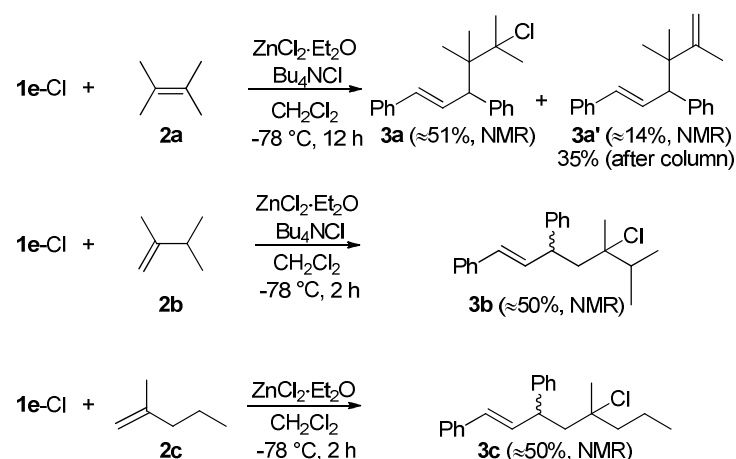
As the nature of the reaction products can be expected not to depend on the substituents X of the aryl groups of **1(a-i)**, product studies were performed with only one representative electrophile for each nucleophile.

The zinc chloride catalyzed reaction of 2,3-dimethylbut-2-ene (**2a**) with **1e-Cl** provided a complex product mixture, which was not identified. When the reaction was carried out in the presence of tetrabutylammonium chloride, a mixture of only two products, (*E*)-5-chloro-4,4,5-trimethyl-1,3-diphenylhex-1-ene (**3a**) and (*E*)-4,4,5-trimethyl-1,3-diphenylhexa-1,5-diene (**3a'**), was formed (Scheme 2). Pure **3a'** (35% yield) was obtained by column chromatography of the crude product; as the isolated yield of **3a'** was higher than its content in the crude mixture, one can conclude that **3a** eliminates HCl on silica.

Under the same conditions, the reaction of **1e-Cl** with 2,3-dimethylbut-1-ene (**2b**) gave (*E*)-5-Chloro-5,6-dimethyl-1,3-diphenylhept-1-ene (**3b**) as a mixture of two diastereomers (dr ca. 1.4:1, ^1H NMR) contaminated by small amounts of byproducts.

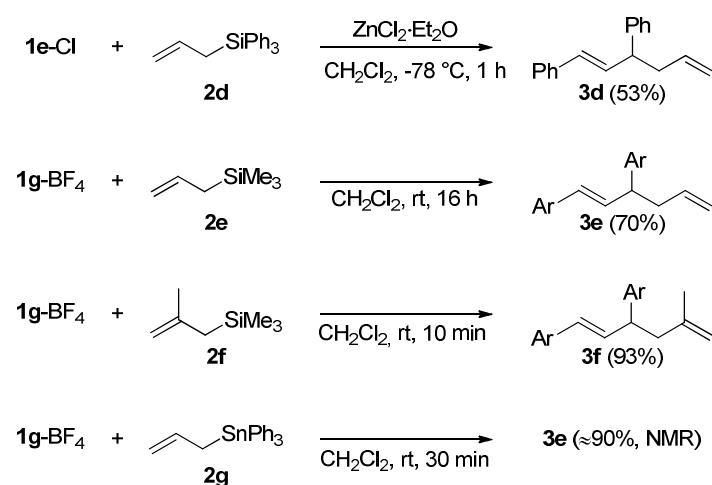
In the case of 2-methylpent-1-ene (**2c**), the addition of Bu_4NCl is not necessary, and the major product of the reaction with **1e-Cl** can be unambiguously identified as (*E*)-5-Chloro-5-methyl-1,3-diphenyloct-1-ene (**3c**, 1.4:1 mixture of two diastereomers, ^1H NMR). Additional signals between δ 4.5 and 6.0 ppm in the ^1H NMR spectrum indicate the formation of dienes, which may be produced via proton elimination from the intermediate carbocation.

Scheme 2.



The combinations of allylsilanes **2(d-f)** and of allyltriphenylstannane (**2g**) with **1e** or **1g** afforded the $\text{S}_{\text{E}}2'$ products **3(d-f)** with moderate to good yields (Scheme 3). Similar results were previously reported for the reaction of **1e-OH** with **2e** under polymer-supported Brønsted acid catalysis.¹⁶

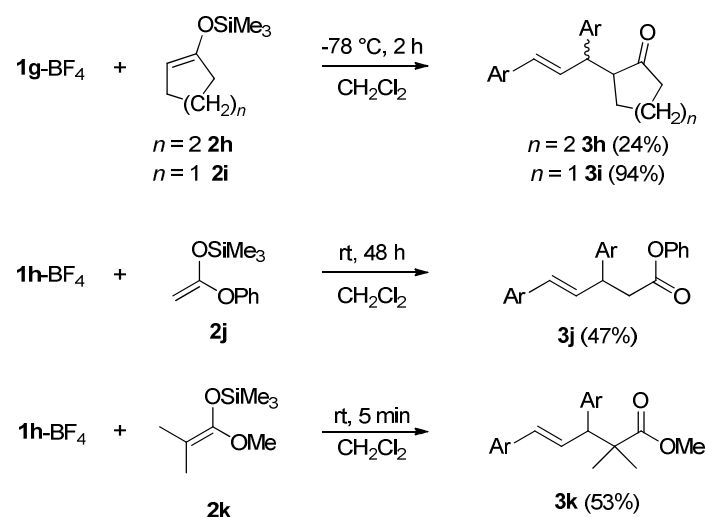
Scheme 3.



Silyl enol ethers and ketene acetals **2(h-k)** react with the allylium tetrafluoroborates **1g-BF₄** and **1h-BF₄** to form the corresponding carbonyl compounds **3(h-k)** (Scheme 4). The low

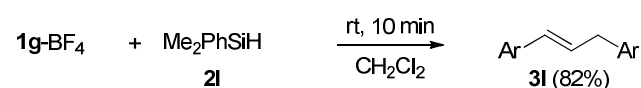
yield of the reaction of **1g**-BF₄ with **2h** is probably due to decomposition of **3h** on the silica column, as the same phenomenon was also observed for the structurally analogous compound **3n'** (see below). The substituted cyclic ketones **3h** and **3i** were formed as mixtures of diastereomers with dr of 1.3:1 and 1.9:1, respectively (based on the ¹H NMR spectra of the crude products).

Scheme 4.



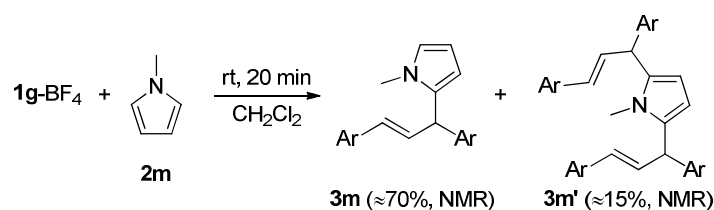
Dimethylphenylsilane (**2l**) reduces **1g**-BF₄ to yield 82% of (*E*)-1,3-bis(4-methoxyphenyl)prop-1-ene (**3l**, Scheme 5).

Scheme 5.



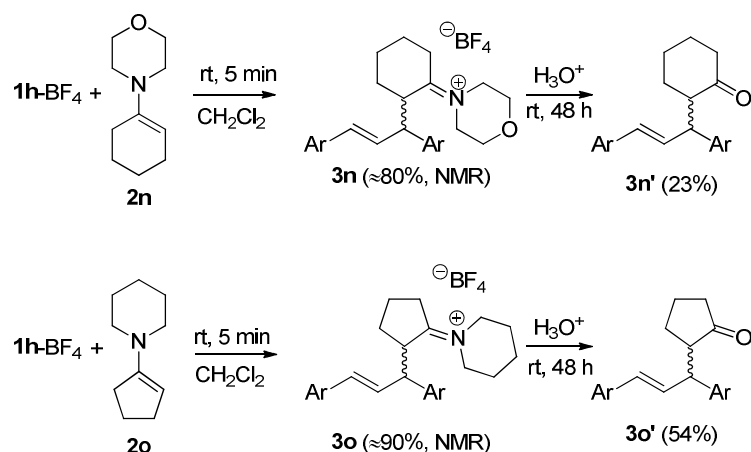
Slow addition of a suspension of **1g**-BF₄ in CH₂Cl₂ to 10 equivalents of 1-methyl-1*H*-pyrrole (**2m**) leads to a 9:1 mixture of (*E*)-2-(1,3-bis(4-methoxyphenyl)allyl)-1-methyl-1*H*-pyrrole (**3m**) and 2,5-bis((*E*)-1,3-bis(4-methoxyphenyl)allyl)-1-methyl-1*H*-pyrrole (**3m'**) (Scheme 6). The formation of the disubstituted product **3m'** even in the presence of a high excess of **2m** can be explained by mixing control,¹⁷ i.e., the diffusional separation of **3m** from the sparsely soluble crystals of **1g**-BF₄ is slow compared with the reaction of **1g**-BF₄ with **3m** ($k_2 > 10^5 \text{ M}^{-1} \text{ s}^{-1}$).

Scheme 6.



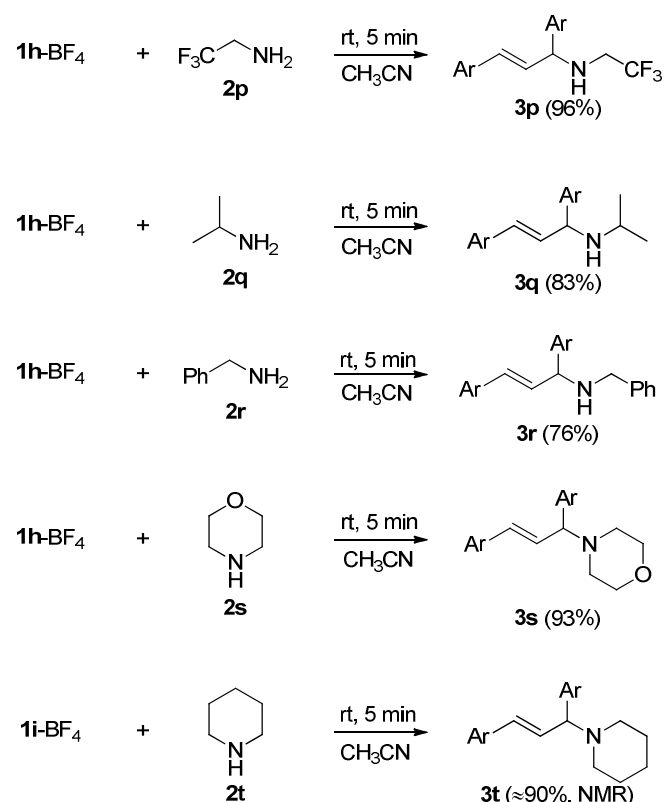
The enamines $2\mathbf{n}$ and $2\mathbf{o}$ react with the allylium tetrafluoroborate $1\mathbf{h}\text{-BF}_4$ to form the iminium salts $3(\mathbf{n,o})\text{-BF}_4$ (characterized by NMR and HRMS) as mixtures of diastereomers (dr ca. 1.2:1, ^1H NMR); their hydrolysis with aqueous acetic acid affords (*E*)-2-(1,3-bis(4-(dimethylamino)phenyl)allyl)cyclohexanone ($3\mathbf{n}'$, 23%) and (*E*)-2-(1,3-bis(4-(dimethylamino)phenyl)allyl)cyclopentanone ($3\mathbf{o}'$, 54%) (Scheme 7). The low yield of $3\mathbf{n}'$ must be due to its partial decomposition on silica, as its precursor $3\mathbf{n}$ is formed almost quantitatively (^1H NMR).

Scheme 7.



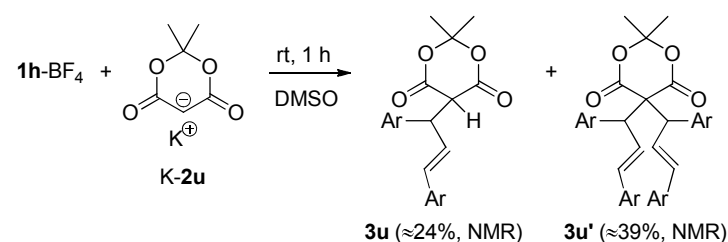
Amines $2(\mathbf{p-t})$ react with $1\mathbf{h}\text{-BF}_4$ and $1\mathbf{i}\text{-BF}_4$ to form (*E*)-1,3-diarylallylamines $3(\mathbf{p-t})$ in good yields (Scheme 8).

Scheme 8.



The combination of **1h-BF₄** with 5 equivalents of the potassium salt of Meldrum's acid (**K-2u**) affords (*E*)-5-(1,3-bis(4-(dimethylamino)phenyl)allyl)-2,2-dimethyl-1,3-dioxane-4,6-dione (**3u**) and 5,5-bis((*E*)-1,3-bis(4-(dimethylamino)phenyl)allyl)-2,2-dimethyl-1,3-dioxane-4,6-dione (**3u'**) in 24% and 39% yield, respectively (Scheme 9). Obviously, **3u** is deprotonated under the reaction conditions and then reacts with a second equivalent of **1h-BF₄** to yield **3u'**. The formation of the double-alkylation product **3u'** indicates that the anion formed by deprotonation of **3u** is more reactive than **2u**. The bisadduct **3u'** is formed exclusively (85% yield of isolated **3u'**), when Meldrum's acid is combined with two equivalents of **1h-BF₄** in the presence of two equivalents of potassium *tert*-butoxide.

Scheme 9.



2.3. Kinetic Experiments

For the investigations of the reactivities of the carbenium ions **1(g-i)**, stock solutions of the isolated tetrafluoroborate salts were used; cations **1(a-f)** were generated in solution as described above. Most of the reactions were studied at 20 °C; in some cases the k_2 values for 20 °C were obtained from the Eyring activation parameters derived from a series of low-temperature measurements. All reactions were studied in those solvents to which the N and s_N parameters of the nucleophiles refer: π -nucleophiles in dichloromethane, amines in acetonitrile, and the carbanion **2u** in DMSO.

The rates were determined by monitoring the decays of the absorbances of the corresponding carbocations in the UV-vis spectra. In case of slow reactions ($\tau_{1/2} > 3$ s), conventional UV-vis spectrophotometry was used, fast reactions (20 ms $< \tau_{1/2} < 3$ s) were followed with stopped-flow devices, and very fast reactions ($\tau_{1/2} < 1$ ms) were investigated by generating the cations by laser-flash irradiation.¹³

All kinetics were performed under pseudo-first-order conditions using the nucleophiles in high excess, resulting in the monoexponential decays of the electrophiles' absorbances. The pseudo-first-order rate constants (k_{obs}) were obtained by least-squares fitting of the time-dependent absorbances (A_t) to the monoexponential function $A_t = A_0 e^{-k_{\text{obs}} t} + C$ (Figure 2a). The plots of the k_{obs} values versus the nucleophile concentrations were linear (Figure 2b), and their slopes yielded the second-order rate constants (k_2), which are summarized in Table 2.

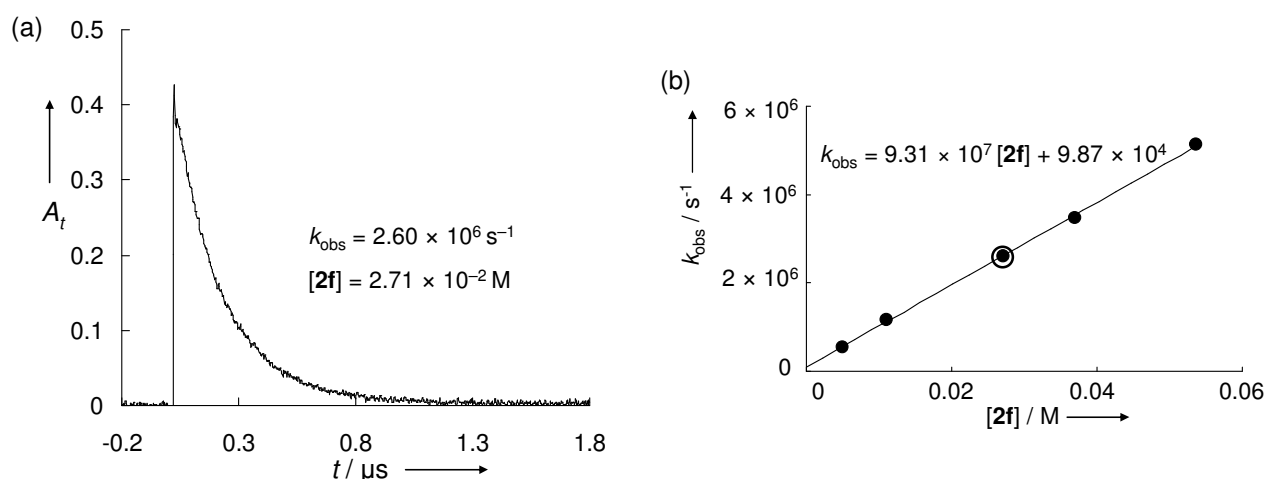


Figure 2. (a) Exponential decay of the absorbance A_t ($\lambda = 500$ nm) and (b) correlation between the pseudo-first-order rate constants k_{obs} and the concentration of **2f** for the reaction between (2-methylallyl)trimethylsilane (**2f**) and the cation **1b** generated by laser-flash photolysis from **1b**- $\text{PPh}_3^+\text{BF}_4^-$ (dichloromethane, 20 °C).

In order to examine whether the rate constants depend on the nature of the counterions, the reaction of **1e** with the cyclohexanone-derived silyl enol ether **2h** was studied with **1e**-PPh₃⁺BF₄⁻ and **1e**-PPh₃⁺TfO⁻ as precursors. The very small difference between the resulting rate constants $k_2(\text{BF}_4^-) = 6.41 \times 10^7 \text{ M}^{-1} \text{ s}^{-1}$ and $k_2(\text{TfO}^-) = 6.57 \times 10^7 \text{ M}^{-1} \text{ s}^{-1}$ confirms the independence of k_2 of the counterion, as previously found for analogous reactions with benzhydrylium ions.¹⁸

Table 2. Second-Order Rate Constants for the Reactions of 1,3-Diarylallylium Ions **1(a-i)** and Nucleophiles **2(a-u)** at 20 °C.

1,3-diarylallylium ion	generation of 1(a-i)	E^a	nucleophile / solvent	N, s_N	$k_2 / \text{M}^{-1} \text{ s}^{-1}$	$k_{\text{calc}} / \text{M}^{-1} \text{ s}^{-1}$	k_2/k_{calc}
1a (X = <i>m,m</i> -F ₂)	<i>b</i>	6.11	2a / CH ₂ Cl ₂	-1.00, 1.40	3.56×10^7	1.41×10^7	2.52
	<i>b</i>		2b / CH ₂ Cl ₂	0.54, 1.00	1.98×10^6	4.43×10^6	0.45
	<i>b</i>		2c / CH ₂ Cl ₂	0.96, 1.00	9.11×10^6	1.16×10^7	0.78
	<i>b</i>		2e / CH ₂ Cl ₂	1.79, 0.94	2.03×10^7	2.64×10^7	0.77
	<i>b</i>		2f / CH ₂ Cl ₂	4.41, 0.96	5.88×10^8 ^c	<i>d</i>	-
	<i>b</i>		2h / CH ₂ Cl ₂	5.21, 1.00	1.06×10^9 ^c	<i>d</i>	-
1b (X = <i>m</i> -F)	<i>b</i>	4.15	2e / CH ₂ Cl ₂	1.79, 0.94	6.99×10^5	3.86×10^5	1.81
	<i>b</i>		2f / CH ₂ Cl ₂	4.41, 0.96	9.31×10^7	1.66×10^8	0.56
1c (X = <i>p</i> -Br)	<i>e</i>	2.85	2d / CH ₂ Cl ₂	-0.13, 1.21	2.93×10^{3f}	1.98×10^3	1.48
	<i>g</i>		2f / CH ₂ Cl ₂	4.41, 0.96	8.65×10^6	9.43×10^6	0.92
	<i>g</i>		2h / CH ₂ Cl ₂	5.21, 1.00	7.86×10^7	1.16×10^8	0.68
1d (X = <i>p</i> -Cl)	<i>b</i>	2.69	2f / CH ₂ Cl ₂	4.41, 0.96	6.57×10^6	-	-
1e (X = H)	<i>h</i>	2.70	2c / CH ₂ Cl ₂	0.96, 1.00	2.88×10^{3f}	4.59×10^3	0.63
	<i>h</i>		2d / CH ₂ Cl ₂	-0.13, 1.21	2.53×10^{3f}	1.29×10^3	1.96
	<i>g</i>		2f / CH ₂ Cl ₂	4.41, 0.96	5.94×10^6	6.71×10^6	0.88
	<i>b</i>		2h / CH ₂ Cl ₂	5.21, 1.00	6.41×10^7 ^b	8.15×10^7	0.79
	<i>g</i>		2h / CH ₂ Cl ₂	5.21, 1.00	6.54×10^7 ^g	8.15×10^7	0.80
1f (X = <i>p</i> -Me)	<i>h</i>	1.23	2c / CH ₂ Cl ₂	0.96, 1.00	5.01×10^1	1.54×10^2	0.33
	<i>h</i>		2d / CH ₂ Cl ₂	-0.13, 1.21	4.98×10^1	2.12×10^1	2.35
	<i>h</i>		2e / CH ₂ Cl ₂	1.79, 0.94	5.03×10^{2f}	6.85×10^2	0.73
	<i>b</i>		2f / CH ₂ Cl ₂	4.41, 0.96	2.24×10^5	2.58×10^5	0.87
	<i>b</i>		2h / CH ₂ Cl ₂	5.21, 1.00	4.56×10^6	2.73×10^6	1.67

Table 2. Continued.

1,3-diarylallylium ion	generation of 1(a-i)	E^a	nucleophile / solvent	N, s_N	$k_2 / \text{M}^{-1} \text{s}^{-1}$	$k_{\text{calc}} / \text{M}^{-1} \text{s}^{-1}$	k_2/k_{calc}
1g ($X = p\text{-OMe}$)	<i>i</i>	-1.45	2e / CH_2Cl_2	1.79, 0.94	6.68×10^{-1}	2.08	0.32
	<i>i</i>		2f / CH_2Cl_2	4.41, 0.96	5.53×10^2	6.90×10^2	0.80
	<i>i</i>		2g / CH_2Cl_2	3.09, 0.90	3.69×10^1	2.98×10^1	1.24
	<i>i</i>		2h / CH_2Cl_2	5.21, 1.00	6.15×10^3	5.72×10^3	1.08
	<i>i</i>		2i / CH_2Cl_2	6.57, 0.93	1.13×10^5	5.74×10^4	1.97
	<i>i</i>		2l / CH_2Cl_2	3.27, 0.73	4.94 ^c	2.12×10^1	0.23
	<i>j</i>		2m / CH_2Cl_2	5.85, 1.03	4.91×10^4	3.38×10^4	1.45
1h ($X = p\text{-NMe}_2$)	<i>i</i>	-7.50	2i / CH_2Cl_2	6.57, 0.93	7.82×10^{-2}	1.37×10^{-1}	0.57
	<i>i</i>		2j / CH_2Cl_2	8.23, 0.81	1.88	3.90	0.48
	<i>i</i>		2k / CH_2Cl_2	9.00, 0.98	1.10×10^2	2.95×10^1	3.73
	<i>i</i>		2n / CH_2Cl_2	11.40, 0.83	8.51×10^3 ^c	1.73×10^3	4.93
	<i>i</i>		2p / CH_3CN	10.13, 0.75	1.29×10^2	9.39×10^1	1.37
	<i>i</i>		2r / CH_3CN	14.29, 0.67	2.22×10^4	3.54×10^4	0.63
	<i>i</i>		2s / CH_3CN	15.65, 0.74	9.34×10^5	1.07×10^6	0.87
1i ($X = \text{jul}$) ^k	<i>i</i>	-9.78	2o / CH_2Cl_2	15.06, 0.82	8.30×10^4 ^c	2.14×10^4	3.88
	<i>i</i>		2q / CH_3CN	13.77, 0.70	4.67×10^2	6.22×10^2	0.75
	<i>i</i>		2s / CH_3CN	15.65, 0.74	2.85×10^4	2.21×10^4	1.29
	<i>i</i>		2t / CH_3CN	17.35, 0.68	1.54×10^5	1.41×10^5	1.09
	<i>i</i>		2u / DMSO	13.91, 0.86	3.38×10^3	3.57×10^3	0.95

^a The E parameters for **1(a-i)** result from the least-squares minimization of $\Delta^2 = \sum(\log k_2 - s_N(N + E))^2$, which uses the second-order rate constants k_2 (this table) and the N and s_N parameters of the nucleophiles **2(a-u)** given in ref 10 and listed in this table. E values with more decimals than given in this table were used for the calculation of k_{calc} by eq 1 and for the correlations in Figures 5, 7, and 9. The use of E parameters given in this table leads to slightly deviating results. ^b Laser-flash photolysis of **1**- $\text{PPh}_3^+\text{BF}_4^-$. ^c Values were not used for determination of E . ^d Diffusion limit approached. ^e From **1**-Cl and GaCl_3 . ^f Extrapolated from rate constants at lower temperature by using the Eyring equation (for details see the Experimental Section). ^g Laser-flash photolysis of **1**- $\text{PPh}_3^+\text{TfO}^-$. ^h From **1**-OTMS and TMSOTf, BCl_3 , or GaCl_3 . ⁱ Isolated tetrafluoroborate salt (**1**- BF_4). ^j From **1g**-OMe and TMSOTf. ^k See Table 1 for definition.

2.4. Determination of the Electrophilicity Parameters E

Figure 3 shows plots of $(\log k_2)/s_N$ versus N for the reactions of the allyl cations **1(a-i)** with the nucleophiles **2(a-u)**. Slopes of 1 were enforced in the drawn correlation lines, as required by eq 1. The electrophilicity parameters E (Table 2) of the cations **1(a-i)** were calculated by minimizing the sum of the squared deviations $\Delta^2 = \sum(\log k_2 - s_N(N + E))^2$ using the nonlinear

solver “What’s Best!”.¹⁹ The good correlations shown in Figure 3, which include rate constants determined in different solvents, confirm that in 1,3-diarylallyl cations, as in benzhydrylium ions, differential solvation of the carbocations is negligible, which allows us to use the same electrophilicity parameters E in different solvents. As explicitly explained in ref 7, the solvent effects on the rate constants are fully incorporated in the nucleophile-specific parameters N and s_N .

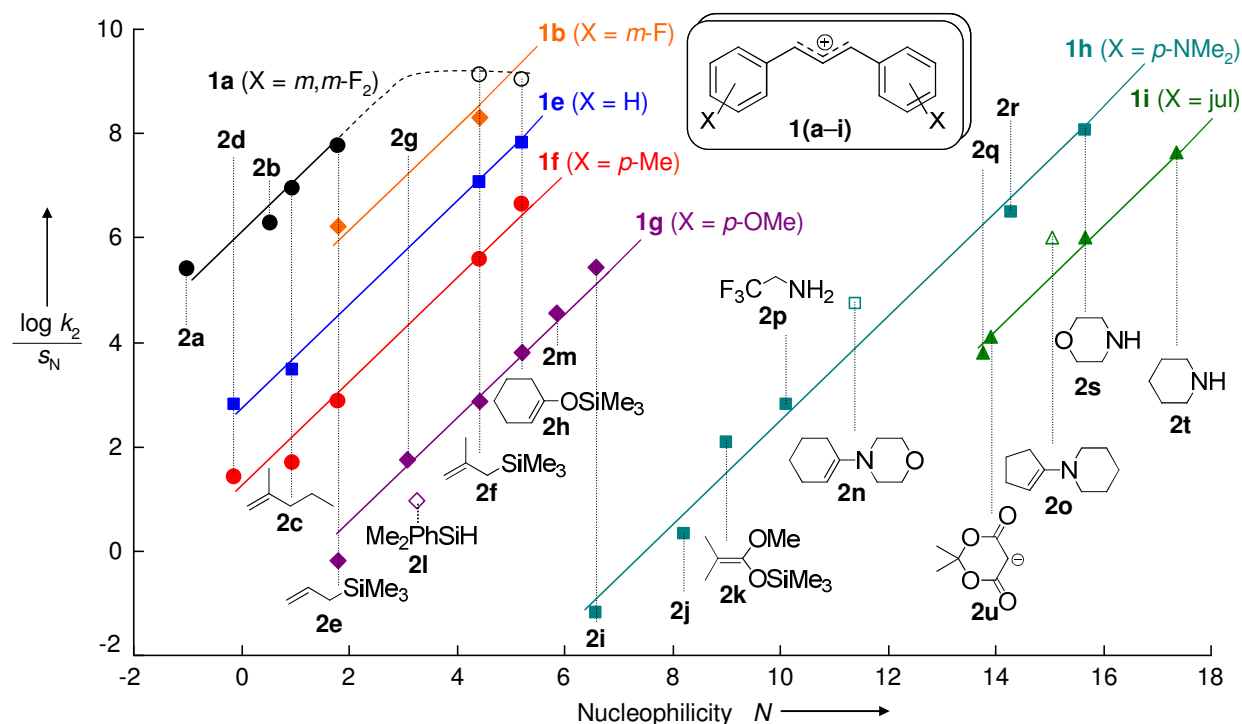


Figure 3. Plot of $(\log k_2)/s_N$ versus N for the reactions of the 1,3-diarylallyl cations **1(a–i)** with the nucleophiles **2(a–u)** (solvents are specified in Table 2). The data points shown with open symbols were not used for the determination of E (see text). The data for cations **1(c–d)** are omitted for clarity.

Though the three-parameter eq 1, which can be employed to predict absolute rate constants in a reactivity range of 40 orders of magnitude can only be expected to be reliable within a factor of 10–100,^{8a} some systematic deviations within this range shown in Figure 3 prompt us also to comment on their possible origin.

In the combinations of **1a** with **2f** and **2h** the diffusion limit is approached; therefore the k_2 values of these reactions were not used for the determination of E .

Dimethylphenylsilane (**2l**) reacts with the (*E*)-1,3-bis(4-methoxyphenyl)allyl cation (**1g**) 4.3 times more slowly than calculated by eq 1 from the E parameter of **1g** (derived from its reactions with carbon nucleophiles) and the N and s_N parameters of **2l**, which were derived

from its reactions with benzhydrylium ions. Similar trends were observed for the reactions of hydride donors with tropylium²⁰ and 1,1,3-triarylallylium ions.²¹ Obviously, hydride donors react generally faster with benzhydrylium ions than with more highly delocalized carbocations.

The amino-substituted allyl cations **1h** and **1i** react with the enamines **2n** and **2o** about 4.5 times faster than expected from their *E* parameters. Possibly, interaction of the nitrogen lone-pair with the other allyl terminus, comparable to the transition state of the aza-Claisen rearrangement,²² accounts for the slightly increased reactivity of the enamines (Figure 4).

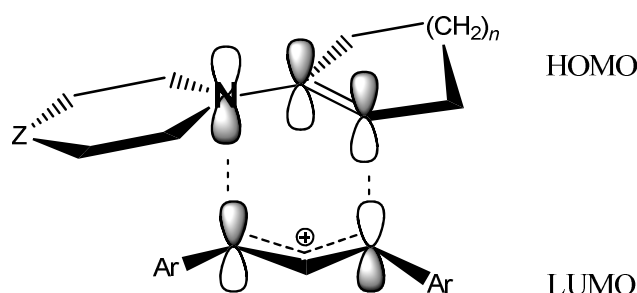


Figure 4. Weak transition state stabilization in reactions between enamines and 1,3-diarylallyl cations.

These deviations are quite moderate, however, so that the inclusion of the rate constants in the least-squares minimization mentioned above would not significantly change the *E* parameters derived for the 1,3-diarylallyl cations.

Because of the low thermodynamic driving force of the reaction of **1h** with 2,2,2-trifluoroethylamine (**2p**), the nucleophile had to be used in very high excess (over 5000 equivalents). Under such conditions, the kinetics may be affected by traces of impurities present in the reagent. However, the good fit of this rate constant to the correlation line indicates the reliability of the value determined in this way.

The relevance of the electrophilicity parameters listed in Table 2 for predicting reaction rates can be examined by comparison with independently determined rate constants. Miranda, Scaiano, and co-workers²³ reported rate constants of the reactions of cation **1e** with a series of nucleophiles, two of which have been characterized by *N* and *s_N*. Substitution of *E*(**1e**) = 2.70 (Table 2) and *N* = 1.23, *s_N* = 0.92 for 2,2,2-trifluoroethanol²⁴ and *N* = 10.3, *s_N* = 0.60 for Cl⁻ in trifluoroethanol^{5a} in eq 1 yield $k_{\text{calc}}(\text{trifluoroethanol}) = 4.1 \times 10^3 \text{ s}^{-1}$ and $k_{\text{calc}}(\text{Cl}^- \text{ in trifluoroethanol}) = 6.3 \times 10^7 \text{ M}^{-1} \text{ s}^{-1}$, respectively. As these numbers agree within factors 1.9 and 3.5 with the experimental data reported in Table 1 of ref 23 ($8.0 \times 10^3 \text{ s}^{-1}$ and 2.2×10^8 ;

$\text{M}^{-1} \text{s}^{-1}$, respectively), the applicability of electrophilicity parameters E derived in this work has been demonstrated.

Figure 5 shows the correlation between the E parameters of **1(a-i)** and Hammett-Brown's σ^\ddagger (σ_m in case of F) parameters²⁵ of the corresponding substituents. The quality of this correlation is comparable to that for benzhydrylium ions.^{8a}

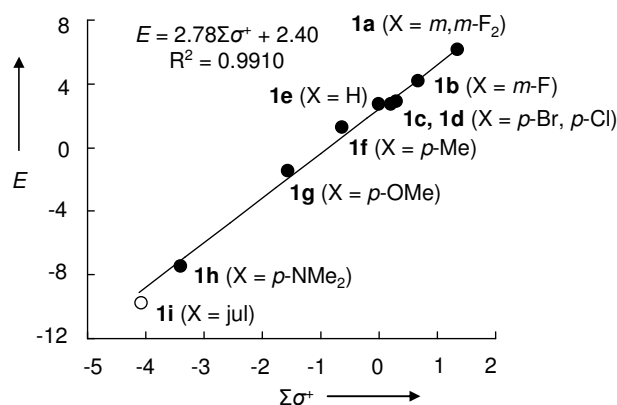
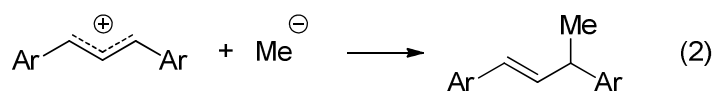


Figure 5. Correlation of the electrophilicity parameters E of the carbocations **1(a-i)** with the sum of the σ^\ddagger parameters²⁵ of the corresponding aryl substituents. Open symbol: **1i** is not included in the correlation, as σ^\ddagger for the julolidyl moiety of **1i** was estimated from the electrophilicities of benzhydrylium ions.^{8a}

2.5. Quantum Chemical Calculations

It has been shown^{9a} that the electrophilicities E of differently substituted benzhydryl cations correlate well with their methyl anion affinities calculated at the B3LYP/6-31G(d,p) level of theory. Thus, it was of interest to examine the analogous correlation for 1,3-diarylallyl cations. As recent work has shown the higher reliability of the MP2 method for such comparisons,²⁶ the methyl anion affinities (eq 2) of the cations **1(a-i)** have now been calculated at the MP2(FC)/6-31+G(2d,p)//B3LYP/6-31G(d,p) level of theory.²⁷



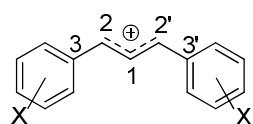
The geometrical parameters listed in Table 3 refer to the most stable conformers of diarylallyl cations **1(a-i)**. In contrast to benzhydryl^{9a} and trityl cations,²⁷ the calculated structures for **1(a-i)** are completely planar (all dihedral angles between ring and allyl carbons and

hydrogens deviate by less than 1.5° from 0° or 180°), in line with the X-ray analysis of **1h**-BF₄.¹⁵

Table 3 shows that the C2–C3 bond lengths ($r_{\text{C2-C3}} = r_{\text{C2'-C3'}}$) of the cations **1(a-i)** decrease while the C1–C2 bond lengths ($r_{\text{C1-C2}} = r_{\text{C1-C2'}}$) increase with higher electron donating ability of the substituents. Figure 6 depicts linear correlations of the bond lengths $r_{\text{C2-C3}}$ and $r_{\text{C1-C2}}$ with Hammett-Brown's σ^+ parameters of the corresponding substituents (σ_m in case of F).^{8a,25} From the significantly higher absolute value of the slope in Figure 6a compared with that in Figure 6b one can derive that substituent variation affects the bonds of the allylic termini to the aryl rings much more than the bond lengths in the allylic fragment. The strong double-bond character of the C2–C3 bond in the 1,3-diarylallyl cations **1** is also reflected by the high rotational barrier ($51 \pm 2 \text{ kJ mol}^{-1}$) for **1h** derived by dynamic NMR spectroscopy (see above).

The bond lengths in the crystal structure of **1h**-BF₄¹⁵ are slightly smaller than those calculated for the gas phase (Figure SX2 in the Supplementary Section, p 88).

Table 3. Characteristic Bond Lengths Between Aromatic and Allylic Carbons in the 1,3-Diarylallyl Cations **1(a-i)** Optimized at the B3LYP/6-31G(d,p) Level of Theory and $\Sigma\sigma^+$ ($\Sigma\sigma_m$) of the Corresponding Substituents.



cation	X	$\Sigma\sigma^{+a}$	$r_{\text{C2-C3}}^b / \text{\AA}$	$r_{\text{C1-C2}}^b / \text{\AA}$
1a	<i>m,m</i> -F ₂	1.36 ^c	1.428	1.39022
1b	<i>m</i> -F	0.68 ^c	1.427	1.39037
1c	<i>p</i> -Br	0.30	1.424	1.39087
1d	<i>p</i> -Cl	0.22	1.424	1.39090
1e	H	0.00	1.425	1.39067
1f	<i>p</i> -Me	-0.62	1.423	1.39089
1g	<i>p</i> -OMe	-1.56	1.419	1.39134
1h	<i>p</i> -NMe ₂	-3.40	1.415	1.39192
1i	jul	-4.06 ^d	1.414	1.39219

^a From ref 25. ^b Values of r with more decimals than given in the table were used for the correlations in Figure 6 and Figure SX2 of the Supplementary Section. The use of the bond lengths given in this table leads to slightly deviating results. ^c σ_m . ^d Estimated value from ref 8a.

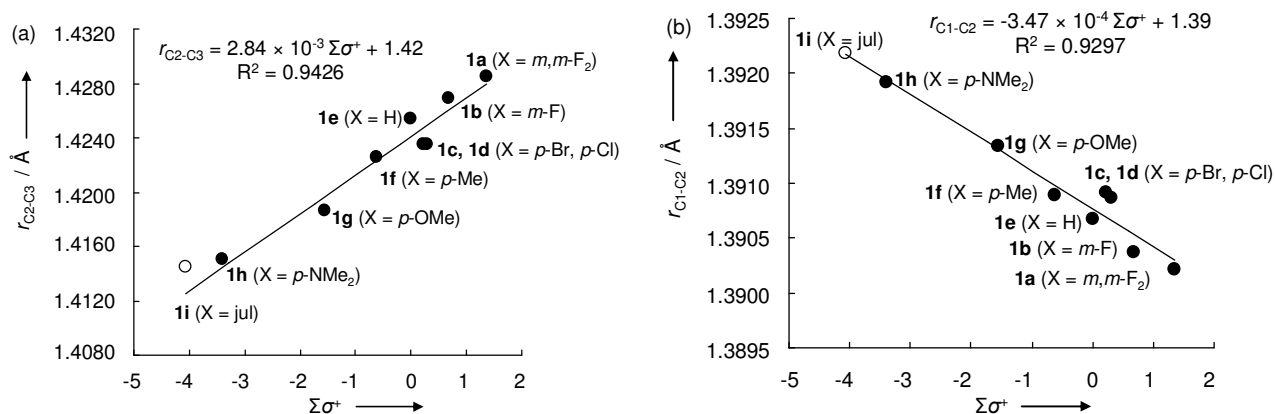


Figure 6. Correlation of the bond lengths a) r_{C2-C3} and b) r_{C1-C2} in cations **1(a-i)** with the sum of the σ^+ parameters of the corresponding substituents.^{8a, 25}

Details of the determinations of the gas-phase methyl anion affinities (ΔH_{298} , ΔG_{298} , Table 4) defined by eq 2 are given in the Experimental Section. Single point calculations were performed at the MP2(FC)/6-31+G(2d,p) level of theory for all allyl cations **1(a-i)** and the corresponding methyl anion adducts **1(a-i)-Me** using the geometries optimized at the B3LYP/6-31G(d,p) level. The resulting MP2 energies were converted to H_{298} and G_{298} using the thermochemical corrections calculated with B3LYP/6-31G(d,p). As cations **1b**, **1g** and **1i** as well as all (*E*)-1,3-diarylbut-1-enes **1(a-i)-Me** have several minima in the conformational space, the Boltzmann distribution was used to calculate their averaged energies.

Table 4. Gas-Phase Methyl Anion Affinities (ΔH_{298} , ΔG_{298} of eq 2) in kJ mol^{-1} , MP2(FC)/6-31+G(2d,p)//B3LYP/6-31G(d,p).^a

cation	X	ΔH_{298}^b	ΔG_{298}^b
1a	<i>m,m</i> -F ₂	-962.44	-976.53
1b	<i>m</i> -F	-931.19	-945.91
1c	<i>p</i> -Br	-912.92	-927.61
1d	<i>p</i> -Cl	-916.12	-930.84
1e	H	-901.07	-915.29
1f	<i>p</i> -Me	-877.42	-891.91
1g	<i>p</i> -OMe	-847.22	-861.40
1h	<i>p</i> -NMe ₂	-782.87	-797.04
1i	Jul	-753.13	-767.29

^a Total energies and thermochemical corrections for the reactants and products can be found in the Experimental Section. ^b The values of ΔH_{298} and ΔG_{298} with more decimals than given in the table were used for the correlations in Figure 7 and Figure SX3 of the Supplementary Section. The use of ΔH_{298} given in this table leads to slightly deviating results.

As expected, the absolute values of ΔH_{298} and ΔG_{298} decrease with increasing electron donating ability of the substituents. Both ΔH_{298} and ΔG_{298} correlate linearly with the sum of the σ^\ddagger parameters of the corresponding substituents^{8a,25} (Figure SX3 in the Supplementary Section, p 89).

The correlation between the electrophilicity parameters E of the allyl cations **1(a–i)** and their ΔH_{298} values (Figure 7) shows that quantum chemically calculated methyl anion affinities can be used for deriving E parameters of further 1,3-diarylallyl cations.

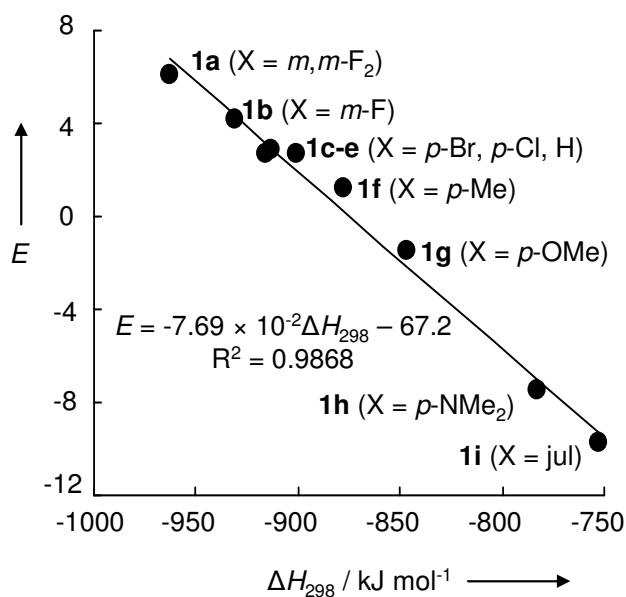


Figure 7. Correlation of the electrophilicities E of the cations **1(a–i)** with their gas-phase methyl anion affinities ΔH_{298} (calculated at MP2(FC)/6-31+G(2d,p)//B3LYP/6-31G(d,p)).

The correlation in eq 3

$$\delta E = -0.0769 \delta \Delta H_{298} \quad (3)$$

(δ describes the effect of a substituent), which is derived from Figure 7, can be transformed into the relationship (eq 4)

$$\delta \Delta G^\ddagger = 0.432 s_N \delta \Delta H_{298} \quad (4)$$

by using eq 1 and the Eyring equation. If one assumes that the substituent effects on the diarylallyl cations in the gas phase ($\delta \Delta H_{298}$) are attenuated to 62% in dichloromethane solution, as previously shown for the analogous benzhydrylium ions,^{9a} one can derive a Brønsted coefficient expressed in eq 5 by dividing the slope of eq 4 by 0.62.

$$\alpha = 0.70 s_N \quad (5)$$

Details of this procedure have been described in ref 9a.

2.6. Comparison with Benzhydryl Cations

The reactivity range covered by 1,3-diarylallyl cations **1(a-i)** (16 orders of magnitude) is slightly smaller than that for analogously substituted diarylmethyl cations⁸ (Figure 8). While amino-substituted 1,3-diarylallyl and diarylmethyl cations show almost identical electrophilicities, 1,3-diarylallyl cations substituted with weaker electron donors are increasingly less electrophilic than analogously substituted diarylmethyl cations.

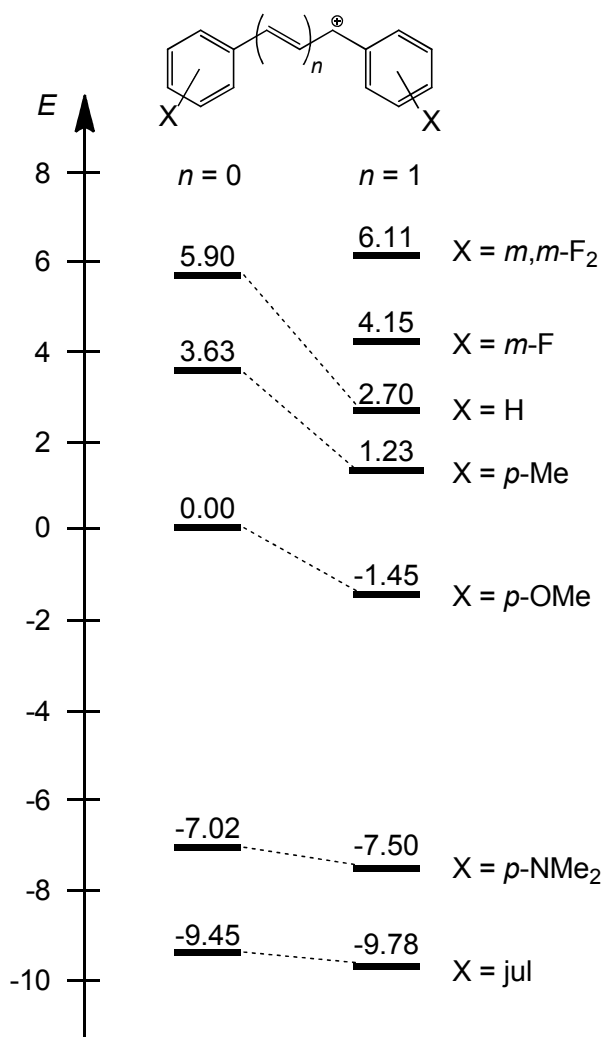


Figure 8. Electrophilicities E of the 1,3-diarylallyl cations ($n = 1$, from Table 2) compared with those of the corresponding benzhydrylium ions ($n = 0$).⁸

As illustrated in Figure 9, the E parameters of 1,3-diarylallyl cations correlate linearly with those of analogously substituted benzhydrylium ions (Figure 9). The slope of this correlation (0.82) reflects that the stabilization of 1,3-diarylallyl cations is less affected by the substituents at the aryl rings, which may be explained by the charge delocalization between C1 and C3 in diarylallyl cations, which reduces the electron demand of the carbenium centers.

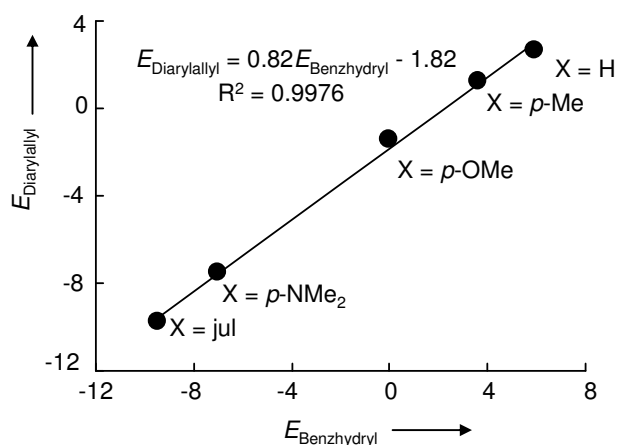


Figure 9. Linear correlation between the E parameters of analogously substituted 1,3-diarylallyl and benzhydryl cations (formula see Figure 8).

3. Conclusions

The rate constants of the reactions of 1,3-diarylallyl cations **1(a-i)** with nucleophiles of a large structural variety can be described by the linear free energy relationship $\log k_2(20\text{ }^\circ\text{C}) = s_N(N + E)$ (eq 1) using N and s_N parameters that have previously been derived from the reactions of the corresponding nucleophiles with benzhydrylium ions.^{8,10} The fact that the correlations used for the determination of the electrophilicity parameters E of **1(a-i)** include rate constants determined in different solvents (CH_2Cl_2 , CH_3CN , DMSO) shows that the E parameters listed in Table 2 can be treated as solvent-independent. As pointed out previously,⁷ this does not mean that all allyl cations **1(a-i)** are solvated to the same extent but that the solvent effects on these rate constants are fully taken account of in the solvent-dependent nucleophile-specific parameters N and s_N of their reaction partners. As the electrophilicity parameters E of **1(a-i)** correlate linearly with the quantum chemically calculated gas-phase methyl anion affinities of these cations and Hammett-Brown's substituent constants σ^+ , these correlations may be employed to estimate reactivities of further 1,3-diarylallyl cations.

4. Experimental Section

4.1. General

Materials for Synthesis. Substituted acetophenones and benzaldehydes with exception of fluorinated ones (synthesis described below) were purchased. The substituted chalcones (**1(a–g)-O**) and chalcols (**1(a–f)-OH**) were synthesized using the general procedures described below. Synthetic procedures have not been optimized for high yields.

Materials for Kinetic Measurements. Dichloromethane (p.a. grade) was subsequently treated with concentrated sulfuric acid, water, 10% NaHCO₃ solution, and again water. After predrying with anhydrous CaCl₂, it was freshly distilled over CaH₂. Acetonitrile (HPLC grade) and DMSO (99.7% purity) were used as received.

Gallium chloride was sublimed in a vacuum and stored under glovebox conditions (dry Ar atmosphere). Trimethylsilyl triflate was used as received.

NMR Spectroscopy. In the ¹H and ¹³C NMR spectra chemical shifts are expressed in δ (ppm) and refer to CDCl₃ (δ_{H} 7.26, δ_{C} 77.0), CD₂Cl₂ (δ_{H} 5.32, δ_{C} 54.0), CD₃CN (δ_{H} 1.94, δ_{C} 1.39), nitrobenzene (δ_{H} 7.50, δ_{C} 148.1), or TMS (δ_{H} 0.00, δ_{C} 0.0) as internal standards. The coupling constants are given in Hz. Abbreviations used are: s (singlet), d (doublet), t (triplet), q (quartet), m (multiplet). In case of ¹³C NMR spectra, these abbreviations refer to the multiplicity in proton-decoupled spectra, and hydrogen multiplicity (based on DEPT or HSQC experiments) is shown as CH₃, CH₂, CH or C to avoid ambiguity.

4.2. Synthetic Procedures

3,5-Difluorobenzaldehyde was prepared according to Olah's procedure:²⁸ To 1-bromo-3,5-difluorobenzene (28.9 g, 150 mmol) a solution of *s*-BuMgCl·LiCl in THF (1.07 M, 140 mL, 150 mmol) was added slowly to keep the temperature of the reaction mixture below 30 °C. The resulting reaction mixture was further stirred at room temperature. GC-MS analysis^{28b} indicated full conversion after 3 h. The reaction mixture was then cooled to –40 °C before DMF (12.7 mL, 12.1 g, 165 mmol) was added dropwise. After stirring overnight at –40 °C, diethyl ether was added. The resulting mixture was successively washed with saturated ammonium chloride solution, water, and brine before it was dried (MgSO₄). Evaporation of solvents followed by distillation under vacuum (75 mbar, 90–110 °C) afforded 3,5-difluorobenzaldehyde (11.2 g, 78.8 mmol, 53%). The ¹H NMR spectrum of the product agreed with previously published data.²⁹

3-Fluoroacetophenone. A small portion of 1-bromo-3-fluorobenzene was added to Mg turnings (1.67 g, 68.5 mmol) and LiCl (2.91 g, 68.5 mmol) in dry THF (35 mL). To initiate the reaction, DIBAL-H (1 M solution in hexane, 2.1 mL, 2.1 mmol) was added. After the exothermic process had started, the remaining portion of 1-bromo-3-fluorobenzene (12.0 g, 68.6 mmol in total) was added dropwise keeping the THF gently boiling. The reaction mixture was kept refluxing until full conversion of 1-bromo-3-fluorobenzene was reached (GC-MS monitoring analogous to the method described in reference 28b), then cooled to room temperature, and added to a suspension of ZnCl₂ (4.67 g, 34.3 mmol) in THF (15 mL). After stirring for 3h, the resulting solution was added dropwise to a solution of acetyl chloride (5.38 g, 68.5 mmol) and [Pd(PPh₃)₄] (50 mg, 0.042 mmol, 0.061 mol%) in diethyl ether (500 mL). Stirring was continued for 12 h before saturated aqueous NH₄Cl solution (250 mL) was added. The organic layer was separated, washed with water and brine, and dried (MgSO₄). Evaporation of solvents followed by distillation (75 mbar) afforded 3-fluoroacetophenone (4.18 g, 30.2 mmol, 44%) as a colorless liquid. The ¹H NMR spectrum agreed with literature data,³⁰ but showed some impurities (probably owing to the product of ZnCl₂-catalyzed attack of acetyl chloride on THF).

3,5-Difluoroacetophenone was synthesized analogously to 3-fluoroacetophenone from 1-bromo-3,5-difluorobenzene (24.6 g, 128 mmol), a solution of *s*-BuMgCl·LiCl in THF (1.07 M, 120 mL, 128 mmol), zinc chloride (8.70 g, 63.8 mmol) and acetyl chloride (9.2 mL, 10 g, 0.13 mol) to give 3,5-difluoroacetophenone (13.2 g, 84.2 mmol, 66%).

General method for the synthesis of (*E*)-1,3-diarylprop-2-en-1-ones (1-O). According to Manolov's procedure,³¹ substituted acetophenones (1 equiv) and benzaldehydes (1 equiv) were dissolved in ethanol (ca. 200 mL ethanol per mol substrate) before an 11% (w/w) aqueous NaOH solution was added (333 mL per mol acetophenone). The resulting mixtures were stirred until precipitates formed (usually after 2 h, otherwise the reaction mixtures were cooled with an ice bath for further 3 h), which were filtered and washed with water until the washing water reacted neutral. Recrystallization of crude products from ethanol gave (*E*)-1,3-diarylprop-2-en-1-ones in 64–88% yields.

(*E*)-1,3-Bis(3,5-difluorophenyl)prop-2-en-1-one (1a-O). From 3,5-difluoroacetophenone (7.18 g, 46.0 mmol) and 3,5-difluorobenzaldehyde (6.53 g, 46.0 mmol) in ethanol (10 mL) and 11% (w/w) aqueous NaOH solution (15 mL): 8.26 g (29.5 mmol, 64%), yellow needles (m.p. 159.0–160.1 °C). ¹H NMR (CDCl₃, 300 MHz): δ 6.89 (tt, ²J_{HF} = 8.7, ⁴J_{HH} = 2.3 Hz, 1 H, H_{Ar}), 7.06 (tt, ²J_{HF} = 8.4, ⁴J_{HH} = 2.4 Hz, 1 H, H_{Ar}), 7.11–7.20 (m, 2 H, H_{Ar}), 7.38 (d, ³J_{HH} = 15.7 Hz, 1 H, ArCHCHCOAr), 7.46–7.57 (m, 2 H, H_{Ar}), 7.72 (d, ³J_{HH} = 15.7 Hz, 1 H,

ArCHCHCOAr). ^{13}C NMR (CDCl_3 , 75.5 MHz): δ 106.1 (t, $J_{\text{CF}} = 25.4$ Hz, CH), 108.5 (t, $J_{\text{CF}} = 25.4$ Hz, CH), 110.9–111.7 (m, $2 \times$ CH), 123.1 (CH), 137.6 (t, $J_{\text{CF}} = 9.5$ Hz, C), 140.6 (t, $J_{\text{CF}} = 7.6$ Hz, C), 143.4 (t, $J_{\text{CF}} = 3.0$ Hz, CH), 163.1 (dd, $J_{\text{CF}} = 252$, $J_{\text{CF}} = 11.0$ Hz, C), 163.3 (dd, $J_{\text{CF}} = 250$, $J_{\text{CF}} = 12.7$ Hz, C), 187.1 ppm (t, $J_{\text{CF}} = 2.5$ Hz, C). ^{19}F NMR (CDCl_3 , 282 MHz): δ -108.7 to -108.6 (m), -107.7 to -107.6 ppm (m). HRMS (EI; positive): calcd 280.0506 ($\text{C}_{15}\text{H}_8\text{F}_4\text{O}$), found 280.0505.

(E)-1,3-Bis(3-fluorophenyl)prop-2-en-1-one (1b-O). From 3-fluoroacetophenone (3.00 g, 21.7 mmol) and 3-fluorobenzaldehyde (2.70 g, 21.7 mmol) in ethanol (5 mL) and 11% (w/w) aqueous NaOH solution (7.5 mL): 3.85 g (15.7 mmol, 65% yield with correction for 10% impurities), yellow solid. ^1H NMR (CDCl_3 , 300 MHz): δ 7.09–7.17 (m, 1 H, H_{ar}), 7.26–7.53 (m, 5 H, H_{ar}) superimposed with 7.46 (d, $^3J_{\text{HH}} = 15.7$ Hz, 1 H, ArCHCHCOAr), 7.68–7.72 (m, 1 H, H_{ar}), 7.78 (d, $^3J_{\text{HH}} = 15.7$ Hz, 1 H, ArCHCHCOAr) superimposed with 7.78–7.82 ppm (m, 1 H, H_{ar}); unknown impurities, which might be the products of the reaction between impurities in 3-fluoroacetophenone and some reagents used for the condensation reaction (NaOH etc.), caused additional resonances in the range of 2–6 ppm. ^{13}C NMR (CDCl_3 , 75.5 MHz): δ 114.5 (d, $J_{\text{CF}} = 21.9$ Hz, CH), 115.3 (d, $J_{\text{CF}} = 22.4$ Hz, CH), 117.6 (d, $J_{\text{CF}} = 21.5$ Hz, CH), 120.0 (d, $J_{\text{CF}} = 21.5$ Hz, CH), 122.6 (CH), 124.2 (d, $J_{\text{CF}} = 3.0$ Hz, CH), 124.6 (d, $J_{\text{CF}} = 2.9$ Hz, CH), 130.3 (d, $J_{\text{CF}} = 7.7$ Hz, CH), 130.5 (d, $J_{\text{CF}} = 8.3$ Hz, CH), 136.9 (d, $J_{\text{CF}} = 7.7$ Hz, C), 140.0 (d, $J_{\text{CF}} = 6.3$ Hz, C), 144.0 (d, $J_{\text{CF}} = 2.8$ Hz, CH), 162.9 (d, $J_{\text{CF}} = 248$ Hz, C), 163.0 (d, $J_{\text{CF}} = 247$ Hz, C), 188.7 ppm (d, $J_{\text{CF}} = 2.2$ Hz, C). ^{19}F NMR (CDCl_3 , 282 MHz): δ -112.34 to -112.26 (m), -111.64 to -111.56 ppm (m) HRMS (EI, positive) calcd 244.0694 ($\text{C}_{15}\text{H}_{10}\text{F}_2\text{O}$), found 244.0694.

General method for the synthesis of (E)-1,3-Diarylprop-2-en-1-ols (1-OH). Similar to the procedure by Dickinson et al.,³² (E)-1,3-diarylprop-2-enones (**1-O**) were dissolved in methanol (ca. 80 mM solutions, in some cases heating or refluxing of the reaction mixture was needed to achieve a homogeneous solution). Subsequently, sodium borohydride (0.5 - 2 equivalents) was added in small portions until the TLC spots of (E)-1,3-diarylprop-2-enone disappeared. After evaporating the methanol the residue were dissolved in EtOAc, washed with water (2 \times), and dried (MgSO_4). Drying in the vacuum afforded (E)-1,3-diarylprop-2-en-1-ols in yields of 89–98%. The resulting alcohols were used without further purification for subsequent syntheses because the excellent crystallization ability of phosphonium salts allows for purification of the cation precursors at the final stage of the synthesis.

(E)-1,3-Bis(3,5-difluorophenyl)prop-2-en-1-ol (1a-OH). From **1a-O** (4.99 g, 17.8 mmol): 4.62 g (16.4 mmol, 92%), colorless oil. ^1H NMR (CDCl_3 , 200 MHz): δ 2.20 (br. s, 1 H, OH),

5.36 (d, $^3J_{\text{HH}} = 6.4$ Hz, 1 H, ArCHCHCH(OH)Ar), 6.29 (dd, $^3J_{\text{HH}} = 15.8, 6.4$ Hz, 1 H, ArCHCHCH(OH)Ar), 6.54–6.81 (m, 3 H, ArCHCHCH(OH)Ar, H_{Ar}), 6.82–7.06 ppm (m, 4 H, H_{Ar}).

(E)-1,3-Bis(3-fluorophenyl)prop-2-en-1-ol (1b-OH). From **1b-O** (1.00 g, 4.09 mmol): 893 mg (3.62 mmol, 89%), colorless oil. ^1H NMR (CDCl₃, 200 MHz): δ 2.07 (br. s, 1 H, OH), 5.37 (d, $^3J_{\text{HH}} = 6.4$ Hz, 1 H, ArCHCHCH(OH)Ar), 6.33 (dd, $^3J_{\text{HH}} = 15.9, 6.4$ Hz, 1 H, ArCHCHCH(OH)Ar), 6.66 (d, $^3J_{\text{HH}} = 15.9$ Hz, 1 H, ArCHCHCH(OH)Ar), 6.88–7.39 ppm (m, 8 H, H_{Ar}).

(E)-1,3-Bis(4-bromophenyl)prop-2-en-1-ol (1c-OH). From **1c-O** (5.00 g, 13.7 mmol): 3.76 g (10.2 mmol, 75%), colorless solid. ^1H NMR (CDCl₃, 200 MHz): δ 2.13 (br. s, 1 H, OH), 5.33 (d, $^3J_{\text{HH}} = 6.3$ Hz, 1 H, ArCHCHCH(OH)Ar), 6.31 (dd, $^3J_{\text{HH}} = 15.8, 6.3$ Hz, 1 H, ArCHCHCH(OH)Ar), 6.61 (d, $^3J_{\text{HH}} = 15.8$ Hz, 1 H, ArCHCHCH(OH)Ar), 7.19–7.32 (m, 4 H, H_{Ar}), 7.37–7.53 ppm (m, 4 H, H_{Ar}).

(E)-1,3-Bis(4-bromophenyl)-3-chloroprop-1-ene (1c-Cl). Synthesized from **1c-OH** (1.00 g, 2.70 mmol) and concentrated HCl by using a procedure described in ref 33: 0.732 g (1.89 mmol, 70%), colorless solid. ^1H NMR (CDCl₃, 300 MHz): δ 5.61 (d, $^3J_{\text{HH}} = 7.2$ Hz, 1 H, ArCHCHCH(Cl)Ar), 6.47 (dd, $^3J_{\text{HH}} = 15.6, 7.2$ Hz, 1 H, ArCHCHCH(Cl)Ar), 6.58 (d, $^3J_{\text{HH}} = 15.6$ Hz, 1 H, ArCHCHCH(Cl)Ar), 7.25–7.29 (m, 2 H, H_{Ar}), 7.35–7.38 (m, 2 H, H_{Ar}), 7.43–7.50 (m, 2 H, H_{Ar}), 7.50–7.60 (m, 2 H, H_{Ar}). ^{13}C NMR (CDCl₃, 75.5 MHz): δ 62.6 (CH), 122.3 (C), 122.5 (C), 128.3 (CH), 129.0 (CH), 129.2 (CH), 131.3 (CH), 131.8 (CH), 131.9 (CH), 134.5 (C), 139.0 ppm (C). Some impurities gave rise to additional resonances in the ^1H and ^{13}C NMR spectra of **1c-Cl** and could neither be removed by distillation nor recrystallization. However, these impurities cannot influence the determination of the second-order rate constants (k_2) due to the fact, that in each kinetic run the same cation precursor concentration was used, so that possible side reactions with these impurities should cause the positive intercept of the k_{obs} vs [Nu] plot and do not affect the slope.

(E)-((1,3-Diphenylallyl)oxy)trimethylsilane (1e-OTMS) was prepared using a procedure analogous to that described in ref 34: Triethylamine (0.83 g, 8.2 mmol) and chlorotrimethylsilane (0.96 mL, 0.82 g, 7.6 mmol) were successively added to a solution of **1e-OH** (1.33 g, 6.32 mmol) in dichloromethane (25 mL) under N₂ atmosphere. The reaction mixture was stirred for further 10 h at ambient temperature. The precipitate formed after addition of diethyl ether (45 mL) was filtered off, and the filtrate was dried in the vacuum providing **1e-OTMS** (1.45 g, 5.12 mmol, 81%) as a yellow oil. The ^1H and ^{13}C NMR spectra of **1e-OTMS** were in agreement with those described in ref 35.

(E)-((1,3-Bis(4-methylphenyl)allyl)oxy)trimethylsilane (1f-OTMS). Analogous to **1e-OTMS**. From **1f-OH** (5.89 g, 24.7 mmol), chlorotrimethylsilane (3.22 g, 29.6 mmol), and triethylamine (3.25 g, 32.1 mmol): 5.89 g (19.0 mmol, 77%), colorless solid (m.p. 36.5–38°C). ^1H NMR (CDCl_3 , 400 MHz): δ 0.16 (m, 9 H, OTMS), 2.34, 2.36 (2 s, 6 H, $2 \times \text{CH}_3$), 5.33 (d, $^3J_{\text{HH}} = 6.5$ Hz, 1 H, $\text{ArCHCHCH}(\text{OTMS})\text{Ar}$), 6.27 (dd, $^3J_{\text{HH}} = 15.8$, 6.6 Hz, 1 H, $\text{ArCHCHCH}(\text{OTMS})\text{Ar}$), 6.58 (d, $^3J_{\text{HH}} = 15.8$, 1 H, $\text{ArCHCHCH}(\text{OTMS})\text{Ar}$), 7.12 (d, $^3J_{\text{HH}} = 8.0$ Hz, 2 H, H_{Ar}), 7.16 (d, $^3J_{\text{HH}} = 8.2$ Hz, 2 H, H_{Ar}), 7.27–7.32 ppm (m, 4 H, H_{Ar}). ^{13}C NMR (CDCl_3 , 101 MHz): δ 0.3 (CH_3), 21.09 (CH_3), 21.14 (CH_3), 75.5 (CH), 126.2 (CH), 126.4 (CH), 128.95 (CH), 129.03 (CH), 129.2 (CH), 132.0 (CH), 134.2 (C), 136.7 (C), 137.2 (C), 140.8 ppm (C). HRMS (EI, positive): calcd 310.1747 ($\text{C}_{20}\text{H}_{26}\text{OSi}$), found 310.1747.

(E)-(1,3-Bis(4-bromophenyl)allyl)oxy)trimethylsilane (1c-OTMS). Prepared analogously to **1e-OTMS** and used for further synthesis without purification and characterization.

General procedure for the synthesis of (E)-(1,3-diarylallyl)triphenylphosphonium tetrafluoroborates (1-PPh₃⁺BF₄⁻). Analogously to ref 13, triphenylphosphine was dissolved in dichloromethane (5 mL), and 50% w/w tetrafluoroboric acid solution in diethyl ether was added (1 equiv). After 5 min stirring at rt, the corresponding diarylallyl alcohols (1 equiv) were added, and the reaction mixtures were stirred for further 30 min. Evaporation of the solvents followed by recrystallization from a $\text{CH}_2\text{Cl}_2/\text{Et}_2\text{O}$ mixture afforded the desired products.

(E)-(1,3-Bis(3,5-difluorophenyl)allyl)triphenylphosphonium tetrafluoroborate (1a-PPh₃⁺BF₄⁻). From **1a-OH** (97.0 mg, 0.343 mmol): 117 mg (0.205 mmol, 60%), colorless crystals (m.p. 225.2–226.3 °C). ^1H NMR (CD_2Cl_2 , 400 MHz): δ 6.11 (dd, $^2J_{\text{HP}} = 15.9$, $^3J_{\text{HH}} = 9.2$ Hz, 1 H, $\text{ArCHCHCH}(\text{P}^+\text{Ph}_3)\text{Ar}$), 6.15–6.27 (m, 1 H, $\text{ArCHCHCH}(\text{P}^+\text{Ph}_3)\text{Ar}$), 6.59–6.72 (m, 2 H, H_{Ar}), 6.71–6.78 (m, 1 H, H_{Ar}), 6.79–6.91 (m, 3 H, H_{Ar}), 6.98 ppm (dd, $^3J_{\text{HH}} = 15.4$, $^4J_{\text{HP}} = 4.6$ Hz, 1 H, $\text{ArCHCHCH}(\text{P}^+\text{Ph}_3)\text{Ar}$), 7.61–7.68 (m, 6 H, H_{Ar}), 7.68–7.75 (m, 6 H, H_{Ar}), 7.82–7.95 ppm (m, 3 H, H_{Ar}). ^{13}C NMR (CD_2Cl_2 , 101 MHz): δ 45.8 (dt, $J_{\text{CP}} = 45.7$, $J_{\text{CF}} = \text{ca. } 2$ Hz, CH), 104.7 (t, $J_{\text{CF}} = 25.7$ Hz, CH), 105.6 (td, $J_{\text{CF}} = 25.0$, $J_{\text{CP}} = 2.5$ Hz, CH), 110.0–110.4 (m, CH), 113.8–114.2 (m, CH), 116.8 (d, $J_{\text{CP}} = 83.1$ Hz, C), 121.4 (d, $J_{\text{CP}} = 6.4$ Hz, CH), 131.1 (d, $J_{\text{CP}} = 12.5$ Hz, CH), 135.1 (d, $J_{\text{CP}} = 9.1$ Hz, CH), 135.7–136.0 (m, C), 136.3 (d, $J_{\text{CP}} = 3.1$ Hz, CH), 138.4 (dt, $J_{\text{CP}} = 12.9$, $J_{\text{CF}} = 3.0$ Hz, CH), 139.0–139.3 (m, C), 162.4–162.6 (m, C), 164.9–165.1 ppm (m, C). ^{19}F NMR (CD_2Cl_2 , 282 MHz): δ –151.10 to –151.05 (m, 3 F, BF_4^-), –151.03 to –151.00 (m, 1 F, BF_4^-), –113.6 to –113.5, –110.7 to –110.6 ppm (2 m, 4 F, F_{Ar}). ^{31}P NMR (CD_2Cl_2 , 162 MHz): δ 23.5 ppm. HRMS (ESI, positive) calcd 527.1546 ($\text{C}_{33}\text{H}_{24}\text{F}_4\text{P}^+$), found 527.1543.

(E)-(1,3-Bis(3-fluorophenyl)allyl)triphenylphosphonium tetrafluoroborate (1b-PPh₃⁺BF₄⁻). From **1b-OH** (298 mg, 1.21 mmol): 520 mg (0.899 mmol, 74%), colorless crystals (m.p. 176.3–177.3 °C). ¹H NMR (CD₂Cl₂, 400 MHz): δ 5.94 (dd, ²J_{HP} = 16.3, ³J_{HH} = 8.9 Hz, 1 H, ArCHCHCH(P⁺Ph₃)Ar), 6.24–6.31 (m, 1 H, ArCHCHCH(P⁺Ph₃)Ar), 6.76 (ddd, ³J_{HF} = 9.7, ³J_{HH} = 2.0, 2.0 Hz, 1 H, H_{Ar}), 6.90–6.98 (m, 4 H, ArCHCHCH(P⁺Ph₃)Ar, H_{Ar}), 7.06–7.09 (m, 1 H, H_{Ar}), 7.09–7.13 (m, 1 H, H_{Ar}), 7.23–7.33 (m, 2 H, 6-H, H_{Ar}), 7.57–7.62 (m, 6 H, H_{Ar}), 7.66–7.71 (m, 6 H, H_{Ar}), 7.83–7.87 ppm (m, 3 H, H_{Ar}). ¹³C NMR (CD₂Cl₂, 101 MHz): δ 46.6 (dd, J_{CP} = 45.0, J_{CF} = 1.9 Hz, CH), 113.6 (dd, J_{CF} = 22.0, J_{CP} = 1.8 Hz, CH), 116.3 (dd, J_{CF} = 21.4, J_{CP} = 1.1 Hz, CH), 117.05 (d, J_{CP} = 82.8 Hz, C), 117.06 (dd, J_{CF} = 20.9, J_{CP} = 3.0 Hz, CH), 117.6 (dd, J_{CF} = 23.0, J_{CP} = 5.9 Hz, CH), 120.6 (d, J_{CP} = 6.3 Hz, CH), 123.5 (dd, J_{CF} = 2.8, J_{CP} = 1.9 Hz, CH), 126.7 (dd, J_{CP} = 6.1, J_{CF} = 3.1 Hz, CH), 130.95 (d, J_{CP} = 12.4 Hz, CH), 130.99 (dd, J_{CF} = ca. 8, J_{CP} = 1.0 Hz, CH), 131.9 (dd, J_{CF} = 8.2, J_{CP} = 2.5 Hz, CH), 134.4 (dd, J_{CF} = 7.4, J_{CP} = 5.3 Hz, C), 135.2 (d, J_{CP} = 9.0 Hz, CH), 136.1 (d, J_{CP} = 3.1 Hz, CH), 138.1 (dd, J_{CF} = 7.7, J_{CP} = 3.0 Hz, C), 138.8 (dd, J_{CP} = 13.0, J_{CF} = 2.6 Hz, CH), 163.4 (dd, J_{CF} = 249, J_{CP} = 2.5 Hz, C), 163.5 ppm (dd, J_{CF} = 246, J_{CP} = 1.1 Hz, C). ¹⁹F NMR (CD₂Cl₂, 282 MHz): δ -150.93 to -150.90 (m, 3 F, BF₄⁻), -150.87 to -150.85 (m, 1 F, BF₄⁻), -113.6 to -113.5, -110.7 to -110.6 ppm (2 m, 2 F, F_{Ar}). ³¹P NMR (CD₂Cl₂, 162 MHz): δ 23.1 ppm. HRMS (ESI, positive) calcd 491.1735 (C₃₃H₂₆F₂P⁺), found 491.1732.

(E)-(1,3-Bis(4-chlorophenyl)allyl)triphenylphosphonium tetrafluoroborate (1d-PPh₃⁺BF₄⁻). From **1d-OH** (600 mg, 2.15 mmol): 721 mg (1.18 mmol, 55%), colorless crystals (149.6–150.4 °C). ¹H NMR (CD₂Cl₂, 400 MHz): δ 5.96 (dd, ²J_{HP} = 16.3, ³J_{HH} = 9.0 Hz, 1 H, ArCHCHCH(P⁺Ph₃)Ar), 6.24–6.32 (m, 1 H, ArCHCHCH(P⁺Ph₃)Ar), 6.92 (dd, ³J_{HH} = 15.4, ⁴J_{HP} = 4.5 Hz, 1 H, ArCHCHCH(P⁺Ph₃)Ar), 6.99–7.09 (m, 2 H, H_{Ar}), 7.21–7.27 (m, 6 H, H_{Ar}), 7.59–7.64 (m, 6 H, H_{Ar}), 7.66–7.71 (m, 6 H, H_{Ar}), 7.83–7.88 ppm (m, 3 H, H_{Ar}). ¹³C NMR (CD₂Cl₂, 101 MHz): δ 46.4 (d, J_{CP} = 44.6 Hz, CH), 117.1 (d, J_{CP} = 82.6 Hz, C), 119.9 (d, J_{CP} = 6.1 Hz, CH), 128.6 (d, J_{CP} = 1.8 Hz, CH), 129.4 (d, J_{CP} = 0.9 Hz, CH), 130.1 (d, J_{CP} = 2.4 Hz, CH), 130.7 (d, J_{CP} = 5.3 Hz, C), 130.9 (d, J_{CP} = 12.3 Hz, CH), 132.1 (d, J_{CP} = 5.9 Hz, CH), 134.5 (d, J_{CP} = 2.9 Hz, C), 135.1 (d, J_{CP} = 9.0 Hz, CH superimposed with signal for C (can be seen in HMBC spectrum)), 135.9 (d, J_{CP} = 3.7 Hz, C), 136.0 (d, J_{CP} = 3.0 Hz, CH), 138.6 ppm (d, J_{CP} = 13.1 Hz, CH). ³¹P NMR (CD₂Cl₂, 162 MHz): δ 22.8 ppm. HRMS (ESI, positive): calcd 523.1144 (C₃₃H₂₆³⁵Cl₂P), found 523.1142; calcd 525.1114 (C₃₃H₂₆³⁵Cl³⁷ClP), found 525.1115; calcd 527.1084 (C₃₃H₂₆³⁷Cl₂P), found 527.1089.

(E)-(1,3-Diphenylallyl)triphenylphosphonium tetrafluoroborate (1e-PPh₃⁺BF₄⁻). From **1e-OH** (310 mg, 1.26 mmol): 671 mg (1.24 mmol, 98%), colorless crystals (m.p. 202.6–203.5

°C). ^1H NMR (CD_2Cl_2 , 400 MHz): δ 5.77 (dd, $^2J_{\text{HP}} = 16.3$ Hz, $^3J_{\text{HH}} = 8.7$ Hz, 1 H, $\text{ArCHCHCH}(\text{P}^+\text{Ph}_3)\text{Ar}$), 6.31–6.39 (m, 1 H, $\text{ArCHCHCH}(\text{P}^+\text{Ph}_3)\text{Ar}$), 6.88 (dd, $^3J_{\text{HH}} = 15.7$, $^4J_{\text{HP}} = 3.9$ Hz, 1 H, $\text{ArCHCHCH}(\text{P}^+\text{Ph}_3)\text{Ar}$), 7.06–7.08 (m, 2 H, H_{Ar}), 7.24–7.33 (m, 7 H, H_{Ar}), 7.39–7.49 (m, 1 H, H_{Ar}), 7.53–7.59 (m, 6 H, H_{Ar}), 7.65–7.70 (m, 6 H, H_{Ar}), 7.83–7.88 ppm (m, 3 H, H_{Ar}). ^{13}C NMR (CD_2Cl_2 , 101 MHz): δ 47.6 (d, $J_{\text{CP}} = 44.2$ Hz, CH), 117.3 (d, $J_{\text{CP}} = 82.5$ Hz, C), 119.7 (d, $J_{\text{CP}} = 6.4$ Hz, CH), 127.2 (d, $J_{\text{CP}} = 1.9$ Hz, CH), 129.3 (d, $J_{\text{CP}} = 1.0$ Hz, CH), 129.5 (d, $J_{\text{CP}} = 1.2$ Hz, CH), 130.07 (d, $J_{\text{CP}} = 3.1$ Hz, CH), 130.10 (d, $J_{\text{CP}} = 2.3$ Hz, CH), 130.7 (d, $J_{\text{CP}} = 6.1$ Hz, CH), 130.8 (d, $J_{\text{CP}} = 12.3$ Hz, CH), 131.9 (d, $J_{\text{CP}} = 5.4$ Hz, C), 135.2 (d, $J_{\text{CP}} = 8.9$ Hz, CH), 135.9 (d, $J_{\text{CP}} = 3.1$ Hz, CH), 136.0 (d, $J_{\text{CP}} = 3.1$ Hz, C), 139.5 ppm (d, $J_{\text{CP}} = 13.0$ Hz, CH). HRMS (ESI, positive) calcd 455.1923 ($\text{C}_{33}\text{H}_{28}\text{P}^+$), found 455.1924.

(E)-(1,3-Di-*p*-tolylallyl)triphenylphosphonium tetrafluoroborate (1f- $\text{PPh}_3^+\text{BF}_4^-$). From **1f-OH** (1.00 g, 4.24 mmol): 1.68 g (2.95 mmol, 69%), colorless crystals (m.p. 188.9–189.9 °C). ^1H NMR (CD_2Cl_2 , 400 MHz): δ 2.30 (s, 3 H, CH_3), 2.35 (d, $^7J_{\text{HP}} = 2.0$ Hz, 3 H, CH_3), 5.68 (dd, $^2J_{\text{HP}} = 16.2$, $^3J_{\text{HH}} = 8.6$ Hz, 1 H, $\text{ArCHCHCH}(\text{P}^+\text{Ph}_3)\text{Ar}$), 6.24–6.31 (m, 1 H, $\text{ArCHCHCH}(\text{P}^+\text{Ph}_3)\text{Ar}$), 6.79 (dd, $^3J_{\text{HH}} = 15.7$, $^4J_{\text{HP}} = 4.8$ Hz, 1 H, $\text{ArCHCHCH}(\text{P}^+\text{Ph}_3)\text{Ar}$), 6.91–6.95 (m, 2 H, H_{Ar}), 7.07–7.15 (m, 4 H, H_{Ar}), 7.15–7.19 (m, 2 H, H_{Ar}), 7.52–7.58 (m, 6 H, H_{Ar}), 7.65–7.70 (m, 6 H, H_{Ar}), 7.83–7.88 ppm (m, 3 H, H_{Ar}). ^{13}C NMR (CD_2Cl_2 , 101 MHz): δ 21.4 (d, $J_{\text{CP}} = 1.1$ Hz, CH_3), 21.5 (s, CH_3), 47.4 (d, $J_{\text{CP}} = 43.9$ Hz, CH), 117.5 (d, $J_{\text{CP}} = 82.3$ Hz, C), 118.6 (d, $J_{\text{CP}} = 6.2$ Hz, CH), 127.1 (d, $J_{\text{CP}} = 1.9$ Hz, CH), 128.7 (d, $J_{\text{CP}} = 5.4$ Hz, C), 129.9 (d, $J_{\text{CP}} = 1.0$ Hz, CH), 130.5 (d, $J_{\text{CP}} = 6.0$ Hz, CH), 130.7 (d, $J_{\text{CP}} = \text{ca. } 1.9$ Hz, CH) superimposed with 130.8 (d, $J_{\text{CP}} = 12.2$ Hz, CH), 133.1 (d, $J_{\text{CP}} = 3.0$ Hz, C), 135.2 (d, $J_{\text{CP}} = 8.8$ Hz, CH), 135.9 (d, $J_{\text{CP}} = 3.0$ Hz, CH), 139.2 (d, $J_{\text{CP}} = 13.1$ Hz, CH), 139.7 (d, $J_{\text{CP}} = 1.4$ Hz, C), 140.4 ppm (d, $J_{\text{CP}} = 3.3$ Hz, C). ^{31}P NMR (CD_2Cl_2 , 162 MHz): δ 22.1 ppm. HRMS (ESI, positive): calcd 483.2236 ($\text{C}_{35}\text{H}_{32}\text{P}^+$), found 483.2235.

General procedure for the synthesis of (E)-(1,3-diarylallyl)triphenylphosphonium triflates (1- $\text{PPh}_3^+\text{TfO}^-$). Triphenylphosphine (1 equiv) and trimethylsilyl triflate (1.2 equiv) were successively added to a dichloromethane solution of (E)-((1,3-diarylallyl)oxy)trimethylsilane (**1-OTMS**). The reaction mixture were stirred for 30 min at rt. After evaporation of the solvent, the crude products were recrystallized from a $\text{CH}_2\text{Cl}_2/\text{Et}_2\text{O}$ mixture affording (diarylallyl)triphenylphosphonium triflate.

(E)-(1,3-Bis(4-bromophenyl)allyl)triphenylphosphonium triflate (1c- $\text{PPh}_3^+\text{TfO}^-$). From **1c-OTMS** (620 mg, 1.41 mmol): 730 mg (0.957 mmol, 68%), colorless crystals (m.p. 228.8–229.9 °C). ^1H NMR (CD_2Cl_2 , 400 MHz): δ 6.19–6.28 (m, 2 H, $\text{ArCHCHCH}(\text{P}^+\text{Ph}_3)\text{Ar}$,

ArCHCHCH(P⁺Ph₃)Ar), 6.91–7.00 (m, 3 H, ArCHCHCH(P⁺Ph₃)Ar, H_{Ar}), 7.16 (d, ³J_{HH} = 8.4 Hz, 2 H, H_{Ar}), 7.42 (d, ³J_{HH} = 8.4 Hz, 4 H, H_{Ar}), 7.61–7.69 (m, 12 H, H_{Ar}), 7.82–7.87 ppm (m, 3 H, H_{Ar}). ¹³C NMR (CD₂Cl₂, 101 MHz): δ 45.9 (d, J_{CP} = 44.4 Hz, CH), 117.3 (d, J_{CP} = 82.6 Hz, C), 120.0 (d, J_{CP} = 6.2 Hz, CH), 121.6 (q, J_{CF} = 321.0 Hz, CF₃SO₃⁻), 123.4 (d, J_{CP} = 1.6 Hz, C), 124.2 (d, J_{CP} = 3.9 Hz, C), 128.9 (d, J_{CP} = 1.8 Hz, CH), 130.9 (d, J_{CP} = 12.3 Hz, CH), 131.3 (d, J_{CP} = 5.3 Hz, C), 132.4 (d, J_{CP} = 1.8 Hz, CH), 132.5 (d, J_{CP} = 3.2 Hz, CH), 133.1 (d, J_{CP} = 2.4 Hz, CH), 135.0 (d, J_{CP} = 2.9 Hz, C), 135.2 (d, J_{CP} = 9.0 Hz, CH), 136.0 (d, J_{CP} = 3.1 Hz, CH), 138.9 ppm (d, J_{CP} = 13.1 Hz, CH). ³¹P NMR (CD₂Cl₂, 162 MHz): δ 22.6 ppm. HRMS (ESI, positive) calcd 611.0133 (C₃₃H₂₆⁷⁹Br₂P⁺), found 611.0136; calcd 613.0113 (C₃₃H₂₆⁷⁹Br⁸¹BrP⁺), found 613.0113; calcd 615.0092 (C₃₃H₂₆⁸¹Br₂P⁺), found 615.0098.

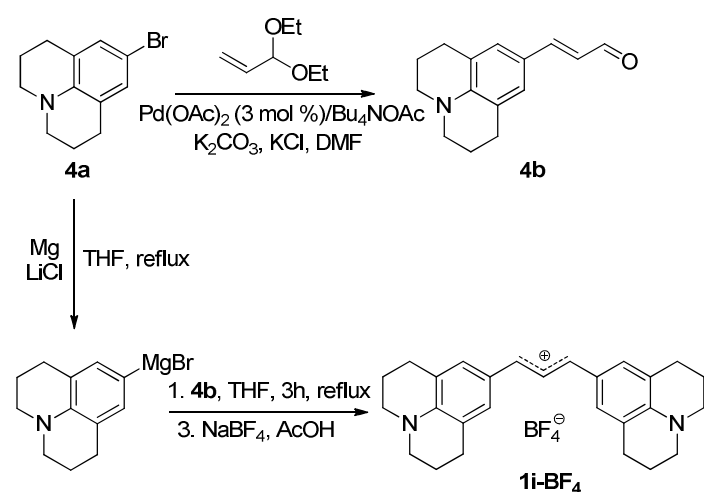
(E)-(1,3-Diphenylallyl)triphenylphosphonium triflate (1e-PPh₃⁺TfO⁻). From **1e-OTMS** (603 mg, 2.14 mmol): 1.01 g (1.66 mmol, 78%), colorless solid (m.p. 201.8–202.9 °C). ¹H NMR (CD₂Cl₂, 400 MHz): δ 5.98 (dd, ²J_{HP} = 16.4, ³J_{HH} = 8.7 Hz, 1 H, ArCHCHCH(P⁺Ph₃)Ar), 6.30–6.38 (m, 1 H, ArCHCHCH(P⁺Ph₃)Ar), 6.91 (dd, ³J_{HH} = 15.7, ⁴J_{HP} = 4.8 Hz, 1 H, ArCHCHCH(P⁺Ph₃)Ar), 7.07–7.11 (m, 2 H, H_{Ar}), 7.24–7.31 (m, 7 H, H_{Ar}), 7.38–7.42 (m, 1 H, H_{Ar}), 7.56–7.61 (m, 6 H, H_{Ar}), 7.64–7.68 (m, 6 H, H_{Ar}), 7.82–7.87 ppm (m, 3 H, H_{Ar}). ¹³C NMR (CD₂Cl₂, 101 MHz): δ 47.2 (d, J_{CP} = 43.9 Hz, CH), 117.5 (d, J_{CP} = 82.5 Hz, C), 119.7 (d, J_{CP} = 6.4 Hz, CH), 121.6 (q, J_{CF} = 321.0 Hz, CF₃SO₃⁻), 127.2 (d, J_{CP} = 1.9 Hz, CH), 129.3 (d, J_{CP} = 0.9 Hz, CH), 129.5 (d, J_{CP} = 1.2 Hz, CH), 130.0 (d, J_{CP} = 3.3 Hz, CH), 130.1 (d, J_{CP} = 2.3 Hz, CH), 130.7 (d, J_{CP} = 6.0 Hz, CH), 130.8 (d, J_{CP} = 12.2 Hz, CH), 132.1 (d, J_{CP} = 5.4 Hz, C), 135.2 (d, J_{CP} = 8.9 Hz, CH), 135.9 (d, J_{CP} = 3.0 Hz, CH), 136.0 (d, J_{CP} = 3.0 Hz, C), 139.5 ppm (d, J_{CP} = 13.0 Hz, CH). ³¹P NMR (162 MHz, CD₂Cl₂): δ 22.7 ppm. HRMS (ESI, positive) calcd 455.1923 (C₃₃H₂₈P⁺), found 455.1921

(E)-1,3-Bis(4-methoxyphenyl)allylium tetrafluoroborate (1g-BF₄). (*E*)-1,3-Bis(4-methoxyphenyl)prop-2-enone **1g-O** (5.00 g, 18.6 mmol) was dissolved in MeOH (250 mL). Sodium borohydride (ca. 1.5 g, ca. 40 mmol) was added in small portions to the resulting solution until complete disappearance of the (*E*)-1,3-bis(4-methoxyphenyl)prop-2-enone spot (TLC). Methanol was evaporated from the reaction solution and the remaining solid was dissolved in diethyl ether and slowly added to a 50% w/w HBF₄ solution in diethyl ether (40 mL, 250 mmol). The resulting suspension was stirred for 1 h at rt, and then the precipitate was filtered and washed with diethyl ether. Recrystallization from a dichloromethane/pentane mixture gave **1g-BF₄** (3.42 g, 10.1 mmol, 54%) as violet crystals. The product is water- and air-sensitive, but it can be stored for several months under glove box conditions (dry Ar atmosphere). ¹H NMR (CD₃CN, 400 MHz): δ 4.07 (s, 6 H, OMe), 7.24 (d, ³J_{HH} = 8.7 Hz, 4 H,

H_{Ar}), 8.18–8.29 (m, 5 H, H_{Ar} , $ArCHCHCH^+Ar$), 8.54 ppm (d, $^3J_{HH} = 13.5$ Hz, 2 H, $ArCHCHCH^+Ar$). ^{13}C NMR (CD_3CN , 101 MHz): δ 58.3 (CH_3), 114.5 (CH), 127.0 (CH), 130.7 (C), 141.4 (CH), 172.9 (C), 176.3 ppm (CH). HRMS (FAB, positive): calcd 253.1229 ($C_{17}H_{17}O_2^+$), found 253.1226. The 1H NMR spectrum of **1g** in 96% H_2SO_4 has previously been reported.³⁶

(E)-1,3-Bis(4-dimethylaminophenyl)allylium tetrafluoroborate (1h-BF₄) was synthesized using Brieskorn's procedure.³⁷ 4-Bromo-*N,N*-dimethylaniline (9.11 g, 45.5 mmol) was added dropwise under Ar atmosphere to lithium (1.20 g, 173 mmol) in dry diethyl ether (100 mL) at ambient temperature. After stirring for 18 h, unreacted lithium was filtered off and (*E*)-3-(4-(dimethylamino)phenyl)propenal (6.00 g, 34.2 mmol) was added dropwise to the filtrate (rt). After refluxing for 3 h, subsequent cooling to rt, and dissolving in conc. acetic acid (250 mL), the reaction mixture was added to a 20% w/w aq solution of sodium tetrafluoroborate (500 mL). A green precipitate formed which was filtered, washed with water and diethyl ether, and dried in the vacuum. Recrystallization from dichloromethane/pentane afforded **1h-BF₄** (7.04 g, 19.2 mmol, 56%) of as a green powder with metallic gloss (m.p. 177–178°C, decomp). In order to obtain crystals suitable for X-ray diffraction analysis, **1h-BF₄** was recrystallized from acetonitrile. 1H NMR (CD_3CN , 400 MHz): δ 3.22 (s, 12 H, 2 \times NMe_2), 6.79–6.95 (m, 4 H, H_{Ar}), 7.65–7.86 ppm (m, 7 H). ^{13}C NMR (CD_3CN , 101 MHz): δ 41.4 (CH_3), 115.0 (CH), 121.2 (CH), 126.2 (C), 137.3 (weak broad peak which becomes sharper at 50°C, CH), 157.7 (C), 161.5 ppm (CH). HRMS (ESI, positive): calcd 279.1856 ($C_{19}H_{23}N_2^+$), found 279.1855.

(E)-1,3-Bis(julolidin-9-yl)allylium tetrafluoroborate (1i-BF₄) was synthesized according to the following scheme:



9-Bromo-1,2,3,5,6,7-hexahydropyrido[3,2,1-ij]quinoline (4a). Julolidine (19.1 g, 110 mmol) was mixed with bromine (5.65 mL, 17.6 g, 110 mmol) in dichloromethane.³⁸ Workup

as described in ref 38 afforded **4a** (22.3 g, 88.3 mmol, 80%). The ^1H NMR spectrum of **4a** agreed with that described in the literature.³⁹

(E)-3-(1,2,3,5,6,7-Hexahydropyrido[3,2,1-ij]quinolin-9-yl)acrylaldehyde (4b). 9-Bromojulolidine **4a** (5.00 g, 19.8 mmol) was reacted with acrolein diethylacetal (7.74 g, 59.4 mmol) in the presence of tetrabutylammonium acetate (8.97 g, 29.7 mmol), potassium acetate (0.97 g, 9.9 mmol), potassium carbonate (4.11 g, 29.7 mmol), potassium chloride (2.96 g, 39.7 mmol), and palladium acetate (133 mg, 0.595 mmol) following a procedure as described in ref 40. The reaction progress was monitored by TLC. After workup, the crude product was purified by column chromatography (silica gel, hexane/EtOAc/ NEt_3 = 91/7/2) affording **4b** (870 mg, 3.82 mmol, 19%). The ^1H NMR spectrum of **4b** was in accord with the one described in ref 41.

(E)-1,3-Bis(julolidin-9-yl)allylium tetrafluoroborate (1i-BF₄). Magnesium (145 mg, 5.95 mmol) and lithium chloride (315 mg, 7.44 mmol) were slurried in THF (5 mL). Then DIBAL-H (1 M solution in hexane, 220 μL , 0.223 mmol) was added to the resulting mixture followed by dropwise addition of freshly sublimated (160 °C, 5×10^{-3} mbar) **4a** (1.87 g, 7.44 mmol). After completion of addition, the resulting mixture was kept gently boiling until GC-MS analysis (analogous to the method described in reference 28b) showed complete conversion of **4a**. A solution of **4b** (780 mg, 3.43 mmol) in THF was added dropwise to the reaction solution and the resulting mixture was refluxed for 3 h. After dissolving in conc. acetic acid (60 mL), the reaction mixture was poured into a 20% w/w aq. solution of sodium tetrafluoroborate (120 mL). A green precipitate formed which was filtered, washed with water and diethyl ether, and dried in the vacuum to yield **1i-BF₄** (0.95 g, 2.0 mmol, 59%) of as dark green powder (m.p. 151.6–152.5 °C, decomp). ^1H NMR (nitrobenzene- d_5 , 400 MHz, 100 °C): δ 1.96–2.02 (m, 8 H, $\text{NCH}_2\text{CH}_2\text{CH}_2$), 2.73–2.79 (m, 8 H, $\text{NCH}_2\text{CH}_2\text{CH}_2$), 3.49–3.55 (m, 8 H, $\text{NCH}_2\text{CH}_2\text{CH}_2$), 7.31 (s, 4 H, H_{Ar}), 7.43 (d, $^3J_{\text{HH}} = 13.3$ Hz, 2 H, $\text{ArCHCHCH}^+\text{Ar}$), 7.67 ppm (t, $^3J_{\text{HH}} = 13.3$ Hz, 1 H, $\text{ArCHCHCH}^+\text{Ar}$). ^{13}C NMR (nitrobenzene- d_5 , 101 MHz, 100 °C): δ 20.6 (CH_2), 26.9 (CH_2), 51.0 (CH_2), 119.0 (CH), 123.5 (C), 125.1 (C), 132.5 (CH), 151.1 (C), 156.5 ppm (CH). HRMS (ESI, positive): calcd 383.2482 ($\text{C}_{27}\text{H}_{31}\text{N}_2^+$), found 383.2479.

4.3 Product Studies

Reaction of 1,3-diphenylallyl cation (1e) with 2,3-dimethylbut-2-ene (2a). Zinc chloride (300 mg, 1.84 mmol), tetrabutylammonium chloride (608 mg, 2.19 mmol), diethyl ether (0.30 mL) and **2a** (402 mg, 4.78 mmol) were dissolved in dichloromethane (5 mL) and cooled to -78 °C. Then **1e-Cl** (500 mg, 2.18 mmol) in dichloromethane (4 mL) was added dropwise.

The reaction solution was stirred at $-78\text{ }^{\circ}\text{C}$ for 2 h and then kept in a $-60\text{ }^{\circ}\text{C}$ fridge for another 12 h. The resulting mixture was quenched with 2 M aqueous ammonia. Diethyl ether was added to the organic phase followed by washing with water, brine, drying (MgSO_4) and evaporation of the solvents in the vacuum. The crude mixture (534 mg) contained (*E*)-5-chloro-4,4,5-trimethyl-1,3-diphenylhex-1-ene (*E*)-5-chloro-4,4,5-trimethyl-1,3-diphenylhex-1-ene (**3a**) (ca. 350 mg, ca. 1.1 mmol, $\approx 50\%$), (*E*)-4,4,5-trimethyl-1,3-diphenylhexa-1,5-diene (**3a'**) (ca. 85 mg, ca. 0.3 mmol, $\approx 14\%$) and $< 20\%$ of other products (all ratios are based on the ^1H NMR spectrum of the crude mixture). A portion of the crude product (298 mg) was purified by column chromatography (silica gel, pentane/EtOAc = 99.3/0.7) affording **3a'** (116 mg, 0.418 mmol). Assuming the same column efficiency for the purification of the whole amount of the crude product one would expect 35% (210 mg, 0.758 mmol) overall yield of **3a'**.

The reaction under identical conditions but without Bu_4NCl afforded a complicated product mixture, which could not be resolved by using column chromatography or distillation.

3a: ^1H NMR (CDCl_3 , 599 MHz): δ 1.02, 1.28 (2 s, $2 \times 3\text{ H}$, $2 \times \text{CH}_3$), 1.64, 1.66 (2 s, $2 \times 3\text{ H}$, $2 \times \text{CH}_3$), 3.87 (d, $^3J_{\text{HH}} = 10.2\text{ Hz}$, 1 H, $\text{PhCHCHCH}(\text{R})\text{Ph}$), 6.36 (d, $^3J_{\text{HH}} = 15.7\text{ Hz}$, 1 H, $\text{PhCHCHCH}(\text{R})\text{Ph}$), 6.71 (dd, $^3J_{\text{HH}} = 15.7, 10.2\text{ Hz}$, 1 H, $\text{PhCHCHCH}(\text{R})\text{Ph}$), 7.16–7.20 (m, 2 H, H_{Ar}), 7.23–7.31 (m, 6 H, H_{Ar}), 7.31–7.34 ppm (m, 2 H, H_{Ar}). ^{13}C NMR (CDCl_3 , 151 MHz): δ 20.9 (CH_3), 23.7 (CH_3), 30.0 (CH_3), 30.2 (CH_3), 45.7 (C), 55.8 (CH), 80.6 (br. s, C), 126.1 (CH), 126.2 (CH), 127.1 (CH), 128.1 (CH), 128.5 (CH), 129.5 (CH), 130.6 (CH), 132.3 (CH), 137.7 (C), 143.9 ppm (C). ^1H and ^{13}C NMR spectra for **3a** were obtained by comparing the spectra of the crude mixture and those of isolated **3a'**. HRMS of the crude mixture (EI, positive): calcd. 312.1639 ($\text{C}_{21}\text{H}_{25}^{35}\text{Cl}$, **3a**), found 312.1631; calcd 276.1873 ($\text{C}_{21}\text{H}_{24}$, **3a'**), found 276.1877.

3a': ^1H NMR (CDCl_3 , 400 MHz): δ 1.01, 1.11 (2 s, $2 \times 3\text{ H}$, $2 \times \text{CH}_3$), 1.77–1.78 (m, 3 H, CH_3), 3.52 (d, $^3J_{\text{HH}} = 9.0\text{ Hz}$, 1 H, $\text{PhCHCHCH}(\text{R})\text{Ph}$), 4.69–4.74 (m, 1 H, $\text{RR}'\text{C}=\text{CH}_2$), 4.77–4.82 (m, 1 H, $\text{RR}'\text{C}=\text{CH}_2$), 6.35 (d, $^3J_{\text{HH}} = 15.7\text{ Hz}$, 1 H, $\text{PhCHCHCH}(\text{R})\text{Ph}$), 6.57 (dd, $^3J_{\text{HH}} = 15.7, 9.0\text{ Hz}$, 1H, $\text{PhCHCHCH}(\text{R})\text{Ph}$), 7.16–7.23 (m, 4 H, H_{Ar}), 7.24–7.29 (m, 4 H, H_{Ar}), 7.32–7.34 ppm (m, 2 H, H_{Ar}). ^{13}C NMR (CDCl_3 , 101 MHz): δ 20.1 (CH_3), 24.1 (CH_3), 25.7 (CH_3), 42.8 (C), 56.2 (CH), 111.3 (CH_2), 126.1 ($2 \times \text{CH}$, superimposed), 127.0 (CH), 127.6 (CH), 128.4 (CH), 129.7 (CH), 130.7 (CH), 131.2 (CH), 137.9 (C), 142.1 (C), 151.2 ppm (C). HRMS (EI, positive): calcd 276.1873 ($\text{C}_{21}\text{H}_{24}$), found 276.1872.

(E)-5-Chloro-5,6-dimethyl-1,3-diphenylhept-1-ene (3b). Zinc chloride (300 mg, 1.84 mmol), tetrabutylammonium chloride (555 mg, 1.99 mmol), diethyl ether (0.30 mL) and 2,3-

dimethylbut-1-ene (**2b**) (370 mg, 4.40 mmol) were dissolved in dichloromethane (5 mL). The mixture was cooled to $-78\text{ }^{\circ}\text{C}$ followed by dropwise addition of **1e-Cl** (455 mg, 1.99 mmol) in dichloromethane (4 mL). After stirring for 30 min, the reaction was quenched with 2 M aq NH_3 . Diethyl ether was added to the organic phase followed by washing with water and brine, drying (MgSO_4), and evaporation of the solvents in the vacuum to afford **3b** (481 mg) as a mixture of two diastereomers (dr ca. 1.4:1) in ca. 70% purity (^1H NMR). Due to the presence of impurities in the crude product the yield could only be estimated to be $\approx 50\%$. ^1H NMR (CDCl_3 , 300 MHz): δ 0.96 (d, $^3J_{\text{HH}} = 6.69$ Hz, 1.29 H, $\text{CH}(\text{CH}_3)_2$), 1.03 (d, $^3J_{\text{HH}} = 6.73$ Hz, 3.42 H, $\text{CH}(\text{CH}_3)_2$), 1.08 (d, $^3J_{\text{HH}} = 6.69$ Hz, 1.29 H, $\text{CH}(\text{CH}_3)_2$), 1.40 (s, 1.71 H, CH_3), 1.48 (s, 1.29 H, CH_3), 1.94–2.10 (m, 1 H, $\text{CH}(\text{CH}_3)_2$), 2.28–2.48 (m, 2 H, CH_2), 3.83–3.92 (m, 1 H, $\text{ArCHCHCH}(\text{R})\text{Ar}$), 6.28–6.47 (m, 2 H, $\text{ArCHCHCH}(\text{R})\text{Ar}$), 7.15–7.38 ppm (m, 10 H, H_{Ar}). ^{13}C NMR (CDCl_3 , 75.5 MHz): δ 18.07 (CH_3), 18.12 (CH_3), 18.16 (CH_3), 18.23 (CH_3), 27.7 (CH_3), 38.8 (CH), 39.2 (CH), 45.9 (CH), 46.2 (CH), 47.7 (CH_2), 48.2 (CH_2), 79.3 (C), 79.5 (C), 126.1 (CH), 126.3 (CH), 126.4 (CH), 127.09 (CH), 127.14 (CH), 127.6 (CH), 127.7 (CH), 128.4 (CH), 128.5 (CH), 128.69 (CH), 128.71 (CH), 129.1 (CH), 129.5 (CH), 134.9 (CH), 135.1 (CH), 137.4 (C), 145.1 (C), 145.4 ppm (C). HRMS (EI, positive): calcd. 312.1639 ($\text{C}_{21}\text{H}_{25}^{35}\text{Cl}$), found 312.1635.

(E)-5-Chloro-5-methyl-1,3-diphenyloct-1-ene (3c). According to procedure described in ref 42, **1e-Cl** (1.25 g, 5.45 mmol) was dissolved in dichloromethane (8 mL). This solution was added dropwise to a mixture of 2-methylpent-1-ene (**2c**) (0.671 g, 7.96 mmol), zinc chloride (300 mg, 1.84 mmol), diethyl ether (0.3 mL), and dichloromethane (10 mL) at $-78\text{ }^{\circ}\text{C}$. After stirring for 30 min, the solution was allowed to warm up and quenched with 2 M aq NH_3 . The organic phase was separated, washed with water and brine, and dried (MgSO_4). Evaporation of solvents in the vacuum afforded **3c** (1.29 g) as a mixture of two diastereomers (dr ca. 1.4:1) of ca. 70% purity (^1H NMR). Due to the presence of impurities in the crude product the yield could only be estimated to be $\approx 50\%$. ^1H NMR (CDCl_3 , 599 MHz): δ 0.84 (t, $^3J_{\text{HH}} = 7.4$ Hz, 1.74 H, $\text{CH}_2\text{CH}_2\text{CH}_3$), 0.87 (t, $^3J_{\text{HH}} = 7.3$ Hz, 1.26 H, $\text{CH}_2\text{CH}_2\text{CH}_3$), 1.34–1.52 (m, 2 H, $\text{CH}_2\text{CH}_2\text{CH}_3$), 1.45 (s, 1.26 H, CH_3), 1.53 (s, 1.74 H, CH_3), 1.65–1.82 (m, 2 H, $\text{CH}_2\text{CH}_2\text{CH}_3$), 2.31–2.44 (m, 2 H, CH_2), 3.78–3.93 (m, 1 H, $\text{PhCHCHCH}(\text{R})\text{Ph}$), 6.35–6.41 (m, 2 H, $\text{PhCHCHCH}(\text{R})\text{Ph}$), 7.16–7.39 ppm (m, 10 H, H_{Ar}). ^{13}C NMR (CDCl_3 , 151 MHz): δ 14.07 (CH_3), 14.10 (CH_3), 18.1 (CH_2), 30.6 (CH_3), 30.8 (CH_3), 46.15 (CH), 46.21 (CH), 46.7 (CH_2), 47.1 (CH_2), 49.5 (CH_2), 49.7 (CH_2), 75.0 (C), 75.1 (C), 126.1 (CH), 126.34 (CH), 126.36 (CH), 127.11 (CH), 127.14 (CH), 127.66 (CH), 127.67 (CH), 128.40 (CH), 128.42 (CH), 128.67 (CH), 128.70 (CH), 129.3 (CH), 129.5 (CH), 134.75 (CH), 134.81 (CH),

137.4 (C), 137.5 (C), 145.0 (C), 145.1 ppm (C). HRMS (EI, positive): calcd 312.1639 (C₂₁H₂₅³⁵Cl), found 312.1638. The Tables SX1 and SX2 of the Supplementary Section (p 90) compare the ¹H and ¹³C resonances found for **3c** with those of the structurally related **3b**.

(E)-1,3-Diphenylhexa-1,5-diene (3d). The allylium ion precursor **1e-Cl** (315 mg, 1.38 mmol) was dissolved in dichloromethane (5 mL). This solution was added dropwise to a mixture of allyltriphenylsilane (**2d**) (436 mg, 1.45 mmol), zinc chloride (100 mg, 0.612 mmol), diethyl ether (0.1 mL) and dichloromethane (7 mL) at -78°C. After stirring for 30 min, the solution was allowed to warm up and quenched with 2 M aq NH₃. The organic phase of the resulting mixture was separated, washed with water and brine, and dried (MgSO₄) followed by evaporation of solvents. The residue was dissolved in pentane and filtered through a paper filter. The filtrate was freed from the solvent and purified by column chromatography (silica gel, pentane/EtOAc = 98.4/1.6) affording **3d** (171 mg, 0.729 mmol, 53%) as a colorless oil. The ¹H and ¹³C NMR spectra of **3d** agreed with those described in ref 16. HRMS (EI, positive): calcd 234.1403 (C₁₈H₁₈), found 234.1418. Anal. Calcd for C₁₈H₁₈: C, 92.26; H, 7.74, found C, 92.10; H, 7.97.

Formation of 3e from 1g-BF₄ and 2g. Allyltriphenylstannane (**2g**) (385 mg, 0.985 mmol) was added successively to a dichloromethane solution of **1g-BF₄** (196 mg, 0.577 mmol) at room temperature. After stirring for 30 min, the reaction mixture was hydrolyzed using 1 M aq NH₃ and then extracted with dichloromethane (2 ×). The combined organic phases were washed with water, dried (MgSO₄) and freed from solvents in the vacuum to yield the crude product (164 mg) for which ¹H and ¹³C NMR spectra showed signals of **3e** and some impurities.

(E)-1,3-Bis(4-methoxyphenyl)-5-methylhexa-1,5-diene (3f). (2-Methylallyl)-trimethylsilane (**2f**) (168 mg, 1.31 mmol) was added to a solution of **1g-BF₄** (223 mg, 0.656 mmol) in dichloromethane (10 mL) at ambient temperature. After fading of the violet color, the reaction mixture was filtered through a short column filled with alumina, and the solvent was evaporated in the vacuum to yield **3f** (190 mg, 0.616 mmol, 93%) as a colorless oil. ¹H NMR (CDCl₃, 300 MHz): δ 1.72 (s, 3 H, CH₃), 2.50 (d, ³J_{HH} = 7.7 Hz, 2 H, CH₂), 3.60 (td, ³J_{HH} = 7.7, 6.8 Hz, 1 H, ArCHCHCH(R)Ar), 3.79, 3.80 (2 s, 2 × 3 H, 2 × OCH₃), 4.67–4.68, 4.73–4.74 (2 m, 2 × 1 H, C=CH₂), 6.18 (dd, ³J_{HH} = 15.8, 6.8 Hz, 1 H, ArCHCHCH(R)Ar), 6.28 (d, ³J_{HH} = 15.9 Hz, 1 H, ArCHCHCH(R)Ar), 6.79–6.83 (m, 2 H, H_{Ar}), 6.85–6.88 (m, 2 H, H_{Ar}), 7.15–7.19 (m, 2 H, H_{Ar}), 7.23–7.28 ppm (m, 2 H, H_{Ar}). ¹³C NMR (CDCl₃, 75.5 MHz): δ 22.5 (CH₃), 44.5 (CH₂), 46.1 (CH), 55.2 (CH₃), 55.3 (CH₃), 112.4 (CH₂), 113.8 (CH), 113.9 (CH),

127.2 (CH), 128.5 (CH), 128.6 (CH), 130.4 (C), 132.1 (CH), 136.4 (C), 143.5 (C), 158.0 (C), 158.8 ppm (C). HRMS (EI, positive): calcd 308.1771 (C₂₁H₂₄O₂), found 308.1762.

(E)-2-(1,3-Bis(4-methoxyphenyl)allyl)cyclohexanone (3h). 1-(Trimethylsilyloxy)cyclohexene (**2h**) (1.00 mL, 204 mg, 1.92 mmol) was added to a stirred solution of **1g**-BF₄ (204 mg, 0.600 mmol) in dichloromethane (10 mL) at -78 °C. After the solution had changed the color from intensive violet to red, the mixture was allowed to warm up, filtered through aluminum oxide using dichloromethane as solvent, and freed from solvents in the vacuum. The crude mixture contained mainly **3h** as mixture of diastereomers (dr 1.3:1, based on ¹H NMR). Purification of the crude product by column chromatography (silica gel, pentane/EtOAc = 85/15) afforded **3h** in three fractions (overall yield of isolated **3h**: 24%).

First diastereomer of 3h: colorless oil, 20.4 mg (58.2 μmol, 10%). ¹H NMR (CDCl₃, 599 MHz): δ 1.37–1.43 (m, 1 H, CH₂), 1.57–1.64 (m, 1 H, CH₂), 1.73–1.86 (m, 3 H, CH₂), 1.90–1.98 (m, 1 H, CH₂), 2.33–2.38 (m, 1 H, CH₂), 2.42–2.46 (m, 1 H, CH₂), 2.79–2.83 (m, 1 H, CH), 3.77 (s, 3 H, OCH₃), 3.79 (s, 3 H, OCH₃), 3.80–3.81 (m, 1 H, ArCHCHCH(R)Ar), 6.25 (d, ³J_{HH} = 15.9 Hz, 1 H, ArCHCHCH(R)Ar), 6.29 (dd, ³J_{HH} = 15.9, 6.5 Hz, 1 H, ArCHCHCH(R)Ar), 6.78–6.80 (m, 2 H, H_{Ar}), 6.85–6.87 (m, 2 H, H_{Ar}), 7.14–7.17 (m, 2 H, H_{Ar}), 7.22–7.25 ppm (m, 2 H, H_{Ar}). ¹³C NMR (CDCl₃, 151 MHz): δ 23.8 (CH₂), 28.5 (CH₂), 32.0 (CH₂), 42.1 (CH₂), 47.4 (CH), 55.21 (CH₃), 55.24 (CH₃), 56.1 (CH), 113.8 (CH), 113.9 (CH), 127.3 (CH), 129.4 (CH), 129.5 (CH), 130.0 (CH), 130.2 (C), 134.1 (C), 158.1 (C), 158.8 (C), 212.7 ppm (C). HRMS (EI, positive): calcd 350.1876 (C₂₃H₂₆O₃), found 350.1864.

Second diastereomer of 3h: colorless oil, 16.0 mg (45.7 μmol, 8%). ¹H NMR (CDCl₃, 599 MHz): δ 1.62–1.70 (m, 2 H, CH₂), 1.70–1.80 (m, 1 H, CH₂), 1.88–1.94 (m, 1 H, CH₂), 1.95–2.01 (m, 1 H, CH₂), 2.14–2.18 (m, 1 H, CH₂), 2.24–2.29 (m, 1 H, CH₂), 2.35–2.39 (m, 1 H, CH₂), 2.81–2.85 (m, 1 H, CH), 3.77 (s, 3 H, OCH₃), 3.79 (s, 3 H, OCH₃), 3.90 (dd, ³J_{HH} = 8.9, 8.9 Hz, 1 H, ArCHCHCH(R)Ar), 6.09 (dd, ³J_{HH} = 15.7, 9.3 Hz, 1 H, ArCHCHCH(R)Ar), 6.37 (d, ³J_{HH} = 15.7 Hz, 1 H, ArCHCHCH(R)Ar), 6.80–6.84 (m, 4 H, H_{Ar}), 7.18–7.20 (m, 2 H, H_{Ar}), 7.25–7.28 ppm (m, 2 H, H_{Ar}). ¹³C NMR (CDCl₃, 151 MHz): δ 24.3 (CH₂), 28.4 (CH₂), 31.8 (CH₂), 42.3 (CH₂), 47.6 (CH), 55.2 (CH₃), 55.3 (CH₃), 55.9 (CH), 113.85 (CH), 113.87 (CH), 127.3 (CH), 128.8 (CH), 129.1 (CH), 130.1 (C), 130.3 (CH), 135.4 (C), 157.9 (C), 158.9 (C), 212.0 ppm (C). HRMS (EI, positive): calcd 350.1876 (C₂₃H₂₆O₃), found 350.1873.

Mixture of first and second diastereomer of 3h: colorless oil (12.8 mg, 36.5 μmol, 6%). ¹H and ¹³C NMR spectra are superpositions of the corresponding spectra of both separately characterized diastereomers.

(E)-2-(1,3-Bis(4-methoxyphenyl)allyl)cyclopentanone (3i) was prepared analogous to **3h** from **1g**-BF₄ (250 mg, 0.735 mmol) and 1-(trimethylsiloxy)cyclopentene (**2i**, 264 mg, 1.69 mmol) as a mixture of diastereomers (dr 1:1.9, based on ¹H NMR of the crude product). After column chromatography (silica gel, pentane/EtOAc = 85/15) three fractions were obtained (overall yield of isolated **3i**: 94%).

First diastereomer of 3i: colorless oil, 28.9 mg (0.0859 mmol, 11%). ¹H NMR (CDCl₃, 599 MHz): δ 1.60–1.68 (m, 1 H, CH₂), 1.69–1.73 (m, 1 H, CH₂), 1.76–1.82 (m, 1 H, CH₂), 1.86–1.92 (m, 1 H, CH₂), 2.08–2.13 (m, 1 H, CH₂), 2.22–2.27 (m, 1 H, CH₂), 2.59–2.63 (m, 1 H, CH), 3.78 (s, 3 H, OCH₃), 3.80 (s, 3 H, OCH₃), 4.00–4.02 (m, 1 H, ArCHCHCH(R)Ar), 6.36 (d, ³J_{HH} = 16.0 Hz, 1 H, ArCHCHCH(R)Ar), 6.43 (dd, ³J_{HH} = 16.0, 6.9 Hz, 1 H, ArCHCHCH(R)Ar), 6.82–6.85 (m, 4 H, H_{Ar}), 7.12–7.15 (m, 2 H, H_{Ar}), 7.29–7.31 ppm (m, 2 H, H_{Ar}). ¹³C NMR (CDCl₃, 151 MHz): δ 20.5 (CH₂), 26.3 (CH₂), 38.8 (CH₂), 46.7 (CH), 53.8 (CH), 55.2 (CH₃), 55.3 (CH₃), 113.6 (CH), 113.9 (CH), 127.3 (CH), 129.53 (CH), 129.54 (CH), 129.9 (CH), 130.2 (C), 133.5 (C), 158.2 (C), 158.9 (C), 219.6 ppm (C). HRMS (EI, positive): calcd 336.1720 (C₂₂H₂₄O₃), found 336.1719.

Second diastereomer of 3i: colorless oil, 4.2 mg (0.012 mmol, 2%). ¹H NMR (CDCl₃, 599 MHz): δ 1.71–1.76 (m, 1 H, CH₂), 1.91–2.06 (m, 3 H, CH₂), 2.16–2.23 (m, 1 H, CH₂), 2.28–2.33 (m, 1 H, CH₂), 2.53–2.57 (m, 1 H, CH), 3.79 (s, 3 H, OCH₃), 3.80 (s, 3 H, OCH₃), 4.03 (dd, ³J_{HH} = 8.4, 4.1 Hz, 1 H, ArCHCHCH(R)Ar), 6.23 (dd, ³J_{HH} = 15.7, 8.4 Hz, 1 H, ArCHCHCH(R)Ar), 6.33 (d, ³J_{HH} = 15.7 Hz, 1 H, ArCHCHCH(R)Ar), 6.80–6.83 (m, 2 H, H_{Ar}), 6.85–6.88 (m, 2 H, H_{Ar}), 7.20–7.24 (m, 2 H, H_{Ar}), 7.24–7.29 ppm (m, 2 H, H_{Ar}). ¹³C NMR (CDCl₃, 151 MHz): δ 20.7 (CH₂), 25.9 (CH₂), 38.9 (CH₂), 47.0 (CH), 55.0 (CH), 55.25 (CH₃), 55.29 (CH₃), 113.86 (CH), 113.91 (CH), 127.2 (CH), 127.4 (CH), 128.9 (CH), 130.1 (C), 131.4 (CH), 135.1 (C), 158.1 (C), 159.0 (C), 219.3 ppm (C). HRMS (EI, positive): calcd 336.1720 (C₂₂H₂₄O₃), found 336.1717.

Mixture of first and second diastereomer of 3i: 214 mg (0.635 mmol, 81%). ¹H and ¹³C NMR spectra are superpositions of the corresponding spectra of both separately characterized diastereomers.

Reaction between 1g-BF₄ and 1-methyl-1H-pyrrole (2m). A suspension of **1g**-BF₄ (162 mg, 0.478 mmol) in dichloromethane was added dropwise to a solution of 1-methyl-1H-pyrrole (**2m**) (578 mg, 7.13 mmol) in dichloromethane (10 mL) at –78 °C. The resulting mixture was allowed to warm up, then washed with brine and water, dried (MgSO₄), and freed from solvents in the vacuum. Based on its ¹H NMR spectrum the crude mixture (183 mg) contained (E)-2-(1,3-bis(4-methoxyphenyl)allyl)-1-methyl-1H-pyrrole (**3m**) (ca. 120 mg,

0.36 mmol, $\approx 70\%$), 2,5-bis(*E*)-1,3-bis(4-methoxyphenyl)-allyl)-1-methyl-1H-pyrrole (**3m'**) (ca. 20 mg, 0.039 mmol, $\approx 15\%$), unreacted 1-methyl-1-*H*-pyrrole (**2m**, ca. 9 mg, 0.1 mmol), and some impurities (ca. 10 % w/w).

3m: ^1H NMR (CDCl_3 , 599 MHz): δ 3.42 (s, 3 H, NCH_3), 3.81 (s, 3 H, OCH_3), 3.82 (s, 3 H, OCH_3), 4.80 (d, $^3J_{\text{HH}} = 6.9$ Hz, ArCHCHCH(R)Ar), 5.93–5.98 (m, 1 H, H_{Ar}), 6.10–6.13 (m, 1 H, H_{Ar}), 6.19 (d, $^3J_{\text{HH}} = 15.8$ Hz, 1 H, ArCHCHCH(R)Ar), 6.47 (dd, $^3J_{\text{HH}} = 15.8, 6.9$ Hz, 1 H, ArCHCHCH(R)Ar), 6.60–6.63 (m, 1 H, H_{Ar}), 6.82–6.90 (m, 4 H, H_{Ar}), 7.09–7.15 (m, 2 H, H_{Ar}), 7.28–7.34 ppm (m, 2 H, H_{Ar}). ^{13}C NMR (CDCl_3 , 151 MHz): δ 33.9 (CH_3), 45.7 (CH), 55.2 (CH_3), 55.3 (CH_3), 106.4 (CH), 107.6 (CH), 113.8 (CH), 113.9 (CH), 122.0 (CH), 127.4 (CH), 129.4 (CH), 129.6 (CH), 130.0 (CH), 130.1 (C), 134.1 (C), 134.2 (C), 158.2 (C) 158.9 ppm (C). HRMS (ESI, positive): calcd 333.1729 ($\text{C}_{22}\text{H}_{23}\text{NO}_2$), found 333.1720.

3m': ^1H NMR (CDCl_3 , 599 MHz): δ 3.61 (s, 3 H, NCH_3), 3.81, 3.82 (2 s, 2 x 6 H, 4 x OCH_3), 4.70 (d, $^3J_{\text{HH}} = 7.6$ Hz, 2 H, ArCHCHCH(R)Ar), 6.34 (s, 2 H, H_{Ar}) overlapped with 6.36 (d, $^3J_{\text{HH}} = 15.7$ Hz, 2 H, ArCHCHCH(R)Ar), 6.48 (dd, $^3J_{\text{HH}} = 15.7, 7.6$ Hz, 2 H, ArCHCHCH(R)Ar), 6.82–6.90 (m, 8 H, H_{Ar}), 7.21–7.28 (m, 4 H, H_{Ar}), 7.30–7.35 ppm (m, 4 H, H_{Ar}). ^{13}C NMR (CDCl_3 , 151 MHz): δ 36.1 (CH_3), 46.6 (CH), 55.21 (CH_3), 55.24 (CH_3), 113.6 (CH), 113.8 (CH), 119.8 (CH), 127.0 (C), 127.3 (CH), 128.8 (CH), 129.2 (CH), 130.5 (C), 131.9 (CH), 137.0 (C), 157.9 (C), 158.7 ppm (C).

(*E*)-4-(2-(1,3-Bis(4-(dimethylamino)phenyl)allyl)cyclohexylidene)morpholin-4-ium

tetrafluoroborate (3n, mixture of diastereomers). The allylium tetrafluoroborate **1h**- BF_4 (68.1 mg, 0.186 mmol) and 1-(*N*-morpholino)cyclohexene (**2n**) (32.5 mg, 0.194 mmol) were mixed in CD_2Cl_2 . The resulting solution was analyzed by NMR and HRMS. ^1H NMR (CD_2Cl_2 , 400 MHz, only characteristic resonances): δ 2.90, 2.93, 2.93, 2.94 (4 s, 12 H, 4 x NMe_2), 5.93 (dd, $^3J_{\text{HH}} = 15.7, 9.9$ Hz, 0.48 H, ArCHCHCH(R)Ar), 6.18 (dd, $^3J_{\text{HH}} = 15.6, 9.5$ Hz, 0.52 H, ArCHCHCH(R)Ar), 6.30 (d, $^3J_{\text{HH}} = 15.7$ Hz, 0.48 H, ArCHCHCH(R)Ar), 6.49 ppm (d, $^3J_{\text{HH}} = 15.6$ Hz, 0.52 H, ArCHCHCH(R)Ar). ^{13}C NMR (CD_2Cl_2 , 101 MHz, only characteristic resonances): δ 40.6, 40.7, 40.78, 40.82, (4 x CH_3 , 2 x NMe_2), 48.0, 48.9 (2 x CH, $\text{CHC}=\text{N}^+$), 50.8, 51.7 (2 x CH, ArCHCHCH(R)Ar), 124.0, 124.8 (2 x CH, ArCHCHCH(R)Ar), 131.6, 133.5 (2 x CH, ArCHCHCH(R)Ar), 195.6, 195.7 ppm (2 x C, $\text{C}=\text{N}^+$); the chemical shifts of $\text{C}=\text{N}^+$ are close to those for products of reactions between benzhydrylium ions and **2n** ($\delta = 195.1$ ppm, see ref 8a). HRMS (ESI, positive): calcd 446.3166 ($\text{C}_{29}\text{H}_{40}\text{N}_3\text{O}$), found 446.3163. Tables SX3 and SX4 of the Supplementary Section (p 91) compare the characteristic ^1H and ^{13}C resonances of compound **3n** listed above with those of the hydrolyzed product **3n'**.

(E)-2-(1,3-Bis(4-(dimethylamino)phenyl)allyl)cyclohexanone (3n'). A solution of **1h**-BF₄ (268 mg, 0.736 mmol) in dichloromethane (30 mL) was prepared. Subsequently, 1-(*N*-morpholino)-cyclohexene (**2n**) (129 mg, 0.772 mmol) and aqueous acetic acid (50 mL of a ca. 2% v/v solution) were added. The resulting mixture was stirred for 48 h at rt. The aqueous phase was separated and extracted with dichloromethane (2 ×). The combined organic phases were then dried (MgSO₄) and freed from solvents. The crude product was purified by column chromatography (silica gel, pentane/EtOAc = 3/1) affording **3n'** in three fractions:

First diastereomer of 3n': yellowish oil, 15.3 mg (0.0406 mmol, 6%). ¹H NMR (CDCl₃, 599 MHz): δ 1.43–1.50 (m, 1 H, CH₂), 1.54–1.63 (m, 1 H, CH₂), 1.70–1.80 (m, 1 H, CH₂), 1.78–1.87 (m, 2 H, CH₂), 1.87–1.95 (m, 1 H, CH₂), 2.28–2.37 (m, 1 H, CH₂), 2.40–2.49 (m, 1 H, CH₂), 2.76–2.83 (m, 1 H, CH), 2.91, 2.92 (2 s, 2 × 6 H, 2 × NMe₂), 3.77 (dd, ³J_{HH} = 9.5, 6.0 Hz, 1 H, ArCHCHCH(R)Ar), 6.16–6.26 (m, 2 H, ArCHCHCH(R)Ar), 6.60–6.65 (m, 2 H, H_{Ar}), 6.68–6.74 (m, 2 H, H_{Ar}), 7.09–7.14 (m, 2 H, H_{Ar}), 7.17–7.21 ppm (m, 2 H, H_{Ar}). ¹³C NMR (CDCl₃, 151 MHz): δ 23.4 (CH₂), 28.5 (CH₂), 31.7 (CH₂), 40.6 (CH₃), 40.7 (CH₃), 41.9 (CH₂), 47.4 (CH), 56.3 (CH), 112.5 (CH), 112.8 (CH), 126.3 (C), 127.1 (CH), 128.2 (CH), 129.0 (CH), 129.5 (CH), 130.2 (C), 149.2 (C), 149.8 (C), 213.2 ppm (C). HRMS (EI, positive): calcd 376.2509 (C₂₅H₃₂N₂O), found 376.2492.

Second diastereomer of 3n': colorless solid, 36.5 mg (0.0969 mmol, 13%). ¹H NMR (CDCl₃, 599 MHz): δ 1.59–1.69 (m, 1 H, CH₂), 1.69–1.77 (m, 1 H, CH₂), 1.77–1.86 (m, 1 H, CH₂), 1.86–2.00 (m, 2 H, CH₂), 2.09–2.17 (m, 1 H, CH₂), 2.21–2.30 (m, 1 H, CH₂), 2.35–2.43 (m, 1 H, CH₂), 2.80–2.85 (m, 1 H, CH), 2.91, 2.94 (2 s, 2 × 6 H, 2 × NMe₂), 3.88 (dd, ³J_{HH} = 9.0, 8.9 Hz, 1 H, ArCHCHCH(R)Ar), 6.03 (dd, ³J_{HH} = 15.6, 9.0 Hz, 1 H, ArCHCHCH(R)Ar), 6.35 (d, ³J_{HH} = 15.6 Hz, 1 H, ArCHCHCH(R)Ar), 6.66 (d, ³J_{HH} = 8.8 Hz, 2 H, H_{Ar}), 6.69 (d, ³J_{HH} = 8.7 Hz, 2 H, H_{Ar}), 7.16 (d, ³J_{HH} = 8.7 Hz, 2 H, H_{Ar}), 7.24 ppm (d, ³J_{HH} = 8.8 Hz, 2 H, H_{Ar}). ¹³C NMR (CDCl₃, 151 MHz): δ 23.9 (CH₂), 28.4 (CH₂), 31.5 (CH₂), 40.6 (CH₃), 40.7 (CH₃), 42.0 (CH₂), 47.5 (CH), 56.0 (CH), 112.5 (CH), 112.8 (CH), 126.2 (C), 127.0 (CH), 127.5 (CH), 128.4 (CH), 130.4 (CH), 131.4 (C), 149.0 (C), 149.8 (C), 212.5 ppm (C). HRMS (EI, positive): calcd 376.2509 (C₂₅H₃₂N₂O), found 376.2502.

Mixture of first and second diastereomer of 3n': yellowish oil, 12.4 mg (0.0239 mmol, 4%). ¹H and ¹³C NMR spectra are superpositions of the corresponding spectra of both separately characterized diastereomers.

Overall yield of **3n'**: 23%. As the ¹H NMR spectrum of the crude product (286 mg, ca. 100%) contains mainly the signals corresponding to the mixture of two diastereomers described

above, the much lower yield of isolated material can be explained by purification problems (partial decomposition of **3n'** on the column).

(E)-1-(2-(1,3-Bis(4-(dimethylamino)phenyl)allyl)cyclopentylidene)piperidin-1-ium tetrafluoroborate (3o, mixture of diastereomers). The allylium tetrafluoroborate **1h**-BF₄ (70.2 mg, 0.192 mmol) and 1-(*N*-piperidino)cyclopentene (**2o**) (30.3 mg, 0.200 mmol) were mixed in CD₂Cl₂. The resulting solution was analyzed by NMR and HRMS. ¹H NMR (CD₂Cl₂, 400 MHz, only characteristic resonances): δ 2.92, 2.93, 2.94, 2.95 (4 s, 12 H, 4 × NMe₂), 6.06 (dd, ³J_{HH} = 15.6, 9.2 Hz, 0.48 H, ArCHCHCH(R)Ar), 6.20 (dd, ³J_{HH} = 15.6, 8.9 Hz, 0.52 H, ArCHCHCH(R)Ar), 6.31 (d, ³J_{HH} = 15.6 Hz, 0.48 H, ArCHCHCH(R)Ar), 6.42 (d, ³J_{HH} = 15.6 Hz, 0.52 H, ArCHCHCH(R)Ar), 6.62–6.75 (m, 4 H, H_{Ar}), 7.06–7.11 (m, 1.04 H, H_{Ar}), 7.11–7.16 (m, 0.96 H, H_{Ar}), 7.21–7.25 (m, 0.96 H, H_{Ar}), 7.26–7.31 ppm (m, 1.04 H, H_{Ar}). ¹³C NMR (CD₂Cl₂, 101 MHz, only characteristic resonances): δ 40.61, 40.68, 40.80, 40.83 (4 × CH₃), 50.2, 51.3 (2 × CH, ArCHCHCH(R)Ar), 52.0, 52.3 (2 × CH, CHC=N⁺), 123.7, 125.4 (2 × CH, ArCHCHCH(R)Ar), 132.0, 133.3 (2 × CH, ArCHCHCH(R)Ar), 198.4, 198.7 ppm (2 × C, C=N⁺). HRMS (ESI, positive): calcd 430.3217 (C₂₉H₄₀N₃), found 430.3219. Tables SX5 and SX6 of the Supplementary Section (pp 91-92) compare the characteristic ¹H and ¹³C resonances of compound **3o** listed above with those of the hydrolyzed product **3o'**.

(E)-2-(1,3-Bis(*N,N*-dimethylaminophenyl)allyl)cyclopentanone (3o'). Analogous to **3n'**; from **1h**-BF₄ (208 mg, 0.568 mmol) and 1-(*N*-piperidino)cyclopentene (**2o**) (90.2 mg, 0.597 mmol). The crude product was purified by column chromatography (silica gel, pentane/EtOAc = 3/1) affording three fractions of **3o'** (overall yield of isolated **3o'**: 54%).

First diastereomer of 3o': colorless oil, 18.6 mg (0.0513 mmol, 9%). ¹H NMR (CDCl₃, 599 MHz): δ 1.65–1.73 (m, 2 H, CH₂), 1.73–1.80 (m, 1 H, CH₂), 1.81–1.92 (m, 1 H, CH₂), 2.07–2.17 (m, 1 H, CH₂), 2.16–2.27 (m, 1 H, CH₂), 2.56–2.66 (m, 1 H, CH), 2.91 (s, 6 H, NMe₂), 2.94 (s, 6 H, NMe₂), 3.99–4.02 (m, 1 H, ArCHCHCH(R)Ar), 6.31–6.38 (m, 2 H, ArCHCHCH(R)Ar), 6.63–6.70 (m, 4 H, H_{Ar}), 7.05–7.10 (m, 2 H, H_{Ar}), 7.23–7.28 ppm (m, 2 H, H_{Ar}). ¹³C NMR (CDCl₃, 151 MHz): δ 20.6 (CH₂), 26.2 (CH₂), 38.9 (CH₂), 40.6 (CH₃), 40.7 (CH₃), 46.6 (CH), 54.0 (CH), 112.5 (CH), 112.6 (CH), 126.3 (C), 127.1 (CH), 127.9 (CH), 129.5 (CH), 129.6 (CH), 129.7 (C), 149.2 (C), 149.8 (C), 220.2 ppm (C). HRMS (EI, positive): calcd 362.2353 (C₂₄H₃₀N₂O), found 362.2363.

Second diastereomer of 3o': colorless oil, 54.8 mg (0.151 mmol, 27%). ¹H NMR (CDCl₃, 599 MHz): δ 1.67–1.77 (m, 1 H, CH₂), 1.93–2.07 (m, 3 H, CH₂), 2.13–2.22 (m, 1 H, CH₂), 2.25–2.33 (m, 1 H, CH₂), 2.50–2.58 (m, 1 H, CH), 2.93, 2.93 (2 s, 2 × 6 H, 2 × NMe₂), 4.01 (dd,

$^3J_{\text{HH}} = 8.5, 3.8$ Hz, 1 H, ArCHCHCH(R)Ar), 6.16 (dd, $^3J_{\text{HH}} = 15.7, 8.5$ Hz, 1 H, ArCHCHCH(R)Ar), 6.31 (d, $^3J_{\text{HH}} = 15.7$ Hz, 1 H, ArCHCHCH(R)Ar), 6.62–6.69 (m, 2 H, H_{Ar}), 6.69–6.77 (m, 2 H, H_{Ar}), 7.17–7.21 (m, 2 H, H_{Ar}), 7.21–7.24 ppm (m, 2 H, H_{Ar}). ^{13}C NMR (CDCl₃, 151 MHz): δ 20.8 (CH₂), 25.7 (CH₂), 39.0 (CH₂), 40.6 (CH₃), 40.8 (CH₃), 46.9 (CH), 55.1 (CH), 112.4 (CH), 112.8 (CH), 125.5 (CH), 126.2 (C), 127.1 (CH), 128.5 (CH), 131.3 (C), 131.5 (CH), 149.2 (C), 149.9 (C), 219.9 ppm (C). HRMS (EI, positive): calcd 362.2353 (C₂₄H₃₀N₂O), found 362.2352.

Mixture of first and second diastereomer of 3o': colorless oil, 36.8 mg (0.101 mmol, 18%). ^1H and ^{13}C NMR spectra are superpositions of the corresponding spectra of both separately characterized diastereomers.

(E)-N-(1,3-Bis(4-(dimethylamino)phenyl)allyl)-2,2,2-trifluoroethylamine (3p) was obtained from **1h**-BF₄ (134 mg, 0.365 mmol), 2,2,2-trifluoroethylamine (**2p**) (75.6 mg, 0.763 mmol), and potassium carbonate (529 mg, 3.83 mmol) by using a procedure described in ref 44: yellow oil, 133 mg (0.352 mmol, 96%). ^1H NMR (CD₂Cl₂, 400 MHz): δ 1.74 (s, 1 H, NH), 2.96, 2.96 (2 s, 2 × 6 H, 2 × NMe₂), 3.29–3.14 (m, 2 H, CH₂), 4.38 (d, $^3J_{\text{HH}} = 7.7$ Hz, 1 H, ArCHCHCH(R)Ar), 6.07 (dd, $^3J_{\text{HH}} = 15.8, 7.7$ Hz, 1 H, ArCHCHCH(R)Ar), 6.51 (d, $^3J_{\text{HH}} = 15.8$ Hz, 1 H, ArCHCHCH(R)Ar), 6.65–6.73 (m, 2 H, H_{Ar}), 6.73–6.80 (m, 2 H, H_{Ar}), 7.18–7.38 ppm (m, 4 H, H_{Ar}). ^{13}C NMR (CDCl₃, 101 MHz): δ 40.8 (CH₃), 41.0 (CH₃), 48.3 (q, $^2J_{\text{CF}} = 30.9$ Hz, CH₂), 64.8 (CH), 112.8 (CH), 113.3 (CH), 125.7 (C), 126.7 (q, $^1J_{\text{CF}} = 278.5$ Hz, CF₃), 127.9 (CH), 128.2 (CH), 128.5 (CH), 130.7 (C), 131.0 (CH), 150.8 (C), 150.9 ppm (C). ^{19}F NMR (CD₂Cl₂, 376 MHz) δ -71.7 to -71.6 ppm (m). HRMS (EI, positive): calcd 377.2073 (C₂₁H₂₆F₃N₃), found 377.2074.

(E)-N-(1,3-Bis(4-(dimethylamino)phenyl)allyl)isopropylamine (3q) was obtained analogously to **3p** from isopropylamine **2q** (129 mg, 1.74 mmol) and **1h**-BF₄ (366 mg, 0.871 mmol) without use of K₂CO₃: red oily solid, 243 mg (0.721 mmol, 83%). ^1H NMR (CDCl₃, 599 MHz): δ 1.08 (d, $^3J_{\text{HH}} = 6.3$ Hz, 3 H, CH₃), 1.10 (d, $^3J_{\text{HH}} = 6.3$ Hz, 3 H, CH₃), 1.35 (br. s, 1 H, NH), 2.83 (qq, $^3J_{\text{HH}} = 6.3$ Hz, 6.3 Hz, 1 H, CH(CH₃)₂), 2.94, 2.94 (2 s, 2 × 6 H, 2 × NMe₂), 4.40 (d, $^3J_{\text{HH}} = 7.4$ Hz, 1 H, ArCHCHCH(R)Ar), 6.12 (dd, $^3J_{\text{HH}} = 15.8, 7.4$ Hz, 1 H, ArCHCHCH(R)Ar), 6.41 (d, $^3J_{\text{HH}} = 15.8$ Hz, 1 H, ArCHCHCH(R)Ar), 6.63–6.69 (m, 2 H, H_{Ar}), 6.72–6.76 (m, 2 H, H_{Ar}), 7.24–7.29 ppm (m, 4 H, H_{Ar}). ^{13}C NMR (CDCl₃, 151 MHz): δ 23.0 (CH₃), 23.4 (CH₃), 40.5 (CH₃), 40.7 (CH₃), 45.4 (CH), 61.9 (CH), 112.4 (CH), 112.7 (CH), 125.9 (C), 127.2 (CH), 127.9 (CH), 129.1 (CH), 129.6 (CH), 131.8 (C), 149.7 (C), 149.8 ppm (C). HRMS (EI, positive): calcd 337.2512 (C₂₂H₃₁N₃), found 337.2512.

(E)-N-(1,3-Bis(4-(dimethylamino)phenyl)allyl)benzylamine (3r) was obtained analogously to **3q** from benzylamine **2r** (150 mg, 1.40 mmol) and **1h**-BF₄ (251 mg, 0.685 mmol). Recrystallization of the crude product from diethyl ether/pentane afforded **3r** (201 mg, 0.522 mmol, 76%) as a pale red solid (m.p. 88.2–90.0 °C, decomp). Evaporation of the solvents from the solution which was left after recrystallization afforded additional 60 mg (0.16 mmol, 23%) of **3r** in lower quality as yellow oil. ¹H NMR (CDCl₃, 599 MHz): δ 1.83 (br. s, 1 H, NH), 2.96, 2.97 (2 s, 2 × 6 H, 2 × NMe₂), 3.81 (d, 1 H, ²J_{HH} = 14.3 Hz, CH₂), 3.84 (d, ²J_{HH} = 14.3 Hz, 1 H, CH₂), 4.33 (d, ³J_{HH} = 7.6 Hz, 1 H, ArCHCHCH(R)Ar), 6.17 (dd, ³J_{HH} = 15.7, 7.6 Hz, 1 H, ArCHCHCH(R)Ar), 6.50 (d, ³J_{HH} = 15.7 Hz, 1 H, ArCHCHCH(R)Ar), 6.68–6.71 (m, 2 H, H_{Ar}), 6.74–6.82 (m, 2 H, H_{Ar}), 7.15–7.50 ppm (m, 9 H, H_{Ar}). ¹³C NMR (CDCl₃, 151 MHz): δ 40.5 (CH₃), 40.7 (CH₃), 51.3 (CH₂), 64.1 (CH), 112.4 (CH), 112.7 (CH), 125.7 (C), 126.7 (CH), 127.2 (CH), 128.0 (CH), 128.1 (CH), 128.3 (CH), 128.8 (CH), 129.7 (CH), 131.3 (C), 140.7 (C), 149.8 (C), 149.9 ppm (C). HRMS (EI, positive): calcd 385.2513 (C₂₆H₃₁N₃), found 385.2528. Anal. Calcd for C₂₆H₃₁N₃: C, 81.00; H, 8.10; N, 10.90; found C, 80.61; H, 8.27; N, 10.65.

(E)-N-(1,3-Bis(4-(dimethylamino)phenyl)allyl)morpholine (3s) was obtained analogously to **3q** from morpholine **2s** (328 mg, 3.77 mmol) and **1h**-BF₄ (329 mg, 0.897 mmol). Pentane (10 mL) was added to the crude product, and the resulting suspension was treated with ultrasound for 30 min. Then the solid residue was filtered and dried in the vacuum affording **3s** (304 mg, 0.831 mmol, 93%) as a pale grey solid (m.p. 76.8–78.1 °C, decomp). ¹H NMR (CDCl₃, 300 MHz): δ 2.37–2.44 (m, 2 H, NCH₂), 2.53–2.60 (m, 2 H, NCH₂), 2.95 (s, 12 H, 2 × NMe₂), 3.68 (d, ³J_{HH} = 8.9 Hz, 1 H, ArCHCHCH(R)Ar), 3.72 (t, ³J_{HH} = 4.7 Hz, 4 H, CH₂O), 6.10 (dd, ³J_{HH} = 15.7, 8.9 Hz, 1 H, ArCHCHCH(R)Ar), 6.45 (d, ³J_{HH} = 15.7 Hz, 1 H, ArCHCHCH(R)Ar), 6.67 (d, ³J_{HH} = 8.8 Hz, 2 H, H_{Ar}), 6.73 (d, ³J_{HH} = 8.8 Hz, 2 H, H_{Ar}), 7.26 (d, ³J_{HH} = 8.8 Hz, 2 H, H_{Ar}), 7.27 ppm (d, ³J_{HH} = 8.8 Hz, 2 H, H_{Ar}). ¹³C NMR (CDCl₃, 75.5 MHz): δ 40.5 (CH₃), 40.7 (CH₃), 52.2 (CH₂), 67.2 (CH₂), 74.4 (CH), 112.4 (CH), 112.7 (CH), 125.7 (C), 127.2 (CH), 127.4 (CH), 128.7 (CH), 129.7 (C), 130.9 (CH), 149.8 (C), 150.0 ppm (C). Anal. Calcd for C₂₃H₃₁N₃O: C, 75.58; H, 8.55; N, 11.50; found C, 75.37; H, 8.60; N, 11.21.

(E)-9,9'-(3-(Piperidin-1-yl)prop-1-ene-1,3-diyl)bis(1,2,3,5,6,7-hexahydropyrido[3,2,1-ij]quinoline) (3t). Piperidine **2t** (12.0 mg, 0.141 mmol) was added to a stirred slurry of **1i**-BF₄ (30.6 mg, 65.1 μmol) and potassium carbonate (98.5 mg, 0.713 mmol) in acetonitrile (10 mL). After fading of the green color, the mixture was diluted with diethyl ether, washed with 2 M NaOH solution and dried (MgSO₄). Evaporation of the solvent gave the crude product

that was analyzed by NMR spectroscopy. Because of the high instability of **3t** in presence of proton sources (reaction between **1i** and piperidine is reversible) further attempts to purify **3t** were not made. ^1H NMR (CD_3CN , 400 MHz): δ 1.36–1.45 (m, 2 H, CH_2), 1.46–1.56 (m, 4 H, CH_2), 1.85–1.92 (m, 8 H, CH_2), 2.30–2.46 (m, 4 H, CH_2), 2.64–2.70 (m, 8 H, CH_2), 3.06–3.11 (m, 8 H, CH_2), 3.47 (d, $^3J_{\text{HH}} = 8.9$ Hz, 1 H, ArCHCHCH(R)Ar), 5.93 (dd, $^3J_{\text{HH}} = 15.9, 8.9$ Hz, 1 H, ArCHCHCH(R)Ar), 6.20 (d, $^3J_{\text{HH}} = 15.9$ Hz, 1 H, ArCHCHCH(R)Ar), 6.68 (s, 2 H, H_{Ar}), 6.74 ppm (s, 2 H, H_{Ar}). ^{13}C NMR (CD_3CN , 101 MHz): δ 23.0 (CH_2), 23.2 (CH_2), 25.7 (CH_2), 27.1 (CH_2), 28.4 (CH_2), 28.5 (CH_2), 50.7 (CH_2), 50.8 (CH_2), 53.4 (CH_2), 75.3 (CH), 122.4 (C), 122.5 (C), 125.75 (C), 125.81 (CH), 127.3 (CH), 128.8 (CH), 130.9 (CH), 131.3 (C), 142.9 (C), 143.4 ppm (C). Though signals of excess piperidine and some other impurities are present in the NMR spectra, these spectra still allow unambiguous identification of **3t** as the major product formed in the reaction.

5,5-Bis(*E*)-1,3-bis(4-(dimethylamino)phenyl)allyl)-2,2-dimethyl-1,3-dioxane-4,6-dione (3u'**)**

A solution of Meldrum's acid (**H-2u**) (62.4 mg, 0.432 mmol) and potassium tert-butoxide (110 mg, 0.900 mmol) in DMSO (2 mL) was added to a suspension of **1h-BF₄** (317 mg, 0.866 mmol) in DMSO at rt. The reaction mixture was stirred for 10 min followed by addition of water. The precipitate was filtered and dried in the vacuum affording **3u'** (255 mg, 0.366 mmol, 85%) as a pale green solid. ^1H NMR (CD_2Cl_2 , 400 MHz): δ 0.66 (s, 6 H, $2 \times \text{CH}_3$), 2.85 (s, 12 H, NMe_2), 2.97 (s, 12 H, NMe_2), 4.18 (d, $^3J_{\text{HH}} = 10.1$ Hz, 2 H, ArCHCHCH(R)Ar), 6.30 (d, $^3J_{\text{HH}} = 15.7$ Hz, 2 H, ArCHCHCH(R)Ar), 6.56–6.67 (m, 4 H, H_{Ar}), 6.68–6.75 (m, 4 H, H_{Ar}), 6.86 (dd, $^3J_{\text{HH}} = 15.7, 10.1$ Hz, 2 H, ArCHCHCH(R)Ar), 7.02–7.12 (m, 4 H, H_{Ar}), 7.26–7.34 ppm (m, 4 H, H_{Ar}). ^{13}C NMR (CD_2Cl_2 , 101 MHz): δ 29.0 (CH_3), 40.88 (CH_3), 40.92 (CH_3), 54.6 (CH), 65.1 (C), 106.3 (C), 112.9 (CH), 113.3 (CH), 122.3 (CH), 126.4 (C), 128.0 (CH), 128.3 (C), 130.3 (CH), 134.5 (CH), 150.8 ($2 \times \text{C}$), 168.1 ppm (C). HRMS (EI, positive): calcd 700.3983 ($\text{C}_{44}\text{H}_{52}\text{N}_4\text{O}_4$), found 700.3998.

Reaction of 1h-BF₄ with the potassium salt of Meldrum's acid (K-2u). According to ref 45, a solution of **1h-BF₄** (104 mg, 0.285 mmol) in DMSO was added dropwise to a solution of **K-2u** (253 mg, 1.39 mmol) in the same solvent at rt. After decolorization followed by addition of water, the precipitate was filtered, washed with water, and dried in the vacuum affording a mixture of (*E*)-5-(1,3-bis(4-(dimethylamino)phenyl)allyl)-2,2-dimethyl-1,3-dioxane-4,6-dione (**3u**) (29 mg, 0.069 mmol, 24%) and **3u'** (39 mg, 0.056 mmol, 39%). The yields of **3u** and **3u'** are based on the signal ratios in the ^1H NMR spectrum and the mass (68.5 mg) of the crude product mixture. **3u**: ^1H NMR (CD_2Cl_2 , 400 MHz): δ 1.51, 1.71 (2 s, 2×3 H, $2 \times \text{CH}_3$), 2.91, 2.94 (2 s, 2×6 H, $2 \times \text{NMe}_2$), 3.95 (br. s, 1 H, COCHCO), 4.55–4.57

(br. m, 1 H, ArCHCHCH(R)Ar), 6.49 (d, $^3J_{\text{HH}} = 16.1$ Hz, 1 H, ArCHCHCH(R)Ar), 6.55–6.80 (m overlapped with signals of **3u'**, 5 H, ArCHCHCH(R)Ar, H_{Ar}), 7.19–7.36 (m overlapped with signals of **3u'**, 4 H, H_{Ar}). ^{13}C NMR (CD₂Cl₂, 101 MHz): δ 28.1 (CH₃), 28.7 (CH₃), 40.8 (CH₃), 40.9 (CH₃), 47.7 (CH), 53.4 (CH), 105.7 (C), 112.8 (CH), 113.0 (CH), 124.8 (CH), 125.7 (C), 127.8 (CH), 128.4 (C), 129.5 (CH), 132.9 (CH), 150.4 (C), 150.8 (C), 165.30 (C), 165.33 ppm (C). The ^1H and ^{13}C NMR spectra of **3u** were obtained comparing the corresponding spectra of the crude mixture with those of isolated **3u'**. HRMS (EI, positive): calcd 422.2200 (C₂₅H₃₀N₂O₄), found 422.2193.

4.4. Determination of the Rate Constants

UV-vis measurements. All reactions were studied using conventional ($\tau_{1/2} > 3$ s) or stopped-flow ($\tau_{1/2} < 3$ s) UV-vis spectroscopy by following the decays of absorbances of the cations. The temperature of all solutions was kept constant during all kinetic studies by using a circulating bath thermostat. At least tenfold excess of nucleophile was used in all reactions studied, so that pseudo-first-order conditions were achieved.

Laser-flash experiments. Solutions of the corresponding triphenylphosphonium salt and nucleophile were irradiated with a 7 ns pulse from a quadrupled Nd:YAG laser (266 nm, 40–60 mJ/pulse), and a Xe lamp was used as probe light for UV-vis detection. The system was equipped with a fluorescence flow cell which allowed complete replacing of the sample volume between subsequent laser pulses. Kinetics were measured by following the decay of the cations. Averaged data obtained from ≥ 48 individual runs were used for further evaluations.

First-order rate constants (k_{obs}) were calculated by least-squares fitting of the absorbance data to a single exponential function $A_t = A_0 e^{-k_{\text{obs}}t} + C$. The second-order rate constants (k_2) were obtained using the slopes of the linear plots of k_{obs} against the nucleophile concentration ([Nu]).

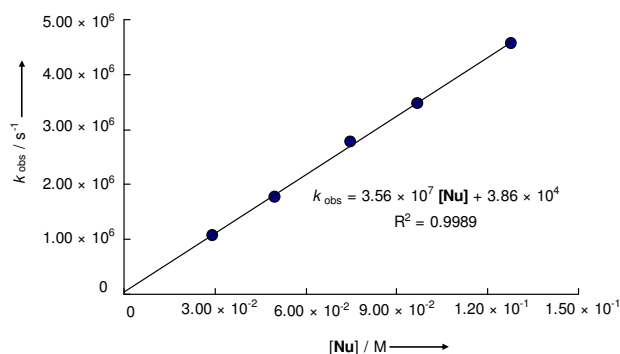
In case of the conventional and stopped-flow measurements, cations **1c–1f** were generated from the corresponding chlorides or trimethylsilyl ethers and Lewis acids. Cation **1g** was used as semi-stable (storable by glovebox conditions at -30 °C) tetrafluoroborate salt. Cations **1h** and **1i** were used as isolated stable tetrafluoroborate salts.

4.5. Kinetic Measurements

4.5.1. Reactions of (*E*)-1,3-bis(3,5-difluorophenyl)allyl cation (**1a**)

Reaction of **1a** with 2,3-dimethyl-but-2-ene (**2a**). **1a** generated from **1a**-PPh₃⁺BF₄⁻ using laser-flash photolysis, $\lambda_{\text{obs}} = 496 \text{ nm}$, CH₂Cl₂, 20 °C, [**1a**-PPh₃⁺BF₄⁻] = $5.27 \times 10^{-5} \text{ M}$.

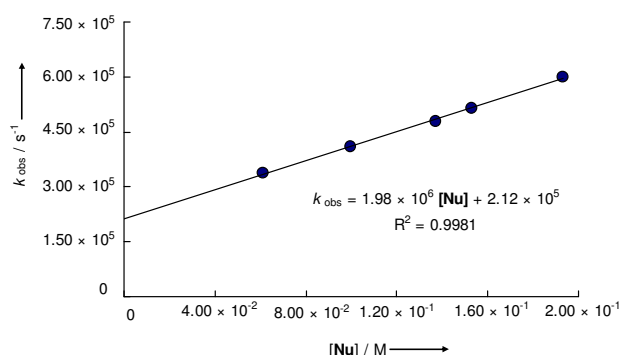
[Nu] / M	$k_{\text{obs}} / \text{s}^{-1}$
2.91×10^{-2}	1.06×10^6
4.99×10^{-2}	1.78×10^6
7.49×10^{-2}	2.78×10^6
9.70×10^{-2}	3.48×10^6
1.28×10^{-1}	4.57×10^6



$$k_2 = 3.56 \times 10^7 \text{ L mol}^{-1} \text{ s}^{-1}$$

Reaction of **1a** with 2,3-dimethylbut-1-ene (**2b**). **1a** generated from **1a**-PPh₃⁺BF₄⁻ using laser-flash photolysis, $\lambda_{\text{obs}} = 496 \text{ nm}$, CH₂Cl₂, 20 °C, [**1a**-PPh₃⁺BF₄⁻] = $5.27 \times 10^{-5} \text{ M}$.

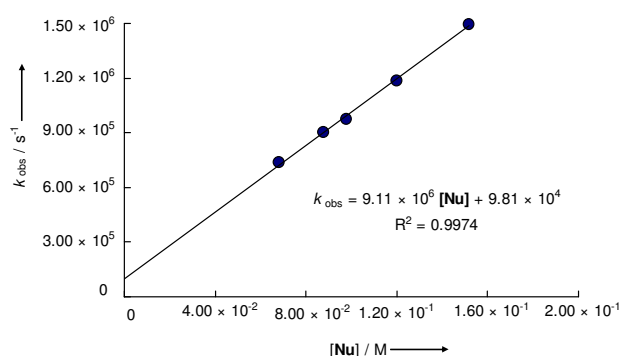
[Nu] / M	$k_{\text{obs}} / \text{s}^{-1}$
6.10×10^{-2}	3.37×10^5
9.96×10^{-2}	4.08×10^5
1.37×10^{-1}	4.78×10^5
1.53×10^{-1}	5.13×10^5
1.93×10^{-1}	6.00×10^5



$$k_2 = 1.98 \times 10^6 \text{ L mol}^{-1} \text{ s}^{-1}$$

Reaction of **1a** with 2-methylpent-1-ene (**2c**). **1a** generated from **1a**-PPh₃⁺BF₄⁻ using laser-flash photolysis, $\lambda_{\text{obs}} = 496 \text{ nm}$, CH₂Cl₂, 20 °C, [**1a**-PPh₃⁺BF₄⁻] = $5.27 \times 10^{-5} \text{ M}$.

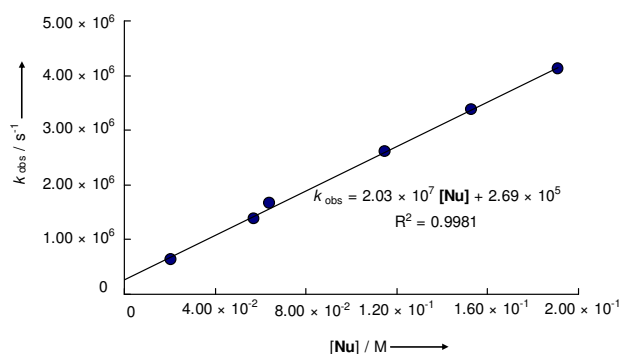
[Nu] / M	$k_{\text{obs}} / \text{s}^{-1}$
6.83×10^{-2}	7.37×10^5
8.80×10^{-2}	9.00×10^5
9.80×10^{-2}	9.72×10^5
1.20×10^{-1}	1.18×10^6
1.52×10^{-1}	1.50×10^6



$$k_2 = 9.11 \times 10^6 \text{ L mol}^{-1} \text{ s}^{-1}$$

Reaction of **1a** with allyltrimethylsilane (**2e**). **1a** generated from **1a**-PPh₃⁺BF₄⁻ using laser-flash photolysis, $\lambda_{\text{obs}} = 496 \text{ nm}$, CH₂Cl₂, 20 °C, [**1a**-PPh₃⁺BF₄⁻] = $5.27 \times 10^{-5} \text{ M}$.

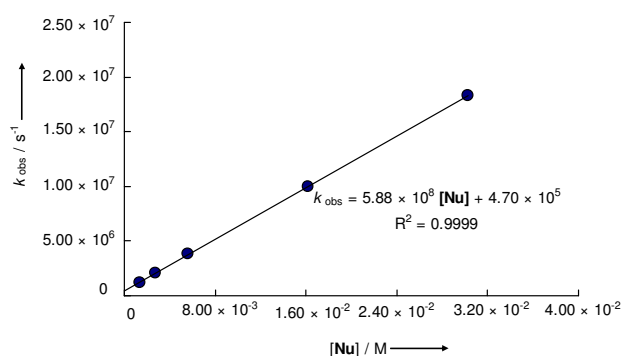
[Nu] / M	$k_{\text{obs}} / \text{s}^{-1}$
2.07×10^{-2}	6.44×10^5
5.70×10^{-2}	1.38×10^6
6.41×10^{-2}	1.67×10^6
1.15×10^{-1}	2.61×10^6
1.53×10^{-1}	3.38×10^6
1.91×10^{-1}	4.11×10^6



$$k_2 = 2.03 \times 10^7 \text{ L mol}^{-1} \text{ s}^{-1}$$

Reaction of **1a** with trimethyl(2-methylallyl)silane (**2f**). **1a** generated from **1a**-PPh₃⁺BF₄⁻ using laser-flash photolysis, $\lambda_{\text{obs}} = 496 \text{ nm}$, CH₂Cl₂, 20 °C, [**1a**-PPh₃⁺BF₄⁻] = $5.27 \times 10^{-5} \text{ M}$.

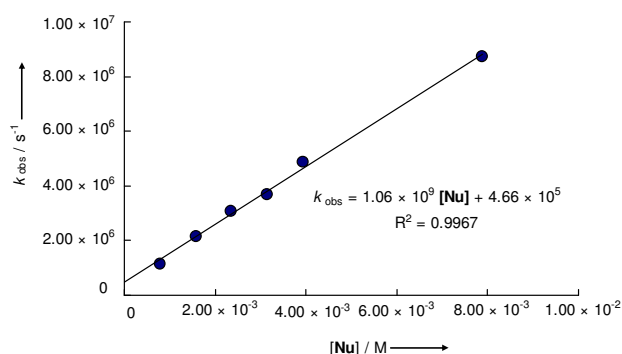
[Nu] / M	$k_{\text{obs}} / \text{s}^{-1}$
1.39×10^{-3}	1.25×10^6
2.78×10^{-3}	2.06×10^6
5.56×10^{-3}	3.83×10^6
1.62×10^{-2}	9.99×10^6
3.03×10^{-2}	1.83×10^7



$$k_2 = 5.88 \times 10^8 \text{ L mol}^{-1} \text{ s}^{-1}$$

Reaction of **1a** with 1-(trimethylsiloxy)cyclohexene (**2h**). **1a** generated from **1a**-PPh₃⁺BF₄⁻ using laser-flash photolysis, $\lambda_{\text{obs}} = 496 \text{ nm}$, CH₂Cl₂, 20 °C, [**1a**-PPh₃⁺BF₄⁻] = $5.27 \times 10^{-5} \text{ M}$.

[Nu] / M	$k_{\text{obs}} / \text{s}^{-1}$
7.87×10^{-4}	1.16×10^6
1.58×10^{-3}	2.14×10^6
2.36×10^{-3}	3.09×10^6
3.15×10^{-3}	3.67×10^6
3.94×10^{-3}	4.87×10^6
7.88×10^{-3}	8.71×10^6

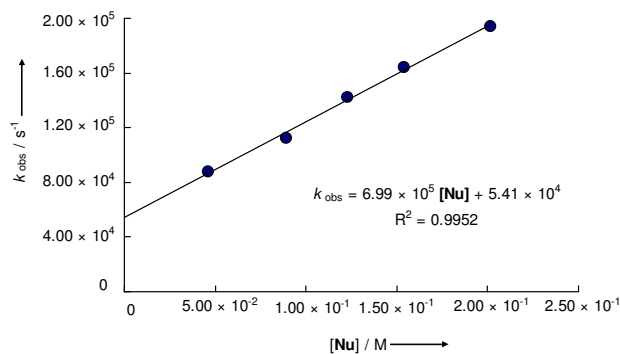


$$k_2 = 1.06 \times 10^9 \text{ L mol}^{-1} \text{ s}^{-1}$$

4.5.2. Reactions of (*E*)-1,3-bis(3-difluorophenyl)allyl cation (**1b**)

Reaction of **1b** with allyltrimethylsilane (**2e**). **1b** generated from **1b**-PPh₃⁺BF₄⁻ using laser-flash photolysis, $\lambda_{\text{obs}} = 500 \text{ nm}$, CH₂Cl₂, 20 °C, [**1b**-PPh₃⁺BF₄⁻] = $5.21 \times 10^{-5} \text{ M}$.

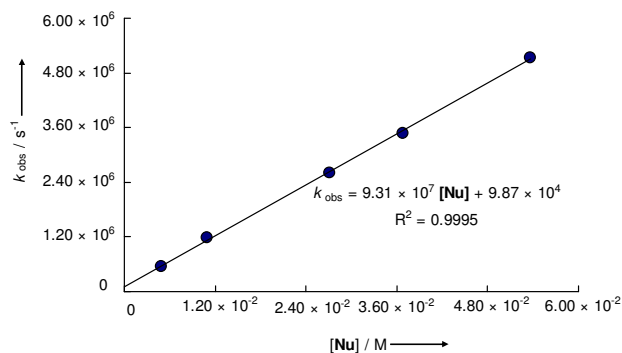
[Nu] / M	$k_{\text{obs}} / \text{s}^{-1}$
4.64×10^{-2}	8.77×10^4
8.90×10^{-2}	1.12×10^5
1.23×10^{-1}	1.42×10^5
1.54×10^{-1}	1.64×10^5
2.02×10^{-1}	1.94×10^5



$$k_2 = 6.99 \times 10^5 \text{ L mol}^{-1} \text{ s}^{-1}$$

Reaction of **1b** with trimethyl(2-methylallyl)silane (**2f**). **1b** generated from **1b**-PPh₃⁺BF₄⁻ using laser-flash photolysis, $\lambda_{\text{obs}} = 500 \text{ nm}$, CH₂Cl₂, 20 °C, [**1b**-PPh₃⁺BF₄⁻] = $5.21 \times 10^{-5} \text{ M}$.

[Nu] / M	$k_{\text{obs}} / \text{s}^{-1}$
4.99×10^{-3}	5.49×10^5
1.10×10^{-2}	1.17×10^6
2.71×10^{-2}	2.60×10^6
3.69×10^{-2}	3.48×10^6
5.37×10^{-2}	5.14×10^6

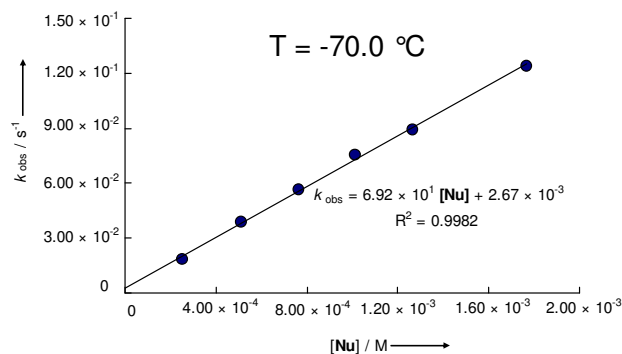


$$k_2 = 9.31 \times 10^7 \text{ L mol}^{-1} \text{ s}^{-1}$$

4.5.3. Reactions of (*E*)-1,3-bis(4-bromophenyl)allyl cation (**1c**)

Reaction of **1c** with allyltriphenylsilane (**2d**). **1c** generated from **1c**-Cl using GaCl₃ as Lewis acid, $\lambda_{\text{obs}} = 551 \text{ nm}$, CH₂Cl₂, -70.0 °C.

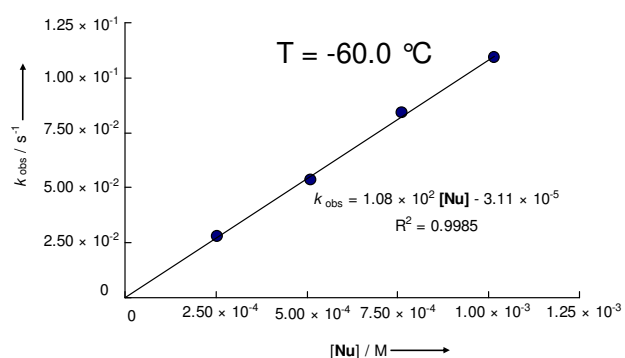
[1c -Cl] / M	[GaCl ₃] / M	[Nu] / M	$k_{\text{obs}} / \text{s}^{-1}$
2.32×10^{-5}	2.15×10^{-3}	2.55×10^{-4}	1.84×10^{-2}
2.32×10^{-5}	2.14×10^{-3}	5.10×10^{-4}	3.86×10^{-2}
2.32×10^{-5}	2.14×10^{-3}	7.63×10^{-4}	5.63×10^{-2}
2.31×10^{-5}	2.13×10^{-3}	1.02×10^{-3}	7.54×10^{-2}
2.31×10^{-5}	2.13×10^{-3}	1.27×10^{-3}	8.93×10^{-2}
2.30×10^{-5}	2.12×10^{-3}	1.77×10^{-3}	1.24×10^{-1}



$$k_2 (-70 \text{ }^\circ\text{C}) = 6.92 \times 10^1 \text{ L mol}^{-1} \text{ s}^{-1}$$

Reaction of **1c** with allyltriphenylsilane (**2d**). **1c** generated from **1c**-Cl using GaCl₃ as Lewis acid, $\lambda_{\text{obs}} = 551 \text{ nm}$, CH₂Cl₂, -60.0 °C.

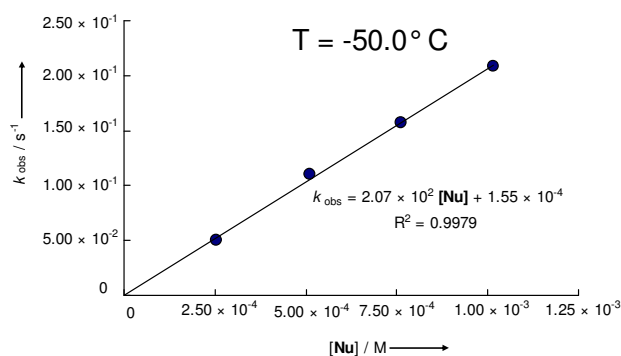
[1c -Cl] / M	[GaCl ₃] / M	[Nu] / M	$k_{\text{obs}} / \text{s}^{-1}$
2.32×10^{-5}	2.15×10^{-3}	2.55×10^{-4}	2.80×10^{-2}
2.32×10^{-5}	2.14×10^{-3}	5.10×10^{-4}	5.35×10^{-2}
2.32×10^{-5}	2.14×10^{-3}	7.63×10^{-4}	8.40×10^{-2}
2.31×10^{-5}	2.13×10^{-3}	1.02×10^{-3}	1.09×10^{-1}



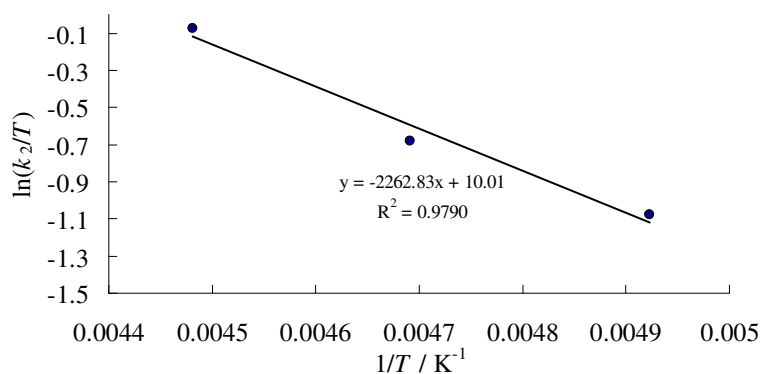
$$k_2 (-60 \text{ }^\circ\text{C}) = 1.08 \times 10^2 \text{ L mol}^{-1} \text{ s}^{-1}$$

Reaction of **1c** with allyltriphenylsilane (**2d**). **1c** generated from **1c**-Cl using GaCl₃ as Lewis acid, $\lambda_{\text{obs}} = 551 \text{ nm}$, CH₂Cl₂, -50.0 °C.

[1c -Cl] / M	[GaCl ₃] / M	[Nu] / M	$k_{\text{obs}} / \text{s}^{-1}$
2.32×10^{-5}	2.15×10^{-3}	2.55×10^{-4}	5.02×10^{-2}
2.32×10^{-5}	2.14×10^{-3}	5.10×10^{-4}	1.10×10^{-1}
2.32×10^{-5}	2.14×10^{-3}	7.63×10^{-4}	1.57×10^{-1}
2.31×10^{-5}	2.13×10^{-3}	1.02×10^{-3}	2.09×10^{-1}



$$k_2 (-50 \text{ }^\circ\text{C}) = 2.07 \times 10^2 \text{ L mol}^{-1} \text{ s}^{-1}$$



Eyring correlation for the second-order rate constants observed for reaction between **1c** and **2d** at variable temperature.

Eyring parameter:

$$\Delta H^\ddagger = (18.8 \pm 2.8) \text{ kJ mol}^{-1}$$

$$\Delta S^\ddagger = (-114.3 \pm 13.0) \text{ J mol}^{-1} \text{ K}^{-1}$$

$$R^2 = 0.9788$$

Arrhenius parameter:

$$E_A = (20.6 \pm 2.79) \text{ kJ mol}^{-1}$$

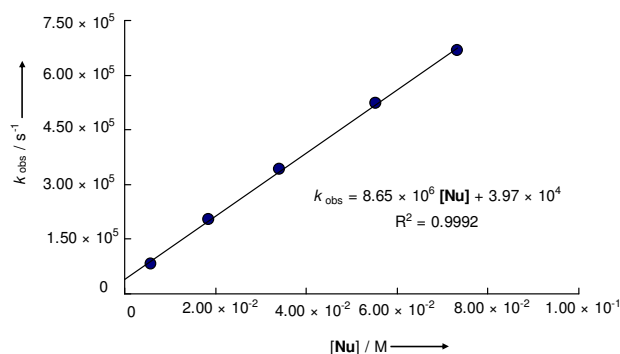
$$\ln A = 16.4 \pm 1.6$$

$$R^2 = 0.9819$$

$$k_2 (20^\circ \text{C}) = 2.93 \times 10^3 \text{ L mol}^{-1} \text{ s}^{-1}$$

Reaction of **1c** with trimethyl(2-methylallyl)silane (**2f**). **1c** generated from **1c**-PPh₃⁺TfO⁻ using laser-flash photolysis, $\lambda_{\text{obs}} = 527 \text{ nm}$, CH₂Cl₂, 20 °C, [**1c**-PPh₃⁺TfO⁻] = $5.55 \times 10^{-5} \text{ M}$.

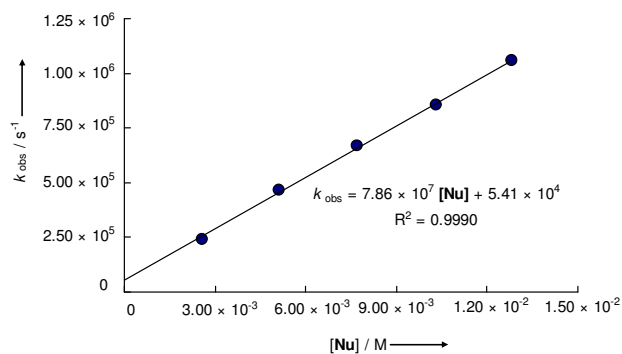
[Nu] / M	$k_{\text{obs}} / \text{s}^{-1}$
5.79×10^{-3}	8.21×10^4
1.86×10^{-2}	2.04×10^5
3.41×10^{-2}	3.42×10^5
5.53×10^{-2}	5.21×10^5
7.33×10^{-2}	6.68×10^5



$$k_2 = 8.65 \times 10^6 \text{ L mol}^{-1} \text{ s}^{-1}$$

Reaction of **1c** with 1-(trimethylsiloxy)cyclohexene (**2h**). **1c** generated from **1c-PPh₃⁺TfO⁻** using laser-flash photolysis, $\lambda_{\text{obs}} = 527 \text{ nm}$, CH_2Cl_2 , $20 \text{ }^\circ\text{C}$, $[\mathbf{1c-PPh}_3^+\text{TfO}^-] = 5.55 \times 10^{-5} \text{ M}$.

[Nu] / M	$k_{\text{obs}} / \text{s}^{-1}$
2.56×10^{-3}	2.44×10^5
5.13×10^{-3}	4.67×10^5
7.69×10^{-3}	6.70×10^5
1.03×10^{-2}	8.56×10^5
1.28×10^{-2}	1.06×10^6

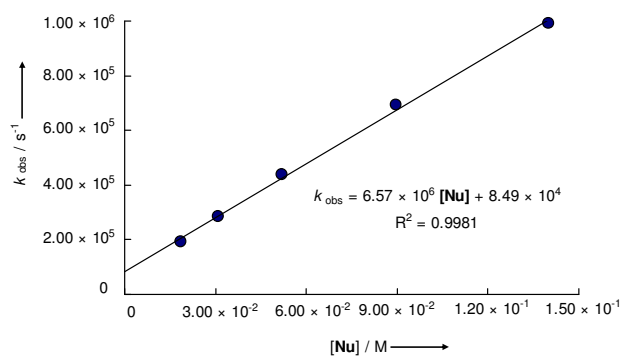


$$k_2 = 7.86 \times 10^7 \text{ L mol}^{-1} \text{ s}^{-1}$$

4.5.4. Reactions of (*E*)-1,3-bis(4-chlorophenyl)allyl cation (**1d**)

Reaction of **1d** with trimethyl(2-methylallyl)silane (**2f**). **1d** generated from **1d-PPh₃⁺BF₄⁻** using laser-flash photolysis, $\lambda_{\text{obs}} = 527 \text{ nm}$, CH_2Cl_2 , $20 \text{ }^\circ\text{C}$, $[\mathbf{1d-PPh}_3^+\text{BF}_4^-] = 8.00 \times 10^{-5} \text{ M}$.

[Nu] / M	$k_{\text{obs}} / \text{s}^{-1}$
1.85×10^{-2}	1.95×10^5
3.09×10^{-2}	2.84×10^5
5.21×10^{-2}	4.37×10^5
8.97×10^{-2}	6.94×10^5
1.40×10^{-1}	9.93×10^5

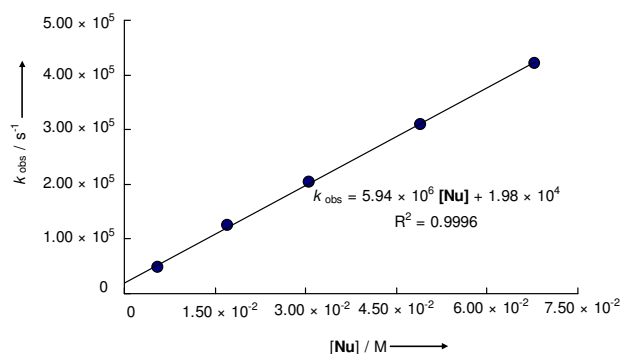


$$k_2 = 6.57 \times 10^6 \text{ L mol}^{-1} \text{ s}^{-1}$$

4.5.5. Reactions of (*E*)-1,3-diphenylallyl cation (**1e**)

Reaction of **1e** with trimethyl(2-methylallyl)silane (**2f**). **1e** generated from **1e-PPh₃⁺TfO⁻** using laser-flash photolysis, $\lambda_{\text{obs}} = 500 \text{ nm}$, CH_2Cl_2 , $20 \text{ }^\circ\text{C}$, $[\mathbf{1e-PPh}_3^+\text{TfO}^-] = 8.47 \times 10^{-5} \text{ M}$.

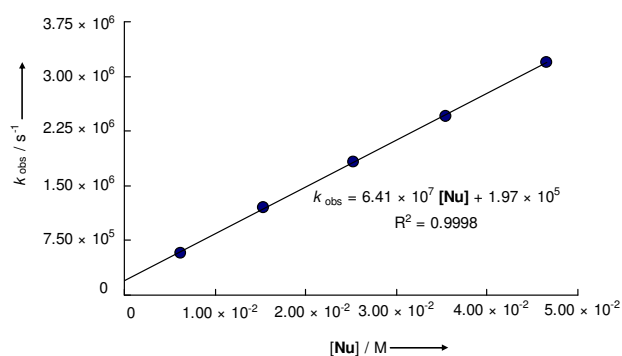
[Nu] / M	$k_{\text{obs}} / \text{s}^{-1}$
5.61×10^{-3}	4.91×10^4
1.71×10^{-2}	1.24×10^5
3.05×10^{-2}	2.04×10^5
4.90×10^{-2}	3.10×10^5
6.78×10^{-2}	4.21×10^5



$$k_2 = 5.94 \times 10^6 \text{ L mol}^{-1} \text{ s}^{-1}$$

Reaction of **1e** with 1-(trimethylsiloxy)cyclohexene (**2h**). **1e** generated from **1e-PPh₃⁺BF₄⁻** using laser-flash photolysis, $\lambda_{\text{obs}} = 488 \text{ nm}$, CH_2Cl_2 , $20 \text{ }^\circ\text{C}$, $[\mathbf{1e-PPh}_3^+\text{BF}_4^-] = 5.42 \times 10^{-5} \text{ M}$.

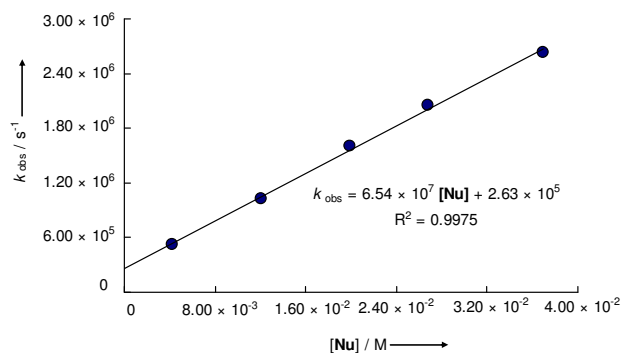
[Nu] / M	$k_{\text{obs}} / \text{s}^{-1}$
6.18×10^{-3}	5.81×10^5
1.53×10^{-2}	1.20×10^6
2.52×10^{-2}	1.82×10^6
3.54×10^{-2}	2.45×10^6
4.66×10^{-2}	3.19×10^6



$$k_2(\text{BF}_4^-) = 6.41 \times 10^7 \text{ L mol}^{-1} \text{ s}^{-1}$$

Reaction of **1e** with 1-(trimethylsiloxy)cyclohexene (**2h**). **1e** generated from **1e-PPh₃⁺TfO⁻** using laser-flash photolysis, $\lambda_{\text{obs}} = 488 \text{ nm}$, CH_2Cl_2 , $20 \text{ }^\circ\text{C}$.

$[\mathbf{1e-PPh}_3^+\text{TfO}^-] / \text{M}$	[Nu] / M	$k_{\text{obs}} / \text{s}^{-1}$
3.44×10^{-5}	4.27×10^{-3}	5.23×10^5
3.44×10^{-5}	1.21×10^{-2}	1.03×10^6
3.44×10^{-5}	1.99×10^{-2}	1.61×10^6
3.44×10^{-5}	2.68×10^{-2}	2.06×10^6
4.30×10^{-5}	3.69×10^{-2}	2.63×10^6

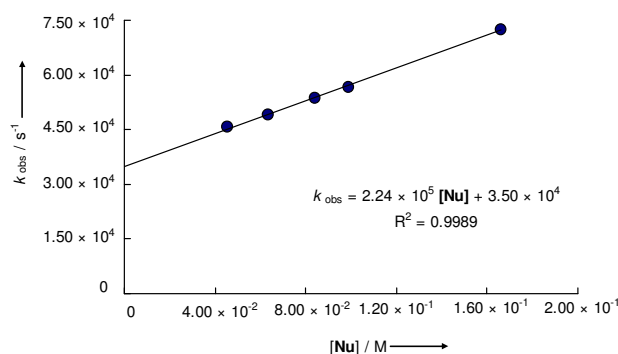


$$k_2(\text{TfO}^-) = 6.54 \times 10^7 \text{ L mol}^{-1} \text{ s}^{-1}$$

4.5.6. Reactions of (*E*)-1,3-di-*p*-tolylallyl cation (**1f**)

Reaction of **1f** with trimethyl(2-methylallyl)silane (**2f**). **1f** generated from **1f**-PPh₃⁺BF₄⁻ using laser-flash photolysis, $\lambda_{\text{obs}} = 524 \text{ nm}$, CH₂Cl₂, 20 °C, [**1f**-PPh₃⁺BF₄⁻] = $7.21 \times 10^{-5} \text{ M}$.

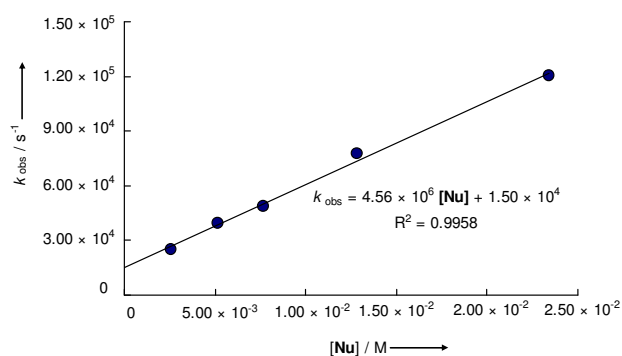
[Nu] / M	$k_{\text{obs}} / \text{s}^{-1}$
4.56×10^{-2}	4.61×10^4
6.35×10^{-2}	4.92×10^4
8.42×10^{-2}	5.37×10^4
9.87×10^{-2}	5.71×10^4
1.66×10^{-1}	7.26×10^4



$$k_2 = 2.24 \times 10^5 \text{ L mol}^{-1} \text{ s}^{-1}$$

Reaction of **1f** with 1-(trimethylsiloxy)cyclohexene (**2h**). **1f** generated from **1f**-PPh₃⁺BF₄⁻ using laser-flash photolysis, $\lambda_{\text{obs}} = 524 \text{ nm}$, CH₂Cl₂, 20 °C, [**1f**-PPh₃⁺BF₄⁻] = $7.21 \times 10^{-5} \text{ M}$.

[Nu] / M	$k_{\text{obs}} / \text{s}^{-1}$
2.56×10^{-3}	2.52×10^4
5.13×10^{-3}	3.92×10^4
7.69×10^{-3}	4.85×10^4
1.28×10^{-2}	7.73×10^4
2.34×10^{-2}	1.20×10^5

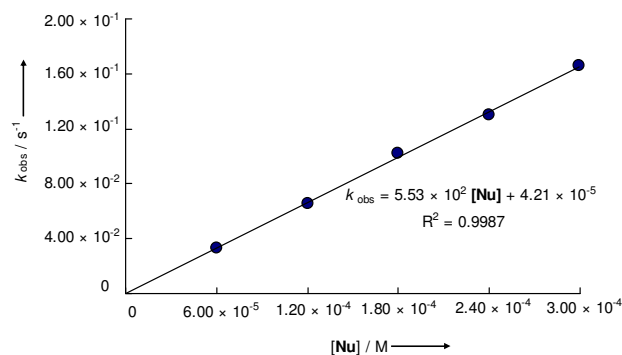


$$k_2 = 4.56 \times 10^6 \text{ L mol}^{-1} \text{ s}^{-1}$$

4.5.7. Reactions of (*E*)-1,3-bis(4-methoxyphenyl)allyl cation (**1g**)

Reaction of **1g** with trimethyl(2-methylallyl)silane (**2f**), $\lambda_{\text{obs}} = 578 \text{ nm}$, CH₂Cl₂, 20 °C.

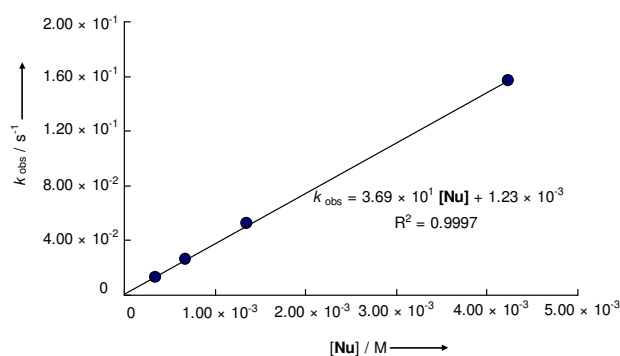
[E] ₀ / M	[Nu] / M	$k_{\text{obs}} / \text{s}^{-1}$
5.81×10^{-6}	6.01×10^{-5}	3.32×10^{-2}
1.16×10^{-5}	1.20×10^{-4}	6.55×10^{-2}
1.16×10^{-5}	1.80×10^{-4}	1.02×10^{-1}
1.16×10^{-5}	2.39×10^{-4}	1.30×10^{-1}
1.16×10^{-5}	2.99×10^{-4}	1.66×10^{-1}



$$k_2 = 5.53 \times 10^2 \text{ L mol}^{-1} \text{ s}^{-1}$$

Reaction of **1g** with allyltriphenylstannane (**2g**), $\lambda_{\text{obs}} = 578 \text{ nm}$, CH_2Cl_2 , $20 \text{ }^\circ\text{C}$.

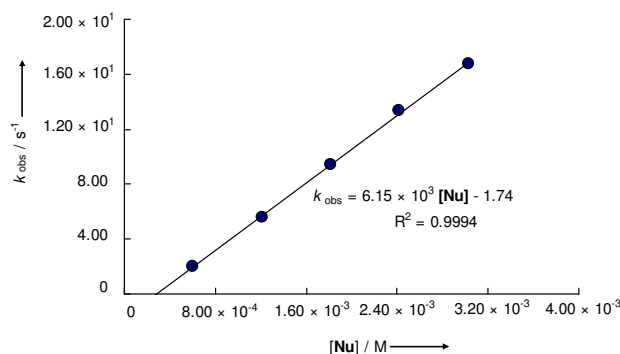
$[\text{E}]_0 / \text{M}$	$[\text{Nu}] / \text{M}$	$k_{\text{obs}} / \text{s}^{-1}$
2.66×10^{-5}	3.40×10^{-4}	1.28×10^{-2}
2.65×10^{-5}	6.78×10^{-4}	2.60×10^{-2}
2.63×10^{-5}	1.35×10^{-3}	5.24×10^{-2}
2.67×10^{-5}	4.24×10^{-3}	1.57×10^{-1}



$$k_2 = 3.69 \times 10^1 \text{ L mol}^{-1} \text{ s}^{-1}$$

Reaction of **1g** with 1-(trimethylsiloxy)cyclohexene (**2h**), stopped-flow device, $\lambda_{\text{obs}} = 578 \text{ nm}$, CH_2Cl_2 , $20 \text{ }^\circ\text{C}$, $[\text{E}]_0 = 2.79 \times 10^{-5} \text{ M}$.

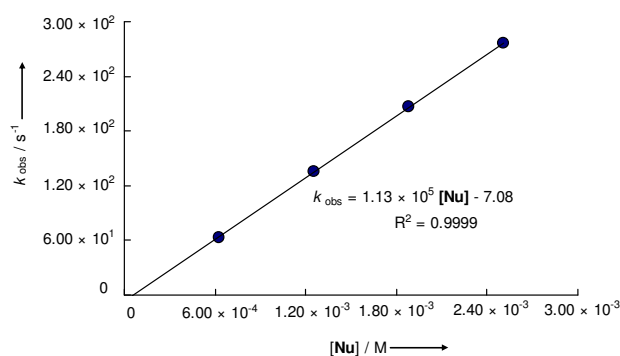
$[\text{Nu}] / \text{M}$	$k_{\text{obs}} / \text{s}^{-1}$
6.05×10^{-4}	2.03
1.21×10^{-3}	5.60
1.82×10^{-3}	9.40
2.42×10^{-3}	1.34×10^1
3.03×10^{-3}	1.68×10^1



$$k_2 = 6.15 \times 10^3 \text{ L mol}^{-1} \text{ s}^{-1}$$

Reaction of **1g** with 1-(trimethylsiloxy)cyclopentene (**2i**), stopped-flow device, $\lambda_{\text{obs}} = 578 \text{ nm}$, CH_2Cl_2 , $20 \text{ }^\circ\text{C}$, $[\text{E}]_0 = 2.79 \times 10^{-5} \text{ M}$.

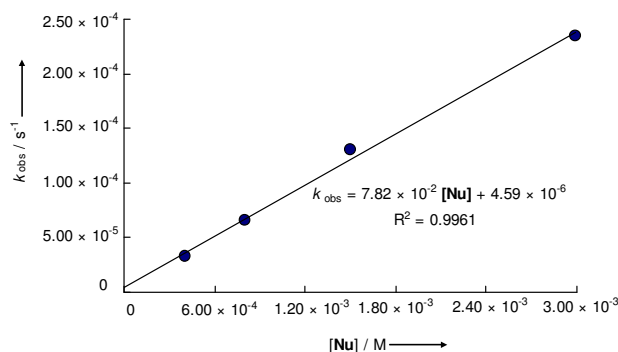
$[\text{Nu}] / \text{M}$	$k_{\text{obs}} / \text{s}^{-1}$
6.26×10^{-4}	6.35×10^1
1.25×10^{-3}	1.35×10^2
1.88×10^{-3}	2.07×10^2
2.51×10^{-3}	2.76×10^2



$$k_2 = 1.13 \times 10^5 \text{ L mol}^{-1} \text{ s}^{-1}$$

4.5.8. Reactions of (*E*)-1,3-bis(4-dimethylaminophenyl)allyl cation (**1h**)Reaction of **1h** with 1-(trimethylsiloxy)cyclopentene (**2i**), $\lambda_{\text{obs}} = 704$ nm, CH_2Cl_2 , 20 °C.

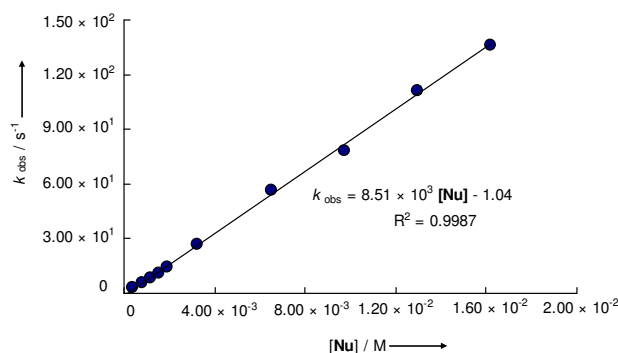
$[\text{E}]_0 / \text{M}$	$[\text{Nu}] / \text{M}$	$k_{\text{obs}} / \text{s}^{-1}$
9.97×10^{-6}	4.04×10^{-4}	3.32×10^{-5}
9.95×10^{-6}	8.05×10^{-4}	6.53×10^{-5}
9.97×10^{-6}	1.50×10^{-3}	1.30×10^{-4}
9.95×10^{-6}	2.99×10^{-3}	2.35×10^{-4}



$$k_2 = 7.82 \times 10^{-2} \text{ L mol}^{-1} \text{ s}^{-1}$$

Reaction of **1h** with 1-(*N*-morpholino)cyclohexene (**2n**), stopped-flow device, $\lambda_{\text{obs}} = 704$ nm, CH_2Cl_2 , 20 °C, $[\text{E}]_0 = 1.07 \times 10^{-5}$ M.

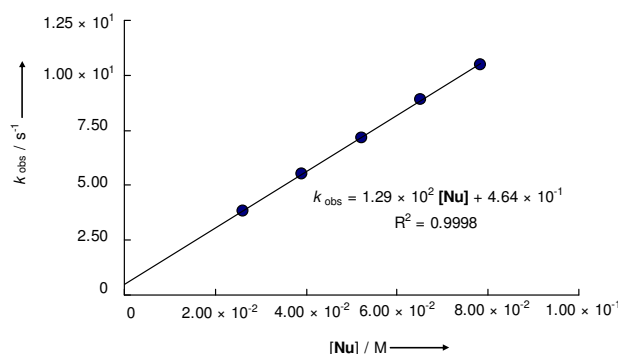
$[\text{Nu}] / \text{M}$	$k_{\text{obs}} / \text{s}^{-1}$
3.85×10^{-4}	3.03
7.71×10^{-4}	5.89
1.16×10^{-3}	8.39
1.54×10^{-3}	1.13×10^1
1.93×10^{-3}	1.45×10^1
6.48×10^{-3}	5.67×10^1
1.30×10^{-2}	1.11×10^2
3.24×10^{-3}	2.68×10^1
9.72×10^{-3}	7.81×10^1
1.62×10^{-2}	1.36×10^2



$$k_2 = 8.51 \times 10^3 \text{ L mol}^{-1} \text{ s}^{-1}$$

Reaction of **1h** with 2,2,2-trifluoroethylamine (**2p**), stopped-flow device, $\lambda_{\text{obs}} = 704$ nm, CH_3CN , 20 °C, $[\text{E}]_0 = 5.37 \times 10^{-6}$ M.

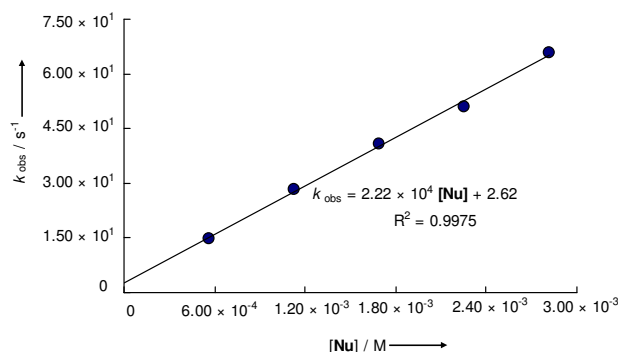
$[\text{Nu}] / \text{M}$	$k_{\text{obs}} / \text{s}^{-1}$
2.61×10^{-2}	3.80
3.91×10^{-2}	5.52
5.22×10^{-2}	7.14
6.52×10^{-2}	8.91
7.83×10^{-2}	1.05×10^1



$$k_2 = 1.29 \times 10^2 \text{ L mol}^{-1} \text{ s}^{-1}$$

Reaction of **1h** with benzylamine (**2r**), stopped-flow device, $\lambda_{\text{obs}} = 704 \text{ nm}$, CH_3CN , $20 \text{ }^\circ\text{C}$, $[\text{E}]_0 = 5.37 \times 10^{-6} \text{ M}$.

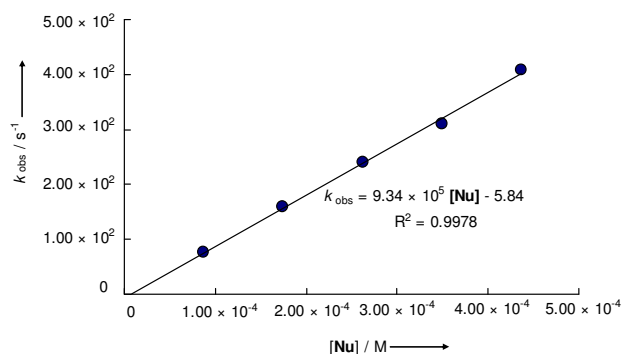
$[\text{Nu}] / \text{M}$	$k_{\text{obs}} / \text{s}^{-1}$
5.63×10^{-4}	1.47×10^1
1.13×10^{-3}	2.82×10^1
1.69×10^{-3}	4.09×10^1
2.25×10^{-3}	5.10×10^1
2.81×10^{-3}	6.57×10^1



$$k_2 = 2.22 \times 10^4 \text{ L mol}^{-1} \text{ s}^{-1}$$

Reaction of **1h** with morpholine (**2s**), stopped-flow device, $\lambda_{\text{obs}} = 704 \text{ nm}$, CH_3CN , $20 \text{ }^\circ\text{C}$, $[\text{E}]_0 = 5.37 \times 10^{-6} \text{ M}$.

$[\text{Nu}] / \text{M}$	$k_{\text{obs}} / \text{s}^{-1}$
8.74×10^{-5}	7.55×10^1
1.75×10^{-4}	1.60×10^2
2.62×10^{-4}	2.41×10^2
3.50×10^{-4}	3.10×10^2
4.37×10^{-4}	4.08×10^2

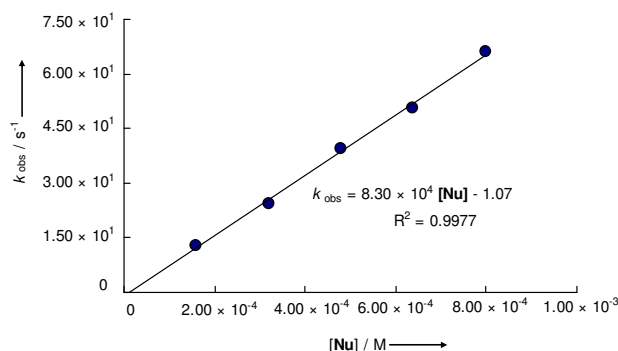


$$k_2 = 9.34 \times 10^5 \text{ L mol}^{-1} \text{ s}^{-1}$$

4.5.9. Reactions of (*E*)-1,3-bis(julolidin-9-yl)allyl cation (**1i**)

Reaction of **1i** with 1-(*N*-piperidino)cyclopentene (**2o**), stopped-flow device, $\lambda_{\text{obs}} = 704 \text{ nm}$, CH_2Cl_2 , $20 \text{ }^\circ\text{C}$, $[\text{E}]_0 = 6.59 \times 10^{-6} \text{ M}$.

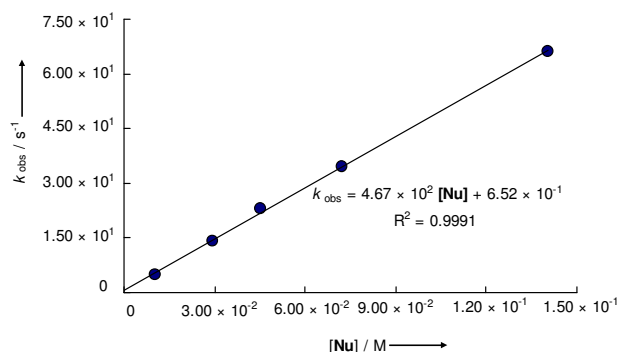
$[\text{Nu}] / \text{M}$	$k_{\text{obs}} / \text{s}^{-1}$
1.60×10^{-4}	1.29×10^1
3.19×10^{-4}	2.45×10^1
4.79×10^{-4}	3.93×10^1
6.39×10^{-4}	5.07×10^1
7.98×10^{-4}	6.61×10^1



$$k_2 = 8.30 \times 10^4 \text{ L mol}^{-1} \text{ s}^{-1}$$

Reaction of **1i** with isopropylamine (**2q**), stopped-flow device, $\lambda_{\text{obs}} = 733 \text{ nm}$, CH_3CN , $20 \text{ }^\circ\text{C}$, $[\text{E}]_0 = 5.10 \times 10^{-6} \text{ M}$.

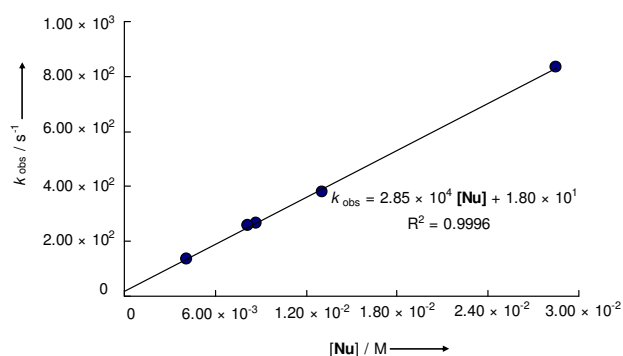
$[\text{Nu}] / \text{M}$	$k_{\text{obs}} / \text{s}^{-1}$
1.04×10^{-2}	4.82
2.94×10^{-2}	1.41×10^1
4.54×10^{-2}	2.30×10^1
7.22×10^{-2}	3.46×10^1
1.41×10^{-1}	6.60×10^1



$$k_2 = 4.67 \times 10^2 \text{ L mol}^{-1} \text{ s}^{-1}$$

Reaction of **1i** with morpholine (**2s**), stopped-flow device, $\lambda_{\text{obs}} = 733 \text{ nm}$, CH_3CN , $20 \text{ }^\circ\text{C}$, $[\text{E}]_0 = 5.10 \times 10^{-6} \text{ M}$.

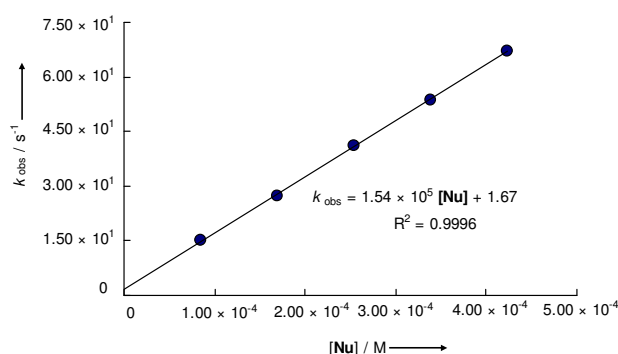
$[\text{Nu}] / \text{M}$	$k_{\text{obs}} / \text{s}^{-1}$
4.08×10^{-3}	1.35×10^2
8.16×10^{-3}	2.57×10^2
8.72×10^{-3}	2.67×10^2
1.30×10^{-2}	3.82×10^2
2.85×10^{-2}	8.32×10^2



$$k_2 = 2.85 \times 10^4 \text{ L mol}^{-1} \text{ s}^{-1}$$

Reaction of **1i** with piperidine (**2t**), stopped-flow device, $\lambda_{\text{obs}} = 733 \text{ nm}$, CH_3CN , $20 \text{ }^\circ\text{C}$, $[\text{E}]_0 = 5.10 \times 10^{-6} \text{ M}$.

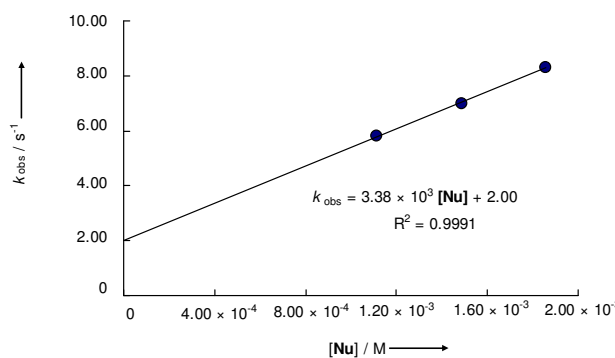
$[\text{Nu}] / \text{M}$	$k_{\text{obs}} / \text{s}^{-1}$
8.46×10^{-5}	1.50×10^1
1.69×10^{-4}	2.73×10^1
2.54×10^{-4}	4.12×10^1
3.38×10^{-4}	5.36×10^1
4.23×10^{-4}	6.71×10^1



$$k_2 = 1.54 \times 10^5 \text{ L mol}^{-1} \text{ s}^{-1}$$

Reaction of **1i** with potassium salt of Meldrum's acid (**2u**), stopped-flow device, $\lambda_{\text{obs}} = 733$ nm, DMSO, 20 °C, $[E]_0 = 5.10 \times 10^{-6}$ M.

[Nu] / M	$k_{\text{obs}} / \text{s}^{-1}$
1.12×10^{-3}	5.79
1.49×10^{-3}	6.98
1.86×10^{-3}	8.30



$$k_2 = 3.38 \times 10^3 \text{ L mol}^{-1} \text{ s}^{-1}$$

4.6. Computational Results

All quantum mechanical calculations were performed by Gaussian 03, Revision D.01.⁴⁶ Geometries was optimized at the B3LYP/6-31G(d,p) level of theory. All stationary points were confirmed being minima by calculations of vibrational frequencies. Thermochemical corrections (B3LYP/6-31G(d,p)) were applied to single point energies from MP2(FC)/6-31G+(2d,p) level calculations to give H_{298} and G_{298} so that:

$$H_{298}(\text{MP2FC}/6-31\text{G}+(2\text{d},\text{p})//\text{B3LYP}/6-31\text{G}(\text{d},\text{p})) = E_{\text{tot}}(\text{MP2FC}/6-31\text{G}+(2\text{d},\text{p})) + H_{298}(\text{B3LYP}/6-31\text{G}(\text{d},\text{p})) - E_{\text{tot}}(\text{B3LYP}/6-31\text{G}(\text{d},\text{p})) \quad (\text{S1})$$

$$G_{298}(\text{MP2FC}/6-31\text{G}+(2\text{d},\text{p})//\text{B3LYP}/6-31\text{G}(\text{d},\text{p})) = E_{\text{tot}}(\text{MP2FC}/6-31\text{G}+(2\text{d},\text{p})) + G_{298}(\text{B3LYP}/6-31\text{G}(\text{d},\text{p})) - E_{\text{tot}}(\text{B3LYP}/6-31\text{G}(\text{d},\text{p})) \quad (\text{S2})$$

G_{298} and H_{298} values for methyl anion were taken from ref 27.

4.6.1. Conformational analysis

Carbocations

In case of **1b**, **1f** and **1i** cations existence of different conformers has to be considered (Figure S1). In these cases, the Boltzmann distribution was used to calculate statistical weights of single conformers; and averaged energies were used for calculations of methyl anion affinities. The relative energies of single conformers and their Boltzmann coefficients are listed in Table S1.

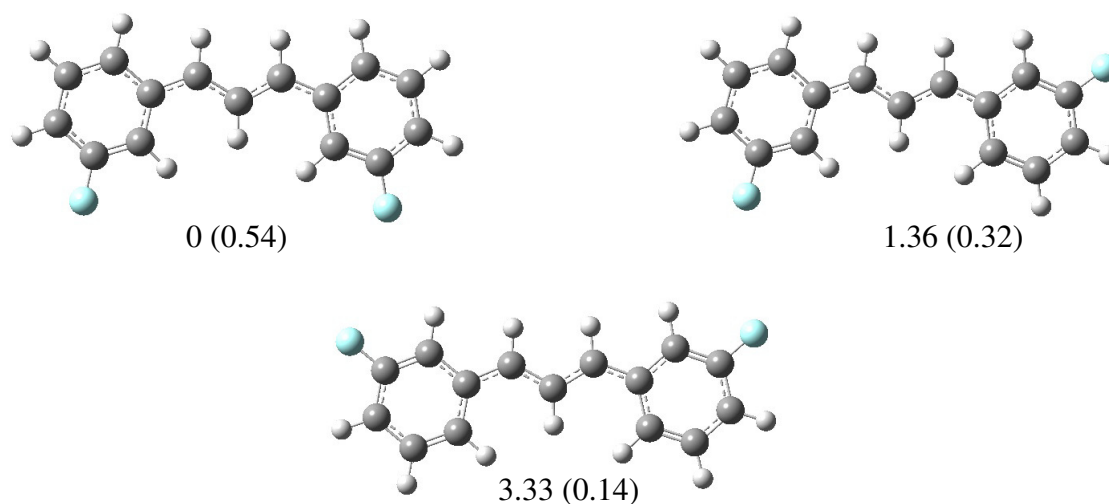


Figure S1. Conformations of **1b** cation with their relative H_{298} values (kJ/mol, MP2FC/6-31G+(2d,p)//B3LYP/6-31G(d,p)) and statistical weights according to Boltzmann distribution (in parentheses).

Table S1. Relative H_{298} and G_{298} (kJ/mol, most stable conformer used as reference point) for conformers of 1,3-diarylallyl cations **1b**, **1g**, **1i** and their statistical weights (according to Boltzmann distribution).

cation (conformer)	$H_{298\text{rel}}$	w_{Hi}^a	$G_{298\text{rel}}$	w_{Gi}^a
1b				
1b (1)	0.000	0.544	0.000	0.526
1b (2)	1.360	0.314	1.169	0.328
1b (3)	3.326	0.142	3.190	0.145
1g				
1g (1)	3.084	0.154	2.712	0.166
1g (2)	1.356	0.310	0.936	0.339
1g (3)	0.000	0.536	0.000	0.495
1i				
1i (1) ^b	2.204	0.164	1.096	0.220
1i (2)	4.640	0.031	3.257	0.046
1i (3) ^b	4.606	0.062	2.992	0.102
1i (4) ^b	2.338	0.155	2.057	0.149
1i (5)	0.000	0.199	0.502	0.140
1i (6) ^b	0.058	0.389	0.000	0.342

^a For the further calculations, the values of w with more decimals than indicated in the table were used. The use of the Boltzmann coefficients from this table leads to slightly different results.

^b There are two enantiomeric conformers of this type which was considered in Boltzmann analysis.

Methyl anion adducts

All methyl anion adducts **1(a-i)-Me** have three basic conformers (Figure S2). In case of compounds **1b-Me**, **1g-Me** and **1i-Me** the number of conformers is higher because of several substituent spatial orientation possibilities (similar to cations **1b**, **1g** and **1i**).

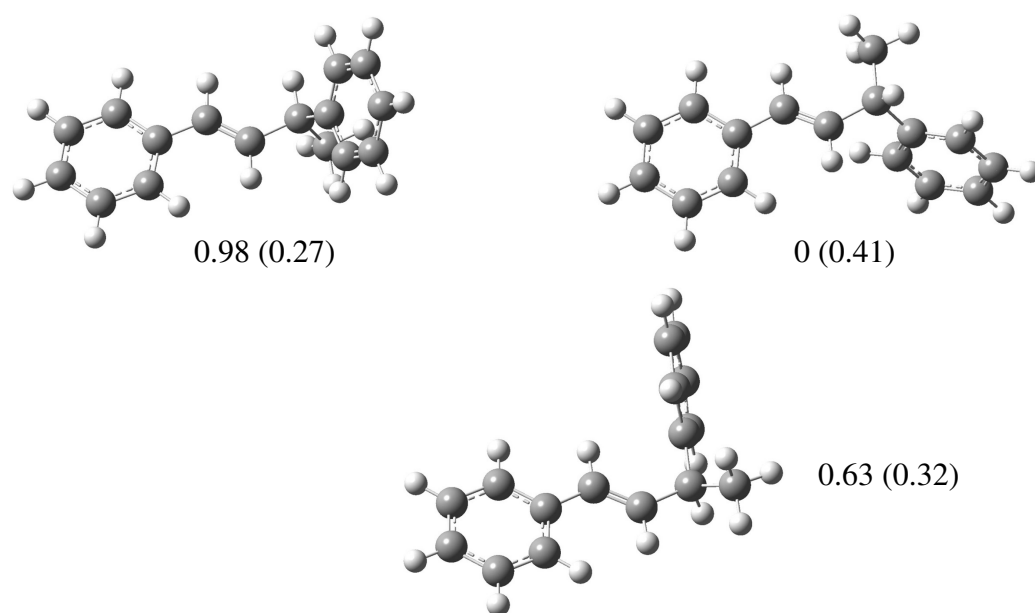


Figure S2. Conformations of **1e-Me** with their relative H_{298} values (kJ/mol, MP2FC/6-31+G(2d,p)//B3LYP/6-31G(d,p)) and statistical weights according to Boltzmann distribution (in parentheses).

The relative energies of single conformers for methyl anion adducts **1(a-i)-Me** and their Boltzmann coefficients are listed in Table S2.

Table S2. Relative H_{298} and G_{298} (kJ/mol, most stable conformer used as reference point) for conformers of the (*E*)-1,3-diarylbut-1-enes **1(a-i)-Me** and their statistical weights (according to the Boltzmann distribution).

(<i>E</i>)-1,3-diarylbut-1-ene (conformer)	$H_{298\text{rel}}$	w_{Hi}^a	$G_{298\text{rel}}$	w_{Gi}^a
1a-Me				
1a-Me (1)	0.765	0.301	0.000	0.405
1a-Me (2)	0.000	0.410	0.540	0.325
1a-Me (3)	0.866	0.289	1.004	0.270
1b-Me				
1b-Me (1)	0.721	0.083	1.993	0.092
1b-Me (2)	0.847	0.079	0.000	0.205
1b-Me (3)	1.124	0.070	1.201	0.126
1b-Me (4)	1.728	0.055	2.301	0.081
1b-Me (5)	0.000	0.111	3.160	0.057
1b-Me (6)	0.245	0.100	2.906	0.063
1b-Me (7)	0.319	0.097	3.046	0.060
1b-Me (8)	0.942	0.076	2.829	0.065
1b-Me (9)	0.862	0.078	3.630	0.047
1b-Me (10)	1.392	0.063	3.772	0.045
1b-Me (11)	0.279	0.099	2.439	0.077
1b-Me (12)	0.548	0.089	2.277	0.082
1c-Me				
1c-Me (1)	1.226	0.238	0.236	0.337
1c-Me (2)	0.127	0.371	0.000	0.371
1c-Me (3)	0.000	0.391	0.601	0.291
1d-Me				
1d-Me (1)	0.000	0.401	0.000	0.494
1d-Me (2)	0.388	0.343	1.299	0.293
1d-Me (3)	1.101	0.257	2.083	0.213
1e-Me				
1e-Me (1)	0.976	0.275	0.000	0.477
1e-Me (2)	0.000	0.408	1.513	0.259
1e-Me (3)	0.626	0.317	1.472	0.264
1f-Me				
1f-Me (1)	0.862	0.294	0.000	0.614
1f-Me (2)	0.000	0.417	4.512	0.100

Table S2: Continued.

(E)-1,3-diarylbut-1-ene (conformer)	$H_{298\text{rel}}$	w_{Hi}^a	$G_{298\text{rel}}$	w_{Gi}^a
1f-Me (continued)				
1f-Me (3)	0.908	0.289	1.894	0.286
1g-Me				
1g-Me (1)	1.870	0.053	0.347	0.095
1g-Me (2)	1.246	0.068	0.117	0.104
1g-Me (3)	1.185	0.070	0.408	0.092
1g-Me (4)	0.769	0.083	0.911	0.075
1g-Me (5)	0.433	0.095	0.000	0.109
1g-Me (6)	0.331	0.099	0.573	0.086
1g-Me (7)	0.000	0.113	1.053	0.071
1g-Me (8)	0.053	0.111	1.426	0.061
1g-Me (9)	0.680	0.086	0.977	0.073
1g-Me (10)	0.441	0.095	0.567	0.087
1g-Me (11)	1.399	0.064	0.678	0.083
1g-Me (12)	1.426	0.064	1.389	0.062
1h-Me				
1h-Me (1)	2.534	0.171	0.373	0.327
1h-Me (2)	0.000	0.476	0.000	0.380
1h-Me (3)	0.747	0.352	0.636	0.294
1i-Me				
1i-Me (1)	0.000	0.098	0.529	0.078
1i-Me (2)	6.707	0.007	5.530	0.010
1i-Me (3)	6.773	0.006	6.121	0.008
1i-Me (4)	0.344	0.086	2.181	0.040
1i-Me (5)	6.059	0.009	6.103	0.008
1i-Me (6)	12.808	0.001	10.481	0.001
1i-Me (7)	12.665	0.001	11.325	0.001
1i-Me (8)	5.745	0.010	4.046	0.019
1i-Me (9)	5.873	0.009	5.657	0.010
1i-Me (10)	12.643	0.001	10.195	0.002
1i-Me (11)	12.682	0.001	10.318	0.002
1i-Me (12)	5.790	0.010	4.041	0.019
1i-Me (13)	0.670	0.075	2.594	0.034
1i-Me (14)	6.769	0.006	5.986	0.009
1i-Me (15)	6.910	0.006	6.717	0.006
1i-Me (16)	0.260	0.088	0.309	0.085
1i-Me (17)	1.395	0.056	0.000	0.097
1i-Me (18)	8.173	0.004	2.065	0.042

Table S2: Continued.

(<i>E</i>)-1,3-diarylbut-1-ene (conformer)	$H_{298\text{rel}}$	w_{Hi}^a	$G_{298\text{rel}}$	w_{Gi}^a
1i-Me (continued)				
1i-Me (19)	8.158	0.004	6.159	0.008
1i-Me (20)	1.367	0.057	1.219	0.059
1i-Me (21)	7.160	0.005	5.597	0.010
1i-Me (22)	14.268	0.000	10.258	0.002
1i-Me (23)	13.385	0.000	8.676	0.003
1i-Me (24)	6.978	0.006	3.134	0.027
1i-Me (25)	7.207	0.005	4.856	0.014
1i-Me (26)	14.162	0.000	7.445	0.005
1i-Me (27)	13.848	0.000	6.236	0.008
1i-Me (28)	7.234	0.005	6.881	0.006
1i-Me (29)	1.427	0.055	0.591	0.076
1i-Me (30)	7.976	0.004	6.116	0.008
1i-Me (31)	8.170	0.004	6.281	0.008
1i-Me (32)	1.380	0.056	1.938	0.044
1i-Me (33)	0.748	0.073	2.924	0.030
1i-Me (34)	6.982	0.006	6.661	0.007
1i-Me (35)	6.968	0.006	6.143	0.008
1i-Me (36)	0.894	0.069	2.746	0.032
1i-Me (37)	6.291	0.008	4.376	0.017
1i-Me (38)	12.712	0.001	9.670	0.002
1i-Me (39)	12.848	0.001	5.815	0.009
1i-Me (40)	6.520	0.007	4.298	0.017
1i-Me (41)	6.527	0.007	7.004	0.006
1i-Me (42)	12.802	0.001	10.528	0.001
1i-Me (43)	13.029	0.001	11.093	0.001
1i-Me (44)	6.681	0.007	7.108	0.005
1i-Me (45)	0.912	0.068	1.814	0.046
1i-Me (46)	6.906	0.006	4.227	0.018
1i-Me (47)	7.253	0.005	6.622	0.007
1i-Me (48)	1.115	0.063	1.776	0.047

^a For the further calculations, the values of w with more decimals than indicated in the table were used. The use of the Boltzmann coefficients from this table leads to slightly different results.

4.6.2. Calculated energies

Table S3. Energy data of the 1,3-diarylallyl cations **1a–i** (in Hartree)^a.

cation (conformer)	B3LYP/6-31G(d,p)			MP2FC/6- 31G+(2d,p)	MP2(FC)/6-31G+(2d,p)// B3LYP/6-31G(d,p)	
	E_{tot}	H_{298}	G_{298}	E_{tot}	H_{298}	G_{298}
1a	-976.103026	-975.886687	-975.948317	-973.678163	-973.461824	-973.523454
1b (1)	-777.652934	-777.421506	-777.478915	-775.584958	-775.353530	-775.410939
1b (2)	-777.652378	-777.421037	-777.478519	-775.584352	-775.353012	-775.410494
1b (3)	-777.651798	-777.420402	-777.477863	-775.583658	-775.352263	-775.409724
1b ^b					-775.353187	-775.410616
1c	-5721.401610	-5721.172621	-5721.235084	-5716.709566	-5716.480577	-5716.543040
1d	-1498.382631	-1498.153175	-1498.213101	-1495.572968	-1495.343512	-1495.403438
1e	-579.199794	-578.953290	-579.006513	-577.487742	-577.241239	-577.294462
1f	-657.851366	-657.546572	-657.610380	-655.890320	-655.585526	-655.649334
1g (1)	-808.273771	-807.956634	-808.021752	-805.994631	-805.677494	-805.742612
1g (2)	-808.274348	-807.957212	-808.022348	-805.995289	-805.678152	-805.743288
1g (3)	-808.274870	-807.957665	-808.022641	-805.995874	-805.678669	-805.743645
1g ^a					-805.678327	-805.743186
1h	-847.196319	-846.793893	-846.867292	-844.706373	-844.303947	-844.377346
1i (1)	-1156.940498	-1156.388339	-1156.468859	-1153.562462	-1153.010303	-1153.090823
1i (2)	-1156.939862	-1156.387636	-1156.468261	-1153.561601	-1153.009375	-1153.090000
1i (3)	-1156.939856	-1156.387640	-1156.468353	-1153.561605	-1153.009388	-1153.090101
1i (4)	-1156.940515	-1156.388315	-1156.468520	-1153.562452	-1153.010252	-1153.090457
1i (5)	-1156.941154	-1156.388996	-1156.468903	-1153.563301	-1153.011142	-1153.091049
1i (6)	-1156.941129	-1156.388990	-1156.469110	-1153.563260	-1153.011121	-1153.091241
1i ^b					-1153.010695	-1153.090831

^a For the further calculations, the values with more decimals than indicated in the table were used. The use of the numbers from this table leads to the slightly different results. ^b Averaged values derived using the Boltzmann distribution

Table S4. Energy data of the (*E*)-1,3-diarylbut-1-enes **1(a-i)**-Me (in Hartree).^a

methyl adduct (conformer)	B3LYP/6-31G(d,p)			MP2FC/6- 31G+(2d,p)	MP2(FC)/6-31G+(2d,p)// B3LYP/6-31G(d,p)	
	E_{tot}	H_{298}	G_{298}	E_{tot}	H_{298}	G_{298}
1a -Me (1)	-1016.280535	-1016.023645	-1016.090918	-1013.744310	-1013.487420	-1013.554693
1a -Me (2)	-1016.280690	-1016.023734	-1016.090510	-1013.744667	-1013.487711	-1013.554487
1a -Me (3)	-1016.279692	-1016.022794	-1016.089723	-1013.744280	-1013.487382	-1013.554311
1a -Me ^b	-	-	-	-	-1013.487528	-1013.554523
1b -Me (1)	-817.818464	-817.546793	-817.609841	-815.638637	-815.366966	-815.430014
1b -Me (2)	-817.818374	-817.546728	-817.610583	-815.638564	-815.366918	-815.430773
1b -Me (3)	-817.818305	-817.546649	-817.610152	-815.638469	-815.366813	-815.430316
1b -Me (4)	-817.818151	-817.546456	-817.609770	-815.638278	-815.366583	-815.429897
1b -Me (5)	-817.818690	-817.546921	-817.609250	-815.639010	-815.367241	-815.429570
1b -Me (6)	-817.818620	-817.546886	-817.609405	-815.638882	-815.367148	-815.429667
1b -Me (7)	-817.818477	-817.546732	-817.609226	-815.638864	-815.367119	-815.429613
1b -Me (8)	-817.818440	-817.546670	-817.609484	-815.638652	-815.366882	-815.429696
1b -Me (9)	-817.817436	-817.545759	-817.608237	-815.638589	-815.366913	-815.429391
1b -Me (10)	-817.817391	-817.545685	-817.608311	-815.638417	-815.366710	-815.429336
1b -Me (11)	-817.817741	-817.546029	-817.608739	-815.638846	-815.367134	-815.429844
1b -Me (12)	-817.817654	-817.545961	-817.608835	-815.638725	-815.367032	-815.429906
1b -Me ^b	-	-	-	-	-815.366955	-815.429835
1c -Me (1)	-5761.561099	-5761.291835	-5761.360238	-5756.756344	-5756.487080	-5756.555483
1c -Me (2)	-5761.561436	-5761.292077	-5761.360151	-5756.756858	-5756.487499	-5756.555573
1c -Me (3)	-5761.560500	-5761.291195	-5761.358992	-5756.756852	-5756.487547	-5756.555344
1c -Me ^b	-	-	-	-	-5756.487376	-5756.555467
1d -Me (1)	-1538.543674	-1538.274022	-1538.339711	-1535.621383	-1535.351731	-1535.417420
1d -Me (2)	-1538.543781	-1538.274049	-1538.339391	-1535.621316	-1535.351583	-1535.416925
1d -Me (3)	-1538.542865	-1538.273173	-1538.338488	-1535.621004	-1535.351312	-1535.416627
1d -Me ^b	-	-	-	-	-1535.351573	-1535.417106
1e -Me (1)	-619.354119	-619.067682	-619.126811	-617.529811	-617.243374	-617.302503
1e -Me (2)	-619.354399	-619.067866	-619.126047	-617.530279	-617.243746	-617.301927
1e -Me (3)	-619.353422	-619.066938	-619.125373	-617.529992	-617.243508	-617.301943
1e -Me ^b	-	-	-	-	-617.243543	-617.302124
1f -Me (1)	-697.995343	-697.650421	-697.720257	-695.923638	-695.578716	-695.648552
1f -Me (2)	-697.995635	-697.650615	-697.718404	-695.924065	-695.579044	-695.646833
1f -Me (3)	-697.994689	-697.649711	-697.718843	-695.923676	-695.578698	-695.647830
1f -Me ^b	-	-	-	-	-695.578819	-695.647738
1g -Me (1)	-848.403765	-848.046997	-848.118090	-846.016188	-845.659420	-845.730513

Table S4: Continued.

methyl adduct (conformer)	B3LYP/6-31G(d,p)			MP2FC/6- 31G+(2d,p)	MP2(FC)/6-31G+(2d,p)// B3LYP/6-31G(d,p)	
	E_{tot}	H_{298}	G_{298}	E_{tot}	H_{298}	G_{298}
1g -Me (2)	-848.403917	-848.047169	-848.118112	-846.016405	-845.659657	-845.730600
1g -Me (3)	-848.404005	-848.047226	-848.118035	-846.016460	-845.659681	-845.730490
1g -Me (4)	-848.404152	-848.047370	-848.117829	-846.016621	-845.659839	-845.730298
1g -Me (5)	-848.404196	-848.047352	-848.118030	-846.016811	-845.659967	-845.730645
1g -Me (6)	-848.404206	-848.047364	-848.117785	-846.016848	-845.660006	-845.730427
1g -Me (7)	-848.404460	-848.047518	-848.117630	-846.017074	-845.660132	-845.730244
1g -Me (8)	-848.404492	-848.047590	-848.117580	-846.017014	-845.660112	-845.730102
1g -Me (9)	-848.403466	-848.046591	-848.116991	-846.016748	-845.659873	-845.730273
1g -Me (10)	-848.403601	-848.046796	-848.117261	-846.016769	-845.659964	-845.730429
1g -Me (11)	-848.403181	-848.046340	-848.117128	-846.016440	-845.659599	-845.730387
1g -Me (12)	-848.403314	-848.046483	-848.117010	-846.016420	-845.659589	-845.730116
1g -Me ^b	-	-	-	-	-845.659820	-845.730377
1h -Me (1)	-887.300072	-886.858220	-886.937694	-884.702408	-884.260556	-884.340030
1h -Me (2)	-887.300664	-886.859329	-886.937980	-884.702856	-884.261521	-884.340172
1h -Me (3)	-887.299727	-886.858428	-886.937121	-884.702536	-884.261237	-884.339930
1h -Me ^b	-	-	-	-	-884.261105	-884.340044
1i -Me (1)	-1197.036023	-1196.445131	-1196.530723	-1193.548237	-1192.957345	-1193.042937
1i -Me (2)	-1197.034554	-1196.443707	-1196.529949	-1193.545637	-1192.954791	-1193.041033
1i -Me (3)	-1197.034592	-1196.443773	-1196.529815	-1193.545584	-1192.954765	-1193.040807
1i -Me (4)	-1197.036033	-1196.445036	-1196.530130	-1193.548211	-1192.957214	-1193.042308
1i -Me (5)	-1197.034909	-1196.443936	-1196.529713	-1193.546010	-1192.955037	-1193.040814
1i -Me (6)	-1197.033427	-1196.442543	-1196.529223	-1193.543351	-1192.952467	-1193.039147
1i -Me (7)	-1197.033383	-1196.442538	-1196.528842	-1193.543366	-1192.952521	-1193.038825
1i -Me (8)	-1197.034856	-1196.443982	-1196.530423	-1193.546031	-1192.955157	-1193.041598
1i -Me (9)	-1197.034882	-1196.443937	-1196.529813	-1193.546053	-1192.955108	-1193.040984
1i -Me (10)	-1197.033399	-1196.442527	-1196.529253	-1193.543402	-1192.952530	-1193.039256
1i -Me (11)	-1197.033425	-1196.442604	-1196.529298	-1193.543336	-1192.952515	-1193.039209
1i -Me (12)	-1197.034837	-1196.443915	-1196.530375	-1193.546062	-1192.955140	-1193.041600
1i -Me (13)	-1197.036061	-1196.445085	-1196.530146	-1193.548066	-1192.957090	-1193.042151
1i -Me (14)	-1197.034584	-1196.443682	-1196.529774	-1193.545669	-1192.954767	-1193.040859
1i -Me (15)	-1197.034611	-1196.443738	-1196.529605	-1193.545586	-1192.954713	-1193.040580
1i -Me (16)	-1197.036024	-1196.445070	-1196.530845	-1193.548200	-1192.957246	-1193.043021
1i -Me (17)	-1197.035672	-1196.444818	-1196.531143	-1193.547668	-1192.956814	-1193.043139
1i -Me (18)	-1197.034166	-1196.443432	-1196.531552	-1193.544967	-1192.954232	-1193.042352

Table S4: Continued.

methyl adduct (conformer)	B3LYP/6-31G(d,p)			MP2FC/6- 31G+(2d,p)	MP2(FC)/6-31G+(2d,p)// B3LYP/6-31G(d,p)	
	E_{tot}	H_{298}	G_{298}	E_{tot}	H_{298}	G_{298}
1i -Me (19)	-1197.034286	-1196.443457	-1196.530012	-1193.545067	-1192.954238	-1193.040793
1i -Me (20)	-1197.035729	-1196.444829	-1196.530679	-1193.547724	-1192.956824	-1193.042674
1i -Me (21)	-1197.034545	-1196.443711	-1196.530100	-1193.545452	-1192.954618	-1193.041007
1i -Me (22)	-1197.033041	-1196.442243	-1196.529564	-1193.542708	-1192.951911	-1193.039232
1i -Me (23)	-1197.033062	-1196.442330	-1196.529917	-1193.542979	-1192.952247	-1193.039834
1i -Me (24)	-1197.034514	-1196.443718	-1196.530976	-1193.545483	-1192.954687	-1193.041945
1i -Me (25)	-1197.034500	-1196.443686	-1196.530375	-1193.545415	-1192.954600	-1193.041289
1i -Me (26)	-1197.032952	-1196.442217	-1196.530569	-1193.542687	-1192.951951	-1193.040303
1i -Me (27)	-1197.032983	-1196.442270	-1196.530963	-1193.542784	-1192.952071	-1193.040764
1i -Me (28)	-1197.034582	-1196.443705	-1196.529633	-1193.545467	-1192.954590	-1193.040518
1i -Me (29)	-1197.035660	-1196.444830	-1196.530942	-1193.547632	-1192.956802	-1193.042914
1i -Me (30)	-1197.034095	-1196.443243	-1196.529745	-1193.545160	-1192.954307	-1193.040809
1i -Me (31)	-1197.034289	-1196.443451	-1196.529964	-1193.545071	-1192.954233	-1193.040746
1i -Me (32)	-1197.035721	-1196.444818	-1196.530399	-1193.547722	-1192.956820	-1193.042401
1i -Me (33)	-1197.035058	-1196.444109	-1196.529074	-1193.548009	-1192.957060	-1193.042025
1i -Me (34)	-1197.033564	-1196.442694	-1196.528610	-1193.545556	-1192.954686	-1193.040602
1i -Me (35)	-1197.033606	-1196.442755	-1196.528863	-1193.545542	-1192.954691	-1193.040799
1i -Me (36)	-1197.035032	-1196.444080	-1196.529168	-1193.547957	-1192.957005	-1193.042093
1i -Me (37)	-1197.033818	-1196.443042	-1196.529565	-1193.545725	-1192.954949	-1193.041472
1i -Me (38)	-1197.032368	-1196.441626	-1196.528578	-1193.543246	-1192.952504	-1193.039456
1i -Me (39)	-1197.032325	-1196.441578	-1196.530050	-1193.543198	-1192.952452	-1193.040924
1i -Me (40)	-1197.033794	-1196.442985	-1196.529625	-1193.545671	-1192.954862	-1193.041502
1i -Me (41)	-1197.033841	-1196.442974	-1196.528586	-1193.545726	-1192.954859	-1193.040471
1i -Me (42)	-1197.032339	-1196.441569	-1196.528229	-1193.543239	-1192.952469	-1193.039129
1i -Me (43)	-1197.032377	-1196.441565	-1196.528096	-1193.543195	-1192.952383	-1193.038914
1i -Me (44)	-1197.033804	-1196.442924	-1196.528555	-1193.545681	-1192.954801	-1193.040432
1i -Me (45)	-1197.035025	-1196.444062	-1196.529512	-1193.547961	-1192.956998	-1193.042448
1i -Me (46)	-1197.033538	-1196.442672	-1196.529486	-1193.545581	-1192.954715	-1193.041529
1i -Me (47)	-1197.033594	-1196.442690	-1196.528724	-1193.545486	-1192.954583	-1193.040617
1i -Me (48)	-1197.035000	-1196.444026	-1196.529568	-1193.547894	-1192.956920	-1193.042462
1i -Me ^b	-	-	-	-	-1192.954694	-1193.041057

^a For the further calculations, the values with more decimals than indicated in the table were used. The use of the numbers from this table leads to the slightly different results. ^b Averaged values derived using Boltzmann distribution

5. Supplementary Section

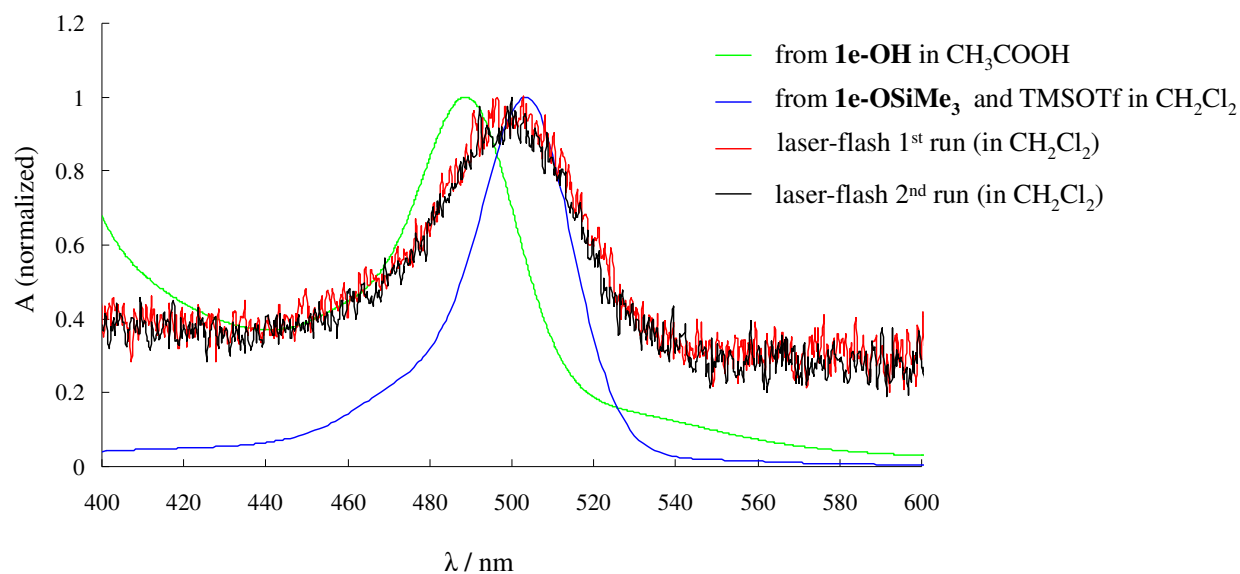


Figure SX1. The UV-vis spectra of cation **1e** generated using different methods.

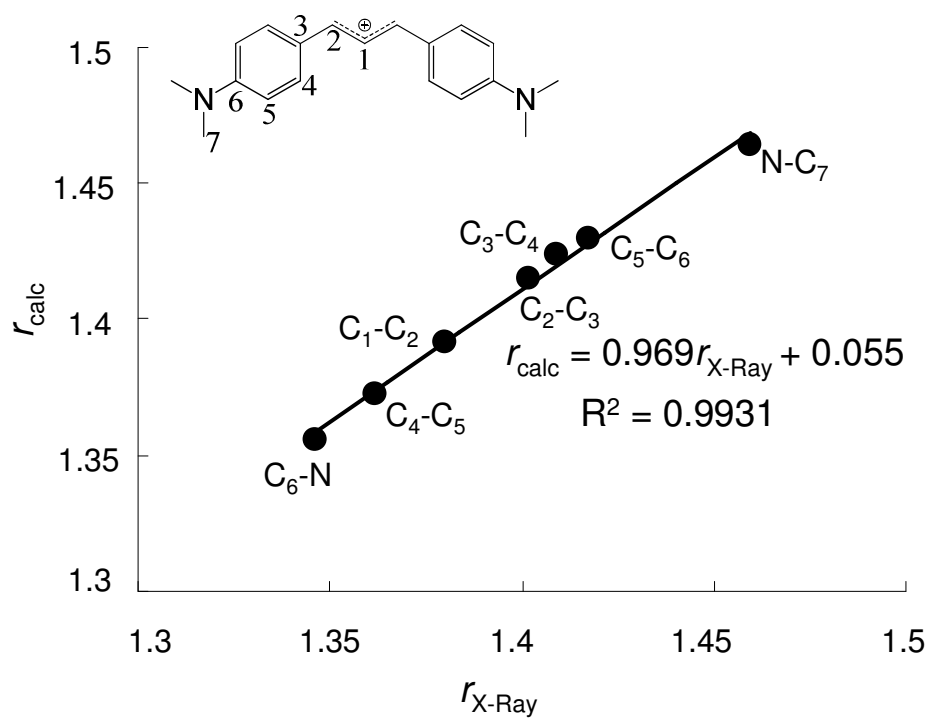


Figure SX2. Calculated averages of gas-phase bond lengths (B3LYP/6-31G(d,p)) in cation **1h** in correlation with the experimental values for the solid state (X-ray).

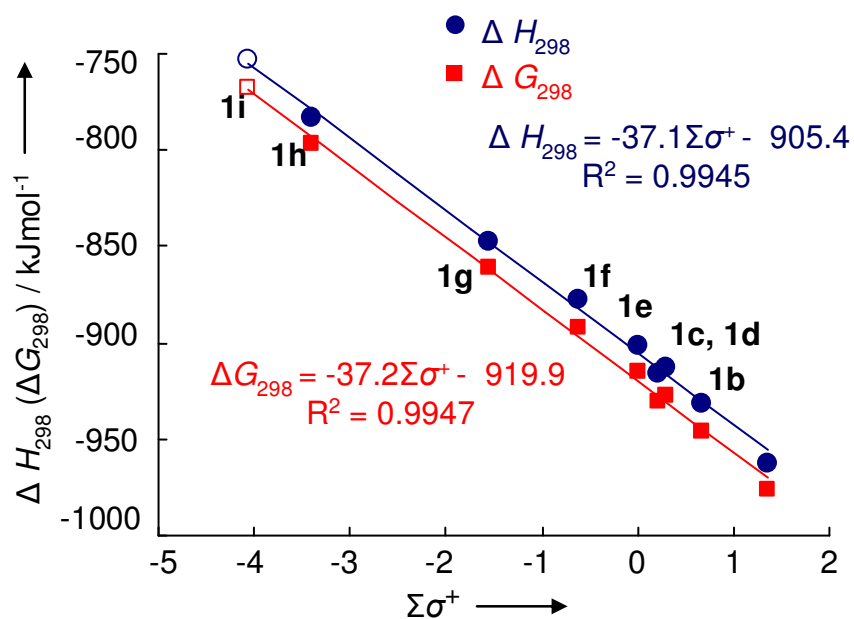


Figure SX3. Correlation between the theoretical gas-phase methyl anion affinities (ΔH_{298} , ΔG_{298}) of the cations **1a-i** and the sum of the sigma parameters of the corresponding substituents. Open symbols: **1i** is not included in the correlation, as σ^+ for the jul moiety was estimated from the electrophilicities of benzhydryl cations.^{8a}

**Table SX1.** The ^1H NMR resonances of compound **3b** compared with those of **3c**.

proton	3b	3c
H _{Ar}	7.15-7.38 (m)	7.16-7.39 (m)
5-H	6.28-6.47 (m)	6.35-6.41 (m)
6-H		
7-H	3.83-3.92 (m)	3.78-3.93 (m)
12-H	2.28-2.48 (m)	2.31-2.44 (m)
14-H	1.94-2.10 (m)	1.65-1.82 (m)
15-H	-	1.34-1.52 (m)
16-H	0.96 (d), 1.03 (d), 1.03(d), 1.08 (d)	0.84 (t), 0.87 (t)
17-H	1.40 (s), 1.48 (s)	1.45 (s), 1.53 (s)

Table SX2. The ^{13}C NMR resonances of compound **3b** compared with those of **3c**.

carbon	3b	3c
C-1		127.11, 127.14
C-11	126.3, 126.4, 127.09, 127.14	126.35, 126.36
C-2	128.69, 128.71	128.67, 128.70
C-3	126.1	126.1
C-4	137.4	137.4, 137.5
C-5	129.1, 129.5	129.3, 129.5
C-6	134.9, 135.1	134.75, 134.81
C-7	45.9, 46.2	46.15, 46.21
C-8	145.1, 145.4	145.0, 145.1
C-9	127.6, 127.7	127.66, 127.67
C-10	128.4, 128.5	128.40, 128.42
C-12	47.7, 48.2	49.5, 49.7
C-13	79.3, 79.5	75.0, 75.1
C-14	38.8, 39.2	46.7, 47.1
C-15	-	18.1
C-16	18.07, 18.12, 18.16, 18.23	14.07, 14.10
C-17	27.7	30.6, 30.8



Table SX3. The characteristic ^1H NMR resonances of compound **3n** (mixture of diastereomers) compared with those of two isolated diastereomers of **3n'**.

proton	3n -dia1	3n -dia2	3n' -dia1	3n' -dia2
1-H, 13-H	2.90, 2.93, 2.93, 2.94 (4 × s)		2.91, 2.92 (2 × s)	2.91, 2.94 (2 × s)
6-H	6.30 (d)	6.49 (d)	6.16-6.26 (m)	6.35 (d)
7-H	5.93 (dd)	6.18 (dd)		6.03 (dd)

Table SX4. The characteristic ^{13}C NMR resonances of compound **3n** (mixture of diastereomers) compared with those of two isolated diastereomers of **3n'**.

carbon	3n -dia1	3n -dia2	3n' -dia1	3n' -dia2
C-1, C-13	40.6, 40.7, 40.78, 40.82		40.6, 40.7	40.6, 40.7
C-6	131.6	133.5	129.5	130.4
C-7	124.8	124.0	128.2	127.5
C-8	51.7	50.8	47.4	47.5
C-14	48.0	48.9	56.3	56.0
C-15	195.6, 195.7		213.8	212.5

The numeration of the diastereomers of compound **3n** may not correspond to those of **3n'**, i. e., the diastereomer 1 of **3n** may produce diastereomer 2 of **3n'**.



Table SX5. The characteristic ^1H NMR resonances of compound **3o** (mixture of diastereomers) compared with those of two isolated diastereomers of **3o'**.

proton	3o -dia1	3o -dia2	3o' -dia1	3o' -dia2
1-H, 13-H	2.93, 2.93, 2.94, 2.95 (4 × s)		2.91, 2.94 (2 × s)	2.93, 2.93 (2 × s)
6-H	6.31 (d)	6.42 (d)	6.31-6.38 (m)	6.31 (d)
7-H	6.06 (dd)	6.20 (dd)		6.16 (dd)

Table SX6. The characteristic ^{13}C NMR resonances of compound **3o** (mixture of diastereomers) compared with those of two isolated diastereomers of **3o'**.

carbon	3o -dia1	3o -dia2	3o' -dia1	3o' -dia2
C-1, C-13	40.6, 40.7, 40.80, 40.83		40.6, 40.7	40.6, 40.8
C-6	132.0	133.3	129.5	131.5
C-7	125.4	123.7	127.9	125.5
C-8	51.3	50.2	46.6	46.9
C-14	52.0	52.3	54.0	55.1
C-15	198.4, 198.7		220.2	219.9

The numeration of the diastereomers of compound **3o** may not correspond to those of **3o'**, i. e., the diastereomer 1 of **3o** may produce diastereomer 2 of **3o'**.

All assignments are made based on analysis of COSY, HSQC and HMBC spectra of the corresponding compounds.

6. References

- (1) (a) DeWolfe, R. H.; Young, W. G. *Chem. Rev.* **1956**, *56*, 753–901. (b) Magid, R. M. *Tetrahedron* **1980**, *36*, 1901–1930. (c) Marshall, J. A. *Chem. Rev.* **1989**, *89*, 1503–1511.
- (2) (a) Bordwell, F. G. *Acc. Chem. Res.* **1970**, *3*, 281–290. (b) Bordwell, F. G.; Mecca, T. G. *J. Am. Chem. Soc.* **1972**, *94*, 5829–5837.
- (3) (a) Bordwell, F. G.; Schexayder, D. A. *J. Org. Chem.* **1968**, *33*, 3240–3246. (b) Bordwell, F. G.; Mecca, T. G. *J. Am. Chem. Soc.* **1972**, *94*, 5825–5829.
- (4) Goering, H. L.; Anderson, R. P. *J. Am. Chem. Soc.* **1978**, *100*, 6469–6474 and references therein.
- (5) (a) Minegishi, S.; Loos, R.; Kobayashi, S.; Mayr, H. *J. Am. Chem. Soc.* **2005**, *127*, 2641–2649. (b) Mayr, H.; Ofial, A. R. *Pure Appl. Chem.* **2009**, *81*, 667–683.
- (6) Phan, T. B.; Nolte, C.; Kobayashi, S.; Ofial, A. R.; Mayr, H. *J. Am. Chem. Soc.* **2009**, *131*, 11392–11401.
- (7) Mayr, H. *Angew. Chem., Int. Ed.* **2011**, *50*, 3612–3618.
- (8) (a) Mayr, H.; Bug, T.; Gotta, M. F.; Hering, N.; Irrgang, B.; Janker, B.; Kempf, B.; Loos, R.; Ofial, A. R.; Remennikov, G.; Schimmel, H. *J. Am. Chem. Soc.* **2001**, *123*, 9500–9512. (b) Lucius, R.; Loos, R.; Mayr, H. *Angew. Chem., Int. Ed.* **2002**, *41*, 91–95. (c) Mayr, H.; Kempf, B.; Ofial, A. R. *Acc. Chem. Res.* **2003**, *36*, 66–77.
- (9) Theoretical treatments of the reactivity parameters: (a) Schindele, C.; Houk, K. N.; Mayr, H. *J. Am. Chem. Soc.* **2002**, *124*, 11208–11214. (b) Wang, C.; Fu, Y.; Guo, Q.-X.; Liu, L. *Chem.—Eur. J.* **2010**, *16*, 2586–2598. (c) Perez, P.; Domingo, L. R.; Aizman, A.; Contreras, R. *Theor. Comput. Chem.* **2007**, *19*, 139–201 and references therein.
- (10) For a database of reactivity parameters E , N , and s_N : www.cup.lmu.de/oc/mayr/DBintro.html.
- (11) (a) Trost, B. M.; Van Vranken, D. L. *Chem. Rev.* **1996**, *96*, 395–422. (b) Trost, B. M. *Chem. Pharm. Bull.* **2002**, *50*, 1–14. (c) Trost, B. M.; Crawley, M. L. *Chem. Rev.* **2003**, *103*, 2921–2943.
- (12) Emer, E.; Sinisi, R.; Capdevila, M. G.; Petruzzello, D.; De Vincentiis, F.; Cozzi, P. G. *Eur. J. Org. Chem.* **2011**, 647–666.
- (13) Ammer, J.; Mayr, H. *Macromolecules* **2010**, *43*, 1719–1723.
- (14) Abraham, R. J.; Fisher, S.; Loftus, P. *Introduction to NMR Spectroscopy*: Chichester, Wiley, 1988.

- (15) CCDC 297424 contains the supplementary crystallographic data for **1h**-BF₄ reported in this paper. These data can be obtained free of charge from the Cambridge Crystallographic Data Centre via www.ccdc.cam.ac.uk/data_request/cif.
- (16) Sanz, R.; Martines A.; Miguel, D.; Alvarez-Gutierrez, J. M.; Rodriguez, F. *Adv. Synth. Catal.* **2006**, *348*, 1841–1845.
- (17) Rys, P. *Acc. Chem. Res.* **1976**, *9*, 345–351.
- (18) (a) Mayr, H.; Schneider, R.; Schade, C.; Bartl, J.; Bederke, R. *J. Am. Chem. Soc.* **1990**, *112*, 4446–4454. (b) Hagen, G.; Mayr, H. *J. Am. Chem. Soc.* **1991**, *113*, 4954–4961.
- (19) "What'sBest! 4.0 Commercial" by Lindo Systems Inc.
- (20) Mayr H.; Müller, K.-H.; Ofial, A. R.; Bühl, M. *J. Am. Chem. Soc.* **1999**, *121*, 2418–2424.
- (21) Mayr, H.; Fichtner, C.; Ofial, A. R. *J. Chem. Soc., Perkin Trans. 2* **2002**, 1435–1440.
- (22) Nubbemeyer, U. *Synthesis* **2003**, 961–1008.
- (23) Miranda, M. A.; Pérez-Prieto, J.; Font-Sanchis, E.; Kónya, K.; Scaiano, J. C. *J. Phys. Chem. A* **1998**, *102*, 5724–5727.
- (24) Minegishi, S.; Kobayashi, S.; Mayr, H. *J. Am. Chem. Soc.* **2004**, *126*, 5174–5181.
- (25) Hansch, C.; Leo, A.; Taft, R. W. *Chem. Rev.* **1991**, *91*, 165–195.
- (26) Wei, Y.; Singer, T.; Mayr, H.; Sastry, G. N.; Zipse, H. *J. Comput. Chem.* **2008**, *29*, 291–297.
- (27) Horn, M.; Mayr, H. *Chem.—Eur. J.* **2010**, *16*, 7478–7487.
- (28) a) Olah, G. A.; Prakash, G. K. S.; Arvanaghi, M. *Synthesis* **1984**, 228–230. b) Samples taken from the reaction mixture were quenched with a solution of iodine in THF. The resulting mixture was dissolved in diethyl ether, washed with aqueous sodium thiosulfate solution, and dried (MgSO₄). GC–MS analysis showed slow disappearance of 1-bromo-3,5-difluorobenzene while the peak of the product of the reaction of the in situ generated (3,5-difluorophenyl)magnesium chloride with iodine, that is, 1,3-difluoro-5-iodobenzene, increased with time.
- (29) SDBSWeb: <http://riodb01.ibase.aist.go.jp/sdbs/> (National Institute of Advanced Industrial Science and Technology, 26.10.2010), SDBS No. 41165, Spectral Code HR2002-00194TS.
- (30) Jones, P. R.; Shelnut, J. G. *J. Org. Chem.* **1979**, *44*, 696–699.
- (31) Manolov, I.; Danchev, N. D. *Arch. Pharm.* **2003**, *336*, 83–94.
- (32) Dickinson, J. M.; Murphy, J. A.; Patterson, C. W.; Wooster, N. F. *J. Chem. Soc., Perkin Trans. 1* **1990**, 1179–1184.

- (33) Hayashi, T.; Yamamoto, A.; Yoshihiko, I.; Nishioka, E.; Miura, H.; Yanagi, K. *J. Am. Chem. Soc.* **1989**, *111*, 6301–6311.
- (34) Quinkert, G.; Schmalz, H.-G.; Walzer, E.; Gross, S.; Kowalczyk-Przewloka, T.; Schierloh, C.; Dürner, G.; Bats, J. W.; Kessler, H. *Liebigs Ann. Chem.* **1988**, 283–315.
- (35) Nudelman, N. S.; García, G. V. *J. Org. Chem.* **2001**, *66*, 1387–1394.
- (36) Pivnenko, N. S.; Grin, L. M.; Lavrushina, O. V.; Pedchenko, N. F.; Lavrushin, V. F., *Theor. Exp. Chem*, **1976**, *11*, 525-529.
- (37) Brieskorn, C.-H.; Otteneder, H. *Chem. Ber.* **1970**, *103*, 363–368.
- (38) Aizensutatsuto, A.; Haamorin, J. Jpn. Kokai Tokkyo Koho 1993, JP 05221932.
- (39) Wang, H.; Lu, Z.; Lord, S. J.; Willets, K. A.; Bertke, J. A.; Bunge, S. D.; Moerner, W. E. Twieg, R. J. *Tetrahedron* **2007**, *63*, 103–114.
- (40) Battistuzzi, G.; Cacchi, S.; Fabrizi, G. *Org. Lett.* **2003**, *5*, 777–780.
- (41) Coe, B. J.; Foxon, S. P.; Harper, E. C.; Harris, J. A.; Helliwell, M.; Raftery, J.; Asselberghs, I.; Clays, K.; Franz, E.; Brunshwig, B. S.; Fitch A. G. *Dyes Pigm.* **2009**, *82*, 171–186.
- (42) Mayr, H.; Pock, R. *Chem. Ber.* **1986**, *119*, 2473–2496 and references therein.
- (43) Liu, Y.; Yao, B.; Deng, C.-L.; Tang R.-Y.; Zhang, X.-G.; Li, J.-H. *Org. Lett.* **2011**, *13*, 1126–1129.
- (44) Kanzian, T.; Nigst, T. A.; Maier, A.; Pichl, S.; Mayr, H. *Eur. J. Org. Chem.* **2009**, 6379–6385.
- (45) Bug, T.; Mayr, H. *J. Am. Chem. Soc.* **2003**, *125*, 12980–12986.
- (46) Gaussian 03, Revision D.01, Frisch, M. J.; Trucks, G. W.; Schlegel, H. B.; Scuseria, G. E.; Robb, M. A.; Cheeseman, J. R.; Montgomery, J. A., Jr.; Vreven, T.; Kudin, K. N.; Burant, J. C.; Millam, J. M.; Iyengar, S. S.; Tomasi, J.; Barone, V.; Mennucci, B.; Cossi, M.; Scalmani, G.; Rega, N.; Petersson, G. A.; Nakatsuji, H.; Hada, M.; Ehara, M.; Toyota, K.; Fukuda, R.; Hasegawa, J.; Ishida, M.; Nakajima, T.; Honda, Y.; Kitao, O.; Nakai, H.; Klene, M.; Li, X.; Knox, J. E.; Hratchian, H. P.; Cross, J. B.; Bakken, V.; Adamo, C.; Jaramillo, J.; Gomperts, R.; Stratmann, R. E.; Yazyev, O.; Austin, A. J.; Cammi, R.; Pomelli, C.; Ochterski, J. W.; Ayala, P. Y.; Morokuma, K.; Voth, G. A.; Salvador, P.; Dannenberg, J. J.; Zakrzewski, V. G.; Dapprich, S.; Daniels, A. D.; Strain, M. C.; Farkas, O.; Malick, D. K.; Rabuck, A. D.; Raghavachari, K.; Foresman, J. B.; Ortiz, J. V.; Cui, Q.; Baboul, A. G.; Clifford, S.; Cioslowski, J.; Stefanov, B. B.; Liu, G.; Liashenko, A.; Piskorz, P.; Komaromi, I.; Martin, R. L.; Fox, D. J.; Keith, T.; Al-Laham, M. A.; Peng, C. Y.; Nanayakkara, A.; Challacombe, M.;

Gill, P. M. W.; Johnson, B.; Chen, W.; Wong, M. W.; Gonzalez, C.; Pople, J. A.; Gaussian, Inc.: Wallingford, CT, 2004.

Chapter 4. Ion Pair Dynamics: Solvolyses of Chiral 1,3-Diarylallyl Carboxylates as a Case Study

Konstantin Troshin and Herbert Mayr

J. Am. Chem. Soc., submitted.

1. Introduction

Control of enantioselectivity by noncovalent interactions has become a major tool in organic synthesis. In particular hydrogen bonding, as in thiourea-catalyzed reactions,¹ and ion-pairing² have extensively been used for stereoselective transformations. An early example for the use of ion-pairing in asymmetric synthesis was reported by Dolling et al.,³ who found that a cinchona-derived quaternary ammonium ion salt can be employed as catalyst for the asymmetric methylation of a substituted indanone under phase-transfer conditions. This pioneering work opened the field of asymmetric phase-transfer catalysis, the scope of which has widely been elaborated by Maruoka and associates.⁴ Protonation of organic substrates by strong chiral Brønsted acids, in particular BINOL-derived phosphoric acid diesters and their derivatives, gives rise to chiral ion pairs or similar structures, which served as chiral electrophiles in a manifold of reactions,⁵ including enantioselective cycloadditions,⁶ electrocyclic reactions,⁷ 1,4-additions,⁸ Friedel-Crafts allylations,⁹ reductions,¹⁰ and ene reactions.¹¹ Hydrogen bonding between the resulting cation and the chiral counteranion often provides additional stabilization of the positively charged electrophilic intermediate and accounts for the augmented enantioselectivity. In some cases it is difficult to differentiate whether chirality is induced by ion-pairing of an achiral cationic electrophile with a chiral counteranion or by activation of neutral electrophiles (e. g., imines or carbonyl compounds) through hydrogen bonding with a chiral Brønsted acid.¹²

However, treatment of prochiral substrates with strong chiral Brønsted acids is not the only method to generate chiral ion pairs for asymmetric counterion-directed synthesis.^{2,13} Ion-pairing was also employed in enantioselective iminium-activated reactions by using achiral ammonium ions with chiral counterions¹⁴ as well as in various asymmetric transition-metal-catalyzed reactions, which utilized the directing effect of chiral counteranions.¹⁵ Ooi demonstrated that transition metal complexes with achiral ligands carrying a quaternary onium moiety can electrostatically be bound to chiral anions to induce asymmetrical palladium catalysis.¹⁶ The general importance of ion-pairing in transition metal-catalyzed

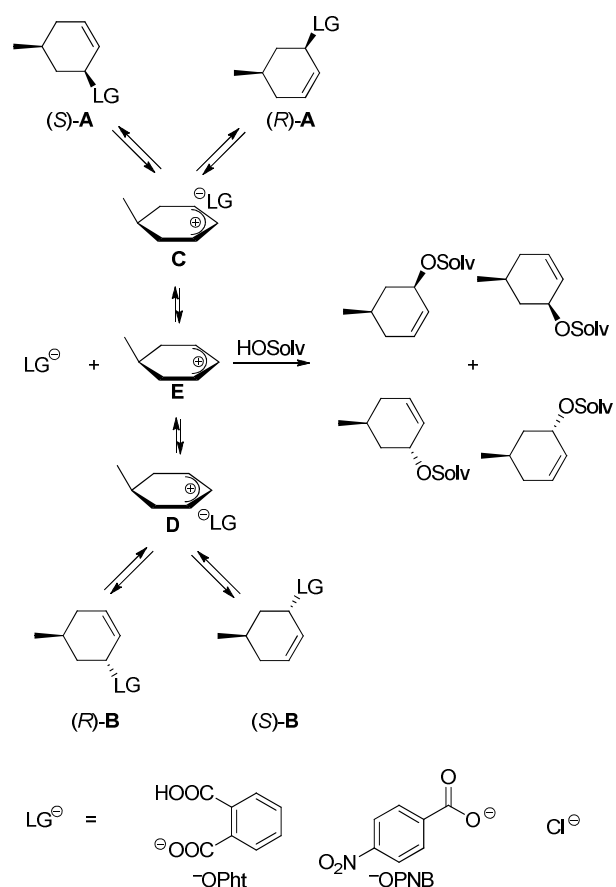
reactions has been reviewed by Macchioni who suggested that ion-pairing should be considered as one of the instruments for tuning catalytic processes.¹⁷

Enantioselective catalysis was furthermore achieved by combining ion-pairing with hydrogen bonding. Examples are reactions catalyzed by chiral ureas which are coordinated to achiral counterions¹⁸ as well as cooperative catalysis, where hydrogen bonding was used to link the complex counterion to the active intermediate, thus providing additional attractive forces within the ion pair.^{19,20}

While the targeted use of ion-pairing in enantioselective synthesis thus reflects recent developments, the importance of ion-pairing for organic reactivity has already been recognized in the 1950s by Winstein and coworkers. Their studies of S_N1 solvolyses²¹ provide the basis of our current understanding of ion pairs and their reactivities.²² Because of their ability to undergo allylic rearrangements, allyl derivatives turned out to be particularly valuable systems for gaining insight in the nature and reactivities of ion pairs.^{21a,22,23} Goering's pioneering investigations of the transformations of optically active allyl derivatives by titrimetric and polarimetric methods as well as product analyses including isotope exchange experiments have become text-book examples²⁴ to demonstrate the role of ion-pairing in S_N1 reactions.

Since the *cis/trans* isomerization of optically active *cis*- and *trans*-5-methylcyclohex-2-enyl 2-carboxybenzoates (**A** \rightleftharpoons **B**, LG = OPht, Scheme 1) in acetonitrile was found to proceed significantly more slowly than the racemization ((*S*)-**A** \rightleftharpoons (*R*)-**A**; (*S*)-**B** \rightleftharpoons (*R*)-**B**),²⁵ Goering proposed the formation of ion pair intermediates (**C**, **D**), in which the anion remains on the same face of the allyl cation as in the substrate. The collapse of these ion pairs (internal return) either regenerates the starting materials or leads to their enantiomers by attack of the anion at the other allylic terminus. The *cis/trans*-isomerization, which requires the migration of the leaving group to the other face of the allyl cation, was proposed to proceed via dissociation of the initial ion pairs to an achiral carbocationic intermediate (**E**) that can be attacked by the leaving group from both faces (Scheme 1).²⁵

Scheme 1. Ion Pair Mechanism Proposed by Goering for Solvolyses and Rearrangements of *cis*- and *trans*-5-Methyl-cyclohex-2-enyl Derivatives^a



^a The descriptors (*R*) and (*S*) for the configuration of C-5 (connected to the methyl group) are omitted.

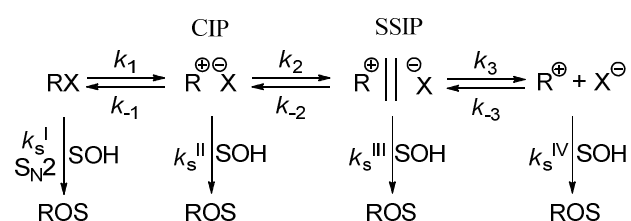
The hydrolyses of *cis*- and *trans*-5-methylcyclohex-2-enyl 2-carboxybenzoates (**A**, **B**, LG = OPht)²⁶ and 4-nitrobenzoates (**A**, **B**, LG = OPNB)²⁷ in aqueous acetone as well as the ethanolyses and acetolyses of *cis*- and *trans*-5-methylcyclohex-2-enyl chlorides (**A**, **B**, LG = Cl)²⁸ were rationalized on the basis of this mechanism. In none of these cases *cis/trans* isomerization of the non-reacted substrates was detected, and the polarimetric rate constant (racemization plus solvolysis) was always larger (factor of 1.1 to 5.07) than the titrimetric rate constant (solvolysis only).

In contrast to the situation described for symmetrical allyl systems in Scheme 1, racemization of unsymmetrical allyl derivatives implies migration of the leaving group to the other face of the allyl cation. As solvolyses of *trans*-3-methyl-1-phenylallyl and *trans*-1-methyl-3-phenylallyl 4-nitrobenzoates in aqueous acetone were later observed to be accompanied by approximately 70% racemization of the unsolvolyzed esters, Goering concluded that the previously investigated stereochemical behavior of cyclohexenyl derivatives (Scheme 1) was

largely dominated by conformational phenomena, which are absent in acyclic derivatives.²⁹ The stereochemistry of S_N1 reactions of acyclic allyl derivatives, which is crucial for the understanding of ion-pairing in general, has, therefore, not conclusively been clarified up to the present time.

Winstein's ion pair mechanism (Scheme 2),³⁰ which has commonly been used to rationalize the course of solvolysis reactions through the intermediacy of contact ion pairs (CIP), solvent separated ion pairs (SSIP), and free ions, has recently been employed to interpret the picosecond dynamics of laser-flash-generated contact ion pairs.

Scheme 2. Classical Winstein Scheme for Solvolysis Reactions.³⁰



It is commonly assumed that such photolytically generated contact ion pairs, which may either be formed directly as the initial cleavage products or through electron transfer in the initially generated geminate radical pairs, are similar to the intermediates in solvolysis reactions.³¹ Vice versa, the rates measured for geminate recombinations of laser-flash photolytically generated ion pairs, were used to discuss structural effects on the rates of internal return during the solvolytic reactions.³²

However, Winstein's solvolysis scheme includes many parameters which could not be unambiguously differentiated with the analytical methods available at that time so that many questions remained open. It is still unclear, for example, whether solvolysis and internal return proceed through the same intermediates or are two independent processes involving different types of ion pairs.³³

A crucial step toward a quantitative description of solvolysis reactions, and of nucleophilic aliphatic substitutions in general, were the investigations of Jencks, Richard, and Tsuji,³⁴⁻³⁶ who used clock-methods to determine rate constants for the attack of solvents on the intermediate carbocations. These authors were not only able to identify the change from S_N1 to S_N2 mechanisms³⁴ but also clarified the dynamics of ion pair dissociation³⁵ and recombination.³⁶

By introducing stopped-flow techniques for determining rates of solvolysis reactions, which occur in the millisecond to second time domain,³⁷ and systematic extension of the data set for

the rates of the reactions of carbocations with solvents³⁸ and other nucleophiles,³⁹ we arrived at linear free energy relationships,^{39,40} which allow one to predict changes of solvolysis mechanisms as the substrates and solvents are altered.⁴¹ Under the same conditions, increasing stabilization of the carbocations led to the change from S_N2 reactions, over S_N1 reactions without and with common ion return, to S_N2C⁺ processes (formation of carbocation occurs faster than its reaction with the solvent) and heterolytic cleavages of esters which proceed with formation of persistent carbocations.⁴¹ Furthermore, we have recently employed femtosecond spectroscopy to investigate the dynamics of free and paired carbocations on the picosecond time scale in collaboration with the Riedle group.⁴²

Combination of all these techniques has provided detailed information about the whole range of carbocation reactivities^{37,43} – from very slow reactions to those occurring within ion pairs which proceed at rates approaching vibrational frequencies. On the other hand, our knowledge about structures and dynamics of intramolecular interconversions of ion pairs has remained crude.

We, therefore, approached the dynamics of ion pair transformations by taking advantage of the special properties of allylic derivatives described above. While titrimetry and polarimetry were the most important analytical tools available to Goering for studying the course of the solvolysis reactions, we now employed chiral HPLC techniques to obtain unprecedented insights in the course of S_N1 reactions and ion-pairing.

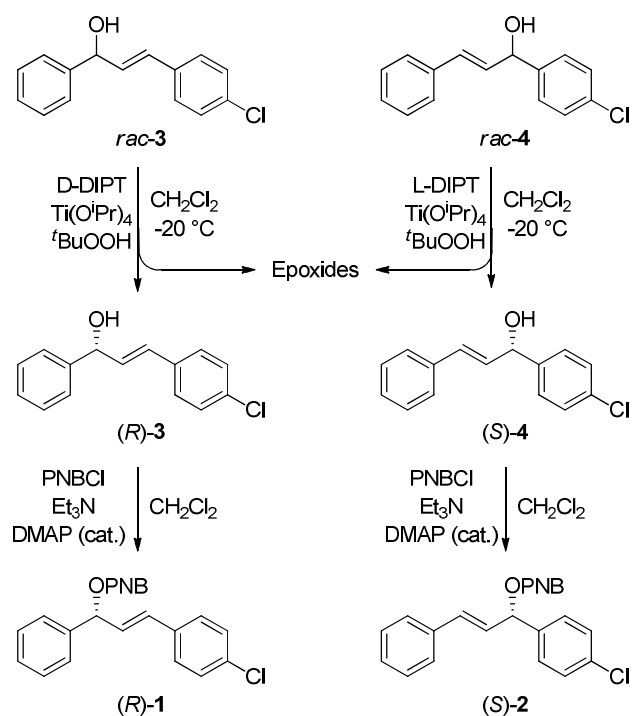
When the enantiopure esters (*R*)-**1** or (*S*)-**2** were dissolved in aqueous acetone (for structures see Scheme 3), mixtures of four isomeric allyl alcohols (hydrolysis products) and of four isomeric allyl 4-nitrobenzoates (starting material and products of ion recombination) were obtained. As we succeeded in separating these eight compounds by HPLC, it was possible to follow the concentrations of each of these individual compounds as a function of time and develop a kinetic model, which quantitatively describes the whole mechanistic scheme.

2. Results

2.1. Synthesis and Chromatographic Separation of the Model Compounds

The regioisomeric alcohols *rac*-**3** and *rac*-**4** were obtained by NaBH₄ reduction of the corresponding chalcones according to ref 44. Sharpless kinetic resolution⁴⁵ of (*rac*)-**3** and *rac*-**4** using D- or L-diisopropyltartrate (D-/L-DIPT), respectively, followed by treatment with 4-nitrobenzoyl chloride in the presence of triethylamine and recrystallization gave the enantiopure (ee > 99%, HPLC) allylic esters (*R*)-**1** and (*S*)-**2** (Scheme 3).

Scheme 3. Synthesis of the Enantiopure Allylic Esters (*R*)-**1** and (*S*)-**2** (PNB = 4-nitrobenzoyl, DIPT = diisopropyltartrate, DMAP = 4-(dimethylamino)pyridine).



As treatment of either (*R*)-**1** or (*S*)-**2** with aqueous acetone may give a mixture of four esters [(*R*)-**1**, (*S*)-**1**, (*R*)-**2**, and (*S*)-**2**] and of four alcohols [(*R*)-**3**, (*S*)-**3**, (*R*)-**4**, and (*S*)-**4**], a complete analysis of the solvolysis mechanism requires monitoring of the concentrations of eight compounds.

Figure 1 shows that mixtures of the racemic compounds **1–4** can be resolved using chiral HPLC (eight peaks in total), which gives the unique possibility of following the time-dependent concentrations of the individual enantiomers.

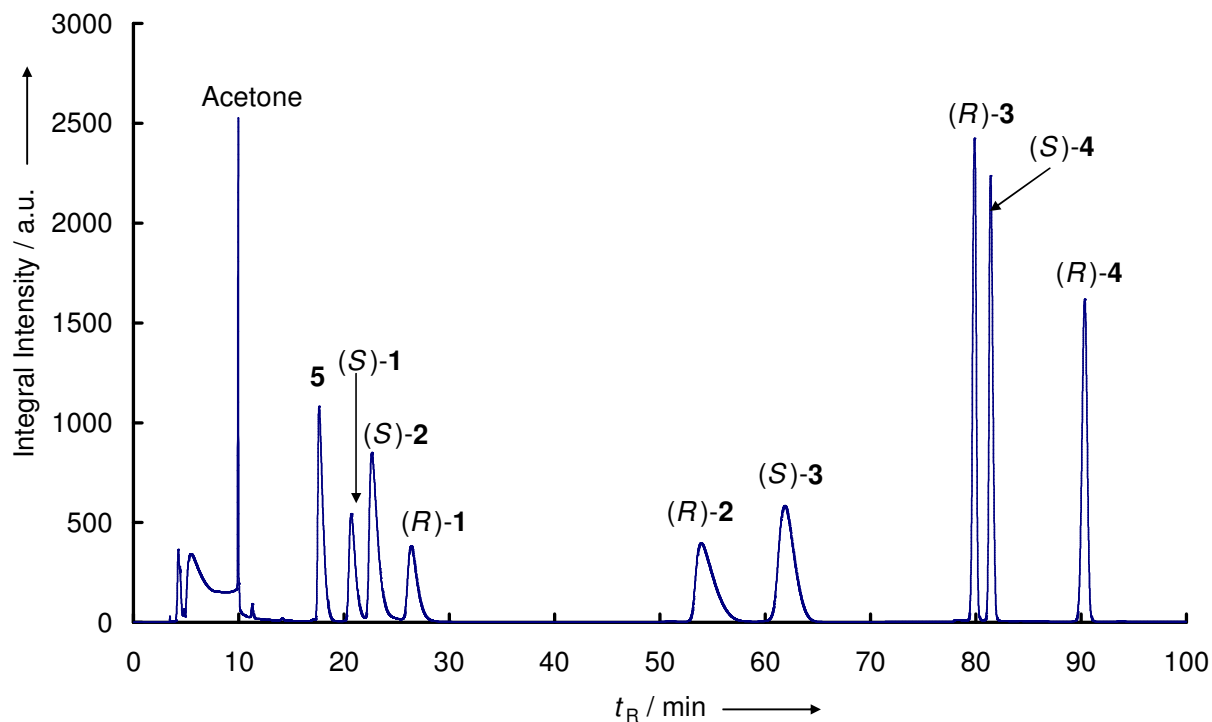


Figure 1. Chromatogram of an artificial mixture of racemic **1–4** and (*E*)-1-(4-methylphenyl)-3-phenylprop-2-en-1-one (**5**) (internal standard). Details of the HPLC method are described in the Experimental Section.

2.2. Kinetic Experiments

General. The 4-nitrobenzoates **1** and **2** were solvolyzed in aqueous acetone at 25 °C with and without addition of various nucleophiles (the experiments are summarized in Table 1).

Table 1. Summary of the HPLC kinetic experiments.

entry	solvent	substrate	[substrate] ₀ /M	additive	[additive] ₀ /M
1	60 % aq acetone	(<i>R</i>)- 1	1.53×10^{-3}	-	-
2	60 % aq acetone	(<i>R</i>)- 1	8.04×10^{-4}	Bu ₄ NOPNB ^a	4.82×10^{-3}
3	60 % aq acetone	(<i>R</i>)- 1	7.82×10^{-4}	Bu ₄ NOPNB ^a	5.25×10^{-2}
4	60 % aq acetone	(<i>R</i>)- 1	8.04×10^{-4}	NaN ₃	7.08×10^{-2}
5	60 % aq acetone	(<i>R</i>)- 1	1.02×10^{-3}	Bu ₄ NCl	1.87×10^{-2}
6	60 % aq acetone	(<i>R</i>)- 1	8.51×10^{-4}	Bu ₄ NCl	1.01×10^{-1}
7	60 % aq acetone	(<i>R</i>)- 1	8.70×10^{-4}	Piperidine	5.42×10^{-2}
8	60 % aq acetone	(<i>R</i>)- 1	8.61×10^{-4}	LiClO ₄	9.46×10^{-3}
9	60 % aq acetone	(<i>S</i>)- 2	7.85×10^{-4}	-	-
10	60 % aq acetone	(<i>S</i>)- 2	7.90×10^{-4}	NaN ₃	7.66×10^{-2}
11	80 % aq acetone	(<i>R</i>)- 1	7.72×10^{-4}	-	-
12	90 % aq acetone	(<i>R</i>)- 1	6.82×10^{-4}	-	-

^a Tetrabutylammonium 4-nitrobenzoate

Aliquots of the reaction mixtures were extracted with dichloromethane or diethyl ether after certain time intervals followed by HPLC analysis. A typical chromatogram obtained during such an experiment is shown in Figure S1 of the Experimental Section (p 132). By using (*E*)-1-(4-methylphenyl)-3-phenylprop-2-en-1-one (**5**) as internal standard, we have determined the time-dependent yields for all compounds present in the mixture.

Solvolyses of (*R*)-1** and (*S*)-**2** in 60% Aqueous Acetone.** Figure 2 shows that both regioisomeric alcohols **3** and **4** are formed as racemates during the solvolysis of (*R*)-**1** in 60% aq acetone. The marginal separation of the graphs for (*R*)-**3** and (*S*)-**3** can be explained by the different shapes of their HPLC signals, and the drift of the baseline caused by the gradient used to shorten the overall elution time. As no isomerization was detectable within 2.75 h when (*S*)-**4** was dissolved in 60% aq acetone containing 2 mM of 4-nitrobenzoic acid (the highest concentration of the acid which can be present at the end of the solvolyses under the experimental conditions used), one can exclude enantioselective formation of **3** and **4** and subsequent isomerization. In line with this observation, the ratio $[3]/[4] = 1.5$ remained constant throughout the reaction. An S_N2 mechanism as well as nucleophilic trapping of the chiral contact ion pairs (CIPs) by water prior to racemization (steps with k_s^I and k_s^{II} in the classical Winstein scheme³⁰) can, therefore, be excluded for this system: both pathways would

result in the formation of enantioenriched products (complete or partial inversion of the configuration).

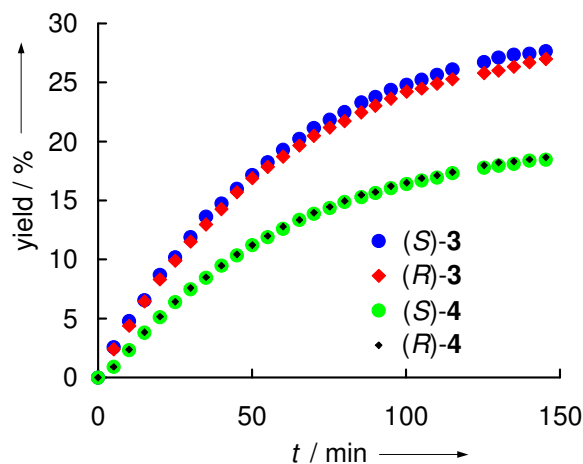


Figure 2. Time-dependent yields of **3** and **4** during the solvolysis of (*R*)-**1** (1.5 mM) in 60% aqueous acetone at 25°C.

Figure 3 shows that the consumption of (*R*)-**1** does not only lead to the formation of the hydrolysis products **3** and **4** discussed above but also to the intermediate appearance of the isomeric 4-nitrobenzoates (*S*)-**2**, (*S*)-**1**, and (*R*)-**2**.

The prevailing formation of (*S*)-**2** indicates that the leaving group stays preferentially at the same face of the plane of the allyl cation which implies that allylic rearrangement occurs predominantly at the contact ion pair stage.

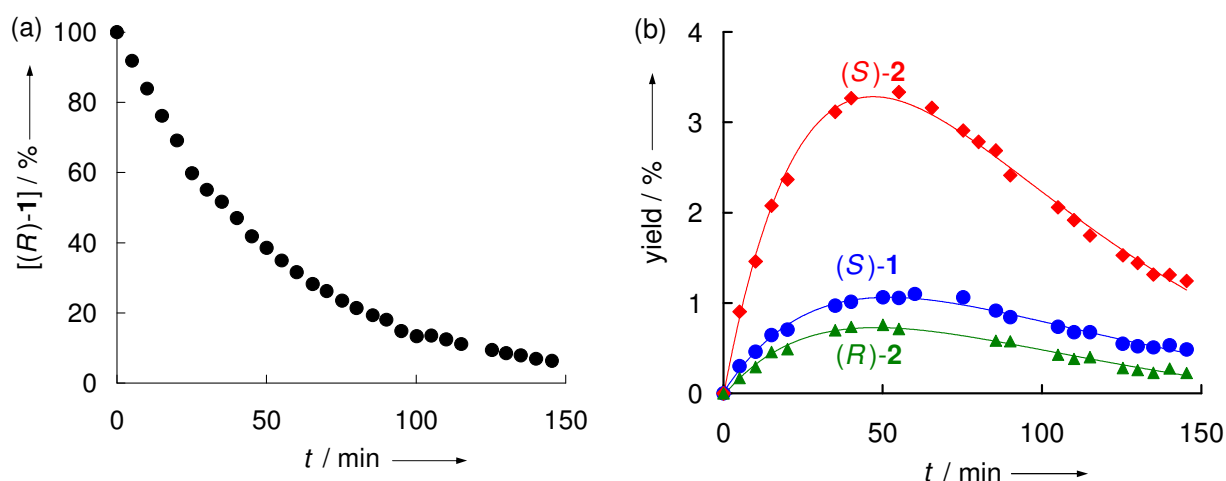


Figure 3. Time-dependent yields of (a) (*R*)-**1** and (b) (*S*)-**2**, (*S*)-**1**, and (*R*)-**2** during solvolysis of (*R*)-**1** (1.5 mM) in 60% aq acetone, 25 °C.

Solvolysis of (*S*)-**2** in 60% aqueous acetone followed exactly the same pattern as the solvolysis of (*R*)-**1** in the same solvent. Both alcohols **3** and **4** were formed as racemates, and the ratio $[3]/[4] = 1.5$ is the same as in the solvolysis of (*R*)-**1**. One can, therefore, conclude that the same achiral intermediates are responsible for the formation of the alcohols **3** and **4** from both precursors **1** and **2**. As addition of 9.5 mM LiClO₄ had no noticeable effect on the time-dependent concentrations of **1-4** during the solvolysis of (*R*)-**1** in 60% aq acetone (see pp 164–165 of the Experimental Section), the participation of SSIPs cannot play a significant role (otherwise special salt effect³⁰ would be expected). Therefore, the alcohols **3** and **4** must be formed via the free 1-(4-chlorophenyl)-3-phenylallylium ions (**6**) or through ion pairs which interconvert more rapidly via **6** than they react with water. The preferred formation of **3** over **4** can be explained by the charge distribution in **6** and does not reflect the relative thermodynamic stabilities of **3** and **4** (a ratio of $[3]/[4] = 0.88$ was obtained by equilibration in the presence of *p*-toluenesulfonic acid, see p 174 for details). According to NBO calculations (p 211 for details), the positive charge is greater on the phenyl-substituted allyl terminus of the 1,3-diarylallyl cation, as phenyl stabilizes carbocations better than 4-chlorophenyl. These observations are consistent with results obtained by Easton et al. for other unsymmetrical allyl derivatives.⁴⁶ The stereospecificity of the allylic rearrangement of (*S*)-**2** in 60% aqueous acetone is also analogous to the previous case: (*R*)-**1** is the major isomerization product followed by (*S*)-**1** and (*R*)-**2** (Figure S30 of the Experimental Section, p 167).

Solvolysis of (*R*)-1** in 80 and 90% Aqueous Acetone.** The rate of consumption of (*R*)-**1** in acetone-water mixtures decreases from 60% to 80% and 90% aq acetone ($k_{\text{rel}} = 73, 7, \text{ and } 1$, respectively) as expected from the solvent ionizing power Y .⁴⁷ Figure 4 shows that the yield of rearranged esters increases considerably with decreasing water content in the solvent and that the sequence $[(S)\text{-}2] > [(S)\text{-}1] > [(R)\text{-}2]$ does not change, which can be explained by decreasing dissociation abilities (ϵ_r ⁴⁸) of the solvents and increasing nucleophilicities of ⁻OPNB from 60% to 80% and 90% aq acetone (as observed for acetate anion³⁷).

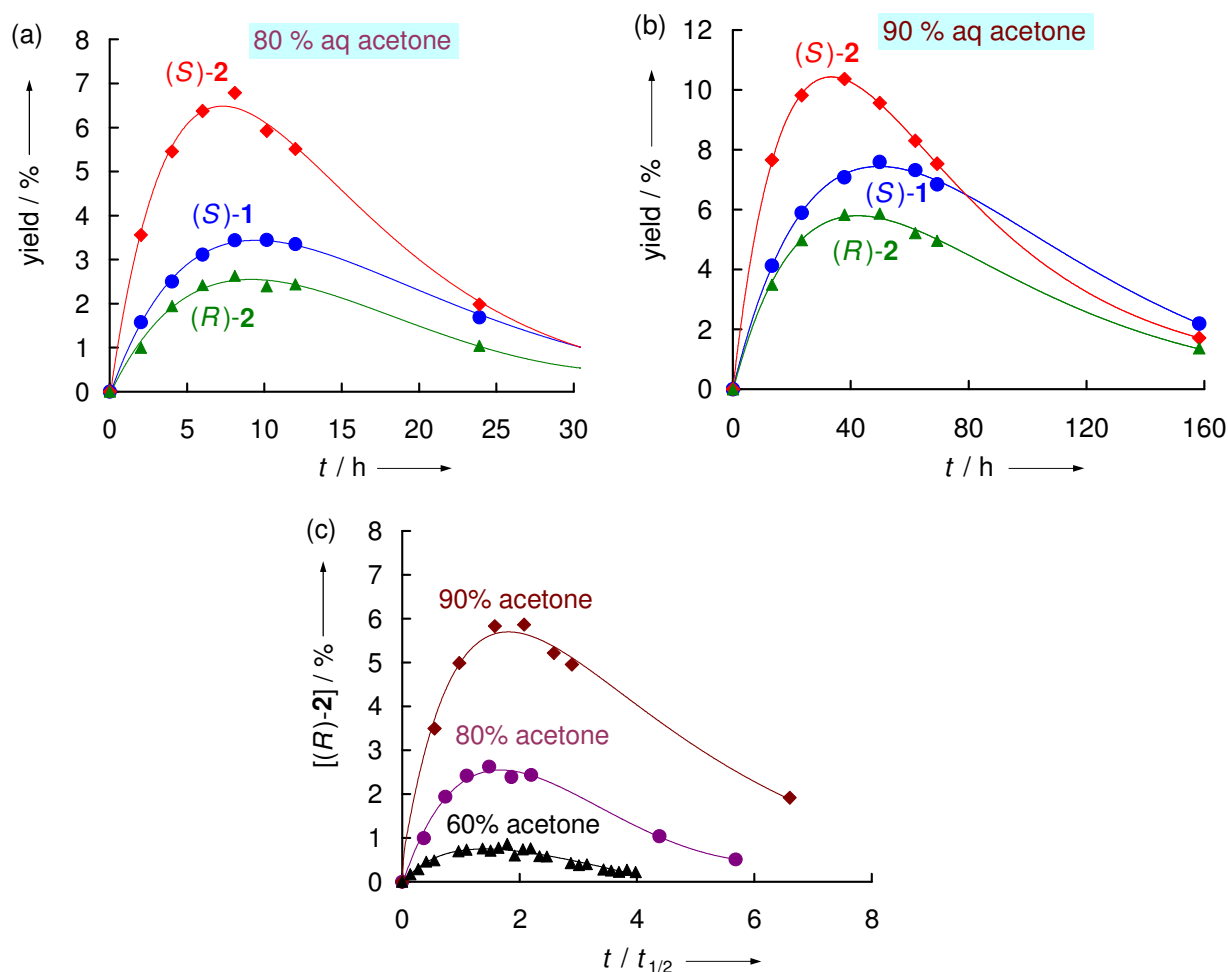


Figure 4. Time-dependent yields of (S)-2, (S)-1, and (R)-2 during solvolysis of (R)-1 in (a) 80% aq acetone ($[(R)-1]_0 = 0.77$ mM) and (b) 90% aq acetone ($[(R)-1]_0 = 0.68$ mM) as well as (c) yields of (R)-2 during solvolyses of (R)-1 in 60 ($[(R)-1]_0 = 1.5$ mM), 80 ($[(R)-1]_0 = 0.77$ mM), and 90% ($[(R)-1]_0 = 0.68$ mM) aq acetone.⁴⁹

Solvolysis of (R)-1 in the Presence of External Nucleophiles. When the solvolysis of (R)-1 in 60% aqueous acetone was performed in the presence of piperidine (54.2 mM), 40% of the allyl cations **6** were intercepted by the amine leading to the formation of the regioisomeric (E)-1,3-diarylallylpiperidines in ca 1:1 ratio (¹H NMR), and the total yield of the alcohols decreased to ca 60%. Non-regioselective formation of 1,3-diarylallylpiperidines can be explained by diffusion-controlled reaction of piperidine with both allylic termini of the cation, which is in agreement with the prediction based on reactivity parameters of piperidine and **6**.⁵⁰ The same product ratio was found for the reaction of piperidine with the free cation **6** in dichloromethane (see p 130 for details).

In the presence of sodium azide (70.8 mM), allyl azide was the major product of the solvolysis reaction of (R)-1 in 60% aqueous acetone, and the total yield of **3** and **4** was only

about 3%. These observations show that the intermediates, which give rise to the formation of **3** and **4**, can almost quantitatively be intercepted by external nucleophiles, which is in agreement with the hypothesis that these intermediates are free 1,3-diarylallyl cations **6**. On the other hand, the various isomerization pathways of (*R*)-**1** were differently affected by external nucleophiles. The yield of (*S*)-**2**, which reached a maximum of 3.2% in the absence of nucleophiles, was only slightly reduced to 2.6% in the presence of piperidine (54.2 mM), and to 2.4% in the presence of NaN₃ (70.8 mM). In contrast, the same concentrations of NaN₃ reduced the formation of (*S*)-**1** by a factor of 2.2 (Figure 5), and [(*R*)-**2**] levels below the detection limit (not shown in Figure 5, see Figure S24a). An analogous situation was observed for the solvolysis of (*S*)-**2** in the presence of 76.6 mM NaN₃ (Figure S33 of the Experimental Section, p 169).

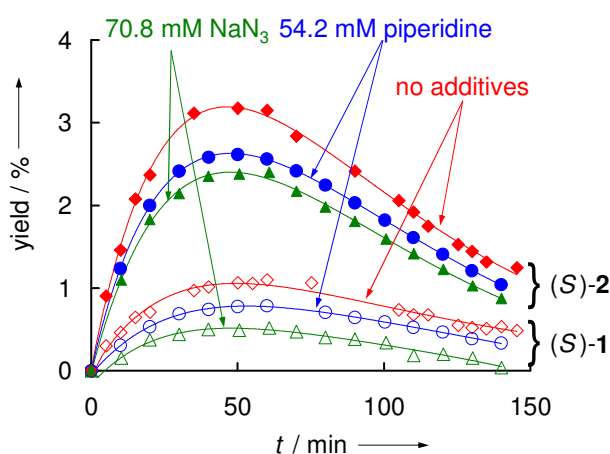


Figure 5. Time-dependent yields of (*S*)-**2** (filled points) and (*S*)-**1** (open points) generated during solvolysis of (*R*)-**1** (0.80 – 1.5 mM) without and with added nucleophiles (60% aq acetone, 25 °C).

Addition of chloride ions reduced the yields of the rearranged diarylallyl 4-nitrobenzoates (*S*)-**1**, (*S*)-**2** and (*R*)-**2** to similar extents (Experimental Section, Figures S19 and S22, pp 159, 161). Since the 1,3-diarylallyl chlorides formed by trapping of the free cation **6** by Cl⁻ undergo fast dissociation to regenerate **6**, the yields of the hydrolysis products **3** and **4** were not affected, however.

Solvolysis of (*R*)-1** in the Presence of Tetrabutylammonium 4-Nitrobenzoate (Common Ion Return).** Small amounts of Bu₄NOPNB (4.8 mM) reduced the rate of consumption of [(*R*)-**1**] in 60% aq acetone by only 7% (Figure S9a of the Experimental Section, p 151), while the yields of (*S*)-**2** (Figure 6a), (*R*)-**2** (Figure 6b) and (*S*)-**1** (Figure 6c) increased by factors of 1.3, 2.5 and 2, respectively. When a high concentration of Bu₄NOPNB (52.5 mM) was

present, the consumption of (*R*)-**1** became significantly slower (factor of 0.65, common ion rate depression), and the yield of (*S*)-**2** increased by a factor of 2.5 (Figure 6a), while the yields of (*R*)-**2** and (*S*)-**1** were approximately 8 (Figure 6b) and 6.5 (Figure 6c) times higher than in the absence of 4-nitrobenzoate. In summary, Bu₄NOPNB additives increased the yields of (*R*)-**2** and (*S*)-**1** by a significantly higher factor than the yield of (*S*)-**2**.

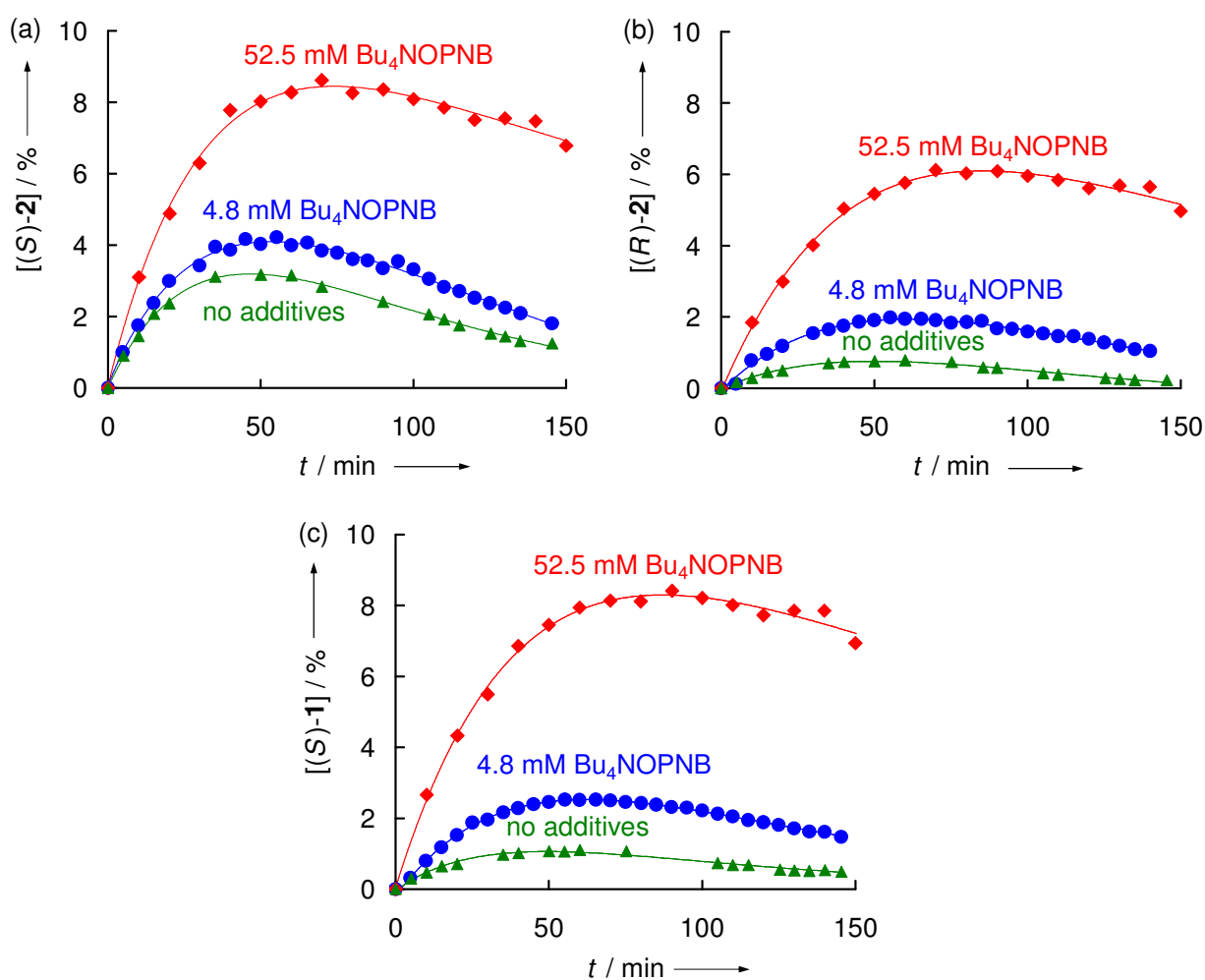
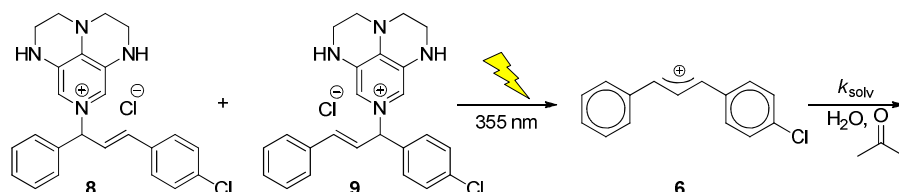


Figure 6. Time-dependent yields of (a) (*S*)-**2**, (b) (*R*)-**2**, and (c) (*S*)-**1** generated during solvolysis of (*R*)-**1** (0.78–1.5 mM) in the presence of various amounts of Bu₄NOPNB (60% aq acetone, 25 °C).

Reaction of the Diarylallyl Cation **6 with Water in Aqueous Acetone.** In order to put the trapping reactions of the intermediate diarylallyl cation **6** on an absolute scale, we have directly measured the rate of consumption of laser flash photolytically generated **6** in 60% aq acetone. As acetone has strong absorption in the UV region, excitation at $\lambda < 310$ nm, as used

in routine laser flash experiments,⁴² was not possible. For that reason, a modified procedure⁵¹ using a mixture of SuperDMAP-derived salts **8** and **9** which can be excited at 355 nm was applied (Scheme 4).

Scheme 4. Laser Flash Photolytic Generation of the 1,3-Diarylallyl Cation **6** in 60% aq Acetone.



The reaction with water was followed spectrophotometrically at the absorption maximum of **6** (510 nm), and the rate constant for the reaction of **6** with water ($k_{\text{solv}} = 1.34 \times 10^7 \text{ s}^{-1}$) was obtained by fitting the time-dependent absorbance to the monoexponential function $A_t = A_0 e^{-k_{\text{solv}} t} + C$. As the k_{solv} values obtained at three different precursor concentrations agreed within the experimental error range ($\pm 5\%$), the influence of the photoleaving group or impurities, which might be present in the stock solution of the precursors, on the reaction kinetics can be excluded.

3. Discussion

Let us now develop a mechanistic scheme which accounts for the experimental findings. The observation that (*S*)-**2** is the preferred rearrangement product during the solvolysis of (*R*)-**1**, and vice versa, (*R*)-**1** is the preferred rearrangement product during the solvolysis of (*S*)-**2** indicates that there is a special pathway interconnecting these two isomers. Can it be a 1,3-sigmatropic rearrangement that avoids the intermediate formation of allyl cations?

If this were the case, decreasing solvent ionizing power,⁴⁷ i.e., changing from 60% aqueous acetone to 80 and 90% aqueous acetone should decrease the yields of esters formed by ionic pathways relative to those generated by a sigmatropic rearrangement. Comparison of Figures 3b, 4a, and 4b shows that the ratio $[(S)\text{-}2]/([(S)\text{-}1] + [(R)\text{-}2])$ even decreases in less ionizing solvents, which clearly rules out a sigmatropic rearrangement of (*R*)-**1** into (*S*)-**2** and vice versa.

In line with Goering's observations for cyclic allyl cations, we, therefore, conclude that the preferred isomerization (*R*)-**1** → (*S*)-**2** proceeds via suprafacial migration of the carboxylate anion at the contact ion pair stage.

Figure 5 shows that the addition of NaN₃ (70.8 mM) and piperidine (54.2 mM) reduces the yield of (*S*)-**2** to a much smaller extent (factors of 1.3 and 1.2, respectively) than that of (*S*)-**1** (factors of 2.2 and 1.5, respectively). (*R*)-**2** shows a similar behavior as (*S*)-**1** (Figure S24a of the Experimental Section, p 163). Cl⁻ ions exert similar effects (Figure S19a of the Experimental Section, p 159). Vice versa, the addition of 4.8 mM Bu₄NOPNB increases the maximum concentration of (*S*)-**2** by a factor of only 1.3 (Figure 6a), while the concentrations of (*R*)-**2** (Figure 6b) and (*S*)-**1** (Figure 6c) grow by factors of 2 to 2.5.

These observations indicate that the isomerizations of the 4-nitrobenzoates (*R,S*)-**1** as well as of (*R,S*)-**2** proceed via two different pathways: one, which is affected by external nucleophiles (including common ions, external return⁵²), and one which is not affected by the presence of external nucleophiles (internal return). The preferred rearrangement of (*R*)-**1** into (*S*)-**2**, where the leaving group stays on the same face of the allyl cation, is rationalized by internal return, which is not 100% stereospecific, however, because part of (*S*)-**1** and (*R*)-**2** must also arise from internal return. The latter conclusion is derived from the observation that 70.8 mM NaN₃ reduces the yield of (*S*)-**1** at the maximum of the curve in Figure 5 to 45% of the value observed in the absence of additives, while the same concentration of azide ions reduces the total yield of the hydrolysis products **3** and **4** from 100% to 3%. If (*S*)-**1** would exclusively be formed through external return, i.e., by trapping of **6** by ⁻OPNB, the yield of (*S*)-**1** should be reduced by a factor of 30, as the yields of the alcohols **3** and **4**.

The isomer (*R*)-**2** shows a similar behavior as (*S*)-**1**, but a precise evaluation of the small quantities of (*R*)-**2** is problematic because of the broadness of the HPLC peak of this isomer (Figure 1). Complementary observations were made for the solvolysis of (*S*)-**2** (see pp 168–169 for details). We, therefore, conclude that the rearrangements through ion pairs do not only proceed via suprafacial migration of carboxylate anion but also via migration of the carboxylate anion to the other face of the allyl cation without dissociation to the free ions.

Table 2 shows that the time-dependent difference $\Delta_t = [(S)\text{-}2]_t - [(R)\text{-}2]_t$ is independent (within experimental error) of the nature and concentration of the external nucleophile. If external nucleophiles were able to attack the CIPs, the value of Δ_t could not be nucleophile-independent. One can, therefore, conclude that the CIPs generated in this system are inert to any additive used in the present work, including strong nucleophiles such as N₃⁻.

Table 2. Difference $\Delta_t = [(S)\text{-}2]_t - [(R)\text{-}2]_t$ at Certain Reaction Times During Solvolysis of (*R*)-**1** in the Presence of Various Additives (60% Aq Acetone, 25 °C).

additive	Δ_t				
	at 10 min	at 20 min	at 40 min	at 50 min	at 60 min
none	1.2	1.9	2.5	2.4	2.4
5 mM Bu ₄ NOPNB	1.0	1.8	2.1	2.1	2.0
52.5 mM Bu ₄ NOPNB	1.3	1.9	2.7	2.6	2.5
54 mM piperidine	1.1	1.8	2.5	2.6	2.4
70.8 mM NaN ₃	1.1	1.8	2.4	2.4	2.4

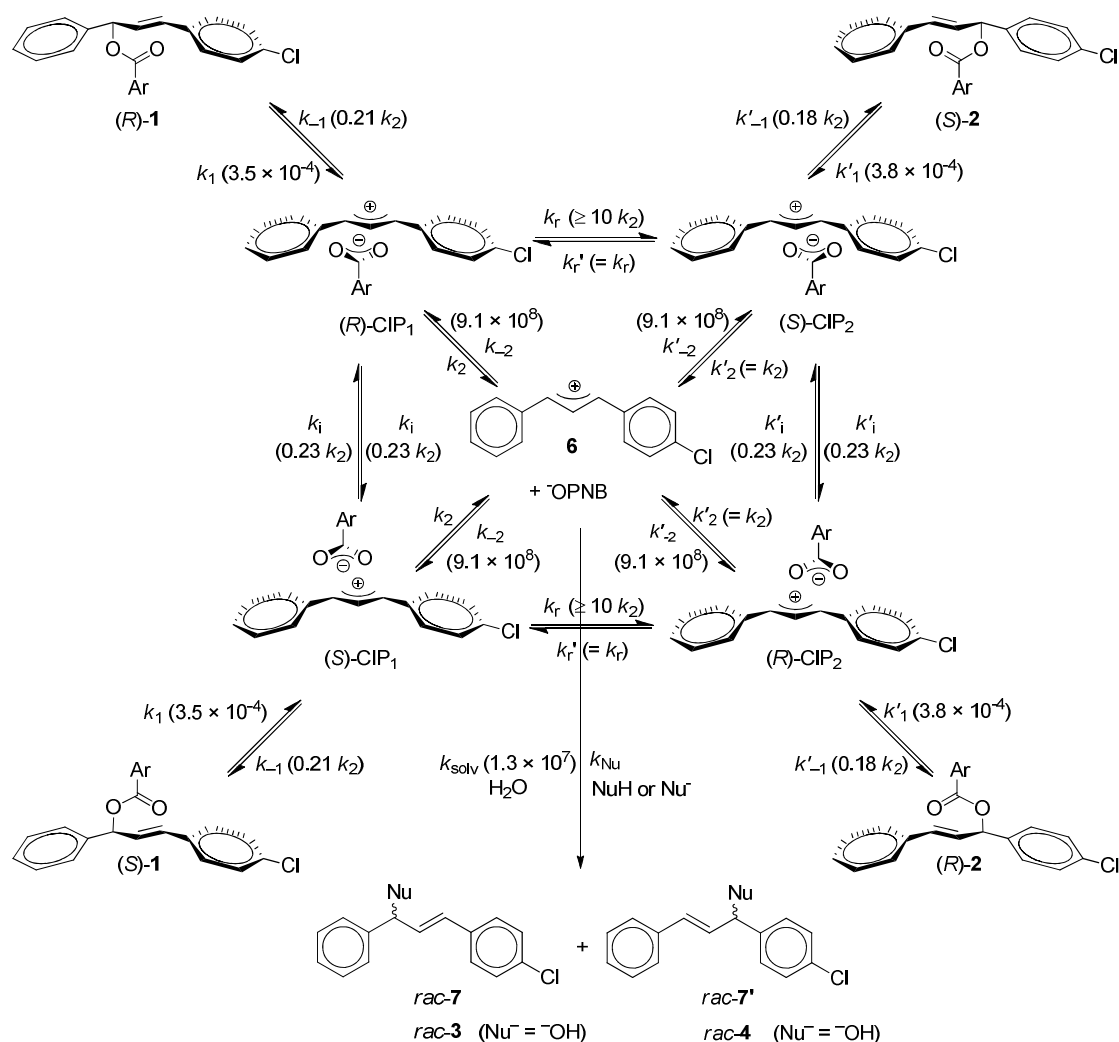
These observations exclude the solvolysis mechanism proposed by Dvorko et al.⁵³ who assumed that the azide anion generally attacks the contact ion pairs rather than SSIPs or CSIPs (cavity separated ion pairs), which are proposed by Dvorko to be intermediates on the way from CIP to SSIP in Scheme 2.

As discussed above, the formation of (*S*)-**1** and (*R*)-**2** from (*R*)-**1** can be suppressed by strong nucleophiles, such as NaN₃, by more than 50 %. Internal return, therefore, is not the major pathway for the formation of these isomers, and external return⁵² must be their main source, particularly when the reactions are carried out in the presence of Bu₄NOPNB. A similar situation is observed when (*S*)-**2** is used as a substrate, where internal return favors the formation of (*R*)-**1** (suprafacial migration product). Table 3 shows that the ratio [(*S*)-**1**]/[(*R*)-**2**] obtained by solvolysis of either (*R*)-**1** or (*S*)-**2** is the same within experimental accuracy, indicating common intermediates from both precursors. This observation definitely excludes that the rearrangements (*R*)-**1** → (*S*)-**1** and (*S*)-**2** → (*R*)-**2** are preferred over the rearrangements (*R*)-**1** → (*R*)-**2** and (*S*)-**2** → (*S*)-**1**, respectively. In other words, when the leaving group migrates to the other face of the allyl cation, it has no preference for the carbon from which it departs. The observation that the ratio [(*S*)-**1**]/[(*R*)-**2**] is comparable to the ratio of the hydrolysis products ([**3**]/[**4**] = 1.5), supports the suggestion that external return of ⁻OPNB (the major source of (*S*)-**1** and (*R*)-**2** in the presence of Bu₄NOPNB) and hydrolysis proceed via the same key intermediates, i.e., the free 1,3-diarylallyl cations **6**.

Table 3. The Ratios [(*S*)-**1**]/[(*R*)-**2**] at Certain Reaction Times During Solvolysis of (*R*)-**1** and (*S*)-**2** in the Presence of Various Additives (60% Aq Acetone, 25 °C).

substrate, additive	[(<i>S</i>)- 1]/[(<i>R</i>)- 2]	
	at 50 min	at 60 min
(<i>R</i>)- 1 , no additive	1.40	1.41
(<i>R</i>)- 1 , 4.8 mM Bu ₄ NOPNB	1.28	1.29
(<i>R</i>)- 1 , 52.5 mM Bu ₄ NOPNB	1.37	1.38
(<i>S</i>)- 2 , no additive	1.35	1.50

A summary of these observations is presented in Scheme 5. The ionization step (k_1 starting from **1** or k'_1 starting from **2**) provides contact ion pairs ((*R*)-CIP₁, (*S*)-CIP₁, (*R*)-CIP₂, (*S*)-CIP₂) which retain the stereochemical and regiochemical information of the covalent substrates, i.e., the 4-nitrobenzoate anion is still on the same face of the carbocationic plane, close to the carbon to which it was covalently bound in the starting material. While these unsymmetrical structures of the ion pairs are in agreement with previous suggestions by Goering⁵⁴ and Thibblin,⁵⁵ the distinction of four different ion pairs is in line with, but not inevitably required by our experimental data. Instead of assuming the rapidly equilibrating pairs (*R*)-CIP₁ \rightleftharpoons (*S*)-CIP₂ and (*S*)-CIP₁ \rightleftharpoons (*R*)-CIP₂, one might also assume that the same chiral ion pair is formed from (*R*)-**1** and (*S*)-**2**, which is enantiomeric to that generated from (*S*)-**1** and (*R*)-**2**. The latter alternative is kinetically equivalent to the mechanism in Scheme 5 (four different CIPs) with $k_r = k'_r = \infty$. According to Scheme 5, the unsymmetrical contact ion pairs can undergo recombination (k_{-1} and k'_{-1}), suprafacial migration (k_r and k'_r), inversion (k_i , k'_i , the anion migrates to the opposite face of the allyl cation), and dissociation with formation of free cations **6** (k_2 , k'_2). The free cations can re-associate with 4-nitrobenzoate anions regenerating the contact ion pairs with the second-order rate constants k_{-2} and k'_{-2} , or react with other nucleophiles (represented in Scheme 5 with the effective first order rate constant k_{Nu} which corresponds to the sum of reactions with all external nucleophiles and water) to produce the racemic products **3**, **4**, **7**, and **7'**. As the alcohols **3** and **4** are formed as racemates, nucleophilic trapping of the chiral CIPs can be excluded in Scheme 5. Trapping of ion pairs by external nucleophiles must be taken into account, however, when ion pairs of less stabilized carbocations are involved.⁵⁶

Scheme 5. Mechanism for the Solvolysis of Allyl 4-Nitrobenzoates **1** and **2**.^a

^a The rate constants shown in parentheses result from the fit described below. All first-order rate constants as well as the pseudo-first-order rate constant k_{solv} are given in s^{-1} and correspond to 60% aq acetone, 25 °C. Second-order rate constants k_{-2} and k'_{-2} are given in $M^{-1} s^{-1}$.

The gross rate constant of the diffusional encounter of **6** with $OPNB^{OPNB}$ (k_{diff}^{OPNB}) is expressed by equation 1.

$$k_{diff}^{OPNB} = 2(k_{-2} + k'_{-2}) \quad (1)$$

The factor of 2 implies that the encounter of **6** with $OPNB^{OPNB}$ is split into two equal pathways leading to the enantiomeric ion pairs.

The interconversions depicted in Scheme 5 can be described by the rate laws in eq 2 to eq 10.

$$\frac{d[(R)-\mathbf{1}]}{dt} = -k_1[(R)-\mathbf{1}] + k_{-1}[(R)-\text{CIP}_1] \quad (2)$$

$$\frac{d[(S)-\mathbf{1}]}{dt} = -k_1[(S)-\mathbf{1}] + k_{-1}[(S)-\text{CIP}_1] \quad (3)$$

$$\frac{d[(R)-\mathbf{2}]}{dt} = -k'_1[(R)-\mathbf{2}] + k'_{-1}[(R)-\text{CIP}_2] \quad (4)$$

$$\frac{d[(S)-\mathbf{2}]}{dt} = -k'_1[(S)-\mathbf{2}] + k'_{-1}[(S)-\text{CIP}_2] \quad (5)$$

$$\frac{d[(R)-\text{CIP}_1]}{dt} = k_1[(R)-\mathbf{1}] + k'_r[(S)-\text{CIP}_2] + k_i[(S)-\text{CIP}_1] + k_{-2}[\mathbf{6}][^- \text{OPNB}] - (k_{-1} + k_r + k_i + k_2)[(R)-\text{CIP}_1] \quad (6)$$

$$\frac{d[(S)-\text{CIP}_1]}{dt} = k_1[(S)-\mathbf{1}] + k'_r[(R)-\text{CIP}_2] + k_i[(R)-\text{CIP}_1] + k_{-2}[\mathbf{6}][^- \text{OPNB}] - (k_{-1} + k_r + k_i + k_2)[(S)-\text{CIP}_1] \quad (7)$$

$$\frac{d[(R)-\text{CIP}_2]}{dt} = k'_1[(R)-\mathbf{2}] + k_r[(S)-\text{CIP}_1] + k'_i[(S)-\text{CIP}_2] + k'_{-2}[\mathbf{6}][^- \text{OPNB}] - (k'_{-1} + k'_r + k'_i + k'_2)[(R)-\text{CIP}_2] \quad (8)$$

$$\frac{d[(S)-\text{CIP}_2]}{dt} = k'_1[(S)-\mathbf{2}] + k_r[(R)-\text{CIP}_1] + k'_i[(R)-\text{CIP}_2] + k'_{-2}[\mathbf{6}][^- \text{OPNB}] - (k'_{-1} + k'_r + k'_i + k'_2)[(S)-\text{CIP}_2] \quad (9)$$

$$\frac{d[\mathbf{6}]}{dt} = k_2[(R)-\text{CIP}_1] + k_2[(S)-\text{CIP}_1] + k'_2[(R)-\text{CIP}_2] + k'_2[(S)-\text{CIP}_2] - (2k_{-2}[^- \text{OPNB}] + 2k'_{-2}[^- \text{OPNB}] + k_{\text{Nu}})[\mathbf{6}] \quad (10)$$

The solution of the system of linear ordinary differential equations 2 to 10 provides the calculated values for the time-dependent concentrations of (R)-**1**, (S)-**1**, (R)-**2**, and (S)-**2** for a given set of parameters (k_1 , k'_1 , k_{-1} , k'_{-1} , k_r , k_i , k'_r , k'_i , k_2 , k'_2 , $k_{-2}[^- \text{OPNB}]$, $k'_{-2}[^- \text{OPNB}]$, k_{Nu}).⁵⁷ In order to determine the individual rate constants shown in Scheme 5, we have simulated the time-dependent concentrations of the four isomeric esters (R)-**1**, (S)-**1**, (R)-**2**, and (S)-**2** during the solvolysis in 60% aq acetone of:

- (R)-**1** (0.80 mM) in the presence of 70.8 mM NaN₃, which provides reliable data for internal return because external return of ⁻OPNB is almost completely suppressed ($k_{-2}[^- \text{OPNB}] \ll k_{\text{Nu}} = k_{\text{N}_3}[\text{N}_3^-] + k_{\text{solv}}$).
- (S)-**2** (0.79 mM) in the presence of 76.6 mM NaN₃.
- (R)-**1** (0.80 mM) in the presence of 4.8 mM Bu₄NOPNB (to keep $k_{-2}[^- \text{OPNB}]$ and $k'_{-2}[^- \text{OPNB}]$ constant during the reaction, which provides the reliable data for external return).

The directly measured rate constant of the reaction of **6** with water in 60% aq acetone ($k_{\text{solv}} = 1.34 \times 10^7 \text{ s}^{-1}$) and the second-order rate constant k_{N_3} ($6.1 \times 10^9 \text{ M}^{-1}\text{s}^{-1}$), which was derived from k_{solv} and the allyl azide/allyl alcohol ratio, were introduced as fixed quantities.

As the free energies of the ion pairs CIP₁ and CIP₂ are closely similar, the corresponding rate constants for diffusion and ion pair reorganization were set equal, i.e., $k'_2 = k_2$, $k'_{-2} = k_{-2}$, $k'_r = k_r$, and $k'_i = k_i$. The small errors introduced by these assumptions are compensated by the relative magnitudes of the recombination rate constants k'_{-1}/k_{-1} .

Minimization of the sum of squared deviations (SSD) between calculated and experimental time-dependent concentrations of all isomeric esters (*R,S*)-**1** and (*R,S*)-**2** yielded the values of the rate constants which fit the experiments most correctly.

As shown in Table SN1 (p 183) of the Experimental Section $k_2 = k'_2$ was arbitrarily set at values between 10^8 and 10^{11} s^{-1} , while the remaining parameters were optimized. The last column of the Table SN1 shows that equally good fits between calculated and experimental concentrations were obtained for the different values of $k_2 = k'_2$. While k_1 , k'_1 , k_{-2} , and k'_{-2} were found to be independent ($\pm 4\%$) of the choice of k_2 in the specified range, k_{-1} , k'_{-1} , and $k_i = k'_i$ were found to be directly proportional to k_2 (Figures SN1 to SN8 of the Experimental Section, pp 184–186), which allowed us to express these rate constants as multiples of k_2 in Scheme 5. For a fixed value of $k_2 = k'_2 = 2 \times 10^{10} \text{ s}^{-1}$, comparable SSDs were obtained for different values of k_r as long as they were greater than $10k_2$, and the values of k_{-1} , k'_{-1} , $k_i = k'_i$ changed insignificantly ($< 7\%$) when $k_r = k'_r$ was varied from $10k_2$ to $500k_2$, (Figures SN9 to SN15, pp 195–197). As a consequence, each value of k_2 entails certain values ($\pm 7\%$) of k_{-1} , k'_{-1} , $k_i = k'_i$ and lower limits for $k_r = k'_r$. The same results were obtained when the steady state approximation was applied to (*R*)-CIP₁, (*S*)-CIP₁, (*R*)-CIP₂, (*S*)-CIP₂, and **6** (Figures SN1a to SN8a of the Experimental Section, pp 188–190). The resulting absolute and relative rate constants are presented in Scheme 5.

The good agreement between calculated and experimental time-dependent concentrations (Figure 7 and Figures SN18 to SN19 of the Experimental Section, pp 198–199) demonstrates that the solvolyses of **1** and **2** can adequately be described by the mechanism presented in Scheme 5.

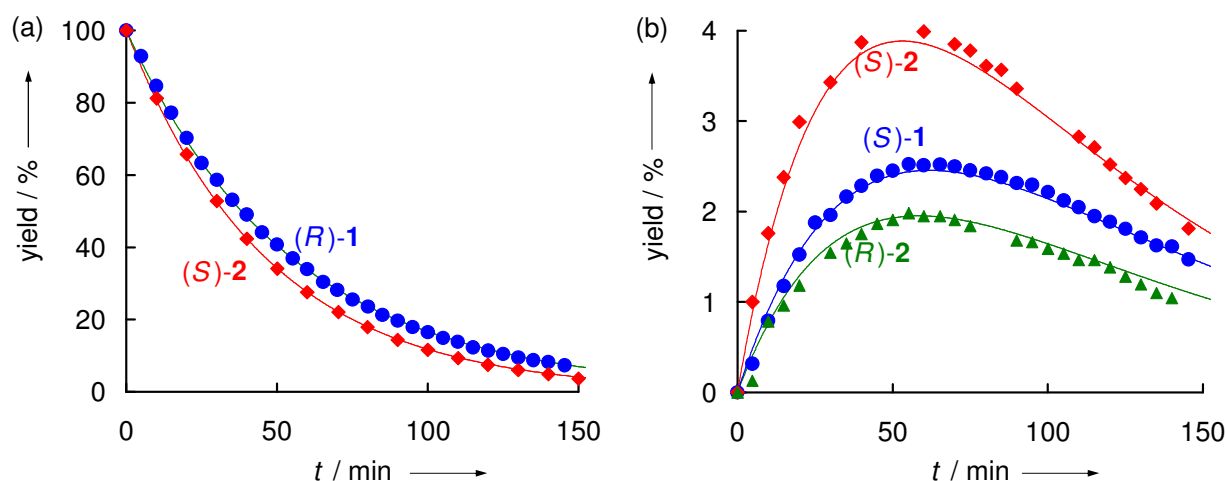


Figure 7. Calculated (solid lines) and experimental time-dependent concentrations of (a) (*R*)-**1** (0.80 mM) and (*S*)-**2** (0.79 mM) during their solvolysis in 60% aq acetone in the presence of 4.8 mM Bu₄NOPNB and 76.6 mM NaN₃, respectively; and (b) of (*S*)-**1**, (*S*)-**2**, and (*R*)-**2** during solvolysis of (*R*)-**1** (0.80 mM) in 60% aq acetone in the presence of 4.8 mM Bu₄NOPNB, 25 °C.

According to Scheme 5, the slowest step of the solvolysis is the initial ionization leading to the CIPs ($k_1 = 3.5 \times 10^{-4} \text{ s}^{-1}$, $k'_1 = 3.8 \times 10^{-4} \text{ s}^{-1}$). Suprafacial migration of the 4-nitrobenzoate anion ($k_r = k'_r > 10k_2$) is the most likely transformation of the CIP, followed by dissociation ($k_2 = k'_2$) and, finally, inversion ($k_i = k'_i = 0.23k_2$) and ion pair collapse ($k_{-1} = 0.21k_2$, $k'_{-1} = 0.18k_2$), which have almost equal rates. This sequence explains the partial stereospecificity of internal return, i.e., the fact that (*S*)-**2** is the major product among the rearranged esters during solvolysis of (*R*)-**1** and vice versa.

Because of the availability of the directly measured rate constant k_{solv} for the reaction of **6** with water (in aq acetone), our experiments provide an accurate value for the diffusional process generating ion pairs from the free ions **6** ($k_{-2} = k'_{-2}$). On the other hand, the rate constants for the diffusional separation of the ion pairs ($k_2 = k'_2$) cannot be derived directly from the experimental data. As values of $10^8 < k_2/\text{s}^{-1} < 10^{11}$ give equally good fits, the value of $k_2 \approx 1.6 \times 10^{10} \text{ s}^{-1}$, which was proposed by Richard and Jencks³⁵ and is mostly used in the literature, appears to be a good choice also for this system.

From the value of $k_{-2} = k'_{-2} = 9.1 \times 10^8 \text{ M}^{-1}\text{s}^{-1}$ one can calculate the second-order rate constant of diffusional migration of 4-nitrobenzoate anion to the free cation **6** using eq 1 ($k_{\text{diff}}^{\text{OPNB}} = 4k_{-2} = 3.6 \times 10^9 \text{ M}^{-1}\text{s}^{-1}$), which is similar to the value of $1.5 \times 10^9 \text{ M}^{-1}\text{s}^{-1}$ reported by Tsuji, Richard, and co-workers for the diffusion of carboxylate anions to the 1-(4-methylphenyl)ethyl cation in 50% v/v TFE-water mixture.^{36a}

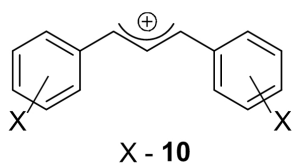
Earlier analyses, which were based on titrimetric, polarimetric, and ^{18}O -exchange rate constants, left the question open whether solvolysis and internal return are two independent processes involving different types of ion pairs.³³ As simulations based on Scheme 5 accurately describe the distribution of the products generated by internal and external return, it is now clear that solvolysis and internal return can be explained by the same intermediates.

A Comprehensive View on Solvolyses of Allyl Carboxylates

The kinetic and stereochemical investigations of the solvolyses of the enantiopure allyl carboxylates (*R*)-**1** and (*S*)-**2** provided detailed information on relative and absolute rates of the individual steps for the system described in Scheme 5. Can one use these results to derive a general scheme of solvolyses of allyl carboxylates?

In previous work,⁴⁴ we have determined the electrophilicity parameters E of the symmetrical 1,3-diarylallyl cations **X-10**, which are listed in Table 4. According to equation 11, the electrophilicity parameters E can be combined with the solvent-dependent nucleophile-specific parameters N and s_N to calculate second-order rate constants for the reactions of carbocations with neutral and anionic nucleophiles³⁹ as well as the first-order rate constants for the reactions of carbocations with the solvents.³⁸

$$\log k (20\text{ }^\circ\text{C}) = s_N(E + N) \quad (11)$$

Table 4. Symmetrical 1,3-Diarylallyl Cations X-**10** and Their Electrophilicity Parameters E .⁴⁴

X- 10	X	E
F ₂ - 10	<i>m,m</i> -F ₂	6.11
F- 10	<i>m</i> -F	4.15
Br- 10	<i>p</i> -Br	2.85
Cl- 10	<i>p</i> -Cl	2.69
H- 10	H	2.70
Me- 10	<i>p</i> -Me	1.23
MeO- 10	<i>p</i> -MeO	-1.45
Me ₂ N- 10	<i>p</i> -Me ₂ N	-7.50

As the 1,3-diphenylallyl cation H-**10** and its dichloro-substituted analogue Cl-**10** have almost the same values of E , the same electrophilicity ($E = 2.70$) can also be assumed for the monochlorinated system **6**.

Rates of Reactions of the Allyl Cations 10 with Aqueous Acetone. Investigations of the nucleophilic reactivities of solvents have shown that acetonitrile/water mixtures with 20% to 90% content of water (v/v) react with equal rates with benzhydrylium ions,³⁸ in accordance with earlier reports by McClelland.⁵⁸ The same relationship seems to hold also for acetone/water mixtures, as 90% ($N = 5.70$, $s_N = 0.85$) and 80% aq acetone ($N = 5.77$, $s_N = 0.87$) were reported to react with similar rates.⁵⁹ Accordingly, the first-order rate constant for the reaction of **6** ($E = 2.70$) with 80% aq acetone calculated by eq 11 ($2.3 \times 10^7 \text{ s}^{-1}$) agrees well with the directly measured rate constant for the reaction of **6** with 60% aqueous acetone ($1.34 \times 10^7 \text{ s}^{-1}$, see above). Equation 11 can thus be employed also to calculate the rate constants for the reactions of **10** with aqueous acetone.

It should be noted that the agreement within a factor of 2 between the calculated and experimental rate constant for the reaction of **6** with aqueous acetone cannot a priori be expected, because deviations up to factors of 10–100 have to be tolerated for predictions of absolute rate constants by equation 11, which covers a reactivity range of 40 orders of magnitude with only three parameters.^{41,60} On the other hand, equation 11 allows one to predict relative reactivities within reaction series, e.g., the relative reaction rates of X-**10**,⁴⁴ with an accuracy better than factor of 2.^{43,60}

Rates of Reactions of the Allyl Cations **10 with the 4-Nitrobenzoate Anion.** In order to apply equation 11, let us first derive the nucleophilicity parameter N for the 4-nitrobenzoate anion (${}^{-}\text{OPNB}$) in 60% aq acetone. At low concentrations of the substrates, as they are usually employed in solvolysis experiments, the concentration of ion pairs (corresponding to encounter-complexes in ion-molecule or molecule-molecule reactions) is small compared with the concentrations of the non-paired reactants, and the rate constant for the recombination of **6** with ${}^{-}\text{OPNB}$ to the covalent products **1** and **2** is given by eq 12, which expresses the rate constants for ion recombination k_{rec} by multiplying the constant of the diffusional association (k_{-2}) with the partitioning factor (forward reaction, k_{-1} , divided by the sum of forward and backward reactions, $k_{-1} + k_2$) and the corresponding term for attack at the other allyl terminus.

$$k_{\text{rec}} = 2k_{-2} \frac{k_{-1}}{k_{-1} + k_2} + 2k'_{-2} \frac{k'_{-1}}{k'_{-1} + k'_2} \quad (12)$$

Substitution of k_{-1} , k'_{-1} , k_{-2} , and k'_{-2} by the absolute values or multiples of k_2 presented in Scheme 5 yields $k_{\text{rec}} = 5.91 \times 10^8 \text{ M}^{-1}\text{s}^{-1}$ for the reaction of **6** with ${}^{-}\text{OPNB}$ in 60% aq acetone. As $k_{\text{rec}} > 10^8 \text{ M}^{-1}\text{s}^{-1}$, i.e., beyond the range which is covered by equation 11, k_{rec} cannot be directly substituted in equation 11 to calculate N .

For the sake of simplicity, let us adjust equation 12 to symmetrically substituted allyl cations, e.g., **10**. For $k'_{-1} = k_{-1}$, $k'_2 = k_2$, and $k'_{-2} = k_{-2}$ equation 12 simplifies to equation 13.

$$k_{\text{rec}} = 4k_{-2} \frac{k_{-1}}{k_{-1} + k_2} \quad (13)$$

In activation-controlled reactions of **10** with ${}^{-}\text{OPNB}$, diffusional separation is much faster than the formation of the covalent esters ($k_2 \gg k_{-1}$), which reduces equation 13 to equation 14.

$$k_{\text{rec}} = 4k_{-2} \frac{k_{-1}}{k_2} \quad (14)$$

It should be noted that equations 13 and 14 correspond to the typical treatment of diffusion- and activation-controlled reactions described in standard textbooks.⁶¹

In order to apply the linear free energy relationship (equation 11) also to reactions which are affected by diffusion rates ($k > 10^8 \text{ M}^{-1}\text{s}^{-1}$), one has to multiply the rate constants calculated by equation 11 (which refer to activation-controlled reactions) with the correction factor f (eq 15) which is obtained by dividing equation 13 by equation 14.

$$f = \frac{k_2}{k_2 + k_{-1}} \quad (15)$$

For $k_{-1} = 0.193k_2$ (average of k_{-1} and k'_{-1} , Scheme 5),⁶² one obtains $f = 0.84$. Division of the experimental rate constant for the reaction of **6** with ${}^-\text{OPNB}$ ($5.91 \times 10^8 \text{ M}^{-1}\text{s}^{-1}$) by $f = 0.84$ leads to $7.04 \times 10^8 \text{ M}^{-1}\text{s}^{-1}$, which can be substituted into eq 11 to derive $N({}^-\text{OPNB}) = 9.94$, using $E(\mathbf{6}) = 2.70$ and $s_N = 0.7$, the typical sensitivity parameter for carboxylate anions in aqueous and polar organic solvents.³⁷ The N and s_N parameters for ${}^-\text{OPNB}$ can now be combined with the E values of X-**10** (Table 4) to calculate the rate constants for the reactions of X-**10** with 4-nitrobenzoate anion in 60% aq acetone.

Probabilities of Internal and External Return. Internal return occurs, when the value of k_{-1} is comparable to or greater than the rate constant of diffusional separation of the ion pairs (k_2). Its probability is given by equation 16.

$$P_{\text{IR}} = \frac{k_{-1}}{k_{-1} + k_2} 100\% \quad (16)$$

From equations 14 and 11 one gets the relationship (17), which allows expressing k_{-1} as a function of E (eq 18).

$$s_N(E + N) = \log 4k_{-2} + \log \frac{k_{-1}}{k_2} \quad (17)$$

$$\log k_{-1} = s_N(E + N) + \log k_2 - \log 4k_{-2} \quad (18)$$

For the sake of simplicity, let us assume that the linear dependence of $\log k_{-1}/k_2$ on E , which is expressed by eqs 17 and 18, also holds for reactions beyond the activation-controlled region (i.e., for reactions where k_{-1} is comparable to k_2).⁶³ One then arrives at Figure 8 which illustrates the increase of the rate of ion pair collapse (k_{-1} , from eq 18) with increasing

electrophilicity E of the allyl cations **X-10** in comparison with the rate constant for diffusional separation (k_2), for which Richard's³⁵ estimate of $1.6 \times 10^{10} \text{ s}^{-1}$ is used.

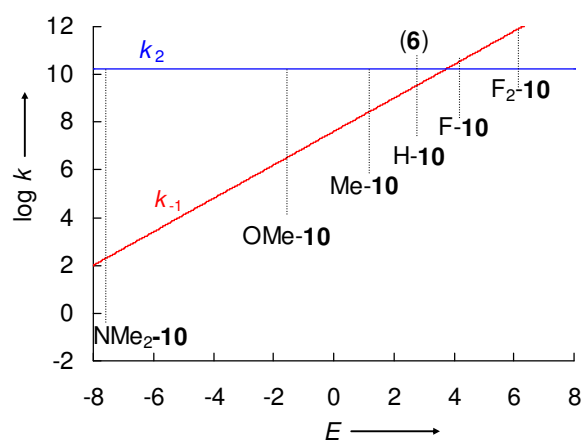


Figure 8. Relationship between internal return (k_{-1} vs k_2) and the electrophilicities E of the carbenium ions **10** during solvolyses of 1,3-diarylallyl 4-nitrobenzoates **10-OPNB** in 60% aq acetone.

One can see that the lines cross at $E \approx 4$, i.e., internal return becomes dominant for the highly electrophilic carbocations on the right of Figure 8. The k_{-1} graph is only slightly below the k_2 line for cation **6**, which reflects the participation of internal return expressed by the k_{-1}/k_2 ratio in Scheme 5. It should be emphasized that this analysis does not depend on the exact magnitude of k_2 . According to eq 18, variation of k_2 would also affect k_{-1} , and shift the crossing point of the two correlation lines in Figure 8 vertically, not horizontally, i.e., the nature of the carbocation (E value) where these lines cross would not be affected. The E value of the crossing point would move slightly, however, when the linear dependence of $\log k_{-1}/k_2$ on E is not followed accurately in the diffusion-controlled range, as assumed above.

The probability of external return is given by the relative rates of the reactions of the free 1,3-diarylallyl cation **10** with 4-nitrobenzoate anion ($k_{\text{rec}}[\text{OPNB}]^-$) and the solvent (k_{solv} , as described by equation 19).

$$P_{\text{ER}} = \frac{k_{\text{rec}}[\text{OPNB}]^-}{k_{\text{rec}}[\text{OPNB}]^- + k_{\text{solv}}} 100\% \quad (19)$$

Figure 9 compares the pseudo-first-order rate constants for the reactions of allyl cations **10** with the 4-nitrobenzoate anion in 60% aq acetone (at $[\text{OPNB}]^- = 5 \text{ mM}$) and with the solvent

calculated by equation 11. The curved part of the k_{rec} graph, which describes the approach to the diffusion limit, was obtained by multiplication of the rate constants calculated by equation 11 with the correction factor f of equation 15. The curvature of the correlation line for the solvent, which is irrelevant for the following discussion, is estimated from preliminary results in our group.⁶⁴

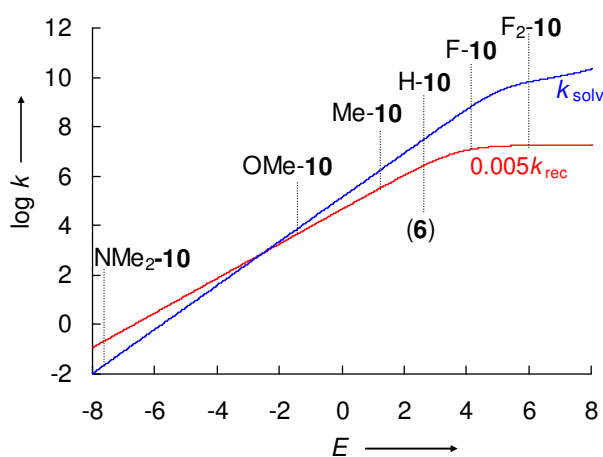


Figure 9. Relationship between external return (k_{rec} vs k_{solv}) and the electrophilicities E of the carbenium ions **10** during solvolyses of 1,3-diarylallyl 4-nitrobenzoates **10**-OPNB in 60% aq acetone (at $[\text{OPNB}] = 5 \text{ mM}$, $25 \text{ }^\circ\text{C}$).

As previously shown for solvolyses of benzhydryl and trityl derivatives,⁴¹ external (common ion) return is faster than the reaction with solvent for highly stabilized carbocations, while highly reactive carbocations are so rapidly trapped by the solvent that the leaving group OPNB^- does not have a chance to compete because of its low concentration, even when the ion combination is diffusion-controlled.

The probabilities of internal return p_{IR} and external return p_{ER} can be calculated by eqs 16 and 19 and are plotted against E in Figure 10.⁶⁵

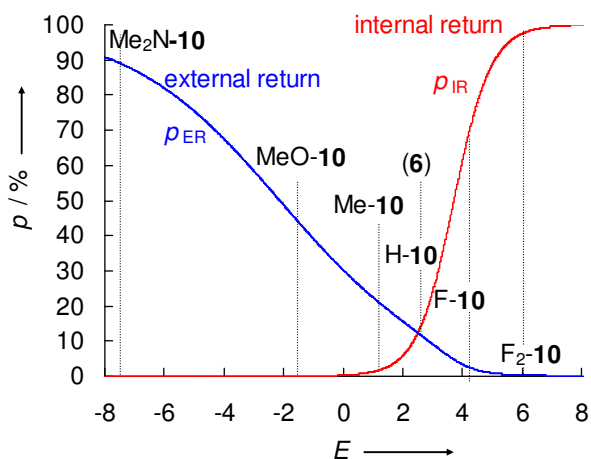


Figure 10. Dependencies of p_{IR} and p_{ER} for solvolyses of 1,3-diarylallyl 4-nitrobenzoates **10**-OPNB in 60% aq acetone (25 °C) on the E values of the cations **10** for $[\text{OPNB}] = 5 \text{ mM}$.

According to Figure 10, solvolyses of 1,3-diarylallyl 4-nitrobenzoates in 60% aq acetone (at $[\text{OPNB}] = 5 \text{ mM}$) which proceed via highly stabilized carbenium ions ($E < 0$, e.g., **Me₂N-10** or **MeO-10**) do not occur with internal return because their diffusional escape from the ion pair cage is faster than ion pair collapse; allylic rearrangements of such systems should proceed completely non-stereospecific. Both external and internal return can be expected for the solvolyses of 4-nitrobenzoates derived from carbenium ions with $1 < E < 5$. While the extent of external and internal return is comparable for **H-10**-OPNB or **6**-OPNB ($p_{\text{IR}} = 16\%$, $p_{\text{ER}} = 11\%$), solvolysis via better stabilized allyl cations ($E < 2.7$) should give more external and those via less stabilized carbocations should give more internal return. Thus, 4-nitrobenzoates derived from carbenium ions with $E > 6$ (e.g., **F₂-10**-OPNB), should solvolyze without external and with a large degree of internal return, i.e., allylic rearrangements of unsymmetrical systems involving carbocations of such high electrophilicities can be expected to be highly stereospecific.

The far right part of Figure 10 has to be seen with some caveat, however, because it is based on the premise that solvent and 4-nitrobenzoate anions only attack at free cations and not at ion pairs, as demonstrated for the solvolysis of **6**-OPNB in this work. It is feasible, however, that in the case of highly electrophilic carbenium ions, direct solvent capture of the CIPs will occur, resulting in a decrease of the probability of internal return.

The scheme presented for 1,3-diarylallyl 4-nitrobenzoates in 60% aq acetone in Figure 10, i.e., increase of p_{IR} and decrease of p_{ER} with increasing electrophilicity E , should analogously hold for other leaving groups and solvents, though the positions of the curves and their shapes will change. Figure 11 illustrates the calculated curves for external and internal return for Br^-

($N = 13.80$, $s_N = 0.60$), a significantly stronger nucleophile^{37,38} (though a weaker Lewis base) than ^-OPNB , in 50% aq acetonitrile ($N = 5.05$, $s_N = 0.89$), a solvent of similar nucleophilicity as aqueous acetone.

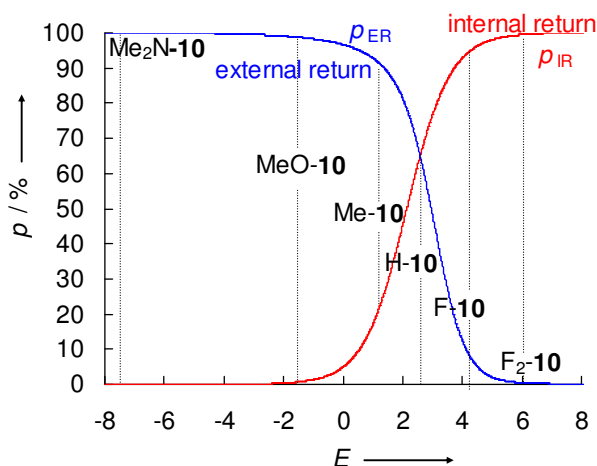


Figure 11. Estimated dependencies of p_{IR} and p_{ER} for solvolyses of 1,3-diarylallyl bromides **10**-Br in 50% aq acetonitrile (25 °C) on the E values of the cations **10** for $[Br^-] = 5$ mM.

One can see that the graph for internal return is similar to that in Figure 10, but shifted to less electrophilic carbocations, implying that internal return plays a greater role because of the higher nucleophilicity of Br^- . The graph for external return is almost the same in the right part of Figures 10 and 11 because both Br^- and ^-OPNB undergo diffusion-controlled reactions with carbocations in this range and have comparable chances to compete with the nucleophilic attack by water. Moving to the left, i.e., to less electrophilic carbocations, leads to a much faster increase of external return in Figure 11, because now the better nucleophile Br^- can more efficiently compete with water than the weaker nucleophile ^-OPNB . It should be noted, however, that the far left part of this graph is hypothetical. Though a fast reaction of Me_2N-10 with Br^- will occur, the reverse reaction can be expected to be even faster, with the result that $Me_2N-10^+Br^-$ will be predominantly ionic in 50% aqueous acetonitrile.

Decrease of the water content in acetone/water and acetonitrile/water mixtures is known to increase the nucleophilicity parameters N of the commonly used anionic leaving groups,^{39,66} resulting in an increase of k_{-1} according to equation 18 and consequently lead to an increase in p_{IR} (eq 16). As an increase of N will also increase k_{rec} (eq 11) and consequently p_{ER} (eq 19; the small decrease of k_{solv} in solvents with a lower content of water will shift p_{ER} in the same direction), also the probability of external return will grow. In line with this analysis, Figures 3 and 4 show an increase of the yields of all isomerization products ((*S*)-**1**, (*R*)-**2**, and (*S*)-**2**)

generated during the solvolysis of (*R*)-**1** when the solvent was changed from 60% to 80% and 90% aq acetone. In the same way, one can rationalize Goering's observations that the ratio k_o/k_t (polarimetric rate constant/titrimetric rate constant) for the solvolyses of *cis*-5-methylcyclohex-2-enyl 2-carboxybenzoate,²⁶ *trans*-5-methylcyclohex-2-enyl 4-nitrobenzoate,^{27b} and 1,3-dimethylallyl 4-nitrobenzoate⁶⁷ in aqueous acetone generally increased with decreasing water content because of the increasing nucleophilicities of the carboxylate ions. The enhancement of internal return with increasing electrophilicities of the carbenium ions is also in agreement with conclusions of Yabe and Kochi, which were derived from the rates of the recombinations of anthracenylium radical cation-trinitromethide ion pairs generated by laser-flash-induced electron transfer in the anthracene-tetranitromethane complexes.³²

4. Conclusions

The time-dependent concentrations of the four isomeric esters (*R,S*)-**1** and (*R,S*)-**2** and the four isomeric alcohols (*R,S*)-**3** and (*R,S*)-**4** measured during the hydrolysis of enantiopure (*R*)-**1** and (*S*)-**2** in aqueous acetone in the presence and absence of external nucleophiles were combined with the measured rate constant for the reaction of the laser-flash photolytically generated allyl cation **6** with water in aqueous acetone in order to develop a complete mechanistic scheme for this solvolysis cascade. As depicted in Scheme 5, the slowest step is the initial ionization leading to the CIPs ($k_1 = 3.5 \times 10^{-4} \text{ s}^{-1}$, $k'_1 = 3.8 \times 10^{-4} \text{ s}^{-1}$). Suprafacial migration of the 4-nitrobenzoate anion ($k_r = k'_r > 10k_2$) is the most likely transformation of the CIP, followed by dissociation ($k_2 = k'_2$) and, finally, inversion ($k_i = k'_i = 0.23k_2$) and ion pair collapse ($k_{-1} = 0.21k_2$, $k'_{-1} = 0.18k_2$). This sequence explains the partial stereospecificity of internal return, i.e., the fact that (*S*)-**2** is the major product among the rearranged esters during solvolysis of (*R*)-**1** and vice versa. As simulations based on Scheme 5 accurately describe the distribution of the products generated by internal and external return, it is now clear that solvolysis and internal return can be explained by the same intermediates.

The results of this work were combined with previously determined electrophilicity parameters *E* for 1,3-diarylallyl cations X-**10** to analyze the role of internal and external return in solvolyses of 1,3-diarylallyl 4-nitrobenzoates. While the parent 1,3-diphenylallyl 4-nitrobenzoate (*E* = 2.7) is predicted to solvolyze with 16% internal and 11% external return,⁶⁵ the contribution of external return increases, and the contribution of internal return decreases with increasing stabilization (decreasing electrophilicity *E*) of the allyl cations (Figure 10).

The correlation equation 11, which calculates rate constants of the reactions of carbocations with nucleophiles from the electrophile-specific parameter *E* and the nucleophile-specific

parameters N and s_N , can be used to estimate the role of internal and external return also for other substrates.

5. Experimental Section

5.1. General

Materials. Acetone (99.8%), hexane, and isopropanol (HPLC grade) were used as received. Double distilled water (impedance 18.2 Ω) was obtained from a water purification system. Tetrabutylammonium chloride and sodium azide were purchased and used without further purification. Tetrabutylammonium 4-nitrobenzoate and tetrabutylammonium benzoate were synthesized by using the procedure described in ref 37. The precursors for laser-flash measurements, **8** and **9**, were generated in situ from the mixture of 1-(4-chlorophenyl)-3-phenylallyl and 3-(4-chlorophenyl)-1-phenylallyl chlorides (**11**) and 1,2,3,4,5,6-hexahydro-1,3a,6,8-tetraazaphenalene (**12**) obtained as reported by David and coworkers.⁶⁸

NMR Spectroscopy. In the ^1H and ^{13}C NMR spectra chemical shifts are expressed in δ (ppm) and refer to CDCl_3 (δ_{H} 7.26, δ_{C} 77.0) or TMS (δ_{H} 0.00, δ_{C} 0.0) as internal standards. The coupling constants are given in Hz. Abbreviations used are: s (singlet), d (doublet), t (triplet), q (quartet), m (multiplet). In complicated cases, signal assignments are based on additional COSY, HSQC and HMBC experiments.

Laser-Flash Experiments. Solutions of **8** and **9** were irradiated with a 7 ns pulse from a quadrupled Nd:YAG laser (355 nm, \sim 50 mJ/pulse), and a xenon lamp was used as probe light for UV/Vis detection. The system was equipped with a fluorescence flow cell which allowed complete replacing of the sample volume between subsequent laser pulses. Kinetics were investigated by following the absorbance decay of the cation **6** ($\lambda = 510$ nm). Averaged data obtained from ≥ 48 individual runs were used for further evaluations.

5.2. Synthetic Procedures

(*E,R*)-3-(4-Chlorophenyl)-1-phenylallyl 4-nitrobenzoate ((*R*)-1**)** was obtained using the following four-step synthesis: (*E*)-3-(4-chlorophenyl)-1-phenyl-prop-2-enone (16.6 g, 68.4 mmol) obtained by a procedure from ref 69 was reduced with sodium borohydride (ca 5.0 g, ca 140 mmol) as described in ref 44 yielding the racemic (*E*)-3-(4-chlorophenyl)-1-phenyl-prop-2-en-1-ol **3** (15.7 g, 64.2 mmol, 94%), the ^1H NMR spectrum of which agreed with literature data.⁷⁰

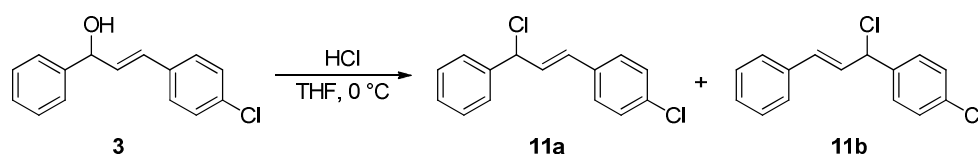
(*R*)-**3** was obtained using the Sharpless epoxidation of racemic **3** (15.5 g, 63.3 mmol) with D-(-)-diisopropyltartrate (1.78 g, 7.60 mmol), titanium (IV) isopropoxide (1.81 g, 6.33 mmol), and ^tBuOOH (8.4 mL of the 4.9 M CH₂Cl₂ solution,⁷¹ 41.1 mmol) at -20 °C as described in ref 72. The crude mixture was freed from the solvents and dissolved in ethanol followed by addition of piperidine (6.3 mL, 5.4 g, 64 mmol) and then refluxed for 10 h. The resulting solution was washed with 0.2 M aq HCl and water and then purified using column chromatography (silica gel, isohexane/diethyl ether) yielding (*R*)-**3** (4.65 g, 19.0 mmol, 30%, > 95% ee as analyzed by HPLC).

(*R*)-**3** (3.00 g, 12.3 mmol) was dissolved in dichloromethane followed by addition of triethylamine (2.7 mL, 2.0 g, 20 mmol), DMAP (195 mg, 1.60 mmol), and 4-nitrobenzoyl chloride (2.96 g, 15.9 mmol). The resulting solution was stirred for 30 min. The reaction mixture was washed with 0.2 M aq HCl and water and freed from the solvent. The crude product was recrystallized twice from dichloromethane/pentane yielding (*R*)-**1** (1.90 g, 4.82 mmol, 39 %, > 99% ee, analyzed by HPLC): yellowish crystals (mp 120.5 - 121.5 °C). ¹H NMR (CDCl₃, 300 MHz): δ 6.42–6.55 (m, 1 H, ArCHCHCH(*R*)Ph), 6.67–6.76 (m, 2 H, ArCHCHCH(*R*)Ph, ArCHCHCH(*R*)Ph), 7.27–7.58 (m, 9 H, H_{Ar}), 8.26–8.36 ppm (m, 4 H, H_{OPNB}). ¹³C NMR (CDCl₃, 75.5 MHz) : δ 77.7 (CH), 123.5 (CH), 127.0 (CH), 127.4 (CH), 128.0 (CH), 128.6 (CH), 128.78 (CH), 128.84 (CH), 130.8 (CH), 132.3 (CH), 134.0 (C), 134.4 (C), 135.6 (C), 138.4 (C), 150.6 (C), 163.7 ppm (C). HRMS (EI+): calcd 393.0762 (C₂₂H₁₆ClNO₄), found 393.0750. The exact configuration of (*R*)-**1** was confirmed by X-ray diffraction analysis (p 212).⁷³

(*E,S*)-**1**-(4-Chlorophenyl)-**3**-phenylallyl 4-nitrobenzoate ((*S*)-**2**) was obtained in a synthetic sequence analogous to that described above for (*R*)-**1** from (*S*)-**4** (2.50 g, 10.2 mmol): 1.63 g (4.14 mmol, 41%, > 99% ee, analyzed by HPLC), colorless powder (mp 105.3 - 106.3 °C). ¹H NMR (CDCl₃, 300 MHz): δ 6.46 (dd, ³J_{HH} = 15.9, 6.9 Hz, 1 H, ArCH(*R*)CHCHPh), 6.70 (d, ³J_{HH} = 6.9 Hz, 1 H, ArCH(*R*)CHCHPh), 6.76 (d, *J* = 15.9 Hz, 1 H, ArCH(*R*)CHCHPh), 7.25–7.53 (m, 9 H, H_{Ar}), 8.24–8.37 ppm (m, 4 H, H_{OPNB}). ¹³C NMR (CDCl₃, 75.5 MHz): δ 77.2 (CH), 123.6 (CH), 126.1 (CH), 126.8 (CH), 128.4 (CH), 128.5 (CH), 128.7 (CH), 129.0 (CH), 130.8 (CH), 134.0 (CH), 134.4 (C), 135.5 (C), 135.6 (C), 137.1 (C), 150.6 (C), 163.6 ppm (C). HRMS (EI+): calcd 393.0762 (C₂₂H₁₆ClNO₄), found 393.0757.

(*E*)-**1**-(4-Methylphenyl)-**3**-phenylprop-2-en-1-one (**5**) was synthesized from 4-methylacetophenone (10.0 g, 74.5 mmol) and benzaldehyde (7.91 g, 74.5 mmol) following the procedure described in ref 44: 9.44 g (42.5 mmol, 57%). The ¹H and ¹³C NMR spectra of **5** agreed with those described in the literature.⁷⁴

Mixture of (*E*)-3-chloro-3-(4-chlorophenyl)-1-phenylprop-1-ene (11a) and (*E*)-3-chloro-1-(4-chlorophenyl)-3-phenylprop-1-ene (11b) was synthesized from **3** (983 mg, 4.02 mmol) using a procedure by Hayashi et al.:⁷⁵ Yellowish oil (811 mg, 3.08 mmol, 77%). ¹H NMR (CDCl₃, 300 MHz): δ 5.62–5.67 (m, 1 H, ArCHCHCH(Cl)Ar'), 6.43–6.69 (m, 2 H, ArCHCHCH(Cl)Ar', ArCHCHCH(Cl)Ar'), 7.24–7.51 ppm (m, 9 H, H_{Ar}). ¹³C NMR (CDCl₃, 75.5 MHz): δ 62.9 (CH), 63.5 (CH), 126.8 (CH), 127.3 (CH), 128.0 (CH), 128.4 (CH), 128.49 (CH), 128.51 (CH), 128.65 (CH), 128.73 (CH), 128.77 (CH), 128.79 (CH), 128.9 (CH), 129.7 (CH), 130.8 (CH), 132.5 (CH), 133.9 (C), 134.2 (C), 134.3 (C), 135.6 (C), 138.8 (C), 140.1 ppm (C). HRMS (EI+): calcd 262.0311 (C₁₅H₁₂Cl₂⁺), found 262.0299.



(*E*)-3-(4-Chlorophenyl)-1-phenylallyl benzoate (13). Triethylamine (400 μ L, 313 mg, 3.09 mmol) and 4-dimethylaminopyridine (DMAP, 35 mg, 0.29 mmol) were added to a solution of **4** (623 mg, 2.55 mmol) in toluene. The resulting mixture was cooled to 0 °C followed by dropwise addition of benzoyl chloride (350 μ L, 424 mg, 3.02 mmol). The reaction progress was followed by TLC. The reaction mixture was quenched with 0.1 M aq HCl, the organic phase was separated, washed with saturated NaHCO₃ solution and water, freed from solvent, and dried *in vacuo* yielding **13** (745 mg, 2.14 mmol, 84%). ¹H NMR (CDCl₃, 200 MHz): δ 6.42 (dd, ³J_{HH} = 15.9, 6.5 Hz, 1 H, ArCHCHCH(OBz)Ph), 6.63–6.78 (m, 2 H, ArCHCHCH(OBz)Ph, ArCHCHCH(OBz)Ph), 7.22–7.61 (m, 12 H, H_{Ar}), 8.05–8.22 (m, 2 H, H_{OBz}).

Synthesis of (*E*)-1-(3-(4-chlorophenyl)-1-phenylallyl)piperidine (14) and (*E*)-1-(1-(4-chlorophenyl)-3-phenylallyl)piperidine (15). Piperidine (240 μ L, 206 mg, 2.42 mmol) was added to a solution of **13** (745 mg, 2.14 mmol) and Pd(PPh₃)₄ (14.7 mg, 12.7 μ mol) in dichloromethane, and the resulting mixture was stirred for 12 h at ambient temperature. After evaporation of the solvent, the crude product was purified with column chromatography (silica gel, pentane/ethyl acetate/triethylamine = 143/10/1). The resulting products were separated in three fractions.

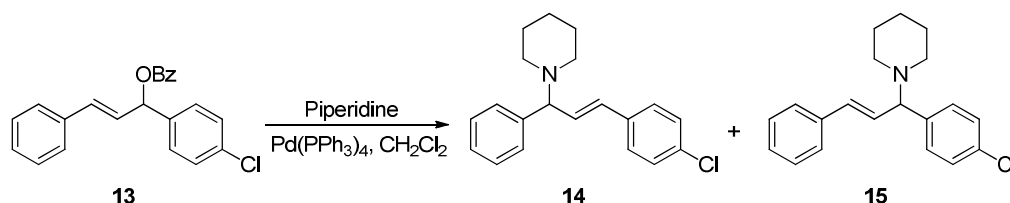
(*E*)-1-(3-(4-Chlorophenyl)-1-phenylallyl)piperidine (14): 220 mg (0.705 mmol, 33%) colorless solid (mp 98.5 – 99.6 °C). ¹H NMR (CDCl₃, 300 MHz): δ 1.35–1.48 (m, 2 H, CH₂CH₂CH₂N), 1.48–1.65 (m, 4 H, CH₂CH₂CH₂N), 2.25–2.39 (m, 2 H, CH₂CH₂CH₂N), 2.39–2.50 (m, 2 H, CH₂CH₂CH₂N), 3.80 (d, ³J_{HH} = 8.5 Hz, 1 H, ArCHCHCH(R)Ph), 6.30

(dd, $^3J_{\text{HH}} = 15.9, 8.5$ Hz, 1 H, ArCHCHCH(R)Ph), 6.47 (d, $^3J_{\text{HH}} = 15.9$ Hz, 1 H, ArCHCHCH(R)Ph), 7.18–7.40 (m, 9 H, H_{Ar}). ^{13}C NMR (CDCl_3 , 75 MHz): δ 24.6 (CH_2), 26.2 (CH_2), 52.7 (CH_2), 74.6 (CH), 127.0 (CH), 127.5 (CH), 128.0 (CH), 128.5 (CH), 128.6 (CH), 129.6 (CH), 132.9 (C), 133.1 (CH), 135.6 (C), 142.1 ppm (C). HRMS (EI+): calcd 311.1435 ($\text{C}_{20}\text{H}_{22}\text{ClN}$), found 311.1434.

(*E*)-1-(1-(4-Chlorophenyl)-3-phenylallyl)piperidine (**15**): 159 mg (0.510 mmol, 24%) colorless solid (mp 90.5 – 92.0 °C). ^1H NMR (CDCl_3 , 300 MHz): δ 1.34–1.49 (m, 2 H, $\text{CH}_2\text{CH}_2\text{CH}_2\text{N}$), 1.48–1.60 (m, 4 H, $\text{CH}_2\text{CH}_2\text{CH}_2\text{N}$), 2.22–2.39 (m, 2 H, $\text{CH}_2\text{CH}_2\text{CH}_2\text{N}$), 2.39–2.53 (m, 2 H, $\text{CH}_2\text{CH}_2\text{CH}_2\text{N}$), 3.80 (d, $^3J_{\text{HH}} = 8.7$ Hz, 1 H, PhCHCHCH(R)Ar), 6.26 (dd, $^3J_{\text{HH}} = 15.8, 8.7$ Hz, 1 H, PhCHCHCH(R)Ar), 6.51 (d, $^3J_{\text{HH}} = 15.8$ Hz, 1 H, PhCHCHCH(R)Ar), 7.16–7.37 (m, 9 H, H_{Ar}). ^{13}C NMR (CDCl_3 , 75 MHz): δ 24.6 (CH_2), 26.2 (CH_2), 52.5 (CH_2), 73.8 (CH), 126.3 (CH), 127.5 (CH), 128.5 (CH), 128.6 (CH), 129.3 (CH), 131.3 (CH), 131.5 (CH), 132.5 (C), 136.8 (C), 141.0 ppm (C). HRMS (EI+): calcd 311.1435 ($\text{C}_{20}\text{H}_{22}\text{ClN}$), found 311.1438.

The assignment of the NMR spectra to the regioisomers **14** and **15** was done based on HSQC, HMBC, and COSY experiments.

Mixture of regioisomers: colorless oil, 149 mg (0.477 mmol, 22%). ^1H and ^{13}C NMR spectra are superpositions of the corresponding spectra of both separately characterized regioisomers.



5.3. NMR Product Studies

Solvolysis of (*R*)-1 in the presence of piperidine. (*R*)-1 (77.1 mg, 0.196 mmol) was added to a solution of piperidine (692 mg, 8.13 mmol) in 60% v/v aq acetone (150 mL), and the resulting mixture was stirred for 4.5 h at 25 °C. Dichloromethane (100 mL) was added, the organic layer was separated, washed twice with water and dried *in vacuo*. Comparison of the ^1H NMR spectrum of the resulting crude mixture with those of isolated **14**, **15**, **3**, and **4** showed that the regioisomeric 1,3-diarylallylpiperidines are present in a ca. 1:1 ratio (based on resonances in region between 6.40 and 6.55 ppm). The allyl alcohol/allyl piperidine ratio was found to be ca. 1.3:1.

Reaction of piperidine with the free carbocation **6 in dichloromethane.** A 50% w/w tetrafluoroboric acid solution in diethyl ether (200 μL , 0.433 mmol) was slowly added to a

solution of **3** (101 mg, 0.413 mmol) in dichloromethane at -78 °C resulting in appearance of an intensive orange color. Piperidine (400 μ L, 344 mg, 4.04 mmol) was added to the resulting mixture at the same temperature, and the reaction solution was allowed to warm up followed by removal of the solvents *in vacuo*. The ratio of regioisomeric 1,3-diarylallyl piperidines [**14**]/[**15**] was found to be ca. 1:1 based on ^1H NMR of the crude mixture.

5.4. HPLC Kinetic Measurements

5.4.1. General procedure

A mixture of the starting material ((*R*)-**1** or (*S*)-**2**) and 1 equiv of **5** (internal standard) was dissolved in dry acetone (2 mL). A small portion of the resulting stock solution (ca 25 μ L) was dissolved in dichloromethane or dry acetone, and then analyzed by HPLC (to obtain the relative concentrations at $t = 0$). The remaining stock solution was injected in the aqueous acetone (150 or 300 mL) containing the corresponding additive. The composition of the acetone-water mixture was calculated so that the reaction mixture contained 60% v/v acetone after the injection of the stock solution. Aliquots of the reaction solution (10 mL) were taken after certain time periods (5 or 10 minutes) and extracted with dichloromethane or diethyl ether. The organic phase was washed with water followed by drying over magnesium sulfate and evaporation of the solvents. The resulting crude mixture was dissolved in dry acetone or dichloromethane and analyzed (diode array detection, the quantitative analysis was applied to chromatograms at $\lambda = 254$ nm) by chiral HPLC (Daicel IB column, 0.46 cm $\phi \times 25$ cm, 5 μ m dp, 25 °C) using the gradient method described in Table S1.

Table S1. Gradient method used for separation of the compounds **1-7** (flow rate 1 mL min $^{-1}$).

retention time	<i>n</i> -hexane / %	isopropanol / %
0	99.1	0.9
72 ^a	99.1	0.9
75	94.9	5.1
95 ^b	94.9	5.1
100	99.1	0.9
120	99.1	0.9

^a The change of solvent composition between two retention times was carried out by continuous ramp. ^b All compounds were eluted from the column at this time. The remaining part of the method just restores the solvent composition and equilibrates the column for the next run.

The exact experimental conditions for the kinetic experiments performed in this work are summarized in Table S2.

A typical chromatogram observed in HPLC kinetic measurements is shown in Figure S1.

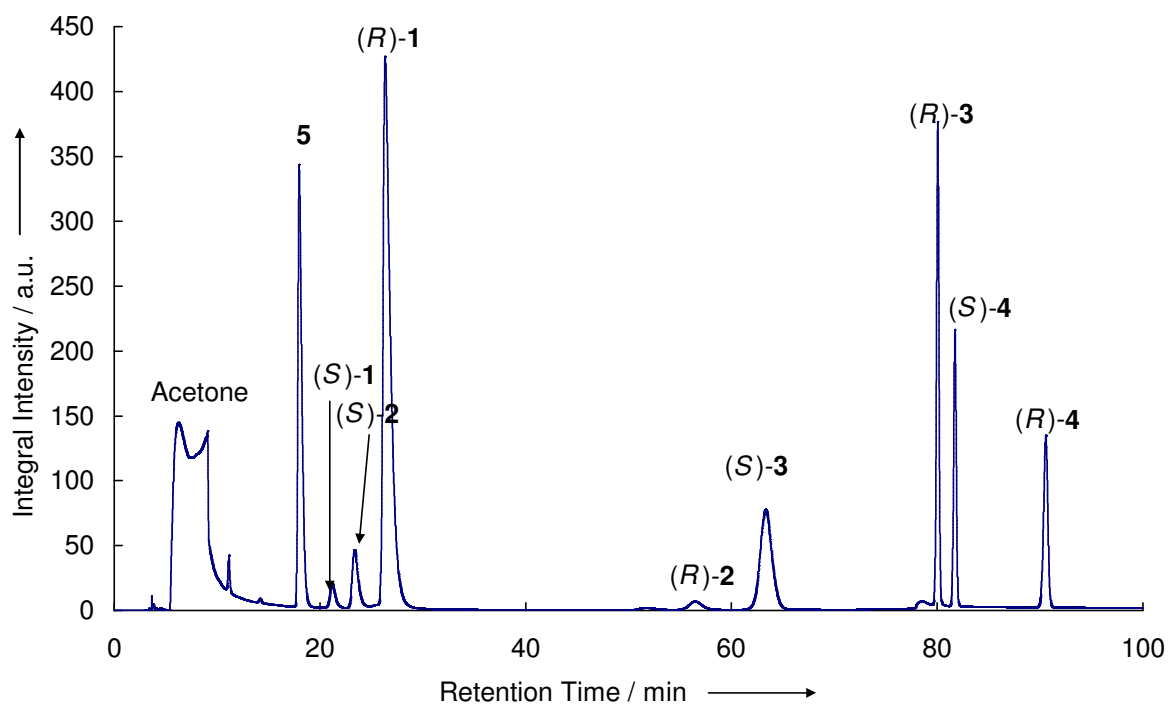


Figure S1. Chromatogram of the reaction mixture quenched 50 min after dissolving (*R*)-**1** in 60% aq acetone.

Table S2. Summary of the HPLC kinetic experiments.

experiment ID	acetone, %	substrate	additive	[substrate] ₀ / M	[S] / M	[additive] ₀ / M	extraction solvent	injection solvent ^e	raw data ^b	normalized data ^b
1	60	(R)-1	-	1.53×10^{-3}	1.53×10^{-3}	-	CH ₂ Cl ₂	acetone	Table S5	Table S5a
2	60	(R)-1	Bu ₄ NOPNB ^c	8.04×10^{-4}	8.89×10^{-4}	4.82×10^{-3}	Et ₂ O ^d	acetone	Table S6	Table S6a
3	60	(R)-1	Bu ₄ NOPNB ^c	7.82×10^{-4}	7.84×10^{-4}	5.25×10^{-2}	Et ₂ O ^d	acetone	Table S7	Table S7a
4	60	(R)-1	NaN ₃	8.04×10^{-4}	1.09×10^{-3}	7.08×10^{-2}	Et ₂ O	CH ₂ Cl ₂	Table S8	Table S8a
5	60	(R)-1	Bu ₄ NCl	1.02×10^{-3}	1.23×10^{-3}	1.87×10^{-2}	CH ₂ Cl ₂	acetone	Table S9	Table S9a
6	60	(R)-1	Bu ₄ NCl	8.51×10^{-4}	8.64×10^{-4}	1.01×10^{-1}	CH ₂ Cl ₂	acetone	Table S10	Table S10a
7	60	(R)-1	Piperidine	8.70×10^{-4}	8.73×10^{-4}	5.42×10^{-2}	CH ₂ Cl ₂	CH ₂ Cl ₂	Table S11	Table S11a
8	60	(R)-1	LiClO ₄	8.61×10^{-4}	9.24×10^{-4}	9.46×10^{-3}	CH ₂ Cl ₂	acetone	Table S12	Table S12a
9	60	(S)-2	-	7.85×10^{-4}	9.30×10^{-4}	-	CH ₂ Cl ₂	acetone	Table S13	Table S13a
10	60	(S)-2	NaN ₃	7.90×10^{-4}	8.49×10^{-4}	7.66×10^{-2}	Et ₂ O	CH ₂ Cl ₂	Table S14	Table S14a
11	80	(R)-1	-	7.72×10^{-4}	8.86×10^{-4}	-	CH ₂ Cl ₂	CH ₂ Cl ₂	Table S15	Table S15a
12	90	(R)-1	-	6.82×10^{-4}	7.99×10^{-4}	-	CH ₂ Cl ₂	CH ₂ Cl ₂	Table S16	Table S16a

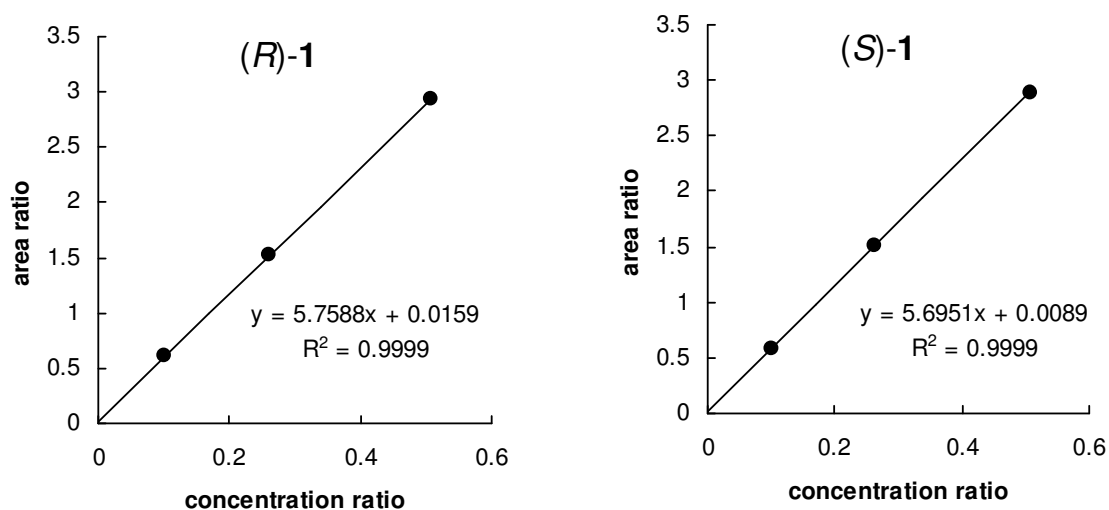
^a The solvent used to dissolve the crude reaction mixture for the injection in the HPLC. As acetone gives a broad peak at t_R between 5 and 10 minutes, it overlaps with the peaks located in this area (diaryllallyl piperidines and azides). Peaks in this area can be analyzed when the samples are dissolved in CH₂Cl₂. ^b The time-dependent concentrations can be found in the given tables (see Section 4.3). ^c Tetrabutylammonium 4-nitrobenzoate. ^d With dichloromethane as the extraction solvent, significant amounts of tetrabutylammonium salt would stay in the organic phase which would cause additional peaks in the chromatogram. This can be avoided by using diethyl ether.

5.4.2. HPLC calibration

The substances **1–4** were calibrated with chalcone **5** as internal standard. The calibration data are listed in Table S3 and the calibration lines are shown on Figures S1-S5.

Table S3. Calibration data for compounds **1–4**.

[5] / M	[(rac)-N] / M	$\frac{[(R)\text{-N}]/[5]}{[(S)\text{-N}]/[5]}$	I_5	$I_{(R)\text{-N}}$	$I_{(S)\text{-N}}$	$I_{(R)\text{-N}}/I_5$	$I_{(S)\text{-N}}/I_5$
N = 1							
2.42×10^{-3}	1.26×10^{-3}	0.261	12665	19417	19125	1.533	1.510
2.79×10^{-3}	2.83×10^{-3}	0.508	17738	51965	51294	2.930	2.892
6.31×10^{-3}	1.27×10^{-3}	0.101	38659	23477	22606	0.607	0.585
N = 2							
2.36×10^{-3}	1.47×10^{-3}	0.310	11523	21366	21186	1.854	1.839
2.07×10^{-3}	2.65×10^{-3}	0.641	9794.5	36211	35895	3.697	3.665
4.67×10^{-3}	1.31×10^{-3}	0.141	22508	18484	17946	0.821	0.797
N = 3							
2.25×10^{-3}	2.61×10^{-3}	0.579	12504	28102	28110	2.247	2.248
2.44×10^{-3}	3.51×10^{-3}	0.720	14489	40012	39696	2.762	2.740
4.57×10^{-3}	2.44×10^{-3}	0.267	22004	21978	22056	0.999	1.002
N = 4							
2.52×10^{-3}	2.84×10^{-3}	0.564	14043	27624	27625	1.967	1.967
2.05×10^{-3}	4.03×10^{-3}	0.983	9040.7	29725	29711	3.288	3.286
4.82×10^{-3}	2.24×10^{-3}	0.232	22728	18466	18440	0.812	0.811

**Figure S2.** Calibration lines for (R)- and (S)-**1** obtained using the Daicel IB column and the gradient method described above.

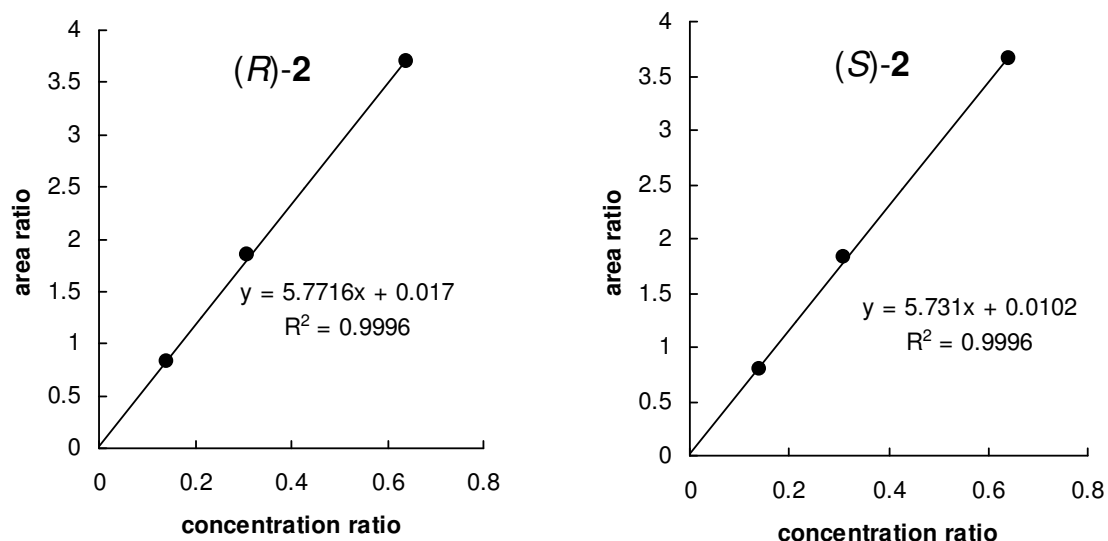


Figure S3. Calibration lines for (R)- and (S)-2 obtained using the Daicel IB column and the gradient method described above.

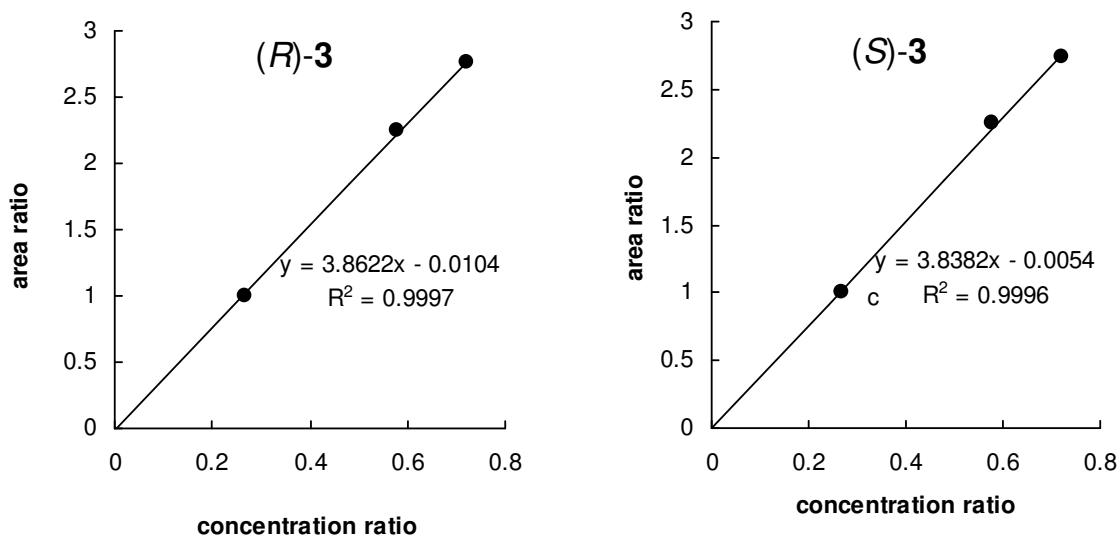


Figure S4. Calibration lines for (R)- and (S)-3 obtained using the Daicel IB column and the gradient method described above.

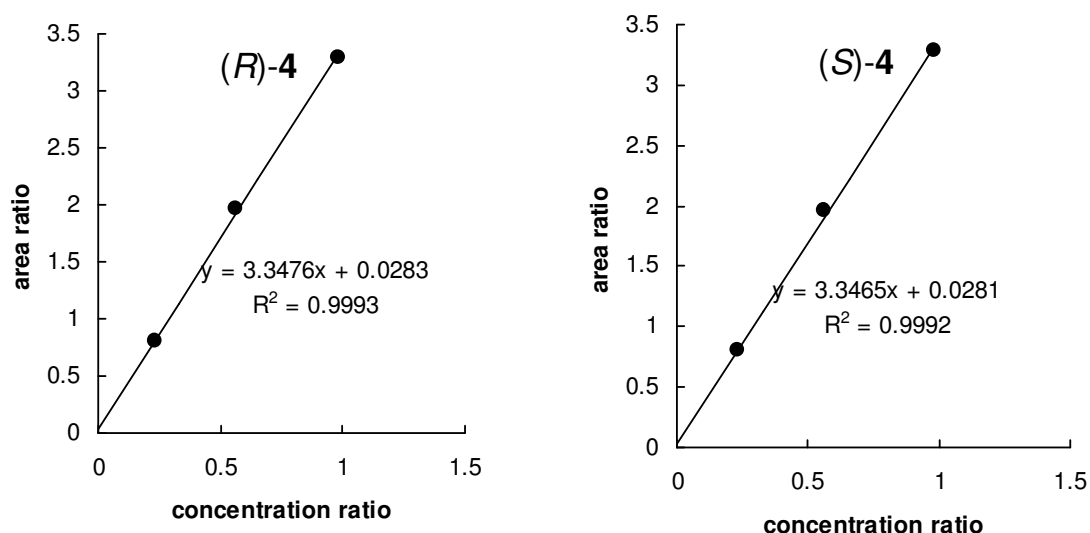


Figure S5. Calibration lines for (*R*)- and (*S*)-**4** obtained using the Daicel IB column and the gradient method described above.

The HPLC characteristics (Daicel IB column and the gradient method described above) of compounds **1-5** as well as **7** and **7'** are summarized in Table S4.

Table S4. Retention times and calibration data for compounds **1-5** and **7**.

compound	retention time (t_R) / min ^a	calibration parameters ^b	
		slope m	intercept b
5 ^c	16.5	1	0
(<i>S</i>)- 1	20.4	5.70	8.89×10^{-3}
(<i>R</i>)- 1	25.2	5.76	1.59×10^{-2}
(<i>S</i>)- 2	22.5	5.73	1.02×10^{-2}
(<i>R</i>)- 2	55.2	5.77	1.70×10^{-2}
(<i>S</i>)- 3	59.6	3.84	-5.45×10^{-3}
(<i>R</i>)- 3	79.0	3.86	-1.04×10^{-2}
(<i>S</i>)- 4	81.1	3.35	2.81×10^{-2}
(<i>R</i>)- 4	90.0	3.35	2.83×10^{-2}
RPip ^d	4.3	<i>e</i>	<i>e</i>
RN ₃ ^d	7.0-8.0	<i>e</i>	<i>e</i>

^a The retention times may vary (± 2 min) in different runs due to the use of the gradient method. ^b The slopes and intercepts of the calibration lines ^c The chalcone **5** was used as internal standard. ^d As the full separation of peaks of single stereoisomers was not possible under the conditions used, the partially separated peaks of all four stereoisomers were treated as one broad peak. ^e Calibration was not performed.

5.4.3. Kinetics of the solvolysis reactions

Raw data

Table S5. Time-dependent relative concentrations of **1-4** (in relative units) for solvolysis of **(R)-1** ($c_0 = 1.53 \times 10^{-3}$ M) in 60% aq acetone, 25 °C.

<i>t</i> / s	[(R)-1]	[(S)-1]	[(R)-2]	[(S)-2]	[(R)-3]	[(S)-3]	[(R)-4]	[(S)-4]
0	1.0600	0.0000	0.0000	0.0000	0.0000	0.0000	0.0000	0.0000
305	1.0100	0.0033	0.0019	0.0099	0.0282	0.0263	0.0099	0.0099
605	0.9200	0.0051	0.0032	0.0160	0.0523	0.0480	0.0254	0.0261
905	0.8290	0.0070	0.0050	0.0226	0.0714	0.0701	0.0413	0.0418
1205	0.7450	0.0076	0.0053	0.0255	0.0937	0.0896	0.0550	0.0556
1505	0.6470	0.0134	0.0101	0.0556	0.1100	0.1070	0.0691	0.0695
1805	0.5890	0.0138	0.0105	0.0444	0.1270	0.1230	0.0799	0.0811
2105	0.5540	0.0104	0.0075	0.0334	0.1460	0.1390	0.0906	0.0911
2405	0.5010	0.0108	0.0078	0.0348	0.1570	0.1520	0.1010	0.1010
2705	0.4450	0.0132	0.0101	0.0377	0.1700	0.1670	0.1100	0.1110
3005	0.4090	0.0113	0.0080	0.0337	0.1820	0.1790	0.1190	0.1190
3305	0.3700	0.0112	0.0076	0.0353	0.1930	0.1890	0.1260	0.1270
3605	0.3360	0.0117	0.0083	0.0335	0.2050	0.1990	0.1340	0.1360
3925	0.3000	0.0128	0.0092	0.0336	0.2150	0.2090	0.1420	0.1420
4205	0.2780	0.0099	0.0064	0.0301	0.2240	0.2170	0.1470	0.1480
4515	0.2520	0.0114	0.0079	0.0312	0.2340	0.2270	0.1540	0.1550
4805	0.2270	0.0117	0.0081	0.0296	0.2390	0.2310	0.1580	0.1590
5131	0.2100	0.0100	0.0063	0.0292	0.2530	0.2440	0.1660	0.1680
5405	0.1930	0.0090	0.0062	0.0258	0.2540	0.2460	0.1670	0.1680
5705	0.1600	0.0138	0.0101	0.0293	0.2630	0.2550	0.1730	0.1750
6012	0.1400	0.0124	0.0088	0.0290	0.2600	0.2540	0.1720	0.1730
6305	0.1460	0.0079	0.0046	0.0222	0.2720	0.2640	0.1800	0.1820
6605	0.1330	0.0072	0.0041	0.0205	0.2740	0.2660	0.1810	0.1830
6905	0.1190	0.0073	0.0043	0.0187	0.2790	0.2700	0.1850	0.1860
7522	0.1010	0.0059	0.0030	0.0164	0.2870	0.2770	0.1910	0.1930
7805	0.0921	0.0057	0.0028	0.0156	0.2930	0.2810	0.1940	0.1970
8101	0.0846	0.0055	0.0025	0.0141	0.2930	0.2820	0.1940	0.1960
8405	0.0750	0.0058	0.0030	0.0142	0.2970	0.2890	0.1990	0.2000
8726	0.0675	0.0052	0.0024	0.0133	0.2950	0.2880	0.1970	0.1990

Table S6. Time-dependent relative concentrations of **1-4** (in relative units) for solvolysis of **(R)-1** ($c_0 = 8.04 \times 10^{-4}$ M) in 60% aq acetone in the presence of 4.8 mM Bu₄NOPNB, 25 °C.

<i>t</i> / s	[(R)-1]	[(S)-1]	[(R)-2]	[(S)-2]	[(R)-3]	[(S)-3]	[(R)-4]	[(S)-4]
0	0.9490	0.0000	0.0000	0.0000	0.0000	0.0000	0.0000	0.0000
290	0.8130	0.0028	0.0011	0.0088	0.0200	0.0193	0.0040	0.0064
593	0.7760	0.0073	0.0072	0.0161	0.0383	0.0375	0.0169	0.0172
894	0.6950	0.0106	0.0087	0.0214	0.0539	0.0529	0.0283	0.0291
1200	0.6410	0.0139	0.0108	0.0273	0.0697	0.0695	0.0399	0.0400
1501	0.9440	0.0280	0.0263	0.0570	0.1350	0.1310	0.0849	0.0856
1800	0.5350	0.0179	0.0141	0.0313	0.0983	0.0971	0.0592	0.0593
2108	0.5030	0.0205	0.0156	0.0374	0.1150	0.1130	0.0711	0.0717
2399	0.4700	0.0219	0.0168	0.0371	0.1270	0.1260	0.0798	0.0799
2700	0.4260	0.0231	0.0180	0.0402	0.1400	0.1390	0.0890	0.0896
3000	0.3820	0.0230	0.0179	0.0378	0.1460	0.1450	0.0930	0.0932
3313	0.3480	0.0238	0.0187	0.0398	0.1560	0.1550	0.1010	0.1010
3601	0.3190	0.0236	0.0183	0.0375	0.1640	0.1640	0.1070	0.1060
3918	0.2856	0.0237	0.0183	0.0382	0.1728	0.1729	0.1135	0.1145
4200	0.2695	0.0239	0.0182	0.0368	0.1830	0.1833	0.1208	0.1208
4500	0.2438	0.0235	0.0176	0.0361	0.1910	0.1905	0.1257	0.1267
4809	0.2279	0.0234	0.0180	0.0349	0.1997	0.1990	0.1313	0.1326
5100	0.2051	0.0229	0.0182	0.0344	0.2045	0.2058	0.1355	0.1361
5400	0.1902	0.0224	0.0162	0.0324	0.2120	0.2111	0.1406	0.1412
5700	0.1748	0.0224	0.0162	0.0346	0.2172	0.2183	0.1451	0.1460
6002	0.1597	0.0215	0.0154	0.0322	0.2224	0.2225	0.1483	0.1483
6307	0.1452	0.0206	0.0149	0.0297	0.2273	0.2286	0.1526	0.1531
6599	0.1357	0.0200	0.0143	0.0277	0.2337	0.2332	0.1561	0.1564
6901	0.1211	0.0192	0.0144	0.0267	0.2404	0.2407	0.1609	0.1611
7201	0.1116	0.0185	0.0136	0.0247	0.2425	0.2425	0.1624	0.1633
7500	0.1043	0.0179	0.0127	0.0235	0.2490	0.2490	0.1672	0.1674
7803	0.0945	0.0170	0.0119	0.0224	0.2538	0.2535	0.1706	0.1713
8102	0.0863	0.0160	0.0109	0.0206	0.2550	0.2545	0.1716	0.1716
8400	0.0812	0.0160	0.0103	0.0222	0.2535	0.2581	0.1737	0.1740
8724	0.0719	0.0143	0.0110	0.0177	0.2558	0.2568	0.1736	0.1744

Table S7. Time-dependent relative concentrations of **1-4** (in relative units) for solvolysis of **(R)-1** ($c_0 = 7.82 \times 10^{-4}$ M) in 60% aq acetone in the presence of 52.5 mM Bu₄NOPNB, 25 °C.

<i>t</i> / s	[(S)-1]	[(R)-1]	[(S)-2]	[(R)-2]	[(S)-3]	[(R)-3]	[(S)-4]	[(R)-4]
0	1.0000	0.0000	0.0000	0.0000	0.0000	0.0000	0.0000	0.0000
607	0.8336	0.0256	0.0177	0.0299	0.0211	0.0211	0.0215	0.0066
1210	0.7280	0.0414	0.0286	0.0467	0.0373	0.0373	0.0371	0.0184
1800	0.7289	0.0583	0.0426	0.0668	0.0541	0.0541	0.0533	0.0291
2400	0.6034	0.0704	0.0517	0.0798	0.0693	0.0693	0.0697	0.0403
3000	0.5512	0.0777	0.0569	0.0836	0.0848	0.0848	0.0854	0.0512
3601	0.4859	0.0839	0.0608	0.0874	0.0996	0.0996	0.1137	0.0609
4200	0.5222	0.0905	0.0680	0.0958	0.1022	0.1022	0.1052	0.0643
4800	0.4584	0.0924	0.0687	0.0940	0.1302	0.1302	0.1288	0.0819
5412	0.4062	0.0954	0.0691	0.0947	0.1431	0.1431	0.1417	0.0909
6000	0.3885	0.0949	0.0688	0.0934	0.1567	0.1567	0.1529	0.0984
6600	0.3823	0.0954	0.0696	0.0935	0.1688	0.1688	0.1652	0.1065
7202	0.3878	0.0958	0.0695	0.0930	0.1824	0.1824	0.1776	0.1155
7800	0.3239	0.0956	0.0692	0.0919	0.1959	0.1959	0.1898	0.1242
8395	0.2878	0.0962	0.0692	0.0915	0.2070	0.2070	0.2039	0.1337
9007	0.3672	0.0898	0.0644	0.0878	0.2085	0.2085	0.2035	0.1343

Table S8. Time-dependent relative concentrations of **1-4** (in relative units) for solvolysis of (*R*)-**1** ($c_0 = 8.04 \times 10^{-4}$ M) in 60% aq acetone in the presence of 70.8 mM NaN₃, 25 °C.

<i>t</i> / s	[(<i>R</i>)- 1]	[(<i>S</i>)- 1]	[(<i>R</i>)- 2]	[(<i>S</i>)- 2]	[(<i>R</i>)- 3] ^a	[(<i>S</i>)- 3] ^a	[(<i>R</i>)- 4]	[(<i>S</i>)- 4]	I_{RN_3}/I_5^b
0	0.8836	0.0000	c	0.0000	0.0000	0.0000	c	c	0.0000
618	0.7179	0.0013	c	0.0097	0.0043	0.0069	c	c	<i>d</i>
1200	0.6158	0.0033	c	0.0162	0.0044	0.0043	c	c	0.9418
1803	0.5025	0.0039	c	0.0189	0.0052	0.0099	c	c	1.3140
2400	0.4134	0.0044	c	0.0208	0.0071	0.0000	c	c	1.6041
3035	0.3354	0.0043	c	0.0210	0.0091	0.0000	c	c	1.8813
3647	0.2601	0.0046	c	0.0212	0.0128	0.0111	c	c	2.0943
4206	0.2318	0.0042	c	0.0192	0.0109	0.0060	c	c	2.2484
4800	0.1904	0.0036	c	0.0175	0.0088	0.0133	c	c	2.4201
5400	0.1559	0.0034	c	0.0160	0.0097	0.0137	c	c	2.5396
6040	0.1269	0.0030	c	0.0141	0.0096	0.0129	c	c	2.6141
6610	0.1043	0.0016	c	0.0125	0.0132	0.0118	c	c	2.7349
7215	0.0868	0.0018	c	0.0108	0.0129	0.0124	c	c	2.8195
7816	0.0698	0.0013	c	0.0091	0.0114	0.0103	c	c	2.8320
8405	0.0575	0.0004	c	0.0077	0.0109	0.0086	c	c	2.8959
9002	0.0515	0.0004	c	0.0069	0.0205	0.0165	c	c	3.1869

^a The precision of the HPLC integration was rather low due to low intensity of the peak, presence of some impurities giving peaks in the same time range as the given compounds, and slight changes in the baseline due to the solvent gradient used to reduce the analysis time. ^b I_{RN_3} and I_5 are the integral areas of peaks corresponding to all diaryllallyl azides and internal standard **5**, respectively. ^c The precision of the HPLC integration was too low to derive reliable values of the time-dependent concentrations. ^d The acetone solution of the quenched probe was injected in the HPLC, therefore, the peak of RN₃ overlapped with that of acetone.

Table S9. Time-dependent relative concentrations of **1-4** (in relative units) for solvolysis of (*R*)-**1** ($c_0 = 1.02 \times 10^{-3}$ M) in 60% aq acetone in the presence of 18.7 mM Bu₄NCl, 25 °C.

<i>t</i> / s	[(<i>R</i>)- 1]	[(<i>S</i>)- 1]	[(<i>R</i>)- 2]	[(<i>S</i>)- 2]	[(<i>R</i>)- 3]	[(<i>S</i>)- 3]	[(<i>R</i>)- 4]	[(<i>S</i>)- 4]
0	0.9157	0.0000	0.0000	0.0000	0.0000	0.0000	0.0000	0.0000
1229	0.5660	0.0025	0.0001	0.0149	0.0813	0.0813	0.0481	0.0485
2400	0.3997	0.0043	0.0016	0.0204	0.1339	0.1358	0.0870	0.0874
3611	0.2755	0.0049	0.0019	0.0209	0.1757	0.1768	0.1161	0.1167
5400	0.1508	0.0040	0.0013	0.0162	0.2143	0.2156	0.1430	0.1437
7200	0.0861	0.0029	0.0004	0.0117	0.2390	0.2406	0.1610	0.1628

Table S10. Time-dependent relative concentrations of **1-4** (in relative units) for solvolysis of (*R*)-**1** ($c_0 = 8.51 \times 10^{-4}$ M) in 60% aq acetone in the presence of 100.7 mM Bu₄NCl, 25 °C.

<i>t</i> / s	[(<i>R</i>)- 1]	[(<i>S</i>)- 1]	[(<i>R</i>)- 2]	[(<i>S</i>)- 2]	[(<i>R</i>)- 3]	[(<i>S</i>)- 3]	[(<i>R</i>)- 4]	[(<i>S</i>)- 4]
0	1.0203	0.0000	0.0000	0.0000	0.0000	0.0000	0.0000	0.0000
1200	0.7233	0.0024	0.0007	0.0190	0.0820	0.0824	0.0493	0.0497
2400	0.5010	0.0041	0.0020	0.0288	0.1404	0.1419	0.0897	0.0907
3600	0.3534	0.0047	0.0021	0.0244	0.1830	0.1866	0.1213	0.1215
5400	0.2035	0.0039	0.0014	0.0246	0.2210	0.2256	0.1483	0.1488

Table S11. Time-dependent relative concentrations of **1-4** (in relative units) for solvolysis of (*R*)-**1** ($c_0 = 8.70 \times 10^{-4}$ M) in 60% aq acetone in the presence of 54.2 mM piperidine, 25 °C.

<i>t</i> / s	[(<i>R</i>)- 1]	[(<i>S</i>)- 1]	[(<i>R</i>)- 2] ^a	[(<i>S</i>)- 2]	[(<i>R</i>)- 3]	[(<i>S</i>)- 3] ^b	[(<i>R</i>)- 4]	[(<i>S</i>)- 4]
0	1.1423	0.0000	0.0000	0.0000	0.0000	0.0000	0.0000	0.0000
600	1.6038	0.0060	0.0020	0.0241	0.0566	0.0845	0.0257	0.0283
1200	1.0944	0.0086	0.0027	0.0324	0.0835	0.1242	0.0444	0.0460
1800	1.1187	0.0139	0.0016	0.0486	0.1378	0.2088	0.0823	0.0849
2405	0.7445	0.0121	0.0018	0.0421	0.1390	0.2070	0.0840	0.0886
3000	0.5940	0.0123	0.0000	0.0413	0.1527	0.2389	0.0959	0.0998
3600	0.5482	0.0139	0.0027	0.0454	0.1908	0.2793	0.1233	0.1274
4200	0.3216	0.0113	0.0013	0.0306	0.1516	0.2293	0.0941	0.0983
4798	0.2735	0.0092	0.0003	0.0294	0.1690	0.2452	0.1063	0.1116
5400	0.2176	0.0082	0.0041	0.0257	0.1721	0.2538	0.1091	0.1141
6015	0.1920	0.0081	0.0013	0.0249	0.1972	0.2892	0.1257	0.1322
6598	0.1415	0.0064	0.0004	0.0196	0.1885	0.2725	0.1173	0.1259
7202	0.1184	0.0058	0.0022	0.0175	0.1922	0.2848	0.1239	0.1287
7800	0.0839	0.0041	0.0000	0.0129	0.1730	0.2511	0.1106	0.1176
8400	0.0755	0.0039	0.0018	0.0122	0.1982	0.2772	0.1245	0.1321

^a The precision of the HPLC integration was too low to derive reliable values of the time-dependent concentrations. ^b The precision of the HPLC integration was rather low due to presence of some impurities giving peaks in the same time range as (*S*)-**3**.

Table S12. Time-dependent relative concentrations of **1-4** (in relative units) for solvolysis of **(R)-1** ($c_0 = 8.61 \times 10^{-4}$ M) in 60% aq acetone in the presence of 9.5 mM LiClO₄, 25 °C.

<i>t</i> / s	[(R)-1]	[(S)-1]	[(R)-2]	[(S)-2]	[(R)-3]	[(S)-3]	[(R)-4]	[(S)-4]
0	1.0387	0.0000	0.0000	0.0013	0.0000	0.0000	0.0000	0.0000
328	0.8996	0.0027	0.0002	0.0109	0.0262	0.0225	0.0083	0.0089
603	0.8325	0.0043	0.0039	0.0162	0.0456	0.0428	0.0224	0.0235
900	0.7719	0.0051	0.0034	0.0195	0.0708	0.0669	0.0393	0.0396
1210	0.6766	0.0098	0.0030	0.0355	0.0840	0.0781	0.0500	0.0500
1805	0.5595	0.0091	0.0071	0.0350	0.1131	0.1115	0.0725	0.0723
2408	0.4615	0.0112	0.0085	0.0401	0.1443	0.1423	0.0943	0.0940
2709	0.4411	0.0108	0.0075	0.0375	0.1522	0.1501	0.1008	0.1005
3600	0.3288	0.0108	0.0074	0.0327	0.1859	0.1992	0.1254	0.1254
3909	0.2921	0.0101	0.0066	0.0328	0.1892	0.1887	0.1293	0.1299
4208	0.2643	0.0102	0.0070	0.0284	0.2121	0.2118	0.1430	0.1430
4514	0.2505	0.0084	0.0050	0.0241	0.2187	0.2157	0.1465	0.1472
4799	0.2327	0.0089	0.0057	0.0266	0.1847	0.1839	0.1307	0.1308
5106	0.1986	0.0105	0.0081	0.0269	0.2148	0.2121	0.1478	0.1486
5706	0.1770	0.0082	0.0045	0.0242	0.2420	0.2356	0.1623	0.1647
6005	0.1593	0.0062	0.0039	0.0183	0.2531	0.2514	0.1715	0.1716
6299	0.1405	0.0075	0.0040	0.0193	0.2428	0.2405	0.1676	0.1686
6600	0.1346	0.0056	0.0035	0.0166	0.2659	0.2650	0.1817	0.1818
6900	0.1215	0.0061	0.0037	0.0166	0.2450	0.2436	0.1724	0.1725
7516	0.1006	0.0056	0.0028	0.0175	0.2336	0.2325	0.1661	0.1659
7800	0.0880	0.0052	0.0031	0.0125	0.2577	0.2563	0.1790	0.1793

Table S13. Time-dependent relative concentrations of **1-4** (in relative units) for solvolysis of (*S*)-**2** ($c_0 = 7.85 \times 10^{-4}$ M) in 60% aq acetone, 25 °C.

<i>t</i> / s	[(<i>S</i>)- 2]	[(<i>R</i>)- 2]	[(<i>S</i>)- 1]	[(<i>R</i>)- 1]	[(<i>R</i>)- 3]	[(<i>S</i>)- 3]	[(<i>R</i>)- 4]	[(<i>S</i>)- 4]
0	0.8641	0.0000	0.0017	0.0000	0.0000	0.0000	0.0000	0.0000
605	0.7251	0.0080	0.0063	0.0190	0.0466	0.0430	0.0235	0.0232
1200	0.5982	0.0091	0.0097	0.0302	0.0833	0.0802	0.0505	0.0503
1800	0.4574	0.0090	0.0091	0.0261	0.1108	0.1117	0.0718	0.0714
2400	0.3700	0.0084	0.0092	0.0276	0.1425	0.1380	0.0899	0.0900
3002	0.3031	0.0073	0.0099	0.0365	0.1596	0.1608	0.1068	0.1063
3600	0.2470	0.0061	0.0091	0.0349	0.1822	0.1794	0.1204	0.1198
4220	0.1983	0.0057	0.0086	0.0326	0.1946	0.1963	0.1319	0.1313
4800	0.1604	0.0048	0.0078	0.0300	0.2075	0.2077	0.1405	0.1395
5400	0.1292	0.0045	0.0071	0.0271	0.2203	0.2180	0.1478	0.1472
6000	0.1045	0.0032	0.0060	0.0234	0.2287	0.2267	0.1540	0.1538
6600	0.0835	0.0032	0.0062	0.0220	0.2343	0.2346	0.1595	0.1597
7200	0.0682	0.0023	0.0051	0.0195	0.2423	0.2430	0.1648	0.1649
7800	0.0554	0.0017	0.0043	0.0165	0.2495	0.2502	0.1702	0.1702
8400	0.0458	0.0011	0.0040	0.0142	0.2605	0.2584	0.1778	0.1782
9000	0.0352	0.0018	0.0041	0.0137	0.2681	0.2680	0.1824	0.1831

Table S14. Time-dependent relative concentrations of **1-4** (in relative units) for solvolysis of (*S*)-**2** ($c_0 = 7.90 \times 10^{-4}$ M) in 60% aq acetone in the presence of 76.6 mM NaN₃, 25 °C.

<i>t</i> / s	[(<i>S</i>)- 2]	[(<i>R</i>)- 2]	[(<i>S</i>)- 1]	[(<i>R</i>)- 1]	[(<i>R</i>)- 3]	[(<i>S</i>)- 3]	[(<i>R</i>)- 4]	[(<i>S</i>)- 4]	$I_{\text{RN3}}/I_{\text{S}}^b$
0	1.0065	<i>a</i>	0.0000	0.0000	<i>a</i>	<i>a</i>	<i>a</i>	<i>a</i>	0.0000
635	0.8457	<i>a</i>	0.0060	0.0186	<i>a</i>	<i>a</i>	<i>a</i>	<i>a</i>	0.4820
1200	0.6544	<i>a</i>	0.0074	0.0279	<i>a</i>	<i>a</i>	<i>a</i>	<i>a</i>	1.1524
1800	0.5472	<i>a</i>	0.0067	0.0291	<i>a</i>	<i>a</i>	<i>a</i>	<i>a</i>	1.5826
2410	0.4488	<i>a</i>	0.0068	0.0313	<i>a</i>	<i>a</i>	<i>a</i>	<i>a</i>	1.9165
2998	0.3663	<i>a</i>	0.0062	0.0315	<i>a</i>	<i>a</i>	<i>a</i>	<i>a</i>	2.2060
3600	0.3003	<i>a</i>	0.0073	0.0308	<i>a</i>	<i>a</i>	<i>a</i>	<i>a</i>	2.4807
4202	0.2446	<i>a</i>	0.0068	0.0300	<i>a</i>	<i>a</i>	<i>a</i>	<i>a</i>	2.7057
4800	0.1977	<i>a</i>	0.0064	0.0270	<i>a</i>	<i>a</i>	<i>a</i>	<i>a</i>	2.8461
5408	0.1646	<i>a</i>	0.0057	0.0257	<i>a</i>	<i>a</i>	<i>a</i>	<i>a</i>	3.0737
6000	0.1299	<i>a</i>	0.0038	0.0227	<i>a</i>	<i>a</i>	<i>a</i>	<i>a</i>	3.0915
6602	0.1037	<i>a</i>	0.0038	0.0198	<i>a</i>	<i>a</i>	<i>a</i>	<i>a</i>	3.1752
7203	0.0837	<i>a</i>	0.0030	0.0170	<i>a</i>	<i>a</i>	<i>a</i>	<i>a</i>	3.2430
7800	0.0688	<i>a</i>	0.0034	0.0152	<i>a</i>	<i>a</i>	<i>a</i>	<i>a</i>	3.3523
8416	0.0564	<i>a</i>	0.0021	0.0131	<i>a</i>	<i>a</i>	<i>a</i>	<i>a</i>	3.3927
9000	0.0447	<i>a</i>	0.0018	0.0109	<i>a</i>	<i>a</i>	<i>a</i>	<i>a</i>	3.4977

^a The precision of the HPLC integration was too low to derive reliable values of the time-dependent concentrations. ^b I_{RN3} is the sum of integral areas of all peaks corresponding to diaryllallyl azides, I_{S} is the integral area of the internal standard **5**.

Table S15. Time-dependent relative concentrations of **1-4** (in relative units) for solvolysis of (*R*)-**1** ($c_0 = 7.72 \times 10^{-4}$ M) in 80% aq acetone, 25 °C.

<i>t</i> / s	[(<i>R</i>)- 1]	[(<i>S</i>)- 1]	[(<i>R</i>)- 2]	[(<i>S</i>)- 2]	[(<i>R</i>)- 3]	[(<i>S</i>)- 3]	[(<i>R</i>)- 4]	[(<i>S</i>)- 4]
0	1.0087	0.0000	0.0000	0.0000	0.0000	0.0000	0.0000	0.0000
7244	0.8162	0.0165	0.0104	0.0374	0.0542	0.0548	0.0305	0.0298
14476	0.6271	0.0260	0.0202	0.0569	0.0957	0.0952	0.0613	0.0600
21600	0.4924	0.0330	0.0257	0.0677	0.1332	0.1331	0.0896	0.0875
29104	0.3675	0.0360	0.0275	0.0711	0.1623	0.1622	0.1114	0.1092
36540	0.2936	0.0364	0.0253	0.0627	0.1882	0.1902	0.1316	0.1295
43200	0.2292	0.0350	0.0255	0.0576	0.2065	0.2057	0.1450	0.1411
86062	0.0492	0.0181	0.0112	0.0212	0.2835	0.2855	0.2027	0.1991
111570	0.0248	0.0107	0.0055	0.0110	0.2998	0.2952	0.2150	0.2103

Table S16. Time-dependent relative concentrations of **1-4** (in relative units) for solvolysis of (*R*)-**1** ($c_0 = 6.82 \times 10^{-4}$ M) in 90% aq acetone, 25 °C.

<i>t</i> / s	[(<i>R</i>)- 1]	[(<i>S</i>)- 1]	[(<i>R</i>)- 2]	[(<i>S</i>)- 2]	[(<i>R</i>)- 3]	[(<i>S</i>)- 3]	[(<i>R</i>)- 4]	[(<i>S</i>)- 4]
0	1.0569	0.0000	0.0000	0.0000	0.0000	0.0000	0.0000	0.0000
47767	0.7487	0.0455	0.0385	0.0845	0.0598	0.0566	0.0353	0.0340
83963	0.5622	0.0650	0.0550	0.1083	0.0983	0.0961	0.0591	0.0591
136220	0.3954	0.0811	0.0668	0.1189	0.1372	0.1443	0.1013	0.1013
179370	0.2854	0.0890	0.0688	0.1121	0.1745	0.1858	0.1289	0.1280
222954	0.2146	0.0871	0.0621	0.0988	0.2043	0.2211	0.1511	0.1510
249529	0.1816	0.0802	0.0581	0.0884	0.2156	0.2286	0.1600	0.1599
569855	0.0356	0.0309	0.0192	0.0241	0.3793	0.3661	0.2807	0.2704

Normalized time-dependent concentrations

In order to compare different experiments, the relative concentrations presented in Tables S5-S16 have been normalized.

In the absence of piperidine or sodium azide, the HPLC samples contain only diaryllallyl 4-nitrobenzoates and alcohols. According to eq S0, the sum of their concentrations, $\Sigma(t)$, must be equal to the initial concentration of substrate (i.e., $[(R)-\mathbf{1}]_0$ or $[(S)-\mathbf{2}]_0$).

$$\Sigma(t) = [(R)-\mathbf{1}](t) + [(S)-\mathbf{1}](t) + [(R)-\mathbf{2}](t) + [(S)-\mathbf{2}](t) + [(R)-\mathbf{3}](t) + [(S)-\mathbf{3}](t) + [(R)-\mathbf{4}](t) + [(S)-\mathbf{4}](t) \quad (\text{S0})$$

Therefore, for these experiments, all relative concentrations derived from the calibration curves were divided by the corresponding $\Sigma(t)$.

As the peak areas of the diaryllallyl azides were not calibrated, the data in Tables S8 and S14 were not divided by $\Sigma(t)$ but by $[(R)-\mathbf{1}]_0$ or $[(S)-\mathbf{2}]_0$.

The integral areas of the internal standard are not fully reliable in the case of solvolysis of $(R)-\mathbf{1}$ in the presence of piperidine due to the peaks of some impurities near to the peak of $\mathbf{5}$. Therefore, the concentrations of the generated esters $(S)-\mathbf{1}$, $(R,S)-\mathbf{2}$ as well as of the four isomeric alcohols $(R,S)-\mathbf{3}$ and $(R,S)-\mathbf{4}$ were derived from the concentrations of the corresponding compounds relative to that of $(R)-\mathbf{1}$, assuming that $(R)-\mathbf{1}$ was consumed with the same rate as in the absence of piperidine ($k = 3.26 \times 10^{-4} \text{ s}^{-1}$), which is justified by the behavior of $(R)-\mathbf{1}$ in the presence of N_3^- . Expression (S1), which describes the calculation of $[(S)-\mathbf{1}](t)$, has analogously been used for calculating the time-dependent concentrations of the other products.

$$[(S)-\mathbf{1}](t) = \frac{[(S)-\mathbf{1}]_{\text{raw}}(t)}{[(R)-\mathbf{1}]_{\text{raw}}(t)} [(R)-\mathbf{1}]_0 e^{-kt} \quad \text{or} \quad [(S)-\mathbf{1}]_{\text{rel}}(t) = \frac{[(S)-\mathbf{1}]_{\text{raw}}(t)}{[(R)-\mathbf{1}]_{\text{raw}}(t)} e^{-kt} \quad (\text{S1})$$

The yields presented in Figures S6-S39, as well as the yields discussed in the main text, were obtained by multiplication of the normalized time-dependent concentrations with 100%.

Table S5a. Normalized time-dependent relative concentrations of **1-4** (in relative units) for solvolysis of (*R*)-**1** ($c_0 = 1.53 \times 10^{-3}$ M) in 60% aq acetone, 25 °C.

<i>t</i> / s	[(<i>R</i>)- 1]	[(<i>S</i>)- 1]	[(<i>R</i>)- 2]	[(<i>S</i>)- 2]	[(<i>R</i>)- 3]	[(<i>S</i>)- 3]	[(<i>R</i>)- 4]	[(<i>S</i>)- 4]
0	1.0000	0.0000	0.0000	0.0000	0.0000	0.0000	0.0000	0.0000
305	0.9187	0.0030	0.0017	0.0090	0.0256	0.0239	0.0090	0.0090
605	0.8394	0.0046	0.0029	0.0146	0.0477	0.0438	0.0232	0.0238
905	0.7618	0.0065	0.0046	0.0208	0.0656	0.0644	0.0380	0.0384
1205	0.6916	0.0071	0.0049	0.0237	0.0870	0.0832	0.0511	0.0516
1505	0.5981	0.0124	0.0093	0.0514	0.1017	0.0989	0.0639	0.0643
1805	0.5512	0.0129	0.0098	0.0415	0.1188	0.1151	0.0748	0.0759
2105	0.5168	0.0097	0.0070	0.0312	0.1362	0.1297	0.0845	0.0850
2405	0.4702	0.0101	0.0074	0.0327	0.1474	0.1427	0.0948	0.0948
2705	0.4182	0.0124	0.0095	0.0354	0.1598	0.1570	0.1034	0.1043
3005	0.3855	0.0106	0.0076	0.0318	0.1715	0.1687	0.1122	0.1122
3305	0.3494	0.0106	0.0071	0.0333	0.1822	0.1785	0.1190	0.1199
3605	0.3159	0.0110	0.0078	0.0315	0.1928	0.1871	0.1260	0.1279
3925	0.2821	0.0120	0.0087	0.0316	0.2021	0.1965	0.1335	0.1335
4205	0.2622	0.0093	0.0060	0.0284	0.2113	0.2046	0.1386	0.1396
4515	0.2350	0.0106	0.0074	0.0291	0.2182	0.2116	0.1436	0.1445
4805	0.2135	0.0110	0.0076	0.0278	0.2247	0.2172	0.1486	0.1495
5131	0.1933	0.0092	0.0058	0.0269	0.2329	0.2246	0.1528	0.1546
5405	0.1805	0.0084	0.0058	0.0241	0.2376	0.2301	0.1562	0.1572
5705	0.1483	0.0128	0.0093	0.0272	0.2437	0.2363	0.1603	0.1622
6012	0.1334	0.0118	0.0084	0.0276	0.2478	0.2421	0.1639	0.1649
6305	0.1353	0.0074	0.0043	0.0206	0.2521	0.2447	0.1669	0.1687
6605	0.1244	0.0068	0.0038	0.0192	0.2564	0.2489	0.1693	0.1712
6905	0.1113	0.0068	0.0040	0.0175	0.2609	0.2525	0.1730	0.1740
7522	0.0940	0.0055	0.0028	0.0153	0.2671	0.2578	0.1778	0.1796
7805	0.0852	0.0052	0.0026	0.0144	0.2710	0.2599	0.1794	0.1822
8101	0.0789	0.0051	0.0023	0.0132	0.2734	0.2632	0.1810	0.1829
8405	0.0693	0.0053	0.0028	0.0131	0.2743	0.2669	0.1838	0.1847
8726	0.0632	0.0049	0.0023	0.0125	0.2764	0.2698	0.1846	0.1864

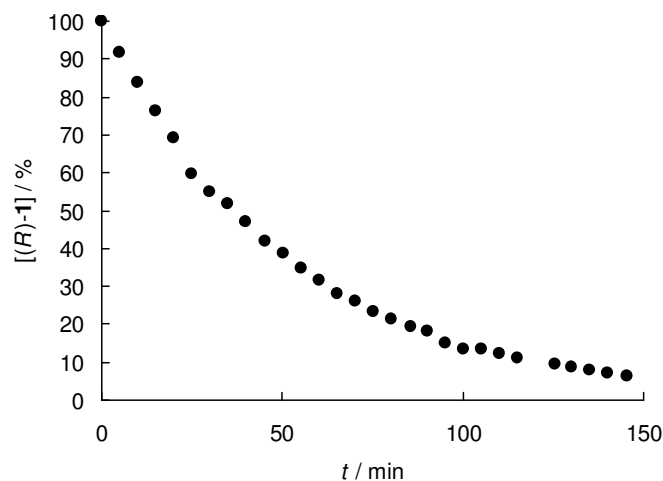


Figure S6. Decay of [(R)-1] ($c_0 = 1.53 \times 10^{-3}$ M) during its solvolysis in 60% aq acetone, 25 °C.

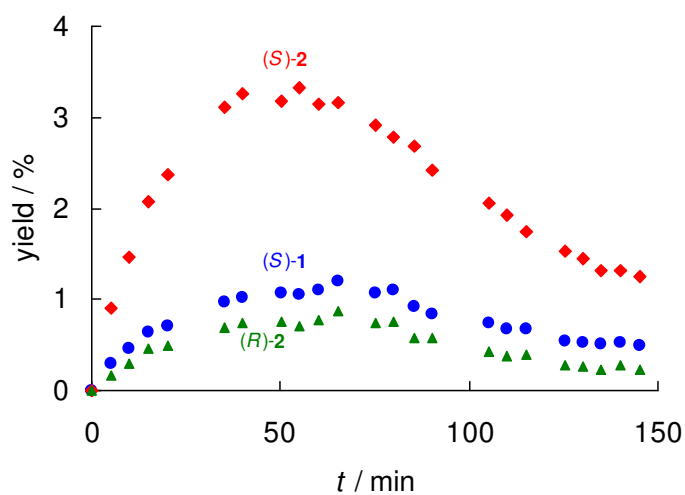


Figure S7. Time-dependent yields of (S)-1, (S)-2 and (R)-2 during solvolysis of (R)-1 ($c_0 = 1.53 \times 10^{-3}$ M) in 60% aqueous acetone, 25 °C.

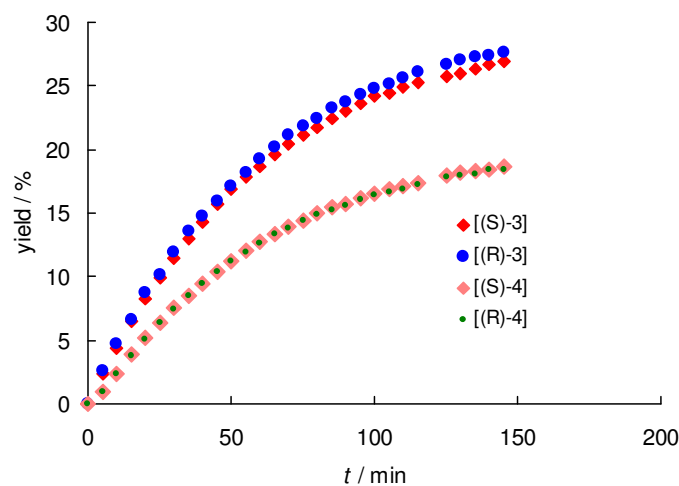


Figure S8. Time-dependent yields of alcohols 3 and 4 during solvolysis of (R)-1 ($c_0 = 1.53 \times 10^{-3}$ M) in 60% aq acetone, 25 °C.

Table S6a. Normalized time-dependent relative concentrations of **1–4** (in relative units) for solvolysis of **(R)-1** ($c_0 = 8.04 \times 10^{-4}$ M) in 60% aq acetone in the presence of 4.8 mM Bu₄NOPNB, 25 °C. Points used for the derivation of microscopic rate constants (for details see below) are shown in **bold**.

t / s	[(R)-1]	[(S)-1]	[(R)-2]	[(S)-2]	[(R)-3]	[(S)-3]	[(R)-4]	[(S)-4]
0	1.0000	0.0000	0.0000	0.0000	0.0000	0.0000	0.0000	0.0000
290	0.9287	0.0032	0.0013	0.0100	0.0228	0.0220	0.0046	0.0074
593	0.8467	0.0079	0.0079	0.0176	0.0418	0.0409	0.0184	0.0188
894	0.7724	0.0118	0.0096	0.0238	0.0599	0.0588	0.0314	0.0323
1200	0.7028	0.0152	0.0118	0.0299	0.0764	0.0762	0.0437	0.0439
1501	0.6328	0.0188	0.0176	0.0382	0.0905	0.0878	0.0569	0.0574
1800	0.5865	0.0196	0.0155	0.0343	0.1078	0.1064	0.0649	0.0650
2108	0.5310	0.0216	0.0165	0.0395	0.1214	0.1193	0.0751	0.0757
2399	0.4903	0.0228	0.0175	0.0387	0.1325	0.1315	0.0833	0.0834
2700	0.4415	0.0239	0.0187	0.0417	0.1451	0.1441	0.0922	0.0929
3000	0.4073	0.0245	0.0191	0.0403	0.1557	0.1546	0.0992	0.0994
3313	0.3689	0.0252	0.0198	0.0422	0.1654	0.1643	0.1071	0.1071
3601	0.3396	0.0251	0.0195	0.0399	0.1746	0.1746	0.1139	0.1128
3918	0.3040	0.0252	0.0195	0.0407	0.1839	0.1840	0.1208	0.1219
4200	0.2818	0.0250	0.0191	0.0385	0.1914	0.1916	0.1263	0.1263
4500	0.2553	0.0246	0.0184	0.0378	0.2000	0.1995	0.1317	0.1327
4809	0.2357	0.0242	0.0186	0.0361	0.2066	0.2058	0.1358	0.1372
5100	0.2131	0.0238	0.0189	0.0357	0.2125	0.2139	0.1408	0.1414
5400	0.1969	0.0232	0.0168	0.0336	0.2194	0.2185	0.1456	0.1461
5700	0.1794	0.0230	0.0166	0.0355	0.2229	0.2240	0.1489	0.1498
6002	0.1646	0.0222	0.0159	0.0332	0.2292	0.2292	0.1529	0.1529
6307	0.1494	0.0212	0.0154	0.0306	0.2338	0.2352	0.1570	0.1575
6599	0.1389	0.0205	0.0147	0.0283	0.2391	0.2387	0.1598	0.1601
6901	0.1231	0.0195	0.0146	0.0271	0.2442	0.2445	0.1634	0.1636
7201	0.1140	0.0188	0.0138	0.0252	0.2477	0.2477	0.1659	0.1668
7500	0.1052	0.0181	0.0128	0.0237	0.2512	0.2513	0.1687	0.1689
7803	0.0950	0.0171	0.0119	0.0225	0.2550	0.2548	0.1715	0.1722
8102	0.0875	0.0162	0.0110	0.0209	0.2585	0.2580	0.1739	0.1740
8400	0.0821	0.0161	0.0104	0.0225	0.2563	0.2610	0.1756	0.1759
8724	0.0719	0.0143	0.0110	0.0177	0.2558	0.2568	0.1736	0.1744

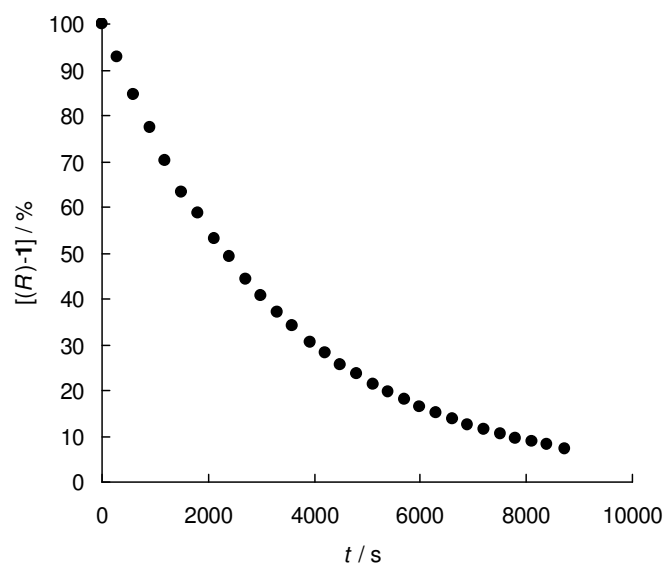


Figure S9. Decay of [(R)-1] ($c_0 = 8.04 \times 10^{-4}$ M) during its solvolysis in 60% aq acetone in the presence of 4.8 mM Bu_4NOPNB , 25 °C.

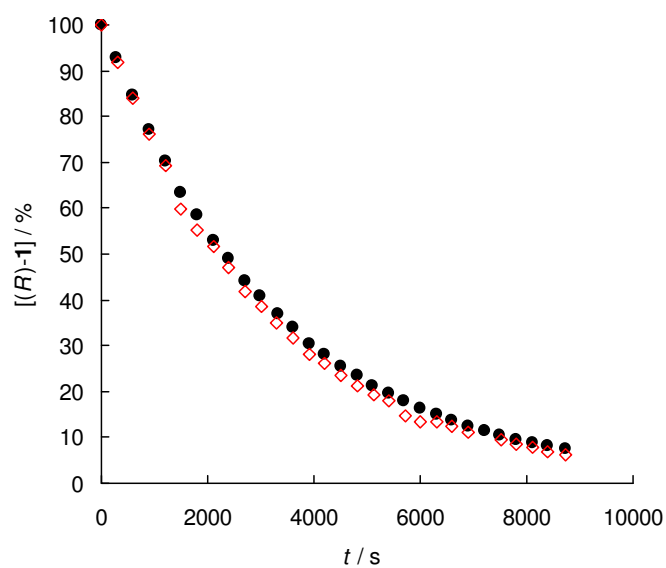


Figure S9a. Decay of [(R)-1] ($c_0 = 8.04 \times 10^{-4}$ M) during its solvolysis in 60% aq acetone in the presence of 4.8 mM Bu_4NOPNB , 25 °C (black circles) compared with those during solvolysis of (R)-1 ($c_0 = 1.53 \times 10^{-3}$ M) in 60% aq acetone in the absence of additives, 25 °C (open red rhombs).

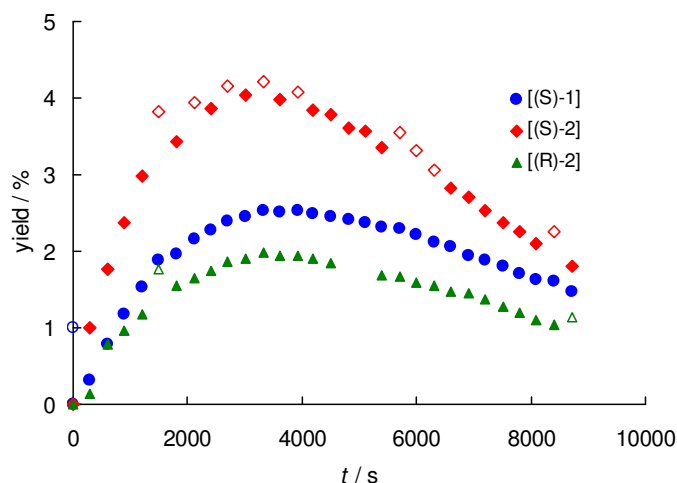


Figure S10. Time-dependent yields of (*S*)-1, (*S*)-2 and (*R*)-2 during solvolysis of (*R*)-1 ($c_0 = 8.04 \times 10^{-4}$ M) in 60% aqueous acetone in the presence of 4.8 mM Bu₄NOPNB, 25 °C. Filled points: data used for the derivation of microscopic rate constants (for details see below).

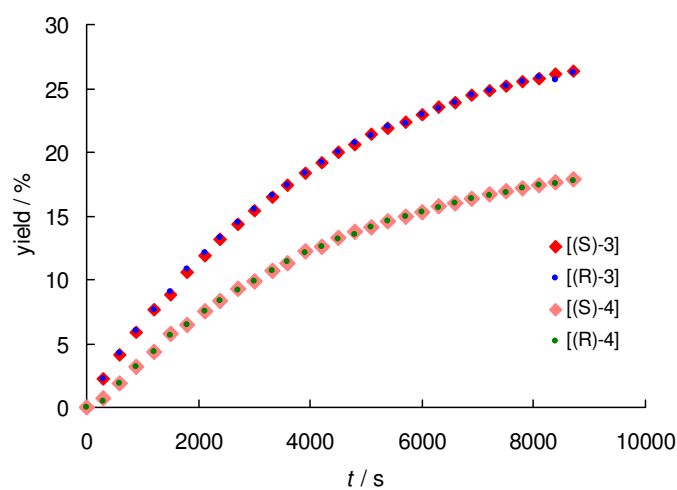


Figure S11. Time-dependent yields of alcohols **3** and **4** during solvolysis of (*R*)-1 ($c_0 = 8.04 \times 10^{-4}$ M) in 60% aq acetone in the presence of 4.8 mM Bu₄NOPNB, 25 °C.

Table S7a. Normalized time-dependent relative concentrations of **1-4** (in relative units) for solvolysis of (*R*)-**1** ($c_0 = 7.82 \times 10^{-4}$ M) in 60% aq acetone in the presence of 52.5 mM Bu₄NOPNB, 25 °C.

<i>t</i> / s	[(<i>R</i>)- 1]	[(<i>S</i>)- 1]	[(<i>R</i>)- 2]	[(<i>S</i>)- 2]	[(<i>R</i>)- 3]	[(<i>S</i>)- 3]	[(<i>R</i>)- 4]	[(<i>S</i>)- 4]
0	1.0000	0.0000	0.0000	0.0000	0.0000	0.0000	0.0000	0.0000
607	0.8657	0.0266	0.0184	0.0310	0.0219	0.0223	0.0072	0.0068
1210	0.7615	0.0433	0.0299	0.0488	0.0390	0.0388	0.0195	0.0192
1800	0.6864	0.0549	0.0401	0.0629	0.0509	0.0502	0.0271	0.0274
2400	0.5879	0.0686	0.0504	0.0778	0.0675	0.0679	0.0408	0.0392
3000	0.5286	0.0745	0.0545	0.0802	0.0813	0.0819	0.0498	0.0491
3601	0.4600	0.0794	0.0576	0.0828	0.0943	0.1076	0.0607	0.0577
4200	0.4696	0.0813	0.0612	0.0862	0.0919	0.0946	0.0574	0.0579
4800	0.4026	0.0812	0.0603	0.0826	0.1144	0.1131	0.0740	0.0719
5412	0.3583	0.0841	0.0609	0.0836	0.1263	0.1250	0.0817	0.0802
6000	0.3364	0.0822	0.0595	0.0809	0.1357	0.1324	0.0877	0.0852
6600	0.3211	0.0801	0.0584	0.0785	0.1418	0.1387	0.0919	0.0894
7202	0.3129	0.0773	0.0561	0.0751	0.1471	0.1433	0.0951	0.0932
7800	0.2660	0.0785	0.0568	0.0755	0.1609	0.1559	0.1044	0.1020
8395	0.2349	0.0785	0.0565	0.0747	0.1690	0.1664	0.1109	0.1091
9007	0.2834	0.0693	0.0497	0.0678	0.1609	0.1571	0.1080	0.1037

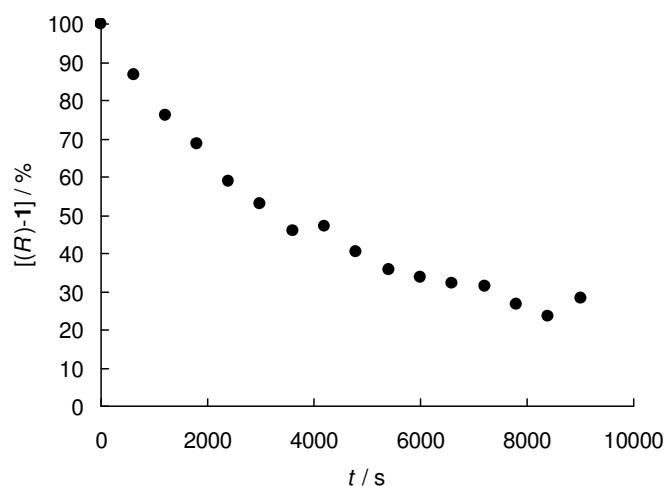


Figure S12. Decay of [(R)-1] ($c_0 = 7.82 \times 10^{-4}$ M) during its solvolysis in 60% aq acetone in the presence of 52.5 mM Bu_4NOPNB , 25 °C.

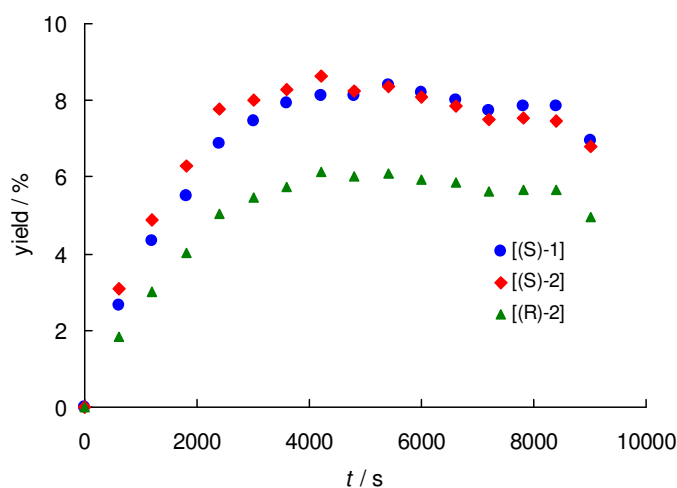


Figure S13. Time-dependent yields of (S)-1, (S)-2 and (R)-2 during solvolysis of (R)-1 ($c_0 = 7.82 \times 10^{-4}$ M) in 60% aqueous acetone in the presence of 52.5 mM Bu_4NOPNB , 25 °C.

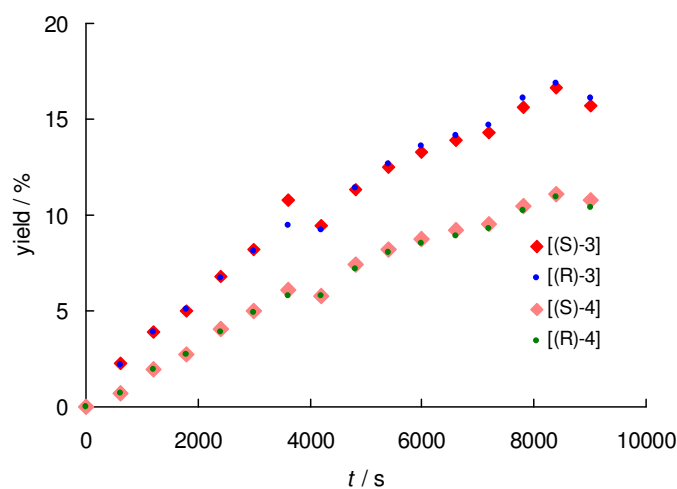


Figure S14. Time-dependent yields of alcohols 3 and 4 during solvolysis of (R)-1 ($c_0 = 7.82 \times 10^{-4}$ M) in 60% aq acetone in the presence of 52.5 mM Bu_4NOPNB , 25 °C.

Table S8a. Normalized time-dependent relative concentrations of **1-4** (in relative units) for solvolysis of (*R*)-**1** ($c_0 = 8.04 \times 10^{-4}$ M) in 60% aq acetone in the presence of 70.8 mM NaN₃, 25 °C. Points used for the derivation of microscopic rate constants (for details see below) are shown in **bold**.

<i>t</i> / s	[(<i>R</i>)- 1]	[(<i>S</i>)- 1]	[(<i>R</i>)- 2]	[(<i>S</i>)- 2]	[(<i>R</i>)- 3]	[(<i>S</i>)- 3] ^{<i>b</i>}	[(<i>R</i>)- 4]	[(<i>S</i>)- 4]	I_{RN3}/I_5^c
0	1.0000	0.0000	<i>a</i>	0.0000	<i>b</i>	0.0000	0.0000	0.0000	0.0000
618	0.8125	0.0015	<i>a</i>	0.0110	<i>b</i>	0.0016	0.0013	0.0012	<i>d</i>
1200	0.6969	0.0038	<i>a</i>	0.0183	<i>b</i>	0.0017	0.0020	0.0028	0.9418
1803	0.5687	0.0044	<i>a</i>	0.0214	<i>b</i>	0.0026	0.0026	0.0030	1.3140
2400	0.4678	0.0050	<i>a</i>	0.0235	<i>b</i>	0.0045	0.0031	0.0030	1.6041
3035	0.3796	0.0049	<i>a</i>	0.0238	<i>b</i>	0.0065	0.0047	0.0039	1.8813
3647	0.2944	0.0052	<i>a</i>	0.0240	<i>b</i>	0.0103	0.0061	0.0056	2.0943
4206	0.2623	0.0047	<i>a</i>	0.0217	<i>b</i>	0.0083	0.0052	0.0041	2.2484
4800	0.2155	0.0040	<i>a</i>	0.0198	<i>b</i>	0.0062	0.0049	0.0042	2.4201
5400	0.1764	0.0038	<i>a</i>	0.0181	<i>b</i>	0.0071	0.0051	0.0045	2.5396
6040	0.1436	0.0034	<i>a</i>	0.0159	<i>b</i>	0.0070	0.0054	0.0045	2.6141
6610	0.1180	0.0019	<i>a</i>	0.0142	<i>b</i>	0.0106	0.0059	0.0049	2.7349
7215	0.0982	0.0020	<i>a</i>	0.0123	<i>b</i>	0.0103	0.0061	0.0051	2.8195
7816	0.0790	0.0015	<i>a</i>	0.0103	<i>b</i>	0.0088	0.0061	0.0050	2.8320
8405	0.0651	0.0004	<i>a</i>	0.0087	<i>b</i>	0.0083	0.0060	0.0050	2.8959
9002	0.0582	0.0004	<i>a</i>	0.0078	<i>b</i>	<i>a</i>	<i>a</i>	<i>a</i>	3.1869

^{*a*} The precision of the HPLC integration was too low to derive reliable values of the time-dependent concentration. ^{*b*} The precision of the HPLC integration was rather low due to low intensity of the peak, presence of some impurities giving peaks in the same time range as (*R*)-**3**, and slight changes in the baseline due to the gradient used to reduce the analysis time. ^{*c*} I_{RN3} and I_5 are the integral areas of peaks corresponding to all diaryllallyl azides and internal standard **5**, respectively. ^{*d*} The acetone solution of the crude mixture was analyzed by HPLC, therefore, the peak of RN₃ was overlapped with that of acetone.

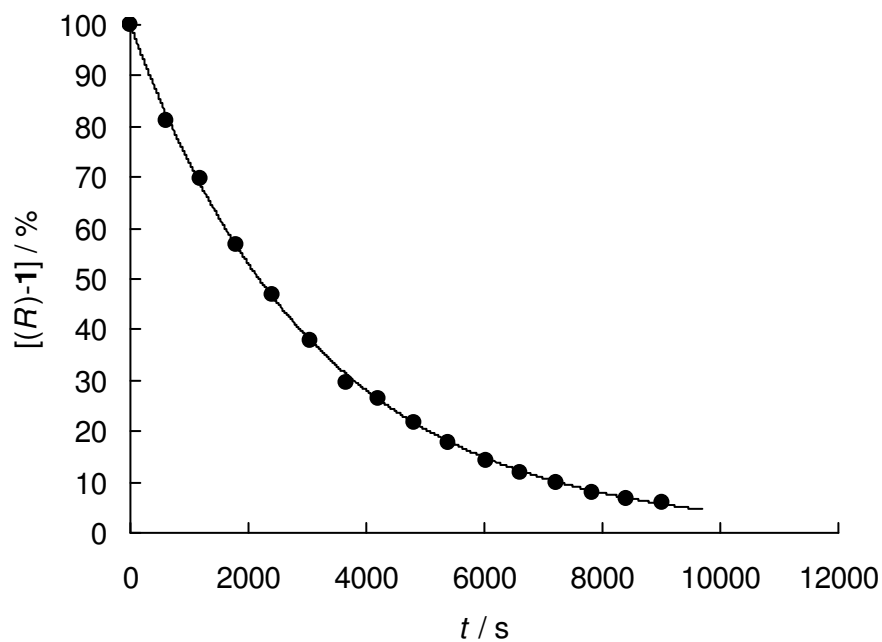


Figure S15. Decay of [(R)-1] ($c_0 = 8.04 \times 10^{-4}$ M) during its solvolysis in 60% aq acetone in the presence of 70.8 mM NaN_3 , 25 °C.

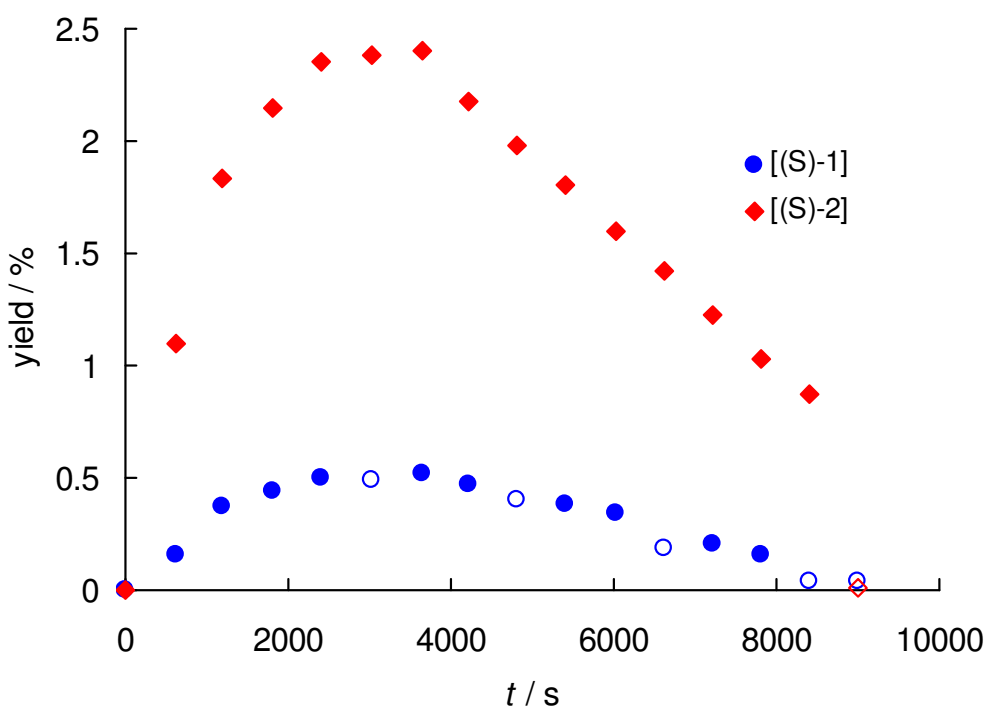


Figure S16. Time-dependent yields of (S)-1 and (S)-2 during solvolysis of (R)-1 ($c_0 = 8.04 \times 10^{-4}$ M) in 60% aqueous acetone in the presence of 70.8 mM NaN_3 , 25 °C. Filled points: data used for the derivation of microscopic rate constants (for details see below).

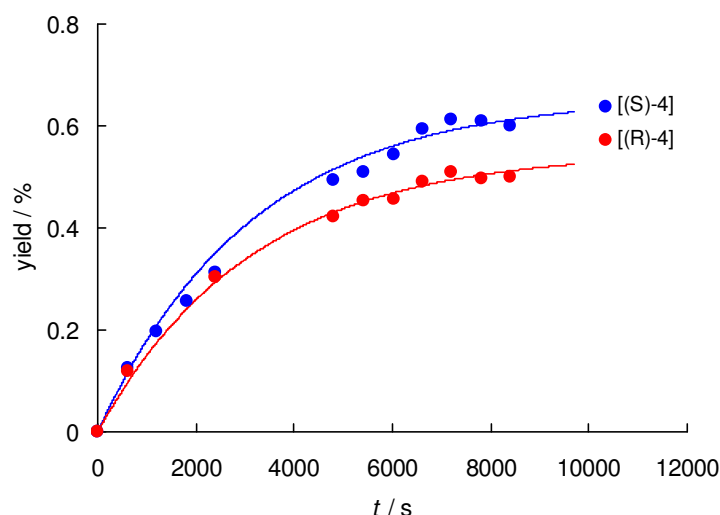


Figure S17. Time-dependent yields of enantiomers of **4** during solvolysis of *(R)*-**1** ($c_0 = 8.04 \times 10^{-4}$ M) in 60% aq acetone in the presence of 70.8 mM NaN₃, 25 °C.

The value of k_{N_3} was derived using the following procedure:

1) The values of $[(R)\text{-1}](t)$ were fitted to a monoexponential function $[(R)\text{-1}](t) = [(R)\text{-1}]_0 e^{-k_{\text{obs}} t}$ yielding the pseudo-first-order rate constant $k_{\text{obs}} = 3.17 \times 10^{-4} \text{ s}^{-1}$. The resulting calculated curve (multiplied with 100%) is shown in Figure S15.

2) The value of k_{obs} was used to fit $[(S)\text{-4}]_{\text{rel}}(t)$ and $[(R)\text{-4}]_{\text{rel}}(t)$ (the precision of the HPLC integration for *(R)*-**3** and *(S)*-**3** was too low) to the monoexponential functions $[(S)\text{-4}]_{\text{rel}}(t) = [(S)\text{-4}]_{\infty \text{rel}}(t)(1 - e^{-k_{\text{obs}} t})$ and $[(R)\text{-4}]_{\text{rel}}(t) = [(R)\text{-4}]_{\infty \text{rel}}(t)(1 - e^{-k_{\text{obs}} t})$ yielding the theoretical concentrations of *(R)*-**4** and *(S)*-**4** at the end of the reaction ($[(R)\text{-4}]_{\infty \text{rel}} = 5.50 \times 10^{-3}$, $[(S)\text{-4}]_{\infty \text{rel}} = 6.58 \times 10^{-3}$). The resulting calculated curves (multiplied with 100%) are shown in Figure S17.

3) The overall yield of the 1,3-diarylallyl alcohols $[\mathbf{3}]_{\infty \text{rel}} + [\mathbf{4}]_{\infty \text{rel}} = 3.02 \times 10^{-2}$ was derived by multiplying the sum $[(R)\text{-4}]_{\infty \text{rel}} + [(S)\text{-4}]_{\infty \text{rel}}$ with 2.5 (the ratio $[\mathbf{3}]/[\mathbf{4}] = 1.5$ found for other experiments means $([\mathbf{3}]+[\mathbf{4}])/[\mathbf{4}] = 2.5$).

4) As 1,3-diarylallyl alcohols and azides are the only products, the total yield of the alcohols is given by eq S2.

$$[\mathbf{3}]_{\infty \text{rel}} + [\mathbf{4}]_{\infty \text{rel}} = \frac{k_{\text{solv}}}{k_{\text{solv}} + k_{N_3}[\text{N}_3^-]} \quad (\text{S2})$$

Eq S2 can be reformulated as eq S3.

$$k_{N_3} = \frac{k_{\text{solv}}}{[\text{N}_3^-]} \left(\frac{1}{[\mathbf{3}]_{\infty \text{rel}} + [\mathbf{4}]_{\infty \text{rel}}} - 1 \right) \quad (\text{S3})$$

Substitution of the values of $k_{\text{solv}} = 1.34 \times 10^7 \text{ s}^{-1}$ and $[\text{N}_3^-] = 70.8 \text{ mM}$ in eq S3 gives $k_{N_3} = 6.1 \times 10^9 \text{ M}^{-1} \text{ s}^{-1}$.

Table S9a. Normalized time-dependent relative concentrations of **1-4** (in relative units) for solvolysis of (*R*)-**1** ($c_0 = 1.02 \times 10^{-3}$ M) in 60% aq acetone in the presence of 18.7 mM of Bu₄NCl, 25 °C.

<i>t</i> / s	[(<i>R</i>)- 1]	[(<i>S</i>)- 1]	[(<i>R</i>)- 2]	[(<i>S</i>)- 2]	[(<i>R</i>)- 3]	[(<i>S</i>)- 3]	[(<i>R</i>)- 4]	[(<i>S</i>)- 4]
0	1.0000	0.0000	0.0000	0.0000	0.0000	0.0000	0.0000	0.0000
1229	0.6716	0.0030	0.0001	0.0177	0.0965	0.0965	0.0570	0.0575
2400	0.4594	0.0050	0.0019	0.0234	0.1539	0.1560	0.1000	0.1005
3611	0.3101	0.0055	0.0021	0.0235	0.1977	0.1990	0.1307	0.1314
5400	0.1697	0.0045	0.0014	0.0182	0.2411	0.2425	0.1608	0.1617
7200	0.0952	0.0032	0.0004	0.0130	0.2642	0.2660	0.1780	0.1799

Table S10a. Normalized time-dependent relative concentrations of **1-4** (in relative units) for solvolysis of (*R*)-**1** ($c_0 = 8.51 \times 10^{-4}$ M) in 60% aq acetone in the presence of 100.7 mM of Bu₄NCl, 25 °C.

<i>t</i> / s	[(<i>R</i>)- 1]	[(<i>S</i>)- 1]	[(<i>R</i>)- 2]	[(<i>S</i>)- 2]	[(<i>R</i>)- 3]	[(<i>S</i>)- 3]	[(<i>R</i>)- 4]	[(<i>S</i>)- 4]
0	1.0000	0.0000	0.0000	0.0000	0.0000	0.0000	0.0000	0.0000
1200	0.7170	0.0024	0.0007	0.0188	0.0812	0.0817	0.0489	0.0493
2400	0.5017	0.0041	0.0020	0.0288	0.1406	0.1421	0.0899	0.0908
3600	0.3545	0.0047	0.0021	0.0245	0.1835	0.1872	0.1216	0.1219
5400	0.2082	0.0040	0.0015	0.0252	0.2261	0.2309	0.1518	0.1523

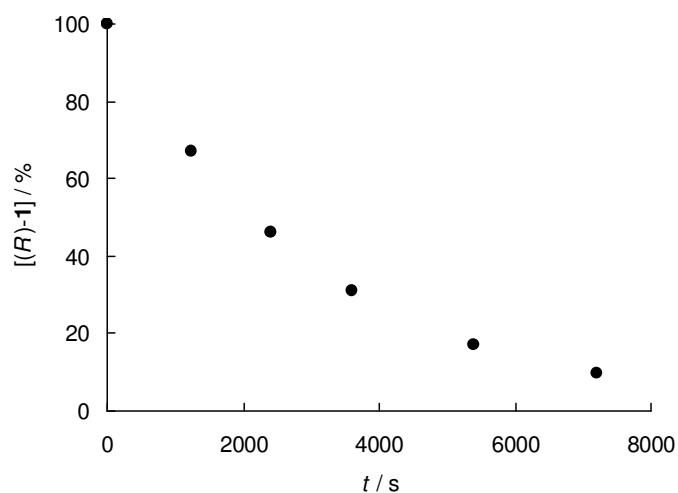


Figure S18. Decay of [(R)-1] ($c_0 = 1.02 \times 10^{-3}$ M) during its solvolysis in 60% aq acetone in the presence of 18.7 mM Bu_4NCl , 25 °C.

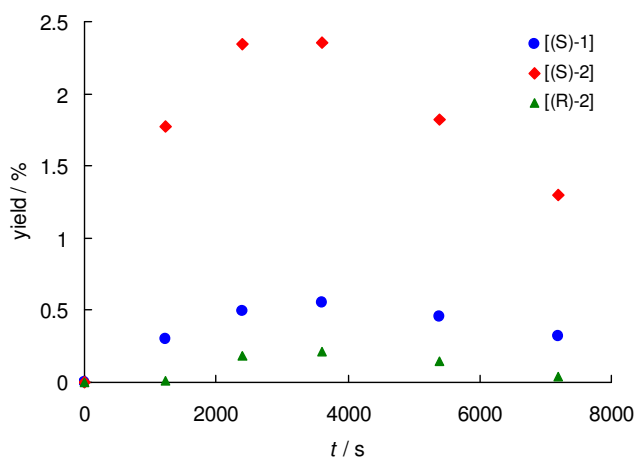


Figure S19. Time-dependent yields of (S)-1, (S)-2 and (R)-2 during solvolysis of (R)-1 ($c_0 = 1.02 \times 10^{-3}$ M) in 60% aqueous acetone in the presence of 18.7 mM Bu_4NCl , 25 °C.

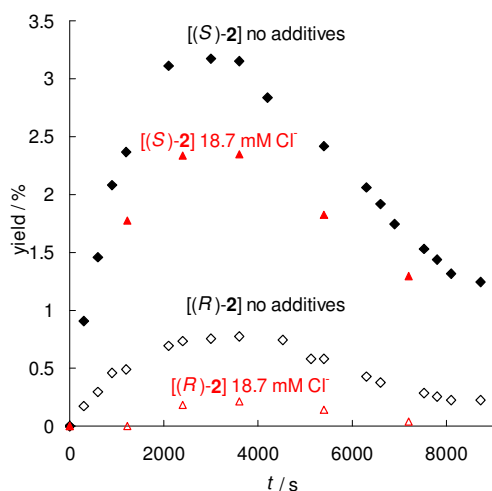


Figure S19a. Time-dependent yields of (S)-2 and (R)-2 during solvolysis of (R)-1 ($c_0 = 1.02 \times 10^{-3}$ M) in 60% aqueous acetone in the presence of 18.7 mM Bu_4NCl , 25 °C compared with those for solvolysis of (R)-1 in 60% aq acetone in the absence of additives, 25 °C.

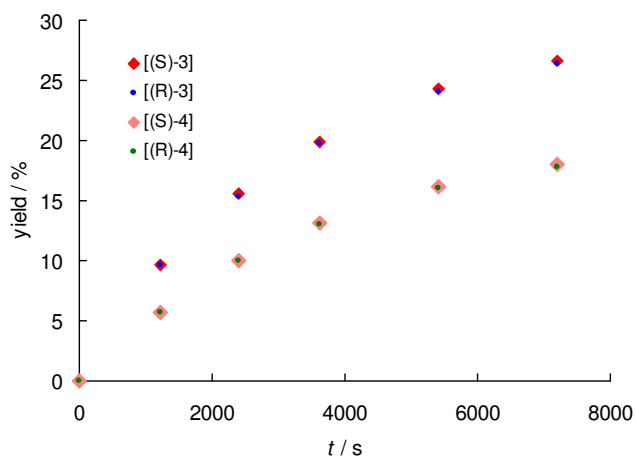


Figure S20. Time-dependent yields of alcohols **3** and **4** during solvolysis of *(R)*-**1** ($c_0 = 1.02 \times 10^{-3}$ M) in 60% aq acetone in the presence of 18.7 mM Bu₄NCl, 25 °C.

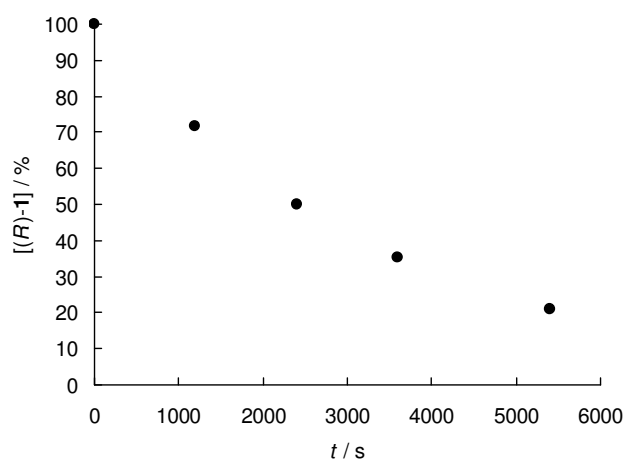


Figure S21. Decay of *[(R)-1]* ($c_0 = 8.51 \times 10^{-4}$ M) during its solvolysis in 60% aq acetone in the presence of 100.7 mM Bu₄NCl, 25 °C.

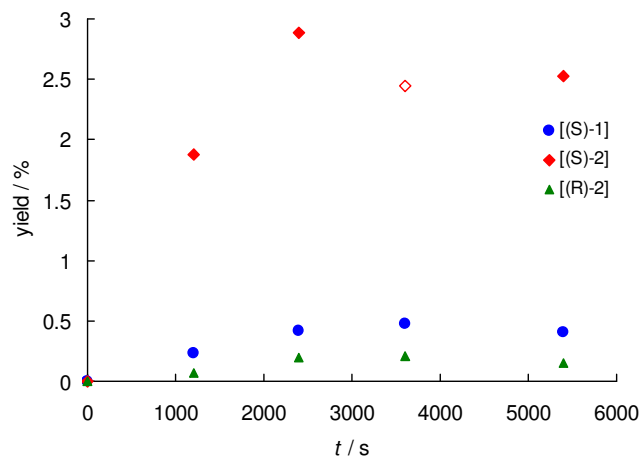


Figure S22. Time-dependent yields of (*S*)-1, (*S*)-2 and (*R*)-2 during solvolysis of (*R*)-1 ($c_0 = 8.51 \times 10^{-4}$ M) in 60% aqueous acetone in the presence of 100.7 mM Bu₄NCl, 25 °C.

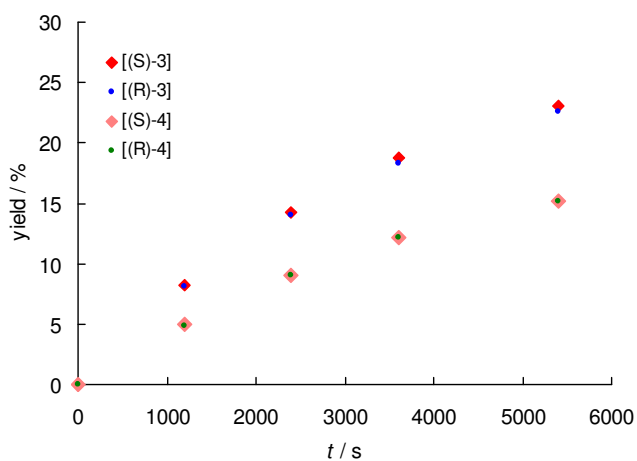


Figure S23. Time-dependent yields of alcohols **3** and **4** during solvolysis of (*R*)-1 ($c_0 = 8.51 \times 10^{-4}$ M) in 60% aq acetone in the presence of 100.7 mM Bu₄NCl, 25 °C.

Table S11a. Normalized time-dependent relative concentrations of **1-4** (in relative units) for solvolysis of **(R)-1** ($c_0 = 8.70 \times 10^{-4}$ M) in 60% aq acetone in the presence of 54.2 mM piperidine, 25 °C.

t / s	[(R)-1]	[(S)-1]	[(R)-2] ^a	[(S)-2]	[(R)-3]	[(S)-3] ^b	[(R)-4]	[(S)-4]
0	1.0000	0.0000	0.0000	0.0000	0.0000	0.0000	0.0000	0.0000
600	0.8223	0.0031	0.0010	0.0124	0.0290	0.0433	0.0132	0.0145
1200	0.6762	0.0053	0.0017	0.0200	0.0516	0.0768	0.0274	0.0284
1800	0.5561	0.0069	0.0008	0.0241	0.0685	0.1038	0.0409	0.0422
2405	0.4566	0.0074	0.0011	0.0258	0.0852	0.1270	0.0515	0.0544
3000	0.3761	0.0078	0.0000	0.0262	0.0967	0.1513	0.0607	0.0632
3600	0.3093	0.0079	0.0015	0.0256	0.1076	0.1576	0.0696	0.0719
4200	0.2543	0.0089	0.0010	0.0242	0.1198	0.1813	0.0744	0.0777
4798	0.2093	0.0071	0.0003	0.0225	0.1293	0.1876	0.0813	0.0854
5400	0.1720	0.0064	0.0033	0.0203	0.1360	0.2006	0.0862	0.0902
6015	0.1407	0.0059	0.0009	0.0182	0.1446	0.2120	0.0921	0.0969
6598	0.1164	0.0053	0.0004	0.0161	0.1550	0.2241	0.0965	0.1036
7202	0.0956	0.0047	0.0018	0.0141	0.1552	0.2300	0.1001	0.1039
7800	0.0786	0.0039	0.0000	0.0121	0.1621	0.2353	0.1036	0.1101
8400	0.0647	0.0034	0.0015	0.0104	0.1699	0.2376	0.1067	0.1132

^a The precision of the HPLC integration was too low to derive reliable values of the time-dependent concentrations. ^b The precision of the HPLC integration was rather low due to presence of some impurities giving peaks in the same time range as for **(S)-3**.

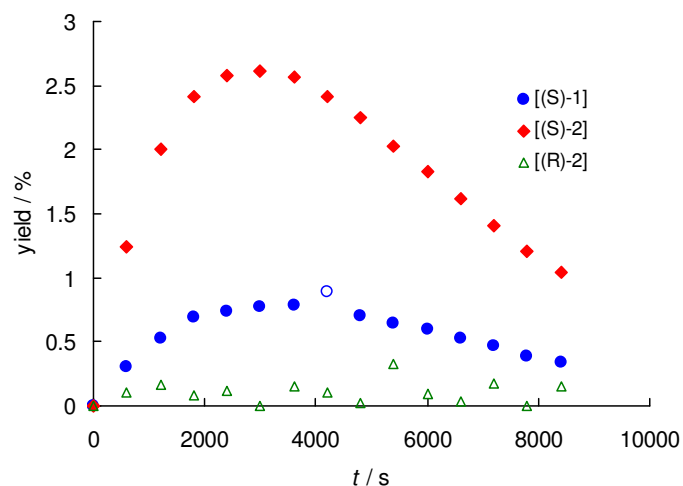


Figure S24. Time-dependent yields of (*S*)-1, (*S*)-2 and (*R*)-2 during solvolysis of (*R*)-1 ($c_0 = 8.70 \times 10^{-4}$ M) in 60% aqueous acetone in the presence of 54.2 mM piperidine, 25 °C.

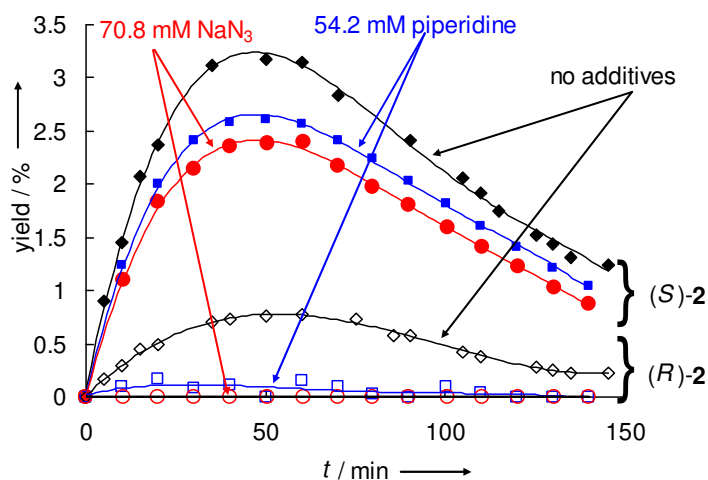


Figure S24a. Time-dependent yields of (*S*)-2 and (*R*)-2 during solvolysis of (*R*)-1 ($c_0 = 8.70 \times 10^{-4}$ M) in 60% aqueous acetone in the presence of piperidine (54.2 mM), NaN_3 (70.8 mM) and in the absence of additives.

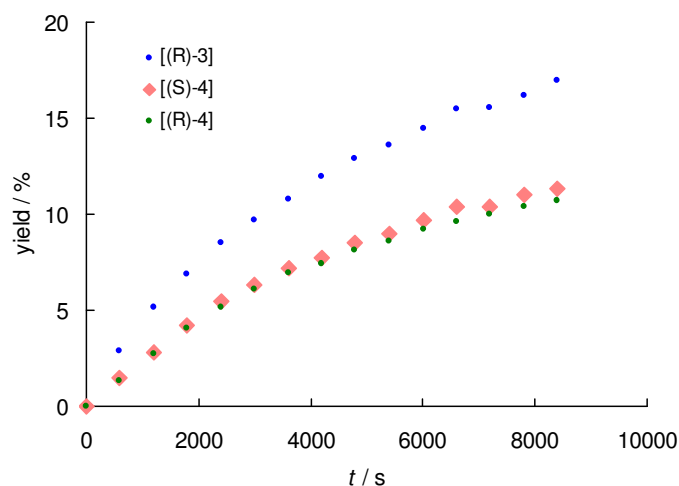


Figure S25. Time-dependent yields of alcohols 3 and 4 during solvolysis of (*R*)-1 ($c_0 = 8.70 \times 10^{-4}$ M) in 60% aq acetone in the presence of 54.2 mM piperidine, 25 °C.

Table S12a. Normalized time-dependent relative concentrations of **1-4** (in relative units) for solvolysis of **(R)-1** ($c_0 = 8.61 \times 10^{-4}$ M) in 60% aq acetone in the presence of 9.5 mM LiClO₄, 25 °C.

t / s	[(R)-1]	[(S)-1]	[(R)-2]	[(S)-2]	[(R)-3]	[(S)-3]	[(R)-4]	[(S)-4]
0	0.9987	0.0000	0.0000	0.0013	0.0000	0.0000	0.0000	0.0000
328	0.9554	0.0028	0.0002	0.0116	0.0278	0.0239	0.0088	0.0094
603	0.8735	0.0045	0.0041	0.0170	0.0479	0.0449	0.0235	0.0247
900	0.7898	0.0052	0.0035	0.0199	0.0725	0.0685	0.0402	0.0405
1210	0.7129	0.0103	0.0032	0.0374	0.0885	0.0823	0.0527	0.0527
1805	0.5937	0.0097	0.0075	0.0371	0.1200	0.1184	0.0769	0.0767
2408	0.4818	0.0117	0.0089	0.0419	0.1506	0.1485	0.0985	0.0981
2709	0.4585	0.0112	0.0078	0.0390	0.1582	0.1561	0.1048	0.1045
3600	0.3367	0.0111	0.0076	0.0334	0.1904	0.2040	0.1284	0.1284
3909	0.3104	0.0107	0.0070	0.0348	0.2011	0.2005	0.1375	0.1380
4208	0.2696	0.0105	0.0071	0.0289	0.2163	0.2160	0.1458	0.1459
4514	0.2564	0.0086	0.0052	0.0247	0.2238	0.2208	0.1500	0.1507
4799	0.2677	0.0102	0.0066	0.0306	0.2125	0.2116	0.1504	0.1505
5106	0.2135	0.0113	0.0087	0.0289	0.2310	0.2280	0.1589	0.1598
5706	0.1808	0.0084	0.0046	0.0247	0.2471	0.2406	0.1657	0.1682
6005	0.1601	0.0063	0.0039	0.0184	0.2542	0.2525	0.1723	0.1724
6299	0.1475	0.0079	0.0042	0.0203	0.2549	0.2525	0.1760	0.1770
6600	0.1327	0.0055	0.0034	0.0164	0.2622	0.2613	0.1792	0.1793
6900	0.1288	0.0064	0.0039	0.0176	0.2596	0.2582	0.1827	0.1828
7516	0.1132	0.0063	0.0032	0.0196	0.2628	0.2616	0.1868	0.1866
7800	0.0933	0.0056	0.0033	0.0133	0.2731	0.2717	0.1898	0.1900

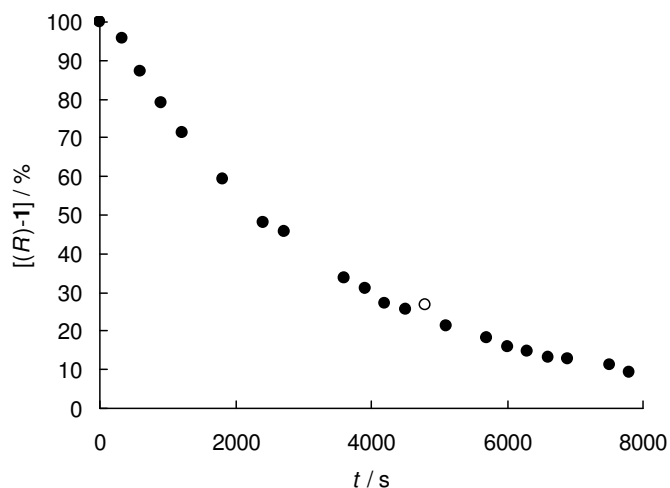


Figure S26. Decay of [(R)-1] ($c_0 = 8.61 \times 10^{-4}$ M) during its solvolysis in 60% aq acetone in the presence of 9.5 mM LiClO₄, 25 °C.

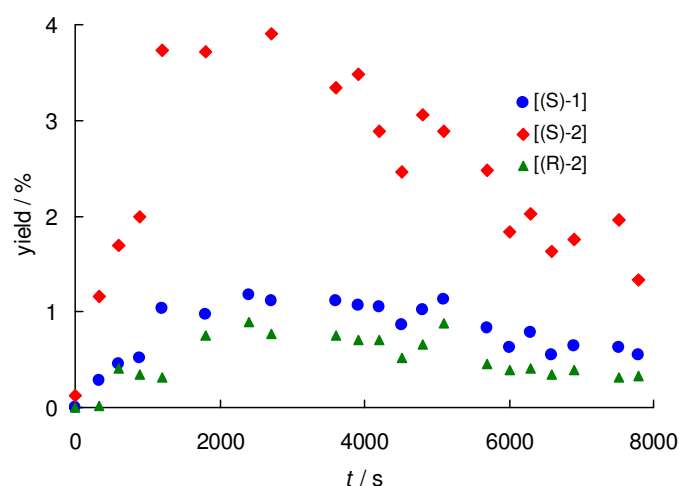


Figure S27. Time-dependent yields of (S)-1, (S)-2 and (R)-2 during solvolysis of (R)-1 ($c_0 = 8.61 \times 10^{-4}$ M) in 60% aqueous acetone in the presence of 9.5 mM LiClO₄, 25 °C.

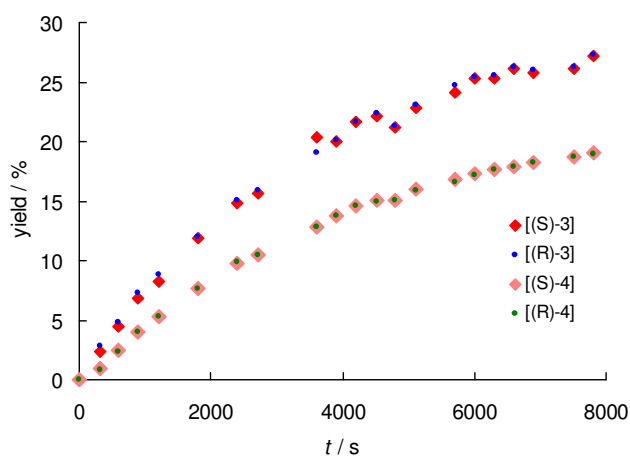


Figure S28. Time-dependent yields of alcohols 3 and 4 during solvolysis of (R)-1 ($c_0 = 8.61 \times 10^{-4}$ M) in 60% aq acetone in the presence of 9.5 mM LiClO₄, 25 °C.

Table S13a. Normalized time-dependent relative concentrations of **1-4** (in relative units) for solvolysis of (S)-**2** ($c_0 = 7.85 \times 10^{-4}$ M) in 60% aq acetone, 25 °C.

t / s	[(S)-2]	[(R)-2]	[(S)-1]	[(R)-1]	[(R)-3]	[(S)-3]	[(R)-4]	[(S)-4]
0	0.9980	0.0000	0.0020	0.0000	0.0000	0.0000	0.0000	0.0000
605	0.8105	0.0090	0.0070	0.0212	0.0521	0.0481	0.0262	0.0259
1200	0.6563	0.0100	0.0106	0.0331	0.0914	0.0880	0.0555	0.0551
1800	0.5274	0.0104	0.0105	0.0301	0.1277	0.1288	0.0827	0.0823
2400	0.4225	0.0096	0.0106	0.0315	0.1627	0.1576	0.1027	0.1028
3002	0.3405	0.0083	0.0111	0.0410	0.1792	0.1806	0.1199	0.1194
3600	0.2748	0.0068	0.0102	0.0388	0.2027	0.1996	0.1339	0.1333
4220	0.2205	0.0064	0.0096	0.0362	0.2164	0.2183	0.1467	0.1460
4800	0.1786	0.0054	0.0087	0.0334	0.2310	0.2313	0.1564	0.1553
5400	0.1433	0.0050	0.0079	0.0300	0.2445	0.2419	0.1640	0.1634
6000	0.1160	0.0035	0.0067	0.0259	0.2541	0.2518	0.1711	0.1709
6600	0.0925	0.0036	0.0068	0.0244	0.2595	0.2598	0.1767	0.1769
7200	0.0749	0.0025	0.0055	0.0214	0.2662	0.2671	0.1811	0.1812
7800	0.0603	0.0019	0.0047	0.0180	0.2718	0.2725	0.1854	0.1854
8400	0.0488	0.0012	0.0042	0.0151	0.2771	0.2749	0.1892	0.1895
9000	0.0368	0.0019	0.0043	0.0144	0.2803	0.2802	0.1907	0.1914

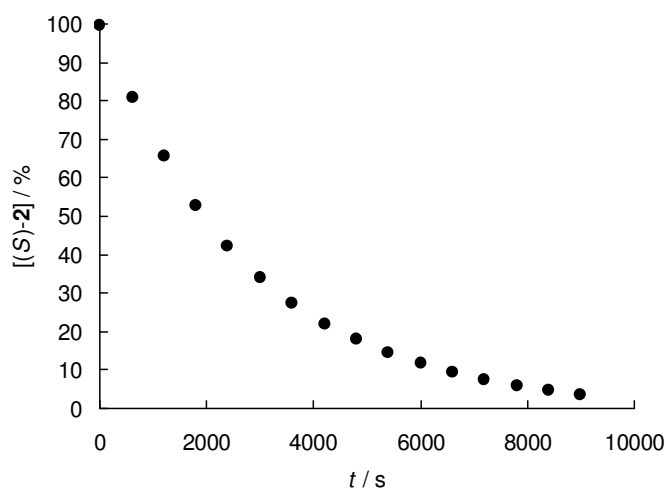


Figure S29. Decay of [(S)-2] ($c_0 = 7.85 \times 10^{-4}$ M) during its solvolysis in 60% aq acetone, 25 °C.

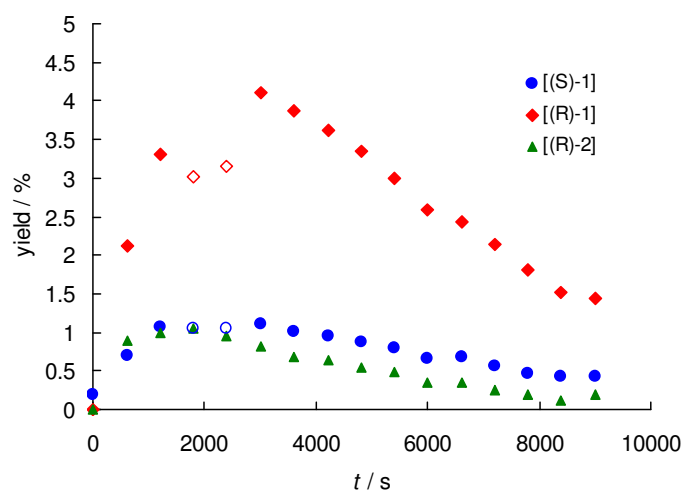


Figure S30. Time-dependent yields of (S)-1, (R)-1 and (R)-2 during solvolysis of (S)-2 ($c_0 = 7.85 \times 10^{-4}$ M) in 60% aqueous acetone, 25 °C.

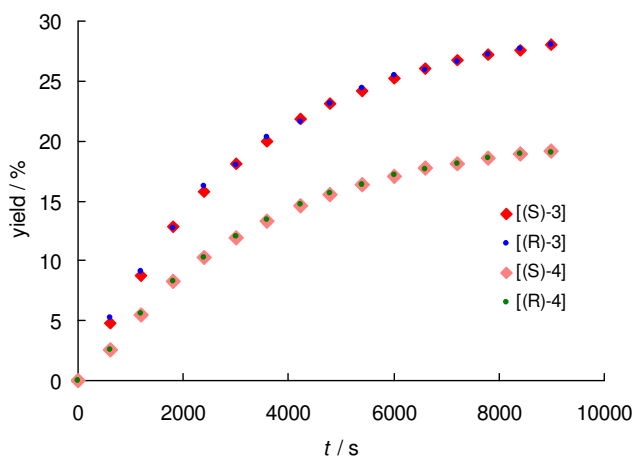


Figure S31. Time-dependent yields of alcohols 3 and 4 during solvolysis of (S)-2 ($c_0 = 7.85 \times 10^{-4}$ M) in 60% aq acetone, 25 °C.

Table S14a. Normalized time-dependent relative concentrations of **1–4** (in relative units) for solvolysis of (S)-**2** ($c_0 = 7.90 \times 10^{-4}$ M) in 60% aq acetone in the presence of 76.6 mM NaN₃, 25 °C. Points used for the derivation of microscopic rate constants (for details see below) are shown in **bold**.

t/s	[(S)-2]	[(R)-2]	[(S)-1]	[(R)-1]	[(R)-3]	[(S)-3]	[(R)-4]	[(S)-4]	I_{RN3}/I_5^b
0	1.0000	<i>a</i>	0.0000	0.0000	<i>a</i>	<i>a</i>	<i>a</i>	<i>a</i>	0.0000
635	0.8402	<i>a</i>	0.0060	0.0185	<i>a</i>	<i>a</i>	<i>a</i>	<i>a</i>	0.4820
1200	0.6501	<i>a</i>	0.0074	0.0277	<i>a</i>	<i>a</i>	<i>a</i>	<i>a</i>	1.1524
1800	0.5437	<i>a</i>	0.0066	0.0289	<i>a</i>	<i>a</i>	<i>a</i>	<i>a</i>	1.5826
2410	0.4459	<i>a</i>	0.0068	0.0311	<i>a</i>	<i>a</i>	<i>a</i>	<i>a</i>	1.9165
2998	0.3639	<i>a</i>	0.0061	0.0313	<i>a</i>	<i>a</i>	<i>a</i>	<i>a</i>	2.2060
3600	0.2983	<i>a</i>	0.0073	0.0306	<i>a</i>	<i>a</i>	<i>a</i>	<i>a</i>	2.4807
4202	0.2431	<i>a</i>	0.0067	0.0298	<i>a</i>	<i>a</i>	<i>a</i>	<i>a</i>	2.7057
4800	0.1964	<i>a</i>	0.0063	0.0268	<i>a</i>	<i>a</i>	<i>a</i>	<i>a</i>	2.8461
5408	0.1635	<i>a</i>	0.0057	0.0255	<i>a</i>	<i>a</i>	<i>a</i>	<i>a</i>	3.0737
6000	0.1290	<i>a</i>	0.0038	0.0226	<i>a</i>	<i>a</i>	<i>a</i>	<i>a</i>	3.0915
6602	0.1030	<i>a</i>	0.0038	0.0197	<i>a</i>	<i>a</i>	<i>a</i>	<i>a</i>	3.1752
7203	0.0832	<i>a</i>	0.0029	0.0169	<i>a</i>	<i>a</i>	<i>a</i>	<i>a</i>	3.2430
7800	0.0683	<i>a</i>	0.0034	0.0151	<i>a</i>	<i>a</i>	<i>a</i>	<i>a</i>	3.3523
8416	0.0560	<i>a</i>	0.0020	0.0130	<i>a</i>	<i>a</i>	<i>a</i>	<i>a</i>	3.3927
9000	0.0444	<i>a</i>	0.0018	0.0108	<i>a</i>	<i>a</i>	<i>a</i>	<i>a</i>	3.4977

^a The precision of the HPLC integration was too low to derive reliable values of the time-dependent concentrations. ^b I_{RN3} and I_5 are the integral areas of peaks corresponding to all diaryllallyl azides and internal standard **5**, respectively.

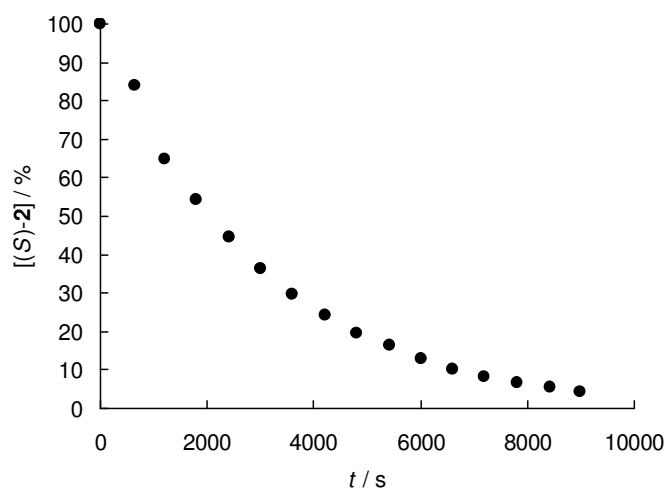


Figure S32. Decay of [(S)-2] ($c_0 = 7.90 \times 10^{-4}$ M) during its solvolysis in 60% aq acetone in the presence of 76.6 mM NaN₃, 25 °C.

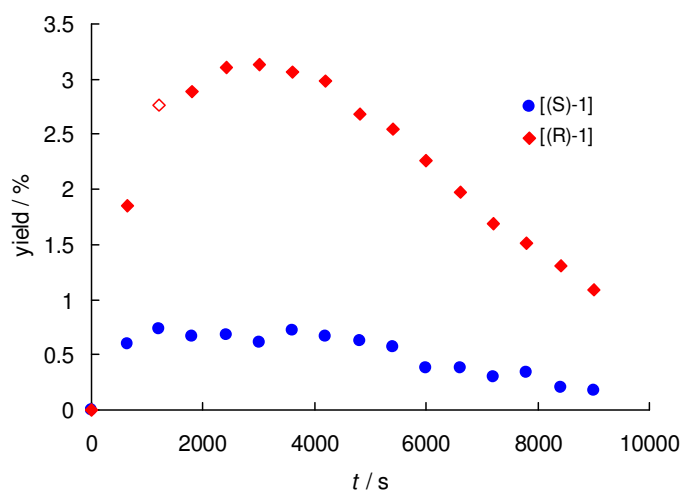


Figure S33. Time-dependent yields of (S)-1 and (R)-1 during solvolysis of (S)-2 ($c_0 = 7.90 \times 10^{-4}$ M) in 60% aqueous acetone in the presence of 76.6 mM NaN₃, 25 °C. Filled points: data used for the derivation of microscopic rate constants (for details see below).

Table S15a. Normalized time-dependent relative concentrations of **1-4** (in relative units) for solvolysis of (*R*)-**1** ($c_0 = 7.72 \times 10^{-4}$ M) in 80% aq acetone, 25 °C.

<i>t</i> / s	[(<i>R</i>)- 1]	[(<i>S</i>)- 1]	[(<i>R</i>)- 2]	[(<i>S</i>)- 2]	[(<i>R</i>)- 3]	[(<i>S</i>)- 3]	[(<i>R</i>)- 4]	[(<i>S</i>)- 4]
0	1.0000	0.0000	0.0000	0.0000	0.0000	0.0000	0.0000	0.0000
7244	0.7775	0.0157	0.0100	0.0356	0.0516	0.0522	0.0291	0.0284
14476	0.6015	0.0250	0.0194	0.0546	0.0918	0.0913	0.0588	0.0575
21600	0.4635	0.0311	0.0242	0.0637	0.1254	0.1253	0.0844	0.0824
29104	0.3510	0.0344	0.0263	0.0679	0.1550	0.1549	0.1064	0.1042
36540	0.2776	0.0345	0.0239	0.0592	0.1780	0.1799	0.1244	0.1225
43200	0.2192	0.0335	0.0244	0.0551	0.1975	0.1968	0.1386	0.1350
86062	0.0460	0.0169	0.0104	0.0198	0.2649	0.2667	0.1893	0.1860
111570	0.0231	0.0100	0.0051	0.0103	0.2796	0.2753	0.2005	0.1961

Table S16a. Normalized time-dependent relative concentrations of **1-4** (in relative units) for solvolysis of (*R*)-**1** ($c_0 = 6.82 \times 10^{-4}$ M) in 90% aq acetone, 25 °C.

<i>t</i> / s	[(<i>R</i>)- 1]	[(<i>S</i>)- 1]	[(<i>R</i>)- 2]	[(<i>S</i>)- 2]	[(<i>R</i>)- 3]	[(<i>S</i>)- 3]	[(<i>R</i>)- 4]	[(<i>S</i>)- 4]
0	1.0000	0.0000	0.0000	0.0000	0.0000	0.0000	0.0000	0.0000
47767	0.6789	0.0413	0.0349	0.0766	0.0542	0.0513	0.0320	0.0308
83963	0.5097	0.0589	0.0499	0.0982	0.0891	0.0871	0.0536	0.0536
136220	0.3449	0.0708	0.0583	0.1037	0.1197	0.1259	0.0884	0.0884
179370	0.2434	0.0759	0.0587	0.0956	0.1488	0.1585	0.1100	0.1091
222954	0.1803	0.0732	0.0522	0.0830	0.1717	0.1858	0.1269	0.1269
249529	0.1549	0.0684	0.0495	0.0754	0.1839	0.1950	0.1365	0.1364
569855	0.0253	0.0219	0.0137	0.0172	0.2697	0.2603	0.1996	0.1923

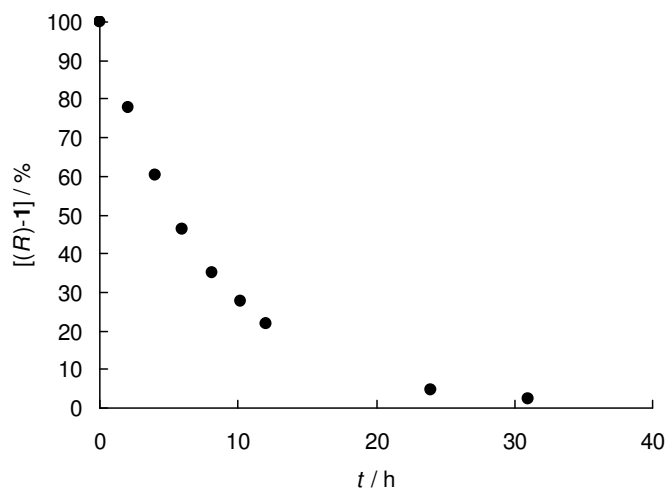


Figure S34. Decay of [(R)-1] ($c_0 = 7.72 \times 10^{-4}$ M) during its solvolysis in 80% aq acetone, 25 °C.

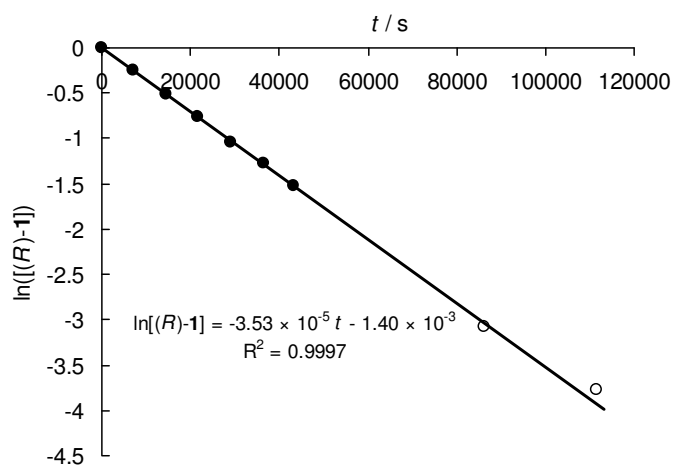


Figure S34a. Plot of $\ln([(R)-1](t))$ vs time for solvolysis of (R)-1 ($c_0 = 7.72 \times 10^{-4}$ M) in 80% aq acetone.

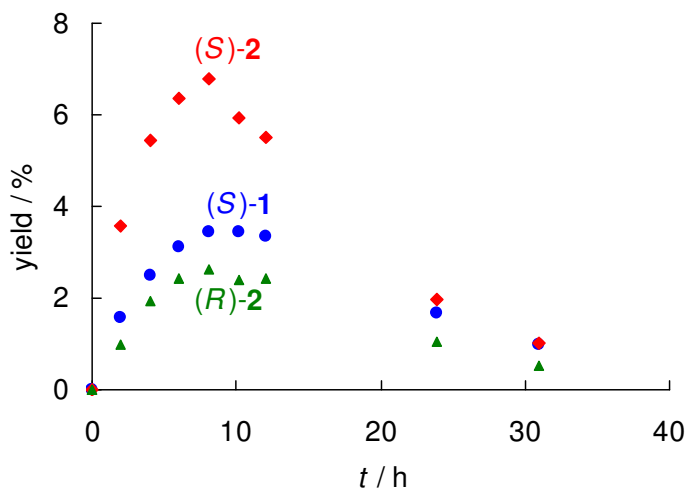


Figure S35. Time-dependent yields of (S)-1, (S)-2 and (R)-2 during solvolysis of (R)-1 ($c_0 = 7.72 \times 10^{-4}$ M) in 80% aqueous acetone, 25 °C.

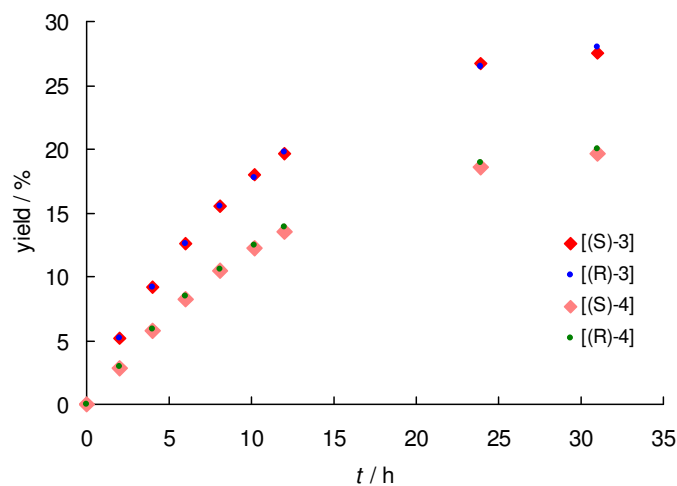


Figure S36. Time-dependent yields of alcohols **3** and **4** during solvolysis of (*R*)-**1** ($c_0 = 7.72 \times 10^{-4}$ M) in 80% aq acetone, 25 °C.

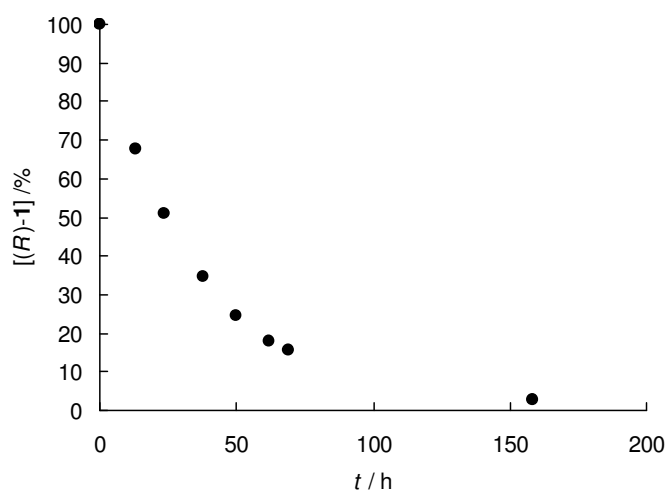


Figure S37. Decay of [(*R*)-**1**] during its solvolysis in 90% ($c_0 = 6.82 \times 10^{-4}$ M) aq acetone, 25 °C.

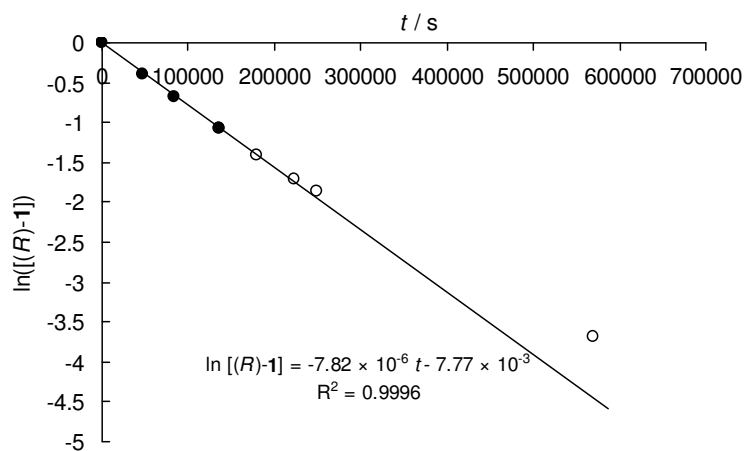


Figure S37a. Plot of $\ln ([(R)-1](t))$ vs time for solvolysis of (*R*)-**1** in 90% aq acetone.

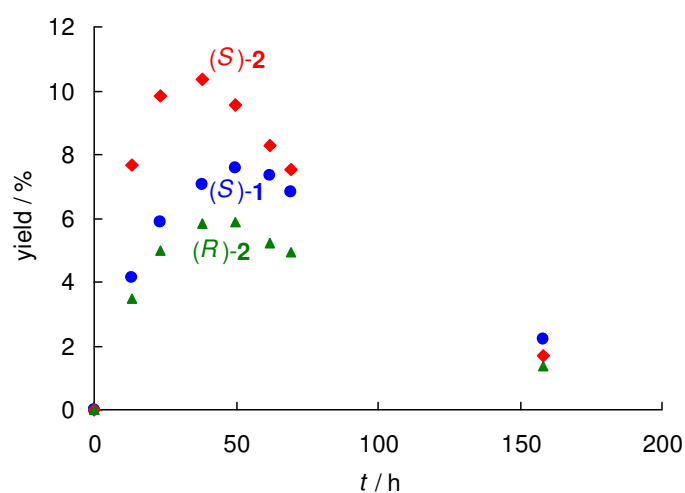


Figure S38. Time-dependent yields of (S)-1, (S)-2 and (R)-2 during solvolysis of (R)-1 ($c_0 = 6.82 \times 10^{-4}$ M) in 90% aqueous acetone, 25 °C.

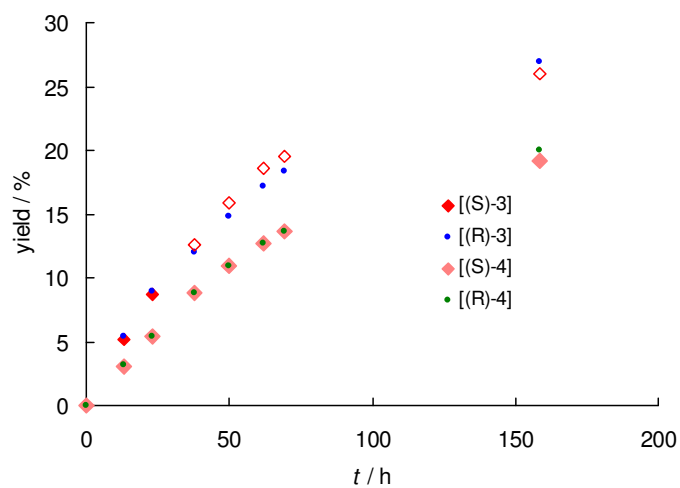


Figure S39. Time-dependent yields of alcohols 3 and 4 during solvolysis of (R)-1 ($c_0 = 6.82 \times 10^{-4}$ M) in 90% aq acetone, 25 °C.

5.5. Isomerization of **3** and **4** in the Presence of Acids

Attempted isomerization of (*S*)-4** in the presence of 4-nitrobenzoic acid.** (*S*)-**4** (12.8 mg, 52.3 μmol , 95% *ee*) was dissolved in 60% aq acetone (25 mL) containing 4-nitrobenzoic acid (9.4 mg, 56.2 μmol , 2.2 mM), and the resulting mixture was stirred for 2h 45min at 25 °C. The reaction solution was worked up in the same manner as for HPLC kinetic measurements and analyzed by HPLC. The resulting chromatogram showed no presence of **3**, and *ee* of (*S*)-**4** was 94.6%.

Isomerization of **3 in the presence of *p*-toluenesulfonic acid.** **3** (26.8 mg, 110 μmol) was dissolved in 60% aq acetone (50 mL) containing *p*-toluenesulfonic acid (47.7 mg, 27.7 μmol , 5.6 mM), and the resulting mixture was stirred at 25 °C. 10 mL aliquots of the reaction solution were worked up in the same manner as HPLC kinetic measurements and analyzed by HPLC. The results are summarized in Table S17.

Table S17. The ratios [3]/[4] observed for isomerization of **3** in 60% aq acetone in the presence of 5.6 mM of *p*-toluenesulfonic acid after certain reaction times.

<i>t</i> / min	[3]/[4]
98	8.14
2800	0.91
7233	0.88

5.6. Reaction of the Free Cation **6** with 60% Aq Acetone

The stock solution of **8** and **9** in acetone (40 mL) was generated in situ from **11** (16.1 mg, 61.2 μmol) and **12** (11.0 mg, 62.4 μmol). The kinetic experiments are summarized in Table S18.

Table S18. Laser-flash determination of k_{solv} .

$[\mathbf{8+9}]_0 / \text{M}$	$k_{\text{obs}} / \text{s}^{-1}$
3.06×10^{-4}	1.40×10^7
4.59×10^{-4}	1.31×10^7
6.12×10^{-4}	1.31×10^7

$$k_{\text{solv}} = 1.34 \times 10^7 \text{ s}^{-1}$$

5.7. Determination of the Microscopic Rate Constants

5.7.1. Direct solution

The kinetic law corresponding to Scheme 5 can be formulated as:

$$\frac{d[(R)-\mathbf{1}]}{dt} = -k_1[(R)-\mathbf{1}] + k_{-1}[(R)-\text{CIP}_1] \quad (\text{S4})$$

$$\frac{d[(S)-\mathbf{1}]}{dt} = -k_1[(S)-\mathbf{1}] + k_{-1}[(S)-\text{CIP}_1] \quad (\text{S5})$$

$$\frac{d[(R)-\mathbf{2}]}{dt} = -k'_1[(R)-\mathbf{2}] + k'_{-1}[(R)-\text{CIP}_2] \quad (\text{S6})$$

$$\frac{d[(S)-\mathbf{2}]}{dt} = -k'_1[(S)-\mathbf{2}] + k'_{-1}[(S)-\text{CIP}_2] \quad (\text{S7})$$

$$\frac{d[(R)-\text{CIP}_1]}{dt} = k_1[(R)-\mathbf{1}] + k'_r[(S)-\text{CIP}_2] + k_i[(S)-\text{CIP}_1] + k_{-2}[\mathbf{6}][^- \text{OPNB}] - (k_{-1} + k_r + k_i + k_2)[(R)-\text{CIP}_1] \quad (\text{S8})$$

$$\frac{d[(S)-\text{CIP}_1]}{dt} = k_1[(S)-\mathbf{1}] + k'_r[(R)-\text{CIP}_2] + k_i[(R)-\text{CIP}_1] + k_{-2}[\mathbf{6}][^- \text{OPNB}] - (k_{-1} + k_r + k_i + k_2)[(S)-\text{CIP}_1] \quad (\text{S9})$$

$$\frac{d[(R)-\text{CIP}_2]}{dt} = k'_1[(R)-\mathbf{2}] + k_r[(S)-\text{CIP}_1] + k'_i[(S)-\text{CIP}_2] + k'_{-2}[\mathbf{6}][^- \text{OPNB}] - (k'_{-1} + k'_r + k'_i + k'_2)[(R)-\text{CIP}_2] \quad (\text{S10})$$

$$\frac{d[(S)-\text{CIP}_2]}{dt} = k'_1[(S)-\mathbf{2}] + k_r[(R)-\text{CIP}_1] + k'_i[(R)-\text{CIP}_2] + k'_{-2}[\mathbf{6}][^- \text{OPNB}] - (k'_{-1} + k'_r + k'_i + k'_2)[(S)-\text{CIP}_2] \quad (\text{S11})$$

$$\frac{d[\mathbf{6}]}{dt} = k_2[(R)-\text{CIP}_1] + k_2[(S)-\text{CIP}_1] + k'_2[(R)-\text{CIP}_2] + k'_2[(S)-\text{CIP}_2] - (2k_{-2}[^- \text{OPNB}] + 2k'_{-2}[^- \text{OPNB}] + k_{\text{Nu}})[\mathbf{6}] \quad (\text{S12})$$

Assuming that $k_{-2}^e = k_{-2}[^- \text{OPNB}]$ and $k'_{-2}^e = k'_{-2}[^- \text{OPNB}]$ do not significantly change during the reaction (which should be the case for experiment in the presence of excess 4-nitrobenzoate due to buffering⁷⁶), this system of differential equations can be rewritten in matrix form as:

$$\frac{d}{dt}Y = AY \quad (\text{S13})$$

where

$$Y = \begin{pmatrix} [(R) - \mathbf{1}] \\ [(S) - \mathbf{1}] \\ [(R) - \mathbf{2}] \\ [(S) - \mathbf{2}] \\ [(R) - \text{CIP}_1] \\ [(S) - \text{CIP}_1] \\ [(R) - \text{CIP}_2] \\ [(S) - \text{CIP}_2] \\ [\mathbf{6}] \end{pmatrix} \quad (\text{S14})$$

and

$$A = \begin{pmatrix} -k_1 & 0 & 0 & 0 & k_{-1} & 0 & 0 & 0 & 0 \\ 0 & -k_1 & 0 & 0 & 0 & k_{-1} & 0 & 0 & 0 \\ 0 & 0 & -k'_1 & 0 & 0 & 0 & k'_{-1} & 0 & 0 \\ 0 & 0 & 0 & -k'_1 & 0 & 0 & 0 & k'_{-1} & 0 \\ k_1 & 0 & 0 & 0 & c_1 & k_i & 0 & k'_r & k_{-2}^e \\ 0 & k_1 & 0 & 0 & k_i & c_1 & k'_r & 0 & k_{-2}^e \\ 0 & 0 & k'_1 & 0 & 0 & k_r & c_2 & k'_i & k_{-2}'^e \\ 0 & 0 & 0 & k'_1 & k_r & 0 & k'_i & c_2 & k_{-2}'^e \\ 0 & 0 & 0 & 0 & k_2 & k_2 & k'_2 & k'_2 & c_3 \end{pmatrix} \quad (\text{S15})$$

where

$$c_1 = -k_{-1} - k_2 - k_r - k_i \quad (\text{S16})$$

$$c_2 = -k'_{-1} - k'_2 - k'_r - k'_i \quad (\text{S17})$$

$$c_3 = -2k_{-2}^e - 2k_{-2}'^e - k_{\text{Nu}} \quad (\text{S18})$$

The changes in k_{-2}^e and $k_{-2}'^e$ do not influence the reaction kinetics in the presence of NaN_3 as $2k_{-2}^e + 2k_{-2}'^e \ll k_{\text{Nu}}$ in this case.

Stating⁷⁷

$$Y(t) = SX(t) \quad (\text{S19})$$

where S is the matrix containing the eigenvectors of matrix A ($[s_1 s_2 s_3 s_4 s_5 s_6 s_7 s_8 s_9]$) one gets:

$$S \frac{dX(t)}{dt} = ASX(t) \quad (\text{S20})$$

which can be rewritten as:

$$\frac{dX(t)}{dt} = S^{-1}ASX(t) = \begin{pmatrix} \lambda_1 & 0 & 0 & 0 & 0 & 0 & 0 & 0 & 0 \\ 0 & \lambda_2 & 0 & 0 & 0 & 0 & 0 & 0 & 0 \\ 0 & 0 & \lambda_3 & 0 & 0 & 0 & 0 & 0 & 0 \\ 0 & 0 & 0 & \lambda_4 & 0 & 0 & 0 & 0 & 0 \\ 0 & 0 & 0 & 0 & \lambda_5 & 0 & 0 & 0 & 0 \\ 0 & 0 & 0 & 0 & 0 & \lambda_6 & 0 & 0 & 0 \\ 0 & 0 & 0 & 0 & 0 & 0 & \lambda_7 & 0 & 0 \\ 0 & 0 & 0 & 0 & 0 & 0 & 0 & \lambda_8 & 0 \\ 0 & 0 & 0 & 0 & 0 & 0 & 0 & 0 & \lambda_9 \end{pmatrix} X(t) \quad (\text{S21})$$

where λ_1 – λ_9 are the eigenvalues of matrix A corresponding to s_1 – s_9 . The latter transformation is obvious considering that $AS = [\lambda_1s_1 \ \lambda_2s_2 \ \lambda_3s_3 \ \lambda_4s_4 \ \lambda_5s_5 \ \lambda_6s_6 \ \lambda_7s_7 \ \lambda_8s_8 \ \lambda_9s_9]$ (this follows directly from definition of eigenvectors) and $S^{-1}S = I_9$ (identity matrix of size 9).

The equation S21 can be rewritten as a system of differential equations with separated variables:

$$\frac{dx_i}{dt} = \lambda_i x_i \quad (\text{S21a})$$

where $i = 1, 2, \dots, 9$ and x_i is the i th element of vector X .

The general solution of system (S21a) is obviously:

$$x_i = C_i e^{\lambda_i t} \quad (\text{S22})$$

where

C_i ($i = 1, 2, \dots, 9$) are the integration constants.

Considering $Y = SX$ one gets the general solution of the system (S13):

$$Y = S \begin{pmatrix} C_1 e^{\lambda_1 t} \\ C_2 e^{\lambda_2 t} \\ C_3 e^{\lambda_3 t} \\ C_4 e^{\lambda_4 t} \\ C_5 e^{\lambda_5 t} \\ C_6 e^{\lambda_6 t} \\ C_7 e^{\lambda_7 t} \\ C_8 e^{\lambda_8 t} \\ C_9 e^{\lambda_9 t} \end{pmatrix} \quad (\text{S23})$$

To find the particular solution with boundary conditions corresponding to the kinetic experiments one should consider:

$$Y(0) = b_1 = \begin{pmatrix} 1 \\ 0 \\ 0 \\ 0 \\ 0 \\ 0 \\ 0 \\ 0 \\ 0 \end{pmatrix} \quad (\text{S24})$$

for solvolysis of (*R*)-**1**, which means that at the initial point of the reaction $[(R)\text{-}\mathbf{1}] = 1$ and other components are not present in the system.

$$Y(0) = b_2 = \begin{pmatrix} 0 \\ 0 \\ 0 \\ 1 \\ 0 \\ 0 \\ 0 \\ 0 \\ 0 \end{pmatrix} \quad (\text{S25})$$

for solvolysis of (*S*)-**2**.

If the ion recombination, i.e., the reaction of **6** with $^-\text{OPNB}$ is considered,

$$Y(0) = b_3 = \begin{pmatrix} 0 \\ 0 \\ 0 \\ 0 \\ 0 \\ 0 \\ 0 \\ 0 \\ 0 \\ 1 \end{pmatrix} \quad (\text{S26})$$

As all exponential terms should be equal to 1 at $t = 0$, one gets:

$$S \begin{pmatrix} C_1 \\ C_2 \\ C_3 \\ C_4 \\ C_5 \\ C_6 \\ C_7 \\ C_8 \\ C_9 \end{pmatrix} = b \quad (\text{S27})$$

Where $b = b_1$ for solvolysis of (*R*)-**1**, $b = b_2$ for solvolysis of (*S*)-**2** and $b = b_3$ for ion recombination.

The solution for system of linear equations (S27) is, obviously:

$$\begin{pmatrix} C_1 \\ C_2 \\ C_3 \\ C_4 \\ C_5 \\ C_6 \\ C_7 \\ C_8 \\ C_9 \end{pmatrix} = S^{-1}b \quad (\text{S28})$$

so that the particular solutions for the system (S13) can be formulated as follows:

$$Y = \begin{pmatrix} [(R) - \mathbf{1}] \\ [(S) - \mathbf{1}] \\ [(R) - \mathbf{2}] \\ [(S) - \mathbf{2}] \\ [(R) - \text{CIP}_1] \\ [(S) - \text{CIP}_1] \\ [(R) - \text{CIP}_2] \\ [(S) - \text{CIP}_2] \\ [\mathbf{6}] \end{pmatrix} = S \begin{pmatrix} (S^{-1}b)_1 e^{\lambda_1 t} \\ (S^{-1}b)_2 e^{\lambda_2 t} \\ (S^{-1}b)_3 e^{\lambda_3 t} \\ (S^{-1}b)_4 e^{\lambda_4 t} \\ (S^{-1}b)_5 e^{\lambda_5 t} \\ (S^{-1}b)_6 e^{\lambda_6 t} \\ (S^{-1}b)_7 e^{\lambda_7 t} \\ (S^{-1}b)_8 e^{\lambda_8 t} \\ (S^{-1}b)_9 e^{\lambda_9 t} \end{pmatrix} \quad (\text{S29})$$

where $(S^{-1}b)_j$ is the j^{th} element of vector $(S^{-1}b)$.

Whereas the formulation of $Y(t)$ as a symbolic expression including microscopic rate constants (k_1, k'_1 , etc.) and time is very complex and human-unreadable, the functions $[(R)-\mathbf{1}](t)$, $[(S)-\mathbf{1}](t)$, $[(R)-\mathbf{2}](t)$, $[(S)-\mathbf{2}](t)$ for a given numerical set of microscopic rate constants $k = (k_1, k'_1, k_{-1}, k'_{-1}, k_r, k_i, k'_r, k'_i, k_2, k'_2, k_{-2}, k'_{-2}, k_{\text{Nu}})$ can be easily found using mathematical programs like MATLAB.⁷⁸

5.7.2. Steady state approximation

Applying the steady-state approximation to the contact ion pairs and the free cation **6**, one can state:

$$\frac{d[(R)-\text{CIP}_1]}{dt} = k_1[(R)-\mathbf{1}] + k'_r[(S)-\text{CIP}_2] + k_i[(S)-\text{CIP}_1] + k_2^e[\mathbf{6}] - (k_{-1} + k_r + k_i + k_2)[(R)-\text{CIP}_1] = 0 \quad (\text{S30})$$

$$\frac{d[(S)-\text{CIP}_1]}{dt} = k_1[(S)-\mathbf{1}] + k'_r[(R)-\text{CIP}_2] + k_i[(R)-\text{CIP}_1] + k_2^e[\mathbf{6}] - (k_{-1} + k_r + k_i + k_2)[(S)-\text{CIP}_1] = 0 \quad (\text{S31})$$

$$\frac{d[(R)-\text{CIP}_2]}{dt} = k'_1[(R)-\mathbf{2}] + k_r[(S)-\text{CIP}_1] + k'_i[(S)-\text{CIP}_2] + k_2^{e'}[\mathbf{6}] - (k'_{-1} + k'_r + k'_i + k'_2)[(R)-\text{CIP}_2] = 0 \quad (\text{S32})$$

$$\frac{d[(S)-\text{CIP}_2]}{dt} = k'_1[(S)-\mathbf{2}] + k_r[(R)-\text{CIP}_1] + k'_i[(R)-\text{CIP}_2] + k_2^{e'}[\mathbf{6}] - (k'_{-1} + k'_r + k'_i + k'_2)[(S)-\text{CIP}_2] = 0 \quad (\text{S33})$$

$$\frac{d[\mathbf{6}]}{dt} = k_2[(R)-\text{CIP}_1] + k_2[(S)-\text{CIP}_1] + k'_2[(R)-\text{CIP}_2] + k'_2[(S)-\text{CIP}_2] - (2k_2^e + 2k_2^{e'} + k_{\text{Nu}})[\mathbf{6}] = 0 \quad (\text{S34})$$

Where $k_2^e = k_{-2}[\text{OPNB}]^-$ and $k_2^{e'} = k'_{-2}[\text{OPNB}]^-$

This system of linear equations can be rewritten in the matrix form:

$$A \begin{pmatrix} [(R)-\text{CIP}_1] \\ [(S)-\text{CIP}_1] \\ [(R)-\text{CIP}_2] \\ [(S)-\text{CIP}_2] \\ [\mathbf{6}] \end{pmatrix} = \begin{pmatrix} -k_1[(R)-\mathbf{1}] \\ -k_1[(S)-\mathbf{1}] \\ -k'_1[(R)-\mathbf{2}] \\ -k'_1[(S)-\mathbf{2}] \\ 0 \end{pmatrix} \quad (\text{S35})$$

where A is the following matrix:

$$A = \begin{pmatrix} -k_{-1} - k_r - k_i - k_2 & k_i & 0 & k'_r & k_2^e \\ k_i & -k_{-1} - k_r - k_i - k_2 & k'_r & 0 & k_2^e \\ 0 & k_r & -k'_{-1} - k'_r - k'_i - k'_2 & k'_i & k_2^{e'} \\ k_r & 0 & k'_i & -k'_{-1} - k'_r - k'_i - k'_2 & k_2^{e'} \\ k_2 & k_2 & k'_2 & k'_2 & -2(k_2^e + k_2^{e'}) - k_{\text{Nu}} \end{pmatrix}$$

The solution of the system (S35) can be formulated as

$$\begin{pmatrix} [(R) - \text{CIP}_1] \\ [(S) - \text{CIP}_1] \\ [(R) - \text{CIP}_2] \\ [(S) - \text{CIP}_2] \\ [\mathbf{6}] \end{pmatrix} = M \begin{pmatrix} -k_1[(R) - \mathbf{1}] \\ -k_1[(S) - \mathbf{1}] \\ -k'_1[(R) - \mathbf{2}] \\ -k'_1[(S) - \mathbf{2}] \\ 0 \end{pmatrix} \quad (\text{S36})$$

where M is A^{-1} .

Concentrations of single enantiomers of $\mathbf{1}$ and $\mathbf{2}$ should have the following time dependencies:

$$\frac{d[(R) - \mathbf{1}]}{dt} = k_{-1}[(R) - \text{CIP}_1] - k_1[(R) - \mathbf{1}] \quad (\text{S37})$$

$$\frac{d[(S) - \mathbf{1}]}{dt} = k_{-1}[(S) - \text{CIP}_1] - k_1[(S) - \mathbf{1}] \quad (\text{S38})$$

$$\frac{d[(R) - \mathbf{2}]}{dt} = k'_{-1}[(R) - \text{CIP}_2] - k'_1[(R) - \mathbf{2}] \quad (\text{S39})$$

$$\frac{d[(S) - \mathbf{2}]}{dt} = k'_{-1}[(S) - \text{CIP}_2] - k'_1[(S) - \mathbf{2}] \quad (\text{S40})$$

Substituting the concentration of $(R)\text{-CIP}_1$ from eq S36 into eq S37 one gets:

$$\frac{d[(R) - \mathbf{1}]}{dt} = -k_1[(R) - \mathbf{1}](k_{-1}m_{11} + 1) - k_{-1}m_{12}k_1[(S) - \mathbf{1}] - k_{-1}m_{13}k'_1[(R) - \mathbf{2}] - k_{-1}m_{14}k'_1[(S) - \mathbf{2}] \quad (\text{S41})$$

where m_{ij} is the element of the matrix M with indices i and j .

Applying the same procedure to eqs (S38) – (S40), one gets the following system of linear ordinary differential equations:

$$\frac{dY(t)}{dt} = NY(t) \quad (\text{S42})$$

where

$$Y(t) = \begin{pmatrix} [(R) - \mathbf{1}](t) \\ [(S) - \mathbf{1}](t) \\ [(R) - \mathbf{2}](t) \\ [(S) - \mathbf{2}](t) \end{pmatrix} \quad (\text{S43})$$

and

$$N = - \begin{pmatrix} k_1 m_{11} k_{-1} + k_1 & k_{-1} m_{12} k_1 & k_{-1} m_{13} k'_1 & k_{-1} m_{14} k'_1 \\ k_{-1} m_{21} k_1 & k_1 m_{22} k_{-1} + k_1 & k_{-1} m_{23} k'_1 & k_{-1} m_{24} k'_1 \\ k'_{-1} m_{31} k_1 & k'_{-1} m_{32} k_1 & k'_1 m_{33} k'_{-1} + k'_1 & k'_{-1} m_{34} k'_1 \\ k'_{-1} m_{41} k_1 & k'_{-1} m_{42} k_1 & k'_{-1} m_{43} k'_1 & k'_1 m_{44} k'_{-1} + k'_1 \end{pmatrix} \quad (\text{S44})$$

Applying the same diagonalization method as described before, the solution of system S42 can be formulated:

$$Y(t) = \begin{pmatrix} [(R) - \mathbf{1}](t) \\ [(S) - \mathbf{1}](t) \\ [(R) - \mathbf{2}](t) \\ [(S) - \mathbf{2}](t) \end{pmatrix} = S \begin{pmatrix} (S^{-1}b)_1 e^{\lambda_1 t} \\ (S^{-1}b)_2 e^{\lambda_2 t} \\ (S^{-1}b)_3 e^{\lambda_3 t} \\ (S^{-1}b)_4 e^{\lambda_4 t} \end{pmatrix} \quad (\text{S45})$$

Where

$$b = b_4 = \begin{pmatrix} 1 \\ 0 \\ 0 \\ 0 \end{pmatrix} \quad (\text{S46})$$

for solvolysis of (R)-1,

$$b = b_5 = \begin{pmatrix} 0 \\ 0 \\ 0 \\ 1 \end{pmatrix} \quad (\text{S47})$$

for solvolysis of (S)-2.

5.7.3. Fitting of the experimental values

The function, which calculates sum of squared deviations $SSD(k)$ between calculated (direct or steady state approach) and experimental values for a given set of parameters k was minimized using the *fminsearch* algorithm of the computer program MATLAB 6.5.⁵⁴

Tables SN1 and SN2 show the values of microscopic rate constants and SSD obtained by direct and steady state methods, respectively, using such an optimization at different fixed values of k_2 . The results are also presented graphically in Figures SN1-SN8 and SN1a-SN8a, respectively.

Table SNI. The values of microscopic rate constants^a (s⁻¹) and SSD obtained by fitting of the experimental data to eq S29 at various fixed values of $k_2 = k'_2$.

k_1	k'_1	k_{-1}	k'_{-1}	k_f	k_i	k'_i	k_r	k_2	k'_2	k_{-2}^e	k_{-2}^b	SSD
3.45×10^{-4}	3.84×10^{-4}	2.10×10^7	1.78×10^7	4.22×10^9	2.33×10^7	2.33×10^7	4.22×10^9	1.00×10^8	1.00×10^8	4.36×10^6	4.36×10^6	1.03×10^{-3}
3.45×10^{-4}	3.84×10^{-4}	4.20×10^7	3.56×10^7	8.39×10^9	4.64×10^7	4.64×10^7	8.39×10^9	2.00×10^8	2.00×10^8	4.37×10^6	4.37×10^6	1.03×10^{-3}
3.45×10^{-4}	3.84×10^{-4}	6.31×10^7	5.34×10^7	1.25×10^{10}	6.98×10^7	6.98×10^7	1.25×10^{10}	3.00×10^8	3.00×10^8	4.36×10^6	4.36×10^6	1.03×10^{-3}
3.45×10^{-4}	3.84×10^{-4}	8.40×10^7	7.12×10^7	1.76×10^{10}	9.31×10^7	9.31×10^7	1.76×10^{10}	4.00×10^8	4.00×10^8	4.37×10^6	4.37×10^6	1.03×10^{-3}
3.45×10^{-4}	3.84×10^{-4}	1.05×10^8	8.90×10^7	2.05×10^{10}	1.17×10^8	1.17×10^8	2.05×10^{10}	5.00×10^8	5.00×10^8	4.37×10^6	4.37×10^6	1.03×10^{-3}
3.45×10^{-4}	3.84×10^{-4}	1.26×10^8	1.07×10^8	2.51×10^{10}	1.42×10^8	1.42×10^8	2.51×10^{10}	6.00×10^8	6.00×10^8	4.35×10^6	4.35×10^6	1.03×10^{-3}
3.45×10^{-4}	3.84×10^{-4}	1.48×10^8	1.25×10^8	2.93×10^{10}	1.63×10^8	1.63×10^8	2.93×10^{10}	7.00×10^8	7.00×10^8	4.37×10^6	4.37×10^6	1.03×10^{-3}
3.45×10^{-4}	3.84×10^{-4}	1.67×10^8	1.42×10^8	3.39×10^{10}	1.85×10^8	1.85×10^8	3.39×10^{10}	8.00×10^8	8.00×10^8	4.35×10^6	4.35×10^6	1.03×10^{-3}
3.45×10^{-4}	3.84×10^{-4}	1.89×10^8	1.60×10^8	3.79×10^{10}	2.12×10^8	2.12×10^8	3.79×10^{10}	9.00×10^8	9.00×10^8	4.36×10^6	4.36×10^6	1.03×10^{-3}
3.45×10^{-4}	3.84×10^{-4}	2.10×10^8	1.78×10^8	4.22×10^{10}	2.34×10^8	2.34×10^8	4.22×10^{10}	1.00×10^9	1.00×10^9	4.37×10^6	4.37×10^6	1.03×10^{-3}
3.45×10^{-4}	3.84×10^{-4}	4.21×10^8	3.57×10^8	8.60×10^{10}	4.73×10^8	4.73×10^8	8.60×10^{10}	2.00×10^9	2.00×10^9	4.35×10^6	4.35×10^6	1.02×10^{-3}
3.47×10^{-4}	3.84×10^{-4}	6.35×10^8	5.34×10^8	1.26×10^{11}	7.09×10^8	7.09×10^8	1.26×10^{11}	3.00×10^9	3.00×10^9	4.38×10^6	4.38×10^6	1.03×10^{-3}
3.45×10^{-4}	3.84×10^{-4}	8.40×10^8	7.11×10^8	1.68×10^{11}	9.72×10^8	9.72×10^8	1.68×10^{11}	4.00×10^9	4.00×10^9	4.37×10^6	4.37×10^6	1.02×10^{-3}
3.46×10^{-4}	3.84×10^{-4}	1.05×10^9	8.89×10^8	2.18×10^{11}	1.17×10^9	1.17×10^9	2.18×10^{11}	5.00×10^9	5.00×10^9	4.34×10^6	4.34×10^6	1.02×10^{-3}
3.46×10^{-4}	3.83×10^{-4}	1.26×10^9	1.07×10^9	2.52×10^{11}	1.45×10^9	1.45×10^9	2.52×10^{11}	6.00×10^9	6.00×10^9	4.36×10^6	4.36×10^6	1.02×10^{-3}
3.44×10^{-4}	3.85×10^{-4}	1.47×10^9	1.25×10^9	2.96×10^{11}	1.68×10^9	1.68×10^9	2.96×10^{11}	7.00×10^9	7.00×10^9	4.40×10^6	4.40×10^6	1.03×10^{-3}
3.45×10^{-4}	3.83×10^{-4}	1.69×10^9	1.42×10^9	3.36×10^{11}	1.85×10^9	1.85×10^9	3.36×10^{11}	8.00×10^9	8.00×10^9	4.37×10^6	4.37×10^6	1.02×10^{-3}
3.48×10^{-4}	3.84×10^{-4}	1.96×10^9	1.62×10^9	3.82×10^{11}	2.10×10^9	2.10×10^9	3.82×10^{11}	9.00×10^9	9.00×10^9	4.41×10^6	4.41×10^6	1.04×10^{-3}
3.46×10^{-4}	3.83×10^{-4}	2.12×10^9	1.80×10^9	4.21×10^{11}	2.35×10^9	2.35×10^9	4.21×10^{11}	1.00×10^{10}	1.00×10^{10}	4.41×10^6	4.41×10^6	1.04×10^{-3}
3.47×10^{-4}	3.84×10^{-4}	4.19×10^9	3.57×10^9	8.42×10^{11}	4.83×10^9	4.83×10^9	8.42×10^{11}	2.00×10^{10}	2.00×10^{10}	4.38×10^6	4.38×10^6	1.02×10^{-3}
3.47×10^{-4}	3.84×10^{-4}	6.29×10^9	5.37×10^9	1.26×10^{12}	7.23×10^9	7.23×10^9	1.26×10^{12}	3.00×10^{10}	3.00×10^{10}	4.53×10^6	4.53×10^6	1.05×10^{-3}
3.47×10^{-4}	3.86×10^{-4}	8.43×10^9	7.12×10^9	1.74×10^{12}	9.71×10^9	9.71×10^9	1.74×10^{12}	4.00×10^{10}	4.00×10^{10}	4.40×10^6	4.40×10^6	1.07×10^{-3}
3.50×10^{-4}	3.85×10^{-4}	1.04×10^{10}	8.94×10^9	2.11×10^{12}	1.21×10^{10}	1.21×10^{10}	2.11×10^{12}	5.00×10^{10}	5.00×10^{10}	4.37×10^6	4.37×10^6	1.02×10^{-3}
3.50×10^{-4}	3.84×10^{-4}	1.27×10^{10}	1.07×10^{10}	2.54×10^{12}	1.46×10^{10}	1.46×10^{10}	2.54×10^{12}	6.00×10^{10}	6.00×10^{10}	4.40×10^6	4.40×10^6	1.02×10^{-3}
3.45×10^{-4}	3.85×10^{-4}	1.47×10^{10}	1.25×10^{10}	2.94×10^{12}	1.63×10^{10}	1.63×10^{10}	2.94×10^{12}	7.00×10^{10}	7.00×10^{10}	4.48×10^6	4.48×10^6	1.05×10^{-3}
3.45×10^{-4}	3.84×10^{-4}	1.68×10^{10}	1.42×10^{10}	3.36×10^{12}	1.95×10^{10}	1.95×10^{10}	3.36×10^{12}	8.00×10^{10}	8.00×10^{10}	4.37×10^6	4.37×10^6	1.07×10^{-3}
3.55×10^{-4}	3.84×10^{-4}	1.91×10^{10}	1.60×10^{10}	3.78×10^{12}	2.20×10^{10}	2.20×10^{10}	3.78×10^{12}	9.00×10^{10}	9.00×10^{10}	4.34×10^6	4.34×10^6	1.05×10^{-3}
3.32×10^{-4}	3.87×10^{-4}	2.12×10^{10}	1.77×10^{10}	4.24×10^{12}	2.31×10^{10}	2.31×10^{10}	4.24×10^{12}	1.00×10^{11}	1.00×10^{11}	4.41×10^6	4.41×10^6	1.23×10^{-3}

^a $k_{\text{solv}} = 1.34 \times 10^7 \text{ s}^{-1}$ and $k_{\text{N}3} = 6.1 \times 10^9 \text{ M}^{-1} \text{ s}^{-1}$ were fixed during the fit. ^bThe values of k_{-2}^e and k_{-2}^b correspond to $[\text{OPNB}] = 4.8 \text{ mM}$.

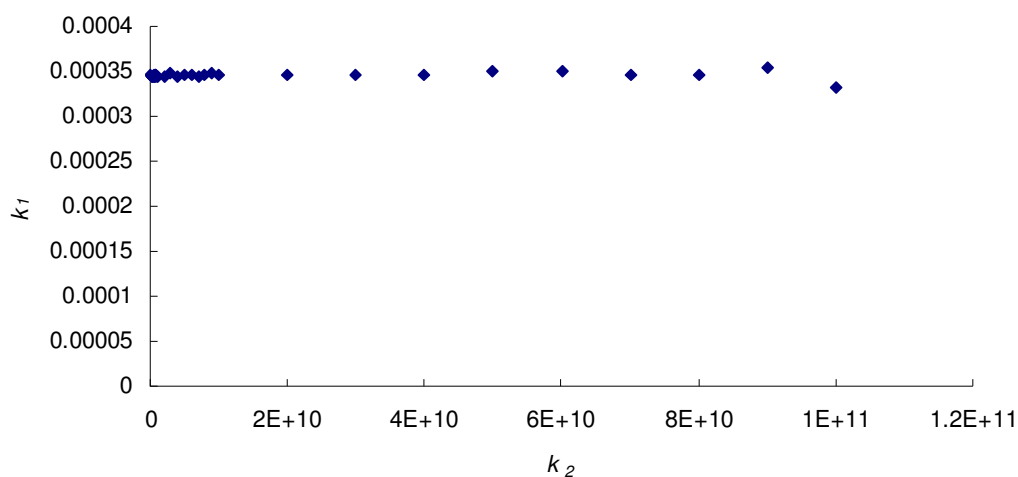


Figure SN1.

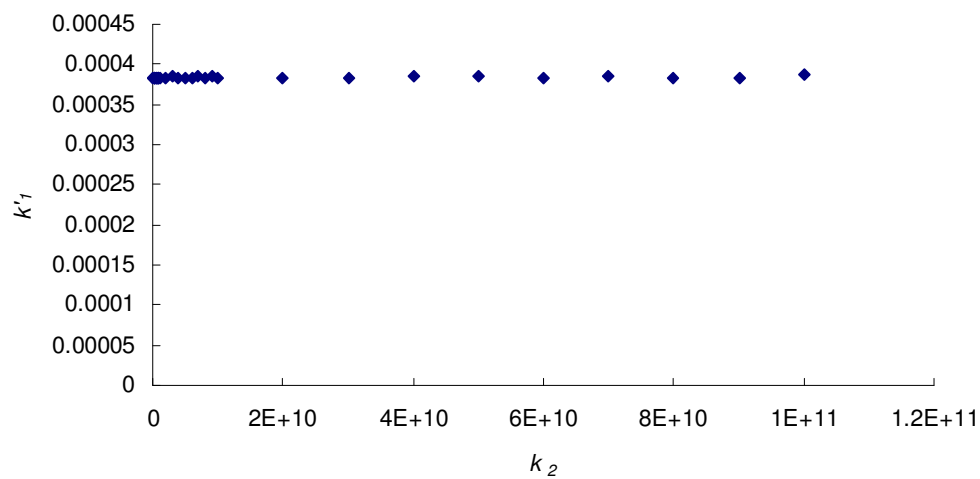


Figure SN2.

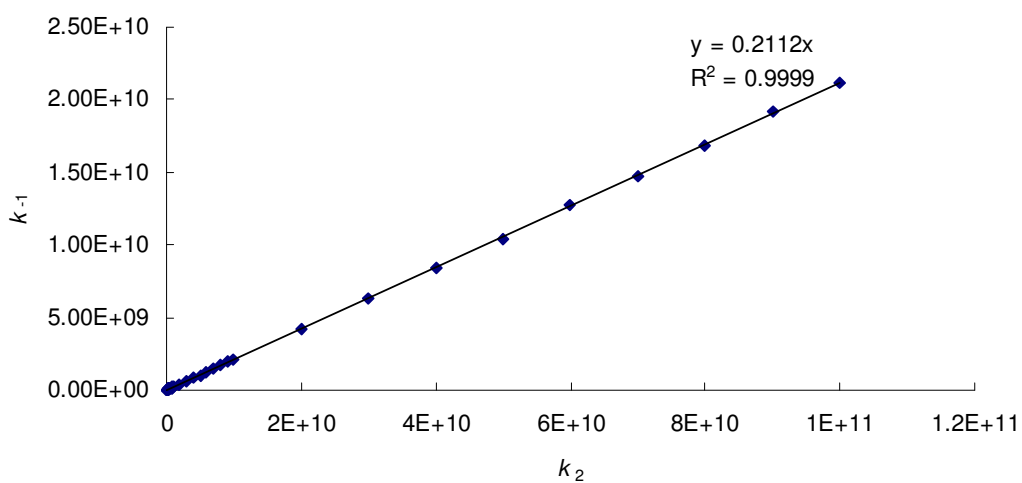


Figure SN3.

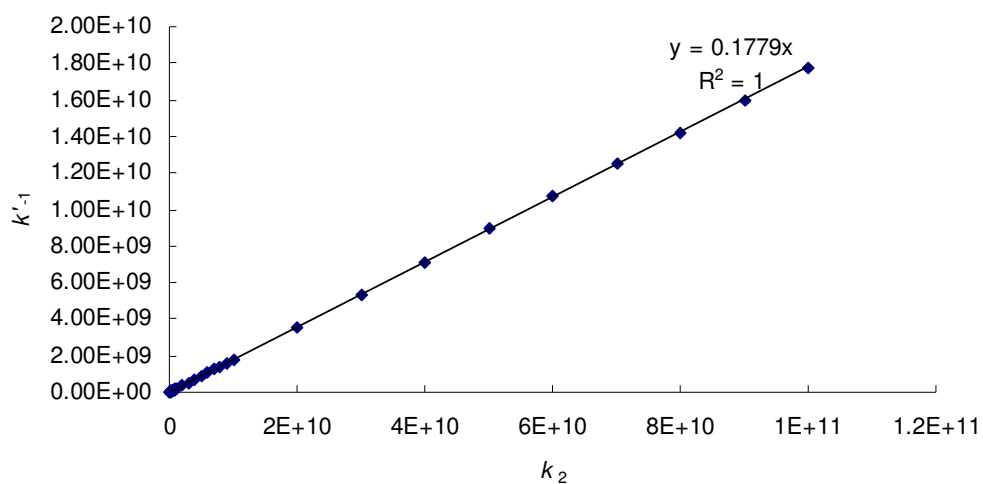


Figure SN4.

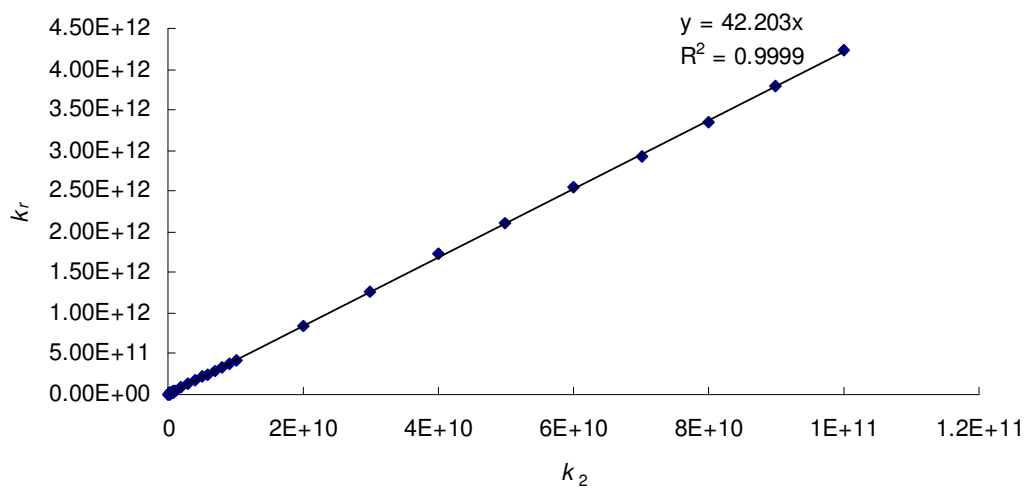


Figure SN5.

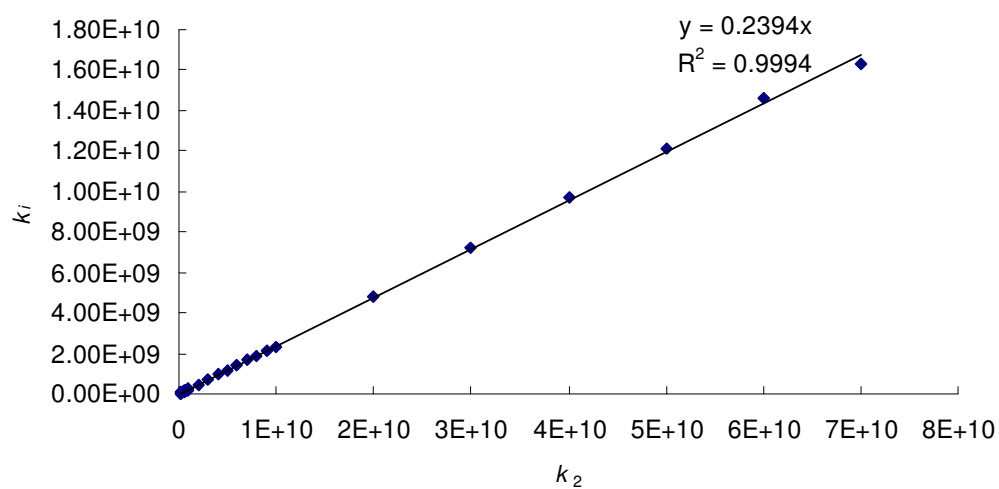


Figure SN6.

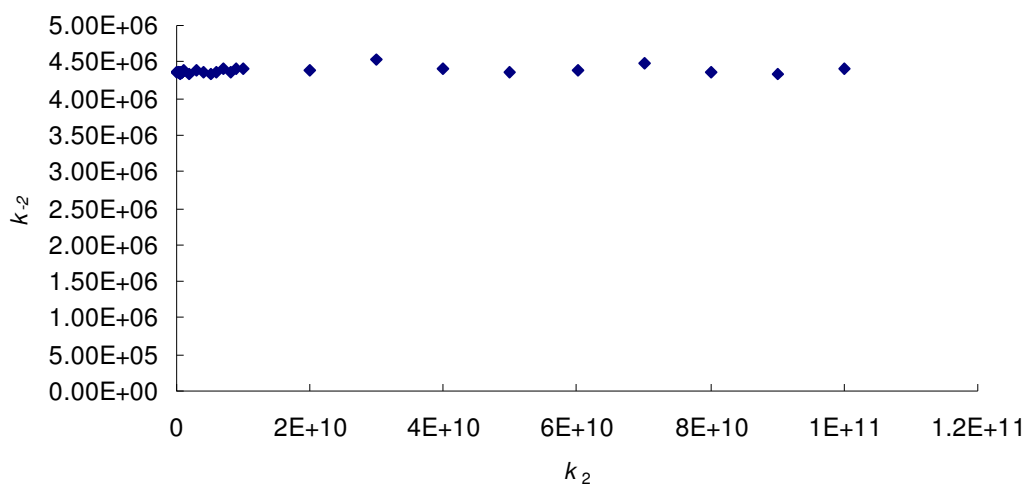


Figure SN7.

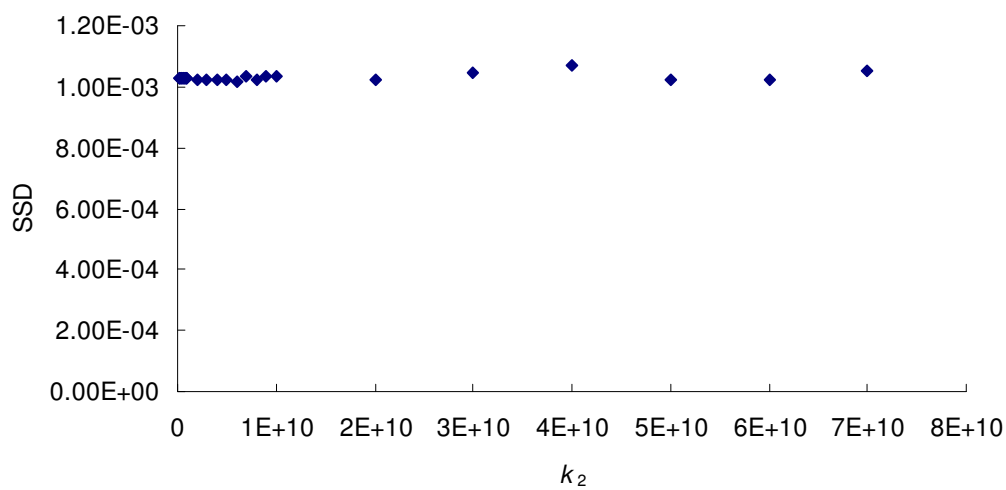


Figure SN8.

Table SN2. The values of microscopic rate constants^a (s⁻¹) and SSD obtained by fitting of the experimental data to eq S45 at various fixed values of $k_2 = k'_2$.

k_1	k_1	k_{-1}	k_c	k_i	k_r	k_i	k_1	k_2	k'_2	k_{-2}^c	k_{-2}^b	k_{-2}^e	SSD
3.45×10^{-4}	3.83×10^{-4}	2.09×10^7	7.10×10^9	2.34×10^7	7.10×10^9	2.34×10^7	1.00×10^8	1.00×10^8	1.00×10^8	4.39×10^6	4.39×10^6	4.39×10^6	1.03×10^{-3}
3.45×10^{-4}	3.83×10^{-4}	4.18×10^7	1.42×10^{10}	4.68×10^7	1.42×10^{10}	4.68×10^7	2.00×10^8	2.00×10^8	2.00×10^8	4.39×10^6	4.39×10^6	4.39×10^6	1.03×10^{-3}
3.45×10^{-4}	3.83×10^{-4}	6.27×10^7	2.13×10^{10}	7.02×10^7	2.13×10^{10}	7.02×10^7	3.00×10^8	3.00×10^8	3.00×10^8	4.39×10^6	4.39×10^6	4.39×10^6	1.03×10^{-3}
3.45×10^{-4}	3.83×10^{-4}	8.36×10^7	2.84×10^{10}	9.36×10^7	2.84×10^{10}	9.36×10^7	4.00×10^8	4.00×10^8	4.00×10^8	4.39×10^6	4.39×10^6	4.39×10^6	1.03×10^{-3}
3.45×10^{-4}	3.83×10^{-4}	1.04×10^8	3.55×10^{10}	1.17×10^8	3.55×10^{10}	1.17×10^8	5.00×10^8	5.00×10^8	5.00×10^8	4.39×10^6	4.39×10^6	4.39×10^6	1.03×10^{-3}
3.45×10^{-4}	3.83×10^{-4}	1.25×10^8	4.26×10^{10}	1.40×10^8	4.26×10^{10}	1.40×10^8	6.00×10^8	6.00×10^8	6.00×10^8	4.39×10^6	4.39×10^6	4.39×10^6	1.03×10^{-3}
3.45×10^{-4}	3.83×10^{-4}	1.46×10^8	4.98×10^{10}	1.64×10^8	4.98×10^{10}	1.64×10^8	7.00×10^8	7.00×10^8	7.00×10^8	4.39×10^6	4.39×10^6	4.39×10^6	1.03×10^{-3}
3.45×10^{-4}	3.83×10^{-4}	1.67×10^8	5.68×10^{10}	1.87×10^8	5.68×10^{10}	1.87×10^8	8.00×10^8	8.00×10^8	8.00×10^8	4.39×10^6	4.39×10^6	4.39×10^6	1.03×10^{-3}
3.45×10^{-4}	3.83×10^{-4}	1.88×10^8	6.39×10^{10}	2.11×10^8	6.39×10^{10}	2.11×10^8	9.00×10^8	9.00×10^8	9.00×10^8	4.39×10^6	4.39×10^6	4.39×10^6	1.03×10^{-3}
3.45×10^{-4}	3.83×10^{-4}	2.09×10^8	7.10×10^{10}	2.34×10^8	7.10×10^{10}	2.34×10^8	1.00×10^9	1.00×10^9	1.00×10^9	4.39×10^6	4.39×10^6	4.39×10^6	1.03×10^{-3}
3.45×10^{-4}	3.83×10^{-4}	4.18×10^8	1.42×10^{11}	4.68×10^8	1.42×10^{11}	4.68×10^8	2.00×10^9	2.00×10^9	2.00×10^9	4.39×10^6	4.39×10^6	4.39×10^6	1.03×10^{-3}
3.45×10^{-4}	3.83×10^{-4}	6.27×10^8	2.13×10^{11}	7.02×10^8	2.13×10^{11}	7.02×10^8	3.00×10^9	3.00×10^9	3.00×10^9	4.39×10^6	4.39×10^6	4.39×10^6	1.03×10^{-3}
3.45×10^{-4}	3.83×10^{-4}	8.36×10^8	2.84×10^{11}	9.36×10^8	2.84×10^{11}	9.36×10^8	4.00×10^9	4.00×10^9	4.00×10^9	4.39×10^6	4.39×10^6	4.39×10^6	1.03×10^{-3}
3.45×10^{-4}	3.83×10^{-4}	1.04×10^9	3.55×10^{11}	1.17×10^9	3.55×10^{11}	1.17×10^9	5.00×10^9	5.00×10^9	5.00×10^9	4.39×10^6	4.39×10^6	4.39×10^6	1.03×10^{-3}
3.45×10^{-4}	3.83×10^{-4}	1.25×10^9	4.26×10^{11}	1.40×10^9	4.26×10^{11}	1.40×10^9	6.00×10^9	6.00×10^9	6.00×10^9	4.39×10^6	4.39×10^6	4.39×10^6	1.03×10^{-3}
3.45×10^{-4}	3.83×10^{-4}	1.46×10^9	4.98×10^{11}	1.64×10^9	4.98×10^{11}	1.64×10^9	7.00×10^9	7.00×10^9	7.00×10^9	4.39×10^6	4.39×10^6	4.39×10^6	1.03×10^{-3}
3.45×10^{-4}	3.83×10^{-4}	1.67×10^9	5.68×10^{11}	1.87×10^9	5.68×10^{11}	1.87×10^9	8.00×10^9	8.00×10^9	8.00×10^9	4.39×10^6	4.39×10^6	4.39×10^6	1.03×10^{-3}
3.45×10^{-4}	3.83×10^{-4}	1.88×10^9	6.39×10^{11}	2.11×10^9	6.39×10^{11}	2.11×10^9	9.00×10^9	9.00×10^9	9.00×10^9	4.39×10^6	4.39×10^6	4.39×10^6	1.03×10^{-3}
3.45×10^{-4}	3.83×10^{-4}	2.09×10^9	7.10×10^{11}	2.34×10^9	7.10×10^{11}	2.34×10^9	1.00×10^{10}	1.00×10^{10}	1.00×10^{10}	4.39×10^6	4.39×10^6	4.39×10^6	1.03×10^{-3}
3.45×10^{-4}	3.83×10^{-4}	4.18×10^9	1.42×10^{12}	4.68×10^9	1.42×10^{12}	4.68×10^9	2.00×10^{10}	2.00×10^{10}	2.00×10^{10}	4.39×10^6	4.39×10^6	4.39×10^6	1.03×10^{-3}
3.45×10^{-4}	3.83×10^{-4}	6.27×10^9	2.13×10^{12}	7.02×10^9	2.13×10^{12}	7.02×10^9	3.00×10^{10}	3.00×10^{10}	3.00×10^{10}	4.39×10^6	4.39×10^6	4.39×10^6	1.03×10^{-3}
3.45×10^{-4}	3.83×10^{-4}	8.36×10^9	2.84×10^{12}	9.36×10^9	2.84×10^{12}	9.36×10^9	4.00×10^{10}	4.00×10^{10}	4.00×10^{10}	4.39×10^6	4.39×10^6	4.39×10^6	1.03×10^{-3}
3.45×10^{-4}	3.83×10^{-4}	1.04×10^{10}	3.55×10^{12}	1.17×10^{10}	3.55×10^{12}	1.17×10^{10}	5.00×10^{10}	5.00×10^{10}	5.00×10^{10}	4.39×10^6	4.39×10^6	4.39×10^6	1.03×10^{-3}
3.45×10^{-4}	3.83×10^{-4}	1.25×10^{10}	4.26×10^{12}	1.40×10^{10}	4.26×10^{12}	1.40×10^{10}	6.00×10^{10}	6.00×10^{10}	6.00×10^{10}	4.39×10^6	4.39×10^6	4.39×10^6	1.03×10^{-3}
3.45×10^{-4}	3.83×10^{-4}	1.46×10^{10}	4.97×10^{12}	1.64×10^{10}	4.97×10^{12}	1.64×10^{10}	7.00×10^{10}	7.00×10^{10}	7.00×10^{10}	4.39×10^6	4.39×10^6	4.39×10^6	1.03×10^{-3}
3.45×10^{-4}	3.83×10^{-4}	1.67×10^{10}	5.68×10^{12}	1.87×10^{10}	5.68×10^{12}	1.87×10^{10}	8.00×10^{10}	8.00×10^{10}	8.00×10^{10}	4.39×10^6	4.39×10^6	4.39×10^6	1.03×10^{-3}
3.45×10^{-4}	3.83×10^{-4}	1.88×10^{10}	6.39×10^{12}	2.11×10^{10}	6.39×10^{12}	2.11×10^{10}	9.00×10^{10}	9.00×10^{10}	9.00×10^{10}	4.39×10^6	4.39×10^6	4.39×10^6	1.03×10^{-3}
3.45×10^{-4}	3.83×10^{-4}	2.09×10^{10}	7.11×10^{12}	2.34×10^{10}	7.11×10^{12}	2.34×10^{10}	1.00×10^{11}	1.00×10^{11}	1.00×10^{11}	4.39×10^6	4.39×10^6	4.39×10^6	1.03×10^{-3}

^a $k_{\text{soliv}} = 1.34 \times 10^7 \text{ s}^{-1}$ and $k_{\text{N3}} = 6.1 \times 10^9 \text{ M}^{-1} \text{ s}^{-1}$ were fixed during the fit. ^b The values of k_{-2}^c and k_{-2}^e correspond to $[\text{OPNB}] = 4.8 \text{ mM}$.

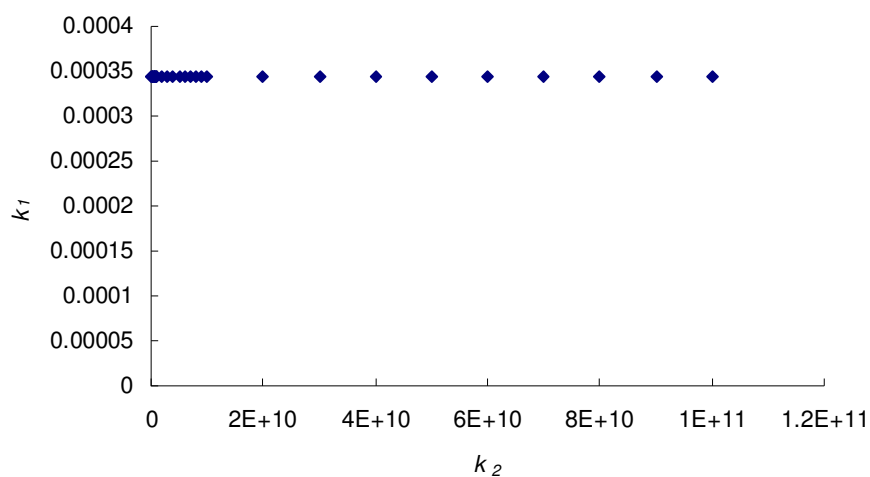


Figure SN1a.

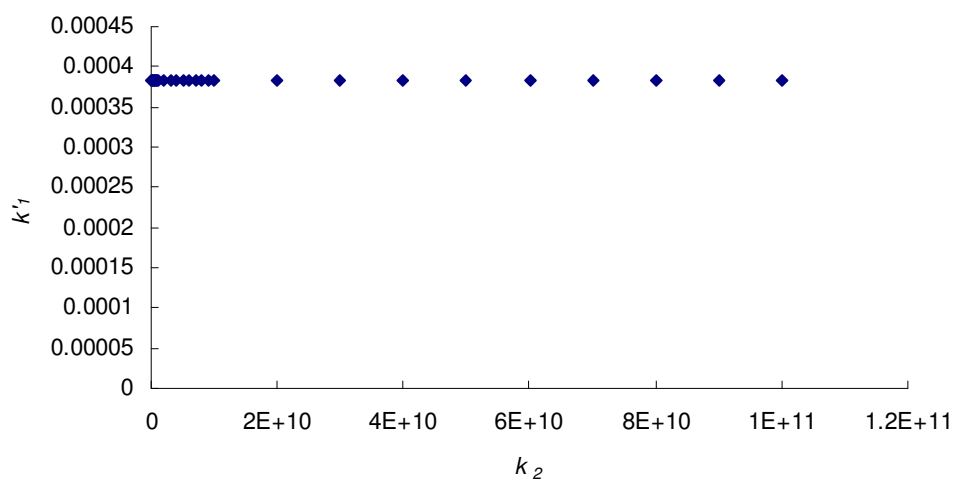


Figure SN2a.

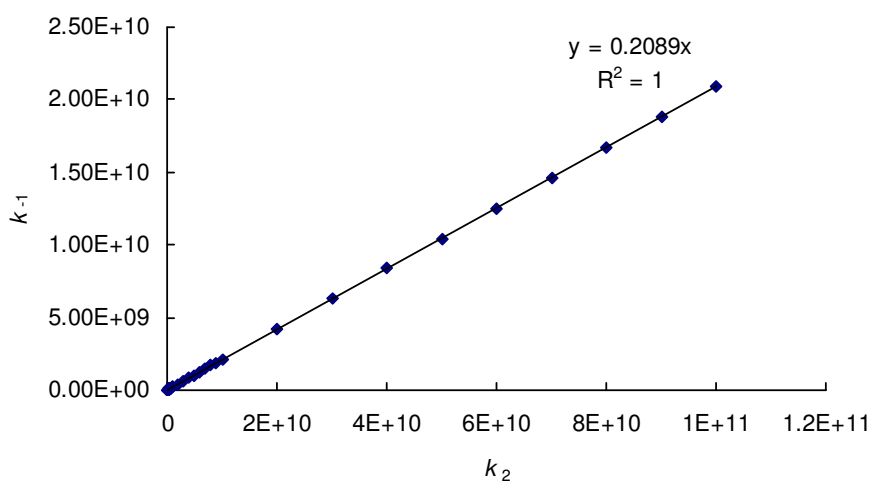


Figure SN3a.

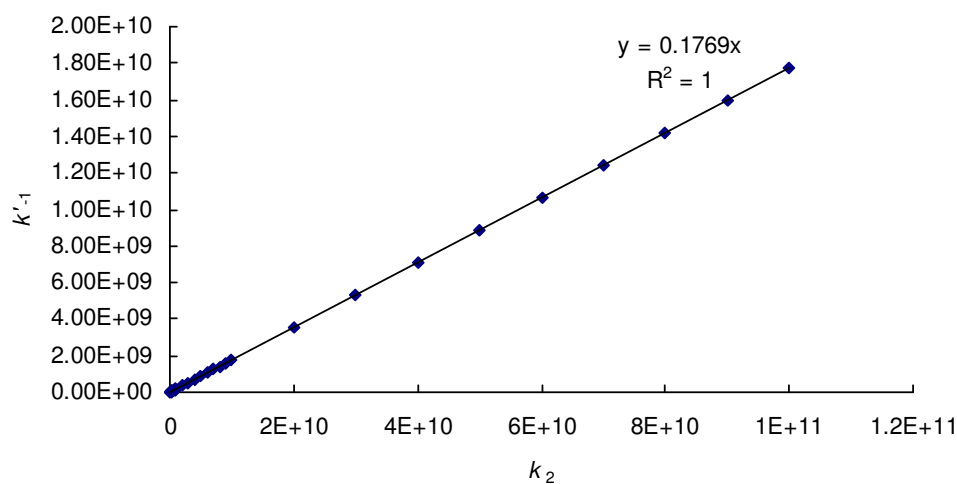


Figure SN4a.

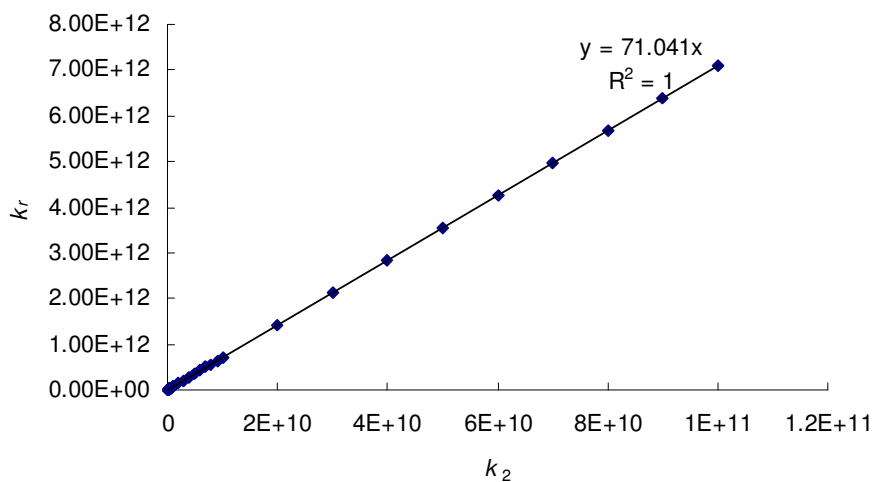


Figure SN5a.

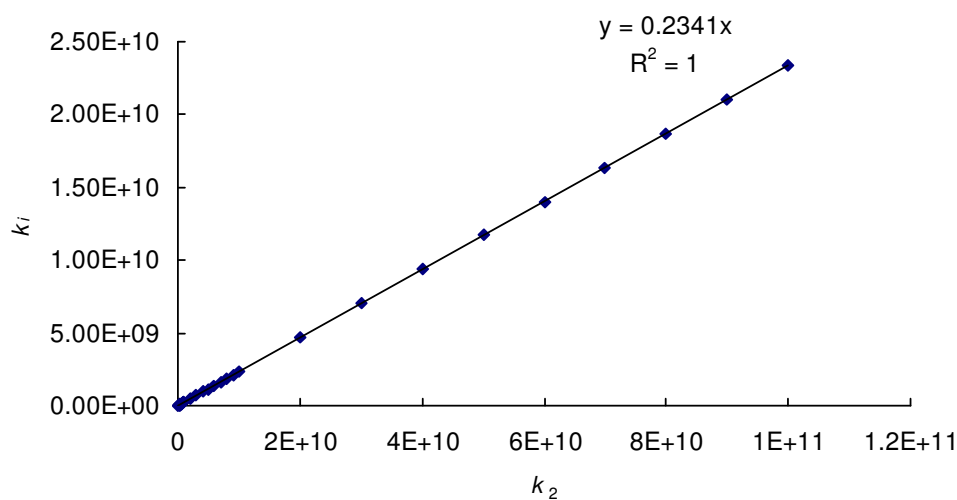
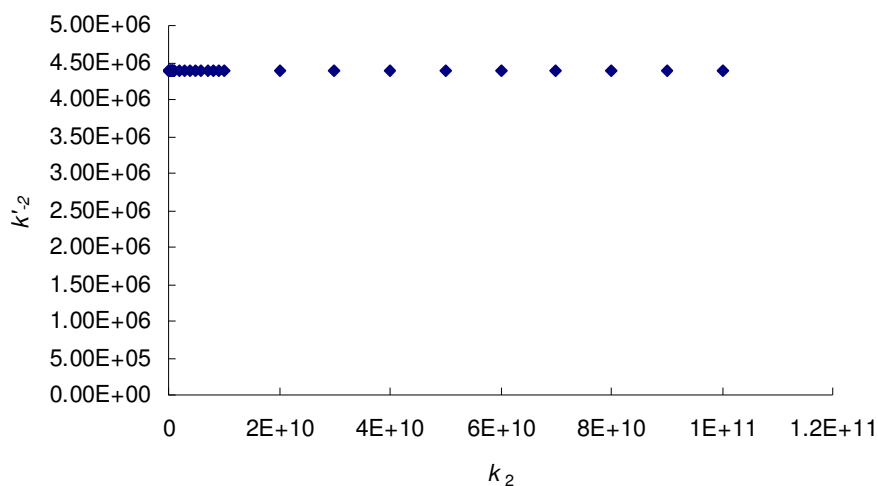
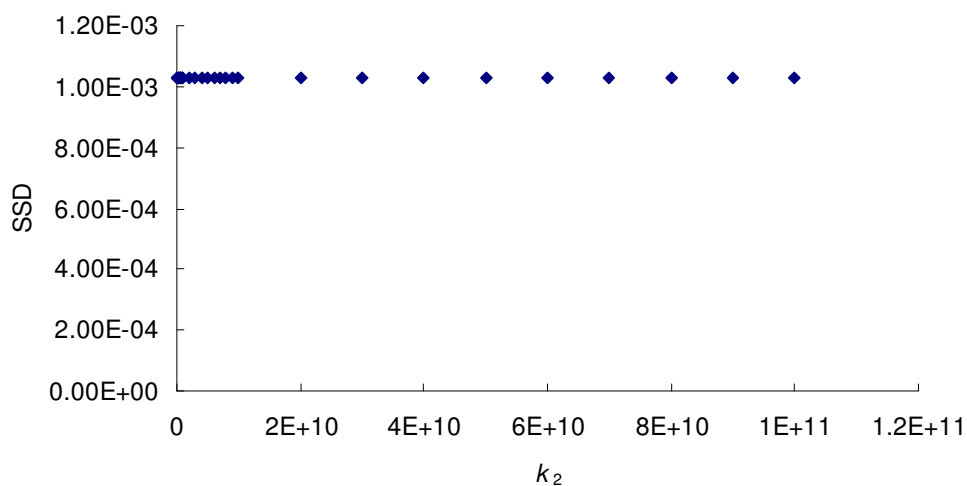


Figure SN6a.

**Figure SN7a.****Figure SN8a.**

The changes in the microscopic rate constants and SSD obtained fitting the experimental values to eq S45 at the fixed value of $k_2 = 2 \times 10^{10} \text{ s}^{-1}$ and different fixed values of k_r are shown in Table SN3 and Figures SN9-SN15. These calculations were only performed using steady state approximation due to large errors in the calculations of eigenvalues and eigenvectors of matrix A by the direct method at high values of $k_r (> 10^{12} \text{ s}^{-1})$.

Table SN3. The values of microscopic rate constants^a (s⁻¹) and SSD obtained by fitting of the experimental data to eq S45 at fixed $k_2 = k'_2 = 2 \times 10^{10} \text{ s}^{-1}$ and various fixed values of $k_r = k'_r$.

k_1	k'_1	k_{-1}	k'_{-1}	k_r	k_i	k'_r	k_i	k_2	k'_2	k_{-2}^e	k_{-2}^b	SSD
4.22×10^{-4}	4.71×10^{-4}	8.13×10^9	8.03×10^9	5.00×10^9	9.40×10^8	5.00×10^9	9.40×10^8	2.0×10^{10}	2.0×10^{10}	2.96×10^6	2.96×10^6	3.15×10^{-3}
4.31×10^{-4}	4.87×10^{-4}	9.32×10^9	9.39×10^9	6.00×10^9	1.18×10^9	6.00×10^9	1.18×10^9	2.0×10^{10}	2.0×10^{10}	2.45×10^6	2.45×10^6	1.83×10^{-3}
4.25×10^{-4}	4.73×10^{-4}	9.00×10^9	8.58×10^9	7.00×10^9	1.22×10^9	7.00×10^9	1.22×10^9	2.0×10^{10}	2.0×10^{10}	2.55×10^6	2.55×10^6	1.56×10^{-3}
4.10×10^{-4}	4.52×10^{-4}	7.60×10^9	7.08×10^9	8.00×10^9	7.35×10^8	8.00×10^9	7.35×10^8	2.0×10^{10}	2.0×10^{10}	3.12×10^6	3.12×10^6	1.78×10^{-3}
4.29×10^{-4}	4.67×10^{-4}	9.97×10^9	8.68×10^9	9.00×10^9	1.79×10^9	9.00×10^9	1.79×10^9	2.0×10^{10}	2.0×10^{10}	2.22×10^6	2.22×10^6	1.13×10^{-3}
4.19×10^{-4}	4.58×10^{-4}	9.32×10^9	8.12×10^9	1.00×10^{10}	1.94×10^9	1.00×10^{10}	1.94×10^9	2.0×10^{10}	2.0×10^{10}	2.31×10^6	2.31×10^6	1.11×10^{-3}
3.79×10^{-4}	4.18×10^{-4}	6.63×10^9	5.71×10^9	2.00×10^{10}	2.87×10^9	2.00×10^{10}	2.87×10^9	2.0×10^{10}	2.0×10^{10}	2.96×10^6	2.96×10^6	1.05×10^{-3}
3.67×10^{-4}	4.06×10^{-4}	5.80×10^9	4.95×10^9	3.00×10^{10}	3.30×10^9	3.00×10^{10}	3.30×10^9	2.0×10^{10}	2.0×10^{10}	3.31×10^6	3.31×10^6	1.04×10^{-3}
3.62×10^{-4}	4.00×10^{-4}	5.38×10^9	4.58×10^9	4.00×10^{10}	3.56×10^9	4.00×10^{10}	3.56×10^9	2.0×10^{10}	2.0×10^{10}	3.53×10^6	3.53×10^6	1.03×10^{-3}
3.58×10^{-4}	3.97×10^{-4}	5.14×10^9	4.36×10^9	5.00×10^{10}	3.74×10^9	5.00×10^{10}	3.74×10^9	2.0×10^{10}	2.0×10^{10}	3.68×10^6	3.68×10^6	1.03×10^{-3}
3.56×10^{-4}	3.94×10^{-4}	4.97×10^9	4.22×10^9	6.00×10^{10}	3.87×10^9	6.00×10^{10}	3.87×10^9	2.0×10^{10}	2.0×10^{10}	3.78×10^6	3.78×10^6	1.03×10^{-3}
3.54×10^{-4}	3.93×10^{-4}	4.85×10^9	4.11×10^9	7.00×10^{10}	3.96×10^9	7.00×10^{10}	3.96×10^9	2.0×10^{10}	2.0×10^{10}	3.86×10^6	3.86×10^6	1.03×10^{-3}
3.53×10^{-4}	3.91×10^{-4}	4.76×10^9	4.04×10^9	8.00×10^{10}	4.04×10^9	8.00×10^{10}	4.04×10^9	2.0×10^{10}	2.0×10^{10}	3.92×10^6	3.92×10^6	1.03×10^{-3}
3.52×10^{-4}	3.90×10^{-4}	4.70×10^9	3.98×10^9	9.00×10^{10}	4.10×10^9	9.00×10^{10}	4.10×10^9	2.0×10^{10}	2.0×10^{10}	3.97×10^6	3.97×10^6	1.03×10^{-3}
3.51×10^{-4}	3.90×10^{-4}	4.64×10^9	3.93×10^9	1.00×10^{11}	4.16×10^9	1.00×10^{11}	4.16×10^9	2.0×10^{10}	2.0×10^{10}	4.02×10^6	4.02×10^6	1.03×10^{-3}
3.48×10^{-4}	3.86×10^{-4}	4.39×10^9	3.72×10^9	2.00×10^{11}	4.42×10^9	2.00×10^{11}	4.42×10^9	2.0×10^{10}	2.0×10^{10}	4.21×10^6	4.21×10^6	1.03×10^{-3}
3.46×10^{-4}	3.85×10^{-4}	4.31×10^9	3.65×10^9	3.00×10^{11}	4.51×10^9	3.00×10^{11}	4.51×10^9	2.0×10^{10}	2.0×10^{10}	4.28×10^6	4.28×10^6	1.03×10^{-3}
3.46×10^{-4}	3.85×10^{-4}	4.27×10^9	3.61×10^9	4.00×10^{11}	4.56×10^9	4.00×10^{11}	4.56×10^9	2.0×10^{10}	2.0×10^{10}	4.31×10^6	4.31×10^6	1.03×10^{-3}
3.46×10^{-4}	3.84×10^{-4}	4.24×10^9	3.59×10^9	5.00×10^{11}	4.60×10^9	5.00×10^{11}	4.60×10^9	2.0×10^{10}	2.0×10^{10}	4.33×10^6	4.33×10^6	1.03×10^{-3}
3.45×10^{-4}	3.84×10^{-4}	4.23×10^9	3.58×10^9	6.00×10^{11}	4.62×10^9	6.00×10^{11}	4.62×10^9	2.0×10^{10}	2.0×10^{10}	4.35×10^6	4.35×10^6	1.03×10^{-3}
3.45×10^{-4}	3.84×10^{-4}	4.21×10^9	3.57×10^9	7.00×10^{11}	4.63×10^9	7.00×10^{11}	4.63×10^9	2.0×10^{10}	2.0×10^{10}	4.36×10^6	4.36×10^6	1.03×10^{-3}
3.45×10^{-4}	3.84×10^{-4}	4.21×10^9	3.56×10^9	8.00×10^{11}	4.64×10^9	8.00×10^{11}	4.64×10^9	2.0×10^{10}	2.0×10^{10}	4.37×10^6	4.37×10^6	1.03×10^{-3}
3.45×10^{-4}	3.84×10^{-4}	4.20×10^9	3.56×10^9	9.00×10^{11}	4.65×10^9	9.00×10^{11}	4.65×10^9	2.0×10^{10}	2.0×10^{10}	4.37×10^6	4.37×10^6	1.03×10^{-3}
3.45×10^{-4}	3.84×10^{-4}	4.19×10^9	3.55×10^9	1.00×10^{12}	4.66×10^9	1.00×10^{12}	4.66×10^9	2.0×10^{10}	2.0×10^{10}	4.38×10^6	4.38×10^6	1.03×10^{-3}

^a $k_{\text{solv}} = 1.34 \times 10^7 \text{ s}^{-1}$ and $k_{\text{N}3} = 6.1 \times 10^9 \text{ M}^{-1} \text{ s}^{-1}$ were fixed during the fit. ^bThe values of k_{-2}^e and k_{-2}^b correspond to $[\text{OPNB}] = 4.8 \text{ mM}$.

Table SN3. Continued.

k_1	k'_1	k_{-1}	k'^{-1}	k_f	k_i	k'_r	k_i	k_2	k'_2	k_{-2}^e	$k_{-2}^{e'}$	SSD
3.44×10^{-4}	3.83×10^{-4}	4.17×10^9	3.53×10^9	2.00×10^{12}	4.70×10^9	2.00×10^{12}	4.70×10^9	2.0×10^{10}	2.0×10^{10}	4.40×10^6	4.40×10^6	1.03×10^{-3}
3.44×10^{-4}	3.83×10^{-4}	4.16×10^9	3.52×10^9	3.00×10^{12}	4.71×10^9	3.00×10^{12}	4.71×10^9	2.0×10^{10}	2.0×10^{10}	4.41×10^6	4.41×10^6	1.03×10^{-3}
3.44×10^{-4}	3.83×10^{-4}	4.16×10^9	3.52×10^9	4.00×10^{12}	4.71×10^9	4.00×10^{12}	4.71×10^9	2.0×10^{10}	2.0×10^{10}	4.41×10^6	4.41×10^6	1.03×10^{-3}
3.44×10^{-4}	3.83×10^{-4}	4.15×10^9	3.52×10^9	5.00×10^{12}	4.72×10^9	5.00×10^{12}	4.72×10^9	2.0×10^{10}	2.0×10^{10}	4.41×10^6	4.41×10^6	1.03×10^{-3}
3.44×10^{-4}	3.83×10^{-4}	4.15×10^9	3.52×10^9	6.00×10^{12}	4.72×10^9	6.00×10^{12}	4.72×10^9	2.0×10^{10}	2.0×10^{10}	4.41×10^6	4.41×10^6	1.03×10^{-3}
3.44×10^{-4}	3.83×10^{-4}	4.15×10^9	3.51×10^9	7.00×10^{12}	4.72×10^9	7.00×10^{12}	4.72×10^9	2.0×10^{10}	2.0×10^{10}	4.41×10^6	4.41×10^6	1.03×10^{-3}
3.44×10^{-4}	3.83×10^{-4}	4.15×10^9	3.51×10^9	8.00×10^{12}	4.72×10^9	8.00×10^{12}	4.72×10^9	2.0×10^{10}	2.0×10^{10}	4.42×10^6	4.42×10^6	1.03×10^{-3}
3.44×10^{-4}	3.83×10^{-4}	4.15×10^9	3.51×10^9	9.00×10^{12}	4.72×10^9	9.00×10^{12}	4.72×10^9	2.0×10^{10}	2.0×10^{10}	4.42×10^6	4.42×10^6	1.03×10^{-3}
3.44×10^{-4}	3.83×10^{-4}	4.15×10^9	3.51×10^9	1.00×10^{13}	4.72×10^9	1.00×10^{13}	4.72×10^9	2.0×10^{10}	2.0×10^{10}	4.42×10^6	4.42×10^6	1.03×10^{-3}
3.44×10^{-4}	3.83×10^{-4}	4.15×10^9	3.51×10^9	2.00×10^{13}	4.73×10^9	2.00×10^{13}	4.73×10^9	2.0×10^{10}	2.0×10^{10}	4.42×10^6	4.42×10^6	1.03×10^{-3}
3.44×10^{-4}	3.83×10^{-4}	4.15×10^9	3.51×10^9	3.00×10^{13}	4.73×10^9	3.00×10^{13}	4.73×10^9	2.0×10^{10}	2.0×10^{10}	4.42×10^6	4.42×10^6	1.03×10^{-3}
3.44×10^{-4}	3.83×10^{-4}	4.14×10^9	3.51×10^9	4.00×10^{13}	4.73×10^9	4.00×10^{13}	4.73×10^9	2.0×10^{10}	2.0×10^{10}	4.42×10^6	4.42×10^6	1.03×10^{-3}
3.44×10^{-4}	3.83×10^{-4}	4.14×10^9	3.51×10^9	5.00×10^{13}	4.73×10^9	5.00×10^{13}	4.73×10^9	2.0×10^{10}	2.0×10^{10}	4.42×10^6	4.42×10^6	1.03×10^{-3}
3.44×10^{-4}	3.83×10^{-4}	4.14×10^9	3.51×10^9	6.00×10^{13}	4.73×10^9	6.00×10^{13}	4.73×10^9	2.0×10^{10}	2.0×10^{10}	4.42×10^6	4.42×10^6	1.03×10^{-3}
3.44×10^{-4}	3.83×10^{-4}	4.14×10^9	3.51×10^9	7.00×10^{13}	4.73×10^9	7.00×10^{13}	4.73×10^9	2.0×10^{10}	2.0×10^{10}	4.42×10^6	4.42×10^6	1.03×10^{-3}
3.44×10^{-4}	3.83×10^{-4}	4.14×10^9	3.51×10^9	8.00×10^{13}	4.73×10^9	8.00×10^{13}	4.73×10^9	2.0×10^{10}	2.0×10^{10}	4.42×10^6	4.42×10^6	1.03×10^{-3}
3.44×10^{-4}	3.83×10^{-4}	4.14×10^9	3.51×10^9	9.00×10^{13}	4.73×10^9	9.00×10^{13}	4.73×10^9	2.0×10^{10}	2.0×10^{10}	4.42×10^6	4.42×10^6	1.03×10^{-3}
3.44×10^{-4}	3.83×10^{-4}	4.14×10^9	3.51×10^9	1.00×10^{14}	4.73×10^9	1.00×10^{14}	4.73×10^9	2.0×10^{10}	2.0×10^{10}	4.42×10^6	4.42×10^6	1.03×10^{-3}

^a $k_{\text{solV}} = 1.34 \times 10^7 \text{ s}^{-1}$ and $k_{\text{N3}} = 6.1 \times 10^9 \text{ M}^{-1} \text{ s}^{-1}$ were fixed during the fit. ^b The values of k_{-2}^e and $k_{-2}^{e'}$ correspond to $[\text{OPNB}] = 4.8 \text{ mM}$.

Table SN4. The differences (in %) between the values of microscopic rate constants obtained by fitting of the experimental data to eq S45 at fixed value of $k_2 = k'_2 = 2 \times 10^{10} \text{ s}^{-1}$ and various fixed values of $k_r = k'_r$, and their values at $k_2 = k'_2 = 2 \times 10^{10} \text{ s}^{-1}$ and $k_r = k'_r = 2 \times 10^{11} \text{ s}^{-1}$ as well as the differences E_{SSD} between current and minimal values of SSD (in % of SSD_{min}).

k_r	k_i/k_2	k_1	k'_1	$k_{1,1}$	$k_{1,2}$	k_r	k_i	k'_i	$k_{r,1}$	$k_{r,2}$	k'_i	$k_{2,1}$	$k_{2,2}$	k'_2	$E_{\text{SSD}}^a / \%$
									$(k_n - k_n(k_r = 2 \times 10^{11}) / k_n(k_r = 2 \times 10^{11})) \cdot 100\%$						
5.00×10^9	0.25	21.40	22.03	85.13	115.92	-97.50	-78.71	-97.50	-78.71	-97.50	-78.71	-29.66	-29.66	-29.66	2.06×10^2
6.00×10^9	0.30	23.88	26.00	112.20	152.52	-97.00	-73.19	-97.00	-73.19	-97.00	-73.19	-41.83	-41.83	-41.83	7.76×10^1
7.00×10^9	0.35	22.21	22.40	105.00	130.71	-96.50	-72.41	-96.50	-72.41	-96.50	-72.41	-39.41	-39.41	-39.41	5.19×10^1
8.00×10^9	0.40	17.95	17.11	72.93	90.60	-96.00	-83.34	-96.00	-83.34	-96.00	-83.34	-25.83	-25.83	-25.83	7.28×10^1
9.00×10^9	0.45	23.26	20.96	127.02	133.62	-95.50	-59.39	-95.50	-59.39	-95.50	-59.39	-47.31	-47.31	-47.31	9.69
1.00×10^{10}	0.50	20.47	18.51	112.14	118.36	-95.00	-55.98	-95.00	-55.98	-95.00	-55.98	-45.01	-45.01	-45.01	8.19
2.00×10^{10}	1.00	9.12	8.26	51.03	53.71	-90.00	-35.04	-90.00	-35.04	-90.00	-35.04	-29.68	-29.68	-29.68	2.09
3.00×10^{10}	1.50	5.68	5.10	31.97	33.27	-85.00	-25.17	-85.00	-25.17	-85.00	-25.17	-21.34	-21.34	-21.34	8.13×10^{-1}
4.00×10^{10}	2.00	4.00	3.56	22.55	23.26	-80.00	-19.31	-80.00	-19.31	-80.00	-19.31	-16.16	-16.16	-16.16	4.05×10^{-1}
5.00×10^{10}	2.50	3.00	2.66	16.91	17.33	-75.00	-15.34	-75.00	-15.34	-75.00	-15.34	-12.65	-12.65	-12.65	2.36×10^{-1}
6.00×10^{10}	3.00	2.33	2.06	13.15	13.42	-70.00	-12.45	-70.00	-12.45	-70.00	-12.45	-10.13	-10.13	-10.13	1.53×10^{-1}
7.00×10^{10}	3.50	1.86	1.63	10.47	10.64	-65.00	-10.24	-65.00	-10.24	-65.00	-10.24	-8.23	-8.23	-8.23	1.07×10^{-1}
8.00×10^{10}	4.00	1.50	1.32	8.46	8.57	-60.00	-8.49	-60.00	-8.49	-60.00	-8.49	-6.76	-6.76	-6.76	7.87×10^{-2}
9.00×10^{10}	4.50	1.23	1.07	6.90	6.97	-55.00	-7.07	-55.00	-7.07	-55.00	-7.07	-5.57	-5.57	-5.57	6.04×10^{-2}
1.00×10^{11}	5.00	1.00	0.88	5.64	5.69	-50.00	-5.89	-50.00	-5.89	-50.00	-5.89	-4.60	-4.60	-4.60	4.79×10^{-2}
2.00×10^{11}	10.00	0.00	0.00	0.00	0.00	0.00	0.00	0.00	0.00	0.00	0.00	0.00	0.00	0.00	1.12×10^{-2}
3.00×10^{11}	15.00	-0.34	-0.29	-1.89	-1.88	50.00	2.21	50.00	2.21	50.00	2.21	1.63	1.63	1.63	4.98×10^{-3}
4.00×10^{11}	20.00	-0.51	-0.44	-2.83	-2.81	100.00	3.37	100.00	3.37	100.00	3.37	2.46	2.46	2.46	2.82×10^{-3}
5.00×10^{11}	25.00	-0.61	-0.52	-3.40	-3.37	150.00	4.09	150.00	4.09	150.00	4.09	2.96	2.96	2.96	1.81×10^{-3}
6.00×10^{11}	30.00	-0.68	-0.58	-3.78	-3.74	200.00	4.57	200.00	4.57	200.00	4.57	3.30	3.30	3.30	1.27×10^{-3}
7.00×10^{11}	35.00	-0.72	-0.62	-4.05	-4.01	250.00	4.92	250.00	4.92	250.00	4.92	3.55	3.55	3.55	9.33×10^{-4}
8.00×10^{11}	40.00	-0.76	-0.65	-4.25	-4.21	300.00	5.19	300.00	5.19	300.00	5.19	3.73	3.73	3.73	7.17×10^{-4}

^a $E_{\text{SSD}} = (\text{SSD} - \text{SSD}_{\text{min}}) / \text{SSD}_{\text{min}} \cdot 100\%$.

Table SN4. Continued.

k_r	k_r/k_2	k_1	k_1'	k_{-1}	k_r	k_i	k_r	k_i	k_r	k_i'	k_2	k_2'	$E_{SSD}^a / \%$
					$(k_n - k_n (k_r = 2 \times 10^{11}) / k_n (k_r = 2 \times 10^{11}) \cdot 100\%$								
9.00×10^{11}	45.00	-0.79	-0.68	-4.41	-4.36	350.00	5.40	350.00	5.40	3.87	3.87	3.87	5.68×10^{-4}
1.00×10^{12}	50.00	-0.81	-0.70	-4.53	-4.49	400.00	5.57	400.00	5.57	3.99	3.99	3.99	4.61×10^{-4}
2.00×10^{11}	100.00	-0.91	-0.78	-5.10	-5.04	900.00	6.33	900.00	6.33	4.51	4.51	4.51	1.17×10^{-4}
3.00×10^{11}	150.00	-0.95	-0.81	-5.29	-5.23	1400.00	6.59	1400.00	6.59	4.68	4.68	4.68	5.20×10^{-5}
4.00×10^{11}	200.00	-0.96	-0.83	-5.39	-5.32	1900.00	6.72	1900.00	6.72	4.77	4.77	4.77	2.93×10^{-5}
5.00×10^{11}	250.00	-0.98	-0.84	-5.44	-5.38	2400.00	6.79	2400.00	6.79	4.82	4.82	4.82	1.88×10^{-5}
6.00×10^{11}	300.00	-0.98	-0.84	-5.48	-5.41	2900.00	6.85	2900.00	6.85	4.85	4.85	4.85	1.30×10^{-5}
7.00×10^{11}	350.00	-0.99	-0.85	-5.51	-5.44	3400.00	6.88	3400.00	6.88	4.88	4.88	4.88	9.56×10^{-6}
8.00×10^{11}	400.00	-0.99	-0.85	-5.53	-5.46	3900.00	6.91	3900.00	6.91	4.90	4.90	4.90	7.31×10^{-6}
9.00×10^{11}	450.00	-0.99	-0.85	-5.54	-5.47	4400.00	6.93	4400.00	6.93	4.91	4.91	4.91	5.77×10^{-6}
1.00×10^{12}	500.00	-1.00	-0.85	-5.56	-5.49	4900.00	6.95	4900.00	6.95	4.92	4.92	4.92	4.67×10^{-6}
2.00×10^{12}	1000.00	-1.01	-0.86	-5.61	-5.54	9900.00	7.03	9900.00	7.03	4.98	4.98	4.98	1.13×10^{-6}
3.00×10^{12}	1500.00	-1.01	-0.87	-5.63	-5.56	14900.00	7.06	14900.00	7.06	4.99	4.99	4.99	4.77×10^{-7}
4.00×10^{12}	2000.00	-1.01	-0.87	-5.64	-5.57	19900.00	7.07	19900.00	7.07	5.00	5.00	5.00	2.48×10^{-7}
5.00×10^{12}	2500.00	-1.01	-0.87	-5.65	-5.58	24900.00	7.08	24900.00	7.08	5.01	5.01	5.01	1.42×10^{-7}
6.00×10^{12}	3000.00	-1.01	-0.87	-5.65	-5.58	29900.00	7.08	29900.00	7.08	5.01	5.01	5.01	8.40×10^{-8}
7.00×10^{12}	3500.00	-1.01	-0.87	-5.65	-5.58	34900.00	7.09	34900.00	7.09	5.01	5.01	5.01	4.92×10^{-8}
8.00×10^{12}	4000.00	-1.01	-0.87	-5.66	-5.58	39900.00	7.09	39900.00	7.09	5.02	5.02	5.02	2.66×10^{-8}
9.00×10^{12}	4500.00	-1.01	-0.87	-5.66	-5.59	44900.00	7.09	44900.00	7.09	5.02	5.02	5.02	1.11×10^{-8}
1.00×10^{13}	5000.00	-1.01	-0.87	-5.66	-5.59	49900.00	7.09	49900.00	7.09	5.02	5.02	5.02	0.00

^a $E_{SSD} = (SSD - SSD_{min}) / SSD_{min} \cdot 100\%$.

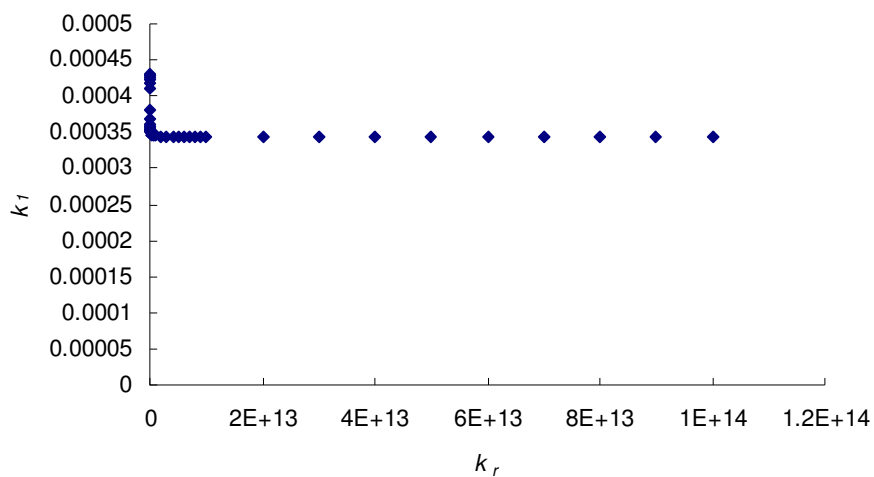


Figure SN9.

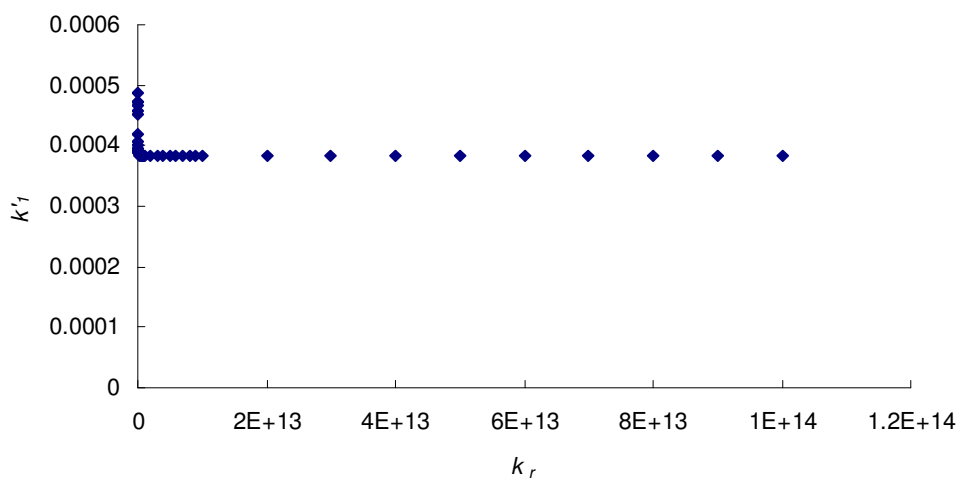


Figure SN10.

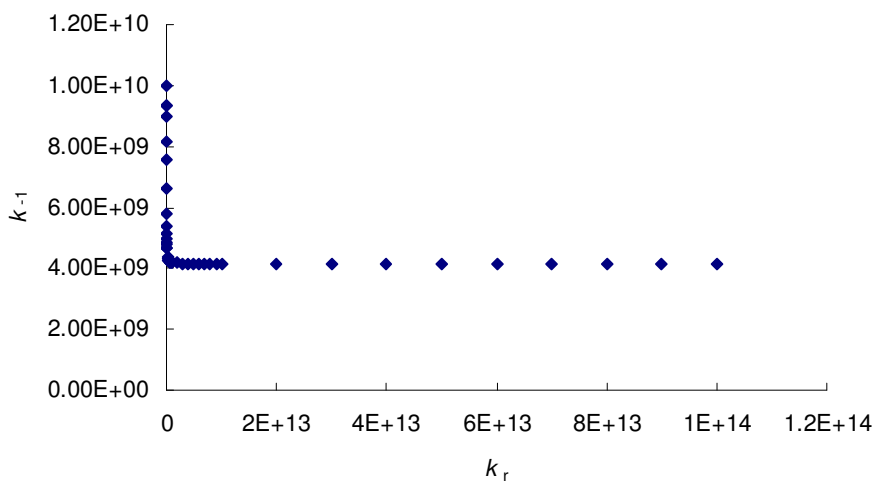


Figure SN11.

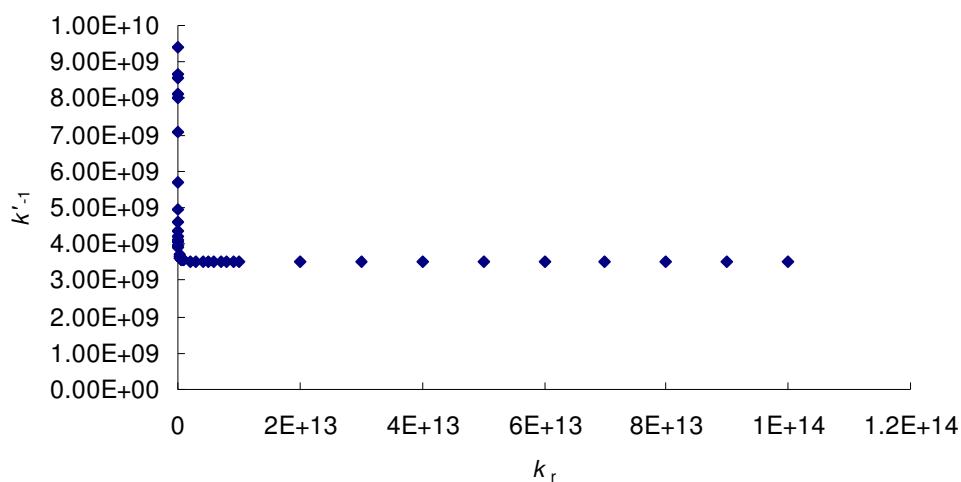


Figure SN12.

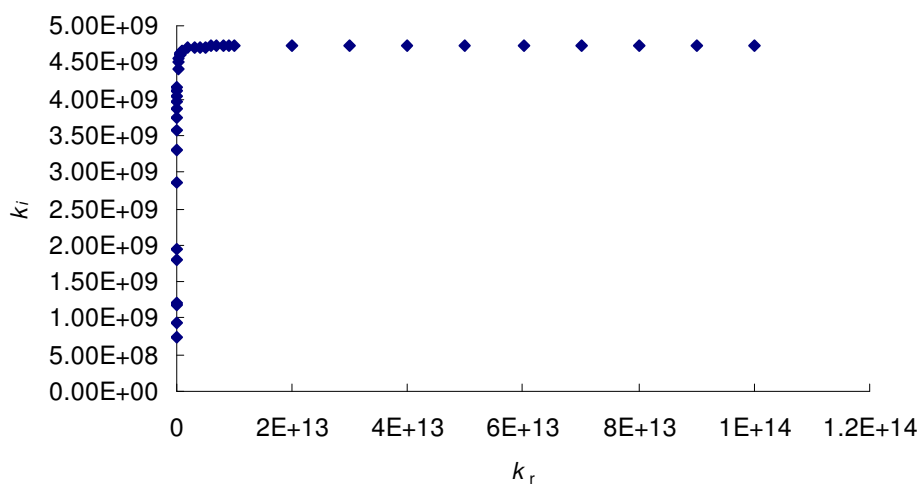


Figure SN13.

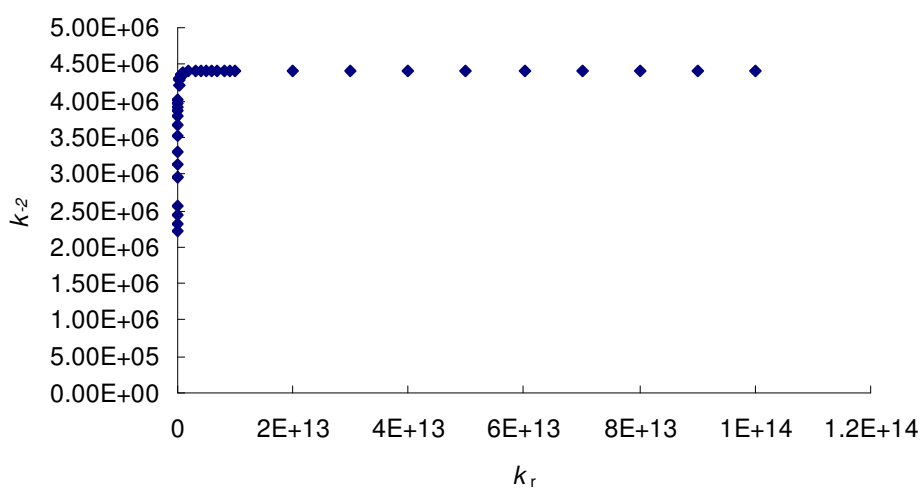


Figure SN14.

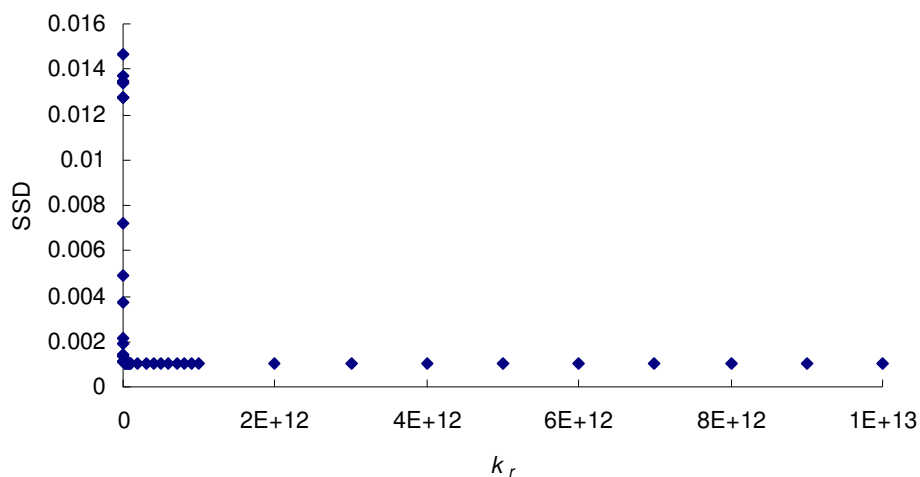


Figure SN15.

Figures SN16-SN22 show the fits of the experimental data based on eq S45 and one of the sets presented in Table SN2.

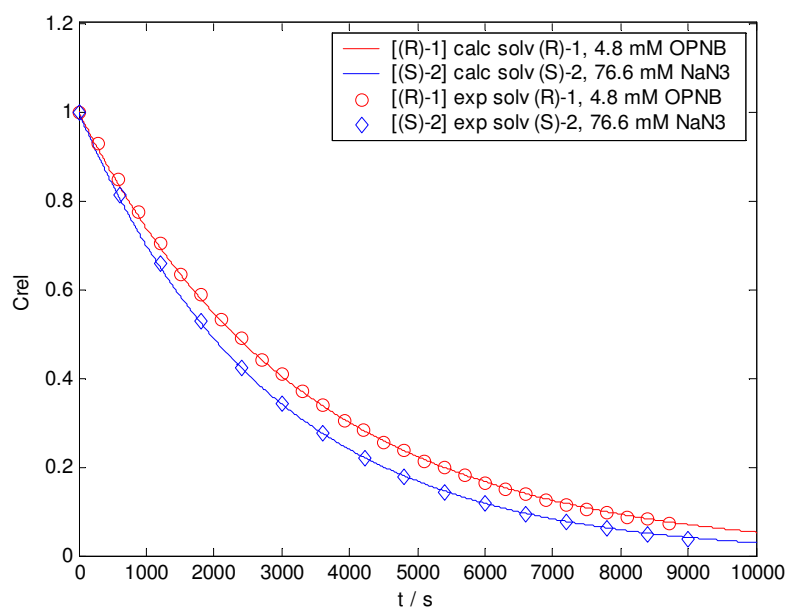


Figure SN16. Experimental (points) and calculated (solid lines) decays of (*R*)-**1** (red) and (*S*)-**2** (blue) in 60% aq acetone, 25 °C.

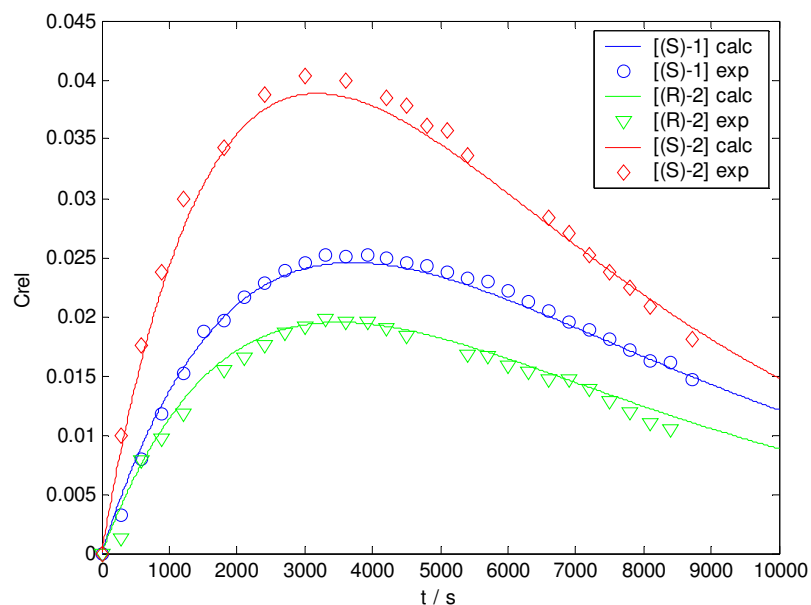


Figure SN17. Experimental (points) and calculated (solid lines) time-dependent relative concentrations of (S)-1 (blue), (R)-2 (green) and (S)-2 (red) during solvolysis of (R)-1 in 60% aq acetone in the presence of 4.8 mM of Bu₄NOPNB, 25 °C.

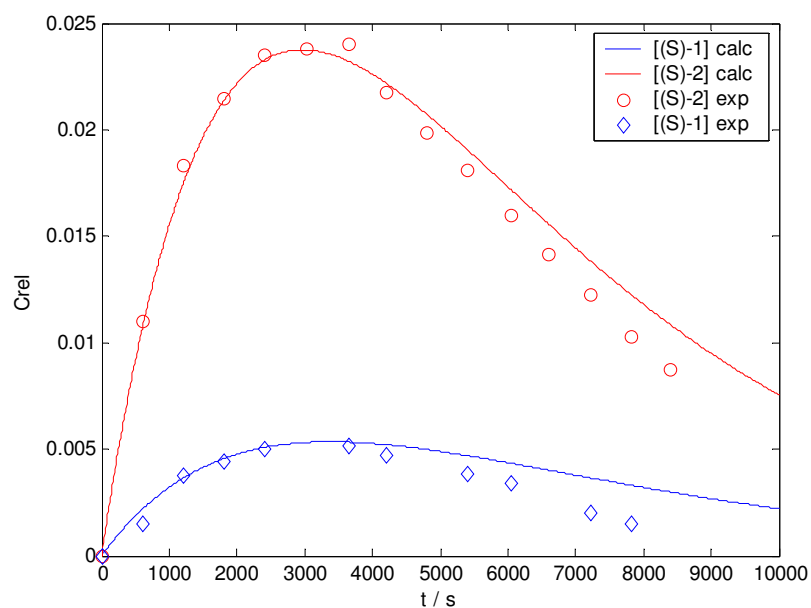


Figure SN18. Experimental (points) and calculated (solid lines) time-dependent relative concentrations of (S)-1 (blue) and (S)-2 (red) during solvolysis of (R)-1 in 60% aqueous acetone in the presence of 70.8 mM NaN₃, 25 °C.

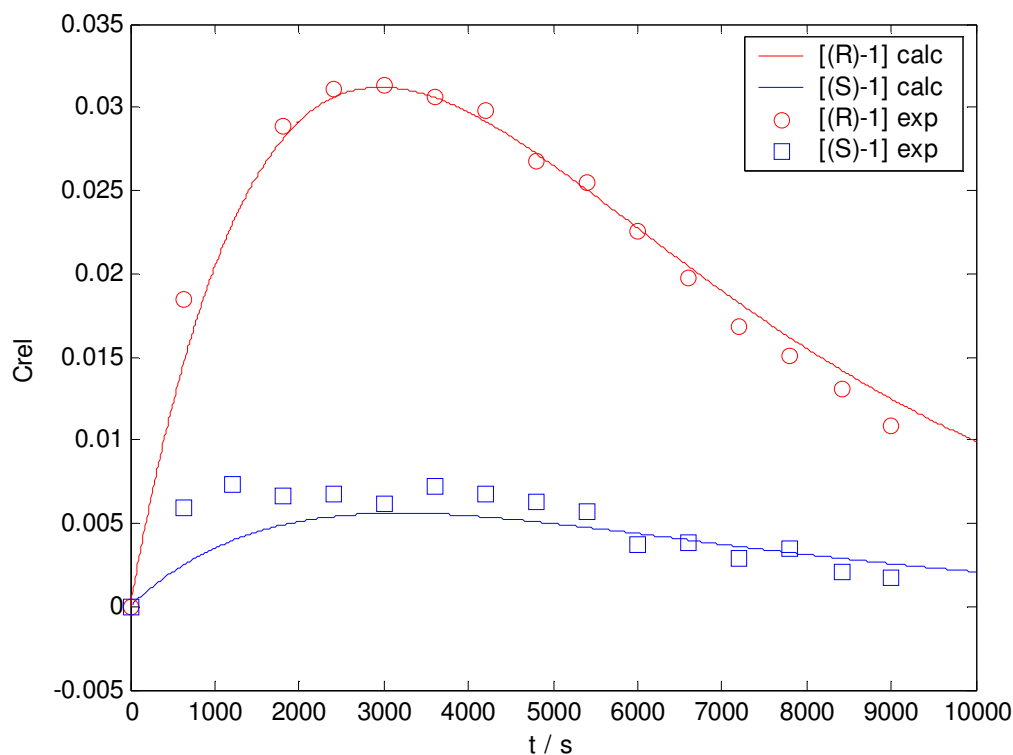


Figure SN19. Experimental (points) and calculated (solid lines) time-dependent relative concentrations of (*S*)-**1** (blue) and (*R*)-**1** (red) during solvolysis of (*S*)-**2** in 60% aqueous acetone in the presence of 76.6 mM NaN_3 , 25 °C.

Figure SN20 shows excellent agreement between calculated (eq S29 or eq S45) and experimental values of [(*R*)-**1**] during its solvolysis in 60% aq acetone in the presence of 70.8 mM NaN_3 . It is noteworthy that these experimental values were not used for the determination of microscopic rate constants.

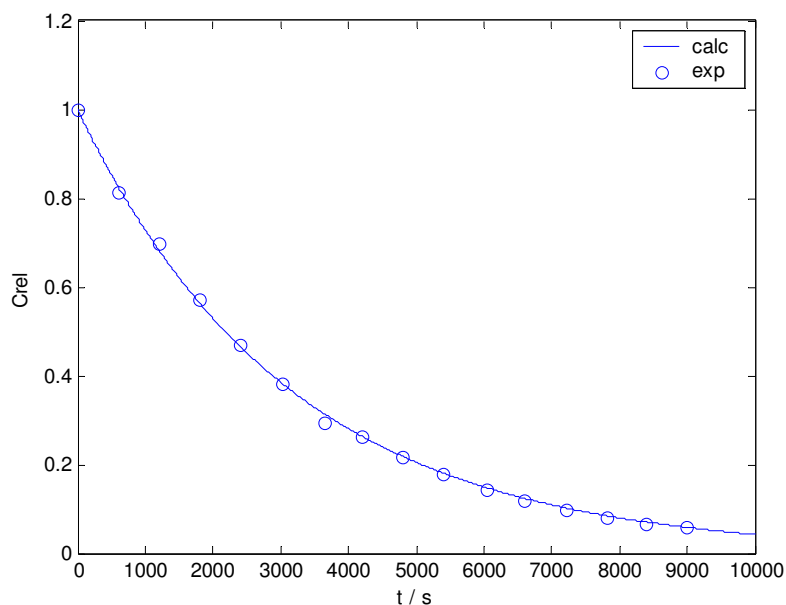


Figure SN20. Experimental (points) and calculated (solid line) values of [(*R*)-**1**] during its solvolysis in 60% aq acetone in the presence of 70.8 mM NaN₃, 25 °C.

Comparison of the integral areas (*I*) of allyl azides RN₃ and chalcone **5** (internal standard) yields the relative concentrations of RN₃, which should be proportional the sum of time-dependent concentrations of the allyl alcohols and azides (i.e., [RN₃]+**3**+**4**) as all these products should be formed with the same rate.

$$I_{\text{RN}_3}(t)/I_5(t) = A([\text{RN}_3](t)+[\mathbf{3}](t)+[\mathbf{4}](t)) \quad (\text{S48})$$

To find the proportionality factor *A*, the time-dependent ratios I_{RN_3}/I_5 , were fitted to the monoexponential function $I_{\text{RN}_3}/I_5 = A(1-e^{-kt}) + C$. Dividing $I_{\text{RN}_3}(t)/I_5(t)$ (the values of $I_{\text{RN}_3}(t)/I_5(t)$ are listed in Tables S8 and S14) by *A* one can get the values of $[\text{RN}_3](t)+[\mathbf{3}](t)+[\mathbf{4}](t)$ which should, on the other hand, correspond to $1-[(R)\text{-}\mathbf{1}](t)-[(S)\text{-}\mathbf{1}](t)-[(R)\text{-}\mathbf{2}](t)-[(S)\text{-}\mathbf{2}](t)$ as the sum of all relative concentrations should correspond to unity.

Figures SN21 and SN22 show good agreement between the values of $[\text{RN}_3](t)+[\mathbf{3}](t)+[\mathbf{4}](t)$ derived as described above from the experimental $I_{\text{RN}_3}(t)/I_5(t)$ values and the values of $1-[(R)\text{-}\mathbf{1}](t)-[(S)\text{-}\mathbf{1}](t)-[(R)\text{-}\mathbf{2}](t)-[(S)\text{-}\mathbf{2}](t)$ calculated using the set of microscopic rate constants with $k_2 = 2 \times 10^{10} \text{ s}^{-1}$ and eq S45.

Good correlations shown in Figures SN20–SN22 demonstrate the internal consistency of calculated data.

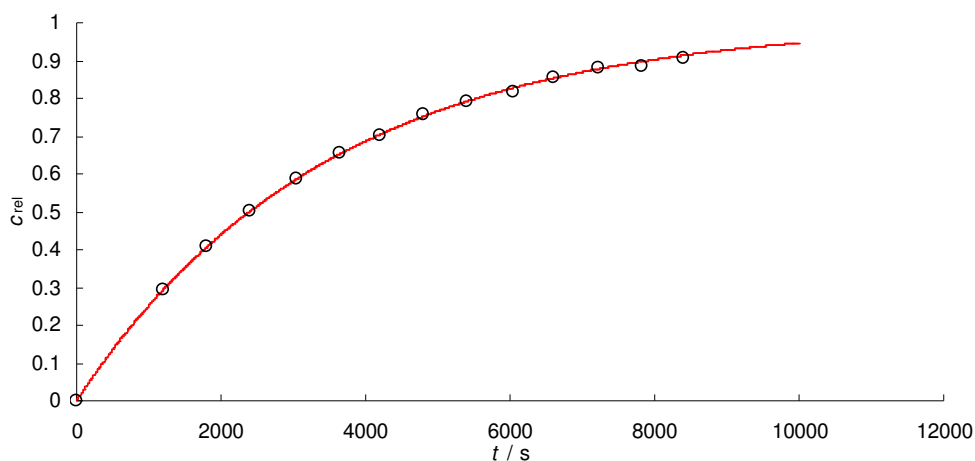


Figure SN21. Calculated (solid line) and experimental (points) values of $[\text{RN}_3](t)+[\mathbf{3}](t)+[\mathbf{4}](t)$ for the solvolysis of (*R*)-**1** in 60% aq acetone in the presence of 70.8 mM NaN_3 .

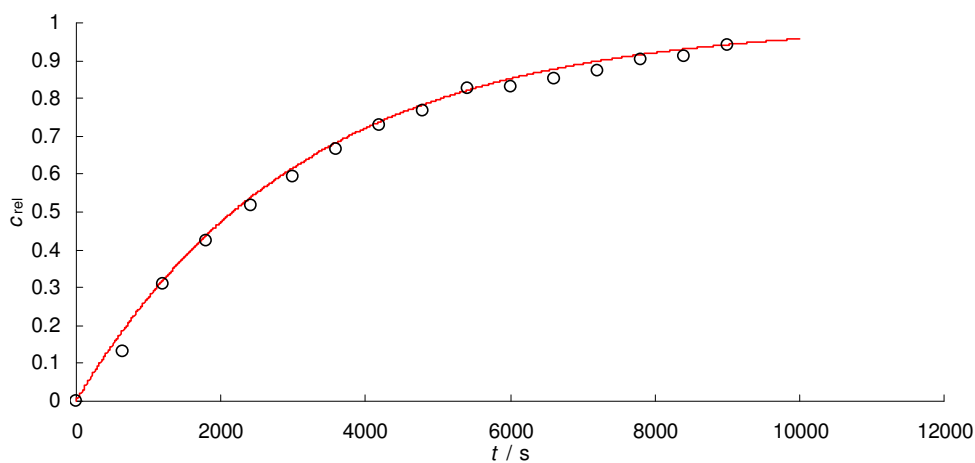


Figure SN22. Calculated (solid line) and experimental (points) values of $[\text{RN}_3](t)+[\mathbf{3}](t)+[\mathbf{4}](t)$ for the solvolysis of (*S*)-**2** in 60% aq acetone in the presence of 76.6 mM NaN_3 .

5.7.4. M-files used for parameter optimization

Direct calculation of the time-dependent concentrations (fitex.m)

```

function [fit1, fit2, fit3, fit4, fit5, fit6, fit7, fit8, fit9, fit10,
fit11, fit12, fit13, fit14, fit15, fit16, fit17, fit18]=
fitex(k1,ks1,km1,kms1,kr,ki,ksr,ksi,k2,ks2,km2,kms2,ksol,t)
c1 = -km1 - k2 - kr - ki;
c2 = -kms1 - ks2 - ksr - ksi;
c3 = -2*km2 -2*kms2 - ksol;
N=[-k1 0 0 0 km1 0 0 0 0; 0 -k1 0 0 0 km1 0 0 0; 0 0 -ks1 0 0 0 kms1 0 0; 0
0 0 -ks1 0 0 0 kms1 0; k1 0 0 0 c1 ki 0 ksr km2; 0 k1 0 0 ki c1 ksr 0 km2;
0 0 ks1 0 0 kr c2 ksi kms2; 0 0 0 ks1 kr 0 ksi c2 kms2; 0 0 0 0 k2 k2 ks2
ks2 c3];
%Formulating matrix for the SLODE
[S,L]=eig(N);
%Eigenvectors and eigenvalues for N
C=S\[1;0;0;0;0;0;0;0;0];
%Boundary conditions for solvolysis of (R)-1
C2=S\[0;0;0;1;0;0;0;0;0];
%Boundary conditions for solvolysis of (S)-2
C3=S\[0;1;0;0;0;0;0;0;0];
C4=S\[0;0;1;0;0;0;0;0;0];
C5=S\[0;0;0;0;0;0;0;0;1];
E=exp(diag(L).*t);
%functions exp(lambdai*t)
E2=C.*E;
%multiplication with constants Ci resolving boundary conditions
Y=S*E2;
%particular solution for solvolysis of (R)-1
fit1=Y(1);
%return [(R)-1]
fit2=Y(2);
%return [(S)-1]
fit3=Y(3);
%return [(R)-2]
fit4=Y(4);
%return [(S)-2]
E3=C2.*E;
Y2=S*E3;
%particular solution for solvolysis of (S)-2
fit5=Y2(1);
%return [(R)-1]
fit6=Y2(2);
%return [(S)-1]
fit7=Y2(3);
%return [(R)-2]
fit8=Y2(4);
%return [(S)-2]
E4=C3.*E;
Y3=S*E4;
E5=C5.*E;
Y5=S*E5;
%particular solution for recombination of cation 6 with -OPNB
fit9=Y5(1);
%return [(R)-1]
fit10=Y5(2);
%return [(S)-1]
fit11=Y5(3);
%return [(R)-2]
fit12=Y5(4);

```



```

%return [(S)-2]
E5=C4.*E;
Y4=S*E5;
fit13=Y5(9);
%return [6]
fit14=Y(5);
fit15=Y(6);
fit16=Y(7);
fit17=Y(8);
fit18=Y(9);

```

Steady state calculation of the time-dependent concentrations (fitf.m)

```

function [fit1, fit2, fit3, fit4, fit5, fit6, fit7, fit8, fit9, fit10,
fit11, fit12, fit13, fit14, fit15, fit16] =
fitf(k1,ks1,km1,kms1,kr,ki,ksr,ksi,k2,ks2,km2,kms2,ksol,t)
c1 = -km1 - k2 - kr - ki;
c2 = -kms1 - ks2 - ksr - ksi;
c3 = -2*km2 -2*kms2 - ksol;
A = [c1 ki 0 ksr km2; ki c1 ksr 0 km2; 0 kr c2 ksi kms2; kr 0 ksi c2 kms2;
k2 k2 ks2 ks2 c3];
%system of linear equations based on steady state approximation
M = inv(A);
%inverted matrix A
N=-[M(1,1)*k1*km1+k1 M(1,2)*k1*km1 M(1,3)*ks1*km1 M(1,4)*ks1*km1;
M(2,1)*k1*km1 M(2,2)*k1*km1+k1 M(2,3)*ks1*km1 M(2,4)*ks1*km1;
M(3,1)*k1*kms1 M(3,2)*k1*kms1 M(3,3)*ks1*kms1+ks1 M(3,4)*ks1*kms1;
M(4,1)*k1*kms1 M(4,2)*k1*kms1 M(4,3)*ks1*kms1 M(4,4)*ks1*kms1+ks1];
%Formulating matrix for the SLODE
[S,L]=eig(N);
%Eigenvectors and eigenvalues for N
C=S\[1;0;0;0];
%Boundary conditions for solvolysis of (R)-1
C2=S\[0;0;0;1];
%Boundary conditions for solvolysis of (S)-2
C3=S\[0;1;0;0];
C4=S\[0;0;1;0];
E=exp(diag(L).*t);
%functions exp(lambdai*t)
E2=C.*E;
%multiplication with constants found resolving boundary conditions
Y=S*E2;
%particular solution for solvolysis of (R)-1
fit1=Y(1);
%return [(R)-1]
fit2=Y(2);
%return [(S)-1]
fit3=Y(3);
%return [(R)-2]
fit4=Y(4);
%return [(S)-2]
E3=C2.*E;
Y2=S*E3;
%particular solution for solvolysis of (S)-2
fit5=Y2(1);
%return [(R)-1]
fit6=Y2(2);
%return [(S)-1]
fit7=Y2(3);
%return [(R)-2]
fit8=Y2(4);

```

```

%return [(S)-2]
E4=C3.*E;
Y3=S*E4;
%particular solution for solvolysis of (S)-1
fit9=Y3(1);
%return [(R)-1]
fit10=Y3(2);
%return [(S)-1]
fit11=Y3(3);
%return [(R)-2]
fit12=Y3(4);
%return [(S)-2]
E5=C4.*E;
Y4=S*E5;
%particular solution for solvolysis of (R)-2
fit13=Y4(1);
%return [(R)-1]
fit14=Y4(2);
%return [(S)-1]
fit15=Y4(3);
%return [(R)-2]
fit16=Y4(4);
%return [(S)-2]

```

Calculation of the SSD by direct method (ssd77exp.m). *To obtain the m-file for steady state replace **fitex** by **fitf**.*

```

function ssd=ssd(k,p)
%argument k - set to optimize
%argument p - set of remaining fit parameters
%structure k or p =(k1,ks1,km1,kms1,kr,ki,ksr,ksi,k2,ks2,km2,kms2,ksol)
k1=k(1);
%free
ks1=k(2);
%free
km1=k(3);
%free
kms1=k(4);
%free
kr=k(5);
%free
ki=k(6);
%free
ksr=k(5);
%bound
ksi=k(6);
%bound
k2=p(9);
%fixed
ks2=p(9);
%fixed
km2=k(11);
%free
kms2=k(11);
%bound
ksol=p(13);
%fixed
kslim=4.45*10^8;
%kNu=ksol+kN3*[N3] in the presence of 70.8 mM NaN3
kslim2=4.81e8;
%kNu=ksol+kN3*[N3] in the presence of 76.6 mM NaN3

```

Chapter 4. Ion Pair Dynamics: Solvolyses of Chiral 1,3-Diaryllallyl Carboxylates as a Case Study

```

rat4=0.0837;
rat4a=0.0823;
%approximate ratio between [OPNB] in two experiments
%experimental data expt - experimental time, expf - experimental
%time-dependent concentration
expt1=[0    290    593    894    1200    1501    1800    2108    2399    2700    3000    3313
        3601    3918    4200    4500    4809    5100    5400    5700    6002    6307    6599    6901
        7201    7500    7803    8102    8400    8724];
expf1=[1.0000    0.9287    0.8467    0.7724    0.7028    0.6328
        0.5865    0.5310    0.4903    0.4415    0.4073    0.3689
        0.3396    0.3040    0.2818    0.2553    0.2357    0.2131
        0.1969    0.1794    0.1646    0.1494    0.1389    0.1231
        0.1140    0.1052    0.0950    0.0875    0.0821    0.0737];
%decay of [(R)-1] during solvolysis of (R)-1 in the presence of 4.8 mM
%Bu4NOPNB
expt2=[0    290    593    894    1200    1501    1800    2108    2399    2700    3000    3313
        3601    3918    4200    4500    4809    5100    5400    5700    6002    6307    6599    6901
        7201    7500    7803    8102    8400    8724];
expf2=[0.0000    0.0032    0.0079    0.0118    0.0152    0.0188
        0.0196    0.0216    0.0228    0.0239    0.0245    0.0252
        0.0251    0.0252    0.0250    0.0246    0.0242    0.0238
        0.0232    0.0230    0.0222    0.0212    0.0205    0.0195
        0.0188    0.0181    0.0171    0.0162    0.0161    0.0147];
%time-dependent concentration of (S)-1 during solvolysis of (R)-1 in the
presence of 4.8 mM
%Bu4NOPNB
expt3=[0    290    593    894    1200    1800    2108    2399    2700    3000    3313    3601
        3918    4200    4500    5400    5700    6002    6307    6599    6901    7201    7500    7803
        8102    8400];
expf3=[0.0000    0.0013    0.0079    0.0096    0.0118    0.0155
        0.0165    0.0175    0.0187    0.0191    0.0198    0.0195
        0.0195    0.0191    0.0184    0.0168    0.0166    0.0159
        0.0154    0.0147    0.0146    0.0138    0.0128    0.0119
        0.0110    0.0104];
%time-dependent concentration of (R)-2 during solvolysis of (R)-1 in the
presence of 4.8 mM
%Bu4NOPNB
expt4=[0    290    593    894    1200    1800    2399    3000    3601    4200    4500    4809
        5100    5400    6599    6901    7201    7500    7803    8102    8724];
expf4=[0.0000    0.0100    0.0176    0.0238    0.0299    0.0343
        0.0387    0.0403    0.0399    0.0385    0.0378    0.0361
        0.0357    0.0336    0.0283    0.0271    0.0252    0.0237
        0.0225    0.0209    0.0181];
%time-dependent concentration of (S)-2 during solvolysis of (R)-1 in the
presence of 4.8 mM
%Bu4NOPNB
expt18=[0    605    1200    1800    2400    3002    3600    4220    4800    5400    6000    6600
        7200    7800    8400    9000];
expf18=[1    0.812108991    0.657633967    0.528438113    0.423385691    0.341137925
        0.275328365    0.220901457    0.178916986    0.143624038    0.116280316
        0.092655727    0.075083996    0.060433001    0.048865865    0.036896571];
%decay of [(S)-2] during solvolysis of (S)-2 in 60% aq acetone in the
%presence of 76.6 mM OPNB
expt6=[0    618    1200    1803    2400    3035    3647    4206    4800    5400    6040    6610
        7215    7816    8405];
expf6=[0    0.010964962    0.018286819    0.021422871    0.023535271    0.023812559
        0.023985867    0.021731369    0.019810788    0.018062054    0.015939271
        0.014169254    0.012272464    0.010278255    0.008731633];
%time-dependent concentration of (S)-2 during solvolysis of (R)-1 in the
presence of 70.8 mM
%NaN3
expt7=[0    618    1200    1803    2400    3647    4206    5400    6040    7215    7816];

```

```

expf7=[0    0.001523894 0.003763449 0.004414718 0.005015038 0.005179516
        0.004728428 0.003837582 0.003395319 0.002018983 0.001522739];
%time-dependent concentration of (S)-1 during solvolysis of (R)-1 in the
presence of 70.8 mM
%NaN3
expt17=[0    635    1200  1800  2410  2998  3600  4202  4800  5408  6000  6602
        7203  7800  8416  9000];
expf17=[0    0.005968557 0.007390913 0.006644261 0.00680473  0.006144405
        0.007255091 0.006733987 0.006324292 0.005680997 0.003752172 0.00379139
        0.00293498  0.003421908 0.002043087 0.001768708];
%time dependent concentration of (S)-1 during solvolysis of (S)-2 in the
%presence of 76.6 mM NaN3
expt19=[0    635    1800 2410  2998  3600  4202  4800  5408  6000  6602  7203
        7800  8416  9000];
expf19=[0    0.018458785 0.028908658 0.031106561 0.031326384 0.030622692
        0.029802943 0.026790943 0.025517046 0.022597432 0.019708861
        0.016855133 0.01506295  0.013022412 0.010835302];
%time dependent concentration of (R)-1 during solvolysis of (S)-2 in the
%presence of 76.6 mM NaN3
f1=0;
f2=0;
f3=0;
f4=0;
f5=0;
f6=0;
f7=0;
f17=0;
f18=0;
f19=0;
ssd=0;
%initialization of calculated concentrations and ssd, resetting the initial
value to zero
for a=[1:1:length(k)]
    if k(a)<0;
        ssd=666;
    end
%rate constants can not be negative. setting ssd to extreme high level when
%k<0
end
if ssd==666
else
for b=[1:1:length(expt1)]
    t=expt1(b);
    [f1(b)                f2(b)                f3(b)                f4(b)
f5(b)]=fitex(k1,ks1,km1,kms1,kr,ki,ksr,ksi,k2,ks2,km2,kms2,ksol,t);
    ssd=ssd+(f1(b)-expf1(b))^2;
end
for b=[1:1:length(expt2)]
    t=expt2(b);
    [f1(b)                f2(b)                f3(b)                f4(b)
f5(b)]=fitex(k1,ks1,km1,kms1,kr,ki,ksr,ksi,k2,ks2,km2,kms2,ksol,t);
    ssd=ssd+(f2(b)-expf2(b))^2;
end
for b=[1:1:length(expt3)]
    t=expt3(b);
    [f1(b)                f2(b)                f3(b)                f4(b)
f5(b)]=fitex(k1,ks1,km1,kms1,kr,ki,ksr,ksi,k2,ks2,km2,kms2,ksol,t);
    ssd=ssd+(f3(b)-expf3(b))^2;
end
for b=[1:1:length(expt4)]
    t=expt4(b);
    [f1(b)                f2(b)                f3(b)                f4(b)
f5(b)]=fitex(k1,ks1,km1,kms1,kr,ki,ksr,ksi,k2,ks2,km2,kms2,ksol,t);

```

```

        ssd=ssd+(f4(b)-expf4(b))^2;
end
for b=[1:1:length(expt18)]
    t=expt18(b);
    [f1(b)          f2(b)          f3(b)          f4(b)          s1          s2          s3
f5(b)]=fitex(k1,ks1,km1,kms1,kr,ki,ksr,ksi,k2,ks2,km2*rat4a,kms2*rat4a,kslim2,t);
    ssd=ssd+(f5(b)-expf18(b))^2;
end
%solvolysis of (S)-2 in the presence of azide-anion (76.6 mM)
for b=[1:1:length(expt6)]
    t=expt6(b);
%f6 is f4 for ksol=kslim which should be so in the presence of the
%azide-anion
    [f1(b)          f2(b)          f7(b)          f6(b)
f5(b)]=fitex(k1,ks1,km1,kms1,kr,ki,ksr,ksi,k2,ks2,km2*rat4,kms2*rat4,kslim,t);
    ssd=ssd+(f6(b)-expf6(b))^2;
end
for b=[1:1:length(expt7)]
    t=expt7(b);
%f6 is f2 for ksol=kslim which should be so in the presence of the
%azide-anion
    [f1(b)          f7(b)          f3(b)          f6(b)
f5(b)]=fitex(k1,ks1,km1,kms1,kr,ki,ksr,ksi,k2,ks2,km2*rat4,kms2*rat4,kslim,t);
    ssd=ssd+(f7(b)-expf7(b))^2;
end
for b=[1:1:length(expt17)]
    t=expt17(b);
    [f1(b)          f2(b)          f3(b)          f4(b)          f18(b)          f17(b)
f19(b)]=fitex(k1,ks1,km1,kms1,kr,ki,ksr,ksi,k2,ks2,km2*rat4a,kms2*rat4a,kslim2,t);
    ssd=ssd+(f17(b)-expf17(b))^2;
end
%[(S)-1] during solvolysis of (S)-2 in the presence of 76.6 mM NaN3
for b=[1:1:length(expt19)]
    t=expt19(b);
    [f1(b)          f2(b)          f3(b)          f4(b)          f19(b)          f18(b)
f17(b)]=fitex(k1,ks1,km1,kms1,kr,ki,ksr,ksi,k2,ks2,km2*rat4a,kms2*rat4a,kslim2,t);
    ssd=ssd+(f19(b)-expf19(b))^2;
end
%[(R)-1] during solvolysis of (S)-2 in the presence of 76.6 mM NaN3
end

```

SSD with fixed k_2 and k_r parameters based on steady state approximation (ssd6rssp.m)

```

function ssd=ssd(k,p)
%argument k - set to optimize
%argument p - set of remaining fit parameters
%structure k or p =(k1,ks1,km1,kms1,kr,ki,ksr,ksi,k2,ks2,km2,kms2,ksol)
k1=k(1);
%free
ks1=k(2);
%free
km1=k(3);
%free
kms1=k(4);
%free
kr=p(5);

```

```

%fixed
ki=k(6);
%free
ksr=p(5);
%fixed
ksi=k(6);
%bound
k2=p(9);
%fixed
ks2=p(9);
%fixed
km2=k(11);
%free
kms2=k(11);
%bound
ksol=p(13);
%fixed
kslim=4.45*10^8;
%kNu=ksol+kaz*[N3] in the presence of 70.8 mM NaN3
kslim2=4.81e8;
%kNu=ksol+kaz*[N3] in the presence of 76.6 mM NaN3
rat4=0.0837;
rat4a=0.0823;
%approximate ratio between [-OPNB] in two experiments
%experimental data expt - experimental time, expf - experimental
%time-dependent concentration
expt1=[0 290 593 894 1200 1501 1800 2108 2399 2700 3000 3313
3601 3918 4200 4500 4809 5100 5400 5700 6002 6307 6599 6901
7201 7500 7803 8102 8400 8724];
expf1=[1.0000 0.9287 0.8467 0.7724 0.7028 0.6328
0.5865 0.5310 0.4903 0.4415 0.4073 0.3689
0.3396 0.3040 0.2818 0.2553 0.2357 0.2131
0.1969 0.1794 0.1646 0.1494 0.1389 0.1231
0.1140 0.1052 0.0950 0.0875 0.0821 0.0737];
%decay of [(R)-1] during solvolysis of (R)-1 in the presence of 4.8 mM
%Bu4NOPNB
expt2=[0 290 593 894 1200 1501 1800 2108 2399 2700 3000 3313
3601 3918 4200 4500 4809 5100 5400 5700 6002 6307 6599 6901
7201 7500 7803 8102 8400 8724];
expf2=[0.0000 0.0032 0.0079 0.0118 0.0152 0.0188
0.0196 0.0216 0.0228 0.0239 0.0245 0.0252
0.0251 0.0252 0.0250 0.0246 0.0242 0.0238
0.0232 0.0230 0.0222 0.0212 0.0205 0.0195
0.0188 0.0181 0.0171 0.0162 0.0161 0.0147];
%time-dependent concentration of (S)-1 during solvolysis of (R)-1 in the
presence of 4.8 mM
%Bu4NOPNB
expt3=[0 290 593 894 1200 1800 2108 2399 2700 3000 3313 3601
3918 4200 4500 5400 5700 6002 6307 6599 6901 7201 7500 7803
8102 8400];
expf3=[0.0000 0.0013 0.0079 0.0096 0.0118 0.0155
0.0165 0.0175 0.0187 0.0191 0.0198 0.0195
0.0195 0.0191 0.0184 0.0168 0.0166 0.0159
0.0154 0.0147 0.0146 0.0138 0.0128 0.0119
0.0110 0.0104];
%time-dependent concentration of (R)-2 during solvolysis of (R)-1 in the
presence of 4.8 mM
%Bu4NOPNB
expt4=[0 290 593 894 1200 1800 2399 3000 3601 4200 4500 4809
5100 5400 6599 6901 7201 7500 7803 8102 8724];
expf4=[0.0000 0.0100 0.0176 0.0238 0.0299 0.0343
0.0387 0.0403 0.0399 0.0385 0.0378 0.0361

```

Chapter 4. Ion Pair Dynamics: Solvolyses of Chiral 1,3-Diaryllallyl Carboxylates as a Case Study

```
0.0357    0.0336    0.0283    0.0271    0.0252    0.0237
0.0225    0.0209    0.0181];
%time-dependent concentration of (S)-2 during solvolysis of (R)-1 in the
presence of 4.8 mM
%Bu4NOPNB
expt18=[0   605   1200  1800  2400  3002  3600  4220  4800  5400  6000  6600
        7200  7800  8400  9000];
expf18=[1   0.812108991 0.657633967 0.528438113 0.423385691 0.341137925
        0.275328365 0.220901457 0.178916986 0.143624038 0.116280316
        0.092655727 0.075083996 0.060433001 0.048865865 0.036896571];
%decay of [(S)-2] during solvolysis of (S)-2 in 60% aq acetone in the
%presence of 76.6 mM OPNB
expt6=[0   618   1200  1803  2400  3035  3647  4206  4800  5400  6040  6610
        7215  7816  8405];
expf6=[0   0.010964962 0.018286819 0.021422871 0.023535271 0.023812559
        0.023985867 0.021731369 0.019810788 0.018062054 0.015939271
        0.014169254 0.012272464 0.010278255 0.008731633];
%time-dependent concentration of (S)-2 during solvolysis of (R)-1 in the
presence of 70.8 mM
%NaN3
expt7=[0   618   1200  1803  2400  3647  4206  5400  6040  7215  7816];
expf7=[0   0.001523894 0.003763449 0.004414718 0.005015038 0.005179516
        0.004728428 0.003837582 0.003395319 0.002018983 0.001522739];
%time-dependent concentration of (S)-1 during solvolysis of (R)-1 in the
presence of 70.8 mM
%NaN3
expt17=[0   635   1200  1800  2410  2998  3600  4202  4800  5408  6000  6602
        7203  7800  8416  9000];
expf17=[0   0.005968557 0.007390913 0.006644261 0.00680473 0.006144405
        0.007255091 0.006733987 0.006324292 0.005680997 0.003752172 0.00379139
        0.00293498 0.003421908 0.002043087 0.001768708];
%time dependent concentration of (S)-1 during solvolysis of (S)-2 in the
%presence of 76.6 mM NaN3
expt19=[0   635   1800  2410  2998  3600  4202  4800  5408  6000  6602  7203
        7800  8416  9000];
expf19=[0   0.018458785 0.028908658 0.031106561 0.031326384 0.030622692
        0.029802943 0.026790943 0.025517046 0.022597432 0.019708861
        0.016855133 0.01506295 0.013022412 0.010835302];
%time dependent concentration of (R)-1 during solvolysis of (S)-2 in the
%presence of 76.6 mM NaN3
kms2=km2;
%for explanation the text
f1=0;
f2=0;
f3=0;
f4=0;
f5=0;
f6=0;
f7=0;
f17=0;
f18=0;
f19=0;
ssd=0;
%initialization of ssd, resetting the initial value to zero
for a=[1:1:length(k)]
    if k(a)<0;
        ssd=666;
    end
%rate constants can not be negative. setting ssd to extreme high level when
%k<0
end
if ssd==666
else
```

```

for b=[1:1:length(expt1)]
    t=expt1(b);
    [f1(b) f2(b) f3(b) f4(b)
f5(b)]=fitf(k1,ks1,km1,kms1,kr,ki,ksr,ksi,k2,ks2,km2,kms2,ksol,t);
    ssd=ssd+(f1(b)-expf1(b))^2;
end
for b=[1:1:length(expt2)]
    t=expt2(b);
    [f1(b) f2(b) f3(b) f4(b)
f5(b)]=fitf(k1,ks1,km1,kms1,kr,ki,ksr,ksi,k2,ks2,km2,kms2,ksol,t);
    ssd=ssd+(f2(b)-expf2(b))^2;
end
for b=[1:1:length(expt3)]
    t=expt3(b);
    [f1(b) f2(b) f3(b) f4(b)
f5(b)]=fitf(k1,ks1,km1,kms1,kr,ki,ksr,ksi,k2,ks2,km2,kms2,ksol,t);
    ssd=ssd+(f3(b)-expf3(b))^2;
end
for b=[1:1:length(expt4)]
    t=expt4(b);
    [f1(b) f2(b) f3(b) f4(b)
f5(b)]=fitf(k1,ks1,km1,kms1,kr,ki,ksr,ksi,k2,ks2,km2,kms2,ksol,t);
    ssd=ssd+(f4(b)-expf4(b))^2;
end
for b=[1:1:length(expt18)]
    t=expt18(b);
    [f1(b) f2(b) f3(b) f4(b) s1 s2 s3
f5(b)]=fitf(k1,ks1,km1,kms1,kr,ki,ksr,ksi,k2,ks2,km2*rat4a,kms2*rat4a,kslim,
2,t);
    ssd=ssd+(f5(b)-expf18(b))^2;
end
%solvolysis of (S)-2 in the presence of azide-anion (76.6 mM)
for b=[1:1:length(expt6)]
    t=expt6(b);
    %f6 is f4 for ksol=kslim which should be so in the presence of the
    %azide-anion
    [f1(b) f2(b) f7(b) f6(b)
f5(b)]=fitf(k1,ks1,km1,kms1,kr,ki,ksr,ksi,k2,ks2,km2*rat4,kms2*rat4,kslim,t
);
    ssd=ssd+(f6(b)-expf6(b))^2;
end
for b=[1:1:length(expt7)]
    t=expt7(b);
    %f6 is f2 for ksol=kslim which should be so in the presence of the
    %azide-anion
    [f1(b) f7(b) f3(b) f6(b)
f5(b)]=fitf(k1,ks1,km1,kms1,kr,ki,ksr,ksi,k2,ks2,km2*rat4,kms2*rat4,kslim,t
);
    ssd=ssd+(f7(b)-expf7(b))^2;
end
for b=[1:1:length(expt17)]
    t=expt17(b);
    [f1(b) f2(b) f3(b) f4(b) f18(b) f17(b)
f19(b)]=fitf(k1,ks1,km1,kms1,kr,ki,ksr,ksi,k2,ks2,km2*rat4a,kms2*rat4a,ksli
m2,t);
    ssd=ssd+(f17(b)-expf17(b))^2;
end
%[(S)-1] during solvolysis of (S)-2 in the presence of 76.6 mM NaN3
for b=[1:1:length(expt19)]
    t=expt19(b);
    [f1(b) f2(b) f3(b) f4(b) f19(b) f18(b)
f17(b)]=fitf(k1,ks1,km1,kms1,kr,ki,ksr,ksi,k2,ks2,km2*rat4a,kms2*rat4a,ksli
m2,t);

```

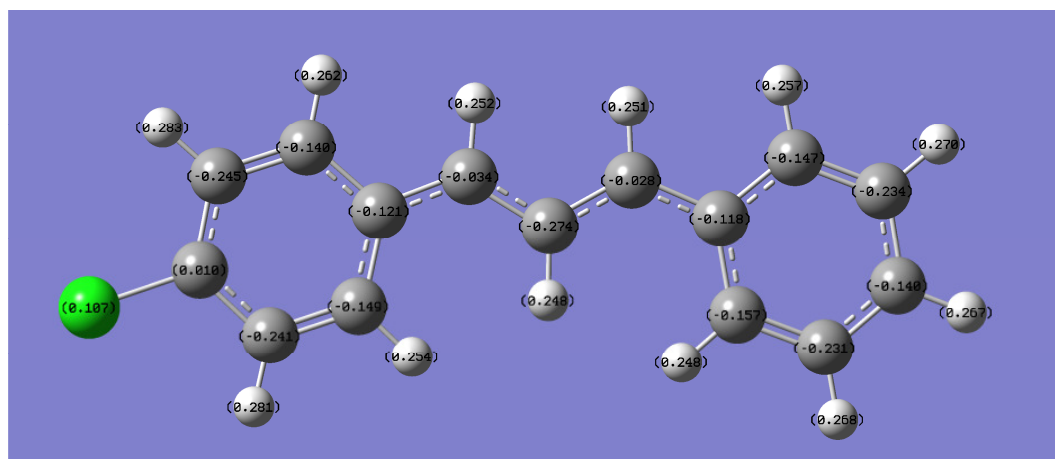


```

    ssd=ssd+(f19(b)-expf19(b))^2;
end
%[(R)-1] during solvolysis of (S)-2 in the presence of 76.6 mM NaN3
end

```

5.8. NPA Calculation for the Cation 6 (B3LYP/6-31G(d,p))

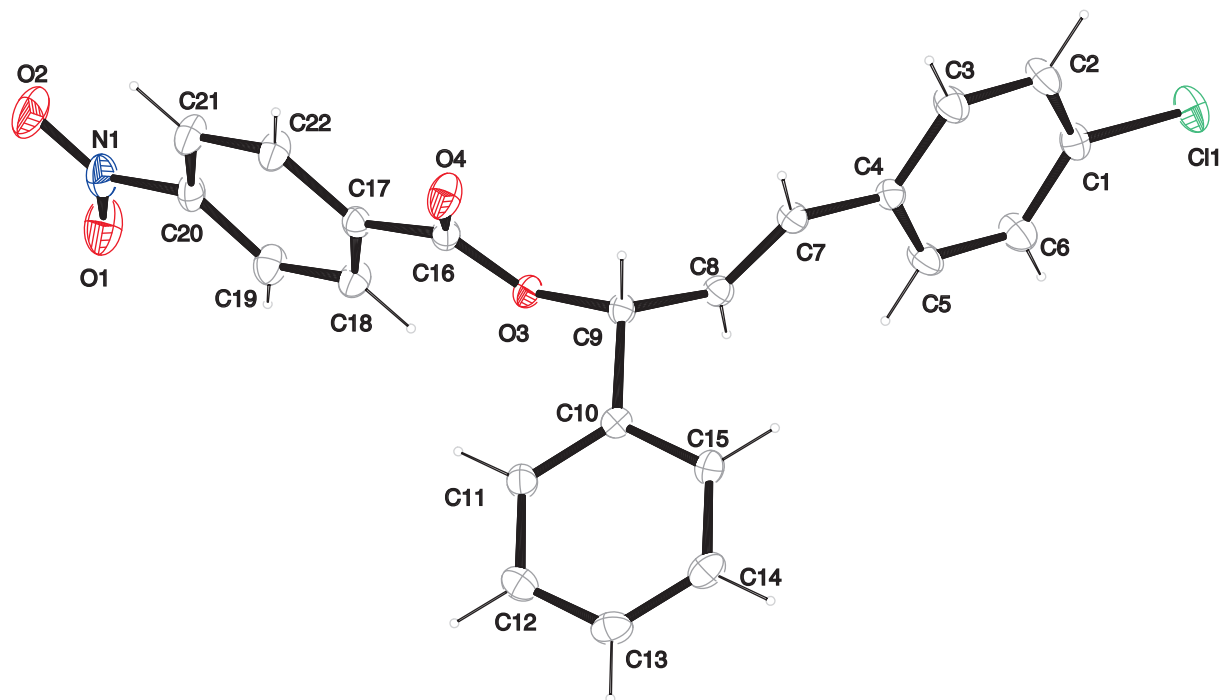


```

1\1\GINC-NODE22\SP\RB3LYP\6-31G(d,p)\C15H12Cl1(1+)\MAY06\23-Mar-2010\
\#P B3LYP/6-31G(d,p) pop=npa geom=check guess=read\H_Cl cation charg
es\1,1\C,0,-0.0054700608,0.,0.0034591621\C,0,0.0047486036,0.,1.407476
557\C,0,1.2072963329,0.,2.091165093\C,0,2.4359276193,0.,1.3768216402\C
,0,2.4014250716,0.,-0.0431653509\C,0,1.1923873576,0.,-0.7206859038\H,0
,1.2052367046,0.,3.1755334767\H,0,3.3363230057,0.,-0.596000017\C,0,3.7
101096742,0.,2.0165533785\H,0,4.5707043379,0.,1.3479915603\C,0,3.98633
27346,0.,3.3791235923\H,0,3.1728321925,0.,4.0962459219\C,0,5.304948752
7,0.,3.82246809\H,0,6.0755343369,0.,3.0521557642\C,0,5.7802903461,0.,5
.164080627\C,0,7.1843519488,0.,5.3815701835\C,0,4.9220721641,0.,6.2976
334873\C,0,7.7121528615,0.,6.6592879622\H,0,7.8545909529,0.,4.52707491
14\C,0,5.4407570348,0.,7.5764316929\H,0,3.8452523015,0.,6.1703872413\C
,0,6.8366957278,0.,7.7557024258\H,0,8.7835108503,0.,6.8221804738\H,0,1
.1740605737,0.,-1.8050768645\H,0,4.7889549009,0.,8.4422958889\H,0,-0.9
317041395,0.,1.9548298803\Cl,0,7.481117462,0.,9.3575918157\H,0,-0.9538
105407,0.,-0.5252793755\Version=AM64L-G03RevD.01\State=1-A'\HF=-1038.
791255\RMSD=1.705e-05\Thermal=0.\Dipole=-0.8338707,0.,-1.8053278\PG=CS
[SG(C15H12Cl1)]\@

```

5.9. Thermal Ellipsoid Plot for (*R*)-1



6. Appendix. Solvolyses of (*R*)-1 and (*S*)-1 in the Presence of Tetrabutylammonium Benzoate

6.1. Discussion

When (*S*)-1⁷⁹ is solvolyzed in 60% aq acetone in the presence of Bu₄NOBz, the yields of the rearranged esters (*R*)-1, (*S*)-2, (*R*)-2 and hydrolysis products ((*R,S*)-3, (*R,S*)-4) decrease following the same pattern as for solvolysis in the presence of other nucleophiles (for details see below). As diaryllallyl benzoates formed by trapping of the intermediates by the ⁻OBz are relatively stable under the reaction conditions, their total yield should be described by eq A1.

$$[\text{ROBz}]_{\infty \text{rel}} = \frac{k_{\text{OBz}}[\text{⁻OBz}]}{k_{\text{OBz}}[\text{⁻OBz}] + k_{\text{solv}}} \quad (\text{A1})$$

According to eq A1, a plot of 1/[ROBz]_{∞rel} vs 1/[⁻OBz] yields $k_{\text{solv}}/k_{\text{OBz}} = 0.0185 \text{ M}$ as the slope of the correlation line (Figure A1).

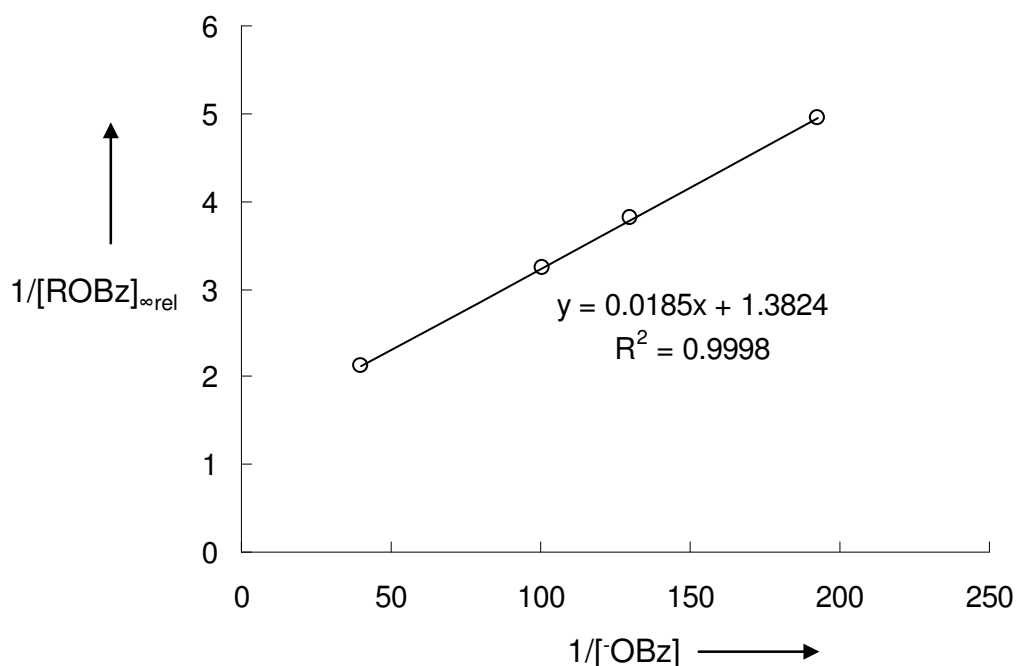


Figure A1. Correlation between 1/[ROBz]_{∞rel} and 1/[⁻OBz] for solvolysis of (*S*)-1 in the presence of various concentrations of Bu₄NOBz in 60% aq acetone at 25 °C.

Substituting $k_{\text{solv}} = 1.34 \times 10^7 \text{ s}^{-1}$ in this ratio yields $k_{\text{OBz}} = 7.24 \times 10^8 \text{ M}^{-1}\text{s}^{-1}$. Comparison of this value with $k_{\text{rec}} = 5.91 \times 10^8 \text{ M}^{-1}\text{s}^{-1}$ and $k_{\text{diff}}^{\text{OPNB}} = 3.6 \times 10^9 \text{ M}^{-1}\text{s}^{-1}$ found for 4-nitrobenzoate anion shows that there is still a relatively high degree of activation control in reaction of **6** with ^-OBz (both anions should have similar diffusional characteristics). A small difference in the reactivities of ^-OBz and $^-\text{OPNB}$ is also expected based on their reactivity parameters.⁸⁰

6.2. Experimental Section

6.2.1 Synthesis of (*E*)-3-(4-chlorophenyl)-1-phenylallyl benzoate

Analogous to **13**. From **3** (513.2 mg, 2.10 mmol), BzCl (310 μL , 424 mg, 2.67 mmol), Et₃N (350 μL , 274 mg, 2.70 mmol), and DMAP (25 mg, 0.20 mmol): 745.2 mg (1.677 mmol, 80%). ¹H NMR (CDCl₃, 300 MHz): δ 6.47 (dd, ³J_{HH} = 16.2, 6.2 Hz, 1 H, ArCHCHCH(OBz)Ph), 6.63 – 6.78 (m, 2 H, ArCHCHCH(OBz)Ph, ArCHCHCH(OBz)Ph), 7.25 - 7.66 (m, 12 H, HAr), 8.11 - 8.24 (m, 2 H, H_{OBz}). ¹³C NMR (CDCl₃, 75 MHz): δ 76.5 (CH), 127.0 (CH), 127.9 (CH), 128.2 (CH), 128.3 (CH), 128.4 (CH), 128.7 (2 \times CH), 129.7 (CH), 130.2 (C), 131.5 (CH), 133.1 (CH), 133.7 (C), 134.7 (C), 139.0 (C), 165.5 ppm (C). HRMS (EI+): calcd 348.0912 (C₂₂H₁₇ClO₂), found 348.0898.

6.2.2 HPLC kinetic measurements

Calibration

As peaks of four stereomeric diarylallyl benzoates can not be completely separated under the conditions used, they were treated as one single broad peak.

Table A1. Calibration data for 1,3-diarylallyl benzoates

[5] / M	[ROBz] / M	[ROBz]/[5]	<i>I</i> ₅	<i>I</i> _{ROBz}	<i>I</i> _{ROBz} / <i>I</i> ₅
3.95×10^{-3}	3.43×10^{-3}	0.870	2284.6	9892.6	4.330
8.38×10^{-3}	2.85×10^{-3}	0.340	1519.1	2249.7	1.481
6.86×10^{-3}	3.71×10^{-3}	0.540	3064.1	7585.8	2.476

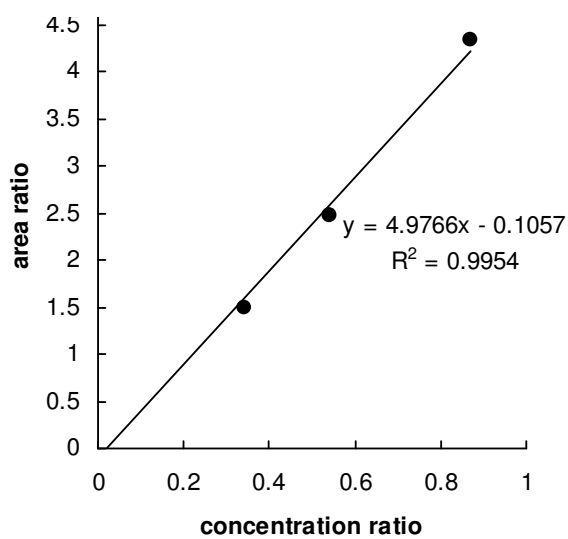


Figure A2. Calibration line for 1,3-diarylallyl benzoates (partially separated peaks of all four stereoisomers are treated as one single broad peak) obtained using the Daicel IB column and the gradient method described above.

Kinetics of the solvolysis reactions

Raw data

Table A2. Time-dependent relative concentrations of **1-4** and diaryllallylbenzoates (in relative units) for solvolysis of (*R*)-**1** ($c_0 = 8.69 \times 10^{-4}$ M) in 60% aq acetone in the presence of 16.2 mM Bu₄NOBz, 25 °C.

<i>t</i> / s	[(<i>R</i>)- 1]	[(<i>S</i>)- 1]	[(<i>R</i>)- 2]	[(<i>S</i>)- 2]	[(<i>R</i>)- 3] ^b	[(<i>S</i>)- 3] ^b	[(<i>R</i>)- 4]	[(<i>S</i>)- 4]	[ROBz] ^a
0	1.1741	0.0000	0.0000	0.0000	0.0000	0.0000	0.0000	0.0000	0.0000
605	1.0108	0.0029	0.0001	0.0173	0.0300	0.0291	0.0130	0.0130	0.0784
1200	0.8213	0.0050	0.0023	0.0244	0.0543	0.0523	0.0279	0.0312	0.1299
1801	0.6637	0.0070	0.0043	0.0288	0.0748	0.0720	0.0423	0.0431	0.1741
2400	0.5641	0.0076	0.0053	0.0309	0.0922	0.0889	0.0543	0.0556	0.2162
3003	0.4472	0.0080	0.0058	0.0320	0.1062	0.1033	0.0647	0.0654	0.2506
3607	0.3679	0.0082	0.0053	0.0311	0.1202	0.1167	0.0738	0.0754	0.2820
4214	0.3098	0.0084	0.0050	0.0309	0.1331	0.1290	0.0831	0.0844	0.3078
4800	0.2553	0.0080	0.0052	0.0288	0.1444	0.1393	0.0901	0.0918	0.3284
5400	0.2110	0.0074	0.0041	0.0262	0.1521	0.1465	0.0954	0.0973	0.3511
5999	0.1792	0.0073	0.0036	0.0254	0.1633	0.1582	0.1040	0.1061	0.3615
6600	0.1458	0.0063	0.0033	0.0216	0.1643	0.1591	0.1047	0.1063	0.3703
7199	0.1200	0.0055	0.0025	0.0187	0.1712	0.1650	0.1090	0.1108	0.3730
7800	0.1015	0.0047	0.0011	0.0169	0.1780	0.1722	0.1141	0.1161	0.3868
8400	0.0840	0.0049	0.0011	0.0158	0.1800	0.1750	0.1158	0.1177	0.4028
9000	0.0650	0.0028	0.0012	0.0095	0.1848	0.1809	0.1205	0.1220	0.3998

^a Sum of the relative concentrations of four stereomeric allylic benzoates.

Table A3. Time-dependent relative concentrations of **1-4** and diaryllallyl benzoates (in relative units) for solvolysis of (S)-**1** ($c_0 = 1.66 \times 10^{-3}$ M) in 60% aq acetone in the presence of 5.2 mM Bu₄NOBz, 25 °C.

<i>t</i> / s	[S]-1]	[R]-1]	[S]-2]	[R]-2]	[S]-3]	[R]-3]	[S]-4]	[R]-4]	[ROBz] ^a
0	1.0236	0.0000	0.0000	0.0000	0.0000	0.0000	0.0000	0.0000	0.0000
1848	0.5739	0.0298	0.0176	0.0369	0.1076	0.1043	0.0770	0.0693	0.0897
2658	0.4238	0.0129	0.0111	0.0349	0.1390	0.1342	0.0947	0.0905	0.1201
3889	0.2992	0.0136	0.0121	0.0370	0.1704	0.1712	0.1173	0.1216	0.1538
5463	0.1839	0.0106	0.0095	0.0269	0.1991	0.2007	0.1404	0.1289	0.1624
7208	0.1089	0.0097	0.0077	0.0223	0.2316	0.2215	0.1450	0.1417	0.1844

^a Sum of the relative concentrations of four stereomeric allylic benzoates.**Table A4.** Time-dependent relative concentrations of **1-4** and diaryllallyl benzoates (in relative units) for solvolysis of (S)-**1** ($c_0 = 1.66 \times 10^{-3}$ M) in 60% aq acetone in the presence of 7.7 mM Bu₄OBz, 25 °C.

<i>t</i> / s	[S]-1]	[R]-1]	[S]-2]	[R]-2]	[S]-3]	[R]-3]	[S]-4]	[R]-4]	[ROBz] ^a
0	1.0236	0.0000	0.0000	0.0000	0.0000	0.0000	0.0000	0.0000	0.0000
1797	0.5515	0.0123	0.0110	0.0420	0.0974	0.0974	0.0596	0.0567	0.1117
2636	0.4030	0.0143	0.0159	0.0453	0.1228	0.1228	0.0728	0.0765	0.1702
3922	0.2610	0.0155	0.0146	0.0432	0.1572	0.1603	0.1052	0.1008	0.1863
5416	0.1662	0.0141	0.0084	0.0238	0.1844	0.1823	0.1168	0.1156	0.2073
7200	0.1149	0.0096	0.0112	0.0259	0.1958	0.1951	0.1262	0.1228	0.2284

^a Sum of the relative concentrations of four stereomeric allylic benzoates.**Table A5.** Time-dependent relative concentrations of **1-4** and diaryllallyl benzoates (in relative units) for solvolysis of (S)-**1** ($c_0 = 1.66 \times 10^{-3}$ M) in 60% aq acetone in the presence of 10.0 mM Bu₄NOBz, 25 °C.

<i>t</i> / s	[S]-1]	[R]-1]	[S]-2]	[R]-2]	[S]-3]	[R]-3]	[S]-4]	[R]-4]	[ROBz] ^a
0	1.0236	0.0000	0.0000	0.0000	0.0000	0.0000	0.0000	0.0000	0.0000
1807	0.5682	0.0092	0.0087	0.0315	0.0862	0.0883	0.0600	0.0534	0.1336
3883	0.3181	0.0097	0.0092	0.0320	0.1509	0.1481	0.0951	0.0928	0.2281
5398	0.1831	0.0096	0.0086	0.0253	0.1722	0.1732	0.1146	0.1038	0.2524
7203	0.1168	0.0067	0.0055	0.0185	0.1817	0.1828	0.1156	0.1189	0.2682

^a Sum of the relative concentrations of four stereomeric allylic benzoates.

Table A6. Time-dependent relative concentrations of **1-4** and diarylallyl benzoates (in relative units) for solvolysis of (*S*)-**1** ($c_0 = 1.66 \times 10^{-3}$ M) in 60% aq acetone in the presence of 24.9 mM Bu₄OBz, 25 °C.

<i>t</i> / s	[<i>S</i>]- 1]	[<i>R</i>]- 1]	[<i>S</i>]- 2]	[<i>R</i>]- 2]	[<i>R</i>]- 3]	[<i>S</i>]- 3]	[<i>R</i>]- 4]	[<i>S</i>]- 4]	[ROBz] ^a
0	1.0236	0.0000	0.0000	0.0000	0.0000	0.0000	0.0000	0.0000	0.0000
1798	0.5588	0.0090	0.0081	0.0326	0.0667	0.0672	0.0413	0.0483	0.1932
2639	0.4373	0.0115	0.0114	0.0362	0.0893	0.0841	0.0547	0.0547	0.2524
3922	0.2850	0.0130	0.0088	0.0342	0.1086	0.1068	0.0675	0.0657	0.3230
7213	0.1049	0.0092	0.0060	0.0204	0.1408	0.1425	0.0909	0.0861	0.4148

^a Sum of the relative concentrations of four stereomeric allylic benzoates.

Normalized time-dependent concentrations

Table A2a. Normalized time-dependent relative concentrations of **1-4** and diarylallylbenzoates (in relative units) for solvolysis of (R)-**1** ($c_0 = 8.69 \times 10^{-4}$ M) in 60% aq acetone in the presence of 16.2 mM Bu₄NOBz, 25 °C.

t/s	[(R)-1]	[(S)-1]	[(R)-2]	[(S)-2]	[(R)-3] ^b	[(S)-3] ^b	[(R)-4]	[(S)-4]	[ROBz] ^a
0	1.0000	0.0000	0.0000	0.0000	0.0000	0.0000	0.0000	0.0000	0.0000
605	0.8461	0.0024	0.0001	0.0145	0.0252	0.0243	0.0108	0.0109	0.0657
1200	0.7151	0.0044	0.0020	0.0212	0.0473	0.0455	0.0243	0.0271	0.1131
1801	0.5979	0.0063	0.0038	0.0259	0.0674	0.0649	0.0381	0.0388	0.1569
2400	0.5059	0.0068	0.0048	0.0277	0.0827	0.0797	0.0487	0.0498	0.1939
3003	0.4128	0.0074	0.0053	0.0295	0.0981	0.0954	0.0597	0.0604	0.2313
3607	0.3404	0.0075	0.0049	0.0288	0.1112	0.1080	0.0683	0.0698	0.2609
4214	0.2839	0.0077	0.0046	0.0283	0.1220	0.1182	0.0761	0.0773	0.2820
4800	0.2339	0.0074	0.0047	0.0264	0.1323	0.1277	0.0826	0.0841	0.3009
5400	0.1933	0.0068	0.0037	0.0240	0.1394	0.1343	0.0875	0.0892	0.3218
5999	0.1616	0.0066	0.0032	0.0229	0.1473	0.1427	0.0938	0.0957	0.3261
6600	0.1348	0.0058	0.0030	0.0200	0.1519	0.1471	0.0968	0.0982	0.3423
7199	0.1116	0.0051	0.0023	0.0173	0.1592	0.1534	0.1013	0.1030	0.3468
7800	0.0930	0.0043	0.0010	0.0155	0.1631	0.1578	0.1045	0.1064	0.3544
8400	0.0765	0.0044	0.0010	0.0144	0.1641	0.1595	0.1055	0.1073	0.3672
9000	0.0598	0.0026	0.0011	0.0087	0.1701	0.1665	0.1109	0.1123	0.3680

^a Sum of the relative concentrations of four stereomeric allylic benzoates.

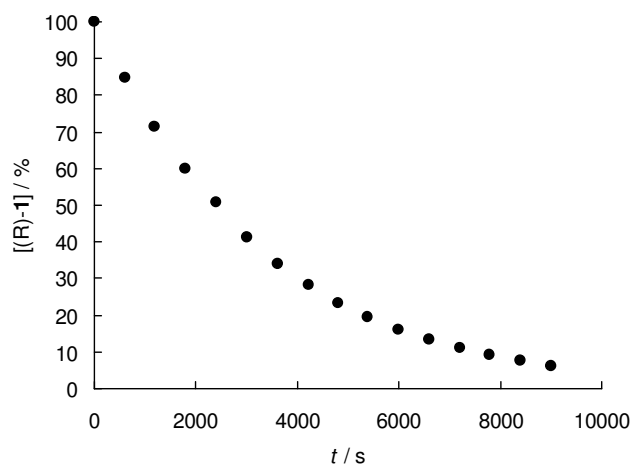


Figure A3. Decay of [(R)-1] ($c_0 = 8.69 \times 10^{-4}$ M) during its solvolysis in 60% aq acetone in the presence of 16.2 mM Bu_4NOBz , 25 °C.

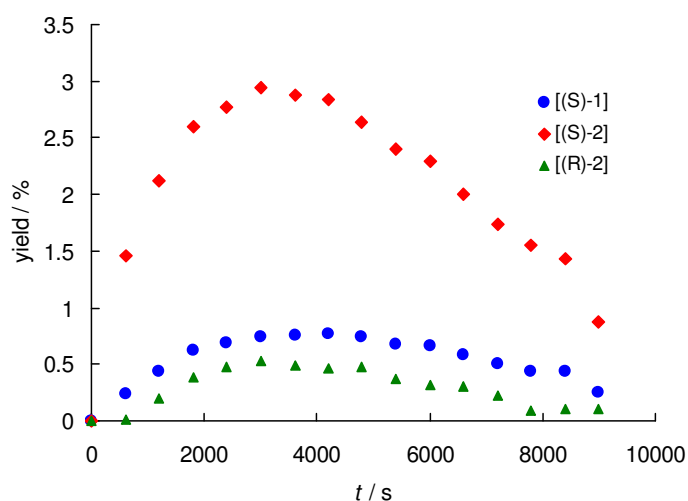


Figure A4. Time-dependent yields of (S)-1, (S)-2 and (R)-2 during solvolysis of (R)-1 ($c_0 = 8.69 \times 10^{-4}$ M) in 60% aqueous acetone in the presence of 16.2 mM Bu_4NOBz , 25 °C.

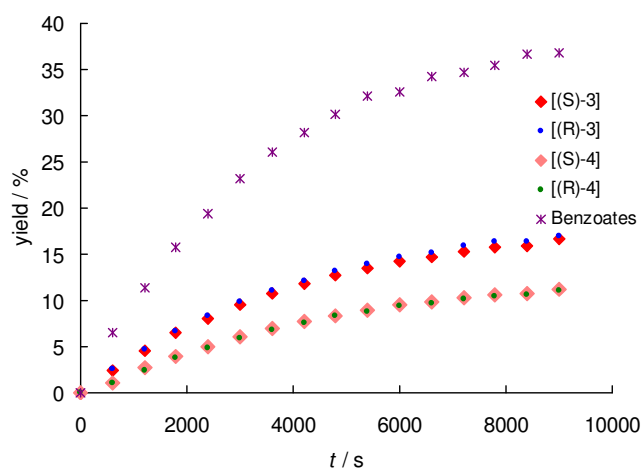


Figure A5. Time-dependent yields of alcohols **3** and **4** and diarylallyl benzoates (ROBz) during solvolysis of (R)-1 ($c_0 = 8.69 \times 10^{-4}$ M) in 60% aq acetone in the presence of 16.2 mM Bu_4NOBz , 25 °C.

Table A3a. Normalized time-dependent relative concentrations of **1-4** and diarylallylbenzoates (in relative units) for solvolysis of (S)-**1** ($c_0 = 1.66 \times 10^{-3}$ M) in 60% aq acetone in the presence of 5.2 mM Bu₄NOBz, 25 °C.

<i>t</i> / s	[S]-1]	[R]-1]	[S]-2]	[R]-2]	[S]-3]	[R]-3]	[S]-4]	[R]-4]	[ROBz] ^a
0	1.0000	0.0000	0.0000	0.0000	0.0000	0.0000	0.0000	0.0000	0.0000
1848	0.5747	0.0298	0.0177	0.0370	0.1077	0.1045	0.0771	0.0694	0.0899
2658	0.4596	0.0139	0.0120	0.0379	0.1507	0.1456	0.1027	0.0981	0.1302
3889	0.3231	0.0147	0.0131	0.0400	0.1840	0.1849	0.1267	0.1313	0.1661
5463	0.2130	0.0122	0.0110	0.0311	0.2306	0.2325	0.1627	0.1493	0.1881
7208	0.1294	0.0115	0.0092	0.0265	0.2753	0.2633	0.1723	0.1684	0.2192

^a Sum of the relative concentrations of four stereomeric allylic benzoates.**Table A4a.** Normalized time-dependent relative concentrations of **1-4** and diarylallylbenzoates (in relative units) for solvolysis of (S)-**1** ($c_0 = 1.66 \times 10^{-3}$ M) in 60% aq acetone in the presence of 7.7 mM Bu₄NOBz, 25 °C.

<i>t</i> / s	[S]-1]	[R]-1]	[S]-2]	[R]-2]	[S]-3]	[R]-3]	[S]-4]	[R]-4]	[ROBz] ^a
0	1.0000	0.0000	0.0000	0.0000	0.0000	0.0000	0.0000	0.0000	0.0000
1797	0.5974	0.0133	0.0119	0.0455	0.1055	0.1004	0.0646	0.0614	0.1210
2636	0.4652	0.0165	0.0184	0.0523	0.1417	0.1338	0.0840	0.0882	0.1964
3922	0.3043	0.0180	0.0170	0.0504	0.1832	0.1869	0.1227	0.1175	0.2171
5416	0.2047	0.0174	0.0104	0.0294	0.2272	0.2246	0.1439	0.1424	0.2554
7200	0.1433	0.0119	0.0139	0.0323	0.2443	0.2435	0.1575	0.1532	0.2850

^a Sum of the relative concentrations of four stereomeric allylic benzoates.**Table A5a.** Normalized time-dependent relative concentrations of **1-4** and diarylallylbenzoates (in relative units) for solvolysis of (S)-**1** ($c_0 = 1.66 \times 10^{-3}$ M) in 60% aq acetone in the presence of 10.0 mM Bu₄NOBz, 25 °C.

<i>t</i> / s	[S]-1]	[R]-1]	[S]-2]	[R]-2]	[S]-3]	[R]-3]	[S]-4]	[R]-4]	[ROBz] ^a
0	1.0000	0.0000	0.0000	0.0000	0.0000	0.0000	0.0000	0.0000	0.0000
1807	0.5468	0.0089	0.0084	0.0303	0.0829	0.0850	0.0577	0.0514	0.1286
3883	0.2935	0.0090	0.0085	0.0295	0.1392	0.1366	0.0878	0.0856	0.2104
5398	0.1756	0.0092	0.0082	0.0243	0.1651	0.1661	0.1099	0.0995	0.2420
7203	0.1151	0.0066	0.0054	0.0182	0.1791	0.1802	0.1140	0.1171	0.2643

^a Sum of the relative concentrations of four stereomeric allylic benzoates.

Table A6a. Normalized time-dependent relative concentrations of **1-4** and diarylallylbenzoates (in relative units) for solvolysis of (S)-**1** ($c_0 = 1.66 \times 10^{-3}$ M) in 60% aq acetone in the presence of 24.9 mM Bu₄NOBz, 25 °C.

<i>t</i> / s	[(S)-1]	[(R)-1]	[(S)-2]	[(R)-2]	[(R)-3]	[(S)-3]	[(R)-4]	[(S)-4]	[ROBz] ^a
0	1.0000	0.0000	0.0000	0.0000	0.0000	0.0000	0.0000	0.0000	0.0000
1798	0.5830	0.0094	0.0084	0.0340	0.0696	0.0701	0.0431	0.0504	0.2016
2639	0.4640	0.0122	0.0121	0.0385	0.0948	0.0892	0.0580	0.0580	0.2679
3922	0.3153	0.0143	0.0098	0.0379	0.1201	0.1181	0.0746	0.0727	0.3573
7213	0.1199	0.0105	0.0069	0.0234	0.1609	0.1629	0.1039	0.0984	0.4742

^a Sum of the relative concentrations of four stereomeric allylic benzoates.

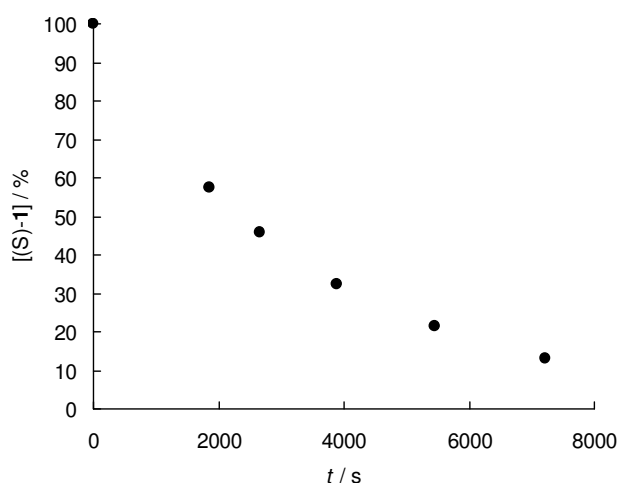


Figure A6. Decay of [(S)-1] ($c_0 = 1.66 \times 10^{-3}$ M) during its solvolysis in 60% aq acetone in the presence of 5.2 mM Bu_4NOBz , 25 °C.

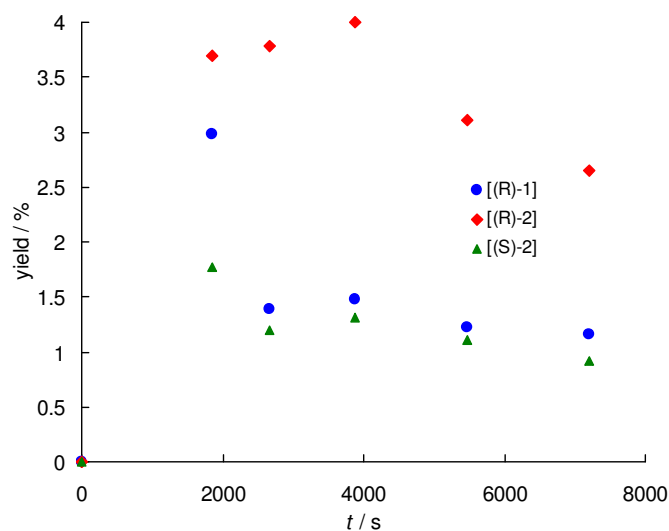


Figure A7. Time-dependent yields of (R)-1, (S)-2 and (R)-2 during solvolysis of (S)-1 ($c_0 = 1.66 \times 10^{-3}$ M) in 60% aqueous acetone in the presence of 5.2 mM Bu_4NOBz , 25 °C.

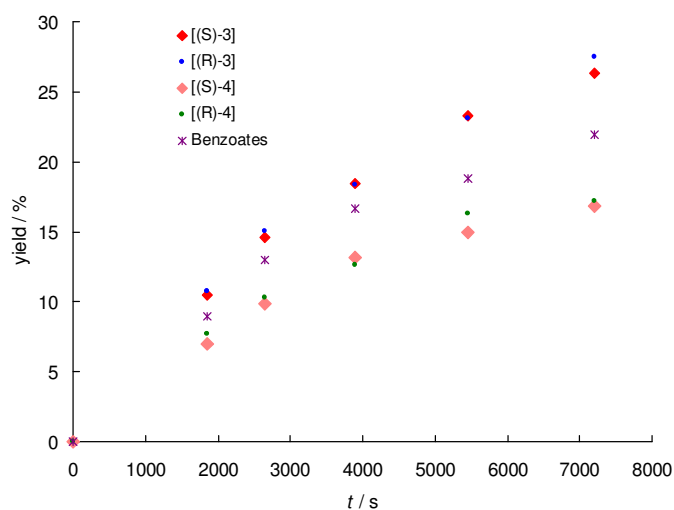


Figure A8. Time-dependent yields of alcohols 3 and 4 and diarylallyl benzoates (ROBz) during solvolysis of (S)-1 ($c_0 = 1.66 \times 10^{-3}$ M) in 60% aq acetone in the presence of 5.2 mM Bu_4NOBz , 25 °C.

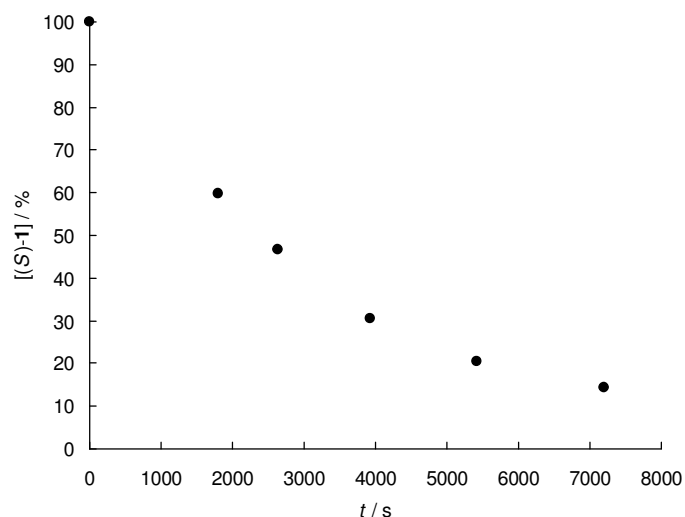


Figure A9. Decay of [(S)-1] ($c_0 = 1.66 \times 10^{-3}$ M) during its solvolysis in 60% aq acetone in the presence of 7.7 mM Bu₄NOBz, 25 °C.

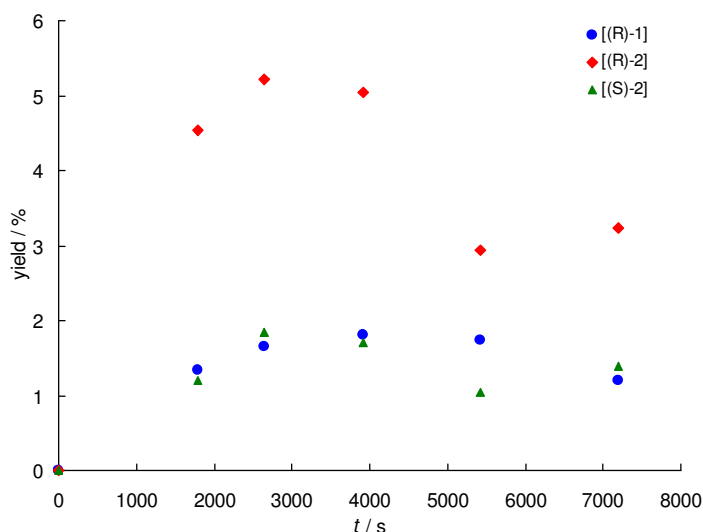


Figure A10. Time-dependent yields of (R)-1, (S)-2 and (R)-2 during solvolysis of (S)-1 ($c_0 = 1.66 \times 10^{-3}$ M) in 60% aqueous acetone in the presence of 7.7 mM Bu₄NOBz, 25 °C.

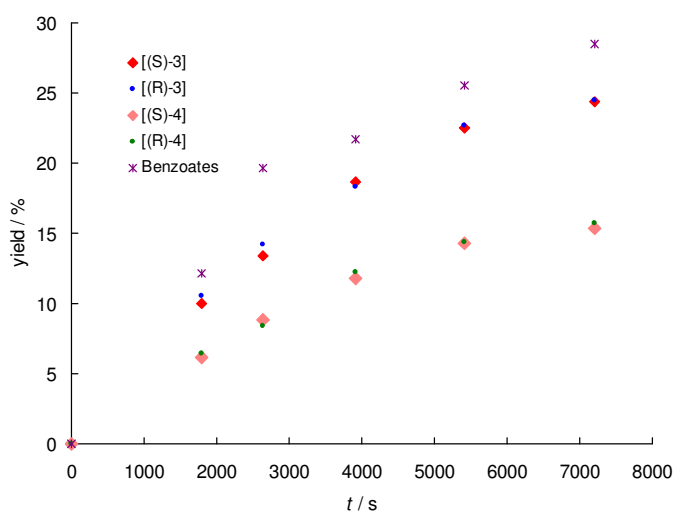


Figure A11. Time-dependent yields of alcohols **3** and **4** and diaryllallyl benzoates (ROBz) during solvolysis of (S)-1 ($c_0 = 1.66 \times 10^{-3}$ M) in 60% aq acetone in the presence of 7.7 mM Bu₄NOBz, 25 °C.

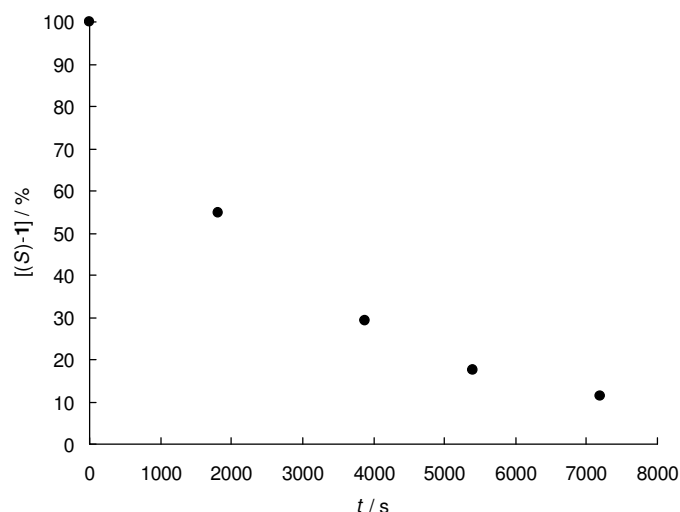


Figure A12. Decay of [(S)-1] ($c_0 = 1.66 \times 10^{-3}$ M) during its solvolysis in 60% aq acetone in the presence of 10.0 mM Bu_4NOBz , 25 °C.

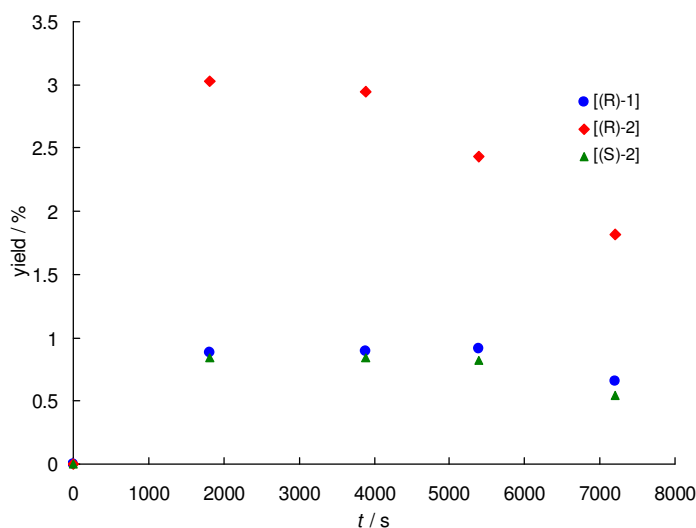


Figure A13. Time-dependent yields of (R)-1, (S)-2 and (R)-2 during solvolysis of (S)-1 ($c_0 = 1.66 \times 10^{-3}$ M) in 60% aqueous acetone in the presence of 10.0 mM Bu_4NOBz , 25 °C.

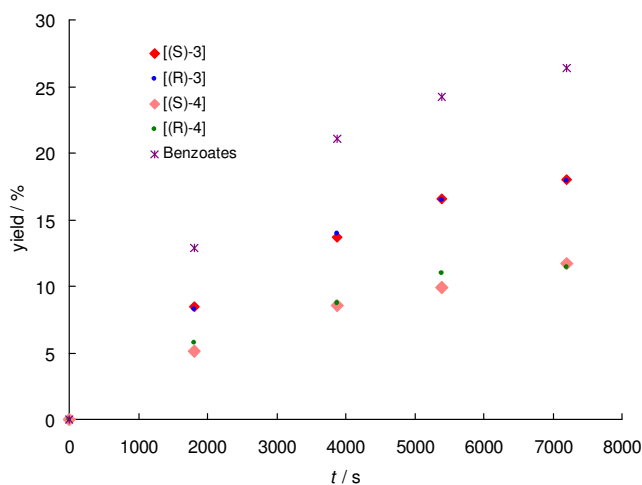


Figure A14. Time-dependent yields of alcohols **3** and **4** and diarylallyl benzoates (ROBz) during solvolysis of (S)-1 ($c_0 = 1.66 \times 10^{-3}$ M) in 60% aq acetone in the presence of 10.0 mM Bu_4NOBz , 25 °C.

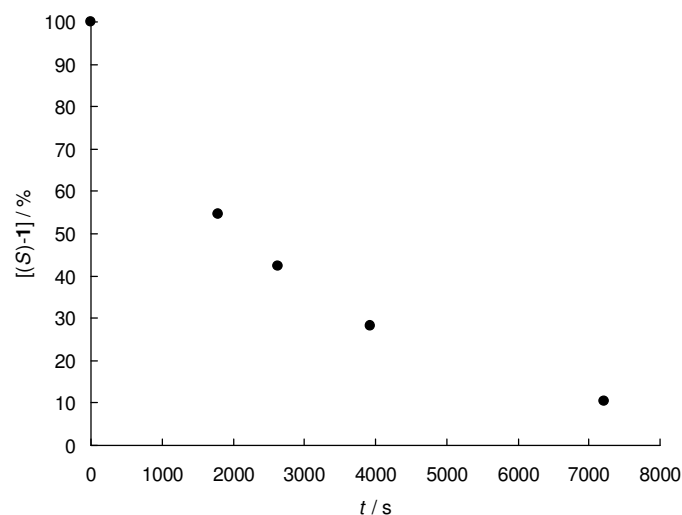


Figure A15. Decay of [(S)-1] ($c_0 = 1.66 \times 10^{-3}$ M) during its solvolysis in 60% aq acetone in the presence of 24.9 mM Bu₄NOBz, 25 °C.

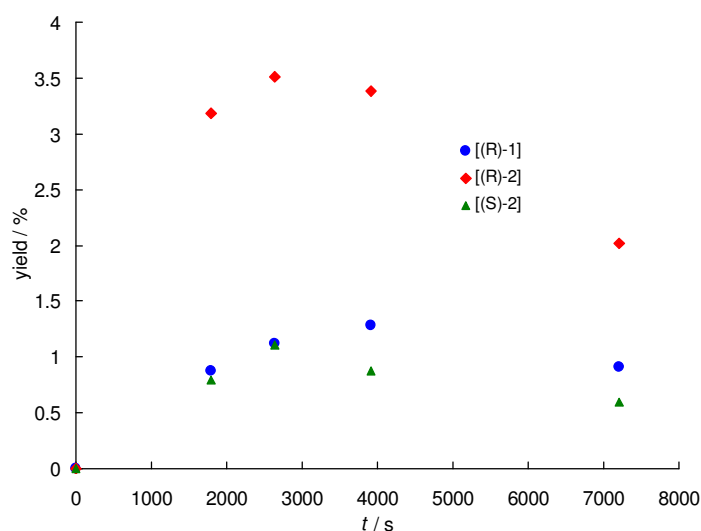


Figure A16. Time-dependent yields of (R)-1, (S)-2 and (R)-2 during solvolysis of (S)-1 ($c_0 = 1.66 \times 10^{-3}$ M) in 60% aqueous acetone in the presence of 24.9 mM Bu₄NOBz, 25 °C.

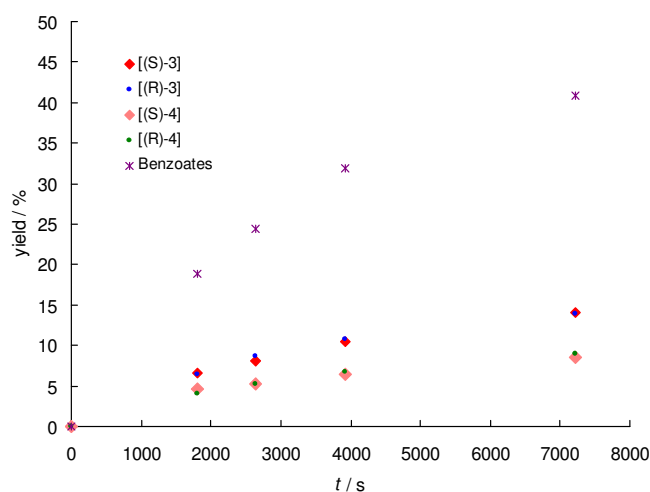


Figure A17. Time-dependent yields of alcohols **3** and **4** and diarylallyl benzoates (ROBz) during solvolysis of (S)-1 ($c_0 = 1.66 \times 10^{-3}$ M) in 60% aq acetone in the presence of 24.9 mM Bu₄NOBz, 25 °C.

7. References

- (1) Kotke, M.; Schreiner, P. R. (Thio)urea organocatalysts. In *Hydrogen Bonding in Organic Synthesis*; Pihko, P. M., Ed.; Wiley, Weinheim, 2009.
- (2) Phipps, R. J.; Hamilton, G. L.; Toste, F. D. *Nat. Chem.* **2012**, *4*, 603–614.
- (3) Dolling, U.-H.; Davis, P.; Grabowski, E. J. J. *J. Am. Chem. Soc.* **1984**, *106*, 446–447.
- (4) (a) Ooi, T.; Maruoka, K. *Angew. Chem., Int. Ed.* **2007**, *46*, 4222–4266. (b) *Asymmetric Phase Transfer Catalysis*; Maruoka, K., Ed.; Wiley, Weinheim, 2008.
- (5) For reviews on use of chiral Brønsted acids see for instance: (a) Akiyama, T. *Chem Rev.* **2007**, *107*, 5744–5758. (b) Rueping, M.; Nachtsheim, B. J.; Ieawsuwan, W.; Atodiresei, I. *Angew. Chem., Int. Ed.*, **2011**, *50*, 6706–6720.
- (6) (a) Nakashima, D.; Yamamoto, H. *J. Am. Chem. Soc.* **2006**, *128*, 9626–9627. (b) Jiao, P.; Nakashima, D.; Yamamoto, H. *Angew. Chem., Int. Ed.* **2008**, *47*, 2411–2413.
- (7) (a) Rueping, M.; Ieawsuwan, W.; Antonchick, A. P.; Nachtsheim, B. J. *Angew. Chem., Int. Ed.* **2007**, *46*, 2097–2100. (b) Müller, S.; List, B. *Angew. Chem., Int. Ed.* **2009**, *48*, 9975–9978.
- (8) Rueping, M.; Nachtsheim, B. J.; Moreth, S. A.; Bolte, M. *Angew. Chem., Int. Ed.* **2008**, *47*, 593–596.
- (9) Rueping, M.; Uria, U.; Lin, M.-Y.; Atodiresei, I. *J. Am. Chem. Soc.* **2011**, *133*, 3732–3735.
- (10) Hoffmann, S.; Seayad, A. M.; List, B. *Angew. Chem., Int. Ed.* **2005**, *44*, 7424–7427.
- (11) Rueping, M.; Theissmann, T.; Kuenkel, A.; Koenigs, R. M. *Angew. Chem., Int. Ed.* **2008**, *47*, 6798–6801.
- (12) Fleischmann, M.; Drettwan, D.; Sugiono, E.; Rueping, M.; Gschwind, R. M. *Angew. Chem., Int. Ed.* **2011**, *50*, 6364–6369.
- (13) (a) Ratjen, L.; Müller, S.; List, B. *Nachr. Chem.* **2010**, *58*, 640–646. (b) Mahlau, M.; List, B. *Isr. J. Chem.* **2012**, *52*, 630–638.
- (14) See, for instance: (a) Mayer, S.; List, B. *Angew. Chem., Int. Ed.* **2006**, *45*, 4193–4195. (b) Martin, N. J. A.; List, B. *J. Am. Chem. Soc.* **2006**, *128*, 13368–13369 (c) Wang, X.; List, B. *Angew. Chem., Int. Ed.* **2008**, *47*, 1119–1122.
- (15) (a) Llewellyn, D. B.; Adamson, D.; Arndtsen, B. A. *Org. Lett.* **2000**, *2*, 4165–4168. (b) Hamilton, G. L.; Kang, E. J.; Mba, M.; Toste, F. D. *Science* **2007**, *317*, 496–499. (c) LaLonde, R. L.; Wang, Z. J.; Mba, M.; Lackner, A. D.; Toste, F. D. *Angew. Chem., Int. Ed.* **2010**, *49*, 598–601. (d) Rauniyar, V.; Wang, Z. J.; Burks, H. E.; Toste, F. D. *J. Am. Chem.*

- Soc.* **2011**, *133*, 8486–8489. (e) Liao, S.; List, B. *Angew. Chem., Int. Ed.* **2010**, *49*, 628–631. It should be noted that in some cases the chiral phosphate may act as ligand and not as counterion for the cationic metal complex. Examples of transformations, where phosphate ions were shown to act as ligands are, for instance: (f) Mukherjee, S.; List, B. *J. Am. Chem. Soc.* **2007**, *129*, 11336–11337. (g) Jiang, G; Halder, R; Fang, Y.; List, B. *Angew. Chem., Int. Ed.* **2011**, *50*, 9752–9755.
- (16) Ohmatsu, K.; Ito, M.; Kunieda, K.; Ooi, T. *Nat. Chem.* **2012**, *4*, 473–477.
- (17) Maccioni, A. *Chem. Rev.* **2005**, *105*, 2039–2074, and references therein.
- (18) (a) Raheem, I. T.; Thiara, P. S.; Peterson, E. A.; Jacobsen, E. N. *J. Am. Chem. Soc.* **2007**, *129*, 13404–13405. (b) Knowles, R. R.; Lin, S.; Jacobsen, E. N. *J. Am. Chem. Soc.* **2010**, *132*, 5030–5032. (c) Brown, A. R.; Kuo, W-H.; Jacobsen, E. N. *J. Am. Chem. Soc.* **2010**, *132*, 9286–9288.
- (19) Xu, H.; Zuend, S. J.; Woll, M. G.; Tao, Y.; Jacobsen, E. N. *Science* **2010**, *327*, 986–990.
- (20) Uraguchi, D; Ueki, Y; Ooi, T. *Science* **2009**, *326*, 120–123.
- (21) (a) Young, W. G.; Winstein, S.; Goering, H. L. *J. Am. Chem. Soc.* **1951**, *73*, 1958–1963. (b) Winstein, S.; Schreiber, K. C. *J. Am. Chem. Soc.* **1952**, *74*, 2165–2170. (c) Winstein, S.; Schreiber, K. C. *J. Am. Chem. Soc.* **1952**, *74*, 2171–2178.
- (22) Raber, D. J.; Harris, J. M.; Schleyer, P. v. R. In *Ions and Ion Pairs in Organic Reactions Vol. 2*; Szwarc, M., Ed.; Wiley: New York, 1974.
- (23) (a) De La Mare, P. B. D.; Vernon, C. A. *J. Chem. Soc.* **1954**, 2504–2510 (b) Sneen, R. A. *J. Am. Chem. Soc.* **1960**, *82*, 4261–4269. (c) Jia, Z. S.; Ottosson, H.; Zeng, X.; Thibblin, A. *J. Org. Chem.* **2002**, *67*, 182–187.
- (24) Smith, M. B.; March, J. *March's Advanced Organic Chemistry*; Wiley, New Jersey, 2007, p 470.
- (25) Goering, H. L., Blanchard, J. P.; Silversmith, E. F. *J. Am. Chem. Soc.* **1954**, *76*, 5409–5418.
- (26) Goering, H. L.; Silversmith, E. F. *J. Am. Chem. Soc.* **1955**, *77*, 1129–1133.
- (27) (a) Goering, H. L.; Silversmith, E. F. *J. Am. Chem. Soc.* **1955**, *77*, 6249–6253. (b) Goering, H. L.; Takahashi Doi, J. *J. Am. Chem. Soc.* **1960**, *82*, 5850–5854.
- (28) Goering, H. L.; Nevitt, T. D.; Silversmith, E. F. *J. Am. Chem. Soc.* **1955**, *77*, 5026–5032.
- (29) (a) Goering, H. L.; Koermer, G. S.; Linsay, E. C. *J. Am. Chem. Soc.* **1971**, *93*, 1230–1234. (b) The importance of conformational factors for 5-methylcyclohex-2-enyl system is demonstrated in: Goering, H. L.; Josephson, R. R. *J. Am. Chem. Soc.* **1962**, *84*, 2779–2785.
- (30) Winstein, S.; Klinedinst Jr., P. E.; Robinson, G. C. *J. Am. Chem. Soc.* **1961**, *83*, 885–895.

- (31) Peters, K. S. *Chem. Rev.* **2007**, *107*, 859–873, and references therein.
- (32) Yabe, T.; Kochi, J. K. *J. Am. Chem. Soc.* **1992**, *114*, 4491–4500.
- (33) (a) Hammett, L. P. *Physical Organic Chemistry*, 2nd ed.; McGraw-Hill: New York, 1970. (b) Bentley, T. W.; Schleyer, P. v. R. *Adv. Phys. Org. Chem.* **1977**, *14*, 1–67.
- (34) Richard, J. P.; Jencks, W. P. *J. Am. Chem. Soc.* **1984**, *106*, 1383–1396.
- (35) Richard, J. P.; Jencks, W. P. *J. Am. Chem. Soc.* **1984**, *106*, 1373–1383.
- (36) (a) Tsuji, Y.; Mori, T.; Richard, J. P.; Amyes, T. L.; Fujio, M.; Tsuno, Y. *Org. Lett.* **2001**, *3*, 1237–1240. (b) Teshima, M.; Tsuji, Y.; Richard, J. P. *J. Phys. Org. Chem.* **2010**, *23*, 730–734.
- (37) Schaller, H. F.; Tishkov, A. A.; Feng, X.; Mayr, H. *J. Am. Chem. Soc.* **2008**, *130*, 3012–3022.
- (38) Minegishi, S.; Kobayashi, S.; Mayr, H. *J. Am. Chem. Soc.* **2004**, *126*, 5174–5181.
- (39) For a review on carbocation-nucleophile combination reactions see: Mayr, H.; Ofial, A. R. *J. Phys. Org. Chem.* **2008**, *21*, 584–595.
- (40) For review on solvolysis reactions see: Streidl, N.; Denegri, B.; Kronja, O.; Mayr, H. *Acc. Chem. Res.* **2010**, *43*, 1537–1549.
- (41) (a) Mayr, H.; Ofial, A. R. *Pure Appl. Chem.* **2009**, *81*, 667–683. (b) Horn, M.; Mayr, H. *J. Phys. Org. Chem.* **2012**, *25*, 979–988.
- (42) Ammer, J.; Sailer, C. F.; Riedle, E.; Mayr, H. *J. Am. Chem. Soc.* **2012**, *134*, 11481–11494.
- (43) Ammer, J.; Nolte, C.; Mayr, H. *J. Am. Chem. Soc.* **2012**, *134*, 13902–13911.
- (44) Troshin, K.; Schindele, C.; Mayr, H. *J. Org. Chem.* **2011**, *76*, 9391–9408 (Chapter 3).
- (45) (a) Roos, G. H. P.; Donovan, R. A. *Synlett* **1996**, 1189–1190. (b) Johnson, R.; Sharpless, K. B. In *Catalytic Asymmetric Synthesis*, 2nd ed.; Ojima, I, Ed.; Wiley: New York, 2000, pp 231–280.
- (46) Easton, A. M.; Habib, M. J. A.; Park, J.; Watts, W. E. *J. Chem. Soc., Perkin Trans. 2* **1972**, 2290–2297.
- (47) (a) Grunwald, E.; Winstein, S. *J. Am. Chem. Soc.* **1948**, *70*, 846–854. (b) Bentley, T. W.; Carter, G. E. *J. Am. Chem. Soc.* **1982**, *104*, 5741–5747. (c) Kevill, D. N.; D’Souza, M. J. *J. Chem. Res.* **2008**, 61–66.
- (48) Åkerlöf, G. *J. Am. Chem. Soc.* **1932**, *54*, 4125–4139.
- (49) The half reaction times were calculated as $t_{1/2} = (\ln 2)/k$ where k is the pseudo-first-order rate constant obtained by fitting $[(R)\text{-1}]_t$ to the monoexponential function $\ln [(R)\text{-2}]_t = -kt + \text{const}$. In the case of 90% aq acetone, only first 40 h of the reaction were evaluated

because re-isomerization of **2** which is formed during the reaction causes upward drifts in the $\ln[(R)-\mathbf{1}]_t$ vs. t plot (see Experimental Section for details).

(50) As discussed in detail below, equation 11 predicts a second-order rate constant of $1.5 \times 10^9 \text{ M}^{-1} \text{ s}^{-1}$ for the reaction of cation **6** with piperidine ($N = 18.44$, $s_N = 0.44$ for piperidine in water and $E = 2.70$ for **6**). An up-to-date database of reactivity parameters E , N , and s_N can be found at www.cup.lmu.de/oc/mayr/DBintro.html.

(51) Whereas 1,6-dibenzyl-1,2,3,4,5,6-hexahydro-1,3a,6,8-tetraazaphenalene was found to be the most universal photoleaving group among a series of variously substituted aminopyridines (Nigst, T. A.; Ammer, J.; Mayr, H. *J. Phys. Chem. A* **2012**, *116*, 8494–8499), its non-benzylated analogon can also be used as well in the present case, as the Lewis acidity of cation **6** is high enough to form stable pyridinium salts with both pyridines.

(52) Goering and Winstein differentiate between *external return*, i.e., the reaction between an added common anion and the free or paired carbocation, which results in the isotope exchange between the substrate and ^{14}C labeled 4-nitrobenzoic acid, and *external ion pair return*, i.e., recombination of the solvent-separated ion pair, which can be suppressed by the addition of strong nucleophiles but does not result in the exchange with isotope-labeled 4-nitrobenzoic acid. As the participation of the SSIPs does not play a significant role in the present case, effects related to *external ion pair return* will be neglected.

(53) Dvorko, G. F.; Ponomareva, E. A. *Russ. J. Gen. Chem.* **2010**, *80*, 1615–1625, and references therein.

(54) Kantner, S. S.; Humski, K.; Goering, H. L. *J. Am. Chem. Soc.* **1982**, *104*, 1693–1697.

(55) Thibblin, A. *J. Chem. Soc., Perkin. Trans. 2* **1987**, 1629–1632.

(56) Tsuji, Y.; Richard, J. P. *Chem. Rec.* **2005**, *5*, 94–106.

(57) The detailed description of the evaluation procedure can be found on pages 175–211.

(58) McClelland, R. A.; Kanagasabapathy, V. M.; Banait, N. S.; Steenken, S. *J. Am. Chem. Soc.* **1989**, *111*, 3966–3972.

(59) Denegri, B.; Minegishi, S.; Kronja, O.; Mayr, H. *Angew. Chem., Int. Ed.* **2004**, *43*, 2302–2305.

(60) Mayr, H.; Bug, T.; Gotta, M. F.; Hering, N.; Irrgang, B.; Janker, B.; Kempf, B.; Loos, R.; Ofial, A. R.; Remennikov, G.; Schimmel, H. *J. Am. Chem. Soc.* **2001**, *123*, 9500–9512.

(61) Atkins, P.; de Paula, J. *Atkins' Physical Chemistry*, 9th ed.; Oxford University Press: Oxford, 2010, p 840.

(62) More decimals of k_{-1}/k_2 and k'_{-1}/k_2 than given in Scheme 5 were used.

(63) While we do not have quantitative evidence for this assumption, picosecond dynamics of laser flash photolytically generated carbenium ions provide qualitative confirmation of it, as the ratio of rates of geminate recombination (corresponding to k_{-1}) and diffusional separation (corresponding to k_2) of photolytically generated ion pairs was reported to increase with increasing reactivity of the carbocation in the ion pair (see refs 32 and 42).

(64) Sailer, C.; Ammer, J.; Riedle, E.; Mayr, H.; unpublished results.

(65) It should be noted that p_{ER} reflects the probability that a free carbenium ion **10** is captured by ^-OPNB and not by the solvent. The probability that CIP generated by ionization of **10**-OPNB gives rise to a rearranged product via external return (e.g., (*S*)-**10**-OPNB from (*R*)-**10**-OPNB) is given by $0.5(1 - p_{IR}/100\%)p_{ER}$. This expression subtracts the fraction of CIPs consumed by internal return and multiplies with 0.5 to account for the fact that in the case of symmetrical allyl cations 50% of external return regenerates the starting material. As p_{IR} and p_{ER} do not correspond to competing processes, the sum of these terms can also be greater than 100%.

(66) Minegishi, S.; Loos, R.; Kobayashi, S.; Mayr, H. *J. Am. Chem. Soc.* **2005**, *127*, 2641–2649.

(67) Goering, H. L.; Pombo, M. M.; McMichael, K. D. *J. Am. Chem. Soc.* **1963**, *85*, 965–970.

(68) De Rycke, N.; Berionni, G.; Couty, F.; Mayr, H.; Goumont, R.; David, O. R. P. *Org. Lett.* **2011**, *13*, 530–533.

(69) Manolov, I.; Danchev, N. D. *Arch. Pharm.* **2003**, *336*, 83–94.

(70) Arai, N.; Azuma, K.; Nii, N.; Ohkuma, T. *Angew. Chem., Int. Ed.* **2008**, *47*, 7457–7460.

(71) The preparation of a solution of tBuOOH in CH_2Cl_2 is described in Gao, Y.; Hanson, R.M.; Klunder, J.M.; Ko, S.Y.; Masamune, H., Sharpless; K.B. *J. Am. Chem. Soc.* **1987**, *109*, 5765–5780.

(72) Roos, G. H. P.; Donovan, A. R. *Synlett* **1996**, 1189–1190.

(73) Troshin, K.; Mayr, H.; Mayer, P. *Acta Crystallogr., Sect. E: Struct. Rep. Online* **2012**, *68*, o2549, p 212.

(74) Wu, H.-F.; Neumann, H.; Spannenberg, A.; Schulz, T.; Jiao, H.; Beller, M. *J. Am. Chem. Soc.* **2010**, *132*, 14596–14602.

(75) Hayashi, T.; Yamamoto, A.; Yoshihiko, I.; Nishioka, E.; Miura, H.; Yanagi, K. *J. Am. Chem. Soc.* **1989**, *111*, 6301–6311.

(76) Using $K_a = 3.89 \times 10^{-4}$ M for 4-nitrobenzoic acid ($pK_a = 3.41$, see Albert, A.; Serjeant, E. P: *Ionization Constants of Acids and Bases*; Wiley: New York, 1962) the additional amount of ^-OPNB , which should be produced by dissociation of 0.8 mM of 4-nitrobenzoic present

in the system at the very end of the solvolysis, can be calculated to be 5.96×10^{-5} M, which is only 1.2% of the initial $[\text{OPNB}] = 4.8$ mM.

(77) The search for general solutions of the systems of linear ordinary differential equations is widely described in the mathematical literature and textbooks. For instance, see: Arens, T.; Hettlich, F.; Karpfinger, C.; Kockelkorn, U.; Lichtenegger, K.; Stachel, H. *Mathematik*, Spektrum Akademischer Verlag: Heidelberg, 2008–2009.

(78) *Matlab*, The MathWorks, Inc., Version 6.5.0.180913a, Release 13, 2002.

(79) The experiments in the presence of Bu_4NOBz have been performed at a different time and could as well have been done with (*R*)-**1** as most of the other experiments.

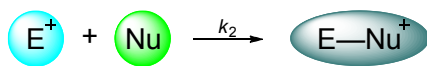
(80) The seemingly big difference between *N* values of OBz^- and OPNB^- in acetonitrile which can be found in ref 37 is almost completely compensated by higher s_{N} value of OPNB^- if cations of high reactivity are considered.

Chapter 5. Electrofugalities of Symmetrical 1,3-Diarylallyl Cations

1. Introduction

In recent work we have demonstrated that the rates of the reactions between electrophiles and nucleophiles as well as the rates of the reverse reactions, i.e., heterolyses of the covalent substrates,¹ correlate well with predictions based on the three-parameter linear free energy relationships (1) and (2), respectively.

Electrophile-nucleophile combinations



$$\log k_2 = s_N(N + E) \quad (1)$$

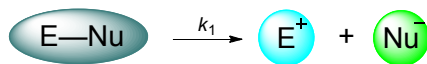
k_2 : second-order rate constant/ $M^{-1}s^{-1}$

s_N : solvent-dependent nucleophile-specific sensitivity parameter

N : solvent-dependent nucleophilicity parameter

E : electrophilicity parameter

Heterolysis reactions



$$\log k_1 = s_f(N_f + E_f) \quad (2)$$

k_1 : first-order rate constant/ s^{-1}

s_f : solvent-dependent nucleofuge-specific sensitivity parameter

N_f : solvent-dependent nucleofugality parameter

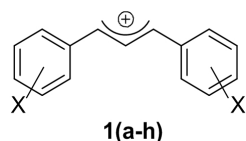
E_f : electrofugality parameter

A series of variously substituted benzhydrylium ions was chosen as reference electrophiles and electrofuges for the construction of comprehensive nucleophilicity and electrophilicity² as well as nucleofugality and electrofugality³ scales.

Due to the occurrence of allylic rearrangements, solvolyses of allyl derivatives were of particular importance for the development of the mechanistic understanding of aliphatic nucleophilic substitutions.⁴ Pioneering studies by Goering brought new insights into structure and reactivities of ion pairs;⁵ however, the mechanistic investigations were limited by the analytical methods available at the time of this research. In a previous study we used the capability of modern HPLC to clarify the ion-pair dynamics during the solvolyses of unsymmetrical 1,3-diarylallyl derivatives and showed how eq 1 can be used to predict the extent of external and internal return during the solvolysis.⁶ We also demonstrated that the

rates of the reactions of 1,3-diarylallyl cations **1(a-h)** with manifold of π - and n -nucleophiles in various solvents can be described by eq 1 and determined the E parameters of 1,3-diarylallyl cations⁷ (Table 1). We now studied the solvolysis rates of various derivatives of cations **1(a-h)** in order to determine their electrofugality parameters E_f according to eq 2. We will subsequently compare the electrofugalities E_f with the corresponding electrophilicity parameters E in order to elucidate general relationships between electrophilicities and electrofugalities.

Table 1. 1,3-Diarylallyl Cations **1(a-h)** and their Electrophilicity Parameters E .⁷

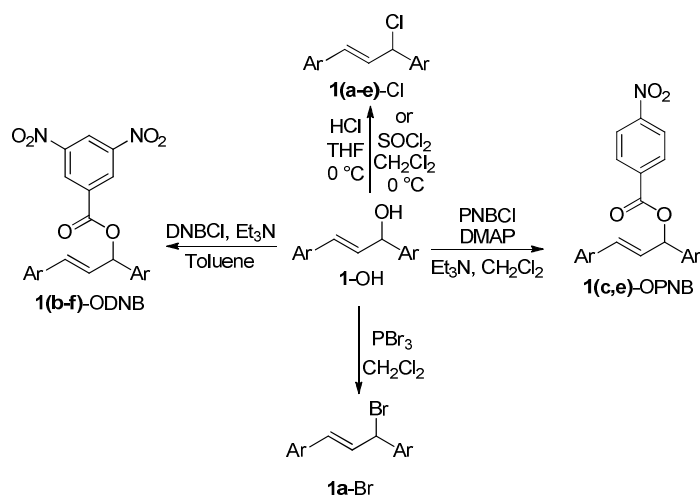


	X	E
1a	<i>m,m</i> -F ₂	6.11
1b	<i>m</i> -F	4.15
1c	<i>p</i> -Br	2.85
1d	<i>p</i> -Cl	2.69
1e	H	2.70
1f	<i>p</i> -Me	1.23
1g	<i>p</i> -OMe	-1.45
1h	<i>p</i> -NMe ₂	-7.50

2. Results and Discussion

2.1 Synthesis of the Substrates

The (*E*)-1,3-diarylallyl chlorides **1(a-e)**-Cl, the bromide **1a**-Br, the 4-nitrobenzoates **1(c,e)**-OPNB, and the 3,5-dinitrobenzoates **1(b-f)**-ODNB were synthesized from the corresponding alcohols (obtained as described in ref 7) by using standard procedures (Scheme 1).

Scheme 1. Syntheses of the Substrates **1(a-f)**-LG.^a

^a Abbreviations used are: DNB = 3,5-dinitrobenzoyl, PNB = 4-nitrobenzoyl, DMAP = 4-dimethylaminopyridine.

The highly reactive (*E*)-1,3-diarylallyl acetates and benzoates **1(g-h)**-OAc and **1(g-h)**-OBz were generated *in situ* by mixing the corresponding (*E*)-1,3-diarylallylium tetrafluoroborates (**1(g-h)**-BF₄) with an excess of the tetrabutylammonium carboxylates until colorless solutions were obtained.

2.2 Kinetic Experiments

As the bis(dimethylamino)-substituted cation **1h** formed by solvolysis of **1h**-OAc or **1h**-OBz in aqueous acetone or acetonitrile is stable under the reaction conditions, the solvolyses of these substrates were followed spectrophotometrically at 704 nm (absorption maximum of **1h**). All other reactions were followed conductimetrically using conventional ($k_1 < 0.15 \text{ s}^{-1}$) or stopped-flow techniques. Because of the direct proportionality between conductivity and concentration of the acid or salt (in the presence of amine additives) produced during the solvolysis (Figure 1 and Figure S2, p 259), the rate constants k_{obs} were obtained by fitting the time-dependent conductivity (κ_t) to the monoexponential function (3).

$$\kappa_t = \kappa_{\infty}(1 - e^{-k_{\text{obs}}t}) + C \quad (3)$$

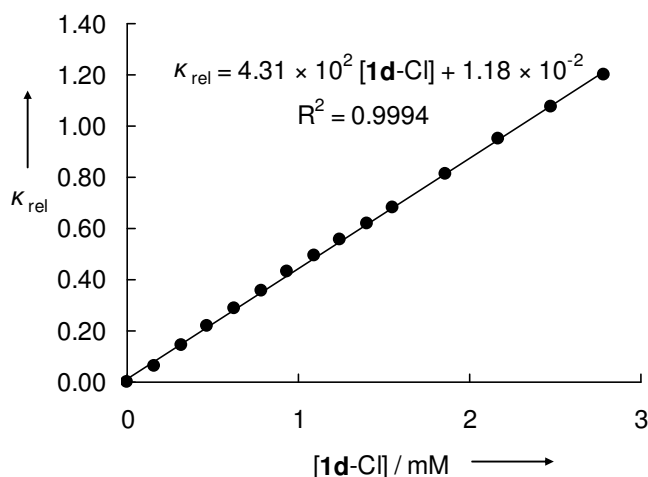
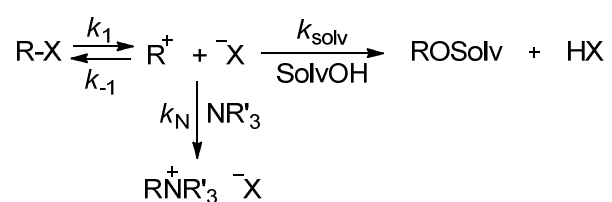


Figure 1. Linear dependence of the relative conductivity κ_{rel} on the concentration of HCl (generated by solvolysis of **1d-Cl** in 60% aq acetone (60A40W)), 25 °C.

As the carboxylic acids produced during solvolyses of diarylallyl carboxylates are only partially dissociated in aqueous acetone and acetonitrile solutions, solvolyses of such substrates were performed in the presence of amines or pyridines to ensure complete dissociation of the generated acids which resulted in a linear dependence of κ on the acid concentration.

In many cases, common ion rate depression (i.e., the recombination of the carbocation with the anion of the leaving group, k_{-1} , Scheme 2) was observed. This led to kinetics (Figure 2a) which did not follow a monoexponential function.

Scheme 2. Simplified Solvolysis Scheme.



The addition of strong neutral nucleophiles (amines, pyridines, phosphines) was shown to suppress the common ion rate depression in benzhydryl halide solvolyses, as these nucleophiles rapidly trap the carbenium ions without attacking the precursor substrates in an $\text{S}_{\text{N}}2$ mode.⁸ In order to confirm that the measured solvolysis rate constants reflect the rates of the heterolysis step, several measurements with increasing concentrations of amines were performed. Although kinetics in the presence of small concentrations of amines or in their

absence did not always follow a monoexponential function, estimates of k_{obs} were derived from the best fit of the experimental curve to the exponential function (eq 3) as depicted in Figure 2a.

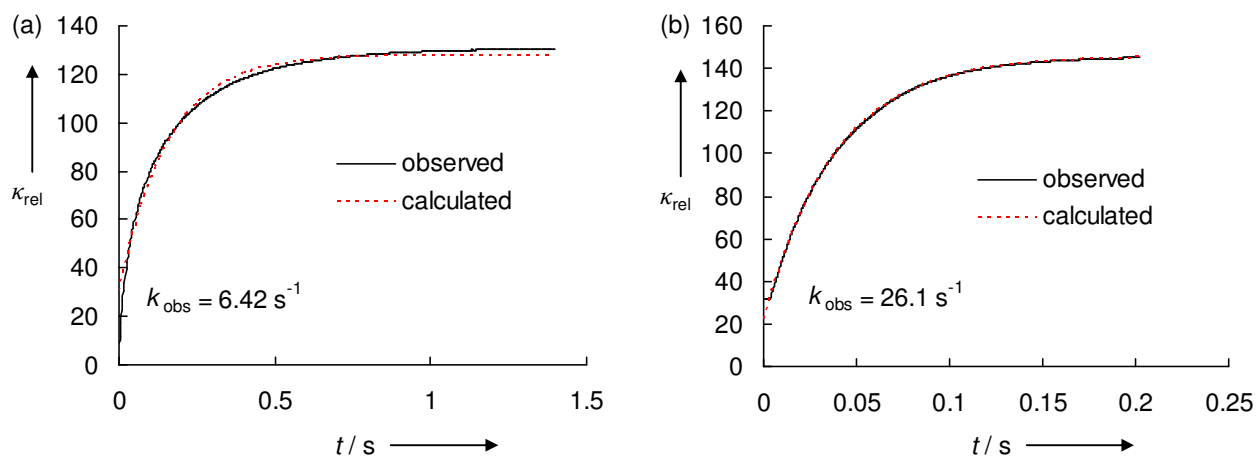


Figure 2. Increase of conductivity during solvolyses of 1,3-diphenylallyl chloride (**1e-Cl**) in 90% aq acetonitrile (90AN10W) at 25 °C (a) in the absence of added nucleophiles and (b) in the presence of 0.30 M 4-(N,N-dimethylamino)pyridine (DMAP).

The quality of the monoexponential fits improved with increasing concentration of amines (Figure 2b) and the values of k_{obs} reached a plateau after an initial increase (Figure 3). The non-linearity of the k_{obs} vs [Nu] plots excludes the operation of $S_{\text{N}}2$ or $S_{\text{N}}2'$ mechanisms, and the plateaus correspond to the concentrations, where the common ion rate depression is completely suppressed because the carbocations generated during the heterolysis step are completely trapped by the solvent or amines before they can recombine with the leaving group. The values of k_{obs} at the plateaus, therefore, correspond to the heterolysis rate constants k_1 . The slight dependence of the heights of the plateaus on the nature of the added nucleophiles,^{8,9} is negligible for the determination of the E_{f} values considering the logarithmic character of eq 2.

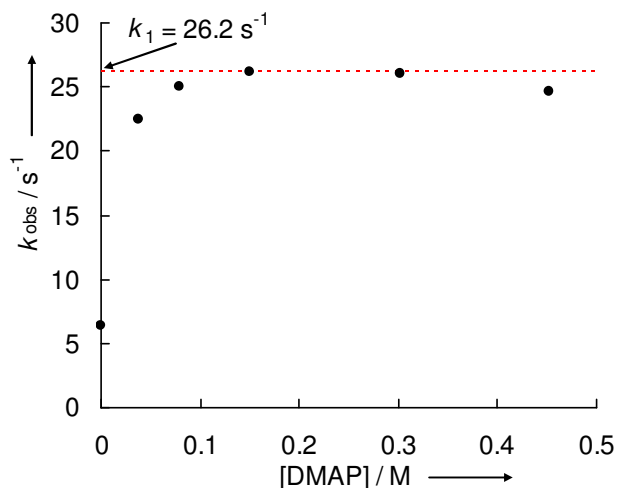


Figure 3. Observed rate constants k_{obs} for the heterolysis of **1e**-Cl at variable concentrations of 4-(N,N-dimethylamino)pyridine (DMAP) in 90% aq acetonitrile (90AN10W) at 25 °C.

The dependence of the common ion return on carbocation electrophilicities and water content in the solvent for the solvolyses of 1,3-diarylallyl chlorides **1(a–e)**-Cl in aq acetonitrile is analogous to that found for solvolyses of benzhydryl⁸ and trityl⁹ derivatives and can be rationalized on the basis of eq 1. The second-order rate constants for the reactions of Cl^- in 60% aq acetonitrile ($N = 12.00$, $s_N = 0.60$)¹⁰ with **1(c–e)** can be calculated (eq 1) to be in the range of $(6.5 - 8.1) \times 10^8 \text{ M}^{-1}\text{s}^{-1}$ and to reach the diffusion limit ($\approx 5 \times 10^9 \text{ M}^{-1}\text{s}^{-1}$) for the reactions with **1(a,b)**. At a substrate concentration of 10^{-2} M , typical for stopped-flow experiments, one would expect the effective recombination rate constants $k_{-1}[\text{Cl}^-]$ at 50% conversion ($[\text{Cl}^-] = 5 \times 10^{-3} \text{ M}$) to be approximately $(3.3 - 4.1) \times 10^6 \text{ s}^{-1}$ for **1(c–e)** and ca. $2.5 \times 10^7 \text{ s}^{-1}$ for **1(a,b)**. These values are comparable with the calculated first-order rate constants for the reactions of **1(c–e)** with water in 60% aq acetonitrile ($N = 5.05$, $s_N = 0.89$)¹¹ $k_{\text{solv}} = (7.7 - 11) \times 10^6 \text{ s}^{-1}$, resulting in common ion rate depression. On the other hand, the diffusionally limited rate constants for the reactions of **1(a,b)** with Cl^- ($5 \times 10^{-3} \text{ M}$) are significantly lower than $k_{\text{solv}}(\mathbf{1a}) = 8.6 \times 10^9 \text{ s}^{-1}$ and $k_{\text{solv}}(\mathbf{1b}) = 1.5 \times 10^8 \text{ s}^{-1}$, resulting in the absence of common ion rate depression in the solvolysis of **1(a,b)**-Cl. Lowering the water concentration in the solvent will increase the nucleophilicity of the leaving group anion (N value of Cl^- is 13.30 in 80% aqueous acetonitrile) and slightly decrease of k_{solv} (for 90% aq acetonitrile, $N = 4.56$, $s_N = 0.94$). Both factors result in increasing common ion rate depression with increasing organic solvent content. The same argumentation is also true for aqueous acetone.

As the typical substrate concentrations used for investigations of solvolyses of **1(c-g)**-OCOR with conventional conductimetry were at least 10 times lower than those used to follow the solvolyses of **1(c-e)**-Cl with stopped-flow techniques, and the nucleophilicities of the carboxylate anions are generally lower than those of the halide anions,^{2e} the extent of common ion return observed for solvolyses of **1(c-g)**-OCOR was much smaller than that for **1(c-e)**-Cl.

By multiplication of the second order rate constant $k_2 = 10^3 \text{ M}^{-1}\text{s}^{-1}$ calculated for the reaction of the bis(dimethylamino)-substituted cation **1h** with acetate anion in 80 % aq acetone using eq 1 ($E = -7.50$, $N = 12.50$, $s_N = 0.60$) with 10^{-3} M (the upper limit of $[\text{Bu}_4\text{NOAc}]$ used in solvolyses of **1h**-OAc), one obtains a first-order recombination rate constant $k_{\text{eff}} = 1 \text{ s}^{-1}$ which is much smaller than the heterolysis rate constants $k_1 \geq 78 \text{ s}^{-1}$ for **1h**-OAc in aqueous acetone and acetonitrile (Table 2). Therefore, the concentration of Bu_4NOAc , which was mixed with **1h**- BF_4 in order to generate **1h**-OAc subsequently subjected to the heterolysis in aqueous solvents, does not have an effect on the observed heterolysis rate constants listed in Table 2. The same is true for heterolyses of **1h**-OBz.

Table 2. Heterolysis Rate Constants k_1 of (*E*)-1,3-Diarylallyl Halides and Carboxylates (at 25 °C).

electrofuge	E_f^a	nucleofuge	solvent ^b	N_f	s_f	k_1 / s^{-1}	k_{calc}^c	k_1/k_{calc}
1a ($X = m,m\text{-F}_2$)	-5.07	Cl^-	90A10W	1.14	1.11	8.95×10^{-5}	4.34×10^{-5}	2.06
		Cl^-	80A20W	2.03	1.05	7.44×10^{-4}	6.43×10^{-4}	1.16
		Cl^-	60A40W	3.30	0.97	1.95×10^{-2}	1.92×10^{-2}	1.02
		Cl^-	90AN10W	2.23	1.08	8.37×10^{-4}	8.57×10^{-4}	0.98
		Cl^-	80AN20W	2.96	1.00	6.86×10^{-3}	7.76×10^{-3}	0.88
		Cl^-	60AN40W	3.84	0.96	6.32×10^{-2}	6.59×10^{-2}	0.96
		Br^-	90A10W	2.29	1.01	1.35×10^{-3}	1.56×10^{-3}	0.87
		Br^-	80A20W	3.01	0.90	1.03×10^{-2}	1.40×10^{-2}	0.74
		Br^-	60A40W	<i>d</i>	<i>d</i>	1.95×10^{-1}	-	-
		Br^-	90AN10W	<i>d</i>	<i>d</i>	1.26×10^{-2}	-	-
		Br^-	80AN20W	<i>d</i>	<i>d</i>	8.83×10^{-2}	-	-
		Br^-	60AN40W	5.23	0.99	5.54×10^{-1}	1.44	0.38
		Br^-	100E	2.93	0.93	1.81×10^{-2}	1.02×10^{-2}	1.77
1b ($X = m\text{-F}$)	-2.70	ODNB^e	80A20W	-2.34	1.10	1.05×10^{-5}	2.86×10^{-6}	3.67
		ODNB	60A40W	-2.20	0.90	7.31×10^{-5}	3.89×10^{-5}	1.88
		ODNB	60AN40W	-2.06	0.97	1.03×10^{-4}	2.41×10^{-5}	4.27

Table 2. Continued.

electrofuge	E_f^a	nucleofuge	solvent ^b	N_f	s_f	k_1 / s^{-1}	k_{calc}^c	k_1/k_{calc}
		Cl ⁻	90A10W	1.14	1.11	6.38×10^{-3}	1.86×10^{-2}	0.34
		Cl ⁻	80A20W	2.03	1.05	9.96×10^{-2}	1.98×10^{-1}	0.50
		Cl ⁻	60A40W	3.30	0.97	2.91	3.82	0.76
		Cl ⁻	90AN10W	2.23	1.08	1.29×10^{-1}	3.11×10^{-1}	0.41
		Cl ⁻	60AN40W	3.84	0.96	8.97	1.24×10^1	0.72
1c (X = <i>p</i> -Br)	-1.37	⁻ OPNB ^f	60A40W	-2.79	1.11	7.76×10^{-5}	2.41×10^{-5}	3.22
		⁻ OPNB	80AN20W	-3.41	0.98	2.77×10^{-5}	2.07×10^{-5}	1.34
		⁻ OPNB	60AN40W	-3.30	0.91	1.18×10^{-4}	5.63×10^{-5}	2.10
		⁻ ODNB	90A10W	-2.68	1.13	2.68×10^{-5}	2.65×10^{-5}	1.01
		⁻ ODNB	60A40W	-2.20	0.90	1.08×10^{-3}	6.12×10^{-4}	1.76
		Cl	90A10W	1.14	1.11	3.01×10^{-1}	5.56×10^{-1}	0.54
		Cl	80A20W	2.03	1.05	3.04	4.93	0.62
		Cl	60A40W	3.30	0.97	4.92×10^1	7.45×10^1	0.66
		Cl	90AN10W	2.23	1.08	4.47	8.49	0.53
		Cl	80AN20W	2.96	1.00	2.40×10^1	3.89×10^1	0.62
1d (X = <i>p</i> -Cl)	-1.23	⁻ ODNB	80A20W	-2.34	1.10	2.30×10^{-4}	1.18×10^{-4}	1.95
		⁻ ODNB	60A40W	-2.20	0.90	1.79×10^{-3}	8.18×10^{-4}	2.19
		⁻ ODNB	60AN40W	-2.06	0.97	1.75×10^{-3}	6.44×10^{-4}	2.72
		Cl	90A10W	1.14	1.11	4.10×10^{-1}	7.95×10^{-1}	0.52
		Cl	80A20W	2.03	1.05	4.34	6.92	0.63
		Cl	90AN10W	2.23	1.08	6.01	1.20×10^1	0.50
		Cl	80AN20W	2.96	1.00	3.34×10^1	5.37×10^1	0.62
1e (X = H)	-0.46	⁻ OPNB	80A20W	-3.40	1.16	6.40×10^{-5}	3.33×10^{-5}	1.92
		⁻ OPNB	60A40W	-2.79	1.11	6.59×10^{-4}	2.47×10^{-4}	2.67
		⁻ OPNB	60AN40W	-3.30	0.91	7.86×10^{-4}	3.79×10^{-4}	2.07
		⁻ ODNB	80A20W	-2.34	1.10	1.06×10^{-3}	8.32×10^{-4}	1.27
		⁻ ODNB	60A40W	-2.20	0.90	6.87×10^{-3}	4.04×10^{-3}	1.70
		⁻ ODNB	90AN10W	<i>d</i>	<i>d</i>	8.61×10^{-4}	-	-
		⁻ ODNB	80AN20W	<i>d</i>	<i>d</i>	2.54×10^{-3}	-	-
		⁻ ODNB	60AN40W	-2.06	0.97	7.36×10^{-3}	3.59×10^{-3}	2.05
		Cl	90A10W	1.14	1.11	1.93	5.69	0.34
		Cl	80A20W	2.03	1.05	1.96×10^1	4.45×10^1	0.44
		Cl	90AN10W	2.23	1.08	2.62×10^1	8.16×10^1	0.32
		Cl	80AN20W	2.96	1.00	1.66×10^2	3.16×10^2	0.53

Table 2. Continued.

electrofuge	E_f^a	nucleofuge	solvent ^b	N_f	s_f	k_1 / s^{-1}	k_{calc}^c	k_1/k_{calc}
1f (X = <i>p</i> -Me)	1.18	⁻ OPNB	80A20W	-3.40	1.16	1.74×10^{-3}	2.66×10^{-3}	0.65
		⁻ OPNB	60A40W	-2.79	1.11	2.04×10^{-2}	1.63×10^{-2}	1.25
		⁻ OPNB	90AN10W	<i>d</i>	<i>d</i>	2.16×10^{-3}	-	-
		⁻ OPNB	80AN20W	-3.41	0.98	6.75×10^{-3}	6.53×10^{-3}	1.03
		⁻ OPNB	60AN40W	-3.30	0.91	2.19×10^{-2}	1.18×10^{-2}	1.86
		⁻ ODNB	90A10W	-2.68	1.13	1.26×10^{-2}	2.02×10^{-2}	0.62
		⁻ ODNB	80A20W	-2.34	1.10	4.30×10^{-2}	5.30×10^{-2}	0.81
		⁻ ODNB	60A40W	-2.20	0.90	1.42×10^{-1}	1.21×10^{-1}	1.17
		⁻ ODNB	90AN10W	<i>d</i>	<i>d</i>	3.51×10^{-2}	-	-
		⁻ ODNB	80AN20W	<i>d</i>	<i>d</i>	8.21×10^{-2}	-	-
		⁻ ODNB	60AN40W	-2.06	0.97	1.92×10^{-1}	1.40×10^{-1}	1.37
1g (X = <i>p</i> -OMe)	2.87	⁻ OAc	80A20W	-4.73	1.18	5.15×10^{-3}	6.39×10^{-3}	0.81
		⁻ OAc	80AN20W	-4.52	1.11	1.22×10^{-2}	1.47×10^{-2}	0.83
		⁻ OAc	60AN40W	-4.18	1.08	6.90×10^{-2}	3.85×10^{-2}	1.79
		⁻ OBz	80A20W	-4.46	1.17	1.32×10^{-2}	1.38×10^{-2}	0.95
		⁻ OBz	80AN20W	-4.19	1.12	2.97×10^{-2}	3.32×10^{-2}	0.89
1h (X = <i>p</i> -NMe ₂)	6.39	⁻ OAc	80A20W	-4.73	1.18	7.85×10^1	9.09×10^1	0.86
		⁻ OAc	60A40W	-4.05	1.17	4.21×10^{2g}	5.47×10^2	0.77
		⁻ OAc	80AN20W	-4.52	1.11	1.48×10^2	1.19×10^2	1.24
		⁻ OAc	60AN40W	-4.18	1.08	2.81×10^2	2.44×10^2	1.15
		⁻ OBz	80A20W	-4.46	1.17	1.57×10^2	1.81×10^2	0.87
		⁻ OBz	60AN40W	-3.92	1.02	3.31×10^2	3.31×10^2	1.00

^a The E_f parameters for **1(a–h)** result from the least-squares minimization of $\Delta^2 = \Sigma(\log k_1 - s_f(N_f + E_f))^2$ which uses the heterolysis rate constants k_1 (this table) and the N_f and s_f parameters of the nucleofuges given in ref 3 and listed in this Table. ^b All solvent compositions are given in vol-%, A = acetone, AN = acetonitrile, E = ethanol, W = water. ^c The values of k_{calc} were obtained using eq 2 and E_f , s_f , and N_f parameters listed in this table. ^d The values of s_f and N_f are not available. ^e ⁻ODNB = 3,5-Dinitrobenzoate. ^f ⁻OPNB = 4-Nitrobenzoate. ^g This rate constant was not included in the correlation since the heterolysis is too fast to derive a reliable value of k_1 .

2.3. Winstein-Grunwald Analysis

The values of $\log k_1$ for the solvolyses of **1-Cl** in various solvents correlate well with the corresponding solvent ionizing powers Y_{Benzyl}^{12} (Figure 4). The m values derived from the correlation lines are slightly smaller than those calculated for solvolyses of benzhydryl

chlorides of similar reactivity in aqueous acetone and acetonitrile ($m = 0.96$ for diphenylmethyl chloride ($E_f = -6.03$), $m = 0.93$ for bis(*p*-tolyl)methyl chloride, ($E_f = -3.44$)).¹³

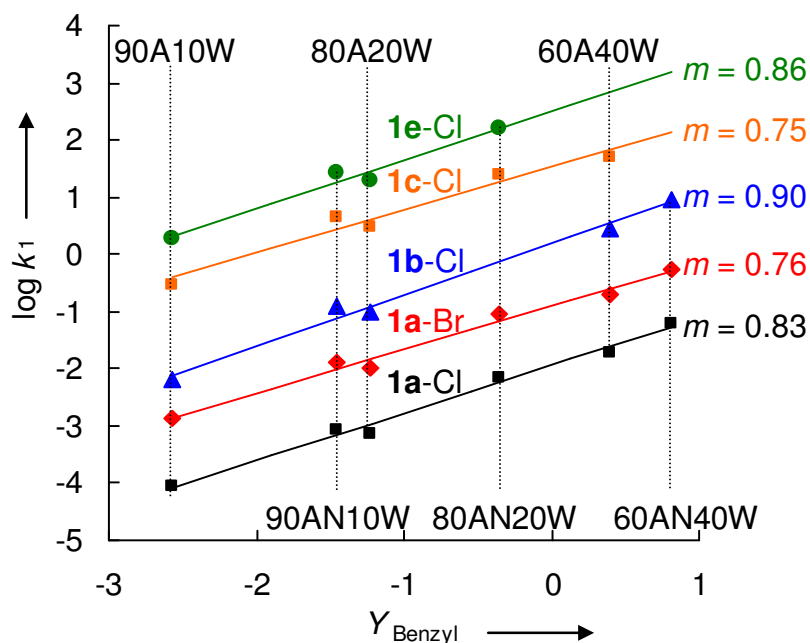


Figure 4. Correlation between the solvolysis rate constants of **1**-Hal in acetone/water and acetonitrile/water mixtures (from Table 2) and the corresponding Y_{Benzyl} values.^{12d} The line for **1d**-Cl ($m = 0.85$) is not shown to avoid overlap.

Increasing cation stability (ca 3 orders of magnitude in electrophilicity) does not change the m -values significantly, and their magnitudes indicate a high carbocation character in the transition states. This conclusion can also be reached by consideration of the rate constants of the reactions of the 1,3-diarylallyl cations with Cl^- (principle of microscopic reversibility). As discussed above, **1e** and the more reactive carbocations **1(a–d)** react with chloride ions in these solvents with second-order rate constants $k_2 > 7 \times 10^8 \text{ M}^{-1}\text{s}^{-1}$, indicating that there is no or only a very small barrier for the ion combination, which is equivalent to a carbocation-like transition state.

A different situation is found for the solvolyses of **1**-OCOR. For all carboxylates (plots for **1**-ODNB and **1**-OPNB are shown in Figure 5), the m values are less than 0.6 and decrease with increasing cation stability, which is most pronounced for the 3,5-dinitrobenzoates.

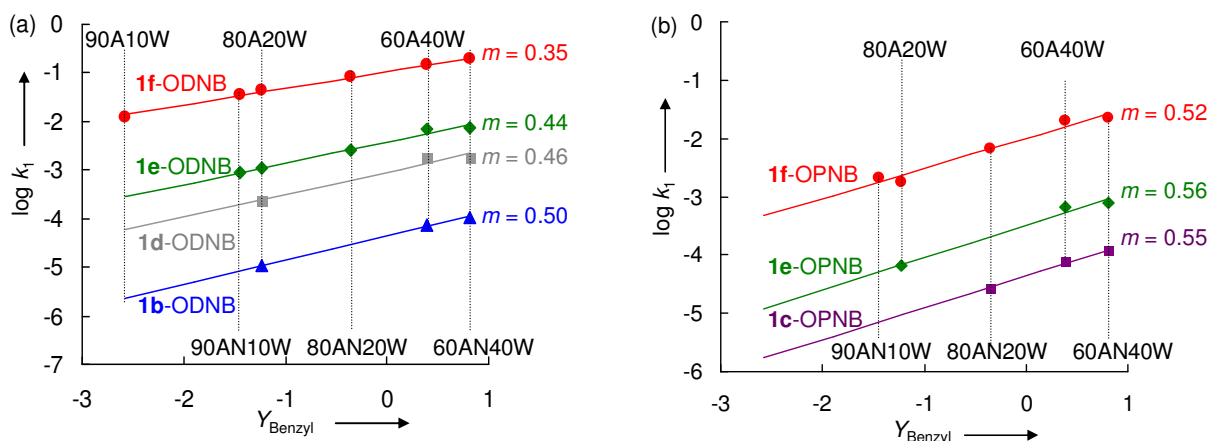


Figure 5. Correlation between the solvolysis rate constants of (a) **1-ODNB** and (b) **1-OPNB** in acetone/water and acetonitrile/water mixtures (from Table 2) and the corresponding Y_{Benzyl} values.^{12d}

This situation is very similar to that for benzhydryl¹⁴ and trityl¹⁵ carboxylates where the m -values of $\text{Ar}_2\text{CH-ODNB}$ were reported to decrease steadily with increasing electrofugalities of the carbocations. As in the benzhydryl and trityl series, the low m -values for allyl carboxylates and their decrease with increasing electrofugality can be rationalized by incompletely developed carbocation character in the transition states.^{14,15} It is noteworthy that the m -values of the allyl carboxylates **1-OCOR** are higher than those of benzhydryl carboxylates of similar reactivities (see p 290), in contrast to the solvolysis rates of **1-Cl** and **1-Br** which are less sensitive to the changes in solvent ionizing power than those of their benzhydryl analogs.

2.4. Hammett Analysis

The heterolysis rates of **1(a-f)-Cl** in 90, 80, and 60% aqueous acetone and acetonitrile correlate with the sum of Hammett-Brown's σ^+ parameters¹⁶ (Figure 6, pp 285–286). The ρ -values (–3.4 to –3.1) are lower than those for benzhydryl derivatives of comparable reactivities (–4.2 to –4.1).¹⁷ As in the benzhydryl series,¹⁴ smaller values of ρ are found for the solvolyses of allyl 4-nitrobenzoates and 3,5-dinitrobenzoates **1-OCOR** (–2.8 < ρ < –2.3, Figure 6) again indicating that the transition states of solvolyses of 1,3-diarylallyl chlorides are more carbocation-like than those for 1,3-diarylallyl carboxylates.

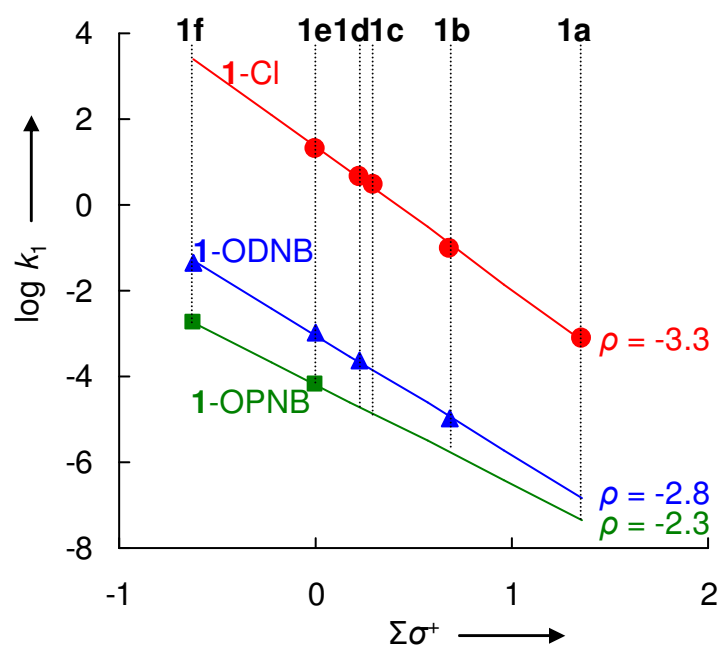


Figure 6. Heterolysis rate constants k_1 of **1-Cl**, **1-ODNB**, and **1-OPNB** in 80% aq acetone (80A20W) in correlation with the sum of σ^+ parameters of the corresponding aryl substituents (σ^+ from ref 16).

2.5 Determination of the Electrofugality Parameters

Figure 7 shows that $\log k_1/s_f$ for the solvolyses of **1(a-h)**-LG correlates linearly with N_f .

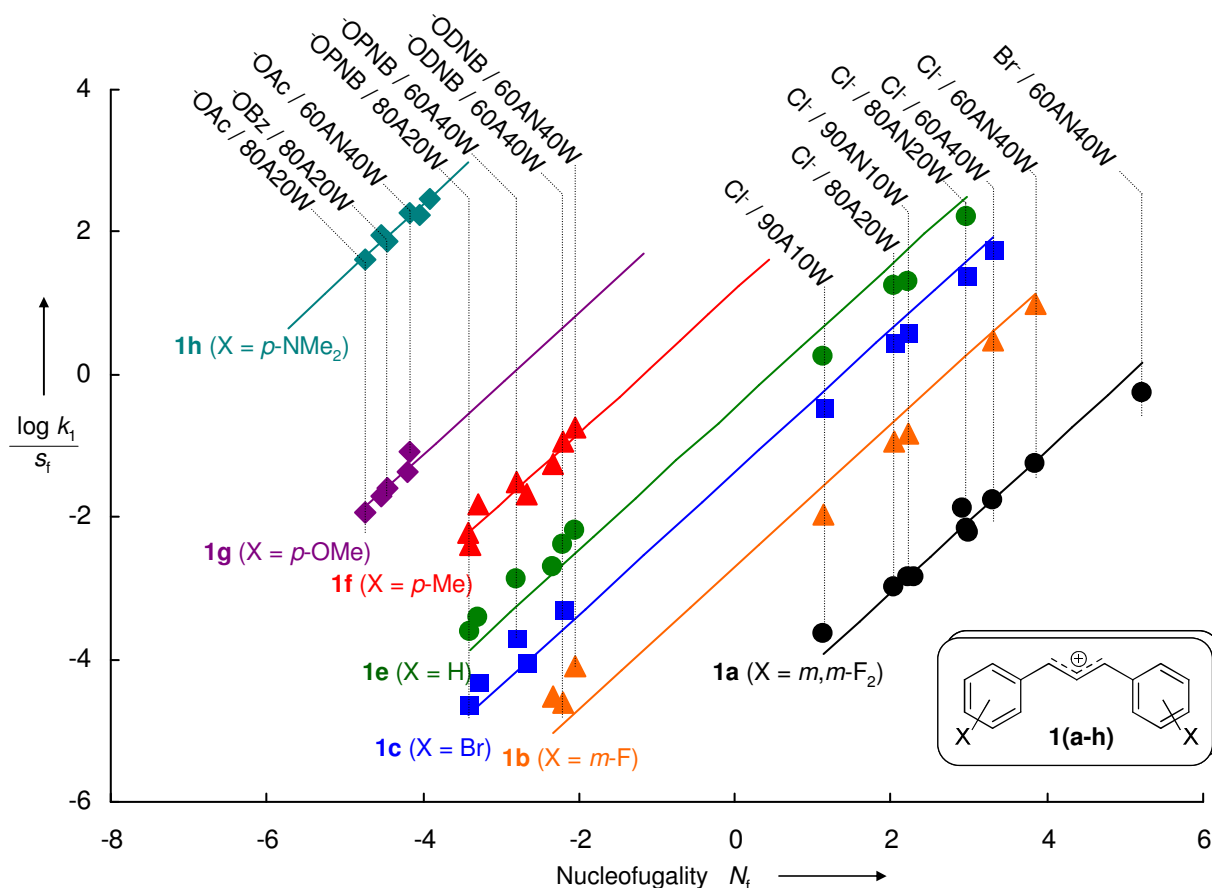


Figure 7. Plot of $(\log k_1)/s_f$ versus N_f for solvolyses of **1(a-h)**-LG in various solvents. Abbreviations used for the solvents are A (acetone), AN (acetonitrile), and W (water). All solvent ratios are given in % v/v (i.e., 80A20W means 80% v/v aq acetone). Abbreviations for leaving groups are: OPNB = 4-nitrobenzoate, ODNB = 3,5-dinitrobenzoate.

By minimizing¹⁸ the sum of the squared deviations $\Delta^2 = \Sigma(\log k_1 - s_f(N_f + E_f))^2$, one can derive the electrofugality parameters E_f for cations **1(a-h)** listed in Table 2, which correspond to the intercepts with the abscissa of the correlation lines in Figure 7.

Since the use of eq 2 enforces slopes of 1.0 for these correlations, carboxylates are generally above and halides are below the correlation lines, when data for both classes of nucleofuges are used for the correlations. As a consequence one would arrive at better predictions of solvolysis rate constants, when different electrofugality parameters would be employed for allyl carboxylates and allyl halides. For the sake of simplicity and unambiguity we refrain from proliferating the number of parameters and refer to the last column of Table 2 which shows that also with a single set of E_f -parameters, experimental and calculated rate constants never deviate by more than a factor of five. As most rate constants agree much better, we consider these deviations tolerable in view of the fact that the 1,3-diarylallyl cations are covering a reactivity range of 12 orders of magnitude.

2.6. Comparison of 1,3-Diarylallyl and Benzhydryl Cations

Depending on the substituents, the electrofugalities of 1,3-diarylallyl cations exceed those of analogously substituted benzhydryl cations by 1.5 to 7.5 orders of magnitude (Figure 8). As for the electrophilicities, the electrofugality range covered by 1,3-diarylallyl cations is smaller than that for analogously substituted benzhydryl systems, and the difference in electrofugalities between the two series decreases with increasing electron donating abilities of the substituents (Figure 8).

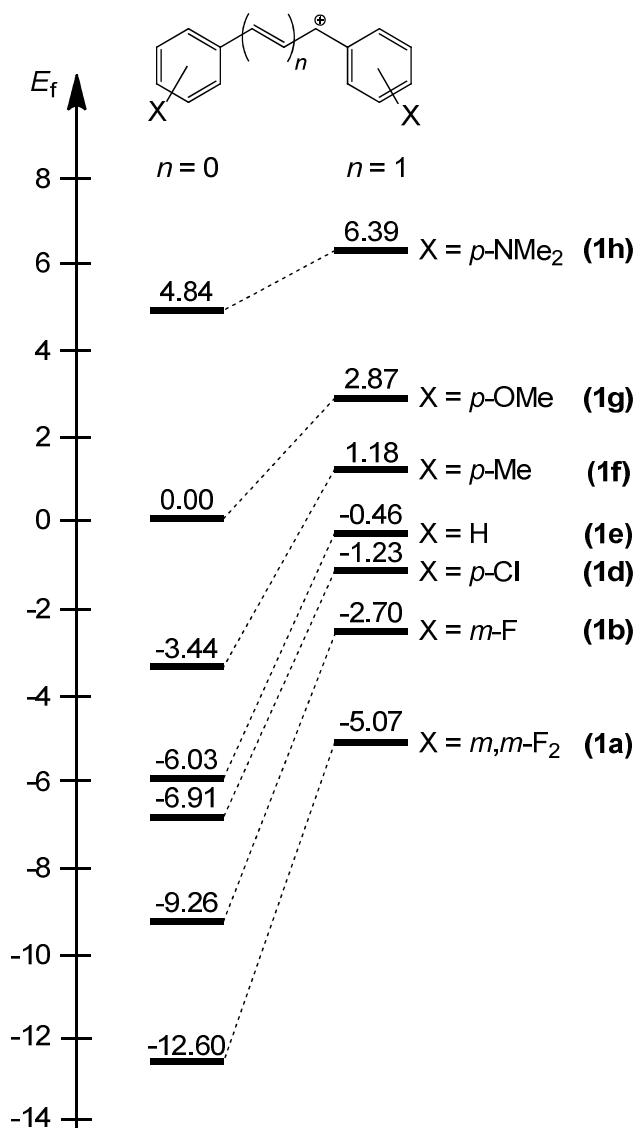


Figure 8. Electrofugalities E_f of **1(a–h)** compared with those of analogously substituted benzhydryl cations.³

The differences can be explained in the same way as in the case of the electrophilicities.⁷ As the electron-demand of the carbenium centers is smaller in the 1,3-diarylallyl cations due to

the charge delocalization over two terminal allylic carbons, substituents have a smaller effect on the rates of their reactions as well as on the rates of their formation.

Figure 9 shows that the electrofugalities of analogously substituted 1,3-diarylallyl and benzhydryl cations are linearly correlated, as previously reported for the corresponding electrophilicities of these carbocations. The slope of this correlation (0.64) reflects the differences in electron demand between the two series which has already been derived from Figure 8.

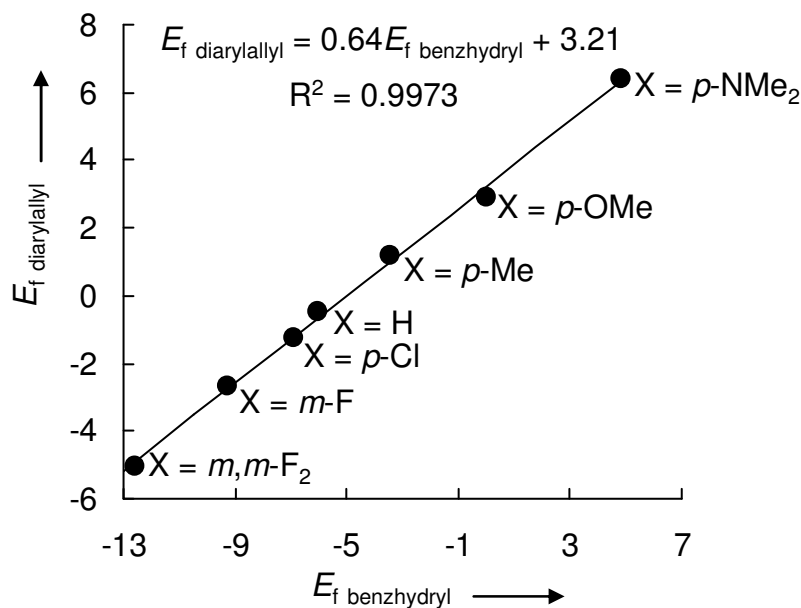
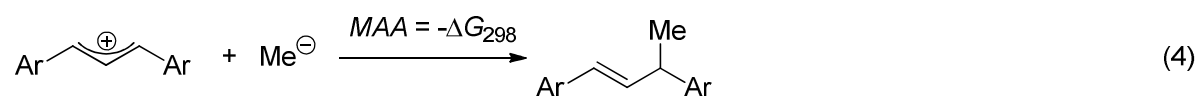


Figure 9. Correlation between the electrofugality parameters E_f of analogously substituted 1,3-diarylallyl and benzhydryl cations.³

As previously reported,⁷ the electrophilicities of **1(a–h)** increase with increasing methyl anion affinities (MAA, eq 4, Figure 10a).



Correspondingly, their electrofugalities decrease with increasing methyl anion affinities (Figure 10b). It is remarkable however, that the red dots are always above the black squares, i.e., that 1,3-diarylallyl cations are both better electrophiles (Figure 10a) and better electrofuges (Figure 10b) than benzhydrylium ions of equal methyl anion affinities.¹⁹ One, therefore, can conclude that the reactions of 1,3-diarylallyl cations proceed with lower intrinsic barriers than the corresponding reactions of benzhydrylium ions, i.e., heterolyses of

diarylallyl derivatives (and the reverse ion recombinations) require less reorganization than the corresponding reactions of benzhydryl derivatives. As a consequence of the different intrinsic barriers, **1(a–h)** are *more electrophilic* than benzhydrylium ions of similar electrofugality and *better electrofuges* than diarylmethyl cations of similar electrophilicity. More specific: The 1,3-bis(*p*-tolyl)allyl cation **1f** is both a better electrophile ($\Delta E = 1.23$) and a better electrofuge ($\Delta E_f = 1.18$) than the 4,4'-dimethoxybenzhydryl cation.

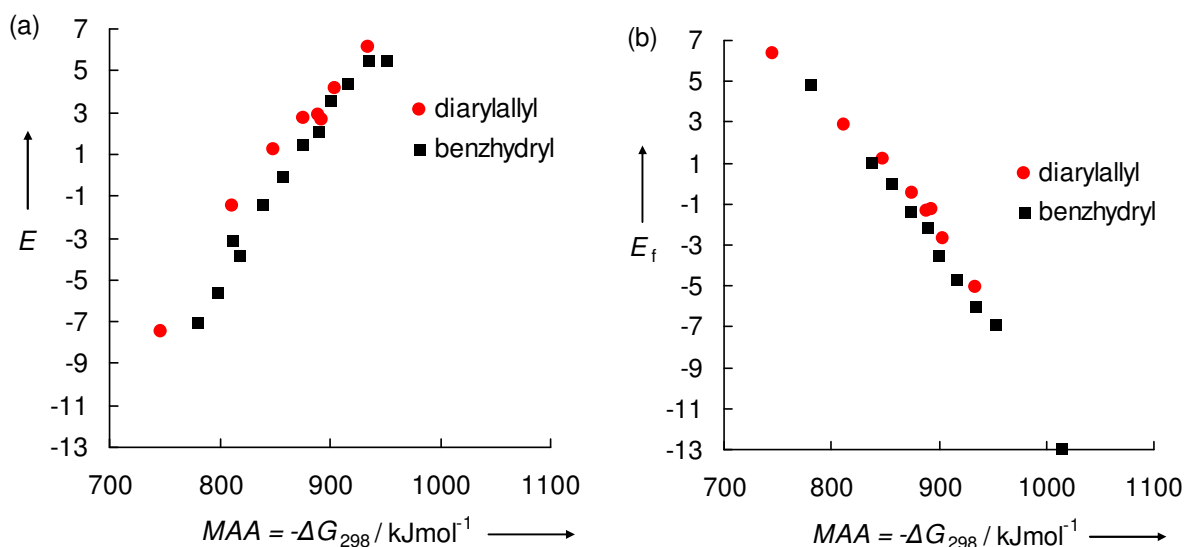


Figure 10. Correlations of (a) electrophilicities and (b) electrofugalities of benzhydryl and 1,3-diarylallyl cations with their calculated (B3LYP/6-31G(d,p) level of theory) gas-phase methyl anion affinities (MAA) as defined in eq 4.

This behavior can quantitatively be explained by Marcus theory²⁰ or the related principle of least nuclear motion:²¹ As the formation of 1,3-diarylallyl cations from covalent precursors as well as their reactions with nucleophiles require less changes of charge densities and related movements of nuclei and solvent molecules than the corresponding processes for benzhydrylium ions of equal Lewis acidities, smaller reorganization energies are needed in the 1,3-diarylallylium than in benzhydrylium series.

Let us now analyze how these differences in intrinsic barriers affect the correlations based on eq 2. When the ion recombination proceeds with diffusion-controlled rate, the activation energy of heterolysis equals ΔG^0 of the reaction (principle of microscopic reversibility). This is the case for many bromides and chlorides derived from acceptor-substituted benzhydrylium and 1,3-diarylallylium ions. As 3,5-dinitrobenzoate and 4-nitrobenzoate anions are less nucleophilic than Cl^- (≥ 100 times), several carbocations undergo diffusion-controlled recombinations with Cl^- , while they undergo activation-controlled reactions with $^-\text{ODNB}$ or

OPNB^- . Consequently, the N_f and s_f values of carboxylates are affected by the intrinsic reactivities of the benzhydrylium ions to a much higher extent than those of Cl^- and Br^- . As the intrinsic reactivities of 1,3-diarylallyl cations are higher (i.e., the electrophile-specific fraction of their intrinsic barrier is lower), the experimental heterolysis rates of the corresponding carboxylates are higher than those predicted based on eq 2 using the N_f and s_f parameters based on diarylmethyl cations (see Figure 7). Acceleration of allyl carboxylate solvolysis by the interaction of the carbonyl oxygen with the other allylic terminus seems to play rather a minor role, since the contact ion pairs for allyl systems have unsymmetrical structures.²²

2.7. Electrophilicity–Electrofugality Relationships

Figure 11 which plots the E_f values of the cations **1(a–h)** versus their electrophilicity parameters E , demonstrates that, similar to the situation with benzhydryl³ and trityl²³ systems, the E_f vs. E correlation for 1,3-diarylallyl cations **1** is not linear. The high intrinsic barriers for the reactions involving cations with strong electron donor groups, which are responsible for the deviation of **1h** from the correlation lines in Figures 10a and 10b, accumulate in Figure 11: Rates of heterolyses, which are smaller than expected based on the MAA, shift **1h** to the left, and the electrophilicity lower than expected from the MAA shifts **1h** downwards.

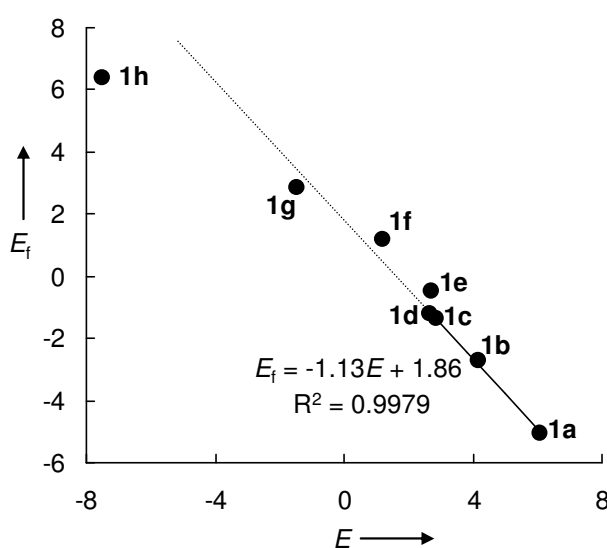


Figure 11. Electrofugality parameters of the cations **1(a–h)** plotted vs their electrophilicities E . The correlation line refers to the acceptor-substituted cations **1(a–d)**.

2.8. Parallel S_N1 and S_N2 Mechanisms in Reactions of **1a-Br** with Amines

From the dependence of the hydrolysis rates of 1,3-diphenylallyl chloride **1e-Cl** in the presence of variable concentrations of DMAP we derived the operation of an S_N1 mechanism, as k_{obs} became independent of the concentration of DMAP when this exceeded a certain value. A different behavior was observed when **1a-Br** was treated with variable amounts of DABCO, piperidine, or morpholine in aqueous acetonitrile and aqueous acetone. As illustrated in Figure 12, one now finds a linear increase of the pseudo-first-order rate constants with increasing amine concentration, indicating S_N2 reactions of the amines with **1a-Br**, which are accompanied by an S_N1 process, the rate constant k_1 of which is given by the identical intercepts of the three correlation lines (eq 5).

$$k_{\text{obs}} = k_1 + k_2[\text{amine}] \quad (5)$$

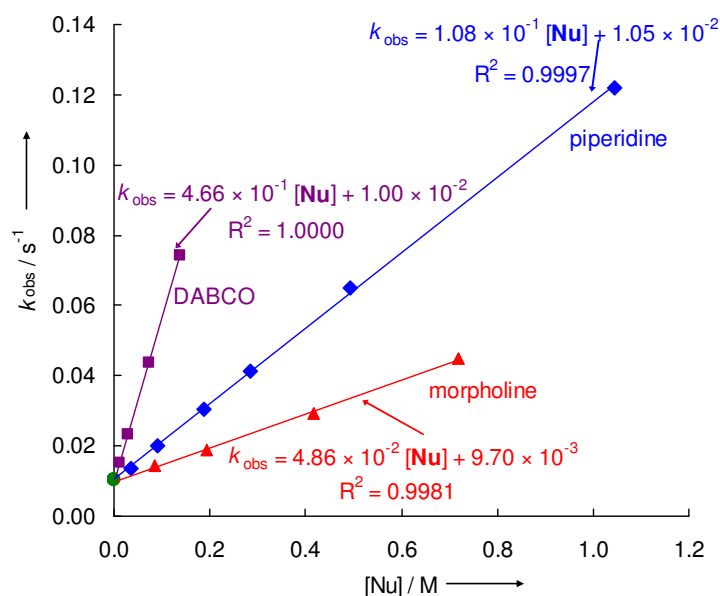


Figure 12. Pseudo-first order rate constants observed for solvolyses of **1a-Br** in 80% aq acetone in the presence of various amine concentrations, 25 °C.

As shown in the Experimental Section (pp 261–265), the operation of the rate law (eq 5) has also been observed for the reaction of **1a-Br** with these three amines in 90% aqueous acetone as well as in 80% and 90% aq acetonitrile.

Table 3, which summarizes these results, shows that in all solvents, DABCO reacts approximately one order of magnitude faster than morpholine, and piperidine is about two

times more reactive than morpholine. A similar reaction sequence for these three amines has previously been reported for their reactions with benzhydryl bromides in DMSO.²⁴

In contrast to the strong solvent effects on the rates of the S_N1 reactions discussed above, the rates of the S_N2 reactions are not or only slightly affected by the solvent polarity. While the nucleophilic substitutions proceed with equal rates in 90% and 80% aqueous acetone, they are even slightly slower in 80% than in 90% aqueous acetonitrile in contrast to the expectations based on the Hughes-Ingold rules, which predict a strong increase of the rates of S_N2 reactions when ions are generated from neutral reactants.²⁵ Obviously, the reduction of the nucleophilicity of the amines by water^{2e} compensates (aq acetone) or overcompensates (aq acetonitrile) the expected acceleration due to the stabilization of the partially ionic transition states by the solvent.

Table 3. First Order Rate Constants (s⁻¹) for the Reactions of **1a**-Br with Aqueous Acetone and Acetonitrile (S_N1 solvolysis) and Second-Order Rate Constants (M⁻¹s⁻¹) for the Reactions of **1a**-Br with Amines in these Solvents, 25 °C.

solvent	k_1 / s^{-1}	$k_2 / \text{M}^{-1}\text{s}^{-1}$		
		DABCO	piperidine	morpholine
90A10W	1.35×10^{-3}	4.97×10^{-1}	1.07×10^{-1}	4.49×10^{-2}
80A20W	1.03×10^{-2}	4.66×10^{-1}	1.08×10^{-1}	4.86×10^{-2}
60A40W	1.95×10^{-1}	$(7.91 \times 10^{-1})^a$	<i>b</i>	<i>b</i>
90AN10W	1.26×10^{-2}	1.23	2.08×10^{-1}	9.40×10^{-2}
80AN20W	8.83×10^{-2}	8.83×10^{-1}	1.46×10^{-1}	<i>b</i>
60AN40W	5.54×10^{-1a}	<i>b</i>	$(3.24 \times 10^{-1})^a$	<i>b</i>

^a Due to the uncertainties caused by the fast reaction with the solvent, the k_2 value cannot be precisely determined and should be considered as an estimate. ^b Not measurable.

As **1a** is by far the least stabilized diarylallyl cation of this series, one can explain why amines, which are present as trapping agents to suppress common ion return (Figures 2 and 3) do not undergo S_N2 reactions with other 1,3-diarylallyl derivatives **1(b-f)**-LG.

2.9. Changes of Solvolysis Mechanisms of Allyl Derivatives

Figure 13 combines the rate constants for the heterolyses of allyl derivatives (k_1 of Scheme 2) with the rate constants for the reactions of the allyl cations with 80% aqueous acetone.

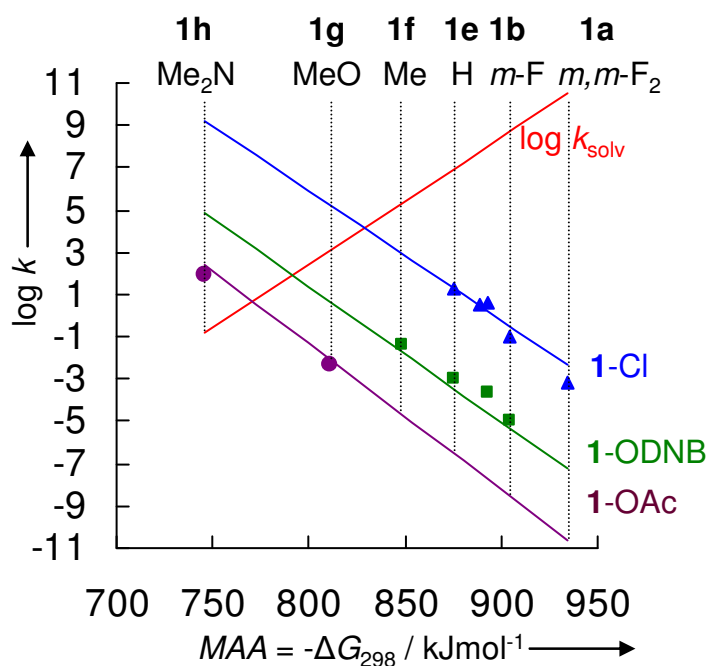


Figure 13. Heterolysis rate constants k_1 for **1-Cl**, **1-ODNB**, and **1-OAc** in 80% aq acetone as well as pseudo-first-order rate constants k_{solv} for the reactions of **1** with the solvent in correlation with calculated (B3LYP/6-31G(d,p) level of theory) gas-phase methyl anion affinities (MAA) of **1**. Experimentally derived values of k_1 (Table 2) are identified by symbols, and the trend lines correspond to k_1 and k_{solv} calculated for **1(a-h)-LG** and **1(a-h)** by eqs 2 and 1, respectively.

One can see that the acceptor-substituted allyl chlorides **1(a,b)-Cl** like the unsubstituted (*E*)-1,3-diphenylallyl chloride **1e-Cl** (as well as **1(c,d)-Cl**) follow the typical S_N1 mechanism: slow formation of the carbocation, followed by rapid trapping by the solvent. Crossing of the two correlation lines is expected for an 1,3-diarylallyl chloride with a reactivity between those of the dimethyl- and dimethoxy-substituted 1,3-diarylallyl chlorides **1f-Cl** and **1g-Cl**. From $\log k$ corresponding to the point of intersection one can derive that heterolysis of the corresponding 1,3-diarylallyl chloride **1-Cl** as well as solvent capture of the generated carbenium ion occur on the sub-millisecond time scale, where measurements of the rates of thermal heterolysis are presently not possible.

As 3,5-dinitrobenzoate anion is a weaker nucleofuge than Cl^- , the correlation line for the heterolysis rate constants of **1-ODNB** is lower, and crossing with the k_{solv} graph occurs for allyl cations slightly better stabilized than the dimethoxy-substituted system **1g**. Because of the smaller $\log k$ for such 3,5-dinitrobenzoates, the build-up of visually detectable carbocation concentrations can be expected, as we have previously observed in the benzhydrylium²⁶ and tritylium^{15,27} series.

Acetate is such a weak leaving group that it was even possible to measure the rate of the heterolytic formation of the highly stabilized dimethylamino-substituted cation **1h** from covalent **1h**-OAc. Though Figure 13 predicts a slow subsequent reaction of **1h** with water, this reaction is reversible, and we have observed the formation of the persistent allyl cation **1h** in aqueous acetone (or acetonitrile).

A complete solvolysis scheme, which includes S_N1 reactions proceeding with external (common ion) and internal return, as well as the turnover to the concerted S_N2 mechanism on one side and to bimolecular substitutions of the S_N2C^+ type on the other, can now be constructed for 1,3-diarylallyl 4-nitrobenzoates. A previous study in our group²⁴ has shown that eq 1 can be applied to predict hypothetical lifetimes τ of carbocations in the presence of nucleophiles. According to Richard and Jencks, an intermediate cannot exist if this lifetime is shorter than the period of a bond vibration (10^{-13} s).²⁸ Applying this criterion to the reactions of **1** with 60% aq acetone ($N = 5.77$, $s_N = 0.87$),²⁹ one can conclude that the S_N2 reaction with this solvent will be enforced for 4-nitrobenzoates derived from cations with $E > 9$.

Eventually, comparison of k_{solv} and k_1 (Figure S6, p 291) shows that the change from the S_N1 to S_N2C^+ mechanism will occur for the solvolyses of 1,3-diarylallyl 4-nitrobenzoates in 60 % aq acetone ($N_f = -2.79$, $s_f = 1.11$) when the electrophilicity of the corresponding carbenium ion reaches $E = -3.9$ ($k_{\text{solv}} = k_1$). When the E value of the cation falls below ca. -6 , formation of stable carbocation solutions is expected (Figure 14).

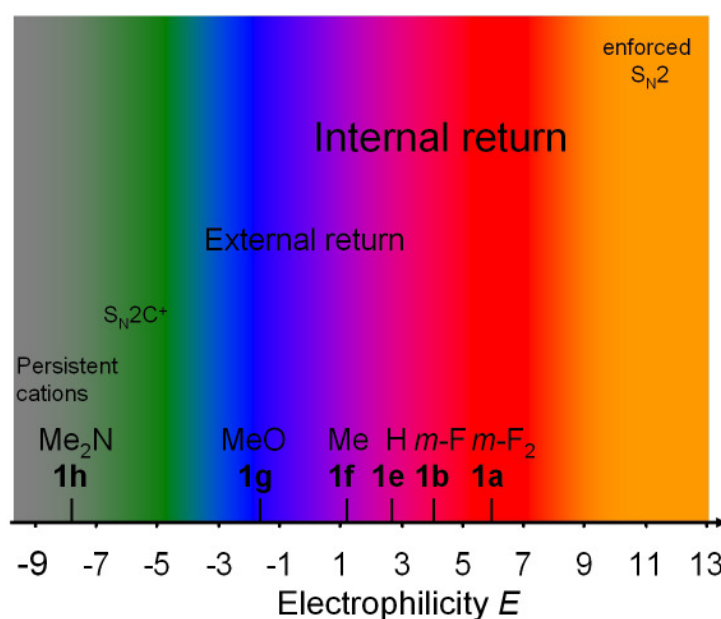


Figure 14. Comprehensive spectrum of 1,3-diarylallyl 4-nitrobenzoate (**1**-OPNB) solvolysis in 60 % aq acetone ($[^-OPNB] = 5$ mM).

3. Conclusions

Though the linear free energy relationship $\log k_1 = s_f(N_f + E_f)$ (eq 2) was found to predict heterolysis rates of 1,3-diarylallyl bromides, chlorides and carboxylates with an accuracy of factor 5 from a single set of E_f parameters and the benzhydrylium-based nucleofuge-specific parameters N_f and s_f , systematic deviations are evident. Thus, the 1,3-diarylallyl carboxylates **1**-ODNB react generally faster while the 1,3-diarylallyl chlorides **1**-Cl react generally more slowly than predicted, when both types of leaving groups were used to determine the electrofugality parameters E_f . As in the benzhydryl and trityl series, solvolyses of 1,3-diarylallyl bromides and chlorides have significantly larger Winstein-Grunwald m -values than carboxylates, which have been explained by late and early transition states. Substituent variation affects solvolysis rates of 1,3-diarylallyl derivatives significantly less than those of benzhydryl derivatives. As the intrinsic barriers for heterolyses of 1,3-diarylallyl derivatives are lower than those for the corresponding benzhydryl heterolyses, one comes to the conclusion that 1,3-diarylallyl derivatives ionize faster than benzhydryl derivatives of same electrophilicity E and that 1,3-diarylallylium ions react faster with nucleophiles than benzhydryl cations of equal electrofugality E_f . The reactivity parameters E and E_f derived in this and preceding investigations have been combined to derive the full mechanistic spectrum of 1,3-diarylallyl solvolyses.

4. Experimental Section

4.1. General

Materials for Kinetic Measurements. Dry ethanol was obtained by distillation of commercially available absolute ethanol from sodium/diethyl phthalate. Piperidine (>99%) and morpholine (>99%) were purchased and distilled prior to use. Acetone (99.8%), acetonitrile (HPLC grade), DMAP (>99%), and DABCO (98%) were purchased and used as received. Double distilled water (impedance 18.2 Ω) was obtained from a water purification system.

NMR Spectroscopy. In the ^1H and ^{13}C NMR spectra chemical shifts are expressed in δ (ppm) and refer to CDCl_3 (δ_{H} 7.26, δ_{C} 77.0), CD_2Cl_2 (δ_{H} 5.32, δ_{C} 54.00), or TMS (δ_{H} 0.00, δ_{C} 0.0) as internal standards. The coupling constants are given in Hz. Abbreviations used are: s (singlet), d (doublet), t (triplet), q (quartet), m (multiplet). In case of ^{13}C spectra, these abbreviations refer to the multiplicity in *hydrogen decoupled* spectra and the hydrogen multiplicity (based

on DEPT or HSQC experiments) is shown as CH₃, CH₂, CH or C to avoid ambiguity. For the compounds containing no fluorine, the letter “s” is omitted.

Determination of the Rate Constants. First-order rate constants (k_{obs}) were calculated by least-squares fitting of the conductivity data to a single exponential function $\kappa_t = \kappa_{\infty} (1 - e^{-k_{\text{obs}}t}) + C$. In the case of **1h**-OCOR, the generation of the free cation **1h** was followed spectrophotometrically at the absorption maximum of **1h** (704 nm), and the resulting time dependent absorbances were fitted to a monoexponential function $A = A_{\infty}(1 - e^{-k_{\text{obs}}t}) + C$. The temperature of the reaction solutions (25 °C) was kept constant during all kinetic studies by using a circulating bath thermostat.

Abbreviations Used for Solvents: A – acetone, AN – acetonitrile, W – water, E – ethanol.

All solvent compositions are given in v/v %.

4.2. Synthetic Procedures

All yields refer to non-optimized procedures.

(E)-3-Bromo-1,3-bis(3,5-difluorophenyl)prop-1-ene (1a-Br) was obtained from **1a-OH** (1.03 g, 3.69 mmol) using a procedure from ref 30: 708 mg (2.05 mmol, 56%), colorless solid (mp 57.0 – 59.5 °C). ¹H NMR (CDCl₃, 300 MHz): δ 5.68 (d, ³J_{HH} = 7.1 Hz, 1 H, ArCHCHCH(Br)Ar), 6.49–6.63 (m, 2 H, ArCHCHCH(Br)Ar, ArCHCHCH(Br)Ar), 6.69–6.83 (m, 2 H, H_{Ar}), 6.86–6.98 (m, 2 H, H_{Ar}), 6.98–7.06 ppm (m, 2 H, H_{Ar}). ¹³C NMR (CDCl₃, 75 MHz): δ 51.4 (t, J_{CF} = 2.3 Hz, CH), 103.9 (t, J_{CF} = 25.6 Hz, CH), 104.2 (t, J_{CF} = 25.2 Hz, CH), 109.5–109.8 (m, CH), 110.6–111.0 (m, CH), 130.6 (s, CH), 130.9 (t, J_{CF} = 2.9 Hz, CH), 138.9 (t, J_{CF} = 9.6 Hz, C), 143.4 (t, J_{CF} = 9.0 Hz, C), 163.0 (dd, J_{CF} = 248.6, 12.7 Hz, C), 163.2 ppm (dd, J_{CF} = 247.2, 12.9 Hz, C). ¹⁹F NMR (CDCl₃, 282 MHz): δ –109.7 to –109.4 (m), –108.4 to –108.1 ppm (m). HRMS (EI+): calcd 265.0635 (C₁₅H₉F₄⁺(M – Br[–])), found 265.0623.

(E)-3-Chloro-1,3-bis(3-fluorophenyl)prop-1-ene (1b-Cl) was synthesized by procedure described in ref 30. From **1b-OH** (530 mg, 2.15 mmol): 378 mg (1.26 mmol, 58%), colorless oil. ¹H NMR (CDCl₃, 400 MHz): δ 5.60 (d, ³J_{HH} = 7.7 Hz, 1 H, ArCHCHCH(Cl)Ar), 6.46 (dd, ³J_{HH} = 15.6, 7.7 Hz, 1 H, ArCHCHCH(Cl)Ar), 6.60 (d, ³J_{HH} = 15.6 Hz, 1 H, ArCHCHCH(Cl)Ar), 6.93–6.99 (m, 1 H, H_{Ar}), 6.99–7.06 (m, 1 H, H_{Ar}), 7.06–7.39 ppm (m, 6 H, H_{Ar}). ¹³C NMR (CDCl₃, 101 MHz): δ 62.3 (d, J_{CF} = 2.0 Hz, CH), 113.3 (d, J_{CF} = 22.3 Hz, CH), 114.5 (d, J_{CF} = 22.7 Hz, CH), 115.2 (d, J_{CF} = 21.4 Hz, CH), 115.5 (d, J_{CF} = 21.2 Hz, CH), 122.8 (d, J_{CF} = 2.8 Hz, CH), 122.9 (d, J_{CF} = 3.0 Hz, CH), 129.7 (d, J_{CF} = 0.5 Hz, CH),

130.1 (d, $J_{CF} = 8.4$ Hz, CH), 130.3 (d, $J_{CF} = 8.3$ Hz, CH), 131.4 (d, $J_{CF} = 2.6$ Hz, CH), 137.9 (d, $J_{CF} = 7.7$ Hz, C), 142.4 (d, $J_{CF} = 7.2$ Hz, C), 162.8 (d, $J_{CF} = 247.2$ Hz, C), 163.0 ppm (d, $J_{CF} = 245.9$ Hz, C). HRMS (EI+): calcd 264.0512 (C₁₅H₁₁ClF₂), found 264.0505.

(E)-3-Chloro-1,3-bis(4-chlorophenyl)prop-1-ene (1d-Cl) was obtained by the procedure from ref 31. From **1d-OH** (487 mg, 1.74 mmol): 344 mg (1.16 mmol, 66%), colorless solid (mp 77.5 – 80.0 °C). ¹H NMR (CDCl₃, 300 MHz): δ 5.59 (d, 1 H, ³J_{HH} = 7.4 Hz, ArCHCHCH(Cl)Ar), 6.44 (dd, ³J_{HH} = 15.7, 7.4 Hz, 1 H, ArCHCHCH(Cl)Ar), 6.56 (d, ³J_{HH} = 15.7 Hz, 1 H, ArCHCHCH(Cl)Ar), 7.22–7.43 ppm (m, 8 H, H_{Ar}). ¹³C NMR (CDCl₃, 75 MHz): δ 62.6 (CH), 128.0 (CH), 128.7 (CH), 128.8 (CH), 128.9 (CH), 129.2 (CH), 131.2 (CH), 134.1 (2 × C), 134.3 (C), 138.5 ppm (C). HRMS (EI+): calcd 296.9999 (C₁₅H₁₁Cl₃+H⁺), found 296.9987.

General procedure for synthesis of 1,3-diarylallyl 3,5-dinitrobenzoates (1-ODNB).

3,5-Dinitrobenzoyl chloride (1 equiv) was added to a stirred solution of the corresponding alcohol **1-OH** (1 equiv) and triethylamine (1.05 equiv) in toluene. After 12 h stirring, the reaction mixture was quenched with 0.1 M aq HCl, the organic layer was separated, washed with saturated NaHCO₃ solution and water, and freed from the solvent. The crude product was purified by recrystallization from a CH₂Cl₂/pentane mixture.

(E)-1,3-Bis(3-fluorophenyl)allyl 3,5-dinitrobenzoate (1b-ODNB). From **1b-OH** (300 mg, 1.22 mmol): 199 mg (0.451 mmol, 37%), yellowish powder (mp 130.0 – 131.5 °C) ¹H NMR (CDCl₃, 300 MHz): δ 6.48 (dd, ³J_{HH} = 15.9, 7.1 Hz, 1 H, ArCHCHCH(ODNB)Ar), 6.67–6.79 (m, 2 H, ArCHCHCH(ODNB)Ar, ArCHCHCH(ODNB)Ar), 6.92–7.03 (m, 1 H, H_{Ar}), 7.03–7.36 (m, 6 H, H_{Ar}), 7.36–7.48 (m, 1 H, H_{Ar}), 9.18–9.22 (m, 2 H, H_{ODNB}), 9.22–9.25 ppm (m, 1 H, H_{ODNB}). ¹³C NMR (CDCl₃, 75 MHz): δ 78.1 (d, $J_{CF} = 2.0$ Hz, CH), 113.3 (d, $J_{CF} = 22.0$ Hz, CH), 114.1 (d, $J_{CF} = 22.5$ Hz, CH), 115.6 (d, $J_{CF} = 21.4$ Hz, CH), 116.0 (d, $J_{CF} = 21.1$ Hz, CH), 122.6 (s, CH), 122.7 (d, $J_{CF} = 3.1$ Hz, CH), 122.9 (d, $J_{CF} = 2.9$ Hz, CH), 126.6 (s, CH), 129.5 (s, CH), 130.2 (d, $J_{CF} = 8.4$ Hz, CH), 130.7 (d, $J_{CF} = 8.2$ Hz, CH), 133.7 (s, C), 133.8 (d, $J_{CF} = 2.6$ Hz, CH), 137.7 (d, $J_{CF} = 7.7$ Hz, C), 140.1 (d, $J_{CF} = 7.1$ Hz, C), 148.7 (s, C), 161.5 (s, C), 163.0 (d, $J_{CF} = 247.5$ Hz, C), 163.1 ppm (d, $J_{CF} = 246.2$ Hz, C). ¹⁹F NMR (CDCl₃, 282 MHz): δ -113.0 to -112.9 (m), -111.5 to -111.4 (m). HRMS (EI+): calcd 440.0814 (C₂₂H₁₄F₂N₂O₆), found 440.0808.

(E)-1,3-Bis(4-bromophenyl)allyl 3,5-dinitrobenzoate (1c-ODNB). From **1c-OH** (1.63 g, 4.43 mmol): 1.05 g (1.87 mmol, 42%), yellowish powder (mp 161.5 – 163.1 °C). ¹H NMR (CD₂Cl₂, 400 MHz): δ 6.51 (dd, ³J_{HH} = 15.9, 7.0 Hz, 1 H, ArCHCHCH(ODNB)Ar), 6.68–6.74 (m, 2 H, ArCHCHCH(ODNB)Ar, ArCHCHCH(ODNB)Ar), 7.29–7.36 (m, 2 H, H_{Ar}),

7.40–7.50 (m, 4 H, H_{Ar}), 7.56–7.62 (m, 2 H, H_{Ar}), 9.18–9.19 (m, 2 H, H_{ODNB}), 9.21–9.22 ppm (m, 1 H, H_{ODNB}). ^{13}C NMR (CD_2Cl_2 , 101 MHz): δ 78.8 (CH), 122.9 (C), 123.2 (CH), 123.3 (C), 127.1 (CH), 128.9 (CH), 129.5 (CH), 130.1 (CH), 132.4 (CH), 132.6 (CH), 133.8 (CH), 134.3 (C), 135.2 (C), 137.7 (C), 149.3 (C), 162.2 ppm (C). HRMS (EI+): calcd 559.9213 ($C_{22}H_{14}Br_2N_2O_6$), found 559.9220.

(E)-1,3-Bis(4-chlorophenyl)allyl 3,5-dinitrobenzoate (1d-ODNB). From **1d-OH** (1.08 g, 3.87 mmol): 0.851 g (1.80 mmol, 47%), colorless powder (mp 150.0 – 151.5 °C). 1H NMR (CD_2Cl_2 , 400 MHz): δ 6.50 (dd, $^3J_{HH} = 15.9, 7.0$ Hz, 1 H, $ArCHCHCH(ODNB)Ar$), 6.66–6.77 (m, 2 H, $ArCHCHCH(ODNB)Ar$, $ArCHCHCH(ODNB)Ar$), 7.29–7.35 (m, 2 H, H_{Ar}), 7.35–7.41 (m, 2 H, H_{Ar}), 7.41–7.46 (m, 2 H, H_{Ar}), 7.47–7.52 (m, 2 H, H_{Ar}), 9.18 (d, $^3J_{HH} = 2.1$ Hz, 2 H, H_{ODNB}), 9.22 ppm (t, $^3J_{HH} = 2.1$ Hz, 1 H, H_{ODNB}). ^{13}C NMR (CD_2Cl_2 , 101 MHz): δ 78.8 (CH), 123.2 (CH), 127.0 (CH), 128.7 (CH), 129.2 (CH), 129.4 (CH), 129.6 (CH), 130.1 (CH), 133.7 (CH), 134.4 (C), 134.7 (C), 134.8 (C), 135.2 (C), 137.2 (C), 149.3 (C), 162.2 ppm (C). HRMS (EI+): calcd 472.0223 ($C_{22}H_{14}Cl_2N_2O_6$), found 472.0225.

(E)-1,3-Diphenylallyl 3,5-dinitrobenzoate (1e-ODNB). From **1e-OH** (1.00 g, 4.76 mmol): 731 mg (1.81 mmol, 38%), colorless powder (mp 154.1 – 155.5 °C). 1H NMR ($CDCl_3$, 300 MHz): δ 6.52 (dd, $^3J_{HH} = 16.0, 7.1$ Hz, 1 H, $PhCHCHCH(ODNB)Ph$), 6.70–6.83 (m, 2 H, $PhCHCHCH(ODNB)Ph$, $PhCHCHCH(ODNB)Ph$), 7.23–7.48 (m, 8 H, H_{Ar}), 7.48–7.56 (m, 2 H, H_{Ar}), 9.15–9.25 ppm (m, 3 H, H_{ODNB}). ^{13}C NMR ($CDCl_3$, 75 MHz): δ 79.3 (CH), 122.4 (CH), 125.9 (CH), 126.8 (CH), 127.1 (CH), 128.6 (CH), 128.7 (CH), 128.9 (CH), 129.0 (CH), 129.5 (CH), 134.1 (C), 134.5 (CH), 135.6 (C), 138.0 (C), 148.7 (C), 161.6 ppm (C). HRMS (EI+): calcd 404.1003 ($C_{22}H_{16}N_2O_6$), found 404.1005.

(E)-1,3-Di-*p*-tolylallyl 3,5-dinitrobenzoate (1f-ODNB). From **1f-OH** (1.00 g, 4.20 mmol): 900 mg (2.08 mmol, 50%), colorless powder (mp 84.5 – 86.0 °C). 1H NMR (CD_2Cl_2 , 400 MHz): δ 2.33 (s, 3 H, CH_3), 2.37 (s, 3 H, CH_3), 6.49 (dd, $^3J_{HH} = 15.9, 7.2$ Hz, 1 H, $ArCHCHCH(ODNB)Ar$), 6.66–6.76 (m, 2 H, $ArCHCHCH(ODNB)Ar$, $ArCHCHCH(ODNB)Ar$), 7.11–7.17 (m, 2 H, H_{Ar}), 7.22–7.28 (m, 2 H, H_{Ar}), 7.28–7.35 (m, 2 H, H_{Ar}), 7.40–7.46 (m, 2 H, H_{Ar}), 9.16–9.23 (m, 3 H, H_{ODNB}). ^{13}C NMR (CD_2Cl_2 , 101 MHz): δ 21.48 (CH_3), 21.51 (CH_3), 80.0 (CH), 123.0 (CH), 125.8 (CH), 127.2 (CH), 127.7 (CH), 129.9 (CH), 130.0 (CH), 130.1 (CH), 133.6 (C), 134.4 (CH), 134.8 (C), 136.0 (C), 139.1 (C), 139.3 (C), 149.2 (C), 162.3 ppm (C). HRMS (EI+): calcd 432.1316 ($C_{24}H_{20}N_2O_6$), 432.1331.

1,3-Diarylallyl 4-nitrobenzoates (1-OPNB) were obtained by the procedure described in ref 6.

(E)-1,3-Bis(4-bromophenyl)allyl 4-nitrobenzoate (1c-OPNB). From **1c-OH** (1.00 g, 2.72 mmol): 477 mg (0.923 mmol, 34%), colorless powder (mp 130.7 – 132.0 °C). ¹H NMR (CD₂Cl₂, 400 MHz): δ 6.47 (dd, ³J_{HH} = 15.9, 6.7 Hz, 1 H, ArCHCHCH(OPNB)Ar), 6.63 (d, ³J_{HH} = 6.7 Hz, 1 H, ArCHCHCH(OPNB)Ar), 6.69 (d, ³J_{HH} = 15.9 Hz, 1 H, ArCHCHCH(OPNB)Ar), 7.25–7.34 (m, 2 H, H_{Ar}), 7.37–7.44 (m, 2 H, H_{Ar}), 7.44–7.51 (m, 2 H, H_{Ar}), 7.52–7.60 (m, 2 H, H_{Ar}), 8.23–8.34 ppm (m, 4 H, H_{OPNB}). ¹³C NMR (CD₂Cl₂, 101 MHz): δ 77.5 (CH), 122.7 (C), 123.0 (C), 124.2 (CH), 127.8 (CH), 128.9 (CH), 129.4 (CH), 131.4 (CH), 132.3 (CH), 132.5 (CH), 132.9 (CH), 135.5 (C), 136.0 (C), 138.3 (C), 151.3 (C), 164.2 ppm (C). HRMS (EI+): calcd 514.9362 (C₂₂H₁₅Br₂NO₄), found 514.9379.

(E)-1,3-Di-*p*-tolylallyl 4-nitrobenzoate (1f-OPNB). From **1f-OH** (1.00 g, 4.20 mmol): 727 mg (1.88 mmol, 45%), colorless powder (mp 92.6 – 94.0). ¹H NMR (CDCl₃, 300 MHz): δ 2.35 (s, 3 H, CH₃), 2.37 (s, 3 H, CH₃), 6.43 (dd, ³J_{HH} = 15.9, 6.9 Hz, 1 H, ArCHCHCH(OPNB)Ar), 6.63–6.75 (m, 2 H, ArCHCHCH(OPNB)Ar), 6.63–6.75 (m, 2 H, ArCHCHCH(OPNB)Ar), 7.07–7.18 (m, 2 H, H_{Ar}), 7.19–7.26 (m, 2 H, H_{Ar}), 7.27–7.33 (m, 2 H, H_{Ar}), 7.34–7.45 (m, 2 H, H_{Ar}), 8.24–8.31 ppm (m, 4 H, H_{OPNB}). ¹³C NMR (CDCl₃, 75 MHz): δ 21.19 (CH₃), 21.21 (CH₃), 78.0 (CH), 123.5 (CH), 125.8 (CH), 126.7 (CH), 127.1 (CH), 129.3 (CH), 129.4 (CH), 130.8 (CH), 133.1 (C), 133.4 (CH), 135.8 (C), 135.9 (C), 138.2 (C), 138.4 (C), 150.5 (C), 163.7 ppm (C). HRMS (EI+): calcd 387.1465 (C₂₄H₂₁NO₄), found 387.1482.

4.3. Kinetic Measurements

General remark: the values of heterolysis rate constants k_1 are shown in **bold**. If several values are marked, their arithmetic mean was used to calculate k_1 .

4.3.1. Calibration curves

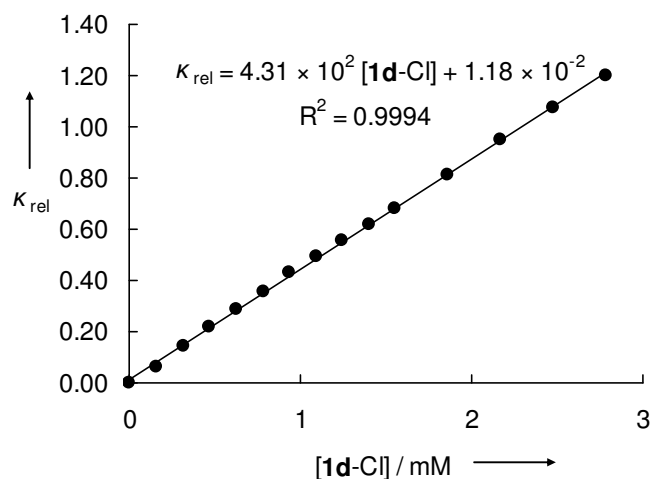


Figure S1. Linear dependence of the relative conductivity κ_{rel} on the concentration of HCl (generated by solvolysis of **1d-Cl** in 60% aq acetone (60A40W)), 25 °C.

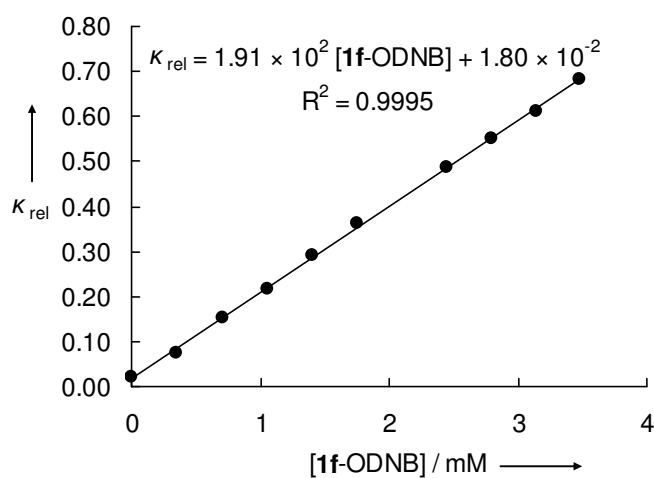


Figure S2. Linear dependence of the relative conductivity κ_{rel} on the concentration of 4-(dimethylamino)pyridin-1-ium 3,5-dinitrobenzoate (generated by solvolysis of **1f-ODNB** in 60% aq acetone (60A40W) in the presence of 19 mM DMAP), 25 °C.

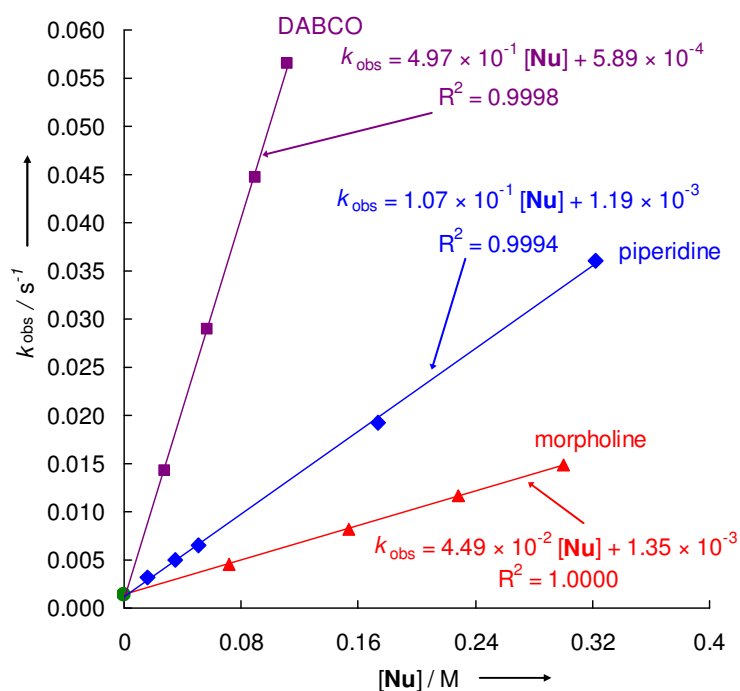
4.3.2. Solvolyses of 1a-LG

Solvolyses of 1a-Cl in various solvents

solvent	nucleophile	[1a-Cl] ₀ / M	[Nu] / M	<i>k</i> _{obs} / s ⁻¹
90A10W	-	4.52 × 10 ⁻⁴	0	8.61 × 10 ⁻⁵
90A10W	piperidine	2.52 × 10 ⁻⁴	7.03 × 10 ⁻³	8.95 × 10⁻⁵
80A20W	-	4.52 × 10 ⁻⁴	0	7.39 × 10 ⁻⁴
80A20W	-	5.04 × 10 ⁻⁴	0	7.27 × 10 ⁻⁴
80A20W	piperidine	2.52 × 10 ⁻⁴	8.21 × 10 ⁻³	7.44 × 10⁻⁴
60A40W	-	4.52 × 10 ⁻⁴	0	1.96 × 10⁻²
60A40W	-	4.52 × 10 ⁻⁴	0	1.94 × 10⁻²
60A40W	piperidine	4.52 × 10 ⁻⁴	4.46 × 10 ⁻¹	1.28 × 10 ⁻²
90AN10W	-	2.48 × 10 ⁻⁴	0	8.37 × 10⁻⁴
90AN10W	piperidine	2.48 × 10 ⁻⁴	1.48 × 10 ⁻²	7.97 × 10 ⁻⁴
80AN20W	-	5.55 × 10 ⁻⁴	0	6.86 × 10⁻³
80AN20W	piperidine	5.55 × 10 ⁻⁴	1.40 × 10 ⁻²	6.70 × 10 ⁻³
80AN20W	piperidine	5.55 × 10 ⁻⁴	3.80 × 10 ⁻²	6.51 × 10 ⁻³
60AN40W	-	2.78 × 10 ⁻⁴	0	6.33 × 10⁻²
60AN40W	-	2.78 × 10 ⁻⁴	0	6.30 × 10⁻²
60AN40W	piperidine	2.78 × 10 ⁻⁴	2.90 × 10 ⁻²	6.00 × 10 ⁻²

Solvolyses of **1a-Br** in 90% aq acetone (90A10W)

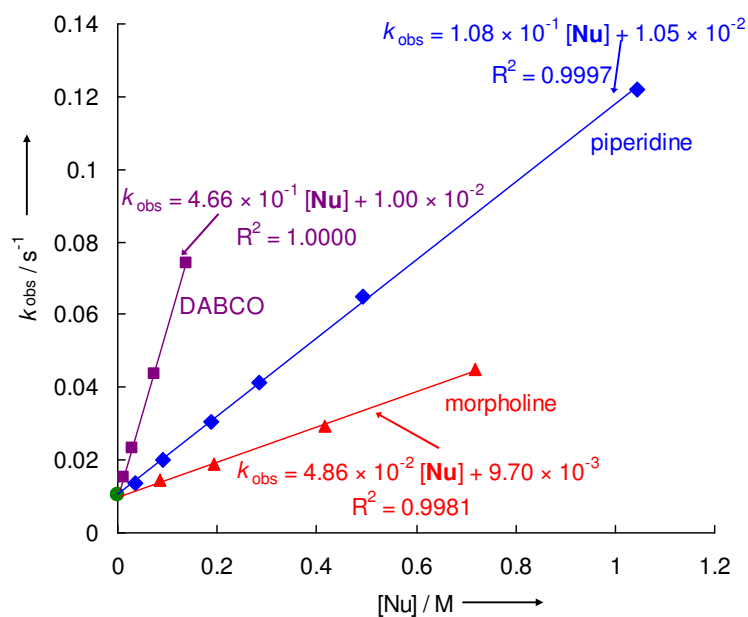
amine	[1a-Br] ₀ / M	[amine] / M	<i>k</i> _{obs} / s ⁻¹
-	4.57 × 10 ⁻⁴	-	1.35 × 10⁻³
morpholine	4.47 × 10 ⁻⁴	7.22 × 10 ⁻²	4.59 × 10 ⁻³
morpholine	4.50 × 10 ⁻⁴	1.54 × 10 ⁻¹	8.25 × 10 ⁻³
morpholine	4.50 × 10 ⁻⁴	2.28 × 10 ⁻¹	1.16 × 10 ⁻²
morpholine	4.50 × 10 ⁻⁴	3.00 × 10 ⁻¹	1.48 × 10 ⁻²
piperidine	4.57 × 10 ⁻⁴	1.60 × 10 ⁻²	3.16 × 10 ⁻³
piperidine	4.56 × 10 ⁻⁴	3.47 × 10 ⁻²	4.99 × 10 ⁻³
piperidine	4.55 × 10 ⁻⁴	5.08 × 10 ⁻²	6.57 × 10 ⁻³
piperidine	4.49 × 10 ⁻⁴	1.74 × 10 ⁻¹	1.93 × 10 ⁻²
piperidine	4.43 × 10 ⁻⁴	3.22 × 10 ⁻¹	3.60 × 10 ⁻²
DABCO	4.50 × 10 ⁻⁴	2.75 × 10 ⁻²	1.43 × 10 ⁻²
DABCO	4.50 × 10 ⁻⁴	5.70 × 10 ⁻²	2.90 × 10 ⁻²
DABCO	4.50 × 10 ⁻⁴	8.96 × 10 ⁻²	4.47 × 10 ⁻²
DABCO	4.50 × 10 ⁻⁴	1.12 × 10 ⁻¹	5.65 × 10 ⁻²



amine	<i>k</i> ₂ / M ⁻¹ s ⁻¹	<i>k</i> _{1ψ} / s ⁻¹
-	-	1.35 × 10 ⁻³
morpholine	4.49 × 10 ⁻²	1.35 × 10 ⁻³
piperidine	1.07 × 10 ⁻¹	1.19 × 10 ⁻³
DABCO	4.97 × 10 ⁻¹	5.89 × 10 ⁻⁴

Solvolyses of **1a-Br** in 80% aq acetone (80A20W)

amine	[1a-Br] ₀ / M	[amine] / M	<i>k</i> _{obs} / s ⁻¹
-	4.67 × 10 ⁻⁴	0	1.03 × 10⁻²
morpholine	4.29 × 10 ⁻⁴	8.50 × 10 ⁻²	1.44 × 10 ⁻²
morpholine	4.24 × 10 ⁻⁴	1.93 × 10 ⁻¹	1.88 × 10 ⁻²
morpholine	4.16 × 10 ⁻⁴	4.18 × 10 ⁻¹	2.93 × 10 ⁻²
morpholine	4.05 × 10 ⁻⁴	7.18 × 10 ⁻¹	4.50 × 10 ⁻²
piperidine	4.65 × 10 ⁻⁴	3.45 × 10 ⁻²	1.38 × 10 ⁻²
piperidine	4.63 × 10 ⁻⁴	9.15 × 10 ⁻²	2.02 × 10 ⁻²
piperidine	4.58 × 10 ⁻⁴	1.87 × 10 ⁻¹	3.04 × 10 ⁻²
piperidine	4.54 × 10 ⁻⁴	2.86 × 10 ⁻¹	4.13 × 10 ⁻²
piperidine	4.44 × 10 ⁻⁴	4.93 × 10 ⁻¹	6.51 × 10 ⁻²
piperidine	4.19 × 10 ⁻⁴	1.04	1.22 × 10 ⁻¹
DABCO	4.17 × 10 ⁻⁴	1.15 × 10 ⁻²	1.54 × 10 ⁻²
DABCO	4.17 × 10 ⁻⁴	2.87 × 10 ⁻²	2.33 × 10 ⁻²
DABCO	4.17 × 10 ⁻⁴	7.21 × 10 ⁻²	4.37 × 10 ⁻²
DABCO	4.17 × 10 ⁻⁴	1.38 × 10 ⁻¹	7.43 × 10 ⁻²

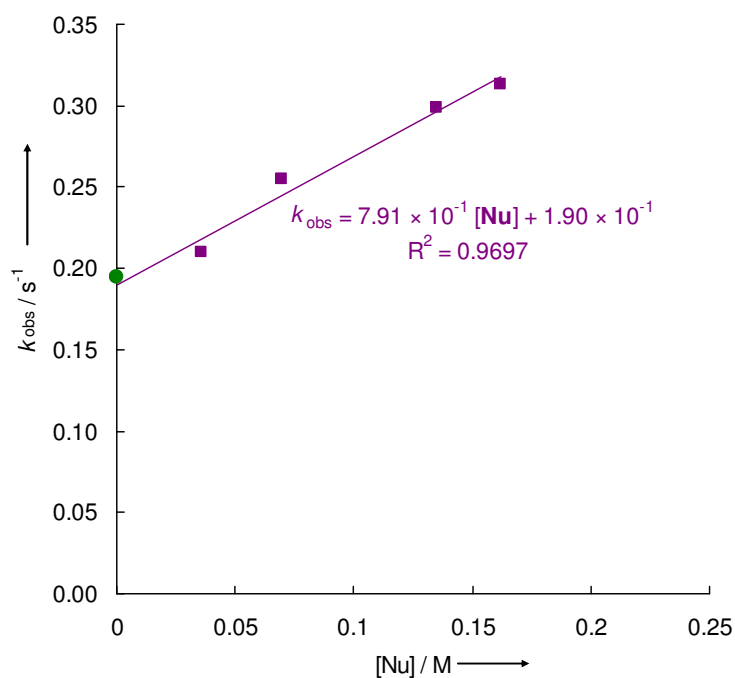


amine	<i>k</i> ₂ / M ⁻¹ s ⁻¹	<i>k</i> _{1ψ} / s ⁻¹
-	-	1.03 × 10 ⁻²
morpholine	4.86 × 10 ⁻²	9.70 × 10 ⁻³
piperidine	1.08 × 10 ⁻¹	1.05 × 10 ⁻²
DABCO	4.66 × 10 ⁻¹	1.00 × 10 ⁻²

Solvolyses of **1a-Br** in 60% aq acetone (60A40W)

amine	[1a-Br] ₀ / M	[amine] / M	$k_{\text{obs}} / \text{s}^{-1}$
-	6.60×10^{-4}	-	1.95×10^{-1}
DABCO	5.39×10^{-4}	3.59×10^{-2}	2.10×10^{-1}
DABCO	5.39×10^{-4}	6.98×10^{-2}	2.55×10^{-1a}
DABCO	5.39×10^{-4}	1.35×10^{-1}	2.99×10^{-1a}
DABCO	5.39×10^{-4}	1.62×10^{-1}	3.13×10^{-1a}

^a The precision in determination of k_{obs} is low due to the technical limits of the conventional conductimetry (the reaction times are close to the lower time limit of the method).

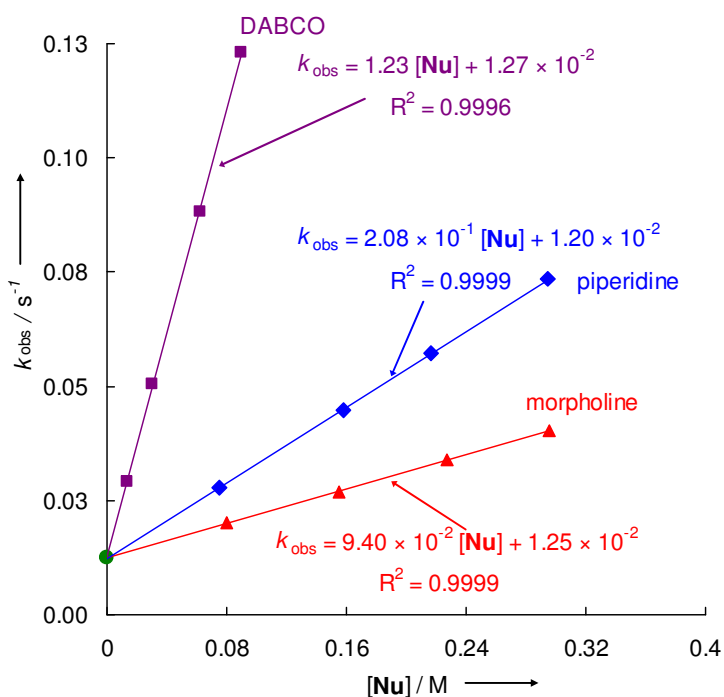


amine	$k_2 / \text{M}^{-1}\text{s}^{-1}$	$k_{1\psi} / \text{s}^{-1}$
-	-	1.95×10^{-1}
DABCO	$(7.91 \times 10^{-1})^a$	$(1.90 \times 10^{-1})^a$

^a An estimated value.

Solvolyses of **1a-Br** in 90% aq acetonitrile (90AN10W)

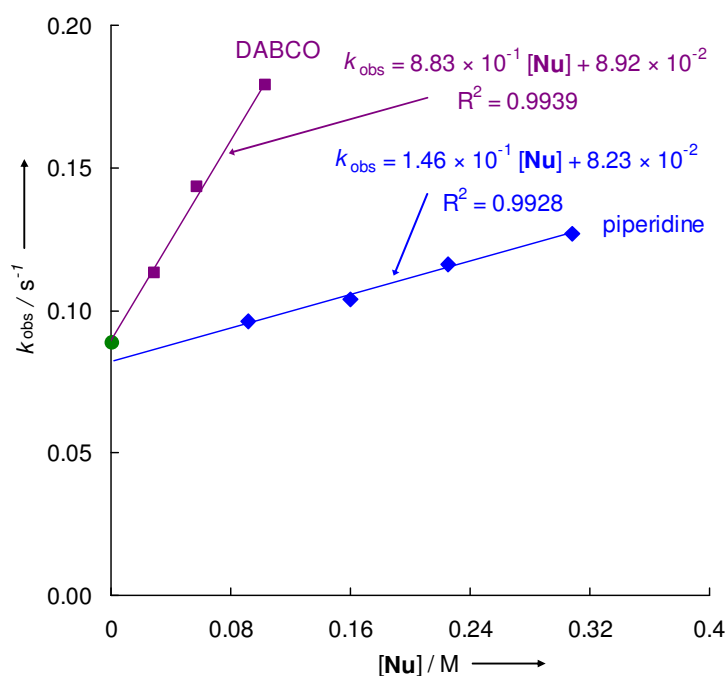
amine	[1a-Br] ₀ / M	[amine] / M	<i>k</i> _{obs} / s ⁻¹
-	4.50 × 10 ⁻⁴	-	1.26 × 10⁻²
morpholine	4.47 × 10 ⁻⁴	7.99 × 10 ⁻²	2.01 × 10 ⁻²
morpholine	4.44 × 10 ⁻⁴	1.55 × 10 ⁻¹	2.70 × 10 ⁻²
morpholine	4.41 × 10 ⁻⁴	2.27 × 10 ⁻¹	3.38 × 10 ⁻²
morpholine	4.39 × 10 ⁻⁴	2.96 × 10 ⁻¹	4.04 × 10 ⁻²
piperidine	4.47 × 10 ⁻⁴	7.56 × 10 ⁻²	2.79 × 10 ⁻²
piperidine	4.43 × 10 ⁻⁴	1.58 × 10 ⁻¹	4.46 × 10 ⁻²
piperidine	4.40 × 10 ⁻⁴	2.17 × 10 ⁻¹	5.72 × 10 ⁻²
piperidine	4.37 × 10 ⁻⁴	2.95 × 10 ⁻¹	7.34 × 10 ⁻²
DABCO	6.60 × 10 ⁻⁴	1.34 × 10 ⁻²	2.91 × 10 ⁻²
DABCO	6.60 × 10 ⁻⁴	3.02 × 10 ⁻²	5.04 × 10 ⁻²
DABCO	6.60 × 10 ⁻⁴	6.23 × 10 ⁻²	8.81 × 10 ⁻²
DABCO	6.60 × 10 ⁻⁴	8.94 × 10 ⁻²	1.23 × 10 ⁻¹



amine	<i>k</i> ₂ / M ⁻¹ s ⁻¹	<i>k</i> _{1ψ} / s ⁻¹
-	-	1.26 × 10 ⁻²
morpholine	9.40 × 10 ⁻²	1.25 × 10 ⁻²
piperidine	2.08 × 10 ⁻¹	1.20 × 10 ⁻²
DABCO	1.23	1.27 × 10 ⁻²

Solvolyses of **1a-Br** in 80% aq acetonitrile (80AN20W)

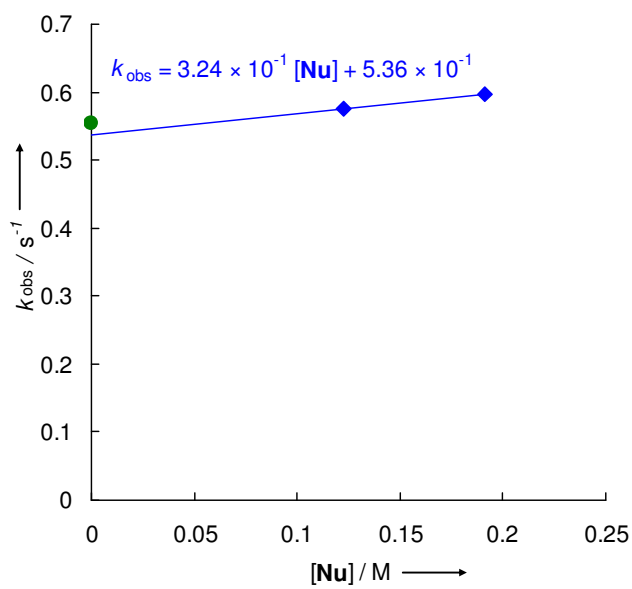
amine	[1a-Br] ₀ / M	[amine] / M	<i>k</i> _{obs} / s ⁻¹
-	6.60 × 10 ⁻⁴	-	8.83 × 10⁻²
piperidine	6.54 × 10 ⁻⁴	9.15 × 10 ⁻²	9.63 × 10 ⁻²
piperidine	3.25 × 10 ⁻⁴	1.60 × 10 ⁻¹	1.04 × 10 ⁻¹
piperidine	3.23 × 10 ⁻⁴	2.25 × 10 ⁻¹	1.16 × 10 ⁻¹
piperidine	3.21 × 10 ⁻⁴	3.08 × 10 ⁻¹	1.27 × 10 ⁻¹
DABCO	6.60 × 10 ⁻⁴	2.90 × 10 ⁻²	1.13 × 10 ⁻¹
DABCO	6.60 × 10 ⁻⁴	5.76 × 10 ⁻²	1.43 × 10 ⁻¹
DABCO	6.60 × 10 ⁻⁴	1.03 × 10 ⁻¹	1.79 × 10 ⁻¹



amine	<i>k</i> ₂ / M ⁻¹ s ⁻¹	<i>k</i> _{1ψ} / s ⁻¹
-	-	8.83 × 10 ⁻²
piperidine	1.46 × 10 ⁻¹	8.23 × 10 ⁻²
DABCO	8.83 × 10 ⁻¹	8.92 × 10 ⁻²

Solvolyses of **1a-Br** in 60% aq acetonitrile (60AN40W)

amine	[1a-Br] ₀ / M	[amine] / M	$k_{\text{obs}} / \text{s}^{-1}$
-	4.91×10^{-3}	0	5.54×10^{-1}
piperidine	4.91×10^{-3}	1.23×10^{-1}	5.76×10^{-1}
piperidine	4.91×10^{-3}	1.91×10^{-1}	5.98×10^{-1}

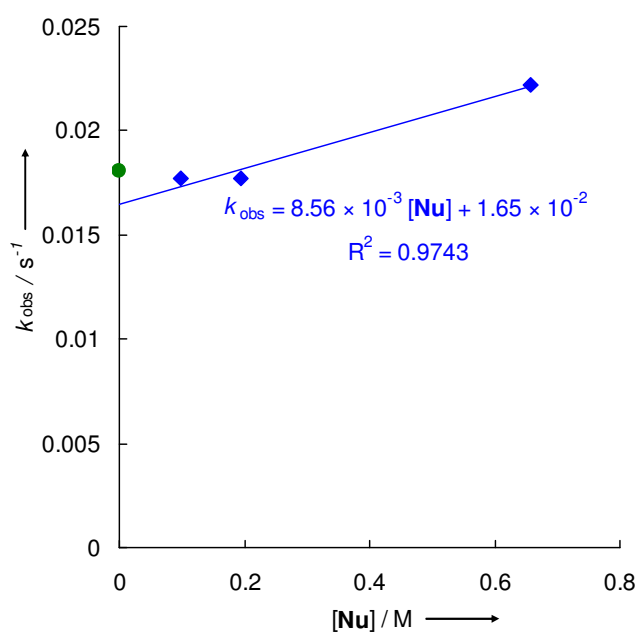


amine	$k_2 / \text{M}^{-1}\text{s}^{-1}$	$k_{1\psi} / \text{s}^{-1}$
-	-	5.54×10^{-1}
piperidine	$(3.24 \times 10^{-1})^a$	$(5.36 \times 10^{-1})^a$

^a An estimated value.

Solvolyses of 1a-Br in ethanol (100E)

amine	[1a-Br] ₀ / M	[amine] / M	k _{obs} / s ⁻¹
-	4.32 × 10 ⁻⁴	0	1.81 × 10⁻²
piperidine	4.28 × 10 ⁻⁴	9.80 × 10 ⁻²	1.77 × 10 ⁻²
piperidine	4.23 × 10 ⁻⁴	1.94 × 10 ⁻¹	1.77 × 10 ⁻²
piperidine	4.04 × 10 ⁻⁴	6.58 × 10 ⁻¹	2.22 × 10 ⁻²



nucleophile	k ₂ / M ⁻¹ s ⁻¹	k _{1ψ} / s ⁻¹
-	-	1.81 × 10 ⁻²
piperidine	(8.56 × 10 ⁻³) ^a	(1.65 × 10 ⁻²) ^a

^a An estimated value.

4.3.3. Solvolyses of 1b-LG

Solvolyses of 1b-ODNB in various solvents

solvent	base ^a	[1b-ODNB] ₀ / M	[base] / M	<i>k</i> _{obs} / s ⁻¹
80A20W	lutidine	1.92 × 10 ⁻⁴	6.20 × 10 ⁻³	1.05 × 10⁻⁵
80A20W	lutidine	2.30 × 10 ⁻⁴	4.65 × 10 ⁻³	1.04 × 10⁻⁵
60A40W	lutidine	2.00 × 10 ⁻⁴	2.86 × 10 ⁻³	7.30 × 10⁻⁵
60A40W	lutidine	2.00 × 10 ⁻⁴	2.86 × 10 ⁻³	7.31 × 10⁻⁵
60AN40W	lutidine	1.92 × 10 ⁻⁴	8.40 × 10 ⁻³	1.04 × 10⁻⁴
60AN40W	lutidine	1.92 × 10 ⁻⁴	7.29 × 10 ⁻³	1.02 × 10⁻⁴

^aAn excess of a Brønsted base (2,6-lutidine) was added to the reaction solution in order to achieve complete dissociation of the 3,5-dinitrobenzoic acid.

Solvolyses of 1b-Cl in various solvents

solvent	nucleophile	[Nu] / M	<i>k</i> _{obs} / s ⁻¹
90A10W	-	-	6.26 × 10 ⁻³
90A10W	piperidine	5.35 × 10 ⁻²	6.38 × 10⁻³
90A10W	piperidine	3.73 × 10 ⁻²	6.38 × 10 ⁻³
80A20W	-	-	9.95 × 10 ⁻²
80A20W	piperidine	2.68 × 10 ⁻²	9.94 × 10 ⁻²
80A20W	piperidine	6.08 × 10 ⁻²	9.96 × 10⁻²
60A40W	-	-	2.91
60A40W	-	-	2.90
60A40W	piperidine	2.78 × 10 ⁻¹	2.35
90AN10W	-	-	1.26 × 10⁻¹
90AN10W	-	-	1.31 × 10⁻¹
60AN40W	-	-	8.97
60AN40W	piperidine	1.47 × 10 ⁻²	8.97
60AN40W	piperidine	7.54 × 10 ⁻²	8.52
60AN40W	piperidine	1.51 × 10 ⁻¹	8.20
60AN40W	piperidine	2.46 × 10 ⁻¹	7.80

4.3.4. Solvolyses of 1c-LG

Solvolyses of 1c-OPNB in various solvents

solvent	nucleophile / base ^a	[1c-OPNB] ₀ / M	[Nu] ([base] ^a) / M	<i>k</i> _{obs} / s ⁻¹
60A40W	lutidine ^a	2.98 × 10 ⁻⁴	5.72 × 10 ⁻³	7.76 × 10⁻⁵
60A40W	DMAP	2.98 × 10 ⁻⁴	1.25 × 10 ⁻²	7.50 × 10 ⁻⁵
60A40W	DMAP	2.98 × 10 ⁻⁴	2.97 × 10 ⁻²	7.71 × 10 ⁻⁵
80AN20W	lutidine ^a	4.57 × 10 ⁻⁴	2.86 × 10 ⁻³	2.77 × 10⁻⁵
80AN20W	piperidine	4.57 × 10 ⁻⁴	6.09 × 10 ⁻³	3.19 × 10 ^{-5a}
60AN20W	lutidine ^a	2.94 × 10 ⁻⁴	5.72 × 10 ⁻³	9.04 × 10 ⁻⁵
60AN40W	piperidine	2.92 × 10 ⁻⁴	5.45 × 10 ⁻²	1.26 × 10 ^{-4b}
60AN40W	<i>n</i> -butylamine	2.92 × 10 ⁻⁴	7.95 × 10 ⁻²	1.18 × 10⁻⁴
60AN40W	<i>n</i> -butylamine	2.91 × 10 ⁻⁴	1.02 × 10 ⁻¹	1.10 × 10 ⁻⁴

^aAn excess of a Brønsted base (2,6-lutidine) was added to a reaction solution in order to achieve complete dissociation of the 4-nitrobenzoic acid. ^bNon-monoexponential increase.

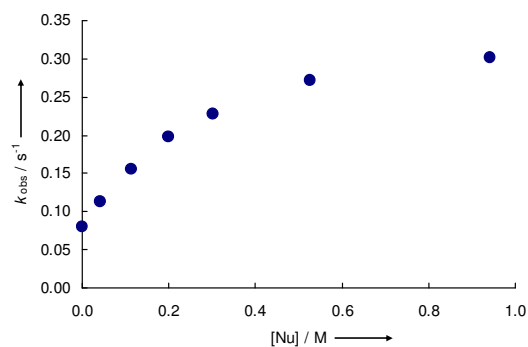
Solvolyses of 1c-ODNB in various solvents

solvent	base	[1c-ODNB] ₀ / M	[base] / M	<i>k</i> _{obs} / s ⁻¹
90A10W	lutidine	7.71 × 10 ⁻⁵	2.97 × 10 ⁻²	2.68 × 10⁻⁵
90A10W	lutidine	2.77 × 10 ⁻⁵	2.86 × 10 ⁻³	2.35 × 10 ⁻⁵
60A40W	lutidine	7.76 × 10 ⁻⁵	5.72 × 10 ⁻³	1.06 × 10⁻³
60A40W	lutidine	7.50 × 10 ⁻⁵	1.25 × 10 ⁻²	1.10 × 10⁻³

Solvolyses of 1c-Cl in 90% aq acetone (90A10W)

Nu	[1c-Cl] ₀ / M	[Nu] / M	<i>k</i> _{obs} / s ⁻¹
DMAP	6.96 × 10 ⁻³	0	8.03 × 10 ⁻²
DMAP	6.96 × 10 ⁻³	4.05 × 10 ⁻²	1.13 × 10 ^{-1a}
DMAP	6.96 × 10 ⁻³	1.14 × 10 ⁻¹	1.55 × 10 ^{-1a}
DMAP	6.96 × 10 ⁻³	2.00 × 10 ⁻¹	1.98 × 10 ^{-1a}
DMAP	6.96 × 10 ⁻³	3.03 × 10 ⁻¹	2.28 × 10 ^{-1a}
DMAP	6.96 × 10 ⁻³	5.27 × 10 ⁻¹	2.72 × 10 ^{-1a}
DMAP	6.96 × 10 ⁻³	9.41 × 10 ⁻¹	3.01 × 10⁻¹

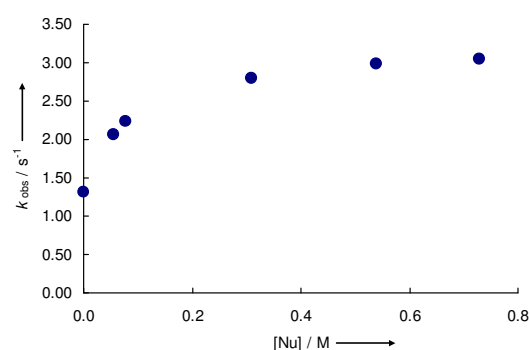
^a *k*_{obs} was obtained from the "best fit" of the nonexponential curve to a monoexponential function.



Solvolyses of 1c-Cl in 80% aq acetone (80A20W)

Nu	[1c-Cl] ₀ / M	[Nu] / M	<i>k</i> _{obs} / s ⁻¹
DMAP	6.96 × 10 ⁻³	0	1.31 ^a
DMAP	6.96 × 10 ⁻³	5.63 × 10 ⁻²	2.07 ^a
DMAP	6.96 × 10 ⁻³	7.84 × 10 ⁻²	2.23 ^a
DMAP	6.96 × 10 ⁻³	3.08 × 10 ⁻¹	2.80 ^a
DMAP	6.96 × 10 ⁻³	5.39 × 10 ⁻¹	2.99
DMAP	6.96 × 10 ⁻³	7.28 × 10 ⁻¹	3.04

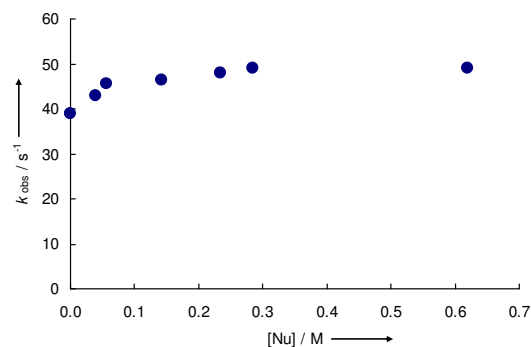
^a *k*_{obs} was obtained from the "best fit" of the nonexponential curve to a monoexponential function.



Solvolyses of 1c-Cl in 60% aq acetone (60A40W).

Nu	[1c-Cl] ₀ / M	[Nu] / M	<i>k</i> _{obs} / s ⁻¹
DMAP	6.96 × 10 ⁻³	0	3.88 × 10 ^{1a}
DMAP	6.96 × 10 ⁻³	3.84 × 10 ⁻²	4.28 × 10 ^{1a}
DMAP	6.96 × 10 ⁻³	5.63 × 10 ⁻²	4.56 × 10 ¹
DMAP	6.96 × 10 ⁻³	1.42 × 10 ⁻¹	4.65 × 10 ¹
DMAP	6.96 × 10 ⁻³	2.34 × 10 ⁻¹	4.79 × 10 ¹
DMAP	6.96 × 10 ⁻³	2.85 × 10 ⁻¹	4.92 × 10¹
DMAP	6.96 × 10 ⁻³	6.20 × 10 ⁻¹	4.91 × 10 ¹

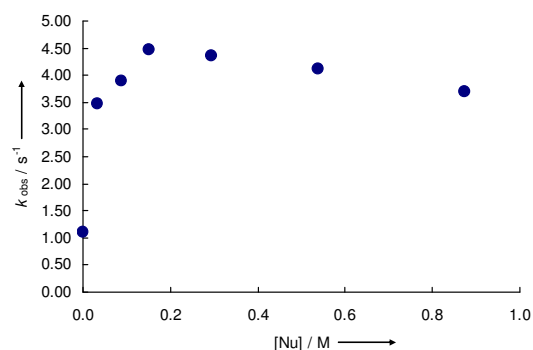
^a *k*_{obs} was obtained from the "best fit" of the nonexponential curve to a monoexponential function.



Solvolyses of **1c-Cl** in 90% aq acetonitrile (90AN10W)

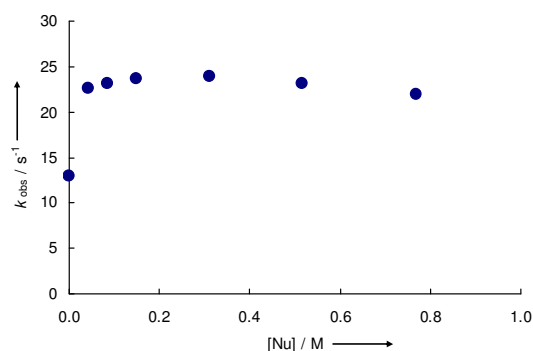
Nu	[1c-Cl] ₀ / M	[Nu] / M	<i>k</i> _{obs} / s ⁻¹
DMAP	6.96 × 10 ⁻³	0	1.11 ^a
DMAP	6.96 × 10 ⁻³	3.26 × 10 ⁻²	3.48 ^a
DMAP	6.96 × 10 ⁻³	8.87 × 10 ⁻²	3.90 ^a
DMAP	6.96 × 10 ⁻³	1.50 × 10 ⁻¹	4.47
DMAP	6.96 × 10 ⁻³	2.95 × 10 ⁻¹	4.36
DMAP	6.96 × 10 ⁻³	5.40 × 10 ⁻¹	4.11
DMAP	6.96 × 10 ⁻³	8.74 × 10 ⁻¹	3.69

^a *k*_{obs} was obtained from the "best fit" of the nonexponential curve to a monoexponential function.

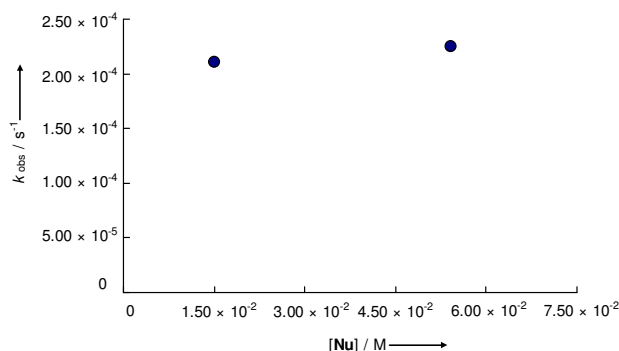
Solvolyses of **1c-Cl** in 80% aq acetonitrile (80AN20W)

Nu	[1c-Cl] ₀ / M	[Nu] / M	<i>k</i> _{obs} / s ⁻¹
DMAP	6.96 × 10 ⁻³	0	1.30 × 10 ^{1a}
DMAP	6.96 × 10 ⁻³	4.15 × 10 ⁻²	2.27 × 10 ^{1a}
DMAP	6.96 × 10 ⁻³	8.39 × 10 ⁻²	2.31 × 10 ¹
DMAP	6.96 × 10 ⁻³	1.48 × 10 ⁻¹	2.37 × 10 ¹
DMAP	6.96 × 10 ⁻³	3.10 × 10 ⁻¹	2.40 × 10¹
DMAP	6.96 × 10 ⁻³	5.16 × 10 ⁻¹	2.31 × 10 ¹
DMAP	6.96 × 10 ⁻³	7.69 × 10 ⁻¹	2.20 × 10 ¹

^a *k*_{obs} was obtained from the "best fit" of the nonexponential curve to a monoexponential function.

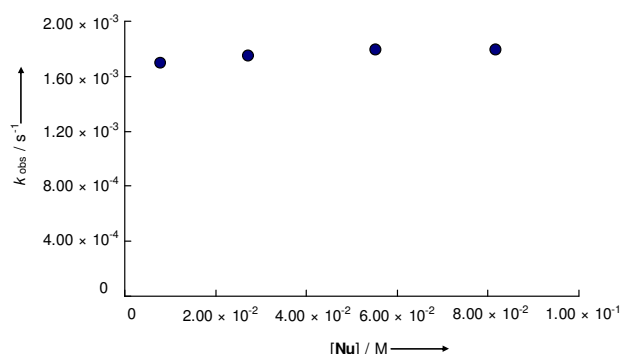
4.3.5. Solvolyses of **1d-LG**Solvolyses of **1d-ODNB** in 80% aq acetone (80A20W)

Nu	[1d-ODNB] ₀ / M	[Nu] / M	<i>k</i> _{obs} / s ⁻¹
DMAP	6.57 × 10 ⁻³	1.50 × 10 ⁻²	2.11 × 10 ⁻⁴
DMAP	6.57 × 10 ⁻³	5.42 × 10 ⁻²	2.30 × 10⁻⁴

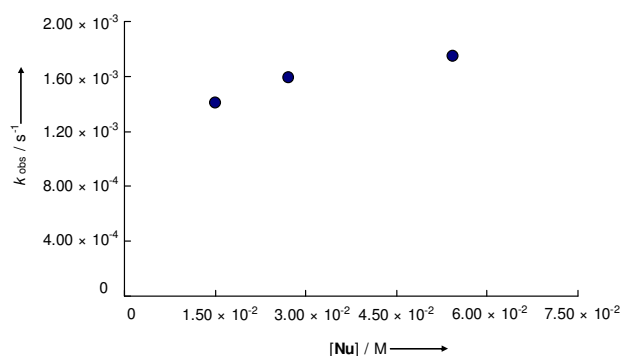


Solvolyses of **1d-ODNB** in 60% aq acetone (60A40W)

Nu	[1d-ODNB] ₀ / M	[Nu] / M	<i>k</i> _{obs} / s ⁻¹
DMAP	6.57 × 10 ⁻³	7.81 × 10 ⁻³	1.69 × 10 ⁻³
DMAP	6.57 × 10 ⁻³	2.72 × 10 ⁻²	1.75 × 10 ⁻³
DMAP	6.57 × 10 ⁻³	5.54 × 10 ⁻²	1.79 × 10⁻³
DMAP	6.57 × 10 ⁻³	8.17 × 10 ⁻²	1.79 × 10 ⁻³

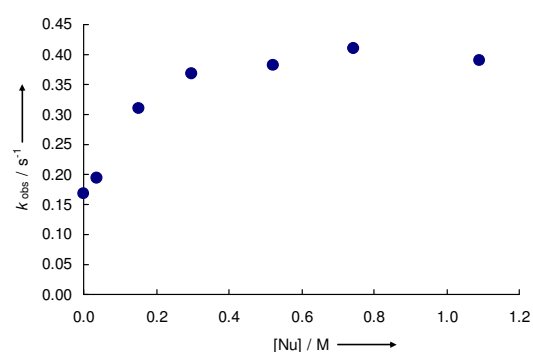
Solvolyses of **1d-ODNB** in 60% aq acetonitrile (60AN40W)

Nu	[1d-ODNB] ₀ / M	[Nu] / M	<i>k</i> _{obs} / s ⁻¹
DMAP	6.57 × 10 ⁻³	1.51 × 10 ⁻²	1.41 × 10 ⁻³
DMAP	6.57 × 10 ⁻³	2.72 × 10 ⁻²	1.59 × 10 ⁻³
DMAP	6.57 × 10 ⁻³	5.43 × 10 ⁻²	1.75 × 10⁻³

Solvolyses of **1d-Cl** in 90% aq acetone (90A10W)

Nu	[1d-Cl] ₀ / M	[Nu] / M	<i>k</i> _{obs} / s ⁻¹
-	1.02 × 10 ⁻²	0	1.68 × 10 ^{-1a}
DMAP	1.02 × 10 ⁻²	3.77 × 10 ⁻²	1.94 × 10 ^{-1a}
DMAP	1.02 × 10 ⁻²	1.52 × 10 ⁻¹	3.10 × 10 ^{-1a}
DMAP	1.02 × 10 ⁻²	2.98 × 10 ⁻¹	3.69 × 10 ^{-1a}
DMAP	1.02 × 10 ⁻²	5.23 × 10 ⁻¹	3.83 × 10 ⁻¹
DMAP	1.02 × 10 ⁻²	7.45 × 10 ⁻¹	4.10 × 10⁻¹
DMAP	1.02 × 10 ⁻²	1.09	3.90 × 10 ⁻¹

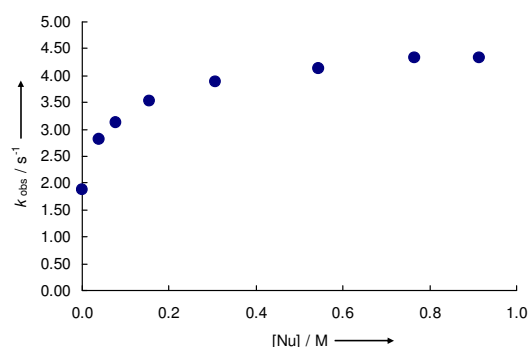
^a *k*_{obs} was obtained from the "best fit" of the nonexponential curve to a monoexponential function.



Solvolyses of **1d-Cl** in 80% aq acetone (80A20W)

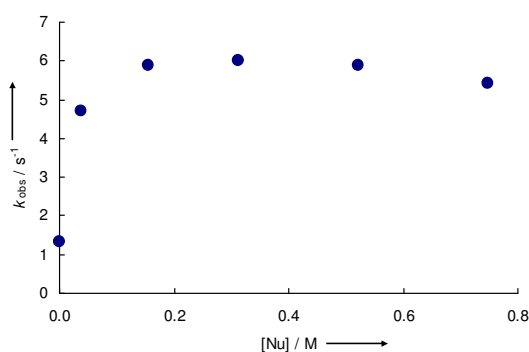
Nu	[1d-Cl] ₀ / M	[Nu] / M	<i>k</i> _{obs} / s ⁻¹
DMAP	1.02 × 10 ⁻²	0	1.87 ^a
DMAP	1.02 × 10 ⁻²	3.87 × 10 ⁻²	2.82 ^a
DMAP	1.02 × 10 ⁻²	7.87 × 10 ⁻²	3.13 ^a
DMAP	1.02 × 10 ⁻²	1.53 × 10 ⁻¹	3.52 ^a
DMAP	1.02 × 10 ⁻²	3.06 × 10 ⁻¹	3.89 ^a
DMAP	1.02 × 10 ⁻²	5.43 × 10 ⁻¹	4.12 ^a
DMAP	1.02 × 10 ⁻²	7.65 × 10 ⁻¹	4.34
DMAP	1.02 × 10 ⁻²	9.14 × 10 ⁻¹	4.33

^a *k*_{obs} was obtained from the "best fit" of the nonexponential curve to a monoexponential function

Solvolyses of **1d-Cl** in 90% aq acetonitrile (90AN10W)

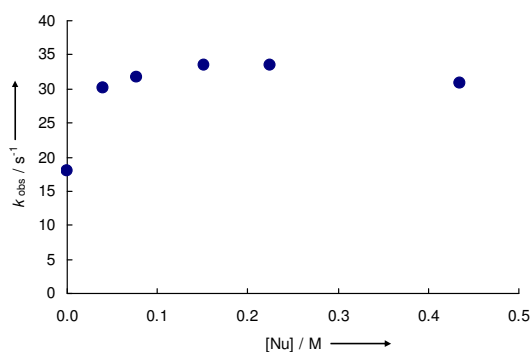
Nu	[1d-Cl] ₀ / M	[Nu] / M	<i>k</i> _{obs} / s ⁻¹
-	1.01 × 10 ⁻²	0	1.34 ^a
DMAP	1.01 × 10 ⁻²	3.78 × 10 ⁻²	4.70 ^a
DMAP	1.01 × 10 ⁻²	1.56 × 10 ⁻¹	5.88
DMAP	1.01 × 10 ⁻²	3.11 × 10 ⁻¹	6.01
DMAP	1.01 × 10 ⁻²	5.21 × 10 ⁻¹	5.88
DMAP	1.01 × 10 ⁻²	7.47 × 10 ⁻¹	5.42

^a *k*_{obs} was obtained from the "best fit" of the nonexponential curve to a monoexponential function.

Solvolyses of **1d-Cl** in 80% aq acetonitrile (80AN20W)

Nu	[1d-Cl] ₀ / M	[Nu] / M	<i>k</i> _{obs} / s ⁻¹
-	1.01 × 10 ⁻²	0	1.80 × 10 ^{1a}
DMAP	1.01 × 10 ⁻²	3.99 × 10 ⁻²	3.02 × 10 ^{1a}
DMAP	1.01 × 10 ⁻²	7.77 × 10 ⁻²	3.17 × 10 ¹
DMAP	1.01 × 10 ⁻²	1.52 × 10 ⁻¹	3.34 × 10¹
DMAP	1.01 × 10 ⁻²	2.25 × 10 ⁻¹	3.34 × 10 ¹
DMAP	1.01 × 10 ⁻²	4.35 × 10 ⁻¹	3.09 × 10 ¹

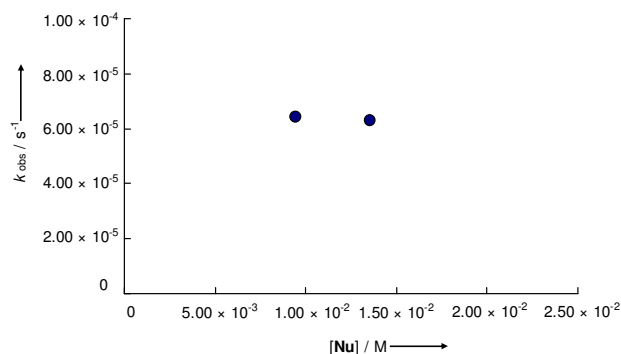
^a *k*_{obs} was obtained from the "best fit" of the nonexponential curve to a monoexponential function.



4.3.6. Solvolyses of 1e-LG

Solvolyses of 1e-OPNB in 80% aq acetone (80A20W)

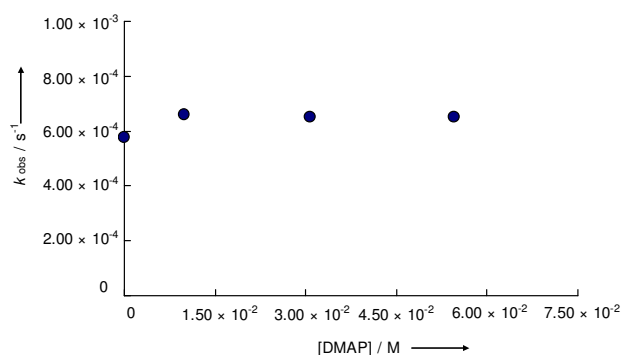
Nu	[Nu] / M	$k_{\text{obs}} / \text{s}^{-1}$
DMAP	9.49×10^{-3}	6.40×10^{-5}
DMAP	1.36×10^{-2}	6.29×10^{-5}



Solvolyses of 1e-OPNB in 60% aq acetone (60A40W)

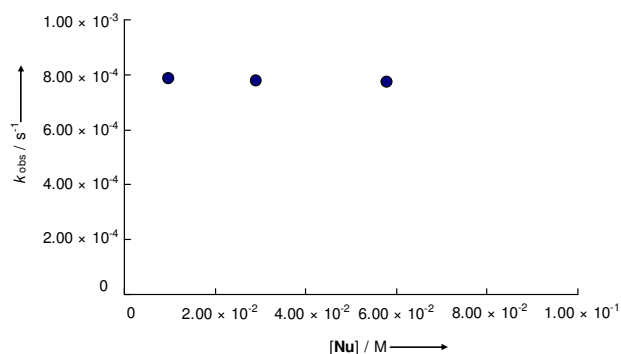
Nu/base	[Nu] / M	$k_{\text{obs}} / \text{s}^{-1}$
lutidine ^a	0	5.76×10^{-4}
DMAP	9.87×10^{-3}	6.59×10^{-4}
DMAP	3.08×10^{-2}	6.51×10^{-4}
DMAP	5.46×10^{-2}	6.51×10^{-4}

^aAn excess of a Brønsted base (2,6-lutidine, 2.86×10^{-3} M) was added to a reaction solution in order to achieve the complete dissociation of the 4-nitrobenzoic acid. As demonstrated in ref 8, efficiency of 2,6-lutidine as carbocation trapping agent is low, so that reaction in the presence of this base can be treated as that "without addition of the nucleophile".



Solvolyses of 1e-OPNB in 60% aq acetonitrile (60AN40W)

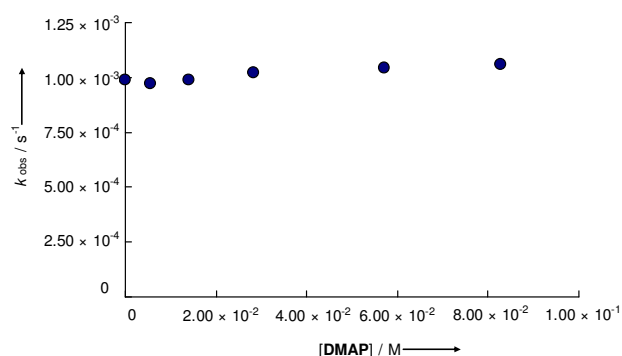
Nu	[Nu] / M	$k_{\text{obs}} / \text{s}^{-1}$
DMAP	9.68×10^{-3}	7.86×10^{-4}
DMAP	2.92×10^{-2}	7.78×10^{-4}
DMAP	5.80×10^{-2}	7.75×10^{-4}



Solvolyses of 1e-ODNB in 80% aq acetone (80A20W)

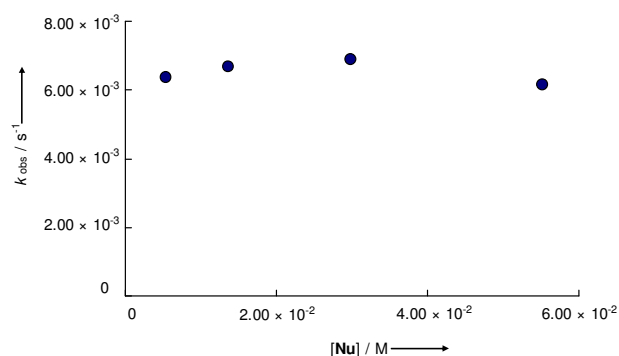
Nu/base	[Nu] / M	$k_{\text{obs}} / \text{s}^{-1}$
lutidine ^a	0	9.88×10^{-4}
DMAP	5.53×10^{-3}	9.71×10^{-4}
DMAP	1.39×10^{-2}	9.89×10^{-4}
DMAP	2.84×10^{-2}	1.02×10^{-3}
DMAP	5.72×10^{-2}	1.04×10^{-3}
DMAP	8.29×10^{-2}	1.06×10^{-3}

^aAn excess of a Brønsted base (2,6-lutidine, 2.86×10^{-3} M) was added to a reaction solution in order to achieve the complete dissociation of the 3,5-dinitrobenzoic acid. As demonstrated in ref 8, efficiency of 2,6-lutidine as carbocation trapping agent is low, so that reaction in the presence of this base can be treated as that "in the absence of nucleophiles".



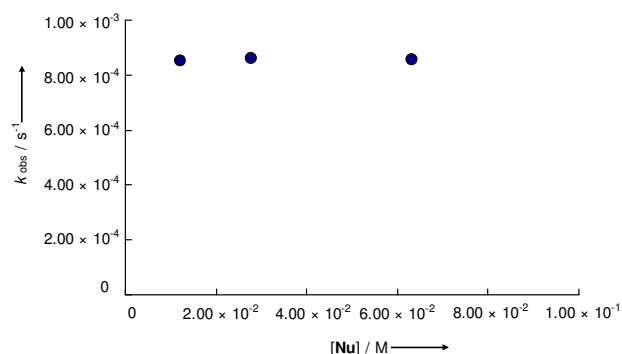
Solvolyses of 1e-ODNB in 60% aq acetone (60A40W)

Nu	[Nu] / M	$k_{\text{obs}} / \text{s}^{-1}$
DMAP	5.39×10^{-3}	6.37×10^{-3}
DMAP	1.36×10^{-2}	6.67×10^{-3}
DMAP	2.99×10^{-2}	6.87×10^{-3}
DMAP	5.53×10^{-2}	6.15×10^{-3}



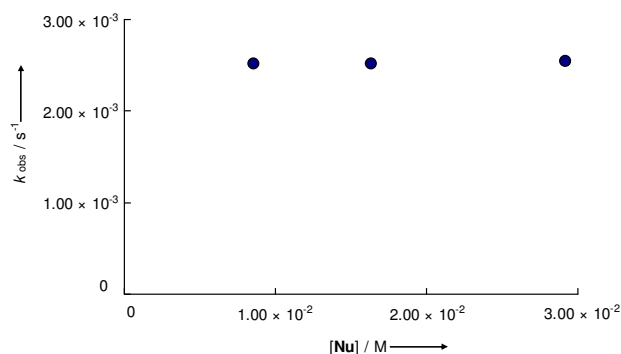
Solvolyses of 1e-ODNB in 90% aq acetonitrile (90AN10W)

Nu	[Nu] / M	$k_{\text{obs}} / \text{s}^{-1}$
DMAP	1.21×10^{-2}	8.52×10^{-4}
DMAP	2.77×10^{-2}	8.61×10^{-4}
DMAP	6.31×10^{-2}	8.58×10^{-4}

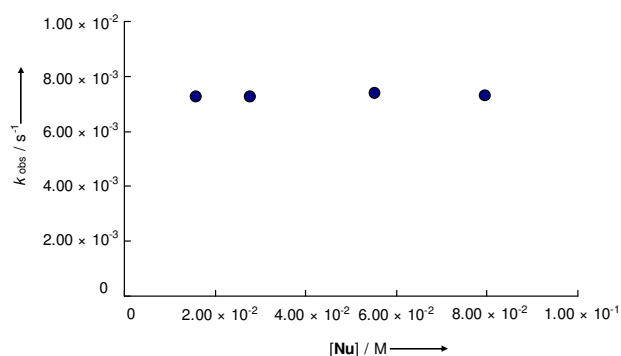


Solvolyses of **1e-ODNB** in 80% aq acetonitrile (80AN20W)

Nu	[Nu] / M	$k_{\text{obs}} / \text{s}^{-1}$
DMAP	8.59×10^{-3}	2.51×10^{-3}
DMAP	1.63×10^{-2}	2.52×10^{-3}
DMAP	2.92×10^{-2}	2.54×10^{-3}

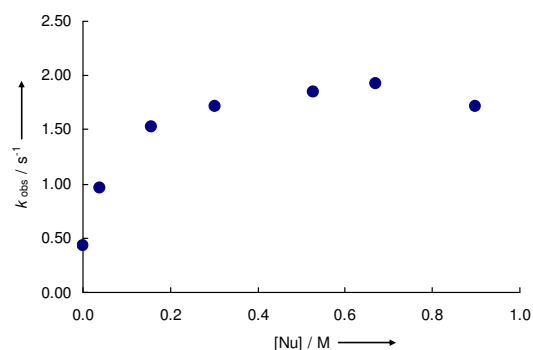
Solvolyses of **1e-ODNB** in 60% aq acetonitrile (60AN40W)

Nu	[Nu] / M	$k_{\text{obs}} / \text{s}^{-1}$
DMAP	1.60×10^{-2}	7.23×10^{-3}
DMAP	2.76×10^{-2}	7.24×10^{-3}
DMAP	5.53×10^{-2}	7.36×10^{-3}
DMAP	7.96×10^{-2}	7.31×10^{-3}

Solvolyses of **1e-Cl** in 90% aq acetone (90A10W)

Nu	[1e-Cl] ₀ / M	[Nu] / M	$k_{\text{obs}} / \text{s}^{-1}$
-	1.37×10^{-2}	0	4.32×10^{-1a}
DMAP	1.37×10^{-2}	3.80×10^{-2}	9.62×10^{-1a}
DMAP	1.37×10^{-2}	1.57×10^{-1}	1.53^a
DMAP	1.37×10^{-2}	3.02×10^{-1}	1.71^a
DMAP	1.37×10^{-2}	5.27×10^{-1}	1.85^a
DMAP	1.37×10^{-2}	6.69×10^{-1}	1.93
DMAP	1.37×10^{-2}	8.99×10^{-1}	1.72

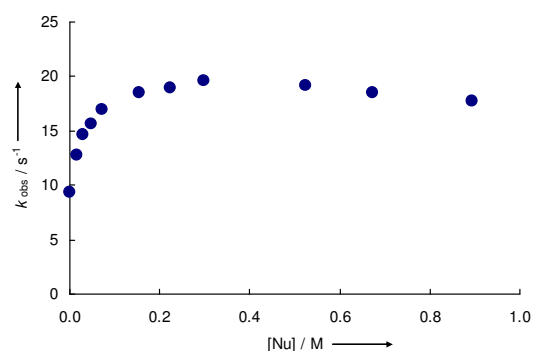
^a k_{obs} was obtained from the "best fit" of the nonexponential curve to a monoexponential function.



Solvolyses of 1e-Cl in 80% aq acetone (80A20W)

Nu	[1e-Cl] ₀ / M	[Nu] / M	<i>k</i> _{obs} / s ⁻¹
-	1.24 × 10 ⁻²	0	9.34 ^a
DMAP	1.24 × 10 ⁻²	1.55 × 10 ⁻²	1.28 × 10 ^{1a}
DMAP	1.24 × 10 ⁻²	3.05 × 10 ⁻²	1.47 × 10 ^{1a}
DMAP	1.24 × 10 ⁻²	4.78 × 10 ⁻²	1.57 × 10 ^{1a}
DMAP	1.24 × 10 ⁻²	7.23 × 10 ⁻²	1.70 × 10 ¹
DMAP	1.24 × 10 ⁻²	1.53 × 10 ⁻¹	1.85 × 10 ¹
DMAP	1.24 × 10 ⁻²	2.23 × 10 ⁻¹	1.89 × 10 ¹
DMAP	1.24 × 10 ⁻²	2.97 × 10 ⁻¹	1.96 × 10¹
DMAP	1.24 × 10 ⁻²	5.25 × 10 ⁻¹	1.92 × 10 ¹
DMAP	1.24 × 10 ⁻²	6.72 × 10 ⁻¹	1.86 × 10 ¹
DMAP	1.24 × 10 ⁻²	8.93 × 10 ⁻¹	1.78 × 10 ¹

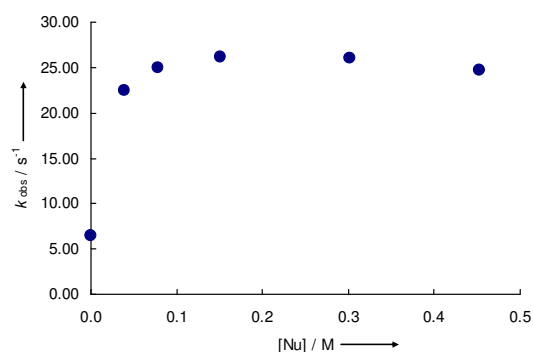
^a *k*_{obs} was obtained from the "best fit" of the nonexponential curve to a monoexponential function.



Solvolyses of 1e-Cl in 90% aq acetonitrile (90AN10W)

Nu	[1e-Cl] ₀ / M	[Nu] / M	<i>k</i> _{obs} / s ⁻¹
-	1.38 × 10 ⁻²	0	6.42 ^a
DMAP	1.38 × 10 ⁻²	3.85 × 10 ⁻²	2.25 × 10 ^{1a}
DMAP	1.38 × 10 ⁻²	7.86 × 10 ⁻²	2.50 × 10 ^{1a}
DMAP	1.38 × 10 ⁻²	1.51 × 10 ⁻¹	2.62 × 10¹
DMAP	1.38 × 10 ⁻²	3.01 × 10 ⁻¹	2.61 × 10 ¹
DMAP	1.38 × 10 ⁻²	4.52 × 10 ⁻¹	2.47 × 10 ¹

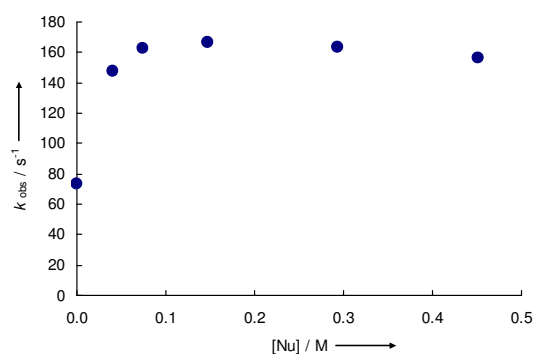
^a *k*_{obs} was obtained from the "best fit" of the nonexponential curve to a monoexponential function.



Solvolyses of 1e-Cl in 80% aq acetonitrile (80AN20W)

Nu	[1e-Cl] ₀ / M	[Nu] / M	<i>k</i> _{obs} / s ⁻¹
-	1.38 × 10 ⁻²	0	7.33 × 10 ^{1a}
DMAP	1.38 × 10 ⁻²	4.00 × 10 ⁻²	1.48 × 10 ^{2a}
DMAP	1.38 × 10 ⁻²	7.37 × 10 ⁻²	1.62 × 10 ²
DMAP	1.38 × 10 ⁻²	1.47 × 10 ⁻¹	1.66 × 10²
DMAP	1.38 × 10 ⁻²	2.93 × 10 ⁻¹	1.64 × 10 ²
DMAP	1.38 × 10 ⁻²	4.51 × 10 ⁻¹	1.57 × 10 ²

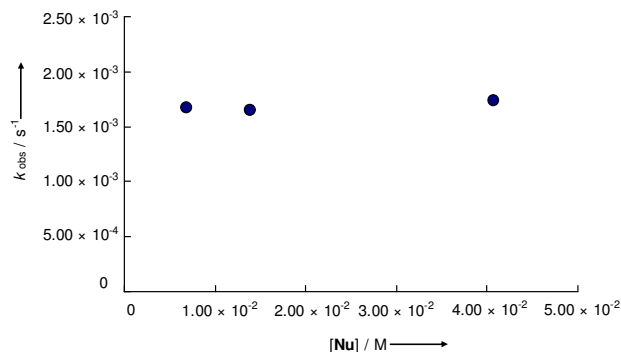
^a *k*_{obs} was obtained from the "best fit" of the nonexponential curve to a monoexponential function.



4.3.7. Solvolyses of 1f-LG

Solvolyses of 1f-OPNB in 80% aq acetone (80A20W)

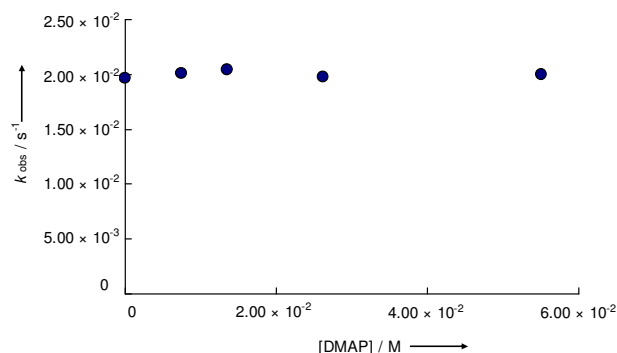
Nu	[1f-OPNB] ₀ / M	[Nu] / M	<i>k</i> _{obs} / s ⁻¹
DMAP	5.97 × 10 ⁻⁴	6.86 × 10 ⁻³	1.67 × 10 ⁻³
DMAP	5.97 × 10 ⁻⁴	1.39 × 10 ⁻²	1.65 × 10 ⁻³
DMAP	5.97 × 10 ⁻⁴	4.07 × 10 ⁻²	1.74 × 10⁻³



Solvolyses of 1f-OPNB in 60% aq acetone (60A40W)

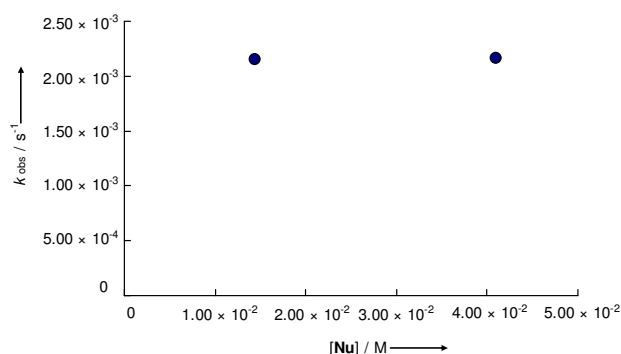
Nu/base	[1f-OPNB] ₀ / M	[Nu] / M	<i>k</i> _{obs} / s ⁻¹
lutidine ^a	5.97 × 10 ⁻⁴	0	1.93 × 10 ⁻²
DMAP	5.97 × 10 ⁻⁴	7.53 × 10 ⁻³	2.01 × 10 ⁻²
DMAP	5.97 × 10 ⁻⁴	1.35 × 10 ⁻²	2.04 × 10⁻²
DMAP	5.97 × 10 ⁻⁴	2.62 × 10 ⁻²	1.98 × 10 ⁻²
DMAP	5.97 × 10 ⁻⁴	5.51 × 10 ⁻²	2.00 × 10 ⁻²

^aAn excess of a Brønsted base (2,6-lutidine, 2.86 × 10⁻³ M) was added to a reaction solution in order to achieve the complete dissociation of the 4-nitrobenzoic acid. As demonstrated in ref 8, efficiency of 2,6-lutidine as carbocation trapping agent is low, so that reaction in the presence of this base can be treated as that "in the absence of nucleophiles".



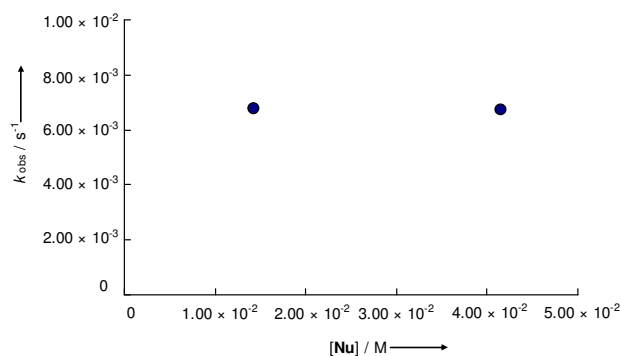
Solvolyses of 1f-OPNB in 90% aq acetonitrile (90AN10W)

Nu	[1f-OPNB] ₀ / M	[Nu] / M	<i>k</i> _{obs} / s ⁻¹
DMAP	6.03 × 10 ⁻⁴	1.44 × 10 ⁻²	2.15 × 10 ⁻³
DMAP	6.03 × 10 ⁻⁴	4.10 × 10 ⁻²	2.16 × 10⁻³



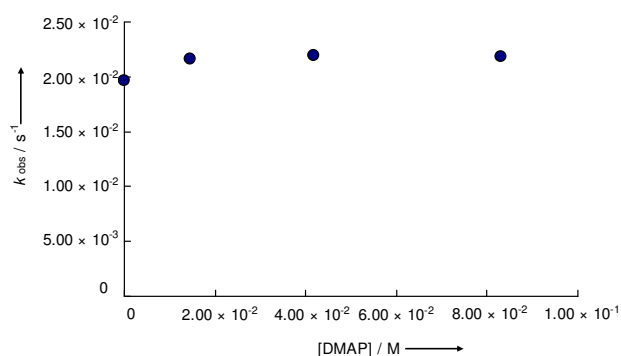
Solvolyses of **1f**-OPNB in 80% aq acetonitrile (80AN20W)

Nu	[1f -OPNB] ₀ / M	[Nu] / M	<i>k</i> _{obs} / s ⁻¹
DMAP	6.03 × 10 ⁻⁴	1.43 × 10 ⁻²	6.75 × 10⁻³
DMAP	6.03 × 10 ⁻⁴	4.16 × 10 ⁻²	6.74 × 10 ⁻³

Solvolyses of **1f**-OPNB in 60% aq acetonitrile (60AN40W)

Nu/base	[Nu] / M	<i>k</i> _{obs} / s ⁻¹
lutidine ^a	0	1.97 × 10 ⁻²
DMAP	1.46 × 10 ⁻²	2.16 × 10 ⁻²
DMAP	4.18 × 10 ⁻²	2.19 × 10⁻²
DMAP	8.30 × 10 ⁻²	2.18 × 10 ⁻²

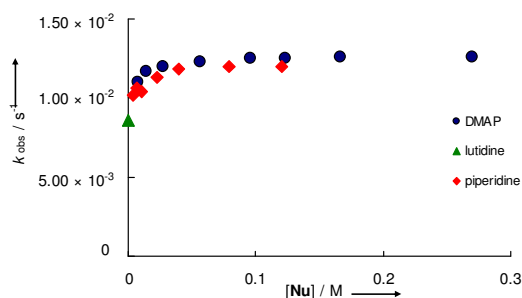
^aAn excess of a Brønsted base (2,6-lutidine, 2.86 × 10⁻³ M) was added to a reaction solution in order to achieve the complete dissociation of the 4-nitrobenzoic acid. As demonstrated in ref 8, efficiency of 2,6-lutidine as carbocation trapping agent is low, so that reaction in the presence of this base can be treated as that "in the absence of nucleophiles".



Solvolyses of **1f-ODNB** in 90% aq acetone (90A10W)

Nu/base	[1f-ODNB] ₀ / M	[Nu] / M	<i>k</i> _{obs} / s ⁻¹
lutidine ^a	5.41 × 10 ⁻⁴	0	8.63 × 10 ^{-3b}
DMAP	5.41 × 10 ⁻⁴	7.53 × 10 ⁻³	1.10 × 10 ^{-2b}
DMAP	5.41 × 10 ⁻⁴	1.39 × 10 ⁻²	1.17 × 10 ^{-2b}
DMAP	5.41 × 10 ⁻⁴	2.75 × 10 ⁻²	1.20 × 10 ⁻²
DMAP	5.41 × 10 ⁻⁴	5.63 × 10 ⁻²	1.23 × 10 ⁻²
DMAP	5.41 × 10 ⁻⁴	9.58 × 10 ⁻²	1.25 × 10 ⁻²
DMAP	5.41 × 10 ⁻⁴	1.23 × 10 ⁻¹	1.25 × 10 ⁻²
DMAP	5.41 × 10 ⁻⁴	1.66 × 10 ⁻¹	1.26 × 10⁻²
DMAP	5.41 × 10 ⁻⁴	2.70 × 10 ⁻¹	1.26 × 10 ⁻²
piperidine	6.10 × 10 ⁻⁴	3.42 × 10 ⁻³	1.02 × 10 ^{-2b}
piperidine	6.10 × 10 ⁻⁴	6.88 × 10 ⁻³	1.06 × 10 ^{-2b}
piperidine	6.10 × 10 ⁻⁴	1.04 × 10 ⁻²	1.04 × 10 ^{-2b}
piperidine	6.10 × 10 ⁻⁴	2.27 × 10 ⁻²	1.13 × 10 ⁻²
piperidine	6.10 × 10 ⁻⁴	3.97 × 10 ⁻²	1.18 × 10 ⁻²
piperidine	6.10 × 10 ⁻⁴	7.93 × 10 ⁻²	1.20 × 10 ⁻²
piperidine	6.10 × 10 ⁻⁴	1.20 × 10 ⁻¹	1.20 × 10 ⁻²

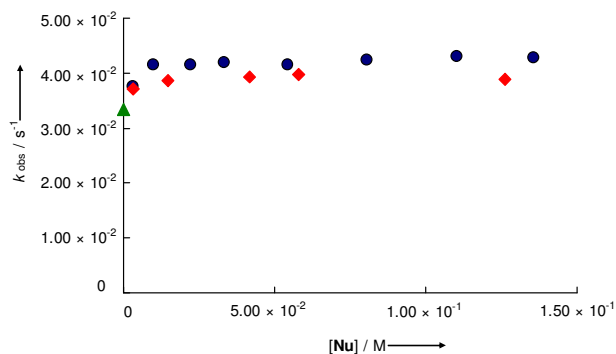
^aAn excess of a Brønsted base (2,6-lutidine, 2.86 × 10⁻³ M) was added to a reaction solution in order to achieve the complete dissociation of the 4-nitrobenzoic acid. As demonstrated in ref 8, efficiency of 2,6-lutidine as carbocation trapping agent is low, so that reaction in the presence of this base can be treated as that "in the absence of nucleophiles". ^b*k*_{obs} was obtained from the "best fit" of the nonexponential curve to a monoexponential function.



Solvolyses of 1f-ODNB in 80% aq acetone (80A20W)

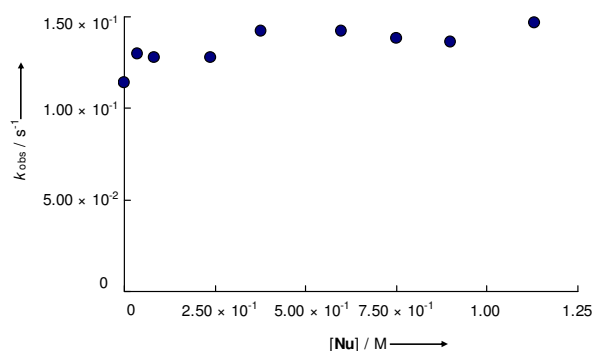
Nu	[1f-ODNB] ₀ / M	[Nu] / M	<i>k</i> _{obs} / s ⁻¹
lutidine ^a	4.33 × 10 ⁻⁴	0	3.34 × 10 ⁻²
DMAP	6.14 × 10 ⁻⁴	3.01 × 10 ⁻³	3.76 × 10 ⁻²
DMAP	6.14 × 10 ⁻⁴	1.01 × 10 ⁻²	4.15 × 10 ⁻²
DMAP	6.14 × 10 ⁻⁴	2.23 × 10 ⁻²	4.15 × 10 ⁻²
DMAP	6.14 × 10 ⁻⁴	3.33 × 10 ⁻²	4.20 × 10 ⁻²
DMAP	6.14 × 10 ⁻⁴	5.42 × 10 ⁻²	4.15 × 10 ⁻²
DMAP	6.14 × 10 ⁻⁴	8.07 × 10 ⁻²	4.24 × 10 ⁻²
DMAP	6.14 × 10 ⁻⁴	1.10 × 10 ⁻¹	4.30 × 10⁻²
DMAP	6.14 × 10 ⁻⁴	1.36 × 10 ⁻¹	4.27 × 10 ⁻²
piperidine	4.33 × 10 ⁻⁴	3.19 × 10 ⁻³	3.71 × 10 ⁻²
piperidine	4.33 × 10 ⁻⁴	1.47 × 10 ⁻²	3.87 × 10 ⁻²
piperidine	4.33 × 10 ⁻⁴	4.15 × 10 ⁻²	3.93 × 10 ⁻²
piperidine	4.33 × 10 ⁻⁴	5.80 × 10 ⁻²	3.98 × 10 ⁻²
piperidine	4.33 × 10 ⁻⁴	1.26 × 10 ⁻¹	3.89 × 10 ⁻²

^aAn excess of a Brønsted base (2,6-lutidine, 2.86 × 10⁻³ M) was added to a reaction solution in order to achieve the complete dissociation of the 4-nitrobenzoic acid. As demonstrated in ref 8, efficiency of 2,6-lutidine as carbocation trapping agent is low, so that reaction in the presence of this base can be treated as that "in the absence of nucleophiles".



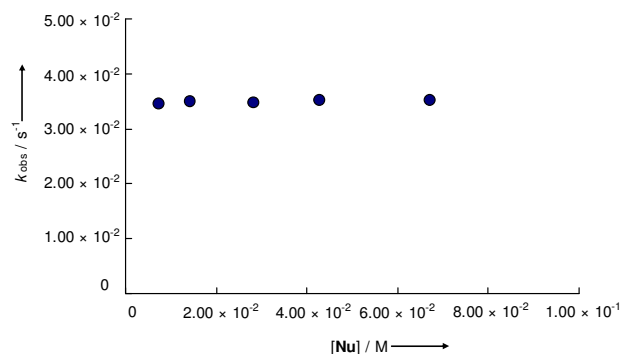
Solvolyses of 1f-ODNB in 60% aq acetone (60A40W)

Nu	[Nu] / M	<i>k</i> _{obs} / s ⁻¹
DMAP	0	1.14 × 10 ⁻¹
DMAP	3.71 × 10 ⁻²	1.30 × 10 ⁻¹
DMAP	8.37 × 10 ⁻²	1.28 × 10 ⁻¹
DMAP	2.38 × 10 ⁻¹	1.28 × 10 ⁻¹
DMAP	3.78 × 10 ⁻¹	1.42 × 10⁻¹
DMAP	5.99 × 10 ⁻¹	1.42 × 10 ⁻¹
DMAP	7.50 × 10 ⁻¹	1.38 × 10 ⁻¹
DMAP	8.99 × 10 ⁻¹	1.36 × 10 ⁻¹
DMAP	1.13	1.47 × 10 ⁻¹



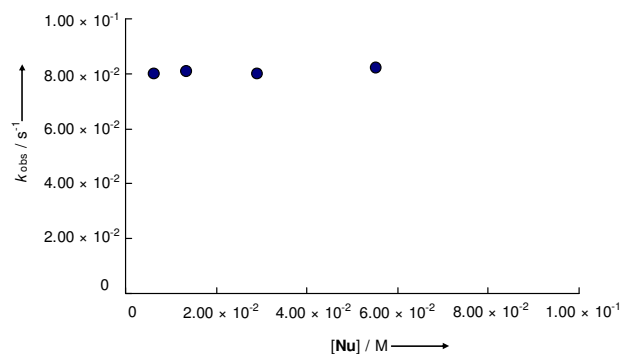
Solvolyses of 1f-ODNB in 90% aq acetonitrile (90AN10W)

Nu	[1f-ODNB] ₀ / M	[Nu] / M	<i>k</i> _{obs} / s ⁻¹
DMAP	5.87 × 10 ⁻⁴	7.32 × 10 ⁻³	3.44 × 10 ⁻²
DMAP	5.87 × 10 ⁻⁴	1.42 × 10 ⁻²	3.49 × 10 ⁻²
DMAP	5.87 × 10 ⁻⁴	2.84 × 10 ⁻²	3.47 × 10 ⁻²
DMAP	5.87 × 10 ⁻⁴	4.29 × 10 ⁻²	3.51 × 10⁻²
DMAP	5.87 × 10 ⁻⁴	6.72 × 10 ⁻²	3.51 × 10 ⁻²



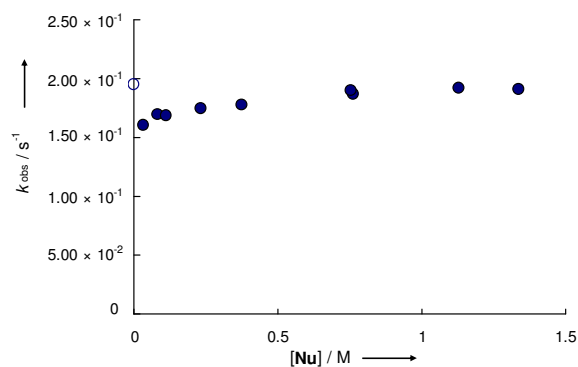
Solvolyses of 1f-ODNB in 80% aq acetonitrile (80AN20W)

Nu	[1f-ODNB] ₀ / M	[Nu] / M	<i>k</i> _{obs} / s ⁻¹
DMAP	5.87 × 10 ⁻⁴	6.32 × 10 ⁻³	7.98 × 10 ⁻²
DMAP	5.87 × 10 ⁻⁴	1.36 × 10 ⁻²	8.06 × 10 ⁻²
DMAP	5.87 × 10 ⁻⁴	2.91 × 10 ⁻²	7.99 × 10 ⁻²
DMAP	5.87 × 10 ⁻⁴	5.54 × 10 ⁻²	8.21 × 10⁻²



Solvolyses of 1f-ODNB in 60% aq acetonitrile (60AN40W)

Nu	[Nu] / M	<i>k</i> _{obs} / s ⁻¹
DMAP	0	1.95 × 10 ^{-1a}
DMAP	3.41 × 10 ⁻²	1.60 × 10 ⁻¹
DMAP	8.20 × 10 ⁻²	1.69 × 10 ⁻¹
DMAP	1.11 × 10 ⁻¹	1.68 × 10 ⁻¹
DMAP	2.35 × 10 ⁻¹	1.75 × 10 ⁻¹
DMAP	3.76 × 10 ⁻¹	1.78 × 10 ⁻¹
DMAP	7.56 × 10 ⁻¹	1.90 × 10 ⁻¹
DMAP	7.64 × 10 ⁻¹	1.87 × 10 ⁻¹
DMAP	1.13	1.92 × 10⁻¹
DMAP	1.34	1.91 × 10 ⁻¹



^a Non monoexponential kinetic

4.3.8. Solvolyses of **1g-LG**

Preparation of the stock solutions of 1g-LG: A solution of Bu₄NLG in dry CH₂Cl₂ was added portionwise to a solution of **1g-BF₄** in the same solvent until complete decolorization of the reaction mixture was achieved. The resulting solutions were used for solvolysis measurements without isolation of unstable **1g-LG** (as only very small volumes of stock solutions were dissolved in aqueous solvent during solvolytic studies (100 μL in 30 mL), the modification of the solvent properties caused by dichloromethane can be neglected).

LG	solvent	nucleophile / base	[1g-LG] ₀ / M	[Nu] / M	<i>k</i> _{obs} / s ⁻¹
OAc	80A20W	lutidine ^a	1.45 × 10 ⁻⁴	0	5.19 × 10⁻³
OAc	80A20W	lutidine ^a	1.45 × 10 ⁻⁴	0	5.11 × 10⁻³
OAc	80AN20W	lutidine ^a	1.45 × 10 ⁻⁴	0	1.23 × 10⁻²
OAc	80AN20W	lutidine ^a	1.45 × 10 ⁻⁴	0	1.21 × 10⁻²
OAc	60AN40W	lutidine ^a	1.45 × 10 ⁻⁴	0	6.93 × 10⁻²
OAc	60AN40W	lutidine ^a	1.45 × 10 ⁻⁴	0	6.86 × 10⁻²
OAc	60AN40W	piperidine	1.45 × 10 ⁻⁴	4.19 × 10 ⁻²	5.39 × 10 ⁻²
OAc	60AN40W	piperidine	1.45 × 10 ⁻⁴	6.98 × 10 ⁻²	5.36 × 10 ⁻²
OBz	80A20W	lutidine ^a	1.28 × 10 ⁻⁴	0	1.30 × 10⁻²
OBz	80A20W	lutidine ^a	1.28 × 10 ⁻⁴	0	1.33 × 10⁻²
OBz	80AN20W	lutidine ^a	1.28 × 10 ⁻⁴	0	2.92 × 10⁻²
OBz	80AN20W	lutidine ^a	1.28 × 10 ⁻⁴	0	3.02 × 10⁻²

^aAn excess of a Brønsted base (2,6-lutidine, 2.86 × 10⁻³ M) was added to a reaction solution in order to achieve the complete dissociation of the carboxylic acids. As demonstrated in ref 8, efficiency of 2,6-lutidine as carbocation trapping agent is low, so that reaction in the presence of this base can be treated as that "in the absence of nucleophiles".

4.3.9. Solvolyses of **1h**-LG

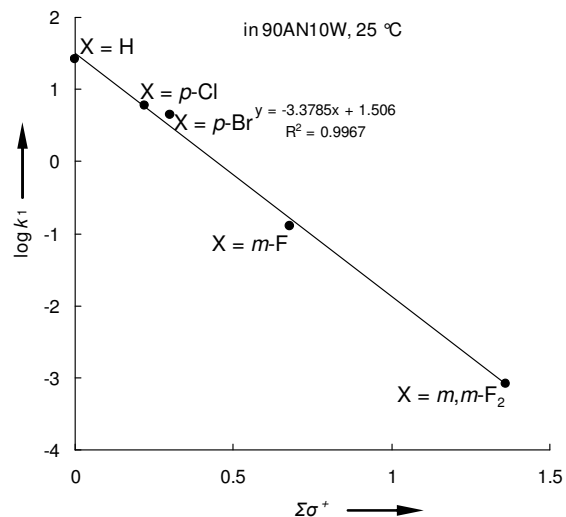
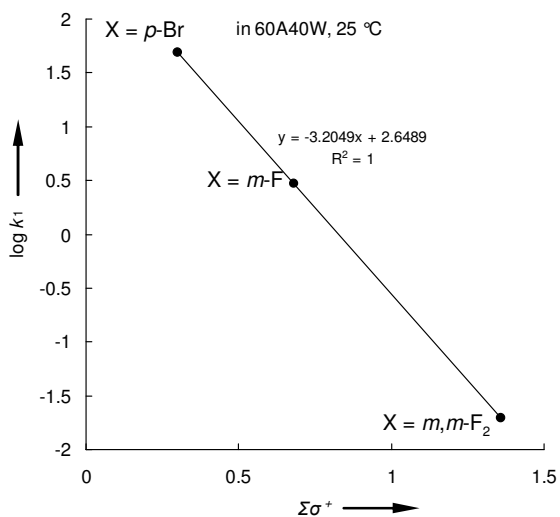
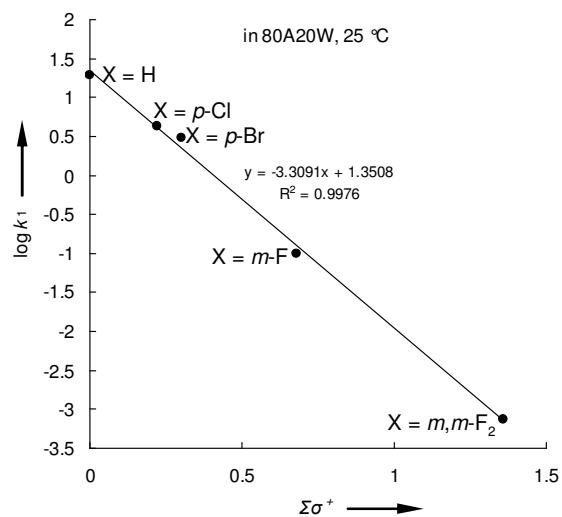
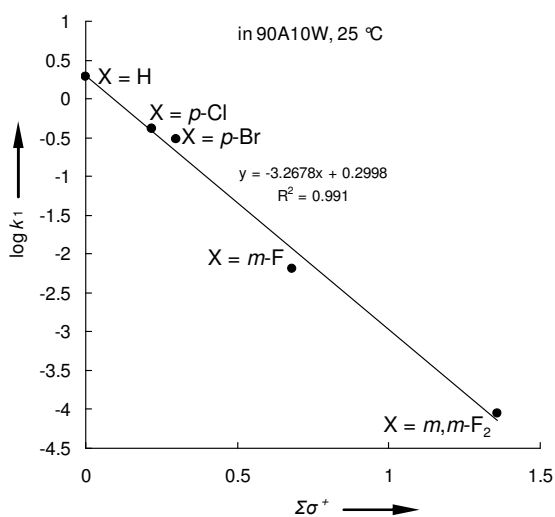
Preparation of the stock solutions of **1h-LG:** A solution of Bu₄NLG in dry acetone or acetonitrile was added to a solution of **1h**-BF₄ in the same solvent leading to the complete decolorization. The resulting solutions were mixed with aqueous acetone or acetonitrile in the stopped-flow device, so that the resulting water contents corresponded to those listed in the following table. The generation of colored cation **1h** was followed spectrophotometrically ($\lambda = 704$ nm).

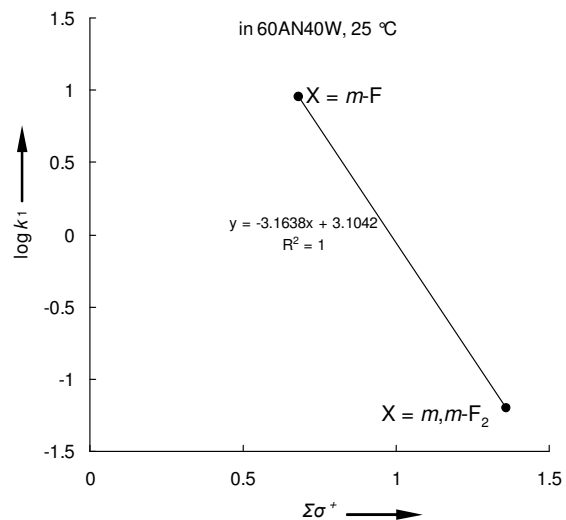
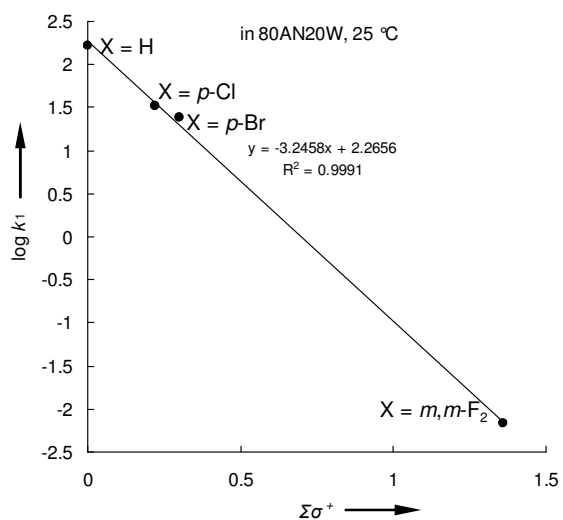
LG	solvent	[1h -BF ₄] / M	[Bu ₄ NOCOR] / M	$k_{\text{obs}} / \text{s}^{-1}$
OAc	80A20W	1.20×10^{-5}	3.50×10^{-4}	7.88×10^1
OAc	80A20W	1.20×10^{-5}	3.50×10^{-4}	7.81×10^1
OAc	80A20W	1.20×10^{-5}	7.00×10^{-4}	7.01×10^1
OAc	80A20W	1.20×10^{-5}	7.00×10^{-4}	6.84×10^1
OAc	60A40W	1.20×10^{-5}	3.50×10^{-4}	4.06×10^2
OAc	60A40W	1.20×10^{-5}	3.50×10^{-4}	4.35×10^2
OAc	80AN20W	1.20×10^{-5}	4.11×10^{-4}	1.49×10^2
OAc	80AN20W	1.20×10^{-5}	4.11×10^{-4}	1.46×10^2
OAc	80AN20W	1.20×10^{-5}	8.21×10^{-4}	1.52×10^2
OAc	80AN20W	1.20×10^{-5}	8.21×10^{-4}	1.46×10^2
OAc	60AN40W	1.20×10^{-5}	4.11×10^{-4}	2.69×10^2
OAc	60AN40W	1.20×10^{-5}	4.11×10^{-4}	2.43×10^2
OAc	60AN40W	1.20×10^{-5}	8.21×10^{-4}	2.85×10^2
OAc	60AN40W	1.20×10^{-5}	8.21×10^{-4}	2.79×10^2
OAc	60AN40W	1.20×10^{-5}	1.64×10^{-3}	2.82×10^2
OAc	60AN40W	1.20×10^{-5}	1.64×10^{-3}	2.76×10^2
OBz	80A20W	1.26×10^{-5}	8.21×10^{-4}	1.58×10^2
OBz	80A20W	1.26×10^{-5}	8.21×10^{-4}	1.56×10^2
OBz	60AN40W	1.26×10^{-5}	7.98×10^{-4}	3.26×10^2
OBz	60AN40W	1.26×10^{-5}	7.98×10^{-4}	3.35×10^2

5. Supplementary Section

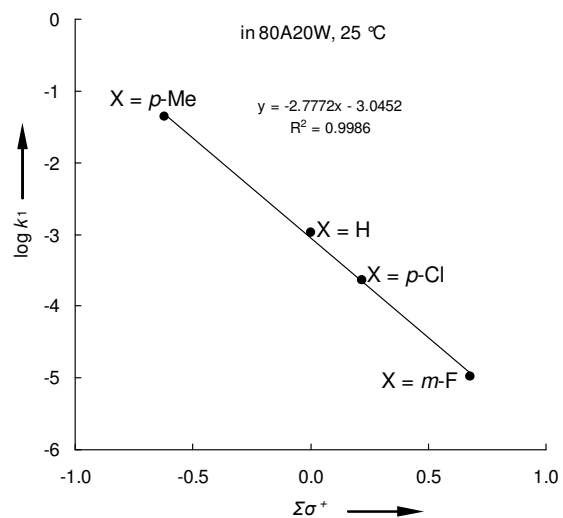
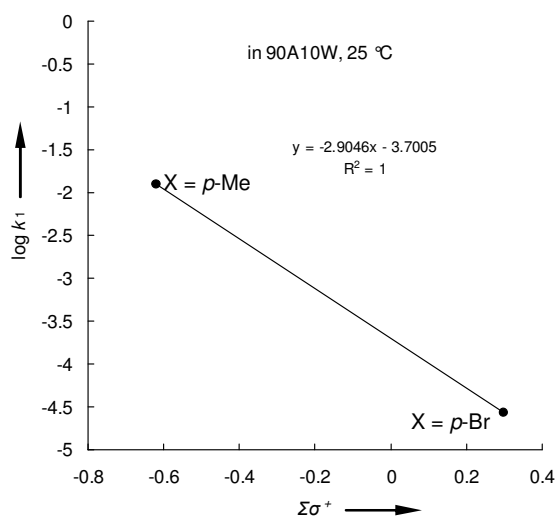
5.1. Hammett Correlations

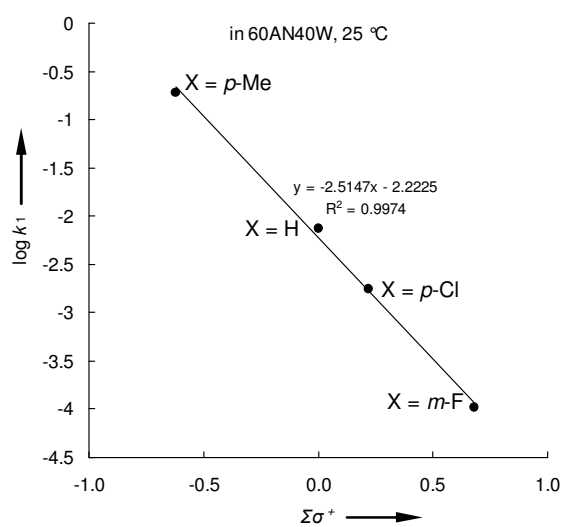
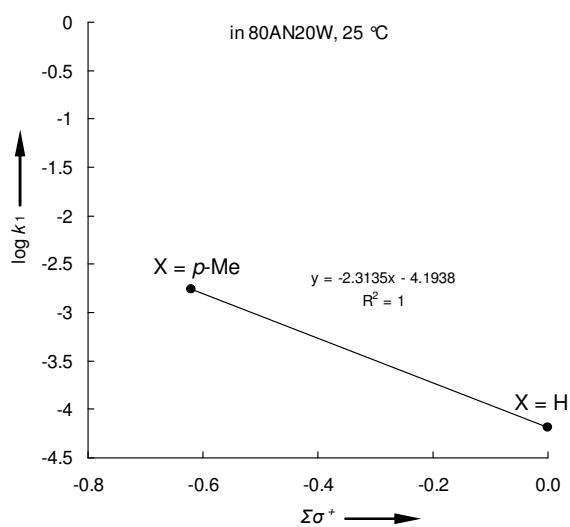
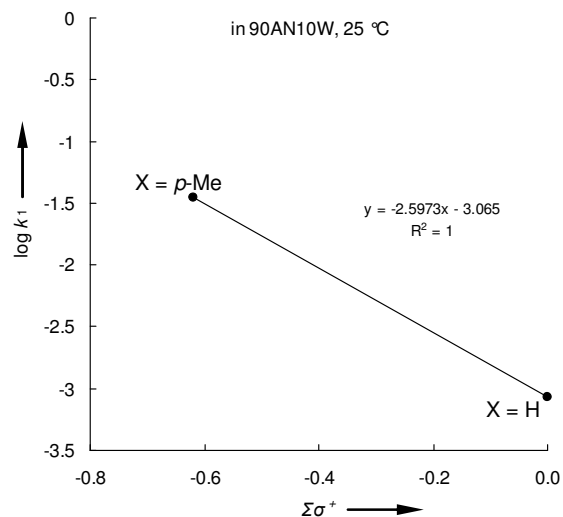
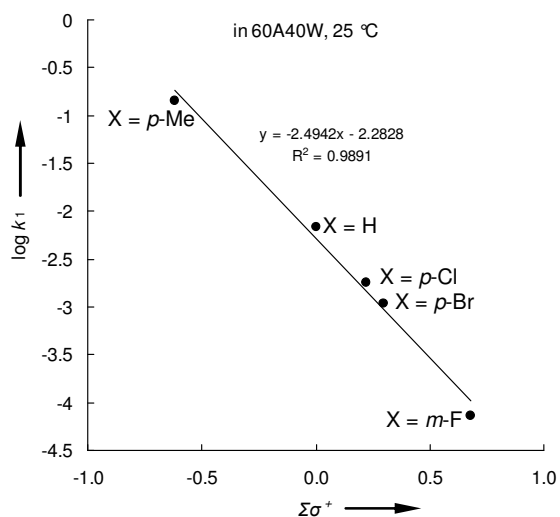
5.1.1. 1,3-Diarylallyl chlorides



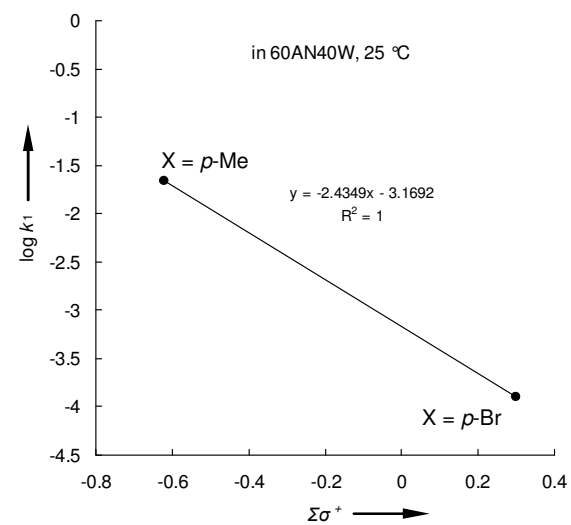
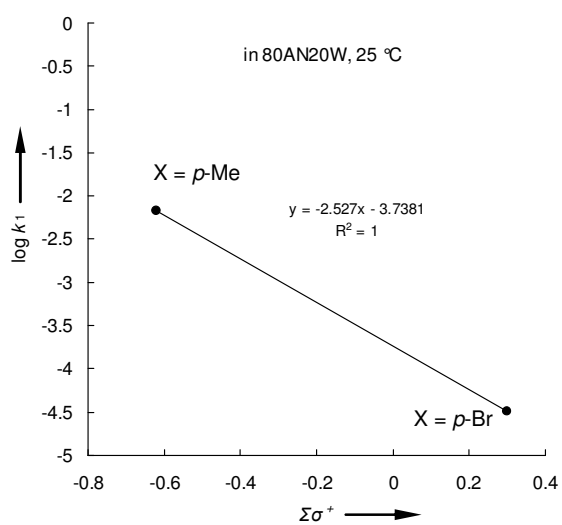
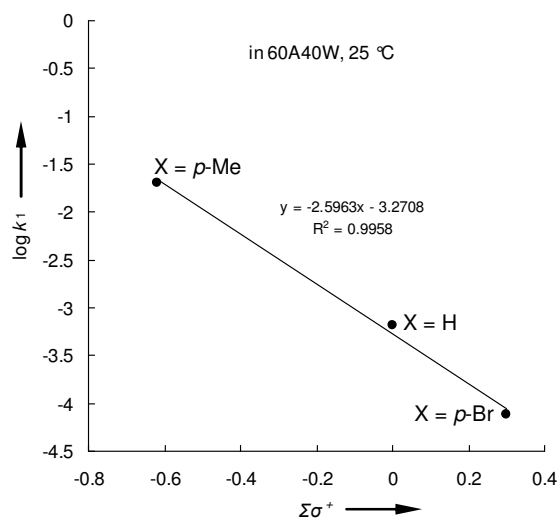
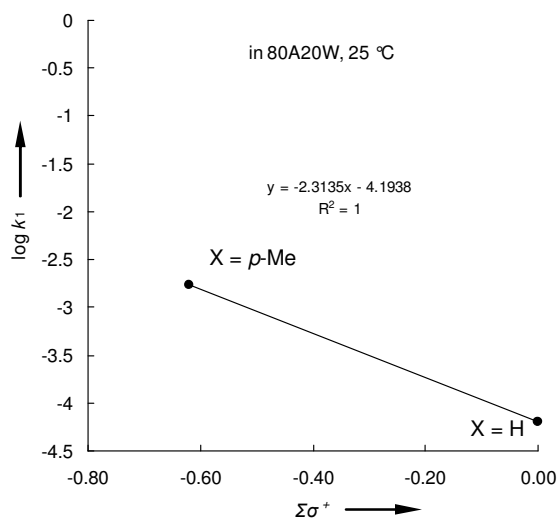


5.1.2. 1,3-Diarylallyl 3,5-dinitrobenzoates





5.1.3. 1,3-Diarylallyl 4-nitrobenzoates



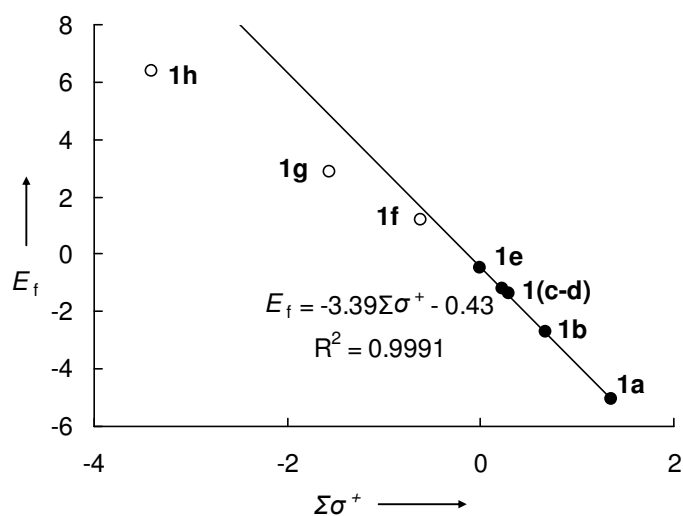
5.1.4. Electrofugality parameters E_f 

Figure S3. Correlation of the electrofugality parameters E_f of the carbocations **1(a-h)** with the sum of the σ^+ parameters¹⁶ of the corresponding aryl substituents.

5.2. Electrofugalities vs Calculated Gas-Phase Methyl Anion Affinities (MP2(FC)/6-31+G(2d,p)//B3LYP/6-31G(d,p) level of theory)⁷

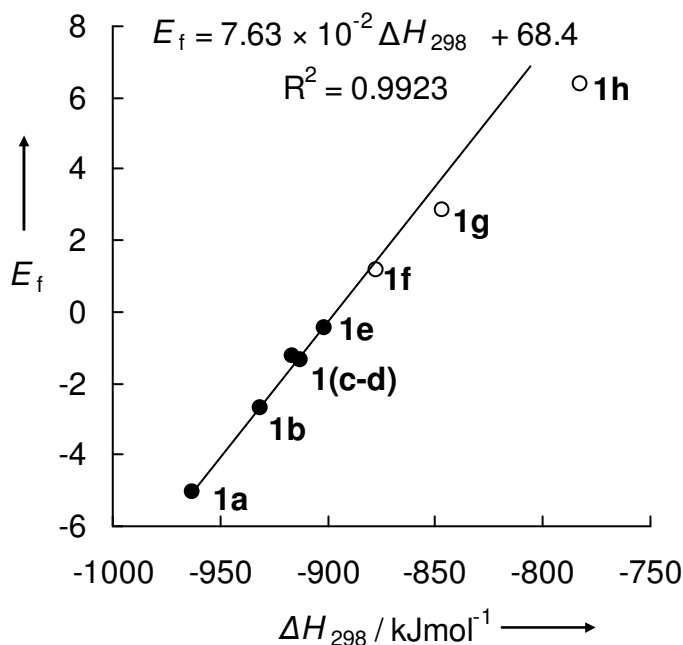


Figure S4. Electrofugalities E of the cations **1(a-h)** in correlation with their calculated gas-phase methyl anion affinities ΔH_{298} (MP2(FC)/6-31+G(2d,p)//B3LYP/6-31G(d,p)).

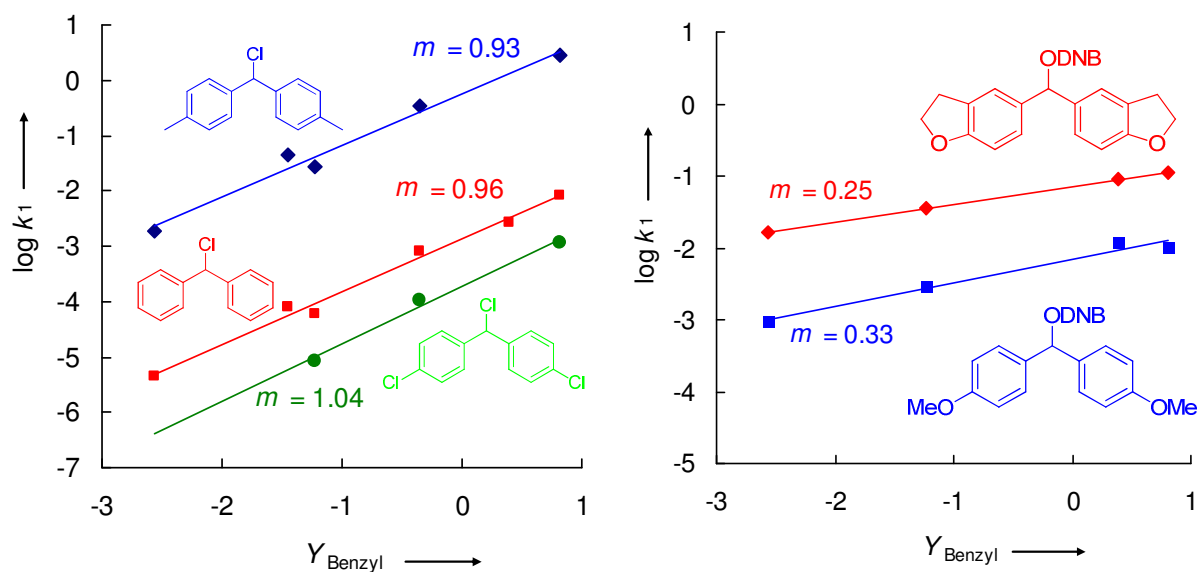
5.3. Winstein-Grunwald Correlations for Benzhydryl Systems^{3,12}

Figure S5. Winstein-Grunwald correlations for solvolyses of benzhydryl chlorides and 3,5-dinitrobenzoates.

5.4. Determination of the S_N2C^+ Region for the Solvolysis of 1,3-Diarylallyl 4-Nitrobenzoates

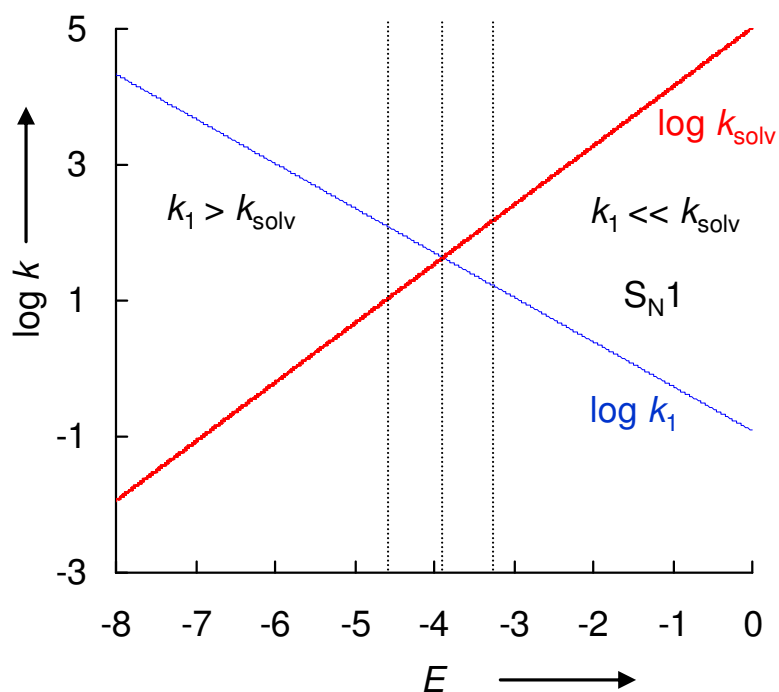


Figure S6. Heterolysis and solvent capture rate constants k_1 and k_{solv} for solvolysis of 1,3-diarylallyl 4-nitrobenzoates **1-OPNB** in 60% aq acetone dependent on the E values of the corresponding cations. The blue line (for $\log k_1$) was calculated assuming that the linear correlation between E_f and E found for **1(f-h)** $E_f = -0.59E + 1.97$ holds in the region $-8 < E < 0$.

6. References

- (1) More precisely, the generation of the free ions from a covalent substrate should be termed as *ionization plus dissociation* (Reichardt, C.; Welton, T. *Solvents and Solvent Effects in Organic Chemistry*, 4th ed, Wiley: Weinheim, 2011, p 52). To avoid the long terms, we will use the term *heterolysis* as a description of this process.
- (2) (a) Mayr, H.; Bug, T.; Gotta, M. F.; Hering, N.; Irrgang, B.; Janker, B.; Kempf, B.; Loos, R.; Ofial, A. R.; Remennikov, G.; Schimmel, H. *J. Am. Chem. Soc.* **2001**, *123*, 9500–9512. (b) Lucius, R.; Loos, R.; Mayr, H. *Angew. Chem., Int. Ed.* **2002**, *41*, 91–95. (c) Mayr, H.; Kempf, B.; Ofial, A. R. *Acc. Chem. Res.* **2003**, *36*, 66–77. (d) Mayr, H.; Ofial, A. R. *J. Phys. Org. Chem.* **2008**, *21*, 584–595. (e) For a database of reactivity parameters E , N , and s_N see: www.cup.lmu.de/oc/mayr/DBintro.html.
- (3) Streidl, N.; Denegri, B.; Kronja, O.; Mayr, H. *Acc. Chem. Res.* **2010**, *43*, 1537–1549.
- (4) See, for instance: (a) Hughes, E. D. *Trans. Faraday Soc.* **1941**, *37*, 603–631. (b) Roberts, J. D.; Young, W. G.; Winstein, S. *J. Am. Chem. Soc.* **1942**, *64*, 2157–2164. (c) Young, W. G.; Winstein, S.; Goering, H. L. *J. Am. Chem. Soc.* **1951**, *73*, 1958–1963. (d) De La Mare, P. B. D.; Vernon, C. A. *J. Chem. Soc.* **1954**, 2504–2510 (e) Sneen, R. A. *J. Am. Chem. Soc.* **1960**, *82*, 4261–4269. (f) Jia, Z. S.; Ottosson, H.; Zeng, X.; Thibblin, A. *J. Org. Chem.* **2002**, *67*, 182–187. For a review see (g) Raber, D. J.; Harris, J. M.; Schleyer, P. v. R. *Ions and Ion Pairs in Organic Reactions Vol. 2*; Szwarc, M., Ed.; Wiley: New York, 1974.
- (5) (a) Goering, H. L., Blanchard, J. P.; Silversmith, E. F. *J. Am. Chem. Soc.* **1954**, *76*, 5409–5418. (b) Goering, H. L.; Silversmith, E. F. *J. Am. Chem. Soc.* **1955**, *77*, 1129–1133. (c) Goering, H. L.; Silversmith, E. F. *J. Am. Chem. Soc.* **1955**, *77*, 6249–6253. (d) Goering, H. L.; Takahashi Doi, J. *J. Am. Chem. Soc.* **1960**, *82*, 5850–5854. (e) Goering, H. L.; Nevitt, T. D.; Silversmith, E. F. *J. Am. Chem. Soc.* **1955**, *77*, 5026–5032. (f) Goering, H. L.; Koermer, G. S.; Linsay, E. C. *J. Am. Chem. Soc.* **1971**, *93*, 1230–1234.
- (6) Troshin, K.; Mayr, H. *J. Am. Chem. Soc.* **2012**, submitted (Chapter 4).
- (7) Troshin, K.; Schindele, C.; Mayr, H. *J. Org. Chem.* **2011**, *76*, 9391–9408 (Chapter 3).
- (8) Streidl, N.; Antipova, A.; Mayr, H. *J. Org. Chem.* **2009**, *74*, 7328–7334.
- (9) Horn, M.; Metz, C.; Mayr, H. *Eur. J. Org. Chem.* **2011**, 6476–6485.
- (10) Minegishi, S.; Loos, R.; Kobayashi, S.; Mayr, H. *J. Am. Chem. Soc.* **2005**, *127*, 2641–2649.
- (11) These values were reported for 50% aq acetonitrile (ref 2e), however, as the differences between the N values of 50% ($N = 5.05$, $s_N = 0.89$) and 80% ($N = 5.02$, $s_N = 0.89$) aq

acetonitrile are marginal and the corresponding s_N values are equal, one would expect similar N and s_N values for 60% aq acetonitrile.

(12) (a) Grunwald, E.; Winstein, S. *J. Am. Chem. Soc.* **1948**, *70*, 846–854. (b) Bentley, T. W.; Carter, G. E. *J. Am. Chem. Soc.* **1982**, *104*, 5741–5747. (c) Kevill, D. N.; D'Souza, M. J. *J. Chem. Res.* **2008**, 61–66. The Y_{benzyl} parameters were taken from (d) Bentley, T. W.; Dauschmidt, J.-P.; Llewellyn, G.; Mayr, H. *J. Org. Chem.* **1992**, *57*, 2387–2392.

(13) Winstein-Grunwald correlations for benzhydryl chlorides are based on the kinetic data from ref 3 and can be found in the Supplementary Section (p 290).

(14) Denegri, B.; Kronja, O. *J. Phys. Org. Chem.* **2009**, 495–503.

(15) Horn, M.; Mayr, H. *Chem.—Eur. J.* **2010**, *16*, 7469–7477.

(16) Hansch, C.; Leo, A.; Taft, R. W. *Chem. Rev.* **1991**, *91*, 165–195.

(17) Streidl, N.; Mayr, H. *Eur. J. Org. Chem.* **2011**, 2498–2506.

(18) *What'sBest!7.0* (May25, 2004), software by Lindo Systems, Inc. 2004 was used for this purpose.

(19) The values obtained at B3LYP/6-31G(d,p) level of theory were used, as they are available both for **1(a–h)** (ref 7) and benzhydrylium ions (from Singer, T. *PhD Dissertation*, Ludwig-Maximilians-Universität, München, **2008**).

(20) (a) Marcus, R. A. *Annu. Rev. Phys. Chem.* **1964**, *15*, 155–196. (b) Marcus, R. A. *J. Phys. Chem.* **1968**, *72*, 891–899. (c) Marcus, R. A. *J. Am. Chem. Soc.* **1969**, *91*, 7224–7225. (d) Albery, W. J.; Kreevoy, M. M. *Adv. Phys. Org. Chem.* **1978**, *16*, 87–157. (e) Albery, W. J. *Annu. Rev. Phys. Chem.* **1980**, *31*, 227–263. (f) Marcus, R. A. *Angew. Chem.* **1993**, *105*, 1161–1172; *Angew. Chem. Int. Ed. Engl.* **1993**, *32*, 1111–1121. (g) Marcus, R. A. *Pure Appl. Chem.* **1997**, *69*, 13–29.

(21) (a) Rice, F. O.; Teller, E. *J. Chem. Phys.* **1938**, *6*, 489–496. (b) Hine, J. *J. Org. Chem.* **1966**, *31*, 1236–1244; (c) Hine, J. *J. Am. Chem. Soc.* **1966**, *88*, 5525–5528; (d) Hine, J. *Adv. Phys. Org. Chem.* **1978**, *15*, 1–61.

(22) (a) Kantner, S. S.; Humski, K.; Goering, H. L. *J. Am. Chem. Soc.* **1982**, *104*, 1693–1697. (b) Thibblin, A. *J. Chem. Soc. Perkin. Trans.2* **1987**, 1629–1632.

(23) Horn, M.; Mayr, H. *Chem.—Eur. J.* **2010**, *16*, 7478–7487.

(24) Phan, T. B.; Nolte, C.; Kobayashi, S.; Ofial, A. R.; Mayr, H. *J. Am. Chem. Soc.* **2009**, *131*, 11392–11401.

(25) Reichardt, C.; Welton, T. *Solvents and Solvent Effects in Organic Chemistry*, 4th ed, Wiley: Weinheim, 2011, p 181.

(26) Schaller, H. F.; Mayr, H. *Angew. Chem.* **2008**, *120*, 4022–4025; *Angew. Chem. Int. Ed.* **2008**, *47*, 3958–3961.

(27) Horn, M.; Mayr, H. *J. Phys. Org. Chem.* **2012**, *25*, 979–988.

(28) Richard, J. P.; Jencks, W. P. *J. Am. Chem. Soc.* **1984**, *106*, 1383–1396.

(29) As acetonitrile-water mixtures of water content between 20 and 80% have almost the same N and s_N values (ref 2e), and 90% ($N = 5.70$, $s_N = 0.85$) and 80% ($N = 5.77$, $s_N = 0.87$) aq acetone are already close in their reactivities, N and s_N parameters of 60% aq acetone can be assumed to be the same as for 80% aq acetone.

(30) Nolte, C.; Mayr, H. *Eur. J. Org. Chem.* **2010**, 1435–1439.

(31) Hayashi, T.; Yamamoto, A.; Yoshihiko, I.; Nishioka, E.; Miura, H.; Yanagi, K. *J. Am. Chem. Soc.* **1989**, *111*, 6301–6311.

Chapter 6. How Does Palladium Coordination Affect the Electrophilicities of Allyl Cations? Development of a Robust Kinetic Method for Following Reactions of $[(\eta^3\text{-Diarylallyl})\text{Pd}(\text{PPh}_3)_2]^+$ with Nucleophiles

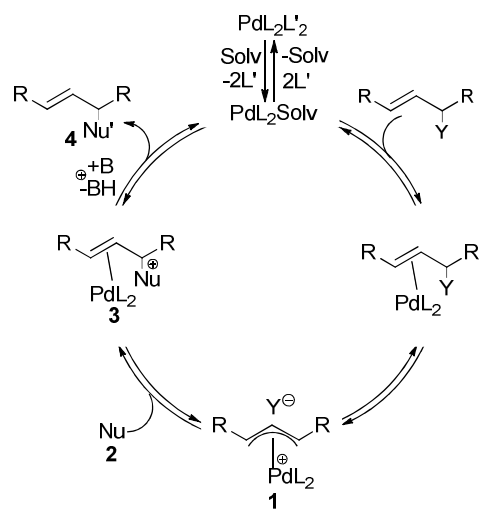
Konstantin Troshin, Peter Mayer, and Herbert Mayr

Organometallics **2012**, *31*, 2416–2424

1. Introduction

The Tsuji–Trost reaction, which often proceeds under mild conditions with high regio- and stereoselectivity, is a powerful synthetic tool for asymmetric allylations of various types of nucleophiles.¹ These reactions have been demonstrated to proceed generally via the cationic $(\eta^3\text{-allyl})\text{palladium}$ complexes (**1**) (Scheme 1). In certain cases, for example, in the presence of chloride ions, neutral $(\eta^1\text{-allyl})\text{palladium}$ species have also been characterized as reactive intermediates.²

Scheme 1. Typical Catalytic Cycle for Tsuji–Trost Allylations.



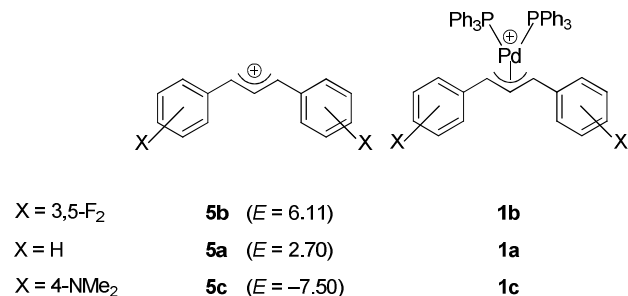
Detailed mechanistic studies on the influence of leaving groups, ligands, and solvents on the formation of the allylpalladium species have been reported.³ Investigations of the reactions of isolated $(\eta^3\text{-allyl})\text{palladium}$ complexes **1** with nucleophiles have shown that the reaction mechanism strongly depends on the nature of the ligands. Jutand et al. reported the reactions of $[(\eta^3\text{-CH}_2\text{CHCH}_2)\text{Pd}(\text{PAr}_3)_2]^+$ ($\text{Ar} = 4\text{-ClC}_6\text{H}_4, 4\text{-MeC}_6\text{H}_4$)⁴ and $[(\eta^3\text{-PhCHCHCHPh})\text{PdL}_2]^+$ ($\text{L} = \text{PPh}_3$ or $\text{L}_2 = \text{dppb}$)⁵ with morpholine and piperidine to proceed via selective attack of

the amines at the allyl ligands, in agreement with earlier work by Kuhn and Mayr.⁶ On the other hand, Crociani et al.⁷ and Canovese et al.⁸ observed that nucleophilic attack at the allyl ligand may be accompanied by reversible coordination of the amines to the metal center. Thus, the formation of pentacoordinated palladium species was found when iminophosphine ligands were employed,⁷ while terdentate (S–N–S), (N–S–N) and (N–N–N) ligands and α -diimines were reversibly replaced by amines.⁸

In recent work⁹ we have studied the kinetics of the reactions of noncoordinated 1,3-diarylallyl cations with nucleophiles and reported that the second-order rate constants can be described by the linear free energy relationship (eq 1), where E is an electrophilicity parameter, N is a nucleophilicity parameter, and s_N is a nucleophile-specific sensitivity parameter (previously termed s).¹⁰ As shown in Chart 1, their electrophilic reactivities differ by more than 13 orders of magnitude, corresponding to relative reaction times of 1 s vs 10^5 to 10^6 years.

$$\log k_2(20\text{ }^\circ\text{C}) = s_N(N + E) \quad (1)$$

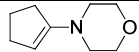
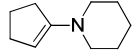
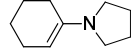
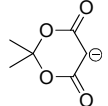
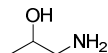
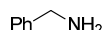
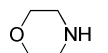
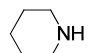
Chart 1. Cationic Palladium Complexes **1(a–c)** and the Corresponding Free 1,3-Diarylallyl Cations **5(a–c)** with Their Electrophilicity Parameters E .^a



^aFrom ref 9.

We have now investigated the kinetics of the reactions of the corresponding $[(\eta^3\text{-}(1,3\text{-diarylallyl})\text{Pd}(\text{PPh}_3)_2)]^+$ complexes **1(a–c)** (Chart 1) with a variety of nucleophiles (Table 1) in order to elucidate how Pd(PPh₃)₂ coordination affects the electrophilic reactivities of 1,3-diarylallyl cations. While products of the reactions of (η^3 -allyl)palladium complexes with most of these nucleophiles have previously been reported,¹¹ there have only been few kinetic investigations.

Table 1. Nucleophiles **2(a–i)** and their Reactivity Parameters N and s_N in Different Solvents.

nucleophile	solvent	N^a	s_N^a
2a 	CH ₂ Cl ₂	13.41	0.82
2b 	CH ₂ Cl ₂	15.06	0.82
2c 	CH ₂ Cl ₂	14.91	0.86
2d 	DMSO	13.91	0.86
2e PPh ₃	CH ₂ Cl ₂	14.33	0.65
2f 	DMSO	15.47	0.65
2g 	CH ₃ CN	14.29	0.67
2h 	CH ₃ CN	15.65	0.74
2i 	CH ₃ CN	17.35	0.68

^a Reactivity parameters from reference 12

2. Results and Discussion

2.1. Synthesis of the Complexes **1(a–c)**

The cationic Pd complexes **1a** and **1b** were synthesized and isolated as tetrafluoroborate salts (**1a**-BF₄ and **1b**-BF₄) by treatment of the corresponding dimeric allylpalladium chlorides (**5(a,b)**-PdCl) with PPh₃ and NaBF₄, as described in ref 13. The triflate **1b**-OTf was obtained analogously by using NaOTf instead of NaBF₄ and characterized by X-ray diffraction analysis (details, see below). Compound **1c**-BF₄ was synthesized by the reaction of (*E*)-1,3-bis(4-dimethylaminophenyl)allylium tetrafluoroborate (**5c**-BF₄) with Pd(PPh₃)₄ in dichloromethane at ambient temperature.

2.2. Kinetic Investigations

All kinetic measurements were performed under pseudo-first-order conditions using the nucleophiles in high excess; the reaction progress was monitored UV–vis spectroscopically at the absorbance maxima of the allyl complexes **1(a–c)**. Freshly prepared solutions of electrophiles were generally required to obtain reproducible results.

Reactions with C-Nucleophiles. Even when the enamines **2a** and **2b** and the potassium salt of Meldrum's acid (**2d**) were used in high excess (10–100 equiv) over the Pd complex **1a**-BF₄

in order to achieve pseudo-first-order kinetics, deviations from the monoexponential decay of the absorbance at 360 nm (absorption maximum of **1a**) were often observed. These deviations were explained by the UV absorptions of the η^2 -Pd complexes **3** (Scheme 1) and their decomposition products. As fumaronitrile is a weak nucleophile, which does not react with **1a** and has previously been shown to strongly coordinate to PdL₂,¹⁴ the kinetics of the reactions of **1a**-BF₄ with nucleophiles were investigated in the presence of fumaronitrile. Under these conditions, the decays of the absorbances at 360 nm were generally monoexponential, when **1a**-BF₄ was combined with more than 10 equiv of various nucleophiles, because the released Pd fragments form stable complexes with fumaronitrile, which do not significantly absorb at 360 nm. The pseudo-first-order rate constants (k_{obs}), which were obtained by least-squares fitting to the function $A_t = A_0 e^{-k_{\text{obs}} t} + C$ (Figure 1a), were found to be independent of the concentration of fumaronitrile. As shown in Figure 1b for the reaction of **1a**-BF₄ with the enamine **2b**, plots of the pseudo-first-order rate constants vs the concentrations of the nucleophiles were linear with the second-order rate constants (k_2) as slopes.

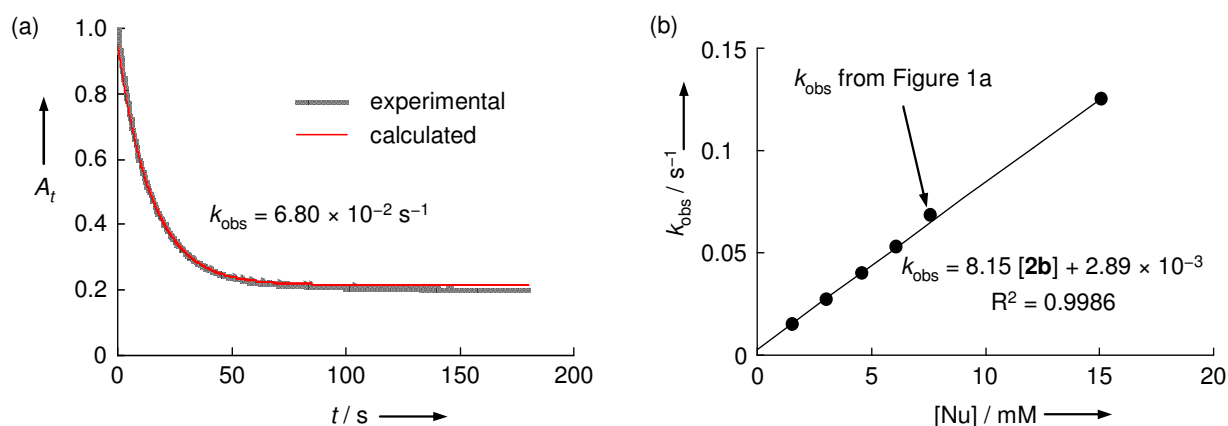
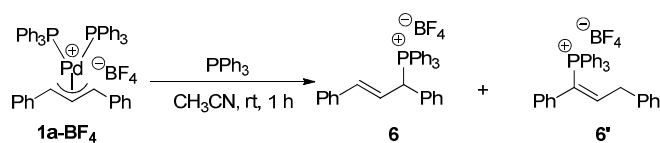


Figure 1. (a) Exponential decay of the absorbance A_t ($\lambda = 360$ nm) and (b) linear correlation between the pseudo-first-order rate constants k_{obs} and the nucleophile concentration for the reaction between the enamine **2b** and **1a**-BF₄ ($6.2 - 6.3 \times 10^{-5}$ M) in the presence of fumaronitrile ($5.7 - 5.8 \times 10^{-4}$ M) in dichloromethane at 20 °C.

Reactions with Triphenylphosphine. The reaction of triphenylphosphine (**2e**) with **1a**-BF₄ in CH₃CN yielded a 2:1 mixture of (*E*)-(1,3-diphenylallyl)triphenylphosphonium tetrafluoroborate (**6**) and (*Z*)-(1,3-diphenylprop-1-en-1-yl)triphenylphosphonium tetrafluoroborate (**6'**) in an overall yield of 54% (Scheme 2).

Scheme 2.



As an independently synthesized sample of the allylphosphonium salt **6** was observed to isomerize to a 4:1 mixture¹⁵ of **6** and **6'** in the presence of 4 mol % of Pd(PPh₃)₄ in acetonitrile at rt, we assume that the reaction of **1a**-BF₄ with PPh₃ proceeds via nucleophilic attack of triphenylphosphine at the allyl ligand to yield **6**, which subsequently undergoes a partial Pd-catalyzed isomerization with formation of a mixture of **6** and **6'**.

The decay of the 360 nm absorbance during the reactions of **1a**-BF₄ with PPh₃ in dichloromethane, acetonitrile, and DMSO was found to be monoexponential, and the linear k_{obs} vs [PPh₃] plots yielded the second-order rate constants $k_2^{\text{PPh}_3}(\text{CH}_2\text{Cl}_2) = 0.366 \text{ M}^{-1} \text{ s}^{-1}$, $k_2^{\text{PPh}_3}(\text{CH}_3\text{CN}) = 0.694 \text{ M}^{-1} \text{ s}^{-1}$, and $k_2^{\text{PPh}_3}(\text{DMSO}) = 0.232 \text{ M}^{-1} \text{ s}^{-1}$ at 20 °C (for details see the Experimental Section, pp 320–321).

Reactions with Amines. Even when fumaronitrile was present, the reactions of the allylpalladium complex **1a**-BF₄ with excess amines often did not follow a first-order rate law. As shown for the reaction of **1a**-BF₄ with benzylamine (**2g**) in Figure 2a, up to 40% of the absorbance at 360 nm decayed by a very fast process, which was followed by a slower secondary reaction; the decay due to the first process increased with increasing concentration of the amine. Fitting the decays for the secondary reactions to the exponential function $A_t = A_0 e^{-k_{\text{obs}} t} + C$ yielded the k_{obs} values, which are plotted against the amine concentrations (Figure 2b). Though the k_{obs} values are poorly reproducible, it is obvious that at low concentrations of amines these values increase with increasing amine concentrations, but do not exceed $7 \times 10^{-3} \text{ s}^{-1}$ even at high concentrations of amines, indicating changes in the reaction mechanism.

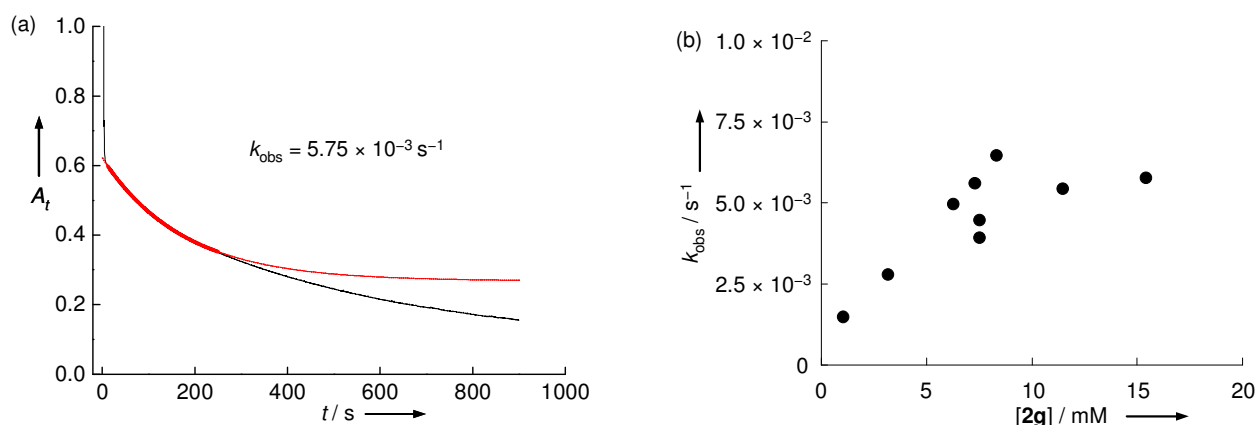


Figure 2. Complex behavior of a mixture of the allylpalladium complex **1a**-BF₄ and benzylamine (**2g**) in acetonitrile at 20 °C. (a) Typical decay of the absorbance at $\lambda = 360$ nm ($[\mathbf{1a}\text{-BF}_4] = 1.0 \times 10^{-4}$ M, $[\mathbf{2g}] = 1.5 \times 10^{-2}$ M, black line). k_{obs} values were achieved by fitting the slow parts of the absorbance decays to the monoexponential function $A_t = A_0 e^{-k_{\text{obs}} t} + C$ (red dashed line, the fit range is shown in bold). (b) Dependence of k_{obs} on the amine concentration.

A rationalization for these observations can be derived from the UV spectra described in Figure 3. When a solution of **1a**-BF₄ in acetonitrile (black dotted curve) is combined with an excess of benzylamine (**2g**), an immediate change of the UV-vis spectrum is observed (red dashed curve). Addition of trifluoroacetic acid immediately after recording the red curve restored the initial absorption spectrum (blue curve, slightly lower than the initial black curve because of dilution), which remained stable at room temperature.

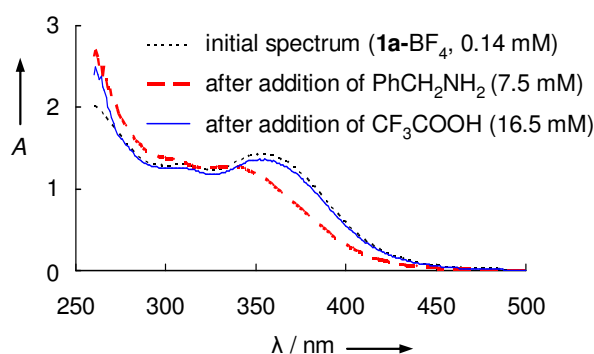
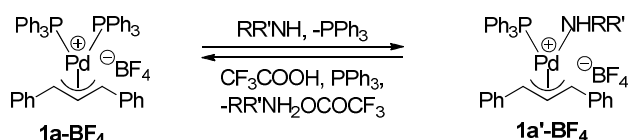


Figure 3. UV-vis evidence for the reversible ligand exchange in the reaction of **1a**-BF₄ with benzylamine (**2g**).

We, therefore, assume that at high concentrations of amines a rapid reversible exchange of Ph₃P by amines yields the complex **1a'**-BF₄, which reverts to **1a**-BF₄ when treated with

CF_3COOH (Scheme 3). An analogous ligand exchange has previously been reported by Canovese et al.⁸ As the amine complexes **1a'** can be assumed to be significantly less electrophilic than **1a**,¹⁶ the limitation of k_{obs} at high amine concentrations (Figure 2) can be explained.

Scheme 3. Reversible Exchange of PPh_3 in **1a** by Amines.



Regeneration of **1a**- BF_4 by addition of CF_3COOH (as shown in Figure 3) occurred only when CF_3COOH was added immediately after the formation of **1a'**- BF_4 . Acidification 15 min after the addition of benzylamine did not restore the original spectrum (Supplementary Figure S4, p 345) indicating the occurrence of an irreversible process, i.e., attack of the amine at the allyl ligand of **1a** or **1a'**.

The formation of **1a'** by ligand exchange, as depicted in Scheme 3, has also been confirmed by a cation-mode ESI mass spectrum¹⁷ of the reaction mixture recorded immediately after addition of benzylamine to the acetonitrile solution of **1a**- BF_4 (Figure 4).

On the basis of these observations, the reactions of the $[(\eta^3\text{-allyl})\text{Pd}(\text{PPh}_3)_2]^+$ complexes with amines can be described by the mechanism depicted in Scheme 4.

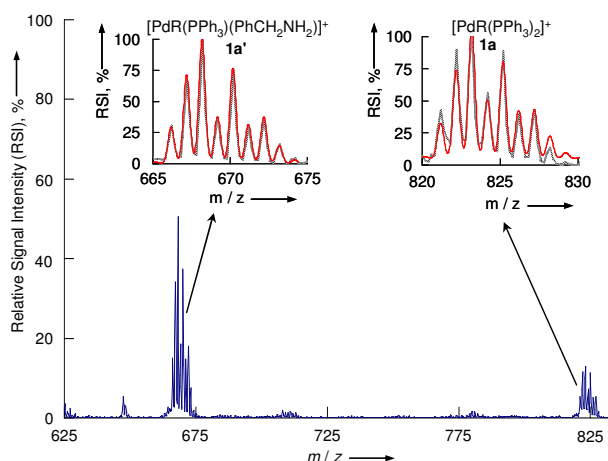
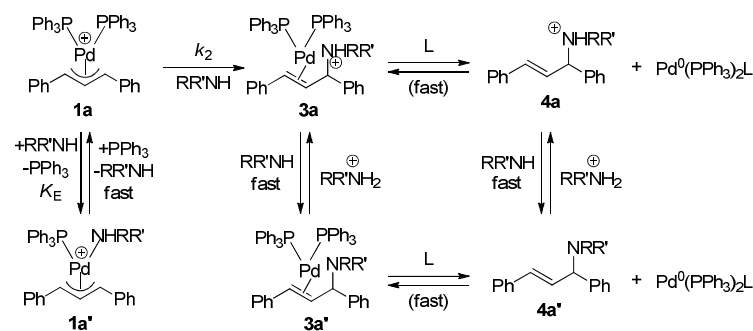


Figure 4. Cation-mode ESI mass spectrum recorded immediately after addition of benzylamine (12 mM) to a 0.2 mM solution of **1a**- BF_4 in acetonitrile. Insets: comparison between experimental (black) and calculated (red) isotopic patterns for peaks at $m/z = 668$ and 823 . $\text{R} = (\eta^3\text{-}(1,3\text{-diphenylallyl}))$.

Scheme 4. Mechanism for Amination of Allylpalladium Complexes.

The amine attacks the palladium complex **1a** either fast and reversibly at Pd to give **1a'** or slowly and irreversibly at the allyl ligand to give **3a**. As the attack of amines at the allyl ligand of **1a'** is significantly slower than that at **1a**, this reaction is neglected in Scheme 4. In the case of low amine concentrations, the complex **1a** is the predominant species in the equilibrium $\mathbf{1a} \rightleftharpoons \mathbf{1a}'$, and the overall reaction rate can be described by eq 2 ($n = 1$).

$$-\frac{d[\mathbf{1a}]}{dt} = k_2[\mathbf{1a}][\text{amine}]^n \quad (2)$$

At high amine concentrations, $[\mathbf{1a}']$ becomes comparable to $[\mathbf{1a}]$, and because of the low reactivity of **1a'** the reaction order n in amine concentration is lowered to $0 \leq n \leq 1$. Apart from a poor reproducibility, a further complication for evaluating kinetics under these conditions is the different absorption coefficients of **1a** and **1a'** at 360 nm. These problems stimulated us to search for a more efficient method of determining the rates of attack of amines at the allyl ligands of $[(\eta^3\text{-allyl})\text{Pd}(\text{PPh}_3)_2]^+$ complexes.

2.3. Four-Component-System for Determining The Rates of the Reactions of $[(\eta^3\text{-Allyl})\text{Pd}(\text{PPh}_3)_2]^+$ with Amines

The exchange of PPh_3 by N ligands upon combination of **1a** with amines was recognized by the change of the UV spectrum of **1a** (black dashed graph vs red graph in Figure 3). In line with the small value of the equilibrium constant K_E ($\approx 4 \times 10^{-3}$, Scheme 4, see Experimental Section, pp 316–318), addition of a small amount of PPh_3 to a mixture of **1a** and **1a'** restored the original spectrum of **1a** (Supplementary Figure S5, p 345). As a consequence, the presence of a small amount of PPh_3 in a mixture of **1a**, **1a'**, and amines shifts the $\mathbf{1a} \rightleftharpoons \mathbf{1a}'$ equilibrium toward **1a**, and the nonexponential decay of the absorbance at 360 nm observed in the absence of PPh_3 (Figure 5a) is replaced by the monoexponential decay shown

in Figure 5b. Analogous behavior was found for reactions of diethylamine with allylpalladium complexes containing diimine ligands.^{8b}

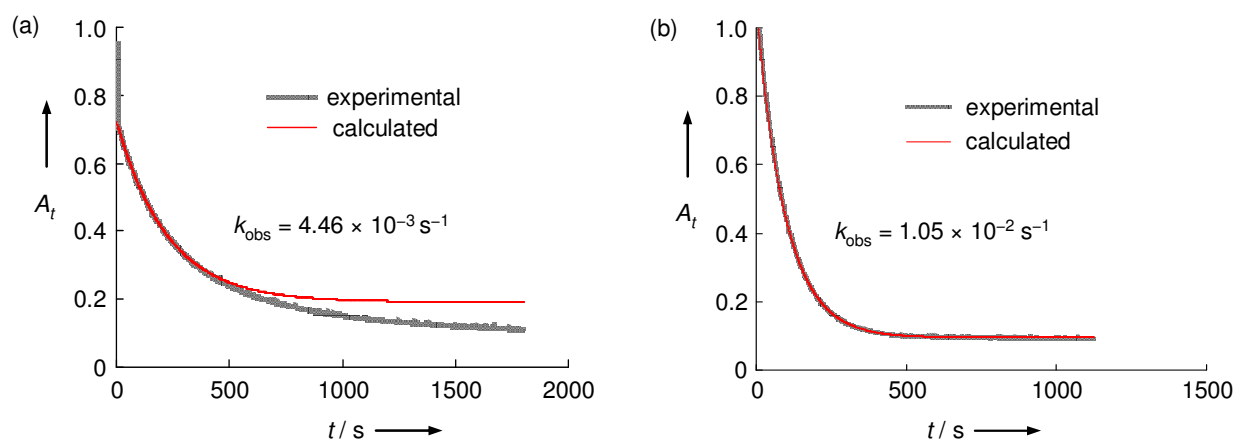


Figure 5. Decays of the absorbances at 360 nm during the reactions of **1a**-BF₄ with benzylamine **2g** (7.5×10^{-2} M) in the presence of fumaronitrile (5.8×10^{-4} M): (a) without PPh₃; (b) in the presence of 1.4×10^{-3} M PPh₃ (acetonitrile, 20 °C).

As discussed above for enamines, all reactions were studied in the presence of fumaronitrile in order to coordinate Pd fragments that are released during these reactions (the whole reaction can be then described with Scheme 4, where L is fumaronitrile). Since the observed rate constants were found to be independent of the fumaronitrile concentration (Supplementary Figure S6, p 346), one can conclude that fumaronitrile is not involved in the rate-determining step.

As triphenylphosphine may also add to the allyl ligand of **1** (see above, Reactions with Triphenylphosphine), the rate constants (k_{obs}) measured for reactions of **1** with amines in the presence of PPh₃ are the sum of the rate constants for the reactions of **1** with amines and PPh₃ (eq 3).

$$k_{\text{obs}} = k_{1\psi}^{\text{amine}} + k_2^{\text{PPh}_3} [\text{PPh}_3] \quad (3)$$

As illustrated by the open symbols in Figure 6, the rate constants k_{obs} determined at a constant amine concentration increased with increasing [PPh₃]. While the strong increase of k_{obs} in the left part of Figure 6 is due to the shift of the equilibrium **1a** \rightleftharpoons **1a'** toward the more electrophilic complex **1a**, the linear increase of k_{obs} in the right part of Figure 6 reflects the attack of PPh₃ at the allyl ligand of **1a**, which was independently determined (see above and in the Experimental Section).

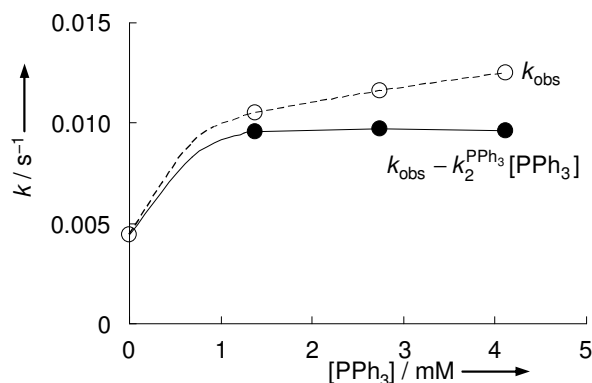


Figure 6. Plot of k_{obs} vs $[\text{PPh}_3]$ for the reaction between **1a** (1.1×10^{-4} M) and benzylamine **2g** (7.52×10^{-2} M) in the presence of fumaronitrile (5.82×10^{-4} M) and variable concentrations of PPh_3 (acetonitrile, 20°C).

As illustrated by the lower plot in Figure 6, subtraction of the contribution of phosphine from k_{obs} yields a plateau for $[\text{PPh}_3] > 1.5$ mM, where $k_{1\psi\text{plateau}}^{\text{amine}}$ reflects the attack of benzylamine at the allyl ligand of complex **1a**. The value of k_2^{amine} can therefore be derived from the slope of a plot of $k_{1\psi\text{plateau}}^{\text{amine}}$ vs [amine] (Figure 7).

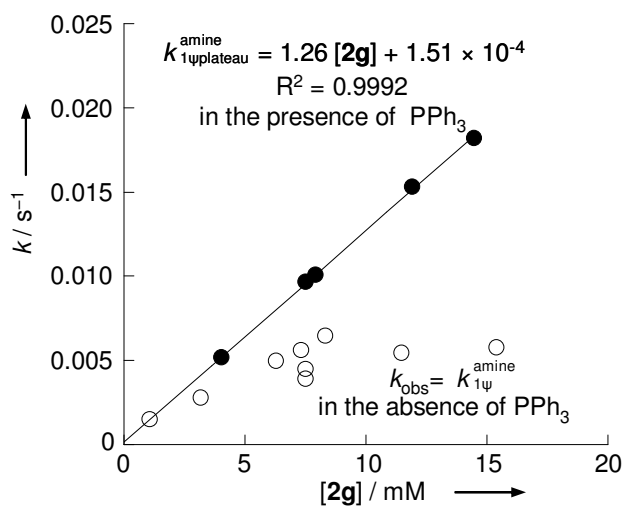


Figure 7. Correlation between the first-order rate constants for the decays of the absorbance at $\lambda = 360$ nm (absorption maximum of **1a**) during the reaction of **1a** ($1.4 - 1.5 \times 10^{-4}$ M) with benzylamine (**2g**) in the absence (open symbols) and presence of PPh_3 ($3.2 \times 10^{-4} - 5.75 \times 10^{-3}$ M, filled symbols) and the amine concentration (acetonitrile, 20°C).

Figure 7 clearly shows that k_{1/PPh_3}^{amine} correlates linearly with the concentration of amines, also in the concentration range in which the poorly reproducible values of k_{obs} measured in the absence of PPh_3 do not increase with increasing [amine].

It is noteworthy that completely different batches of all components were used for the kinetic measurements shown in Figure 7, which indicates excellent reproducibility of the individual rate constants k_{1/PPh_3}^{amine} and contrasts the scatter of k_{obs} determined in the absence of PPh_3 . Obviously, side reactions, which have different weight with different batches of reagents and are responsible for the scatter of the rate constants determined in the absence of triphenylphosphine, can completely be suppressed using the four-component kinetic method. When PPh_3 was present, reproducible kinetic data could also be obtained with solutions of **1a**- BF_4 that have been stored for several hours. Decomposition of **1a**- BF_4 , which is responsible for the poor reproducibility of the kinetic data obtained in the absence of triphenylphosphine, is indicated by the change of the UV-vis spectra of solutions of **1a**- BF_4 in acetonitrile within a few hours. Addition of 3 equiv of triphenylphosphine to such aged solutions fully regenerates the original UV-vis spectrum of **1a** and, therefore, makes reliable kinetic measurements possible.

As the phosphonium ions **6** and **6'** do not react with benzylamine in the absence of Pd complexes, we can exclude that (*E*)-*N*-benzyl-1,3-diphenylprop-2-en-1-amine (**7**), which is the only isolable product of the reaction of **1a**- BF_4 with benzylamine in the presence of PPh_3 and fumaronitrile, is produced via initial attack of PPh_3 at the allyl ligand of **1a** and subsequent noncatalyzed reaction of **6/6'** with the amine. Since the phosphonium salts **6** and **6'** do react with benzylamine in the presence of palladium complexes, **6** and **6'** are not among the reaction products, even when high concentrations of PPh_3 are present in the reaction of **1a**- BF_4 with benzylamine.

Addition of triphenylphosphine has an even stronger effect on the reaction of **1a**- BF_4 with piperidine (**2i**) than on the reaction with benzylamine discussed above. Supplementary Figure S7 (p 346) as well as Figure 8 illustrate that the problem of low reproducibility of the kinetics in the absence of PPh_3 (Figure 8, open symbols) is solved when the reactions are studied in the presence of triphenylphosphine (Figure 8, filled symbols).

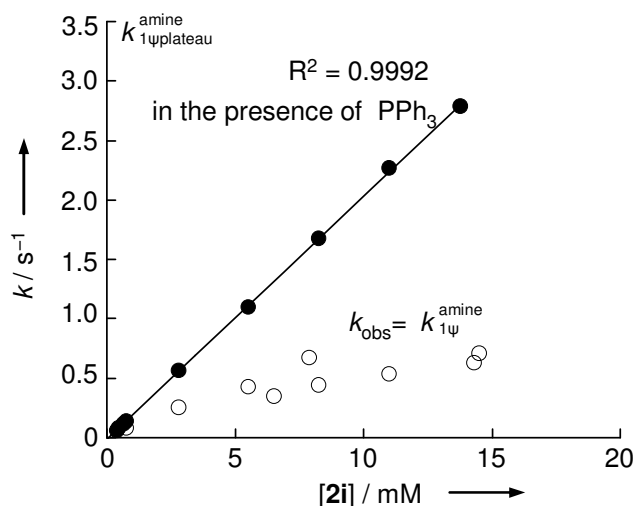


Figure 8. Correlation between the first-order rate constants for the decay of the absorbance at $\lambda = 360$ nm (absorption maximum of **1a**) during the reaction of **1a** ($4.5\text{--}7.9 \times 10^{-4}$ M) with piperidine (**2i**) in the absence (open symbols) and presence of PPh_3 (3.7×10^{-4} to 9.70×10^{-3} M, filled symbols) and the amine concentration (acetonitrile, 20°C).

Similar results were found for the reactions of the complexes **1(a–c)** with a variety of other amines. Only in rare cases were deviations from the second-order rate law, i.e., first-order with respect to **1** and first-order with respect to nucleophile **2**, observed when PPh_3 was present. Thus, for reasons that presently are not exactly known,¹⁸ the reaction of morpholine (**2h**) with **1a-BF₄** was found to be of mixed first- and second-order in amine concentration.

2.4. Determination of Electrophilicity Parameters E for **1(a–c)**

Using the four-component system developed above (additives of PPh_3 and fumaronitrile to mixtures of **1** and **2**), rate constants for the reactions of the allylpalladium complexes **1(a–c)** with a variety of C-, N-, and P-nucleophiles have been determined (Table 2).

Table 2. Second-Order Rate Constants (in $M^{-1} s^{-1}$) for the Reactions of (η^3 -Diarylallyl)palladium Complexes **1(a–c)** with the Nucleophiles **2(a–i)** at 20 °C (solvents are specified in Table 1) and the Resulting Electrophilicity Parameters E .

complex	E^a	Nu	k_2	k_{calc}^a	k_2/k_{calc}
1a	-14.14	2a	1.99×10^{-1}	2.51×10^{-1}	0.79
		2b	8.15	5.66	1.44
		2d	$1.49^{b,c}$	6.32×10^{-1}	2.36
		2e	$3.66 \times 10^{-1}{}^c$	1.33	0.28
		2f	4.52^d	7.30	0.62
		2g	1.26^d	1.26	1.00
		2h	$1.07 \times 10^1{}^{c,d,e}$	1.31×10^1	0.82
		2i	$2.05 \times 10^2{}^d$	1.52×10^2	1.35
1b	-14.21	2a	2.63×10^{-1}	2.51×10^{-1}	1.05
		2d	$2.98^{b,c}$	6.32×10^{-1}	4.71
		2f	3.39^d	7.30	0.46
		2g	1.13^d	1.13	1.00
		2i	$2.10 \times 10^2{}^d$	1.37×10^2	1.54
1c	-14.46	2c	2.05	2.44	0.84
		2f	5.67^f	4.54	1.25
		2g	$7.79 \times 10^{-1}{}^f$	7.71×10^{-1}	1.01
		2i	$6.67 \times 10^1{}^{c,e,f}$	9.25×10^1	0.72

^a The E parameters for **1(a–c)** result from the least-squares minimization of $\Delta^2 = \Sigma(\log k_2 - s_N(N + E))^2$ which uses the second-order rate constants k_2 (this table) and the N and s_N parameters of the nucleophiles **2(a–i)** listed in Table 1. E values with more decimals than given in this table were used for the calculation of k_{calc} by eq 1. The use of E parameters given in this table leads to slightly deviating results. ^b The kinetic data are only of moderate quality. ^c This value was not used for the determination of E . ^d Four-component kinetic method used. ^e Mixed first- and second-order in nucleophile. ^f The rate constant was determined in the presence of PPh_3 . Fumaronitrile must not be added, as it causes immediate release of the free (E)-1,3-bis(4-dimethylaminophenyl)allylium ion (**5c**).

Figure 9 shows a plot of $(\log k_2/s_N)$ versus N (for the N and s_N values see Table 1) for the reactions of complex **1a** with nucleophiles **2**. As required by eq 1, the slope of 1.0 was enforced in the drawn correlation line.

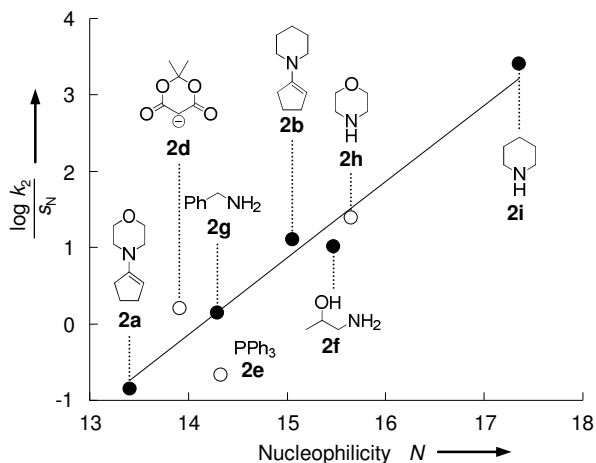


Figure 9. Plot of $(\log k_2)/s_N$ vs N for the reactions of the complex **1a** with the nucleophiles **2(a–i)** (solvents are specified in Table 1). Open points correspond to the rate constants which were not used for the determination of E .

The electrophilicity parameters E (Table 2) of the allylpalladium complexes **1(a–c)** were calculated by minimizing the sum of the squared deviations $\Delta^2 = \sum(\log k_2 - s_N(N + E))^2$ with the nonlinear solver “What’s Best!”¹⁹ using the rate constants listed in Table 2 and the N and s_N values derived from the reactions of corresponding nucleophiles with benzhydrylium ions (Table 1). Because of the lower accuracy of the second-order rate constants for **2d** and **2h**, these k_2 values were not used for the determination of the E parameters. Triphenylphosphine was also not included in the correlation in order to have comparable reference nucleophiles for all three allylpalladium complexes. The proximity of these points to the correlation line implies that the calculated E values would not be significantly changed if these rate constants were included in the correlation.

It is remarkable that the second-order rate constants of reactions of **1(a–c)** with C-, N-, and P-nucleophiles performed in three different solvents can be predicted within a factor of five by using eq 1. This observation indicates that the N and s_N values of the nucleophiles, determined on the basis of their reactions with benzhydrylium ions and therefore incorporating the solvent effects on the stabilities of the diarylmethyl cations (as the E values were defined as solvent-independent),¹⁰ can be applied for the relatively accurate prediction of the reactivities of these nucleophiles even toward electrophiles of widely different nature.

2.5. Comparison of the Allylpalladium Complexes **1(a–c)** with the Free Diarylallyl Cations **5(a–c)**

The structural data listed in Table 3, which are based on X-ray diffraction analysis or quantum chemical calculations, show significant differences between the palladium complexes **1a** and **1b** and the corresponding free cations **5a** and **5b**. While the bond lengths in the allylic fragments of the complexes **1(a,b)** and the free cations **5(a,b)** are almost identical, the bonds between the terminal allyl and the aromatic carbons are significantly longer in the complexes **1(a,b)** than in the free cations. Conjugative stabilization of the positive charge by the aryl rings is thus indicated to be much more important in the free diarylallyl cations **5(a,b)** than in the palladium complexes **1(a,b)**. The smaller conjugative interaction between the aromatic rings and the allyl fragments in the complexes **1(a,b)** is also reflected by the torsional angles of approximately 20° for C2–C3–C4–C5 and C2–C1–C10–C11, while they are close to 0° in the free cations **5(a–c)**. The planar configuration of the allyl fragment in the free cations **5(a,b)** is only slightly disturbed in the Pd complexes **1(a,b)**, as shown by the torsional angles C1–C2–C3–C4 and C3–C2–C1–C10 which deviate by less than 5° from planarity.

Table 3. Geometrical Parameters of the (η^3 -Diarylallyl)palladium Complexes **1(a–b)** and Free Diarylallyl Cations **5(a–c)**.^a

	Pd complexes		free cations			
	1a ^b	1b ^c	5a ^d	5b ^d	5c ^e	5c ^d
bond lengths (Å)						
r_{C1C10}	1.484	1.466	1.425	1.428	1.391	1.415
r_{C3C4}	1.473	1.476	1.425	1.428	1.413	1.415
r_{C1C2}	1.397	1.403	1.391	1.390	1.386	1.392
r_{C2C3}	1.391	1.393	1.391	1.390	1.374	1.392
torsional angles (°)						
C2C3C4C5	-13.14	-19.54	0.00	-0.008	3.13	0.00
C2C1C10C11	27.48	16.09	0.00	0.00	-1.69	0.00
C1C2C3C4	-177.02	-174.94	180.00	180.00	174.37	179.99
C3C2C1C10	-175.14	179.32	0.00	-180	-177.96	180.00

^a For the numbering of atoms see Figure 10. ^b X-ray data from ref 13. ^c X-ray data from this work. ^d B3LYP/6-31G(d,p) data from ref 9. ^e X-ray data from ref 9.

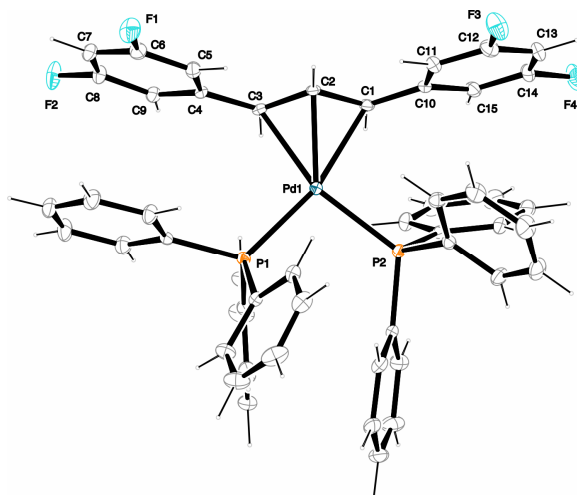


Figure 10. X-ray structure of complex **1b-OTf**. The triflate anion and acetone (cosolvent for crystallization), which were found in the unit cell, are omitted in this figure and are depicted in the Experimental Section (p 344).

Chart 2 shows that the tremendous differences in the electrophilicities of the differently substituted free allyl cations **5(a–c)** are leveled in the corresponding palladium complexes **1(a–c)** all of which have similar electrophilic reactivities. Comparison of the two columns in Chart 2 shows that Pd(PPh₃)₂ coordination of the highly reactive allyl cation **5b** reduces the electrophilic reactivity by 20 orders of magnitude, while the reactivity of the stabilized allyl cation **5c** is only reduced by 7 orders of magnitude.

Chart 2. Electrophilicities of Complexes **1(a–c)** and the Corresponding Free 1,3-Diarylallyl Cations **5(a–c)**.

		<i>E</i> (from ref 9)	<i>E</i> (this work)
X = 3,5-F ₂	5b	6.11	1b -14.21
X = H	5a	2.70	1a -14.14
X = 4-NMe ₂	5c	-7.50	1c -14.46

Jutand et al. reported small differences between the rate constants of the reactions of $[(\eta^3\text{-(CH}_2\text{CHCH}_2)\text{Pd(PAr}_3)_2]^+$ and $[\eta^3\text{-(PhCHCHCHPh)Pd(PPh}_3)_2]^+$ with morpholine in DMF.^{4,5} This observation may a priori be explained by a compensation of electronic acceleration and steric retardation of the nucleophilic attack by the phenyl substituents. As the data in Chart 2 show that electronic substituent effects do not modify the electrophilicities of

allylpalladium complexes, we can conclude that steric effects also play a minor role. In line with this conclusion the rate constants for the reactions of piperidine (**2i**) with **1(a–c)** (205, 210, and $66.7 \text{ M}^{-1}\text{s}^{-1}$, Table 2) are similar to that for the reaction of piperidine with the $[(\eta^3\text{-1-phenylallyl})\text{Pd}(\text{PPh}_3)_2]^+$ complex⁶ ($30.9 \text{ M}^{-1}\text{s}^{-1}$).²⁰

Since the reactivities of the allylpalladium complexes $[(\eta^3\text{-RCHCHCHR})\text{PdL}_2]^+$ are obviously not related to the reactivities of the free allyl cations $[\text{RCHCHCHR}]^+$, the designation of the former species as “palladium-stabilized allyl cations” may be misleading.

As bimolecular reactions at room temperature take place only within acceptable times, when $k_2 (20 \text{ }^\circ\text{C}) > 10^{-5} \text{ M}^{-1}\text{s}^{-1}$, one can derive that nucleophiles with $N > 9$ are suitable substrates for Tsuji–Trost reactions via $[(\eta^3\text{-allyl})\text{Pd}(\text{PPh}_3)_2]^+$ complexes. Weaker nucleophiles may react, however, if another reaction mechanism is followed or other ligands are used, e.g., in reactions with indoles²¹ ($N \approx 5\text{--}7$) which have been suggested^{21a} to proceed via the precoordination of the indole to the metal.

3. Conclusions

Contrary to previous assumptions,⁵ secondary and primary amines were found to attack not only the allyl ligand but also the central metal in reactions with $[(\eta^3\text{-allyl})\text{Pd}(\text{PPh}_3)_2]^+$ complexes. Since the products of the latter reaction, in which one PPh_3 ligand is reversibly replaced by an amine molecule, are considerably less electrophilic than the $\text{Pd}(\text{PPh}_3)_2$ -coordinated species, complex kinetics were encountered. Small amounts of PPh_3 were shown to suppress the ligand exchange, giving rise to the high reproducibility of the kinetic measurements of these reactions.

Substitution of the previously reported^{12–16} nucleophile-specific parameters N and s_N and the second-order rate constants k_2 for the reactions of **1(a–c)** with various nucleophiles in the correlation $\log k_2 = s_N(N + E)$ (eq 1) allowed us to derive the electrophilicities $E \approx -14$ for the $[(\eta^3\text{-diarylallyl})\text{Pd}(\text{PPh}_3)_2]^+$ almost independent of the nature of the substituents and to compare them with the reactivities of other important classes of electrophiles²² (Figure 11).

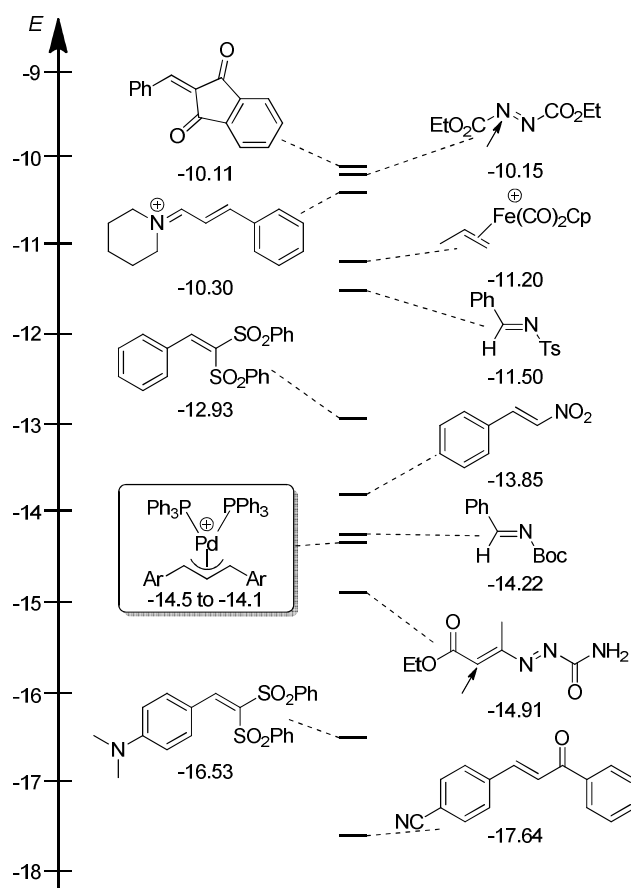


Figure 11. Comparison of the electrophilicities of the allylpalladium complexes **1(a–c)** and electron-deficient π -systems of similar reactivity.²²

4. Experimental Section

4.1. General

Materials for Kinetic Measurements. Dichloromethane (p.a. grade) was subsequently treated with concentrated sulfuric acid, water, 10% NaHCO₃ solution, and again water. After predrying with anhydrous CaCl₂, it was freshly distilled over CaH₂. Acetonitrile (HPLC grade) and DMSO (99.7% purity) were used as received.

NMR Spectroscopy. In the ¹H and ¹³C NMR spectra chemical shifts are expressed in δ (ppm) and refer to CD₂Cl₂ (δ_{H} 5.32, δ_{C} 54.00), DMSO (δ_{H} 2.50, δ_{C} 39.50), and CD₃CN (δ_{H} 1.94, δ_{C} 1.39) as internal standards. The coupling constants are given in Hz. Abbreviations used are s (singlet), d (doublet), t (triplet), q (quartet), m (multiplet). In the case of ¹³C NMR spectra, these abbreviations refer to the multiplicity in hydrogen decoupled spectra, and the hydrogen multiplicity (based on DEPT or HSQC experiments) is shown as CH₃, CH₂, CH or C to avoid ambiguity.

4.2. Synthetic Procedures

(*E*)-3-chloro-1,3-bis(3,5-difluorophenyl)prop-1-ene (5b-Cl). Prepared from (*E*)-1,3-bis(3,5-difluorophenyl)prop-2-en-1-ol (4.58 g, 16.2 mmol) and thionyl chloride (2.71 g, 22.8 mmol) in dichloromethane (20 mL) using the procedure from ref 23: 3.82 g (12.7 mmol, 78%); colorless oil. ^1H NMR (CDCl_3 , 599 MHz): δ 5.54 (d, $^3J_{\text{HH}} = 7.7$ Hz, 1 H, $\text{ArCHCHCH}(\text{Cl})\text{Ar}$), 6.41 (dd, $^3J_{\text{HH}} = 15.6$, 7.7 Hz, 1 H, $\text{ArCHCHCH}(\text{Cl})\text{Ar}$), 6.57 (d, $^3J_{\text{HH}} = 15.6$ Hz, 1 H, $\text{ArCHCHCH}(\text{Cl})\text{Ar}$), 6.71–6.81 (m, 2 H, H_{Ar}), 6.89–6.93 (m, 2 H, H_{Ar}), 6.98–7.02 ppm (m, 2 H, H_{Ar}). ^{13}C NMR (CDCl_3 , 151 MHz): δ 61.2 (t, $J_{\text{CF}} = 2.2$ Hz, CH), 103.4 (s, CH), 103.8 (t, $J_{\text{CF}} = 25.5$ Hz, CH), 103.9 (t, $J_{\text{CF}} = 2.9$ Hz, CH), 104.1 (t, $J_{\text{CF}} = 25.2$ Hz, CH), 109.6 (dd, $J_{\text{CF}} = 20.3$, 5.3 Hz, CH), 110.5 (dd, $J_{\text{CF}} = 20.8$, 5.6 Hz, CH), 138.7 (t, $J_{\text{CF}} = 9.5$ Hz, C), 143.3 (t, $J_{\text{CF}} = 8.7$ Hz, C), 163.0 (dd, $J_{\text{CF}} = 251$, 12.0 Hz, C), 163.2 ppm (dd, $J_{\text{CF}} = 249$, 13.6 Hz, C).

[Pd(1,3-bis(3,5-difluorophenyl)- π -allyl)(μ -Cl)]₂ (5b-PdCl). Prepared from palladium (II) chloride (400 mg, 2.26 mmol), 5b-Cl (2.70 g, 8.98 mmol), and lithium chloride (405 mg, 9.55 mmol) following the procedure described in ref 24: 834 mg (1.02 mmol, 90%); yellow powder; mp 247.8–249.2 °C (decomp). ^1H NMR (DMSO, 400 MHz): δ 5.20 (d, $^3J_{\text{HH}} = 11.8$ Hz, 4 H, ArCHCHCHAr), 7.09 (t, $J = 11.8$ Hz, 2 H, ArCHCHCHAr), 7.17–7.34 (m, 4 H, H_{Ar}), 7.40–7.64 ppm (m, 8 H, H_{Ar}). ^{13}C NMR (DMSO, 101 MHz): δ 80.7 (s, CH), 103.4 (t, $J_{\text{CF}} = 26.0$ Hz, CH), 109.5 (s, CH), 111.4–111.6 (m, CH), 141.5 (t, $J_{\text{CF}} = 10.1$ Hz, C), 162.7 ppm (dd, $J_{\text{CF}} = 245.1$, 13.5 Hz, C). ^{19}F NMR (DMSO, 376 MHz): δ –110.7 to –110.4 ppm (m). HRMS (ESI+, acetonitrile–water as eluents): calcd. 453.0201 ($\text{C}_{19}\text{H}_{15}\text{F}_4\text{N}_2^{106}\text{Pd}^+$, $[\text{C}_6\text{H}_3\text{F}_2\text{CHCHCHC}_6\text{H}_3\text{F}_2\text{Pd}(\text{CH}_3\text{CN})_2]^+$), found 453.0202.

(*E*)-[(η^3 -1,3-Bis(3,5-difluorophenyl)allyl)Pd(PPh₃)₂]⁺BF₄[–] (1b-BF₄). Synthesized according to ref 13 from 5b-PdCl (420 mg, 0.516 mmol), triphenylphosphine (542 mg, 2.07 mmol), and NaBF₄ (568 mg, 5.17 mmol): 605 mg (0.615 mmol, 60%); yellow powder; mp 170–172 °C (decomp). ^1H NMR (CD_2Cl_2 , 400 MHz): δ 5.45–5.51 (m, 2 H, ArCHCHCHAr), 6.38–6.51 (m, 7 H, ArCCHCHAr , H_{Ar}), 7.11–7.16 (m, 12 H, *o*-PPh₃), 7.19–7.23 (m, 12 H, *m*-PPh₃), 7.34–7.38 ppm (m, 6 H, *p*-PPh₃). ^{13}C NMR (CD_2Cl_2 , 101 MHz): δ 91.1 (t, $J_{\text{CP}} = 15.0$ Hz, CH), 103.7 (t, $J_{\text{CF}} = 25.6$ Hz, CH), 111.3–111.9 (m, CH), 113.8 (t, $J_{\text{CP}} = 7.3$ Hz, CH), 129.3–129.4 (m, CH), 129.6 (d, $J_{\text{CP}} = 22.1$ Hz, C), 131.5 (s, CH), 134.1–134.2 (m, CH), 139.4–139.6 (m, C), 163.2 ppm (dd, $J_{\text{CF}} = 248$, 13.0 Hz, C). ^{31}P NMR (CD_2Cl_2 , 162 MHz): δ 27.5 ppm. ^{19}F NMR (CD_2Cl_2 , 376 MHz): δ –150.63 to –150.62 (m, 3 F, BF₄), –150.58 to –150.57 (m, 1 F, BF₄), –110.32 to –110.28 ppm (m, 4 F, F_{Ar}). HRMS (ESI+): calcd 895.1492 ($\text{C}_{51}\text{H}_{39}\text{F}_4\text{P}_2^{106}\text{Pd}^+$), found 895.1498.

(E)-[(η^3 -1,3-Bis(3,5-difluorophenyl)allyl)Pd(PPh₃)₂]⁺TfO⁻ (1b-OTf**). Analogous to **1b-BF₄**. From **5b**-PdCl (186 mg, 0.228 mmol), PPh₃ (242 mg, 0.923 mmol), and sodium triflate (393 mg, 2.28 mmol): 205 mg (0.196 mmol, 43%); yellow needles; mp 206.5–208.5 °C (decomp). To obtain crystals suitable for X-ray diffraction analysis, **1b-OTf** was recrystallized from acetone/Et₂O.**

(E)-[(η^3 -1,3-Bis(4-(dimethylamino)phenyl)allyl)Pd(PPh₃)₂]⁺BF₄⁻ (1c-BF₄**). Pd(PPh₃)₄ (871 mg, 0.754 mmol) and **5c-BF₄** (268 mg, 0.732 mmol) were mixed in the solid state followed by addition of dichloromethane (10 mL). The resulting solution was stirred for 10 min at rt, then pentane (ca 50 mL) was added. After 2 h cooling (4 °C), the precipitate was filtered, washed with pentane, and dried in vacuo to yield **1c-BF₄**: 476 mg (0.477 mmol, 65%); red powder; mp 162.0–164.0 °C (decomp). ¹H NMR (CD₂Cl₂, 400 MHz): δ 2.91 (s, 12 H, 2 \times NMe₂), 5.48–5.53 (m, 2 H, ArCHCHCHAr), 6.11 (t, ³J_{HH} = 12.4 Hz, 1 H, ArCHCHCHAr), 6.26–6.28 (m, 4 H, H_{Ar}), 6.71–6.73 (m, 4 H, H_{Ar}), 7.00–7.04 (m, 12 H, *o*-PPh₃), 7.13–7.17 (m, 12 H, *m*-PPh₃), 7.32–7.36 ppm (m, 6 H, *p*-PPh₃). ¹³C NMR (CD₂Cl₂, 101 MHz): δ 40.5 (s, CH₃), 98.7 (t, J_{CP} = 11.7 Hz, CH), 101.3 (t, J_{CP} = ca 6 Hz, CH), 112.4 (s, CH), 122.0 (t, J_{CP} = 4.1 Hz, C), 129.1–129.2 (m, CH), 130.0 (s, CH), 130.9 (s, CH), 131.2 (d, J_{CP} = 19.3 Hz, C), 134.0–134.1 (m, CH), 151.4 ppm (s, C). HRMS (ESI, positive): calcd 909.2713 (C₅₅H₅₃N₂P₂¹⁰⁶Pd⁺), found 909.2721.**

4.3. Product Studies

Reaction of 1a-BF₄ with Triphenylphosphine (2e). Triphenylphosphine (553 mg, 2.11 mmol) was added to a solution of **1a-BF₄** (315 mg, 0.346 mmol) in acetonitrile (10 mL). After 1 h of stirring (rt), the precipitate was filtered off, and the filtrate was dried in vacuo. Diethyl ether (50 mL) was added to the solid residue, and the resulting slurry was placed in an ultrasonic bath for 20 min. The remaining solid was filtered and recrystallized from CH₂Cl₂/Et₂O yielding a 2:1 mixture of (*E*)-(1,3-diphenylallyl)-triphenylphosphonium tetrafluoroborate (**6**) and (*Z*)-(1,3-diphenylprop-1-en-1-yl)triphenylphosphonium tetrafluoroborate (**6'**). The ¹H and ¹³C NMR spectra of **6'** were obtained comparing the spectra of the mixture with those of isolated **6**.⁹

6': ¹H NMR (CD₂Cl₂, 400 MHz): δ 3.62 (dd, ³J_{HH} = 7.5, ⁴J_{HP} = 3.0 Hz, 2 H, CH₂), 6.93–7.02 (m, 3 H, =CH, H_{Ar}), 7.05–7.10 (m, 2 H, H_{Ar}, overlapped with H_{Ar} of **6**), 7.26–7.36 (m, 5 H, H_{Ar} overlapped with H_{Ar} of **6**), 7.38–7.45 (m, 7 H, *o*-PPh₃, H_{Ar}, overlapped with H_{Ar} of **6**), 7.62–7.70 (m, 6 H, *m*-PPh₃, overlapped with *m*-PPh₃ of **6**), 7.83–7.88 ppm (m, 3 H, *p*-PPh₃ overlapped with *p*-PPh₃ of **6**). ¹³C NMR (CD₂Cl₂, 101 MHz): δ 38.0 (d, J_{CP} = 14.4 Hz, CH₂),

117.4 (d, $J_{CP} = 88.9$ Hz, C), 124.5 (d, $J_{CP} = 77.9$ Hz, C), 127.7 (s, CH), 129.0 (s, CH), 129.6 (s, CH), 130.4 (d, $J_{CP} = 2.5$ Hz, CH), 130.08–130.13 (m, overlapped with resonance of **6**, CH), 130.7 (m, overlapped with resonance of **6**, CH), 130.9 (d, $J_{CP} = 12$ Hz, CH), 131.5 (d, $J_{CP} = 9.5$ Hz, C), 135.1 (d, $J_{CP} = 10.1$ Hz, CH), 136.1 (d, $J_{CP} = 3.0$ Hz, CH), 137.2 (d, $J_{CP} = 1.8$ Hz, C), 157.4 ppm (d, $J_{CP} = 10.1$ Hz, CH). ^{31}P NMR (CD_2Cl_2 , 162 MHz): δ 24.5 ppm.

Isomerization of 6 in the Presence of $\text{Pd}(\text{PPh}_3)_4$. $\text{Pd}(\text{PPh}_3)_4$ (8.4 mg, 7.3 μmol) and **6** (104 mg, 0.192 mmol) were mixed in the solid state, and acetonitrile (10 mL) was added. After 15 h of stirring (ambient temperature), the reaction mixture was freed from the solvent, yielding a 4:1 mixture of **6** and **6'** (based on ^1H NMR).

Reaction of **1a- BF_4 with Benzylamine (2g) in the Presence of Triphenylphosphine and Fumaronitrile.** A solution containing benzylamine (151 mg, 1.41 mmol), triphenylphosphine (185 mg, 0.706 mmol), and fumaronitrile (17 mg, 0.22 mmol) in acetonitrile (5 mL) was added to a solution of **1a**- BF_4 (199 mg, 0.218 mmol) in the same solvent (5 mL). After 1 h of stirring (rt), the precipitate was filtered off and the filtrate was dried in vacuo. (*E*)-*N*-Benzyl-1,3-diphenylprop-2-en-1-amine (**7**) was found to be the only allylic product in the crude mixture (^1H NMR). Column chromatography (MPLC, silica gel, isohexane/EtOAc = 93/7, flow rate 25 mL/min) afforded **7** (35.4 mg, 0.118 mmol, 54%), the ^1H and ^{13}C NMR spectra of which agreed with literature data.^{24,25}

Isomerization of 6 in the Presence of Benzylamine (2g). The phosphonium salt **6** (29.6 mg, 54.6 μmol) was dissolved in CD_3CN (0.5 mL). Then a solution of benzylamine (43.6 mg, 0.407 mmol) in the same solvent (0.2 mL) was added. ^1H and ^{31}P NMR spectra of the reaction mixture taken 2 and 5 min after mixing, respectively, showed resonances corresponding to a mixture of **6**, **6'**, and benzylamine. After 24 h, no traces of **7** were found, and the ratio between **6** and **6'** (ca 1:5) remained unchanged.

Reaction of 6 with benzylamine in the presence of $\text{Pd}(\text{PPh}_3)_4$. The phosphonium salt **6** (29.3 mg, 0.0540 mmol) and $\text{Pd}(\text{PPh}_3)_4$ (7.3 mg, 6.1 μmol) were dissolved in CD_3CN (0.5 mL). Then a solution of benzylamine (39.6 mg, 370 μmol) in the same solvent (0.2 mL) was added. The ^1H NMR spectrum of the reaction mixture taken 20 min after mixing showed resonances corresponding to a mixture of **7**, **6** and **6'** in a ratio of ca. 1:0.3:0.6. After a reaction time of 6 h, the **7**:**6**:**6'** ratio reached 1:0.04:0.13.

4.4. Estimation of the Equilibrium Constant of the Ligand Exchange (K_E) between **1a** and Benzylamine (**2g**)

The equilibrium constant of the amine – phosphine exchange at Pd (II) (see Schemes 2 and 3 of the main text of the manuscript) was estimated based on the absorbance data for the reactions between **1a**-BF₄ and benzylamine (the initial fast decay in the absorbance – time curve, see Figure 2a). Assuming that **1a** and **1a'** are the only two components in the reaction mixture absorbing at 360 nm (which should be the case at the very beginning of the reaction, where the concentrations of **3a**, **3a'** and other palladium-containing species are negligible), one can state (eq S1):

$$A_t = \varepsilon_{1a} l [\mathbf{1a}] + \varepsilon_{1a'} l [\mathbf{1a'}] \quad (\text{S1})$$

where A_t is the absorbance of the reaction mixture at the certain time t , l is the optical path length (0.5 cm), $[\mathbf{1a}]$ and $[\mathbf{1a'}]$ are the concentrations, and ε_{1a} and $\varepsilon_{1a'}$ are the molar absorption coefficients of **1a** and **1a'**, respectively.

As the overall reaction is significantly slower than the ligand exchange, the sum of concentrations of **1a** and **1a'** should be approximately equal to the starting concentration of **1a** corrected for dilution ($[\mathbf{1a}]_0$). Consequently, eq S1 can be transformed to

$$A_t = \varepsilon_{1a} l [\mathbf{1a}] + \varepsilon_{1a'} l ([\mathbf{1a}]_0 - [\mathbf{1a}]) \quad (\text{S2})$$

Combination of all terms containing $[\mathbf{1a}]$ and division by the corresponding coefficient result in

$$[\mathbf{1a}] = \frac{A_t - \varepsilon_{1a'} l [\mathbf{1a}]_0}{\varepsilon_{1a} l - \varepsilon_{1a'} l} \quad (\text{S3})$$

ε_{1a} ($2.0 \times 10^4 \text{ M}^{-1} \text{ cm}^{-1}$) can be measured directly, and the value of $\varepsilon_{1a'}$ ($\sim 9.2 \times 10^3 \text{ M}^{-1} \text{ cm}^{-1}$) can be estimated dividing the absorbance of the reaction mixture after injection of a big amount of the amine (A_t^∞) by $[\mathbf{1a}]_0 l$, assuming that the equilibrium is almost completely shifted toward **1a'** in this case. This assumption is justified by the observation that the values of A_t for $[\mathbf{2g}] = 0.22 \text{ M}$ and $[\mathbf{2g}] = 0.37 \text{ M}$ do not differ significantly.

Without addition of external triphenylphosphine, the ligand exchange can be described by eq S4

$$K_E = \frac{([\mathbf{1a}]_0 - [\mathbf{1a}])^2}{[\mathbf{1a}][\mathbf{2g}]} \quad (\text{S4})$$

which can be rewritten as

$$\frac{([\mathbf{1a}]_0 - [\mathbf{1a}])^2}{[\mathbf{1a}]} = K_E [\mathbf{2g}] \quad (\text{S5})$$

Indeed, the plot of the values of $\frac{([\mathbf{1a}]_0 - [\mathbf{1a}])^2}{[\mathbf{1a}]}$ calculated using eq S3 and listed in Table S1 versus benzylamine concentration (Figure S1) is linear and its slope gives an estimate for the K_E value (4×10^{-3}). The last column in the Table S1 corresponds to ratios $x = \frac{[\mathbf{1a}']}{[\mathbf{1a}] + [\mathbf{1a}]}$ calculated using this value of K_E . This ratio reaches 93% for the amine concentration used for estimation of $\varepsilon_{\mathbf{1a}'}$ (last entry in the table), showing internal consistency of the estimation method.

Table S1. Estimation of the K_E value for the reaction of **1a** with **2g**

[2g] / M	A_0	A_t	$[\mathbf{1a}]_0$ / M	$[\mathbf{1a}]$ / M	$([\mathbf{1a}]_0 - [\mathbf{1a}])^2 / [\mathbf{1a}]$ / M	x / %
4.29×10^{-3}	1.12	0.880	1.12×10^{-4}	6.77×10^{-5}	2.90×10^{-5}	31.5
8.56×10^{-3}	1.09	0.804	1.09×10^{-4}	5.64×10^{-5}	4.84×10^{-5}	41.2
1.28×10^{-2}	1.12	0.782	1.11×10^{-4}	5.01×10^{-5}	7.48×10^{-5}	47.6
1.70×10^{-2}	0.83	0.549	8.24×10^{-5}	3.15×10^{-5}	8.21×10^{-5}	50.4
2.13×10^{-2}	1.07	0.705	1.06×10^{-4}	4.04×10^{-5}	1.06×10^{-4}	56.2
2.55×10^{-2}	1.10	0.722	1.09×10^{-4}	4.13×10^{-5}	1.10×10^{-4}	57.3
3.38×10^{-2}	1.15	0.724	1.13×10^{-4}	3.78×10^{-5}	1.50×10^{-4}	62.2
5.03×10^{-2}	1.18	0.694	1.15×10^{-4}	3.07×10^{-5}	2.31×10^{-4}	69.0
8.25×10^{-2}	1.16	0.637	1.11×10^{-4}	2.32×10^{-5}	3.35×10^{-4}	76.9
2.22×10^{-1}	1.09	0.534	1.06×10^{-4}	<i>a</i>	<i>a</i>	89.5
3.65×10^{-1}	1.10	0.485 ^b	1.06×10^{-4}	-	-	93.2

^aThe precision of determination is too low. ^bThis value was used as A_t^∞

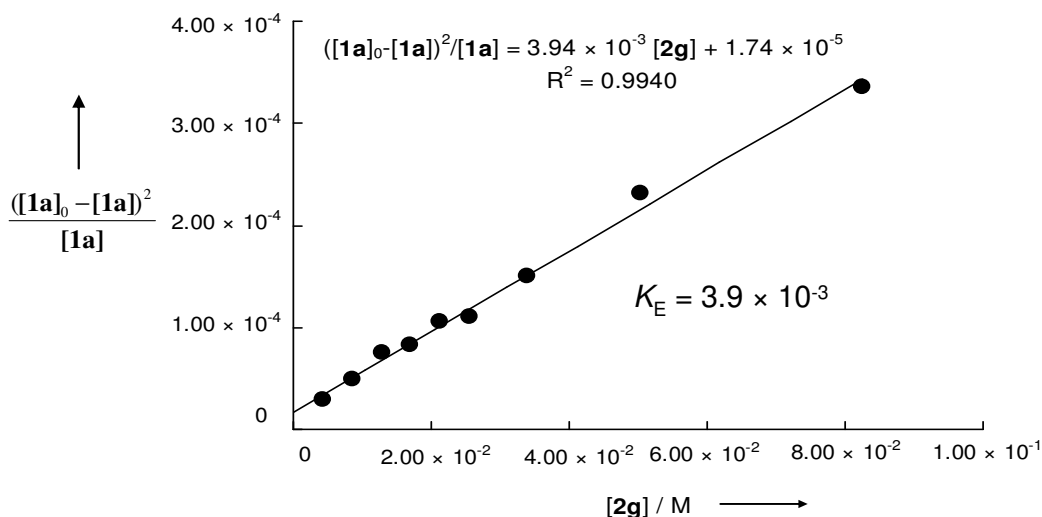


Figure S1. Estimation of the K_E value for the reaction of **1a** with **2g**.

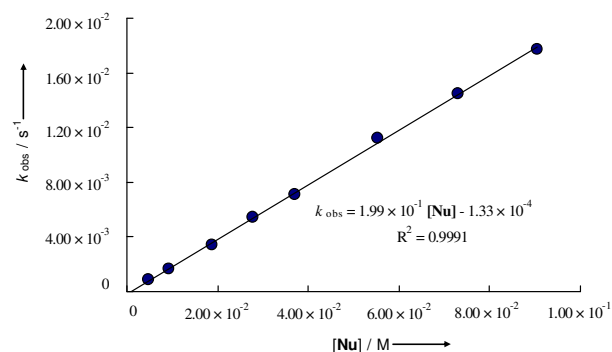
4.5. Kinetic Measurements

All reactions were studied using conventional ($\tau_{1/2} > 5$ s) or stopped-flow ($\tau_{1/2} < 5$ s) UV–vis spectroscopy by following the decays of absorbances of the complexes **1(a–c)** on their maximum absorption wavelengths. The temperature of the solutions was kept constant during all kinetic studies by using a circulating bath thermostat. At least a ten-fold excess of the nucleophile over the electrophile was used in all reactions studied, such that pseudo-first-order conditions were achieved.

Reaction of **1a** with 1-(*N*-morpholino)cyclopentene (**2a**), $\lambda_{\text{obs}} = 360$ nm, dichloromethane, 20 °C, conventional UV–vis spectrometry.

[1a] / M	[Nu] / M	$k_{\text{obs}}^a / \text{s}^{-1}$
1.19×10^{-4}	4.71×10^{-3}	8.79×10^{-4}
1.18×10^{-4}	9.39×10^{-3}	1.70×10^{-3}
1.18×10^{-4}	1.87×10^{-2}	3.41×10^{-3}
1.18×10^{-4}	2.79×10^{-2}	5.48×10^{-3}
1.17×10^{-4}	3.71×10^{-2}	7.11×10^{-3}
1.16×10^{-4}	5.52×10^{-2}	1.12×10^{-2}
1.15×10^{-4}	7.30×10^{-2}	1.45×10^{-2}
1.14×10^{-4}	9.06×10^{-2}	1.77×10^{-2}

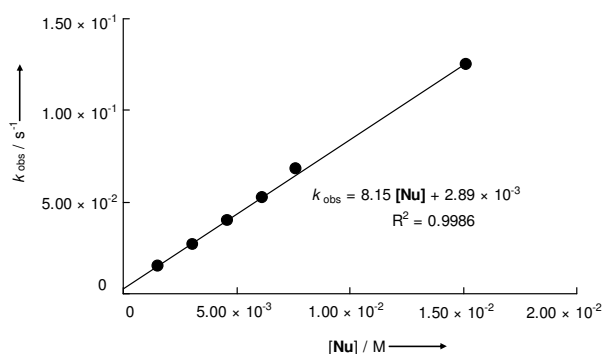
^a Absorbance decays were fitted only to 80–90% conversion in order to achieve proper monoexponential fits.



$$k_2 = 1.99 \times 10^{-1} \text{ M}^{-1} \text{ s}^{-1}$$

Reaction of **1a** with 1-(*N*-piperidino)cyclopentene (**2b**) in the presence of fumaronitrile (fn), $\lambda_{\text{obs}} = 360$ nm, dichloromethane, 20 °C, conventional UV–vis spectrometry.

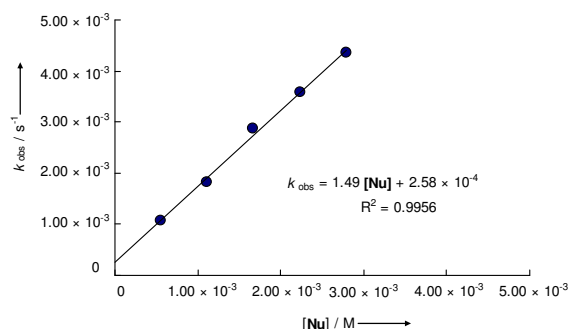
[1a] / M	[fn] / M	[Nu] / M	$k_{\text{obs}} / \text{s}^{-1}$
6.32×10^{-5}	5.80×10^{-4}	1.54×10^{-3}	1.52×10^{-2}
6.30×10^{-5}	5.78×10^{-4}	3.07×10^{-3}	2.70×10^{-2}
6.29×10^{-5}	5.77×10^{-4}	4.60×10^{-3}	4.00×10^{-2}
6.28×10^{-5}	5.76×10^{-4}	6.12×10^{-3}	5.24×10^{-2}
6.27×10^{-5}	5.75×10^{-4}	7.63×10^{-3}	6.80×10^{-2}
6.20×10^{-5}	5.69×10^{-4}	1.51×10^{-2}	1.25×10^{-1}



$$k_2 = 8.15 \text{ M}^{-1} \text{ s}^{-1}$$

Reaction of **1a** with potassium salt of Meldrum's acid (**2d**) in the presence of fumaronitrile (fn), $\lambda_{\text{obs}} = 360$ nm, DMSO, 20 °C, conventional UV–vis spectrometry.

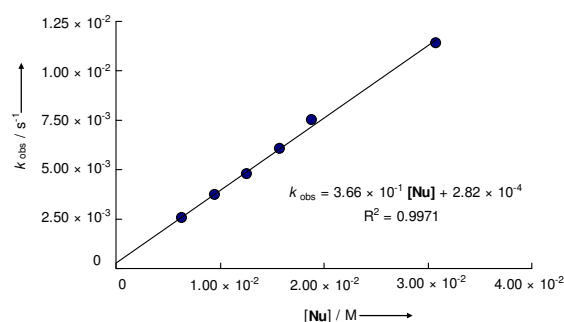
[1a] / M	[fn] / M	[Nu] / M	$k_{\text{obs}} / \text{s}^{-1}$
5.87×10^{-5}	5.39×10^{-4}	5.57×10^{-4}	1.08×10^{-3}
5.86×10^{-5}	5.39×10^{-4}	1.11×10^{-3}	1.82×10^{-3}
5.86×10^{-5}	5.38×10^{-4}	1.67×10^{-3}	2.88×10^{-3}
5.85×10^{-5}	5.38×10^{-4}	2.23×10^{-3}	3.59×10^{-3}
5.85×10^{-5}	5.38×10^{-4}	2.79×10^{-3}	4.35×10^{-3}



$$k_2 = 1.49 \text{ M}^{-1} \text{ s}^{-1}$$

Reaction of **1a** with triphenylphosphine (**2e**) in the presence of fumaronitrile (fn), $\lambda_{\text{obs}} = 360$ nm, dichloromethane, 20 °C, conventional UV–vis spectrometry.

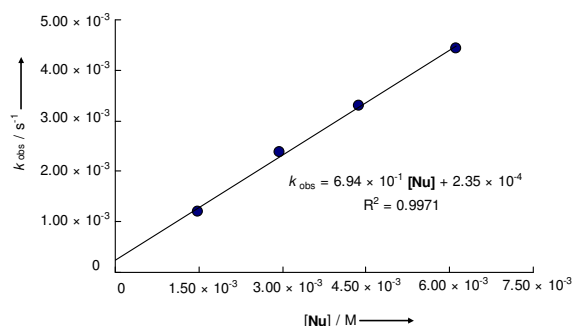
[1a] / M	[fn] / M	[PPh ₃] / M	$k_{\text{obs}} / \text{s}^{-1}$
1.11×10^{-4}	6.29×10^{-4}	6.37×10^{-3}	2.53×10^{-3}
1.11×10^{-4}	6.26×10^{-4}	9.52×10^{-3}	3.75×10^{-3}
1.10×10^{-4}	6.24×10^{-4}	1.26×10^{-2}	4.78×10^{-3}
1.10×10^{-4}	6.21×10^{-4}	1.57×10^{-2}	6.05×10^{-3}
1.09×10^{-4}	6.19×10^{-4}	1.88×10^{-2}	7.48×10^{-3}
1.61×10^{-4}	6.08×10^{-4}	3.08×10^{-2}	1.14×10^{-2}



$$k_2 = 3.66 \times 10^{-1} \text{ M}^{-1} \text{ s}^{-1}$$

Reaction of **1a** with triphenylphosphine (**2e**) in the presence of fumaronitrile (fn), $\lambda_{\text{obs}} = 360$ nm, acetonitrile, 20 °C, conventional UV–vis spectrometry.

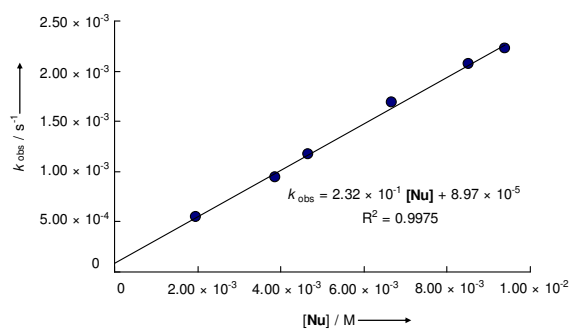
[1a] / M	[fn] / M	[PPh ₃] / M	$k_{\text{obs}} / \text{s}^{-1}$
1.48×10^{-4}	4.65×10^{-4}	1.48×10^{-3}	1.19×10^{-3}
1.47×10^{-4}	4.61×10^{-4}	2.94×10^{-3}	2.37×10^{-3}
1.46×10^{-4}	4.57×10^{-4}	4.38×10^{-3}	3.30×10^{-3}
1.44×10^{-4}	4.50×10^{-4}	6.12×10^{-3}	4.44×10^{-3}



$$k_2 = 6.94 \times 10^{-1} \text{ M}^{-1} \text{ s}^{-1}$$

Reaction of **1a** with triphenylphosphine (**2e**) in the presence of fumaronitrile (fn), $\lambda_{\text{obs}} = 360$ nm, DMSO, 20 °C, conventional UV-vis spectrometry.

[1a] / M	[fn] / M	[PPh ₃] / M	$k_{\text{obs}} / \text{s}^{-1}$
6.70×10^{-5}	5.22×10^{-4}	1.95×10^{-3}	5.47×10^{-4}
9.95×10^{-5}	5.17×10^{-4}	3.86×10^{-3}	9.48×10^{-4}
9.91×10^{-5}	5.14×10^{-4}	4.66×10^{-3}	1.17×10^{-3}
9.83×10^{-5}	5.10×10^{-4}	6.67×10^{-3}	1.69×10^{-3}
9.75×10^{-5}	5.06×10^{-4}	8.51×10^{-3}	2.07×10^{-3}
9.68×10^{-5}	1.00×10^{-3}	9.38×10^{-3}	2.23×10^{-3}

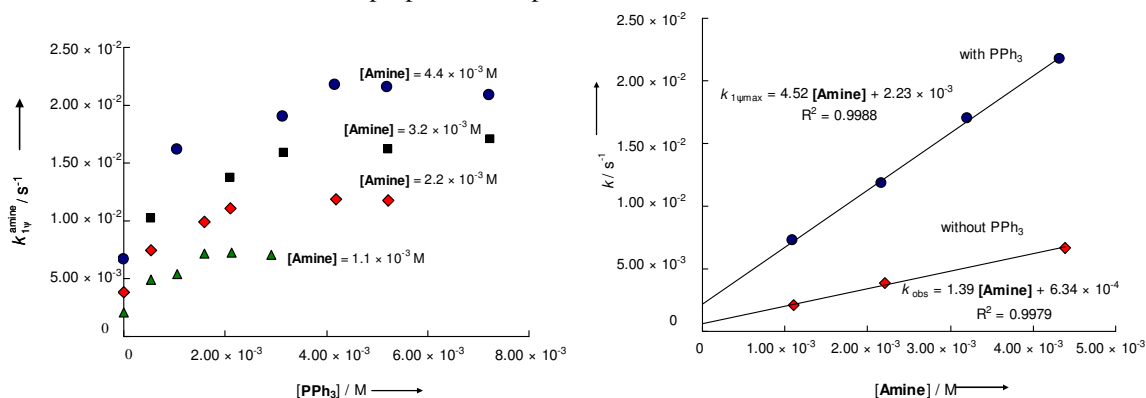


$$k_2 = 2.32 \times 10^{-1} \text{ M}^{-1} \text{ s}^{-1}$$

Reaction of **1a** with 1-amino-2-propanol (**2f**) in the presence of fumaronitrile (fn) and triphenylphosphine, $\lambda_{\text{obs}} = 360 \text{ nm}$, DMSO, $20 \text{ }^\circ\text{C}$, conventional UV-vis spectrometry. The values of $k_{1\psi}^{\text{amine}}$ and corresponding concentrations of all components are written in **bold**.

[1a] / M	[fn] / M	[Amine] / M	[PPh ₃] / M	$k_{\text{obs}} / \text{s}^{-1}$	$k_{1\psi}^{\text{PPh}_3} / \text{s}^{-1}$	$k_{1\psi}^{\text{amine}} / \text{s}^{-1}$
1.10×10^{-4}	5.42×10^{-4}	1.10×10^{-3}	0	2.09×10^{-3}	0	2.09×10^{-3}
1.10×10^{-4}	5.41×10^{-4}	1.10×10^{-3}	5.33×10^{-4}	5.02×10^{-3}	1.24×10^{-4}	4.90×10^{-3}
1.10×10^{-4}	5.40×10^{-4}	1.10×10^{-3}	1.06×10^{-3}	5.66×10^{-3}	2.47×10^{-4}	5.41×10^{-3}
1.09×10^{-4}	6.77×10^{-4}	1.10×10^{-3}	1.59×10^{-3}	7.53×10^{-3}	3.69×10^{-4}	7.16×10^{-3}
1.09×10^{-4}	5.37×10^{-4}	1.09×10^{-3}	2.12×10^{-3}	7.76×10^{-3}	4.92×10^{-4}	7.27×10^{-3}
1.09×10^{-4}	6.74×10^{-4}	1.09×10^{-3}	2.92×10^{-3}	7.75×10^{-3}	6.76×10^{-4}	7.07×10^{-3}
1.10×10^{-4}	6.80×10^{-4}	2.21×10^{-3}	0	3.82×10^{-3} ^b	0	3.82×10^{-3}
1.46×10^{-4}	6.77×10^{-4}	2.19×10^{-3}	5.31×10^{-4}	7.55×10^{-3}	1.23×10^{-4}	7.43×10^{-3}
1.09×10^{-4}	6.75×10^{-4}	2.19×10^{-3}	1.59×10^{-3}	1.03×10^{-2}	3.68×10^{-4}	9.93×10^{-3}
1.09×10^{-4}	6.74×10^{-4}	2.19×10^{-3}	2.11×10^{-3}	1.16×10^{-2}	4.90×10^{-4}	1.11×10^{-2}
1.08×10^{-4}	6.69×10^{-4}	2.17×10^{-3}	4.20×10^{-3}	1.28×10^{-2}	9.74×10^{-4}	1.18×10^{-2}
1.08×10^{-4}	6.66×10^{-4}	2.16×10^{-3}	5.22×10^{-3}	1.30×10^{-2}	1.21×10^{-3}	1.18×10^{-2}
1.13×10^{-4}	6.77×10^{-4}	3.29×10^{-3}	5.31×10^{-4}	1.03×10^{-2}	1.23×10^{-4}	1.02×10^{-2}
1.12×10^{-4}	6.73×10^{-4}	3.27×10^{-3}	2.11×10^{-3}	1.42×10^{-2}	4.89×10^{-4}	1.37×10^{-2}
1.12×10^{-4}	6.70×10^{-4}	3.26×10^{-3}	3.15×10^{-3}	1.66×10^{-2}	7.31×10^{-4}	1.59×10^{-2}
1.11×10^{-4}	6.65×10^{-4}	3.23×10^{-3}	5.21×10^{-3}	1.74×10^{-2}	1.21×10^{-3}	1.62×10^{-2}
1.10×10^{-4}	6.59×10^{-4}	3.21×10^{-3}	7.24×10^{-3}	1.87×10^{-2}	1.68×10^{-3}	1.70×10^{-2}
1.13×10^{-4}	6.77×10^{-4}	4.39×10^{-3}	0	6.70×10^{-3}	0	6.70×10^{-3}
1.13×10^{-4}	6.74×10^{-4}	4.37×10^{-3}	1.06×10^{-3}	1.64×10^{-2}	2.45×10^{-4}	1.62×10^{-2}
1.12×10^{-4}	6.69×10^{-4}	4.34×10^{-3}	3.15×10^{-3}	1.97×10^{-2}	7.29×10^{-4}	1.90×10^{-2}
1.11×10^{-4}	6.66×10^{-4}	4.32×10^{-3}	4.18×10^{-3}	2.27×10^{-2}	9.70×10^{-4}	2.17×10^{-2}
1.11×10^{-4}	6.63×10^{-4}	4.30×10^{-3}	5.20×10^{-3}	2.28×10^{-2}	1.21×10^{-3}	2.16×10^{-2}
1.10×10^{-4}	6.58×10^{-4}	4.27×10^{-3}	7.23×10^{-3}	2.26×10^{-2}	1.67×10^{-3}	2.09×10^{-2}

^a $k_{1\psi}^{\text{PPh}_3} = k_2^{\text{PPh}_3}(\text{DMSO}) \cdot [\text{PPh}_3] = 0.232 \cdot [\text{PPh}_3]$. ^b The absorbance decay was fitted only to 80% conversion in order to achieve proper monoexponential fit.



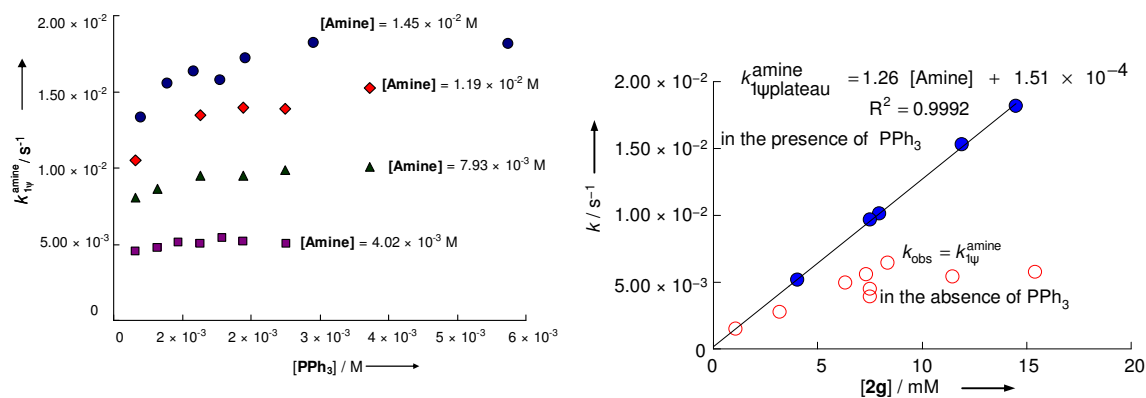
$$k_2 = 4.52 \text{ M}^{-1} \text{ s}^{-1}$$

Reaction of **1a** with benzylamine (**2g**) in the presence of fumaronitrile and triphenylphosphine (fn), $\lambda_{\text{obs}} = 360 \text{ nm}$, acetonitrile, $20 \text{ }^\circ\text{C}$, conventional UV-vis spectrometry.

[1a] / M	[fn] / M	[Amine] / M	[PPh ₃] / M	$k_{\text{obs}} / \text{s}^{-1}$	$k_{1\psi}^{\text{PPh}_3} / \text{s}^{-1}$	$k_{1\psi}^{\text{amine}} / \text{s}^{-1}$	$x, \%$
1.37×10^{-4}	0	1.07×10^{-3}	0	$1.48 \times 10^{-3}{}^b$	0	1.48×10^{-3}	16.2
1.36×10^{-4}	0	3.19×10^{-3}	0	$2.78 \times 10^{-3}{}^b$	0	2.78×10^{-3}	26.3
1.34×10^{-4}	0	6.31×10^{-3}	0	$4.96 \times 10^{-3}{}^b$	0	4.96×10^{-3}	35.0
1.33×10^{-4}	0	7.33×10^{-3}	0	$5.59 \times 10^{-3}{}^b$	0	5.59×10^{-3}	37.2
1.33×10^{-4}	0	8.34×10^{-3}	0	$6.45 \times 10^{-3}{}^b$	0	6.45×10^{-3}	39.1
1.04×10^{-4}	0	1.15×10^{-2}	0	$5.75 \times 10^{-3}{}^b$	0	5.75×10^{-3}	48.0
1.04×10^{-4}	0	1.54×10^{-2}	0	$5.43 \times 10^{-3}{}^b$	0	5.43×10^{-3}	52.8
1.39×10^{-4}	5.31×10^{-4}	4.06×10^{-3}	3.18×10^{-4}	4.77×10^{-3}	2.21×10^{-4}	4.55×10^{-3}	4.8
1.39×10^{-4}	5.30×10^{-4}	4.05×10^{-3}	6.34×10^{-4}	5.16×10^{-3}	4.40×10^{-4}	4.72×10^{-3}	2.5
1.38×10^{-4}	5.29×10^{-4}	4.05×10^{-3}	9.50×10^{-4}	5.75×10^{-3}	6.59×10^{-4}	5.09×10^{-3}	1.7
1.38×10^{-4}	5.28×10^{-4}	4.04×10^{-3}	1.26×10^{-3}	5.95×10^{-3}	8.74×10^{-4}	5.08×10^{-3}	1.3
1.38×10^{-4}	5.27×10^{-4}	4.03×10^{-3}	1.58×10^{-3}	6.46×10^{-3}	1.10×10^{-3}	5.36×10^{-3}	1.0
1.38×10^{-4}	5.26×10^{-4}	4.02×10^{-3}	1.89×10^{-3}	6.47×10^{-3}	1.31×10^{-3}	5.16×10^{-3}	0.8
1.37×10^{-4}	5.24×10^{-4}	4.00×10^{-3}	2.51×10^{-3}	6.86×10^{-3}	1.74×10^{-3}	5.12×10^{-3}	0.6
1.13×10^{-4}	0	7.52×10^{-3}	0	$3.90 \times 10^{-3}{}^b$	0	3.90×10^{-3}	39.9
1.25×10^{-4}	5.81×10^{-4}	7.52×10^{-3}	0	$4.46 \times 10^{-3}{}^b$	0	4.46×10^{-3}	38.5
1.13×10^{-4}	5.81×10^{-4}	7.52×10^{-3}	1.37×10^{-3}	1.05×10^{-2}	9.51×10^{-4}	9.55×10^{-3}	2.1
1.13×10^{-4}	5.81×10^{-4}	7.52×10^{-3}	2.74×10^{-3}	1.16×10^{-2}	1.90×10^{-3}	9.70×10^{-3}	1.1
1.13×10^{-4}	5.81×10^{-4}	7.52×10^{-3}	4.11×10^{-3}	1.25×10^{-2}	2.85×10^{-3}	9.65×10^{-3}	0.7
1.39×10^{-4}	5.30×10^{-4}	8.11×10^{-3}	3.17×10^{-4}	8.27×10^{-3}	2.20×10^{-4}	8.05×10^{-3}	9.0
1.38×10^{-4}	5.29×10^{-4}	8.09×10^{-3}	6.33×10^{-4}	9.07×10^{-3}	4.39×10^{-4}	8.63×10^{-3}	4.8
1.38×10^{-4}	5.27×10^{-4}	8.06×10^{-3}	1.26×10^{-3}	1.04×10^{-2}	8.74×10^{-4}	9.53×10^{-3}	2.5
1.37×10^{-4}	5.25×10^{-4}	8.03×10^{-3}	1.88×10^{-3}	1.09×10^{-2}	1.30×10^{-3}	9.60×10^{-3}	1.7
1.37×10^{-4}	5.23×10^{-4}	7.99×10^{-3}	2.50×10^{-3}	1.17×10^{-2}	1.74×10^{-3}	9.97×10^{-3}	1.3
1.36×10^{-4}	5.19×10^{-4}	7.93×10^{-3}	3.72×10^{-3}	1.28×10^{-2}	2.58×10^{-3}	1.02×10^{-2}	0.8
1.38×10^{-4}	5.29×10^{-4}	1.21×10^{-2}	3.17×10^{-4}	1.07×10^{-2}	2.20×10^{-4}	1.05×10^{-2}	12.7
1.38×10^{-4}	5.26×10^{-4}	1.21×10^{-2}	1.26×10^{-3}	1.44×10^{-2}	8.74×10^{-4}	1.35×10^{-2}	3.7
1.37×10^{-4}	5.24×10^{-4}	1.20×10^{-2}	1.88×10^{-3}	1.53×10^{-2}	1.30×10^{-3}	1.40×10^{-2}	2.5
1.36×10^{-4}	5.22×10^{-4}	1.20×10^{-2}	2.50×10^{-3}	1.57×10^{-2}	1.74×10^{-3}	1.40×10^{-2}	1.9
6.80×10^{-5}	5.20×10^{-4}	1.19×10^{-2}	3.73×10^{-3}	1.80×10^{-2}	2.59×10^{-3}	1.54×10^{-2}	1.3
1.48×10^{-4}	0	1.47×10^{-2}	3.99×10^{-4}	$1.60 \times 10^{-2}{}^b$	2.77×10^{-4}	1.57×10^{-2}	12.4
1.47×10^{-4}	4.61×10^{-4}	1.46×10^{-2}	3.96×10^{-4}	1.36×10^{-2}	2.75×10^{-4}	1.33×10^{-2}	12.4
1.46×10^{-4}	9.17×10^{-4}	1.45×10^{-2}	3.94×10^{-4}	1.33×10^{-2}	2.73×10^{-4}	1.30×10^{-2}	12.4
1.45×10^{-4}	1.81×10^{-3}	1.43×10^{-2}	3.89×10^{-4}	1.19×10^{-2}	2.70×10^{-4}	1.16×10^{-2}	12.4
1.46×10^{-4}	4.57×10^{-4}	1.45×10^{-2}	7.86×10^{-4}	1.61×10^{-2}	5.45×10^{-4}	1.56×10^{-2}	6.8
1.45×10^{-4}	4.54×10^{-4}	1.44×10^{-2}	1.17×10^{-3}	1.72×10^{-2}	8.12×10^{-4}	1.64×10^{-2}	4.7
1.44×10^{-4}	4.50×10^{-4}	1.43×10^{-2}	1.55×10^{-3}	1.69×10^{-2}	1.08×10^{-3}	1.58×10^{-2}	3.5
1.43×10^{-4}	4.47×10^{-4}	1.41×10^{-2}	1.92×10^{-3}	1.86×10^{-2}	1.33×10^{-3}	1.73×10^{-2}	2.9
1.46×10^{-4}	4.57×10^{-4}	1.45×10^{-2}	2.92×10^{-3}	2.03×10^{-2}	2.03×10^{-3}	1.83×10^{-2}	1.9
1.44×10^{-4}	4.50×10^{-4}	1.45×10^{-2}	5.75×10^{-3}	2.23×10^{-2}	3.99×10^{-3}	1.83×10^{-2}	1.0

^a $k_{1\psi}^{\text{PPh}_3} = k_2^{\text{PPh}_3} (\text{CH}_3\text{CN}) \cdot [\text{PPh}_3] = 0.694 \cdot [\text{PPh}_3]$. ^b „Best monoexponential fit“ of non-first order absorbance decay.

The values of $k_{1\psi\text{plateau}}^{\text{amine}}$ and corresponding concentrations of all components are written in **bold**.



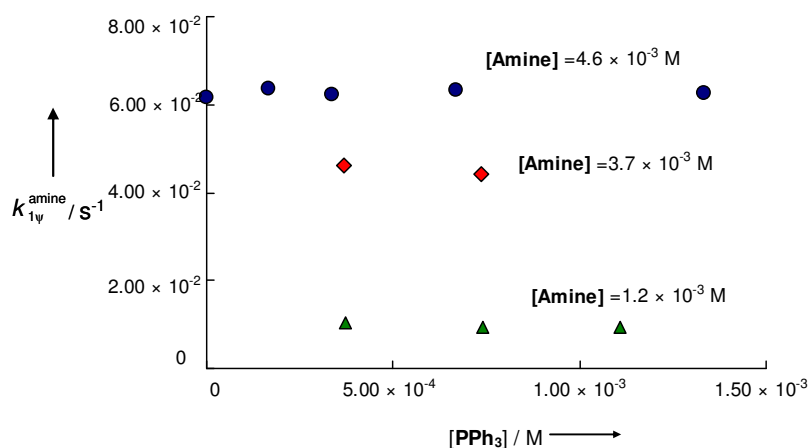
$$k_2 = 1.26 \text{ M}^{-1} \text{ s}^{-1}$$

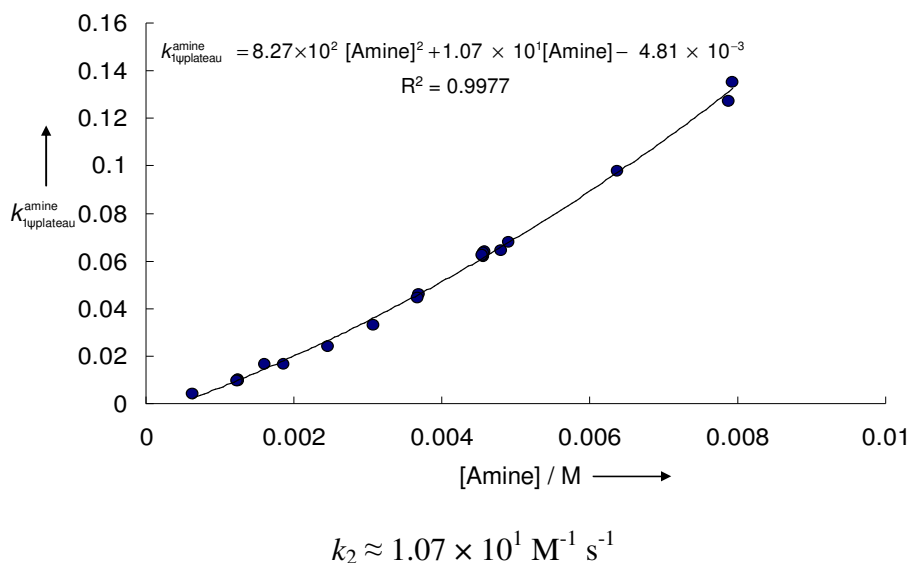
The ratios $x = \frac{[\mathbf{1a}']}{[\mathbf{1a}] + [\mathbf{1a}]'}$ corresponding to the moment immediately after addition of benzylamine to the reaction mixture, which can be calculated using the K_E value estimated above, are also in agreement with data shown on the right top figure. For instance, in case of every measurement used for $k_{1\psi\text{plateau}}^{\text{amine}}$ derivation, this ratio is less than 2%, whereas for the reaction corresponding to the right bottom point on the Figure 10 it reaches 53%; and in case of the lowest amine concentration used for the measurements in the absence of PPh_3 , $x = 16\%$, which explains that the corresponding point even lies on the $k_{1\psi\text{plateau}}^{\text{amine}} - [\text{Amine}]$ correlation line.

Reaction of **1a** with morpholine (**2h**) in the presence of fumaronitrile (fn) and triphenylphosphine, $\lambda_{\text{obs}} = 360$ nm, CH_3CN , 20 °C, conventional UV–vis spectrometry. The values of $k_{1\psi}^{\text{amine}}$ and corresponding concentrations of all components are written in **bold**.

[1a] / M	[fn] / M	[Amine] / M	[PPh ₃] / M	$k_{\text{obs}} / \text{s}^{-1}$	$k_{1\psi}^{\text{PPh}_3} / \text{s}^{-1}$	$k_{1\psi}^{\text{amine}} / \text{s}^{-1}$
4.45×10^{-5}	4.59×10^{-4}	6.24×10^{-4}	3.73×10^{-4}	4.17×10^{-3}	2.59×10^{-4}	3.91×10^{-3}
4.44×10^{-5}	4.58×10^{-4}	1.24×10^{-3}	3.73×10^{-4}	1.05×10^{-2}	2.59×10^{-4}	1.02×10^{-2}
8.83×10^{-5}	4.55×10^{-4}	1.24×10^{-3}	7.41×10^{-4}	9.98×10^{-3}	5.14×10^{-4}	9.47×10^{-3}
8.81×10^{-5}	4.54×10^{-4}	1.23×10^{-3}	1.11×10^{-3}	1.02×10^{-2}	7.69×10^{-4}	9.43×10^{-3}
8.84×10^{-5}	4.87×10^{-4}	1.61×10^{-3}	3.41×10^{-4}	1.66×10^{-2}	2.36×10^{-4}	1.64×10^{-2}
8.83×10^{-5}	4.55×10^{-4}	1.86×10^{-3}	3.70×10^{-4}	1.68×10^{-2}	2.57×10^{-4}	1.65×10^{-2}
8.81×10^{-5}	4.54×10^{-4}	2.47×10^{-3}	3.70×10^{-4}	2.43×10^{-2}	2.56×10^{-4}	2.40×10^{-2}
8.79×10^{-5}	4.53×10^{-4}	3.08×10^{-3}	3.69×10^{-4}	3.33×10^{-2}	2.56×10^{-4}	3.30×10^{-2}
8.77×10^{-5}	4.52×10^{-4}	3.69×10^{-3}	3.68×10^{-4}	4.63×10^{-2}	2.55×10^{-4}	4.60×10^{-2}
8.75×10^{-5}	4.51×10^{-4}	3.68×10^{-3}	7.35×10^{-4}	4.48×10^{-2}	5.10×10^{-4}	4.43×10^{-2}
8.72×10^{-5}	1.02×10^{-4}	4.57×10^{-3}	0	6.16×10^{-2b}	0	6.16×10^{-2}
6.55×10^{-5}	1.02×10^{-4}	4.58×10^{-3}	1.68×10^{-4}	6.38×10^{-2}	1.17×10^{-4}	6.37×10^{-2}
6.54×10^{-5}	1.02×10^{-4}	4.57×10^{-3}	3.36×10^{-4}	6.25×10^{-2}	2.33×10^{-4}	6.23×10^{-2}
6.53×10^{-5}	1.02×10^{-4}	4.56×10^{-3}	6.70×10^{-4}	6.38×10^{-2}	4.65×10^{-4}	6.33×10^{-2}
6.50×10^{-5}	1.02×10^{-4}	4.55×10^{-3}	1.34×10^{-3}	6.34×10^{-2}	9.27×10^{-4}	6.25×10^{-2}
8.77×10^{-5}	4.83×10^{-4}	4.80×10^{-3}	3.38×10^{-4}	6.47×10^{-2}	2.34×10^{-4}	6.45×10^{-2}
8.74×10^{-5}	4.50×10^{-4}	4.90×10^{-3}	3.67×10^{-4}	6.83×10^{-2}	2.54×10^{-4}	6.80×10^{-2}
8.74×10^{-5}	4.81×10^{-4}	6.38×10^{-3}	3.37×10^{-4}	9.80×10^{-2}	2.34×10^{-4}	9.78×10^{-2}
8.63×10^{-5}	1.01×10^{-4}	7.88×10^{-3}	3.32×10^{-4}	1.35×10^{-1}	2.31×10^{-4}	1.27×10^{-1}
8.70×10^{-5}	4.79×10^{-4}	7.94×10^{-3}	3.35×10^{-4}	1.35×10^{-1}	2.33×10^{-4}	1.35×10^{-1}

^a $k_{1\psi}^{\text{PPh}_3} = k_2^{\text{PPh}_3} (\text{CH}_3\text{CN}) \cdot [\text{PPh}_3] = 0.694 \cdot [\text{PPh}_3]$. ^b „Best monoexponential fit“ of non-first order absorbance decay.



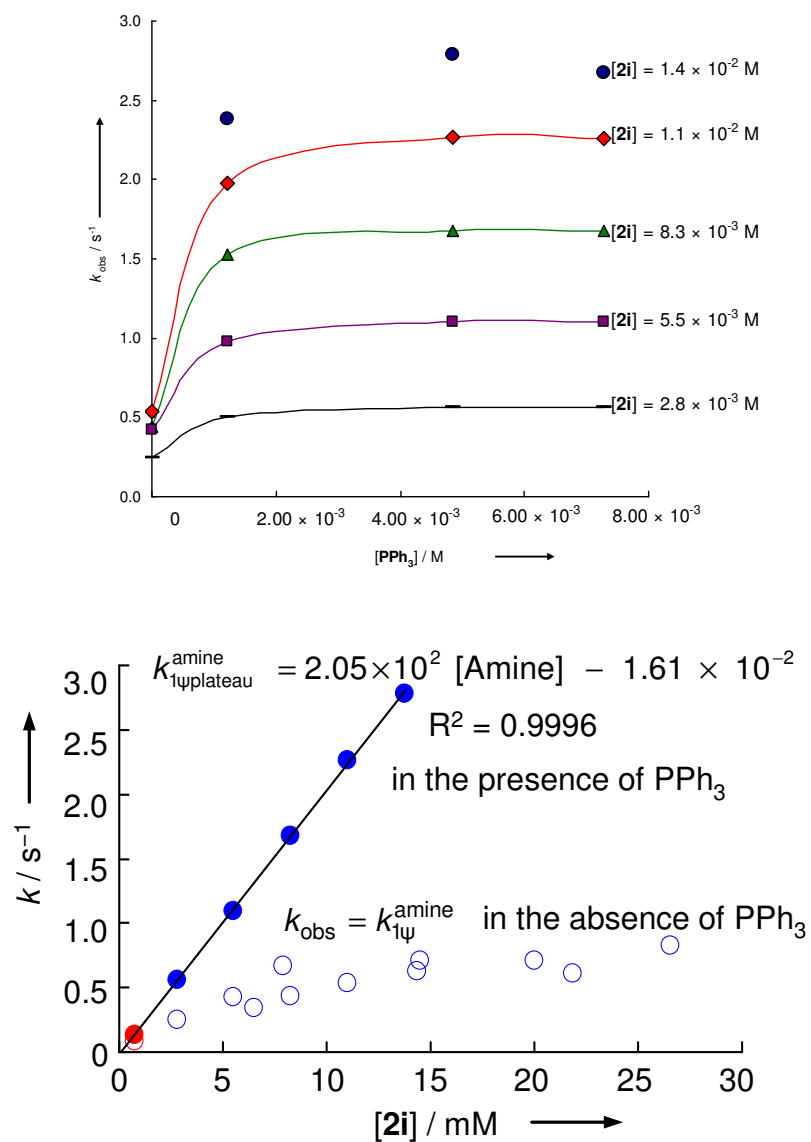


The mixed first and second order in nucleophile was reported for reactions of amines with cationic allylpalladium complexes carrying iminophosphine ligands.⁷ This kinetic behavior was rationalized with possibility of reversible coordination of one amine molecule on the central metal forming pentacoordinated palladium species, which also can act as electrophiles towards amines. Considering this pathway and the attack of amines at the allyl ligand of the initial complex, one can derive the rate law with mixed first and second order in nucleophile. For more details see ref 7.

Reaction of **1a** with piperidine (**2i**) in the presence of fumaronitrile (fn) and triphenylphosphine, $\lambda_{\text{obs}} = 360 \text{ nm}$, CH_3CN , $20 \text{ }^\circ\text{C}$, conventional UV-vis and stopped-flow measurements. The values of $k_{1\psi_{\text{max}}}$ and corresponding concentrations of all components are written in **bold**. Due to the highest precision only stopped-flow-derived $k_{1\psi_{\text{max}}}$ values were used for determination of k_2 .

[1a] / M	[fn] / M	[Amine] / M	[PPh ₃] / M	$k_{\text{obs}} / \text{s}^{-1}$	$k_{1\Psi}^{\text{PPh}_3} / \text{s}^{-1}$	$k_{1\Psi}^{\text{amine}} / \text{s}^{-1}$
7.29×10^{-5}	0	7.55×10^{-4}	0	$8.10 \times 10^{-2 a, b}$	0	8.10×10^{-2}
7.38×10^{-5}	0	6.52×10^{-3}	0	$3.44 \times 10^{-1 a, c}$	0	3.44×10^{-1}
5.33×10^{-5}	0	7.99×10^{-3}	0	$6.70 \times 10^{-1 a, c}$	0	6.70×10^{-1}
5.33×10^{-5}	0	1.43×10^{-2}	0	$6.27 \times 10^{-1 a, c}$	0	6.27×10^{-1}
7.38×10^{-5}	0	1.45×10^{-2}	0	$7.09 \times 10^{-1 a, c}$	0	7.09×10^{-1}
7.38×10^{-5}	0	2.00×10^{-2}	0	$7.13 \times 10^{-1 a, c}$	0	7.13×10^{-1}
5.33×10^{-5}	0	2.18×10^{-2}	0	$6.11 \times 10^{-1 a, c}$	0	6.11×10^{-1}
7.38×10^{-5}	0	2.65×10^{-2}	0	$8.26 \times 10^{-1 a, c}$	0	8.26×10^{-1}
5.33×10^{-5}	0	3.39×10^{-2}	0	$7.34 \times 10^{-1 a, c}$	0	7.34×10^{-1}
7.38×10^{-5}	0	4.09×10^{-2}	0	$8.18 \times 10^{-1 a, c}$	0	8.18×10^{-1}
7.38×10^{-5}	0	5.41×10^{-2}	0	$7.80 \times 10^{-1 a, c}$	0	7.80×10^{-1}
5.33×10^{-5}	0	5.83×10^{-2}	0	$6.94 \times 10^{-1 a, c}$	0	6.94×10^{-1}
7.38×10^{-5}	0	1.29×10^{-1}	0	$8.51 \times 10^{-1 a, c}$	0	8.51×10^{-1}
4.37×10^{-5}	4.58×10^{-4}	3.86×10^{-4}	3.73×10^{-4}	$6.14 \times 10^{-2 b}$	2.59×10^{-4}	6.11×10^{-2}
4.37×10^{-5}	4.57×10^{-4}	4.82×10^{-4}	3.72×10^{-4}	$8.09 \times 10^{-2 b}$	2.58×10^{-4}	8.06×10^{-2}
4.36×10^{-5}	4.57×10^{-4}	5.78×10^{-4}	3.72×10^{-4}	$9.88 \times 10^{-2 b}$	2.58×10^{-4}	9.85×10^{-2}
4.35×10^{-5}	4.56×10^{-4}	5.76×10^{-4}	7.42×10^{-4}	$9.73 \times 10^{-2 b}$	5.15×10^{-4}	9.68×10^{-2}
4.35×10^{-5}	4.55×10^{-4}	5.75×10^{-4}	1.11×10^{-3}	$9.48 \times 10^{-2 b}$	7.71×10^{-4}	9.40×10^{-2}
4.36×10^{-5}	4.56×10^{-4}	6.73×10^{-4}	3.71×10^{-4}	$1.13 \times 10^{-1 b}$	2.58×10^{-4}	1.13×10^{-1}
4.35×10^{-5}	4.56×10^{-4}	7.69×10^{-4}	3.71×10^{-4}	$1.34 \times 10^{-1 b}$	2.58×10^{-4}	1.34×10^{-1}
4.35×10^{-5}	4.55×10^{-4}	7.67×10^{-4}	7.41×10^{-4}	$1.36 \times 10^{-1 b}$	5.14×10^{-4}	1.35×10^{-1}
7.86×10^{-5}	6.94×10^{-4}	2.80×10^{-3}	0	$2.49 \times 10^{-1 a, c}$	0	2.49×10^{-1}
7.86×10^{-5}	6.94×10^{-4}	2.80×10^{-3}	1.21×10^{-3}	$5.07 \times 10^{-1 c}$	8.42×10^{-4}	5.06×10^{-1}
7.86×10^{-5}	6.94×10^{-4}	2.80×10^{-3}	4.85×10^{-3}	$5.66 \times 10^{-1 c}$	3.37×10^{-3}	5.63×10^{-1}
7.86×10^{-5}	6.94×10^{-4}	2.80×10^{-3}	7.27×10^{-3}	$5.68 \times 10^{-1 c}$	5.05×10^{-3}	5.63×10^{-1}
7.86×10^{-5}	6.94×10^{-4}	5.51×10^{-3}	0	$4.23 \times 10^{-1 a, c}$	0	4.23×10^{-1}
7.86×10^{-5}	6.94×10^{-4}	5.51×10^{-3}	1.21×10^{-3}	$9.83 \times 10^{-1 c}$	8.42×10^{-4}	9.82×10^{-1}
7.86×10^{-5}	6.94×10^{-4}	5.51×10^{-3}	4.85×10^{-3}	1.10^c	3.37×10^{-3}	1.10
7.86×10^{-5}	6.94×10^{-4}	5.51×10^{-3}	7.27×10^{-3}	1.10^c	5.05×10^{-3}	1.09
7.86×10^{-5}	6.94×10^{-4}	8.26×10^{-3}	0	$4.38 \times 10^{-1 a, c}$	0	4.38×10^{-1}
7.86×10^{-5}	6.94×10^{-4}	8.26×10^{-3}	1.21×10^{-3}	1.53^c	8.42×10^{-4}	1.53
7.86×10^{-5}	6.94×10^{-4}	8.26×10^{-3}	4.85×10^{-3}	1.68^c	3.37×10^{-3}	1.68
7.86×10^{-5}	6.94×10^{-4}	8.26×10^{-3}	7.27×10^{-3}	1.68^c	5.05×10^{-3}	1.67
7.86×10^{-5}	6.94×10^{-4}	1.10×10^{-2}	0	$5.35 \times 10^{-1 a, c}$	0	5.35×10^{-1}
7.86×10^{-5}	6.94×10^{-4}	1.10×10^{-2}	1.21×10^{-3}	1.98^c	8.42×10^{-4}	1.98
7.86×10^{-5}	6.94×10^{-4}	1.10×10^{-2}	4.85×10^{-3}	2.27^c	3.37×10^{-3}	2.27
7.86×10^{-5}	6.94×10^{-4}	1.10×10^{-2}	7.27×10^{-3}	2.26^c	5.05×10^{-3}	2.25
7.86×10^{-5}	6.94×10^{-4}	1.38×10^{-2}	1.21×10^{-3}	2.38^c	8.42×10^{-4}	2.38
7.86×10^{-5}	6.94×10^{-4}	1.38×10^{-2}	4.85×10^{-3}	2.80^c	3.37×10^{-3}	2.80
7.86×10^{-5}	6.94×10^{-4}	1.38×10^{-2}	7.27×10^{-3}	2.67^c	5.05×10^{-3}	2.66
7.86×10^{-5}	6.94×10^{-4}	1.38×10^{-2}	9.70×10^{-3}	2.83^c	6.74×10^{-3}	2.82

^a „Best monoexponential fit“ of non-first order absorbance decay. ^b Conventional UV–vis measurements. ^c Stopped-flow measurements.

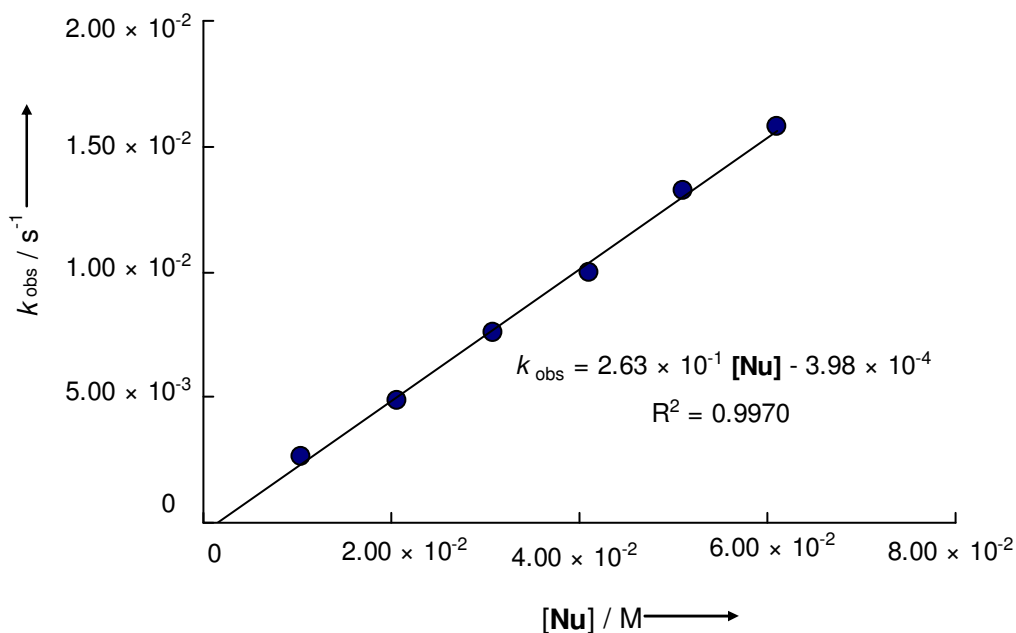


Red points: conventional UV-vis measurements (only one point for each series is shown for to avoid overlapping), blue points: stopped-flow measurements.

$$k_2 = 2.05 \times 10^2 \text{ M}^{-1} \text{ s}^{-1}$$

Reaction of **1b** with 1-(N-morpholino)cyclopentene (**2a**) in the presence of fumaronitrile (fn), $\lambda_{\text{obs}} = 357$ nm, dichloromethane, 20 °C, conventional UV-vis spectrometry. To revert the partial decomposition of the electrophile proceeding slowly in the stock solution, small amounts of PPh_3 were added.

[1b] / M	[PPh_3] / M	[fn] / M	[Nu] / M	$k_{\text{obs}} / \text{s}^{-1}$
1.25×10^{-4}	3.13×10^{-4}	6.02×10^{-4}	1.04×10^{-2}	2.64×10^{-3}
1.24×10^{-4}	3.11×10^{-4}	5.98×10^{-4}	2.07×10^{-2}	4.90×10^{-3}
1.24×10^{-4}	3.09×10^{-4}	5.96×10^{-4}	3.09×10^{-2}	7.60×10^{-3}
1.23×10^{-4}	3.08×10^{-4}	5.93×10^{-4}	4.10×10^{-2}	9.95×10^{-3}
1.23×10^{-4}	3.07×10^{-4}	5.91×10^{-4}	5.11×10^{-2}	1.32×10^{-2}
1.22×10^{-4}	3.06×10^{-4}	5.88×10^{-4}	6.10×10^{-2}	1.58×10^{-2}

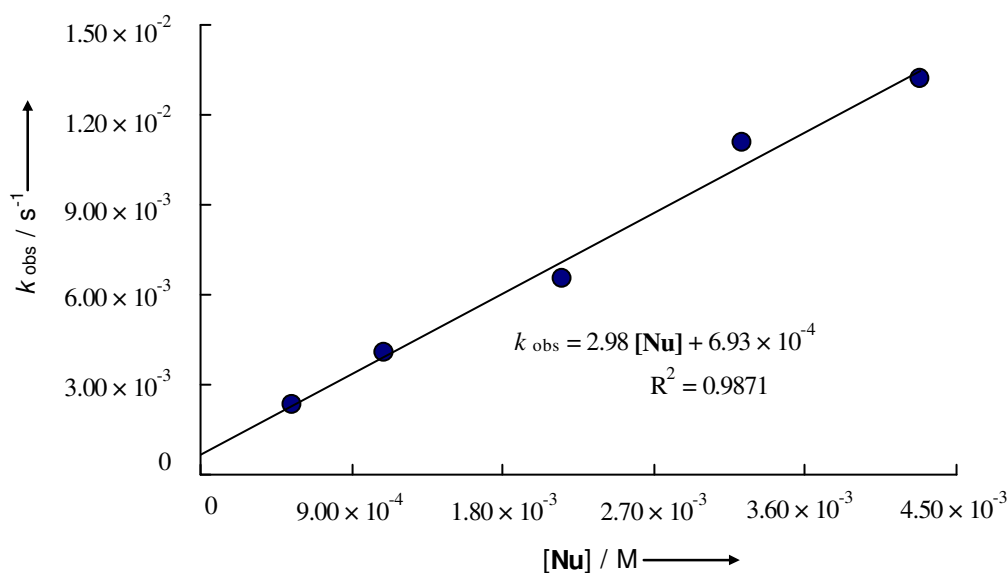


$$k_2 = 2.63 \times 10^2 \text{ M}^{-1} \text{ s}^{-1}$$

Reaction of **1b** with potassium salt of Meldrum's acid (**2d**) in the presence of fumaronitrile (fn), $\lambda_{\text{obs}} = 357 \text{ nm}$, DMSO, 20 °C, conventional UV-vis spectrometry. To turn back the partial, slowly proceeding decomposition of the electrophile in the stock solution, small amounts of PPh_3 were added.

[1b] / M	[PPh_3] / M	[fn] / M	[Nu] / M	$k_{\text{obs}}^a / \text{s}^{-1}$
7.75×10^{-5}	4.27×10^{-4}	5.86×10^{-4}	5.46×10^{-4}	2.35×10^{-3}
1.16×10^{-4}	4.25×10^{-4}	5.84×10^{-4}	1.09×10^{-3}	4.08×10^{-3}
1.15×10^{-4}	4.23×10^{-4}	5.81×10^{-4}	2.16×10^{-3}	6.51×10^{-3}
1.15×10^{-4}	4.21×10^{-4}	5.79×10^{-4}	3.23×10^{-3}	1.11×10^{-2}
1.14×10^{-4}	4.20×10^{-4}	5.77×10^{-4}	4.29×10^{-3}	1.32×10^{-2}

^a „Best monoexponential fit“ of non-first order absorbance decay.

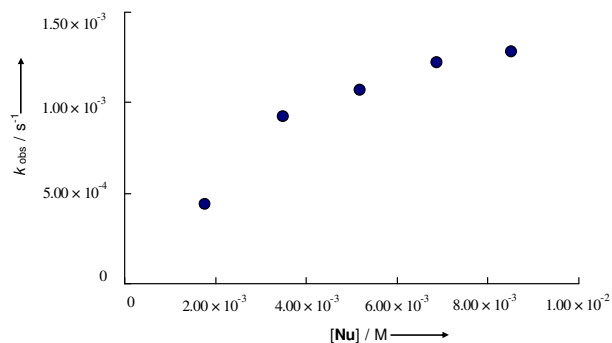


$$k_2 \approx 2.98 \text{ M}^{-1} \text{ s}^{-1}$$

Due to the low quality of single runs and the k_{obs} vs [Nu] correlation, this k_2 value should be considered only as rough estimate.

Reaction of **1b** with triphenylphosphine (**2e**) in the presence of fumaronitrile (fn), $\lambda_{\text{obs}} = 360$ nm, DMSO, 20 °C, conventional UV–vis spectrometry.

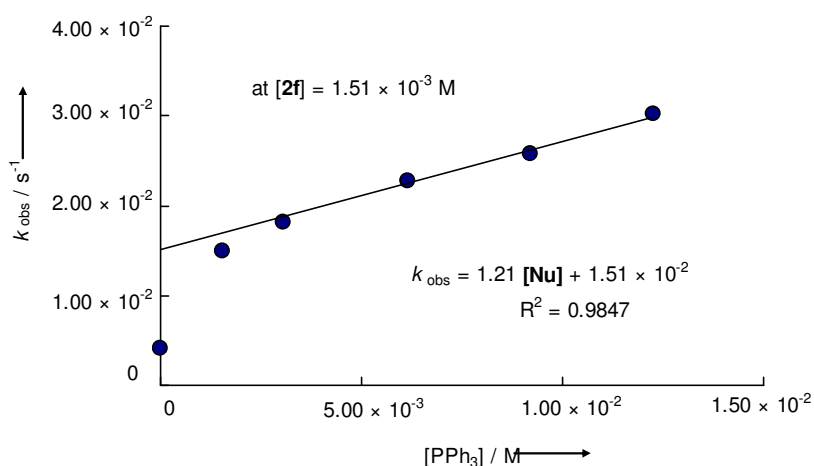
[1b] / M	[fn] / M	[PPh ₃] / M	$k_{\text{obs}} / \text{s}^{-1}$
1.22×10^{-4}	6.00×10^{-4}	1.76×10^{-3}	4.35×10^{-4}
1.21×10^{-4}	5.96×10^{-4}	3.49×10^{-3}	9.20×10^{-4}
1.20×10^{-4}	5.91×10^{-4}	5.19×10^{-3}	1.07×10^{-3}
1.19×10^{-4}	5.86×10^{-4}	6.87×10^{-3}	1.22×10^{-3}
1.18×10^{-4}	5.81×10^{-4}	8.52×10^{-3}	1.28×10^{-3}



Reaction of **1b** with 1-amino-2-propanol (**2f**) in the presence of fumaronitrile (fn) and triphenylphosphine, $\lambda_{\text{obs}} = 355$ nm, DMSO, 20 °C, conventional UV–vis spectrometry.

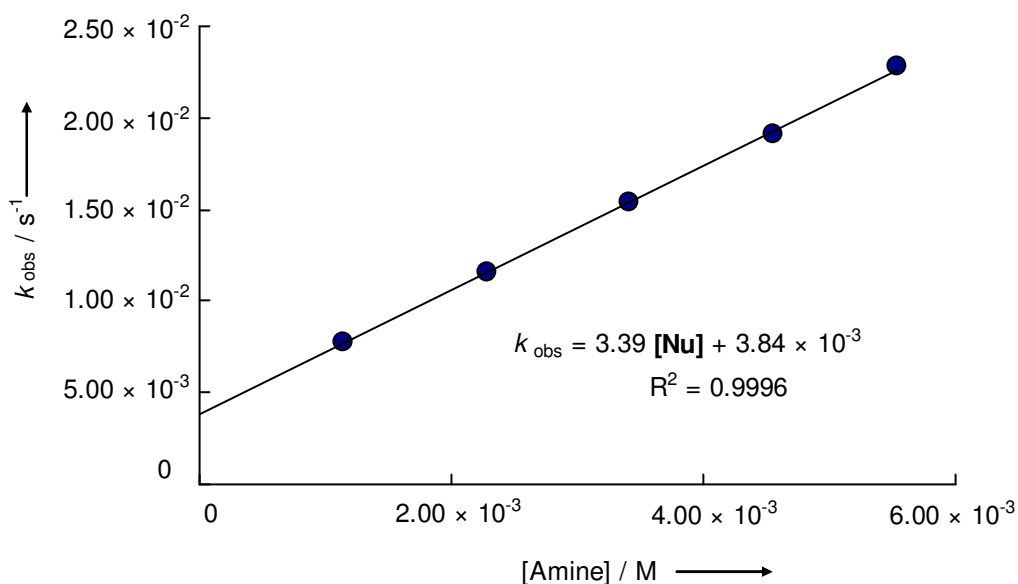
[1b] / M	[PPh ₃] / M	[fn] / M	[Amine] / M	$k_{\text{obs}} / \text{s}^{-1}$
1.29×10^{-4}	0	7.10×10^{-4}	5.54×10^{-3}	$4.06 \times 10^{-3}{}^a$
1.29×10^{-4}	1.53×10^{-3}	7.10×10^{-4}	5.54×10^{-3}	1.49×10^{-2}
1.29×10^{-4}	3.07×10^{-3}	7.10×10^{-4}	5.54×10^{-3}	1.82×10^{-2}
1.29×10^{-4}	6.13×10^{-3}	7.10×10^{-4}	5.54×10^{-3}	$2.28 \times 10^{-2}{}^b$
1.29×10^{-4}	9.20×10^{-3}	7.10×10^{-4}	5.54×10^{-3}	2.57×10^{-2}
1.29×10^{-4}	1.23×10^{-2}	7.10×10^{-4}	5.54×10^{-3}	3.02×10^{-2}

^a „Best monoexponential fit“ of non-first order absorbance decay.



As the $k_{\text{obs}}\text{-[PPh}_3\text{]}$ dependence is linear even at the highest amine concentration used, when $[\text{PPh}_3] > 3 \text{ mM}$ (see Figure above), these values of k_{obs} correspond to $k_{1\psi}^{\text{amine}} + k_{1\psi}^{\text{PPh}_3}$. As all the values were measured at almost the same $[\text{PPh}_3]$, the second term should be constant and the slope of k_{obs} vs $[\text{Amine}]$ plots gives k_2^{amine} .

[1b] / M	[PPh ₃] / M	[fn] / M	[Amine] / M	$k_{\text{obs}} / \text{s}^{-1}$
1.33×10^{-4}	6.33×10^{-3}	7.33×10^{-4}	1.14×10^{-3}	7.75×10^{-3}
1.12×10^{-4}	6.32×10^{-3}	7.32×10^{-4}	2.28×10^{-3}	1.16×10^{-2}
1.12×10^{-4}	6.31×10^{-3}	7.30×10^{-4}	3.42×10^{-3}	1.54×10^{-2}
1.12×10^{-4}	6.29×10^{-3}	7.29×10^{-4}	4.55×10^{-3}	1.91×10^{-2}
1.29×10^{-4}	6.13×10^{-3}	7.10×10^{-4}	5.54×10^{-3}	2.28×10^{-2}

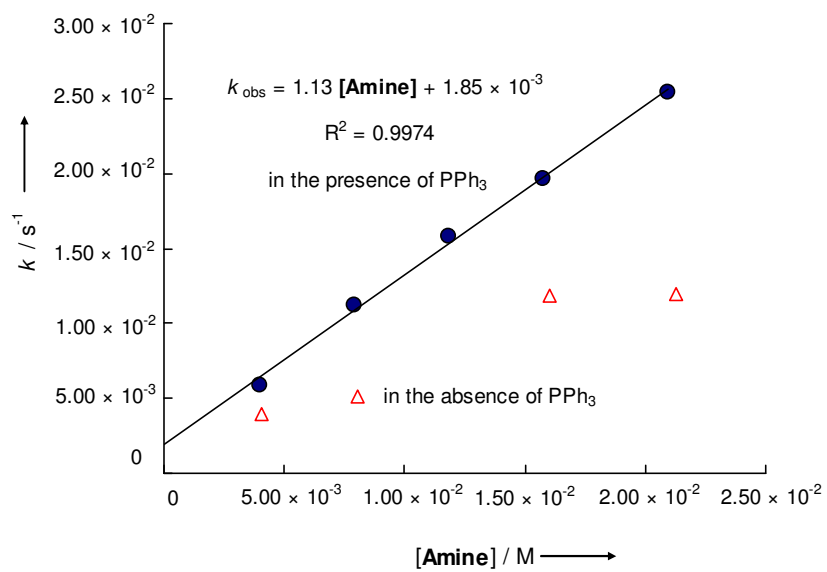


$$k_2 = 3.39 \text{ M}^{-1} \text{ s}^{-1}$$

Reaction of **1b** with benzylamine (**2g**) in the presence of fumaronitrile (fn) and triphenylphosphine, $\lambda_{\text{obs}} = 357 \text{ nm}$, acetonitrile, $20 \text{ }^\circ\text{C}$, conventional UV–vis spectrometry. The values of k_{obs} used for the determination of k_2^{amine} and corresponding concentrations of all components are written in **bold**.

[1b] / M	[fn] / M	[Amine] / M	[PPh ₃] / M	$k_{\text{obs}} / \text{s}^{-1}$
1.23×10^{-4}	6.04×10^{-4}	4.03×10^{-3}	0	3.91×10^{-3a}
1.23×10^{-4}	6.02×10^{-4}	4.02×10^{-3}	8.82×10^{-4}	5.52×10^{-3}
1.22×10^{-4}	5.99×10^{-4}	4.00×10^{-3}	1.76×10^{-3}	5.74×10^{-3}
1.21×10^{-4}	5.94×10^{-4}	3.97×10^{-3}	3.48×10^{-3}	5.90×10^{-3b}
1.23×10^{-4}	6.03×10^{-4}	8.05×10^{-3}	0	5.84×10^{-3a}
1.23×10^{-4}	6.02×10^{-4}	8.03×10^{-3}	4.41×10^{-4}	9.18×10^{-3}
1.22×10^{-4}	6.00×10^{-4}	8.02×10^{-3}	8.80×10^{-4}	9.96×10^{-3}
1.22×10^{-4}	5.98×10^{-4}	7.99×10^{-3}	1.75×10^{-3}	1.08×10^{-2}
1.21×10^{-4}	5.93×10^{-4}	7.92×10^{-3}	3.48×10^{-3}	1.12×10^{-2b}
1.23×10^{-4}	6.02×10^{-4}	1.21×10^{-2}	0	6.96×10^{-3a}
1.22×10^{-4}	6.00×10^{-4}	1.20×10^{-2}	4.40×10^{-4}	1.36×10^{-2}
1.22×10^{-4}	5.97×10^{-4}	1.20×10^{-2}	1.75×10^{-3}	1.51×10^{-2}
1.21×10^{-4}	5.92×10^{-4}	1.19×10^{-2}	3.47×10^{-3}	1.58×10^{-2b}
1.22×10^{-4}	6.00×10^{-4}	1.60×10^{-2}	0	1.18×10^{-2a}
1.20×10^{-4}	5.93×10^{-4}	1.58×10^{-2}	1.74×10^{-3}	1.90×10^{-2}
7.00×10^{-5}	5.91×10^{-4}	1.58×10^{-2}	3.46×10^{-3}	1.96×10^{-2b}
1.36×10^{-4}	5.10×10^{-4}	2.13×10^{-2}	0	1.20×10^{-2a}
1.35×10^{-4}	5.06×10^{-4}	2.11×10^{-2}	2.08×10^{-3}	2.44×10^{-2}
1.34×10^{-4}	5.02×10^{-4}	2.09×10^{-2}	4.14×10^{-3}	2.54×10^{-2b}
1.33×10^{-4}	4.98×10^{-4}	2.08×10^{-2}	6.15×10^{-3}	2.55×10^{-2}

^a „Best monoexponential fit“ of non-first order absorbance decay. ^b The figure left below shows that at $[\text{PPh}_3] > 3 \times 10^{-3} \text{ M}$ the plateau is reached. Therefore the k_{obs} values measured in this concentration region correspond to $k_{1\psi\text{plateau}}^{\text{amine}} + k_{1\psi}^{\text{PPh}_3}$, and the latter term should be constant at the same $[\text{PPh}_3]$.



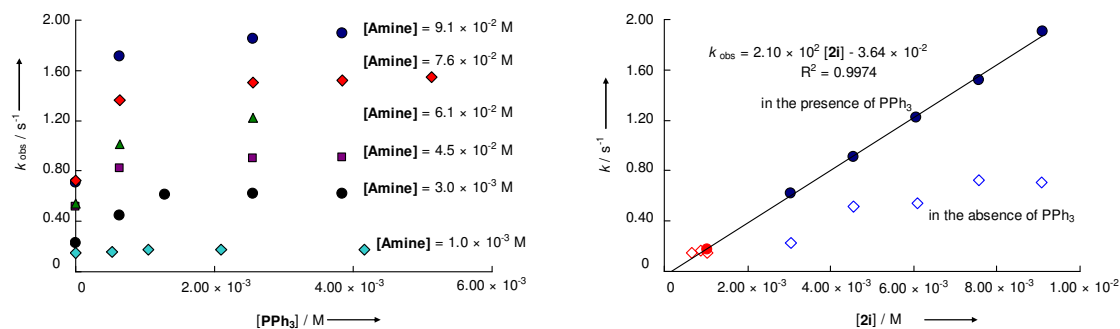
$$k_2 = 1.13 \text{ M}^{-1} \text{ s}^{-1}$$

Reaction of **1b** with piperidine (**2i**) in the presence of fumaronitrile (fn), $\lambda_{\text{obs}} = 357$ nm, acetonitrile, 20 °C, conventional UV–vis and stopped-flow measurements. Due to the higher precision only stopped-flow-derived k_{obs} (which also represent $k_{1\psi}^{\text{amine}}$ as $k_{1\psi}^{\text{PPh}_3} \ll k_{1\psi}^{\text{amine}}$) values were used for determination of k_2 (these values are written in **bold**).

[1b]	[fn] / M	[Amine] / M	[PPh ₃] / M	$k_{\text{obs}} / \text{s}^{-1}$
6.30×10^{-5}	0	6.62×10^{-4}	0	$1.48 \times 10^{-1 a}$
6.30×10^{-5}	0	8.82×10^{-4}	0	$1.69 \times 10^{-1 a}$
8.06×10^{-5}	5.13×10^{-4}	1.04×10^{-3}	0	$1.49 \times 10^{-1 a}$
8.05×10^{-5}	5.12×10^{-4}	1.04×10^{-3}	5.28×10^{-4}	$1.58 \times 10^{-1 b}$
8.03×10^{-5}	5.11×10^{-4}	1.04×10^{-3}	1.05×10^{-3}	$1.76 \times 10^{-1 b}$
8.00×10^{-5}	5.09×10^{-4}	1.04×10^{-3}	2.10×10^{-3}	$1.78 \times 10^{-1 b}$
7.93×10^{-5}	5.05×10^{-4}	1.03×10^{-3}	4.16×10^{-3}	$1.72 \times 10^{-1 b}$
9.61×10^{-5}	6.99×10^{-4}	3.04×10^{-3}	0	$2.31 \times 10^{-1 c}$
9.61×10^{-5}	6.99×10^{-4}	3.04×10^{-3}	6.40×10^{-4}	$4.49 \times 10^{-1 c}$
9.61×10^{-5}	6.99×10^{-4}	3.04×10^{-3}	1.28×10^{-3}	$6.12 \times 10^{-1 c}$
9.61×10^{-5}	6.99×10^{-4}	3.04×10^{-3}	2.56×10^{-3}	$6.19 \times 10^{-1 c}$
9.61×10^{-5}	6.99×10^{-4}	3.04×10^{-3}	3.84×10^{-3}	$6.21 \times 10^{-1 c}$
9.61×10^{-5}	6.99×10^{-4}	4.54×10^{-3}	0	$5.18 \times 10^{-1 c}$
9.61×10^{-5}	6.99×10^{-4}	4.54×10^{-3}	6.40×10^{-4}	$8.21 \times 10^{-1 c}$
9.61×10^{-5}	6.99×10^{-4}	4.54×10^{-3}	2.56×10^{-3}	$8.99 \times 10^{-1 c}$
9.61×10^{-5}	6.99×10^{-4}	4.54×10^{-3}	3.84×10^{-3}	$9.08 \times 10^{-1 c}$
9.61×10^{-5}	6.99×10^{-4}	6.07×10^{-3}	0	$5.38 \times 10^{-1 c}$
9.61×10^{-5}	6.99×10^{-4}	6.07×10^{-3}	6.40×10^{-4}	1.01^c
9.61×10^{-5}	6.99×10^{-4}	6.07×10^{-3}	2.56×10^{-3}	1.22^c
9.61×10^{-5}	6.99×10^{-4}	7.57×10^{-3}	0	$7.21 \times 10^{-1 c}$
9.61×10^{-5}	6.99×10^{-4}	7.57×10^{-3}	6.40×10^{-4}	1.37^c
9.61×10^{-5}	6.99×10^{-4}	7.57×10^{-3}	2.56×10^{-3}	1.50^c
9.61×10^{-5}	6.99×10^{-4}	7.57×10^{-3}	3.84×10^{-3}	1.52^c
9.61×10^{-5}	6.99×10^{-4}	7.57×10^{-3}	5.12×10^{-3}	1.55^c
9.61×10^{-5}	6.99×10^{-4}	9.09×10^{-3}	0	$7.05 \times 10^{-1 c}$
9.61×10^{-5}	6.99×10^{-4}	9.09×10^{-3}	6.40×10^{-4}	1.72^c
9.61×10^{-5}	6.99×10^{-4}	9.09×10^{-3}	2.56×10^{-3}	1.85^c
9.61×10^{-5}	6.99×10^{-4}	9.09×10^{-3}	3.84×10^{-3}	1.90^c

^a „Best monoexponential fit“ of non-first order absorbance decay. ^b

Conventional UV–vis measurements. ^c Stopped-flow measurements.

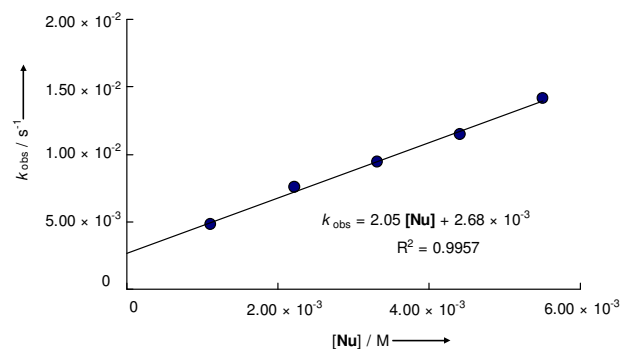


Red points: conventional UV–vis measurements, blue points: stopped-flow measurements.

$$k_2 = 2.10 \times 10^2 \text{ M}^{-1} \text{ s}^{-1}$$

Reaction of **1c** with 1-(N-pyrrolidino)cyclohexene (**2c**), $\lambda_{\text{obs}} = 455 \text{ nm}$, dichloromethane, $20 \text{ }^\circ\text{C}$, conventional UV–vis spectrometry. To turn back the partial, slowly proceeding decomposition of the electrophile in the stock solution, small amounts of PPh_3 were added.

$[1c] / \text{M}$	$[\text{PPh}_3] / \text{M}$	$[\text{Nu}] / \text{M}$	$k_{\text{obs}} / \text{s}^{-1}$
1.34×10^{-4}	1.86×10^{-4}	1.11×10^{-3}	4.79×10^{-3}
1.34×10^{-4}	1.85×10^{-4}	2.22×10^{-3}	7.57×10^{-3}
1.34×10^{-4}	1.85×10^{-4}	3.32×10^{-3}	9.41×10^{-3}
1.33×10^{-4}	1.84×10^{-4}	4.42×10^{-3}	1.15×10^{-2}
1.33×10^{-4}	1.84×10^{-4}	5.51×10^{-3}	1.41×10^{-2}

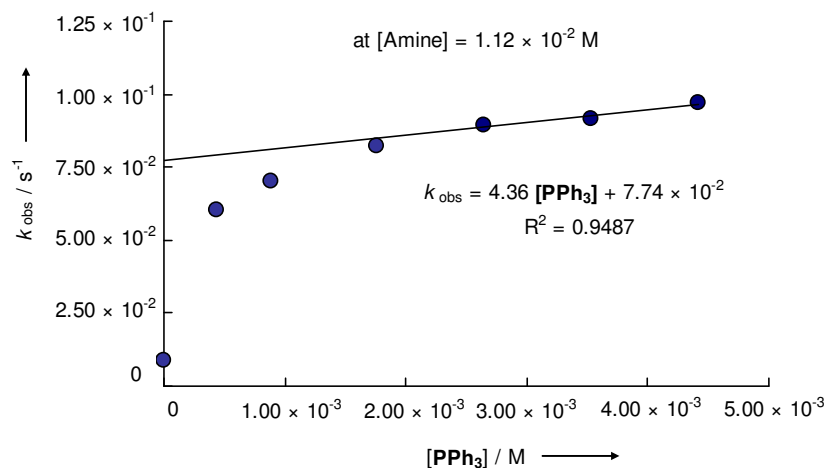


$$k_2 = 2.05 \text{ M}^{-1} \text{ s}^{-1}$$

Reaction of **1c** with 1-amino-2-propanol (**2f**) in the presence and triphenylphosphine, $\lambda_{\text{obs}} = 455 \text{ nm}$, DMSO, $20 \text{ }^\circ\text{C}$, conventional UV–vis spectrometry.

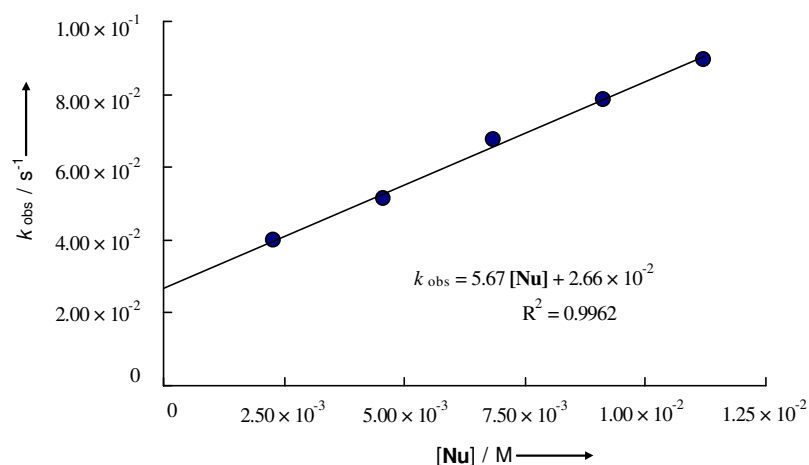
$[1c] / \text{M}$	$[\text{PPh}_3] / \text{M}$	$[\text{Amine}] / \text{M}$	$k_{\text{obs}} / \text{s}^{-1}$
9.83×10^{-5}	0	1.12×10^{-2}	$8.77 \times 10^{-3}{}^a$
9.83×10^{-5}	4.41×10^{-4}	1.12×10^{-2}	6.01×10^{-2}
9.83×10^{-5}	8.83×10^{-4}	1.12×10^{-2}	7.01×10^{-2}
9.83×10^{-5}	1.77×10^{-3}	1.12×10^{-2}	8.25×10^{-2}
9.83×10^{-5}	2.65×10^{-3}	1.12×10^{-2}	8.95×10^{-2}
9.83×10^{-5}	3.53×10^{-3}	1.12×10^{-2}	9.18×10^{-2}
9.83×10^{-5}	4.41×10^{-3}	1.12×10^{-2}	9.72×10^{-2}

^a „Best monoexponential fit“ of non-first order absorbance decay



As the $k_{\text{obs}}\text{-[PPh}_3]$ dependence is linear even at the highest amine concentration used, when $[\text{PPh}_3] > 2$ mM (see Figure above), these values of k_{obs} correspond to $k_{1\psi\text{plateau}}^{\text{amine}} + k_{1\psi}^{\text{PPh}_3}$. As all the values were measured at the almost the same $[\text{PPh}_3]$, the second term should be constant and the slope of k_{obs} vs [Amine] plot gives k_2^{amine} .

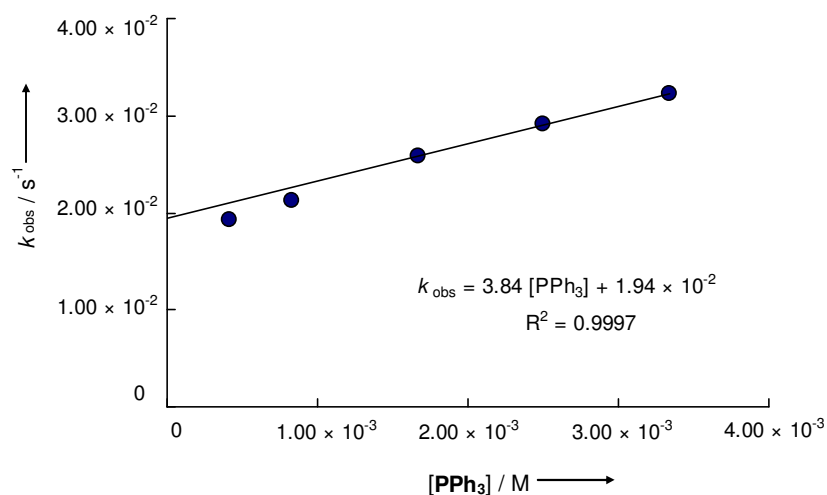
[1c] / M	[PPh ₃] / M	[Amine] / M	$k_{\text{obs}} / \text{s}^{-1}$
1.01×10^{-4}	2.71×10^{-3}	2.29×10^{-3}	3.98×10^{-2}
1.00×10^{-4}	2.71×10^{-3}	4.58×10^{-3}	5.11×10^{-2}
8.03×10^{-5}	2.70×10^{-3}	6.86×10^{-3}	6.74×10^{-2}
6.69×10^{-5}	2.70×10^{-3}	9.13×10^{-3}	7.85×10^{-2}
9.83×10^{-5}	2.65×10^{-3}	1.12×10^{-2}	8.95×10^{-2}



$$k_2 = 5.67 \text{ M}^{-1} \text{ s}^{-1}$$

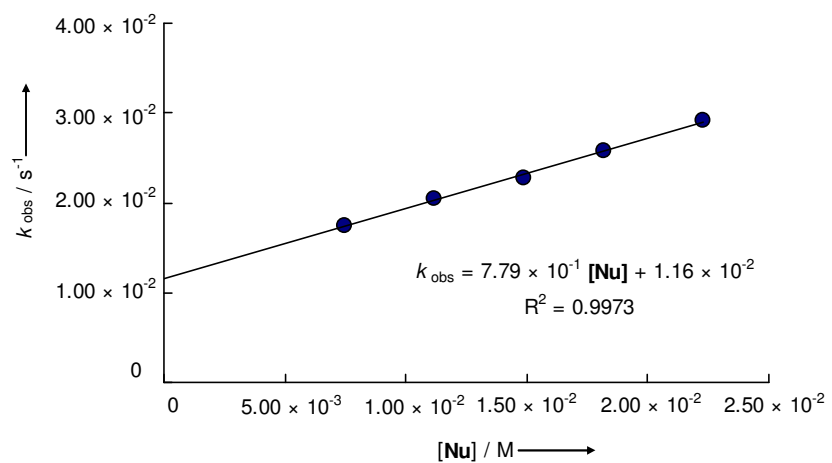
Reaction of **1c** with benzylamine (**2g**) in the presence of triphenylphosphine, $\lambda_{\text{obs}} = 460$ nm, acetonitrile, 20 °C, conventional UV-vis spectrometry.

[1c] / M	[PPh ₃] / M	[Amine] / M	$k_{\text{obs}} / \text{s}^{-1}$
1.18×10^{-4}	4.17×10^{-4}	1.82×10^{-2}	1.92×10^{-2}
1.18×10^{-4}	8.34×10^{-4}	1.82×10^{-2}	2.12×10^{-2}
1.18×10^{-4}	1.67×10^{-3}	1.82×10^{-2}	2.58×10^{-2}
1.18×10^{-4}	2.50×10^{-3}	1.82×10^{-2}	2.91×10^{-2}
1.18×10^{-4}	3.34×10^{-3}	1.82×10^{-2}	3.22×10^{-2}



As the $k_{\text{obs}}\text{-[PPh}_3\text{]}$ dependence is linear even at the one of the highest amine concentration used, when $[\text{PPh}_3] > 1.7$ mM (see Figure above), these values of k_{obs} correspond to $k_{1\psi\text{plateau}}^{\text{amine}} + k_{1\psi}^{\text{PPh}_3}$. As all the values were measured at the almost the same $[\text{PPh}_3]$, the second term should be constant and the slope of $k_{\text{obs}}\text{-[Amine]}$ plot gives k_2^{amine} .

[1c] / M	[PPh ₃] / M	[Amine] / M	$k_{\text{obs}} / \text{s}^{-1}$
1.21×10^{-4}	1.72×10^{-3}	7.50×10^{-3}	1.75×10^{-2}
1.21×10^{-4}	1.72×10^{-3}	1.12×10^{-2}	2.05×10^{-2}
1.21×10^{-4}	1.71×10^{-3}	1.49×10^{-2}	2.28×10^{-2}
1.18×10^{-4}	1.67×10^{-3}	1.82×10^{-2}	2.58×10^{-2}
1.20×10^{-4}	1.70×10^{-3}	2.23×10^{-2}	2.91×10^{-2}



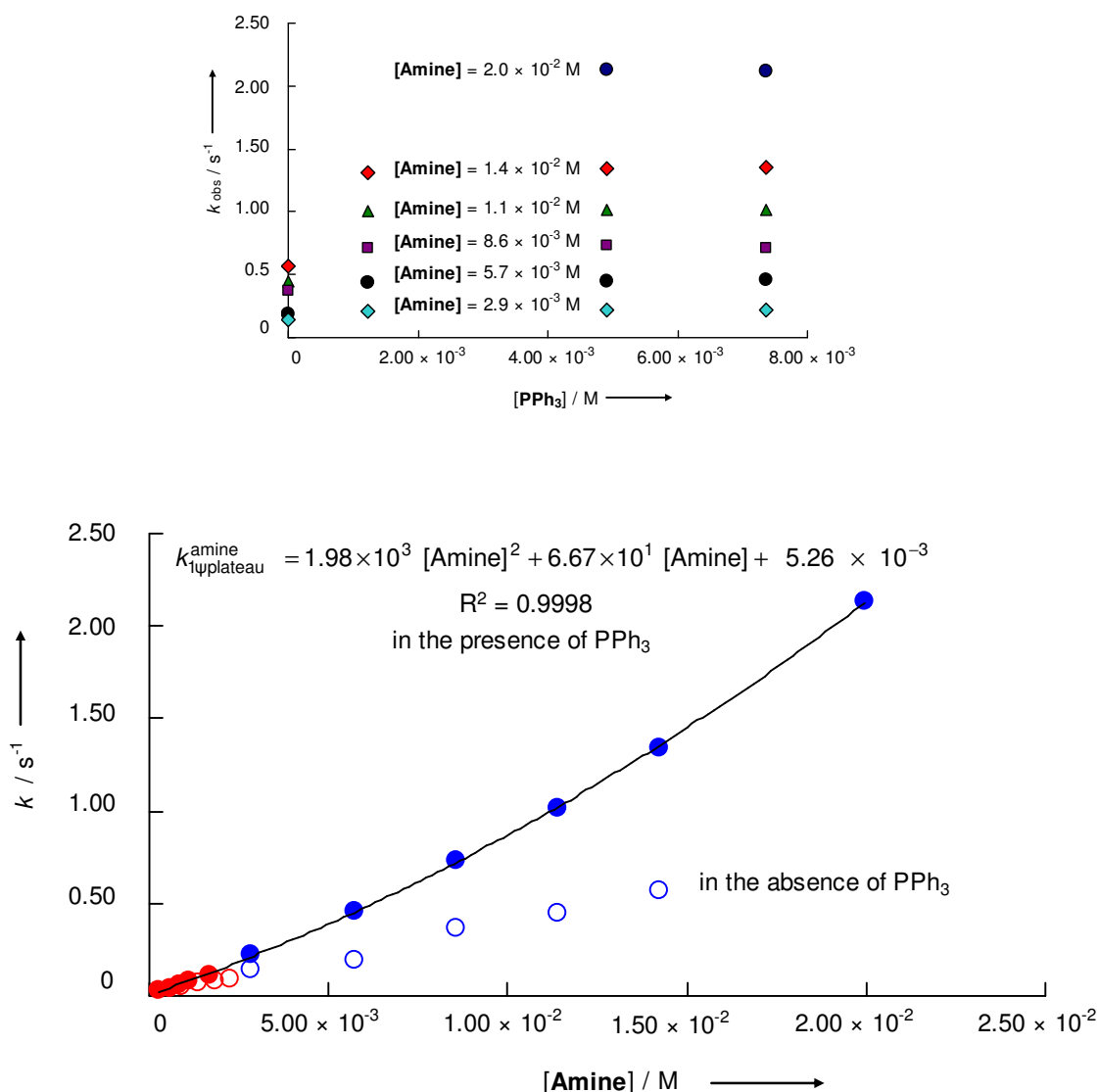
$$k_2 = 7.79 \times 10^{-1} \text{ M}^{-1} \text{ s}^{-1}$$

Reaction of **1c** with piperidine (**2i**), $\lambda_{\text{obs}} = 357$ nm, acetonitrile, 20 °C, conventional UV–vis and stopped-flow measurements. Due to the highest precision only stopped-flow-derived k_{obs} values (which also represent $k_{1\psi}^{\text{amine}}$ as $k_{1\psi}^{\text{PPh}_3} \ll k_{1\psi}^{\text{amine}}$) were used for determination of k_2 (these values are written in **bold**).

[1c] / M	[Amine] / M	[PPh ₃] / M	$k_{\text{obs}} / \text{s}^{-1}$
1.14×10^{-4}	9.15×10^{-4}	0	$4.69 \times 10^{-2 a, b}$
1.13×10^{-4}	1.37×10^{-3}	0	$7.20 \times 10^{-2 a, b}$
1.13×10^{-4}	1.82×10^{-3}	0	$8.03 \times 10^{-2 a, b}$
1.13×10^{-4}	2.27×10^{-3}	0	$9.35 \times 10^{-2 a, b}$
1.15×10^{-4}	1.12×10^{-3}	8.45×10^{-4}	$8.36 \times 10^{-2 b}$
1.15×10^{-4}	1.68×10^{-3}	8.42×10^{-4}	$1.12 \times 10^{-1 b}$
7.50×10^{-5}	2.85×10^{-3}	0	$1.41 \times 10^{-1 a, c}$
7.50×10^{-5}	2.85×10^{-3}	1.23×10^{-3}	$2.06 \times 10^{-1 c}$
7.50×10^{-5}	2.85×10^{-3}	4.91×10^{-3}	$2.20 \times 10^{-1 c}$
7.50×10^{-5}	2.85×10^{-3}	7.36×10^{-3}	$2.23 \times 10^{-1 c}$
7.50×10^{-5}	5.70×10^{-3}	0	$1.90 \times 10^{-1 a, c}$
7.50×10^{-5}	5.70×10^{-3}	1.23×10^{-3}	$4.42 \times 10^{-1 c}$
7.50×10^{-5}	5.70×10^{-3}	4.91×10^{-3}	$4.53 \times 10^{-1 c}$
7.50×10^{-5}	5.70×10^{-3}	7.36×10^{-3}	$4.59 \times 10^{-1 c}$
7.50×10^{-5}	8.55×10^{-3}	0	$3.66 \times 10^{-1 a, c}$
7.50×10^{-5}	8.55×10^{-3}	1.23×10^{-3}	$7.11 \times 10^{-1 c}$
7.50×10^{-5}	8.55×10^{-3}	4.91×10^{-3}	$7.34 \times 10^{-1 c}$
7.50×10^{-5}	8.55×10^{-3}	7.36×10^{-3}	$7.13 \times 10^{-1 c}$
7.50×10^{-5}	1.14×10^{-2}	0	$4.43 \times 10^{-1 a, c}$
7.50×10^{-5}	1.14×10^{-2}	1.23×10^{-3}	1.00^c
7.50×10^{-5}	1.14×10^{-2}	4.91×10^{-3}	1.02^c
7.50×10^{-5}	1.14×10^{-2}	7.36×10^{-3}	1.01^c
7.50×10^{-5}	1.43×10^{-2}	0	$5.67 \times 10^{-1 a, c}$
7.50×10^{-5}	1.43×10^{-2}	1.23×10^{-3}	1.31^c
7.50×10^{-5}	1.43×10^{-2}	4.91×10^{-3}	1.34^c
7.50×10^{-5}	1.43×10^{-2}	7.36×10^{-3}	1.35^c
7.50×10^{-5}	2.00×10^{-2}	4.91×10^{-3}	2.13^c
7.50×10^{-5}	2.00×10^{-2}	7.36×10^{-3}	2.12^c

^a „Best monoexponential fit“ of non-first order absorbance decay. ^b

Conventional UV–vis measurements. ^c Stopped-flow measurements.



Red points: conventional UV–vis measurements, blue points: stopped-flow measurements.

$$k_2 \approx 6.67 \times 10^1 \text{ M}^{-1} \text{ s}^{-1}$$

The mixed first and second order in nucleophile was reported for reactions of amines with cationic allylpalladium complexes carrying iminophosphine ligands.⁷ This kinetic behavior was rationalized with possibility of reversible coordination of one amine molecule on the central metal forming pentacoordinated palladium species, which also can act as electrophiles towards amines. Considering this pathway and the attack of amines at the allyl ligand of the initial complex, one can derive the rate law with mixed first and second order in nucleophile. For more details see ref 7.

4.6. ESI Experiments

4.6.1. Sample preparation and settings

A 12.2 mM solution of corresponding benzylamine (**2g**) in acetonitrile was added to a 0.2 mM solution of **1a**-BF₄ in same solvent and the resulting mixture was immediately injected in the HCT quadrupole ion trap mass-spectrometer (Bruker Daltonik).

Instrument settings: backing pressure of the nebulizer gas $p(\text{N}_2) \approx 0.7$ bar, voltage of the ESI capillary $V_{\text{ESI}} \approx -4.0$ kV, temperature of the drying gas $\theta(\text{N}_2) = 60$ °C (at a flow rate of 5 L min⁻¹), voltage of the capillary exit $V_{\text{ce}} \approx +117$ V, voltage of the skimmer $V_{\text{sk}} \approx +40$ V. The ions were then transferred into the instrument's three-dimensional quadrupole ion trap by means of two octopole ion guides with voltage offsets of $V(\text{Oct 1 DC}) \approx +12$ V and $V(\text{Oct 2 DC}) \approx 2$ V. The quadrupole trap was filled with helium (Air Liquide, 99.999% purity, estimated pressure $p(\text{He}) \approx 2$ mtorr) and operated at trap drive level of 50. The Compass 1.3 software package was used to manipulate the ions in the trap to afford their detection in simple MS experiments and their mass selection (isolation width of 1.5 amu), kinetic excitation (by applying an excitation voltage with an amplitude V_{exc}), and detection in fragmentation experiments.

4.6.2. Spectra

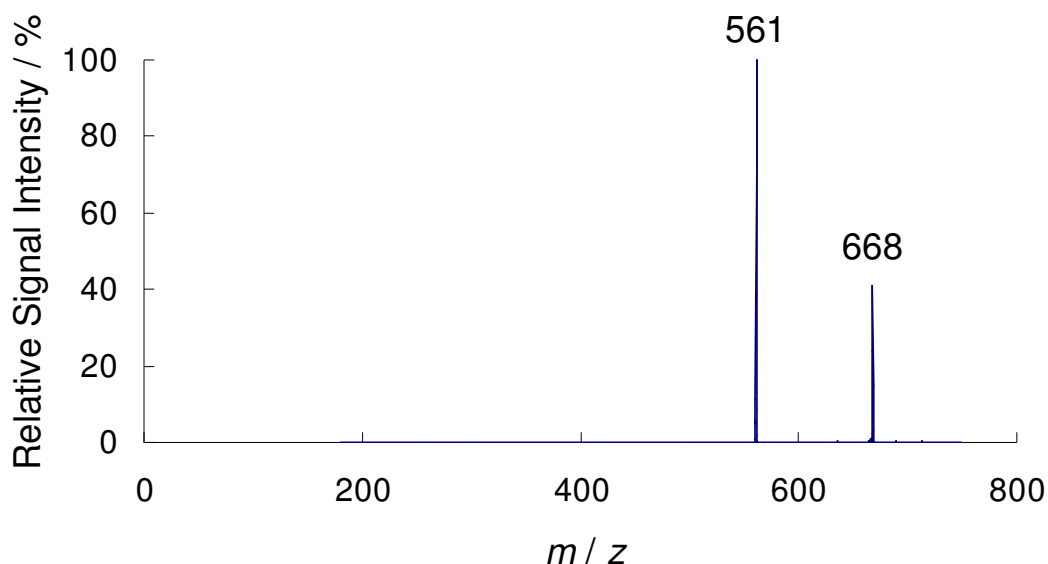


Figure S2. MS-MS for peak at 668 m/z (complex **1a'**).

The ESI-MS spectrum and comparisons between theoretical and experimental isotopic distributions for characteristic peaks can be found in the main text of the chapter.

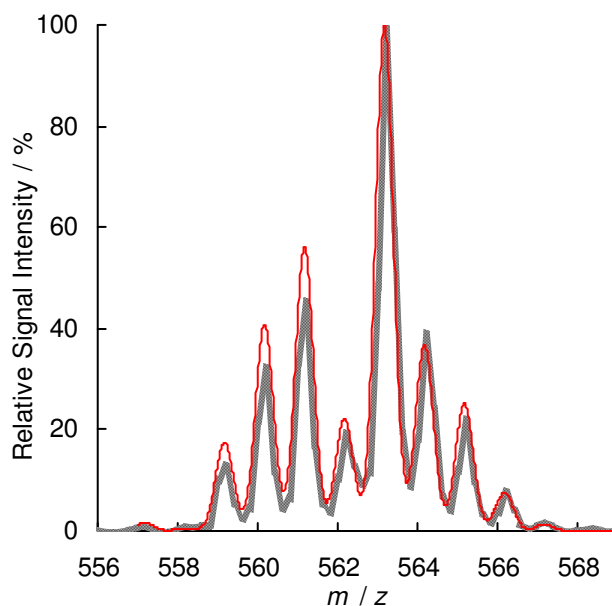
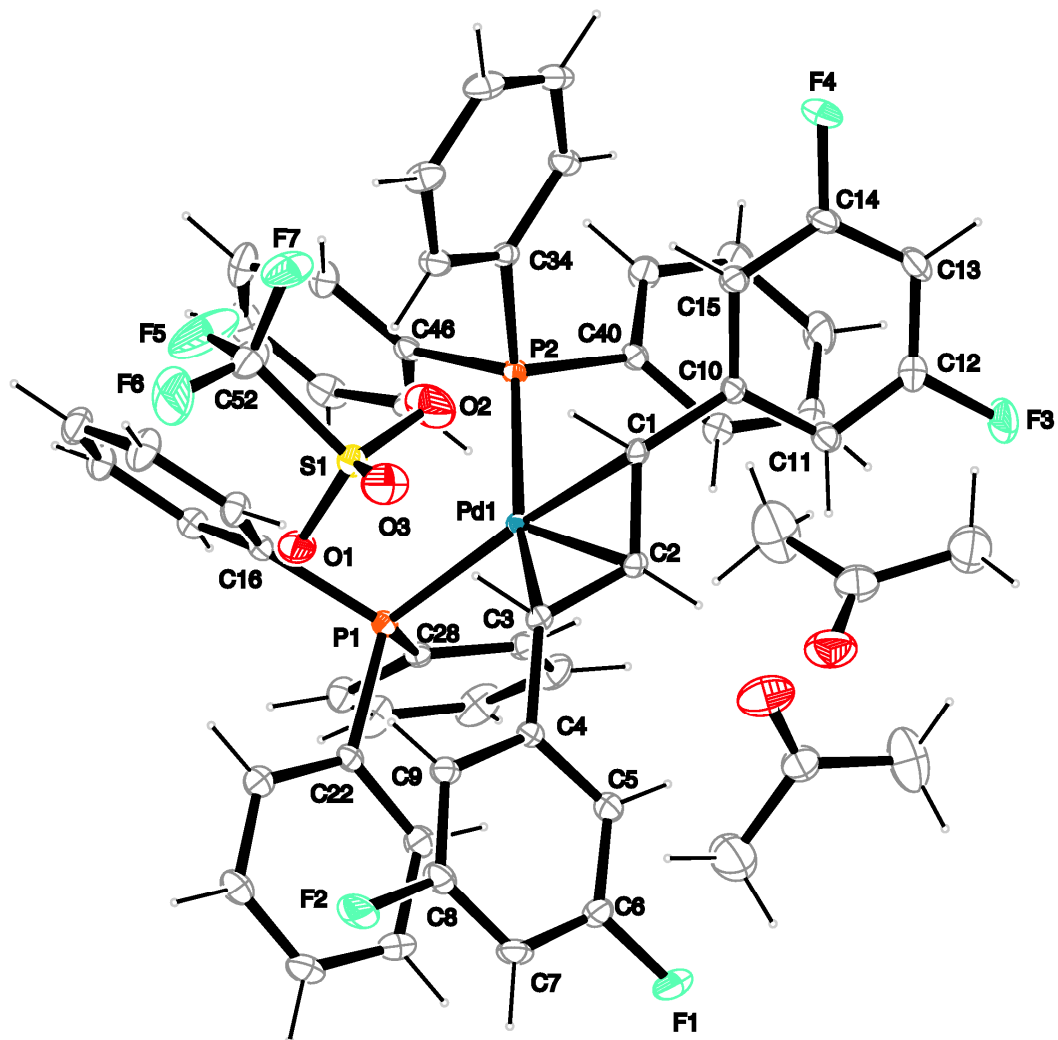


Figure S3. Comparison between experimental (black) and calculated (red) isotopic patterns for peak at 561 m/z. This signal corresponds to a mixture of $[(\text{PhCHCHCHPh})\text{Pd}(\text{PPh}_3)]^+$ and $[\text{Li}(\text{PPh}_3\text{O})_2]^+$ cation. The presence of the latter species in the spectrum can be explained by the oxidation of triphenylphosphine under ESI ionization conditions and subsequent coordination of triphenylphosphine oxide on lithium ions, which were present in the spectrometer due to unrelated experiments with lithium organic species.

4.7. Thermal Ellipsoid Plot for the Compound 1b-TfO



5. Supplementary Section

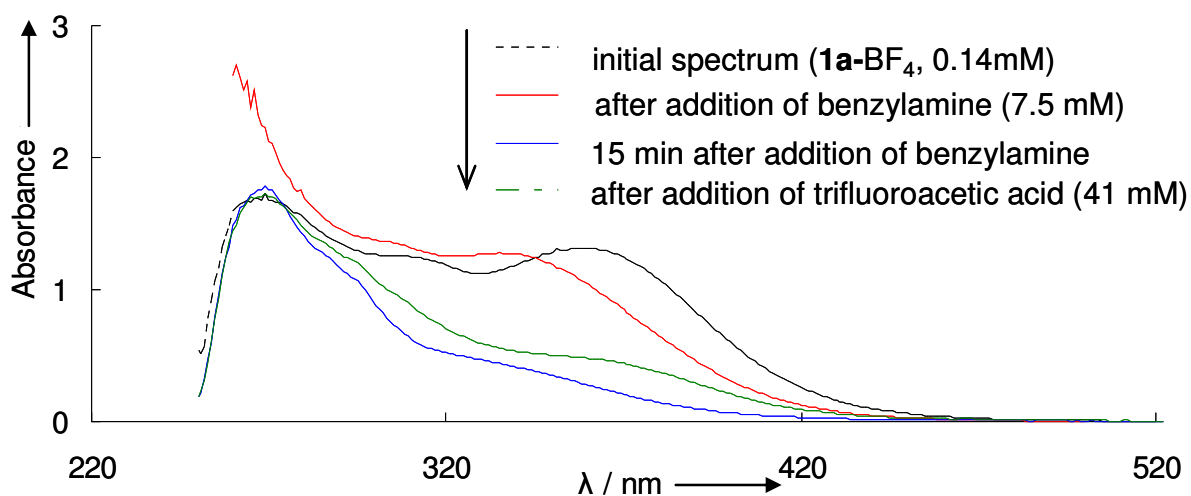


Figure S4. The irreversibility of the reaction of **1a** with benzylamine (**2g**).

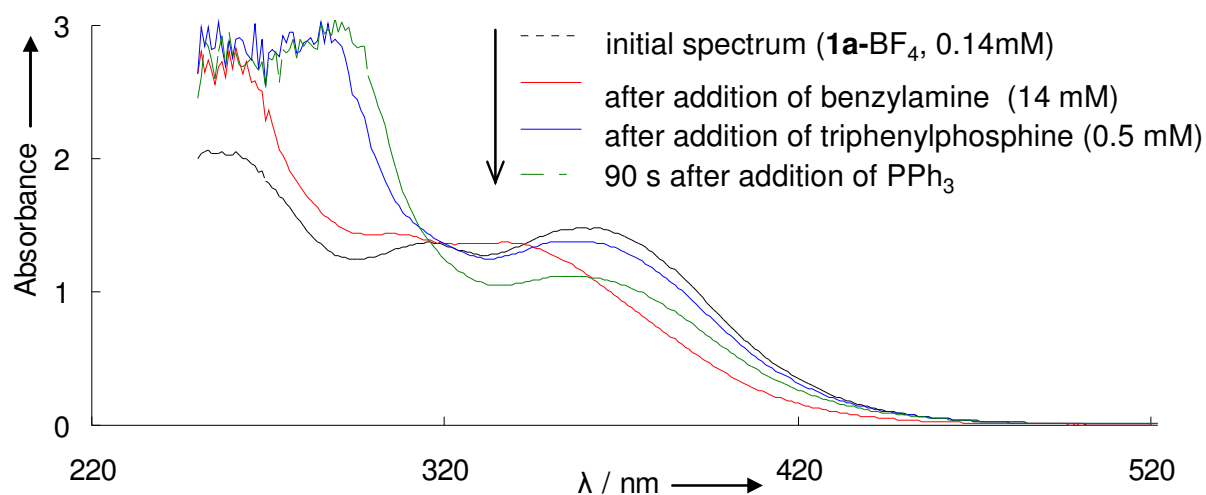


Figure S5. The reversibility of the amine-phosphine ligand exchange demonstrated by addition of PPh₃ to a mixture of **1a-BF₄** and benzylamine (**2g**).

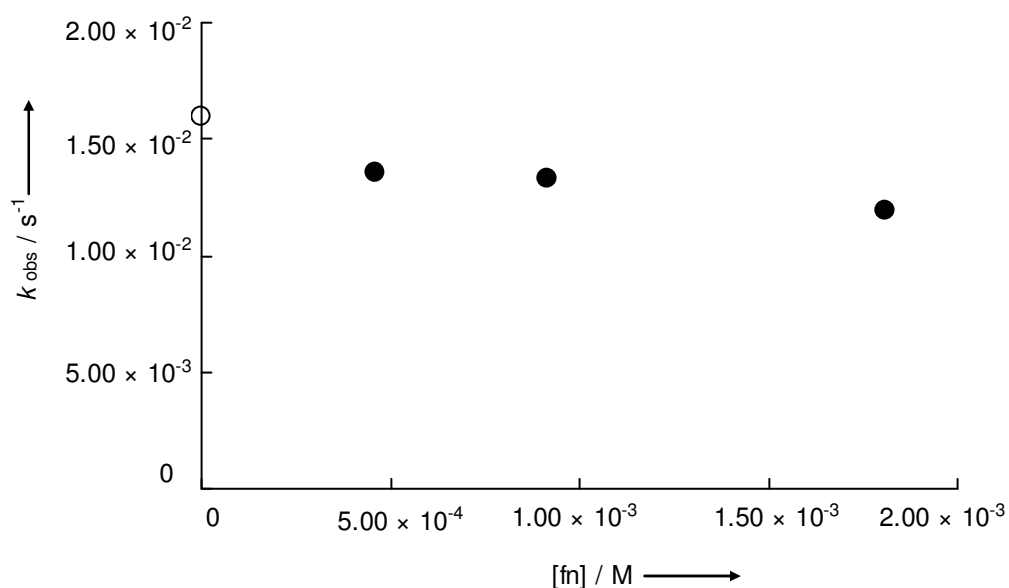


Figure S6. Rate constants of the reaction of **1a**-BF₄ (0.15 mM) with benzylamine (1.5 mM) in the presence of triphenylphosphine (0.4 mM) and various concentrations of fumaronitrile (fn). Open point corresponds to the non-first-order kinetic in the absence of fumaronitrile.

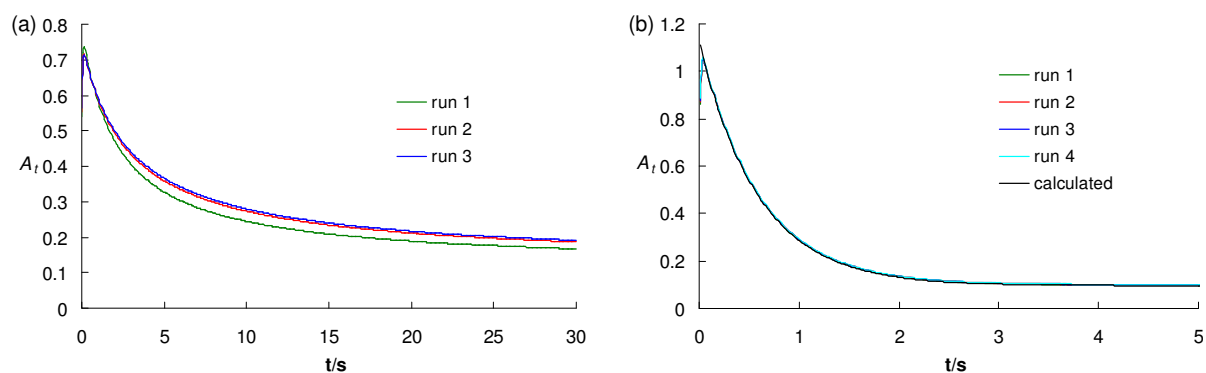


Figure S7. Kinetics of the reaction between **1a**-BF₄ and piperidine (8.3×10^{-3} M) in the presence of fumaronitrile (6.94×10^{-4} M) (a) without addition of triphenylphosphine (b) with addition of 4.85×10^{-3} M PPh₃.

6. References

- (1) (a) Trost, B. M.; Van Vranken, D. L. *Chem. Rev.* **1996**, *96*, 395–422. (b) Trost, B. M. *Chem. Pharm. Bull.* **2002**, *50*, 1–14. (c) Trost, B. M.; Crawley, M. L. *Chem. Rev.* **2003**, *103*, 2921–2943.
- (2) Jutand, A. *Appl. Organomet. Chem.* **2004**, *18*, 574–582, and references therein.
- (3) Jutand, A. *Eur. J. Inorg. Chem.* **2003**, 2017–2040.
- (4) Cantat, T.; Génin, E.; Giroud, C.; Meyer, G.; Jutand, A. *J. Organomet. Chem.* **2003**, *687*, 365–376.
- (5) Amatore, C.; Génin, E.; Jutand, A.; Mensah, L. *Organometallics* **2007**, *26*, 1875–1880; and references therein.
- (6) Kuhn, O.; Mayr, H. *Angew. Chem., Int. Ed.* **1999**, *38*, 343–346.
- (7) Crociani, B.; Antonaroli, S.; Bandoli, G.; Canovese, L.; Visentin, F.; Uguagliati, P. *Organometallics* **1999**, *18*, 1137–1147; and references therein.
- (8) (a) Canovese, L.; Visentin, F.; Chessa, G.; Niero, A.; Uguagliati, P. *Inorg. Chim. Acta* **1999**, *293*, 44–52. (b) Crociani, B.; Antonaroli, S.; Di Bianca, F.; Canovese, L.; Visentin, F.; Uguagliati, P. *J. Chem. Soc., Dalton Trans.* **1994**, 1145–1151.
- (9) Troshin, K.; Schindele, C.; Mayr, H. *J. Org. Chem.* **2011**, *76*, 9391–9408 (Chapter 3).
- (10) Mayr, H. *Angew. Chem., Int. Ed.* **2011**, *50*, 3612–3618.
- (11) For catalytic reactions see e.g.: (a) Enamines: Zhao, X.; Lui, D.; Xie, F.; Zhang, W. *Tetrahedron* **2009**, *65*, 512–517. (b) Carbanions: Ross, J.; Chen, W.; Xu, L.; Xiao, J. *Organometallics* **2001**, *20*, 138–142. (c) Amines: Faller, J. W.; Wilt, J. C. *Org. Lett.* **2005**, *7*, 633–636. For stoichiometric reactions see e.g., refs 5 and 6.
- (12) For N and s_N of (a) Enamines **2a–c**: Kempf, B.; Hampel, N.; Ofial, A. R.; Mayr, H. *Chem.–Eur. J.* **2003**, *9*, 2209–2218. (b) Carbanion **2d**: Lucius, R.; Loos, R.; Mayr, H. *Angew. Chem., Int. Ed.* **2002**, *41*, 91–95. (c) Phosphine **2e**: Kempf, B., Mayr, H. *Chem. Eur. J.* **2005**, *11*, 917–927 (d) Amine **2f**: Phan, T. B.; Nolte, C.; Kobayashi, S.; Ofial, A. R.; Mayr, H. *J. Am. Chem. Soc.* **2009**, *131*, 11392–11401. (e) Amines **2g–i**: Kanzian, T.; Nigst, T. A.; Maier, A.; Pichl, S.; Mayr, H. *Eur. J. Org. Chem.* **2009**, 6379–6385.
- (13) Amatore, C.; Bahsoun, A. A.; Jutand, A.; Mensah, L.; Meyer, G.; Ricard, L. *Organometallics* **2005**, *24*, 1569–1577.
- (14) Antonaroli, S.; Crociani, B. *J. Organomet. Chem.* **1998**, *560*, 137–146.
- (15) This ratio was found after 15 h of reaction time and probably does not correspond to the equilibrium mixture.

- (16) Åkermark, B.; Åkermark, G.; Hegedus, L. S.; Zetterberg, K. *J. Am. Chem. Soc.* **1981**, *103*, 3037–3040.
- (17) For detailed description of the method used, see: Putau, A.; Koszinowski, K. *Organometallics* **2010**, *29*, 3593–3601, and the Experimental Section.
- (18) An explanation for the higher reaction order in amine in a similar reaction was proposed in reference 7.
- (19) "What'sBest! 4.0 Commercial" by Lindo Systems Inc.
- (20) Even though the reactions of **1(a–c)** with **2i** were performed in acetonitrile and that of (η^3 -1-phenylallyl)Pd(PPh₃)₂ in dichloromethane, a direct comparison is possible, because amines were shown to have almost the same reactivity in these solvents: Ammer, J.; Baidya, M.; Kobayashi, S.; Mayr, H. *J. Phys. Org. Chem.* **2010**, *23*, 1029–1035.
- (21) (a) Mo, H.; Bao, W. *Adv. Synth. Catal.* **2009**, *351*, 2845–2849. (b) Ma, S.; Yu, S.; Peng, Z.; Guo, H. *J. Org. Chem.* **2006**, *71*, 9865–9868. (c) Usui, I.; Schmidt, S.; Keller, M.; Breit, B. *Org. Lett.* **2008**, *10*, 1207–1210.
- (22) For a database of reactivity parameters E , N , and s_N : www.cup.lmu.de/oc/mayr/DBintro.html.
- (23) Nolte, C.; Mayr, H. *Eur. J. Org. Chem.* **2010**, 1435–1439.
- (24) Hayashi, T.; Yamamoto, A.; Yoshihiko, I.; Nishioka, E.; Miura, H.; Yanagi, K. *J. Am. Chem. Soc.* **1989**, *111*, 6301–6311.
- (25) Breeden, S.; Wills, M. *J. Org. Chem.* **1999**, *64*, 9735–9738.